

HYDROGEN EMBRIITTLEMENT:

Prevention and Control

Louis Raymond, *editor*



STP 962

STP 962

Hydrogen Embrittlement: Prevention and Control

Louis Raymond, editor



ASTM
1916 Race Street
Philadelphia, PA 19103

Library of Congress Cataloging-in-Publication Data

Hydrogen embrittlement: prevention and control/[edited by] Louis Raymond.

(ASTM special technical publication; 962)

Papers from the Second National Symposium on Test Methods for Hydrogen Embrittlement: Prevention and Control, sponsored by ASTM Subcommittee F7.4 on Hydrogen Embrittlement and held in Los Angeles, May 24-26, 1985.

Includes bibliographies and index.

"ASTM publication code number (PCN) 04-962000-26."

ISBN 0-8031-0959-8

1. Metals—Hydrogen embrittlement—Congresses. 2. Metals—Testing—Congresses. I. Raymond, Louis, 1934–. II. National Symposium on Test Methods for Hydrogen Embrittlement: Prevention and Control (2nd: 1985: Los Angeles) III. ASTM Subcommittee F7.4 on Hydrogen Embrittlement. IV. Series.

TA460.H89 1988

620.1'623—dc19

88-3490
CIP

Copyright © by AMERICAN SOCIETY FOR TESTING AND MATERIALS 1988

NOTE

The Society is not responsible, as a body,
for the statements and opinions
advanced in this publication.

Peer Review Policy

Each paper published in this volume was evaluated by three peer reviewers. The authors addressed all of the reviewers' comments to the satisfaction of both the technical editor(s) and the ASTM Committee on Publications.

The quality of the papers in this publication reflects not only the obvious efforts of the authors and the technical editor(s), but also the work of these peer reviewers. The ASTM Committee on Publications acknowledges with appreciation their dedication and contribution of time and effort on behalf of ASTM.

Foreword

This publication, *Hydrogen Embrittlement: Prevention and Control*, contains papers presented at the Second National Symposium on Test Methods for Hydrogen Embrittlement: Prevention and Control, which was held in Los Angeles 24–26 May 1985. The symposium was sponsored by ASTM Subcommittee F7.4 on Hydrogen Embrittlement. Louis Raymond, Ph.D., L. Raymond & Associates, presided as symposium chairman and was editor of this publication.

Contents

Introduction—L. RAYMOND	1
 SECTION 1: OVERVIEW	
Opening Remarks—C. SONNINO	7
Overview: Sections 1 and 2—A. A. ANCTIL	8
Hydrogen Embrittlement Test Methods: Current Status and Projections—L. RAYMOND	10
Electrochemical Aspects of Hydrogen in Metals—J. J. DELUCCIA	17
 SECTION 2: CURRENT STANDARDS AND PROJECTIONS	
Hydrogen Embrittlement Coverage by U.S. Government Standardization Documents—E. T. CLEGG	37
Other ASTM Committees and ISO Committees Involved in Hydrogen Embrittlement Test Methods—A. W. GROBIN, JR.	46
Specifications for Hydrogen Control Testing of Materials—D. J. COATES	55
Accelerated Acceptance Testing for Hydrogen Embrittlement Control—R. V. DREHER	60
Assessment of the Degree of Hydrogen Embrittlement Produced in High-Strength 4340 Steel by Plating-and-Baking Processes Using Slow Strain Rate Testing—W. J. POLLOCK	68
Panel Discussion: Sections 1 and 2	81
 SECTION 3: HYDROGEN IN STEEL AND TITANIUM	
Opening Remarks—R. FRICIONI	89
Electrochemical Sensor for the Determination of Hydrogen in Metals by Potential Measurements—A. MACKOR, C. W. DE KREUK, AND J. SCHOONMAN	90
The Barnacle Electrode Method to Determine Diffusible Hydrogen in Steels—D. A. BERMAN AND V. S. AGARWALA	98
The Development of an In-Situ Sensor for Measuring the Hydrogen Content of Liquid Iron—T. OHTSUBO, H. KAWASE, AND S. YAMAZAKI	105

A Study of the Effect of Voids on Hydrogen Diffusion Through Electroslag Refined Steel—M. WANG AND P. G. SHEWMON	117
Panel Discussion: Section 3	125
Summary: Section 3—R. FRICIONI	128
 SECTION 4: RELATIVE SUSCEPTIBILITY	
Overview: Section 4—D. R. MCINTYRE	133
Sensitivity of Steels to Degradation in Gaseous Hydrogen—H. J. CIALONE AND J. H. HOLBROOK	134
Discussion	151
The Present Status of the Disk Pressure Test for Hydrogen Embrittlement—J.-P. FIDELLE	153
Discussion	171
Screening Tests for Hydrogen Stress Cracking Susceptibility—W. R. CRUMLY	173
Ranking Materials for Extreme Sour Gas Service Using the Slow Strain Rate Method—D. R. MCINTYRE	178
A Bent Beam Test Method for Hydrogen Sulfide Stress Corrosion Cracking Resistance—D. O. COX	190
Discussion	198
Selection of Petroleum Industry Materials Through Use of Environmental Cracking Tests—S. W. CIARALDI	200
Discussion	212
 SECTION 5: HYDROGEN IN WELDING	
Overview: Section 5—J. BLACKBURN	217
In Situ Measurement of Hydrogen in Weld Heat Affected Zones Thru Mass Spectrometry and Computer Analysis—G. M. PRESSOUYRE, V. LEMOINE, D. J. M. DUBOIS, J.-B. LEBLOND, P. R. SAILLARD, AND F. M. FAURE	219
Testing of Welding Electrodes for Diffusible Hydrogen and Coating Moisture—T. A. SIEWERT	238
Diffusible Hydrogen Testing by Gas Chromatography—M. A. QUINTANA AND J. R. DANNECKER	247
Panel Discussion: Gas Chromatography	269
The Effect of Weld Metal Diffusible Hydrogen on the Cracking Susceptibility of HY-80 Steel—R. J. WONG	274

In-Process Prediction of the Diffusible Hydrogen Content of Gas-Metal Arc—D. R. WHITE AND W. G. CHIONIS	287
Panel Discussion: Diffusible Hydrogen	299
 SECTION 6: PREVENTION AND CONTROL: CASE HISTORIES	
Overview: Section 6—W. FIELD	303
Prevention of Hydrogen Embrittlement by Surface Films—G. T. MURRAY	304
Discussion	316
Hydrogen Embrittlement and Relief Treatment Study of Zinc Phosphate-Coated Submunitions—G. P. VOORHIS	318
Discussion	334
Examination of Cadmium-Plated Aircraft Fasteners for Hydrogen Embrittlement—M. LEVY AND G. A. BRUGGEMAN	335
Discussion	341
Proof Test Logic for Hydrogen Embrittlement Control—W. E. KRAMS	343
Discussion	349
 SECTION 7: RESEARCH IN PROGRESS	
Quantitative Analysis of Critical Concentrations for Hydrogen-Induced Cracking—G. M. PRESSOUYRE AND F. M. FAURE	353
Assessment of the Degree of Hydrogen Embrittlement Produced in Plated High-Strength 4340 Steel by Paint Strippers Using Slow Strain Rate Testing—W. J. POLLOCK AND C. GREY	372
The Hydrogen Embrittlement Susceptibility of Ferrous Alloys: The Influence of Strain on Hydrogen Entry and Transport—J. R. SCULLY AND P. J. MORAN	387
Hydrogen Transport, Microstructure, and Hydrogen-Induced Cracking in Austenitic Stainless Steels—T. PERNG AND C. ALTSTETTER	403
Temperature Dependence of Fatigue Crack Propagation in Niobium-Hydrogen Alloys—N. POLVANICH AND K. SALAMA	417
Index	429

Introduction

A proliferation of test methods relative to hydrogen embrittlement prevention and control has been generated since the publication of *Hydrogen Embrittlement Testing, ASTM STP 543*. As a result, only one voluntary consensus standard, ASTM Method for Mechanical Hydrogen Embrittlement Testing of Plating Processes and Aircraft Maintenance (F 519-77), has been generated since that time. Over 30 other standards, either federal, military, international, or industrial, have incorporated variations on this single test standard to provide some semblance of consistency throughout the industry.

A recent rash of failures due to hydrogen embrittlement, including failures in alloys other than high-strength steels, has caused a revitalized interest in this activity. The need for more standard test methods has never been more apparent. To this end, it was felt that the time had come to put together a symposium bringing in experts throughout the world to provide ASTM with a state-of-the-art review of the technology, its applications, and a focus on how to prevent hydrogen embrittlement failures in the future. These failures can be prevented either: (1) by eliminating the sources of hydrogen in the making of alloys (primarily steel); (2) by the manufacturing of hardware; or (3) by the ultimate generation of hydrogen under different environmental conditions generally associated with dissimilar metals producing galvanic couples that are primarily used as sacrificial anodes to prevent corrosion.

As of this writing, hydrogen embrittlement has now been documented as the cause for failure in high-strength aluminum alloys, specifically aged to avoid stress corrosion cracking, for such critical applications as main rotor fittings for helicopter blades. Fractures have occurred, as with steel, simply with time after being exposed to moisture in a storage box that encounters common atmospheric temperatures. These failures are found with a prestressed T-73 specifically designed to eliminate susceptibility to stress corrosion cracking overage condition for a 7000 series aluminum alloy.

The response to the call for papers in 1984 was expansive. The papers were divided primarily into seven sections:

1. Overview or state-of-the-art tutorial.
2. Existing standards, both on a national and international scale.
3. Hydrogen introduced during the making of steel or other alloys.
4. Methods for measuring the relative susceptibility of other metals and alloys to hydrogen-assisted stress cracking.
5. Hydrogen induced during welding.
6. The application of coupon test techniques to the testing of actual hardware.
7. Research in progress, which will be the foundation of future research and direct the activities of universities and other research institutes in future research activities.

This volume meets the purposes for which it was organized, provides the reader with a state-of-the-art review with specific details, and offers many new ideas.

Section 1 is an overview section that provides a backdrop for topics related to the processing of steel and titanium, service environment, manufacturing and processing, prevention and control, and research in progress.

Section 2 examines current standards and their significance and identifies qualifying factors in the use and interpretation of their results. The main focus is on the introduction of hydrogen

2 HYDROGEN EMBRITTLEMENT

during manufacturing and processing, about which most of the specifications are written. ASTM Standard F 519 clearly illustrates that the standard is written solely to ensure that no hydrogen is introduced into the steel during a plating operation or during the use of maintenance chemicals in the cleaning of high-strength steels. Other technical societies have been surveyed to see how they use a variety of hydrogen embrittlement processing and control standards.

Section 3 focuses on the measurement of the hydrogen introduced during the making of steel, which can be measured as a total or diffusible hydrogen. This section summarizes advances in vacuum fusion and electrochemical methods for the measurement of both the total and diffusible hydrogen.

Section 4 provides a variety of new tests encompassing testing in high-pressure hydrogen gas environments to hydrogen sulfide stress cracking conditions encountered in the petroleum industry. The methods appear to focus on accelerated and rapid testing techniques that would be more consistent with the scheduling or time constraints of industry, with a concern about the cost impact to such controls.

Section 5 is dedicated totally to advances in hydrogen embrittlement prevention and control in welding. Real-time monitoring techniques of hydrogen during the weld metal deposition are described in addition to post-weld methods of hydrogen analysis, including mechanical tests that provide constraints that rank or evaluate hydrogen stress cracking susceptibility in welds.

Section 6 focuses on applying our knowledge of the behavior of hydrogen under sustained loads in production applications, whether these loads are externally induced or through residual stresses from processing, to actual hardware such as submunitions, fasteners, and hydraulic actuators.

Section 7 identifies research in progress related to a broad range of applications from slow strain rate tension testing to hydrogen-assisted fatigue failures in niobium. Methods of measuring hydrogen in fabricated hardware and their precision and accuracy are discussed. This STP provides a variety of new proposed test methods, interpretation of data, and use in a variety of fields that include petroleum, nuclear, aircraft, and space, in addition to the more common military applications of high-strength steels.

The STP serves as a foundation for any manufacturer involved in the plating of parts for corrosion protection and provides an awareness of the sensitivity of these parts to the environment relative to any embrittling factors that might be produced because of conditions for environmentally assisted fracture that are not commonly identified. The most prominent experts in the field of hydrogen embrittlement have contributed to this STP and can be readily identified with regard to any further information or specific details of their work that might support the prevention and control of hydrogen embrittlement failures in any new applications.

In summary, we are encountering an era where high-strength materials are being selected for applications based on ballistic impact, wear resistance, hardened surfaces for implementation of accelerated manufacturing techniques (as with self-drilling fasteners), and even hard-facing for improved wear resistance. All these methods in one way or another eventually require corrosion protection systems or the introduction of dissimilar metals. Because of the types of fabrication employed to produce hard surfaces or high-strength materials, residual stresses are inherent to the manufactured hardware. All of these factors in combination provide a potential for hydrogen embrittlement failure which cannot be ignored. Routine, conventional 3-h to 23-h baking treatments at 375°F (190.5°C) are no longer sufficient to prevent embrittlement failures with hydrogen, especially in-service.

The articles in this STP provide us with an awareness of the problems and the tools with which to address the prevention and control of any hydrogen stress assisted failures. Only by implementing this knowledge and properly interpreting test results can unanticipated hydrogen embrittlement failures of fracture critical parts be avoided. Therefore, this STP is not the com-

pletion or summary of a large amount of work that puts the problem of hydrogen embrittlement prevention and control to rest, but instead should be considered as the foundation for developing standards that will help us avoid costly life-threatening catastrophic failures in the future.

Louis Raymond, Ph.D.,

L. Raymond & Associates, P.O. Box 7925,
Newport Beach, CA 92658-7925; symposium chairman and editor.

Section 1: Overview

Opening Remarks

It is important for a better understanding of the mechanism of hydrogen embrittlement to mention the most accepted related theories. The influence of the hydrogen dissolved in the metallic lattice was emphasized for the first time by Professors Bastien and Azou in France in 1951 at the Ecole Centrale, then from 1958 to 1960 by Professor Troiano at the Case Western Institute in Cleveland.

They believe that under the influence of a stress gradient, the hydrogen atoms, or better, the hydrogen protons (being the electrons lost in the free electron cloud in the metallic lattice) diffuse to the regions with the highest tensile stresses, then reduce the cohesive force in the metal. Evidence was found that the hydrogen moves in the metal with a transport mechanism. When irreversible plastic deformations take place, the dislocations move, carrying along the protons, which pile up at obstacles as nonmetallic inclusions and form a microcrack at the head of the pileup. This explains the hydrogen embrittlement subsurface cracking. We then have to make a distinction between diffusible hydrogen that is free to diffuse out and trapped hydrogen that is attached to the dislocations, which is free to move only when the temperature is sufficiently high to increase the mobility of the dislocations. This temperature level corresponds to the recovery stage of annealing and has to be reached for hydrogen embrittlement relief.

LECO, and now a large contingency from Japan, have lead the way in separately measuring diffusible or mobile hydrogen and trapped or the total hydrogen concentration in steel. Their standards will be published separately by ASTM Committee E03 on Chemical Analysis of Metals, although in cooperation and in sanction with Subcommittee F07.04 on Hydrogen Embrittlement. Another recent approach is by David Berman, who addressed the use of the "bar-nacle" electrode to measure diffusible hydrogen in plated hardware. Similar concerns in welding are being addressed by the AWS. The use of gas chromatography and in-situ monitoring of hydrogen during welding were discussed in this symposium. Jean-Paul Fidelle, of France, updates the use of the disk pressure test for measurement of the relative susceptibility of steels to hydrogen embrittlement from a gaseous hydrogen environment. Numerous test techniques are constantly being devised and older techniques are being revised as more precise analytical tools become available.

Carlo Sonnino,

Emerson Electric Co., St. Louis, MO; chairman, Session 1.

Overview: Sections 1 and 2

The symposium on hydrogen embrittlement began with an overview session which provided the backdrop for topics related to the processing of steel and titanium, service environment, manufacturing and processing, prevention and control, and research in progress.

Louis Raymond, in his paper, writes about the current status and future projections related to hydrogen embrittlement test methods. He points out that many test methods are employed for the prevention and control of hydrogen embrittlement; however, only a few have been standardized, notably ASTM Standard F 519-77, Method for Mechanical Hydrogen Embrittlement Testing of Plating Processes and Aircraft Maintenance Chemicals. He then discusses proposed ASTM hydrogen embrittlement test standards falling into three categories: (1) hydrogen introduced while making steel; (2) hydrogen introduced during manufacturing and processing of hardware; and (3) hydrogen introduced during service or environmental exposure. When the source of hydrogen cannot be eliminated, you must measure the relative susceptibility of a candidate material as a function of that environment. Standards being proposed are related to the disk pressure test for high-pressure gases, the slow strain rate tension test for aggressive hydrogen sulfide, and the rising step load test with potentiostatic control in an aqueous environment to measure relative susceptibility as a function of melting practice, alloy additions, and processing. A summary is given on three general approaches used to evaluate the potential problem of hydrogen embrittlement in finished hardware. These approaches center on sustained load testing, the Barnacle electrode, and acoustic emission. Raymond concludes by emphasizing that future research and development efforts for standard test methods should concentrate on quantitative analysis using fracture mechanics and accelerated small specimen tests.

John J. DeLuccia's paper on electrochemical aspects of hydrogen in metals contains a review of the electrode kinetics of the hydrogen evolution reaction and the entry of electrolytic hydrogen into metals as it affects hydrogen embrittlement. The paper starts with a historic perspective, citing the findings of Cailletet in 1864 and Bodenstein in 1922 and moves quickly to recent work on the mechanisms and kinetics of hydrogen embrittlement. An excellent review of elementary electrochemistry follows, describing exchange current density, polarization (and mechanisms of), hydrogen in crack tips, the mathematics of hydrogen permeation techniques, and deviations from simple diffusion behavior. Summarizing, the author points out that the electrochemical discharge of hydrogen ions at a metallic surface occurring during electroplating, electromachining, pickling and cleaning, and corrosion can provide the hydrogen source for embrittlement. Polarization of the electrochemical discharge and recombination reactions will increase the probability of hydrogen embrittlement. In addition, the presence of innocuous electrolytes in surface crevices can act as potent sources of hydrogen. The paper contains 50 references.

Edward T. Clegg's paper is divided into two main topics: (1) a complete explanation of the Department of Defense (DOD) specifications and standards program; and (2) a summary of DOD standardization documents related to hydrogen embrittlement. He describes the DOD standardization organizational structure starting with the Secretary of Defense and culminating with each service and a defense logistics agency departmental standardization office, DEPSO. The DEPSO in turn delegates program responsibility to standardization offices located at military installations having the necessary expertise. A description of hydrogen embrittlement, cause and effect, is given. This is followed by specifics related to government standardization documents on post heat treatments, surface preparation, sampling procedures, specimen and

parts selection, and inspection techniques. Clegg concludes by listing practical steps to minimize hydrogen embrittlement. An appendix to his paper contains a list of related government specifications, standards, and handbooks.

Allen W. Grobin, Jr. gives a liaison report from ASTM Committee B08 on Metallic and Inorganic Coatings to ASTM Committee F07.04 on Hydrogen Embrittlement. Two B08 subcommittees are involved with hydrogen embrittlement: (1) B08.02 on substrate preparation to avoid embrittlement in metallic coating processes and shot peening; and (2) B08.10 on test methods for embrittlement in plated parts and for the evaluation of plating solutions. Committee B08 also prepares standards on low embrittlement processes (that is, mechanical plating, vacuum, and ion vapor deposited coatings) and administers the U.S. Technical Advisory Group for the International Standards Organization Technical Committee (ISO/TC 107) on Metallic and Nonorganic Coatings. ISO/TC 107 is preparing draft proposals to avoid/test for hydrogen embrittlement. In addition, Committee B08 works closely with Committee F16 on test methods and product specifications to detect fastener embrittlement. Grobin gives a balloting summary of proposed methods to prevent and detect embrittlement related to steel heat treatments prior to and after surface coatings and inclined wedge and notched spring tests.

The paper by David J. Coates examines some of the techniques and test methods for monitoring and control of hydrogen-induced failure of materials developed by the Society of Automotive Engineers/Aerospace Material Specifications (SAE/AMS), Industrial Fasteners Institute (IFI), American Welding Society (AWS), and National Association of Corrosion Engineers (NACE). He cites specific examples, such as SAE ARP-1525 providing test methods for determining hydrogen embrittlement effects in metals resulting from aircraft maintenance chemicals; IFI-113 having hydrogen embrittlement test procedures for quality control in the manufacture of steel self-tapping screws; AWS A4-3 having standard procedures to determine the amount of diffusible hydrogen in martensitic, bainitic, and ferritic weld metal produced by arc welding; and NACE TM-01-77 test method to determine a metals resistance to sulfide stress cracking. Coates' concluding remarks stress the importance of having a basic understanding of the applicability of test method results to "in-service" situations and the limitations of any given test method. He sees a need for increased intersociety agreement on existing specifications and test methods related to hydrogen embrittlement.

Robert Dreher addresses the importance of accelerated testing to meet production schedules. The standard 200-h sustained load tests are too long, creating as much as a 2-month delay before being scheduled for testing by a commercial laboratory. If one of the three samples ruptures before 200 h, the test must be repeated, further extending the delay to where production hardware is often installed before the testing is completed. Therefore, not only must the test time be accelerated, but the acceptance criteria revised to resolve any disputes within a much shorter time.

W. J. Pollock addresses Dreher's concerns by proposing a modification to ASTM Method for Mechanical Hydrogen Embrittlement Testing of Plating Processes and Aircraft Maintenance Chemicals (F 519) that accelerates the test by using the type 1a specimen, but in a slow strain rate (displacement controlled) notched tension test. Pollock supplies an abundance of data, evaluating a large number of platings and coatings in order to substantiate his position.

Albert A. Anctil,

Army Materials Technology Laboratory,
Watertown, MA; Cochairman, Section 1.

Hydrogen Embrittlement Test Methods: Current Status and Projections

REFERENCE: Raymond, L., “Hydrogen Embrittlement Test Methods: Current Status and Projections,” *Hydrogen Embrittlement: Prevention and Control*, ASTM STP 962, L. Raymond, Ed., American Society for Testing and Materials, Philadelphia, 1988, pp. 10–16.

ABSTRACT: This paper reviews the current standardized test methods for controlling the possibility of hydrogen embrittlement in high-strength steels as a result of different manufacturing and processing variables such as the use of maintenance chemicals or plating processes. The standards are addressed from the point of view of: (1) basic concepts for acceptance; (2) type of loading; (3) significance of time-to-failure and magnitude of stress; (4) future trends, which include the use of fracture mechanics concepts and methods for small-specimen, accelerated testing. Finally, newly proposed standards and new areas requiring hydrogen embrittlement controls are identified.

KEY WORDS: sustained load, step load, slow strain rate, tension, bending, fracture mechanics, accelerated testing, electrochemical methods, platings, maintenance chemicals, barnacle electrode

Current ASTM Standards

Although many test methods are employed for the prevention and control of hydrogen embrittlement, only a very limited number have been standardized by ASTM. Others have been developed out of necessity, primarily by hardware manufacturers in an attempt to prevent a costly recall because of the plated bolt, piston, or other piece of hardware that experiences tensile stresses in service or residual stresses from heat treatment. Military (MIL) specifications address embrittlement control in specific plating processes such as electroless nickel coating (MIL-C-26074B 1971) and electrodeposited chromium plating (MIL-C-23422 1978). Fastener societies have standards that usually include a section that addresses embrittlement control by sustained testing of the plated fastener, such as the International Fastener Institute’s “Steel Self-Drilling Tapping Screws” (IFI 113).

The major problem with these approaches is that they are not always consistent with each other; nor are they easily understood within the context of critical test parameters required to establish the validity of the test.

Basic Concepts for Acceptance

Current test methods are all relative and based on a GO–NO GO criterion, for example, ASTM Method for Mechanical Hydrogen Embrittlement Testing of Plating Processes and Aircraft Maintenance Chemicals (F 519-77), which states that mechanical coupons be made of air-melted Type 4340 steel, heat treated to 52 to 54 Rockwell Hardness (C scale) (HRC). This steel is used because it is considered the “worst case,” or more susceptible to hydrogen embrittlement than other commercially used steels. Four different types of coupons can be used; each

¹President and principal consultant, L. Raymond & Associates, Newport Beach, CA 92658-7925.

must be installed with the part during plating. If the notched coupons (Type 01) or smooth ring (Type 02) maintain the prescribed loads for 200 h, the parts are considered nonembrittled or acceptable for use.

The major objection to the current standard is that the test takes too much time and consequently is too expensive. Others claim that the coupon does not represent the part, especially when the test coupons break in less than 200 h and are cause to have the entire lot of parts rejected.

Types of Loading

The loads in ASTM F 519 are either tension or bending and are applied with either the use of a sustained or creep rupture loading frame or a self-loading fixture. The notched round tensile bar, Type 01a, requires a 12-kip loading frame. Type 01b is a notched round tensile bar with a self-loading frame used to apply the tensile stress. The specimen diameter is obviously reduced to 0.19 in. (0.48 cm) from a 0.15 in. (0.38 cm) diameter or 0.33 in. (0.84 cm) reduced diameter section for the Type 01a.

The other coupons use self-loading fixtures to apply bending loads to either a notched round bar (Type 01c) or a notched ring (Type 01d). The entire specimen is not plated because an escape path for the hydrogen is required during baking. In all cases, the notch detail is critical and crush grinding is required to make the notch.

Finally, a smooth ring is loaded in bending with an internal loading bar, that is, diametrically located (Type 02a).

In all cases, the test load is maintained constant throughout.

TTF and Magnitude of Stress

The time-to-failure (TTF) is not recorded except that if no failure occurs after 200 h, the test is discontinued and the parts are considered to be nonembrittled. The basis for this criterion is the classic work performed by Troiano [1]. Examining Fig. 1, it can be deduced that at 75% of

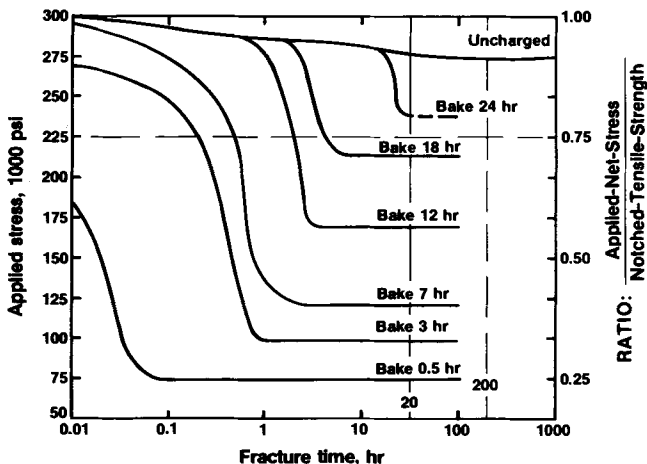


FIG. 1—The effect of baking at 300°F (149°C) on the time-to-failure at a given level of applied stress and stress ratio of notched specimens of 4340 steel heat-treated to a strength level of 230 ksi (1586 MPa).

12 HYDROGEN EMBRITTLEMENT

the notched tensile strength, rupture will occur in less than 200 h. Examining Fig. 1 more closely also shows that 20 h with no fracture essentially provides the same information.

Obviously, the original test data, that is, the basis for the standard, were generated only under tensile load, and, therefore, equivalent loads had to be established for the bend specimens. For the notched bend bar (Type 01c), the specified load is described to be 75% of the number of turns required to break the test bar before it has been plated. Other values have been proposed, but insufficient documentation of data exists to clearly establish a lower value.

Maintenance Chemicals

The test coupons for evaluating maintenance chemicals as a source of hydrogen are identical to those previously described, except that the coupons are stressed before they are exposed to the chemical, not afterwards as in the case of the plating baths. In both cases the test coupons are baked before they are stressed, but in the case of the chemicals, the baking is before exposure to hydrogen, whereas in the case of the plating, the baking is after exposure just prior to stressing in air.

Because of the more severe test conditions, 150 h has been found to be an adequate test time instead of 200 h. It should be recognized that if the test coupons were stressed prior to exposure to a plating bath, they would always fracture during plating in the bath because electrolytic plating produces much more hydrogen than maintenance chemicals, even in so-called "low hydrogen baths."

As with the plating coupons, the loads are maintained constant during the test, and after 150 h without fracture the maintenance chemical is considered to be nonembrittling.

Proposed Standards

Since the First International ASTM Symposium on Hydrogen Embrittlement Test Methods [2], testing and development have proceeded to produce several proposed standards. The grouping is in three general categories: (1) hydrogen introduced during the making of steel; (2) hydrogen introduced during the manufacturing and processing of hardware, which includes welding; and (3) hydrogen introduced during service or environmental exposure, which includes material selection or the measurement of a material's relative susceptibility to hydrogen embrittlement.

Hydrogen in Steel

Section 3 of this text focuses on measurement of hydrogen introduced in the making of steel. Several standards have been proposed, primarily a result of developments at Leco with their RH-101 model for the measurement of residual hydrogen in steel, and their DH-102 model for the measurement of diffusible hydrogen in steel. The Barnacle Electrode is also being considered for use in the measurement of diffusible hydrogen in steel, but primarily for comparison to a part after some manufacturing and processing steps.

Manufacturing and Processing

ASTM F 519 is being further evaluated with regard to reducing the test time by incorporating step loading techniques that incrementally increase the stress, thereby requiring less time for failure to occur. The advantage to this modification in loading procedure is that the test will become more discriminating with regard to the severity of embrittlement caused by the residual hydrogen from the plating bath or, for that matter, the maintenance chemicals. The disadvantage to this approach is with the smooth Type 02a ring, wherein several additional specimens

would be required at the different load levels because of the impracticality of increasing the load using a spacer bar.

The acceptance criteria are being influenced by this procedure, inasmuch as if one of three specimens fail at the initial 75% load, then the requirement will be to increase the load to the specimens that passed the initial screening. If the two remaining coupons pass the higher load requirements, then the bath is considered nonembrittling. If they fail, then the bath is considered to be embrittling.

Material Selection

Section 4 of the proceedings features papers that reflect a major activity since the majority of proposed standards are in this area. Hydrogen problems have become more encompassing than with the high-strength steels and have presented new problems to the military, and petroleum, nuclear, and aerospace industries with regard to selection of the best or most fracture-resistant material for their specific application. In many cases, the source of hydrogen cannot be eliminated. Therefore, the answer has been to measure the relative susceptibility of a material as a function of the environment.

The standards being proposed are as follows:

Gaseous, High Pressure: The Disk Pressure Test has been used to evaluate a large number of alloys, including super-, aluminum-, titanium-, nickel-, and cobalt-alloys.

H2S: The Slow Strain Rate Tensile Test is being used to evaluate the relative susceptibility of low-hardness stainless steels to the aggressive hydrogen sulfide-bearing environments found in the petroleum industry.

Electrochemical: Rising Step Load with Potentiostatic Control in an Aqueous Environment Test is being used to measure the relative susceptibility of different steels to hydrogen embrittlement with emphasis on melting practice, alloy additions, and thermomechanical processing variables.

Welding

Section 5 of the proceedings focuses on recent developments in monitoring the effects of hydrogen during welding. The effort is concurrent and in cooperation with members of the American Welding Society, where emphasis is on measuring the residual hydrogen in a standard test coupon by gas chromatography.

Real-time, in situ measurements of hydrogen during deposition of the weld are being proposed. Also, mechanical constraint tests are discussed and research activities are examining refinements in acoustic emission analysis.

Finished Hardware

Once the most suitable material is selected for a particular environment and test coupons are used to monitor and thus provide quality assurance with regard to hydrogen pickup during manufacturing and processing, the piece of finished hardware is assumed to be free of hydrogen of sufficient quantity to eliminate the potential problem of hydrogen embrittlement. This does not mean that the part will not fail by hydrogen embrittlement under actual service conditions where exposure to handling could scratch the surface and generate hydrogen in the field in the presence of moisture.

But once a field failure is attributed to hydrogen embrittlement, all of the other parts become suspect. Likewise, if two or more test coupons fail, the parts are to be rejected, but, because of the cost impact, the results of the test coupons are challenged with regard to actually representing the hardware. Under these circumstances, no choice remains but to test the hardware.

Because of these possibilities, some disciplines resort to going directly to destructive testing of a sample size from a lot of actual hardware. Such is the case with the fastener industry.

Section 6 of this text addresses some specific applications and approaches to testing actual hardware within the guidelines of ASTM standards or MIL specifications. Three general approaches are taken:

Sustained Load Testing of Hardware: Attempt to load the actual hardware in such a manner that the maximum tensile stress closely approaches the service loads. Testing times and techniques should approach those specified in ASTM F 519.

Barnacle Electrode: Measure residual hydrogen in the plated or welded steel part after removal of plating and compare current density of the electrode to a piece of the heat-treated steel before processing. As an upper bound, an as-plated piece can be similarly analyzed.

Acoustic Emission: Employ the step-loading technique and listen to acoustic emissions at each increasing load level to ascertain the extent of microcracking or subcritical crack growth and to clearly establish progressively increasing acoustical activity. Obviously, such results would be the cause for rejection.

Future Projections

The direction for the future is toward (1) quantitative analysis employing fracture mechanics and (2) accelerated, small-specimen tests to meet the needs of accelerated production schedules and accurate failure analysis determinations that require a quick response.

Quantitative Analysis

Obviously, more quantitative than relative measurements of susceptibility are primarily directed at material selection processes that incorporate fracture mechanics as part of the design process. The threshold stress intensity for stress corrosion cracking, or K_{Isc} , is the property that is measured. When the specific crack growth mechanism is by hydrogen-assisted stress cracking, the designation is K_{Ihem} . This property allows the design stress level to be related to the level of nondestructive testing (NDT) or detectable flaw size; it allows for the use of a proof test logic to establish the structural integrity or life in the same manner as with fatigue analysis. In general, the major problem with the classical fracture mechanic approach is the extensive time and prohibitive cost of testing. To overcome these obstacles, the tendency has been toward short time or accelerated test techniques that closely approximate the results of the more restrictive ASTM Test Method for Plane-Strain Fracture Toughness of Metallic Materials (E 399-83) test procedures. At a minimum, the results bracket the critical variables in establishing an extensive program consistent with ASTM E 399.

Accelerated Testing

Rising Step Load: Approaches to accelerated, small-specimen testing emphasize the use of a rising step load and a potentiostat to generate hydrogen in a specified aqueous environment [3]. A good correlation has been demonstrated for this approach with the use of modified HY-130-type steels in Fig. 2. The potentiostat can electrochemically simulate galvanic coupling found under service conditions or controlled amounts of hydrogen in different aqueous environments. This combination of test parameters and the use of a Charpy-sized specimen in bending, identical to ASTM F 519, Type 01c, allows for the measurement of K_{Ihem} in less than 8 h with one specimen as compared to the more conventional fracture mechanics stress corrosion tests such as with: (1) the cantilever beam (CB), which requires several specimens (as many as twelve), each requiring their own loading frame; or (2) the wedge opening load (WOL) specimen that can take as much as 5000 h for one specimen and can require several to determine K_{Ihem} . The

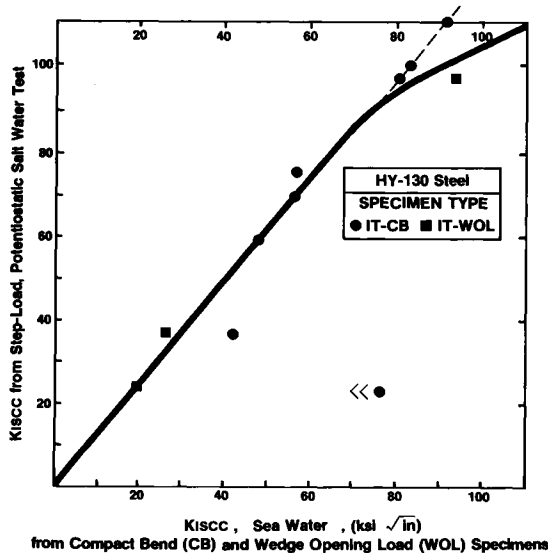


FIG. 2—The correlation between accelerated, rising step load test results and long-term, conventional stress corrosion testing is shown to be quite accurate for a series of weld and base samples of Type HY-130 steel.

validity of the measurements being made with the WOL specimen are currently being challenged because the arrest time and corresponding geometry of the test specimen are material dependent.

Slow Strain Rate Tensile: Primarily used for relative measurements of susceptibility in hydrogen environments, attempts are being made to relate the changes in the shape of the tensile curve to $K_{I_{hem}}$, which is similar to the approaches used in estimating the fracture toughness from tensile ductility parameters. The method is also finding applicability in higher strength steels and is being considered for use as a modification to F 519 as discussed in greater detail later in this book.

Galvanic Coupling: Depending on the mixed potential generated by the galvanic couple produced by dissimilar metals such as is the case with an electroplated or cadmium-plated steel bolt, in-service failures can be prevented or unknowingly be produced by an excellent corrosion protection system that overprotects but produces sufficient hydrogen to cause an embrittlement or time delay intergranular failure. The potential of the coating or the corrosion protection systems that depend on the coating being a sacrificial anode must be measured relative to the steel bolt to avoid a potential in-service problem with hydrogen embrittlement [4]. John J. De Luccia discusses these concepts in more detail in his tutorial presented in this text entitled "Electrochemical Aspects of Hydrogen in Metals."

Finally, the effects of a hydrogen-producing environment on fatigue crack initiation, growth, and the crack growth threshold stress intensity are being investigated using test methods that employ the concepts of accelerated, small-specimen test methods. Initial results have shown that galvanic protection of austenitic stainless steels in seawater will raise the fatigue threshold, but will degrade or lower the fatigue threshold for martensitic Type 410 stainless steels. In other words, the electrochemical effect can drive the fatigue threshold in opposite directions depending on the type of stainless steel.

Many other interesting concepts that also indicate the direction of new test methods and

techniques were presented at the symposium. Section 7 of this text touches on concepts considered to be "research in progress." The use of conventional electrochemical permeation techniques similar to the Barnacle Electrode to measure the critical concentrations for hydrogen-induced cracking are being investigated. In addition, research is being conducted on the role of hydrogen in fatigue crack propagation as a function of temperature; and the influence of strain and plasticity on hydrogen entry and transport as related to the hydrogen embrittlement susceptibility of ferrous alloys. The results of these research studies should provide a good foundation for the next ASTM international symposium on test methods for hydrogen embrittlement.

References

- [1] Troiano, A. R., "The Role of Hydrogen and Other Interstitials of the Mechanical Behavior of Metals," *Transactions American Society for Metals*, Vol. 52, 1960, pp. 54-80.
- [2] *Hydrogen Embrittlement Testing*, ASTM STP 543, L. Raymond, ed., American Society for Testing and Materials, Philadelphia, 1972.
- [3] Raymond, L., "Tests for Hydrogen Embrittlement," *Metals Handbook*, Vol. 8: *Mechanical Testing*, 9th ed., American Society for Metals, Metals Park, OH, 1985, pp. 537-543.
- [4] Dull, D. L., and Raymond, L., "A Test Procedure to Evaluate the Relative Susceptibility of Materials to Stress Corrosion Cracking," *Corrosion*, Vol. 29, No. 2, May 1973, pp. 205-212.

Electrochemical Aspects of Hydrogen in Metals

REFERENCE: DeLuccia, J. J., "Electrochemical Aspects of Hydrogen in Metals," *Hydrogen Embrittlement: Prevention and Control*, ASTM STP 962, L. Raymond, Ed., American Society for Testing and Materials, Philadelphia, 1988, pp. 17-34.

ABSTRACT: This is a review of the electrode kinetics of the hydrogen evolution reaction and the entry of electrolytic hydrogen into metals as it affects hydrogen embrittlement. Basic electrochemical parameters (for example, exchange current density, activation and concentration polarization, and coverage) are described for the determination of a rate and mechanism for the hydrogen evolution reaction. Hydrogen coverage dependence on overpotential and current is discussed with reference to the Langmuir adsorption isotherm. Reactions responsible for the electrolytic production of hydrogen in aqueous solutions are described for corrosion processes that occur in occluded regions on or below the surface of the metal. Hydrogen adsorption-absorption processes and electrochemical hydrogen permeation test techniques for the determination of the susceptibility of metals to internal hydrogen embrittlement are presented.

KEY WORDS: hydrogen embrittlement, hydrogen evolution kinetics, hydrogen permeation, electrochemical technique, corrosion, hydrogen diffusion, hydrogen trapping mechanism

In 1864 Caillietet discovered that a small amount of the hydrogen liberated when an iron specimen was immersed in dilute sulfuric acid was absorbed by the metal [1]. In 1922, Bodenstein found that the quantity of nascent (atomic) hydrogen entering iron could be varied by the application of a cathodic current [2]. These two simple observations demonstrated that hydrogen atoms produced electrochemically may enter the metallic lattice and permeate through the metal. It is the entry of these hydrogen atoms into the lattice of the metal that causes embrittlement and, as a result, possibly catastrophic failure of structures in service environments. It is generally observed that if large amounts of hydrogen are absorbed, there may be a general loss in ductility. Internal bursts or blisters may be realized if large amounts of hydrogen collect in localized areas [3,4]. Small amounts of dissolved hydrogen may also react with microstructural features of alloys to produce catastrophic failures at applied stresses far below the yield strength. All of the just-cited phenomena are collectively referred to as hydrogen embrittlement [4-9].

The effect of nascent hydrogen on mechanical properties of a given metal or alloy will depend upon the hydrogen-metal system in question, especially on the solubility of hydrogen. Some metals form solid solutions with hydrogen. This is indicated by the facts that: (a) the solubility of hydrogen changes as the square root of the pressure (Sievert's law); and (b) the metal dissolves more hydrogen as the temperature increases. These metals, for example, iron (Fe), platinum (Pt), nickel (Ni), cobalt (Co), copper (Cu), aluminum (Al), and silver (Ag) are considered endothermic occluders. In the case where the solubility decreases as the temperature increases, the metal is referred to as an exothermic occluder. These metals, for example, titanium (Ti),

¹Division manager, Aerospace Materials Division, Air Vehicle and Crew Systems Technology Department, Naval Air Development Center, Warminster, PA 18974-5000.

zirconium (Zr), vanadium (V), thorium (Th), and palladium (Pd), usually form compounds with the hydrogen, that is, they are hydride formers [3,10]. When hydrogen is dissolved in the metal lattice, endothermic occluders, it is considered to be present as a screened proton, that is, the valence electron joins the electron cloud of the metal. In exothermic occluders, hydrogen atoms are believed not to be completely ionized and as such are much larger than protons. Thus, their presence in interstitial positions tends to distort the lattice [5].

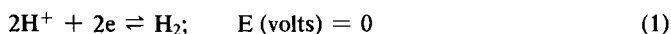
The sources of electrolytic hydrogen in metals are many. It can be introduced during cleaning, pickling, or electroplating processes, or it may be picked up from the service environment as a result of cathodic protection or corrosion reactions [6,7,9,11-15]. It is the unavoidable electrode reaction proceeding simultaneously with these processes where hydrogen ions or water molecules are discharged. The reaction which produces hydrogen electrolytically in acidic solutions is the discharge of hydrogen ions and water. In alkaline solutions, the breakdown of water produces hydrogen atoms and hydroxyl ions. It should be emphasized that high-strength metals are the most susceptible to hydrogen embrittlement (HE). The most important factors tending to promote HE are the hydrogen content of the metal, the tendency of the material to absorb hydrogen, and the hydrogen-metal interaction. The applied stress and the amount of hydrogen in a metal influence the sensitivity to HE [3].

The purpose of this paper is to give a summary of the mechanisms and kinetics of the electrochemical hydrogen evolution reaction as they may affect embrittlement. Electrolytic hydrogen production during corrosion processes will be reviewed with particular emphasis on those reactions which take place at occluded areas, for example, crack tips, crevices, and pits. The diffusion of hydrogen into the metallic lattice and the electrochemical permeation test techniques will be described.

Elementary Electrochemistry

Exchange Current Density

As hydrogen is reacted at an electrode surface, there is a certain kinetic effect even though the reaction is at equilibrium. For example, the reaction in Eq 1 can occur on a platinum electrode



in a solution of acid at 1 atm of hydrogen gas (H_2) pressure. It has an electrode potential, E (corroding tendency), of zero. As can be seen by Fig. 1 and Eq 2, when this reaction is in equilibrium, the

$$\text{rate of oxidation} = \text{rate of reduction} = \frac{io}{ZF} \quad (2)$$

where

- Z = number of electrons transferred,
- F = Faraday's constant, $96.5 \times 10^3 \text{ C}$
- io = exchange current density, A/m^2 .

The equilibrium exchange current density, io , implies an equal number of electrons going in both directions. These electrons, however, produce no net current. The magnitude of this electron flow in either direction is known as the exchange current density, io . It is defined as the electrochemical equilibrium rate constant and reflects the kinetic properties (catalytic activity) of a particular electrode material. The exchange current density is characteristic of the metal

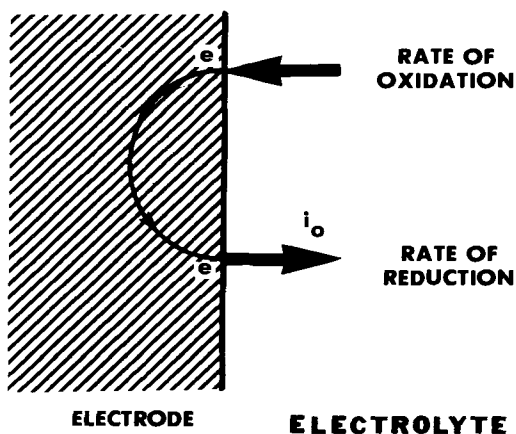


FIG. 1—Pictorial representation of the exchange current density.

and the reaction taking place on its surface and may vary by many orders of magnitude. The value of i_o will determine the reaction reversibility of an electrode-electrolyte interface. Some values are presented in Table 1. An electrode with a large value of i_o for a particular reaction on the order of 10 A/m^2 means that an even larger net current density must be passed before any appreciable deviation of the electrode potential from the equilibrium value occurs. Such a system would be considered highly reversible. Conversely, a system with a small i_o , on the order of 10^{-4} A/m^2 , demonstrates irreversible behavior since small net currents will upset the established equilibrium. Thus, the value of the exchange current density indicates how stable the hydrogen evolution reaction is on a metal surface. For this reaction on Pt, the i_o is large (see Table 1). Since Pt is so stable, it is usually the electrode of choice for hydrogen evolution. It is, in fact, the basis of the standard hydrogen reference electrode. When any electrode deviates from reversibility, the electrode experiences polarization.

TABLE 1—The Exchange-current density i_o for the hydrogen-evolution reaction [16].

Metal	$-\log i_o [\text{amp cm}^{-2}] \text{ in } 1 \text{ M H}_2\text{SO}_4$
Palladium	3.0
Platinum	3.1
Rhodium	3.6
Iridium	3.7
Nickel	5.2
Gold	5.4
Tungsten	5.9
Niobium	6.8
Titanium	8.2
Cadmium	10.8
Manganese	10.9
Thallium	11.0
Lead	12.0
Mercury	12.3

Polarization

Polarization represents a change in potential, E , with net current flow, that is, the exchange current density is exceeded. This overpotential is a deviation from the reversible (equilibrium) potential. It is also a measure of

$$E_{\text{reversible}} - E_{\text{actual}} = \eta \text{ (Overpotential)} \quad (3)$$

irreversibility. Thus, the overpotential of a reaction is that potential in excess of the equilibrium potential required to pass a current, I , for a reaction. It is also related to the slowing of the rate of a process. It is the extra potential that must be supplied to cause the reaction to proceed at a finite rate or current density. Polarization for our purposes can be divided in two main categories: activation and concentration polarization. Activation polarization η_{act} is the kinetically produced overpotential corresponding to the interfacial reactions at the electrode. If concentration polarization exists, the discharge/charge reaction at the electrical double layer is hindered. Concentration polarization, η_{conc} , is the change in potential due to the depletion of the layer of reactive ionic species next to the electrode (diffusion layer). Activation polarization is usually depicted on a voltage versus $\log i$ curve as shown in Fig. 2. The straight line portion is governed by the Tafel equation

$$i = i_o \exp \frac{-z\alpha\eta F}{RT} \quad (4)$$

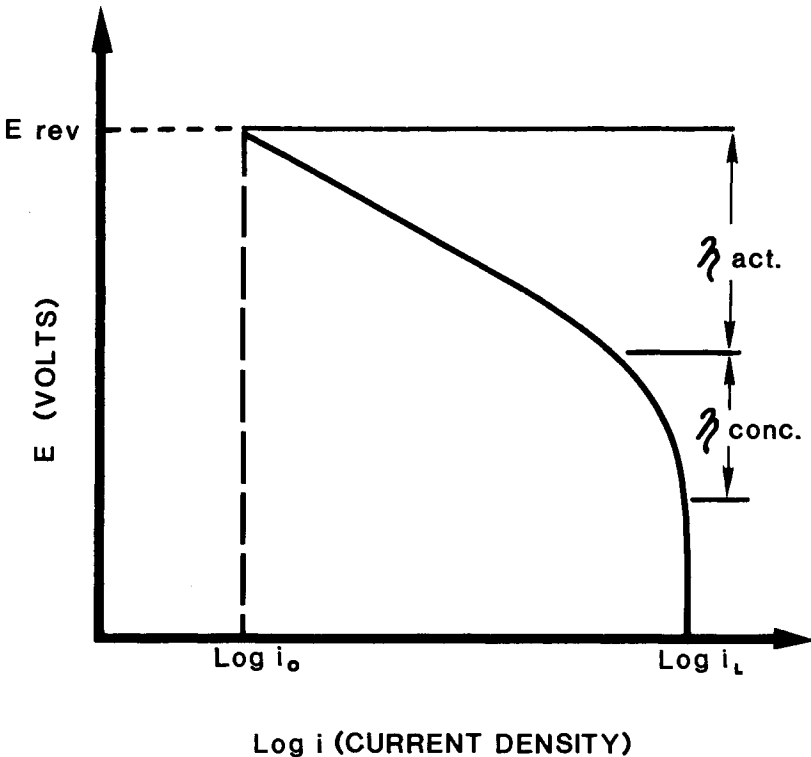


FIG. 2—General example of activation and concentration polarization at a cathode.

where

- i = current density, A/m²,
- z = number of electrons transferred,
- α = transfer coefficient (symmetry factor),
- R = gas constant, 8.31 J/mol · °K,
- T = temperature, °K,
- η = activation overpotential, volts.

Thus, one can see that the activation overvoltage, η_{act} , is a function of the current density, i . This equation can be rewritten in the more familiar form

$$\eta_{\text{act}} = \beta \log \frac{i}{i_0} \quad (5)$$

where β is a constant which will be described later. Concentration polarization, η_{conc} , being mass transfer limited, is dependent on the concentration of reactive species. For example, η_{conc} for Eq 1 is

$$\eta_{\text{conc}} = \frac{-2.3RT}{zF} \log_{10} \frac{p_{\text{H}_2}}{[\text{H}^+]^2} \quad (6)$$

where

- p_{H_2} = the pressure of hydrogen gas in atmospheres, and
- $[\text{H}^+]$ = the molecular concentration of hydrogen ions.

Figure 2 also shows a limiting current density that results after concentration polarization. The limiting current density is

$$i_L = \frac{FC^0D}{\delta} \quad (7)$$

where

- D = diffusion coefficient of reacting species,
- i_L = limiting current density, A/m²,
- C^0 = bulk concentration of reactive species mol/m³, and
- δ = diffusion layer thickness, m.

and is the result of the transport process in the bulk of the electrolyte, which cannot supply the reactive ions to the diffusion layer at a faster rate. Once the limiting current density for the reaction has been reached, no increase in overpotential can change this condition. This is shown in Fig. 2.

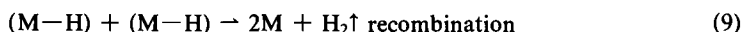
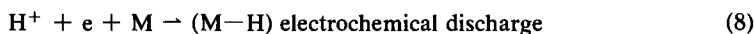
On passage of current across a metal-electrolyte interface, the equilibrium potential difference at the interface is usually changed and the electrode becomes polarized. In order to measure this change, a reference electrode of defined potential is required. A description of several reference electrodes and their use can be found in Refs 17, 18, and 19. With polarization, the efficiency of energy conversion (chemical to electrical) is a function of the current density, i . Therefore, if the objective is the efficient conversion of chemical to electrical energy, a low η process is generally considered desirable, since less energy is expended in carrying out the reaction, for example, batteries and electroplating. There are times when a large overvoltage is preferable, for example with corrosion, since it slows down the rate of attack.

It is important to note that when an anode polarizes, it becomes more cathodic (potential shifts to the more noble direction). When a cathode polarizes, it becomes more anodic (shifts in the less noble direction), for example, Fig. 2. The intersection of the anodic and cathodic polarization lines results in a steady state electrochemical rate process such as corrosion (anodic dissolution) or electroplating (cathodic deposition). Another effect that can contribute to cell polarization is circuit resistance.

Mechanism of Polarization

There are many proposed mechanisms for polarization. A more appropriate one employs the double layer theory [16,20]. For example, dipping a piece of metal into a highly concentrated electrolyte containing ions of the metal results in the formation of an electrical double layer at the metal-electrolyte interface. The simplest model for this double layer is that of a plate capacitor at the interface, the so-called Helmholtz double layer. The most important step in an electrode process is the charge transfer reaction or, in other words, the transfer of charge through the double layer. The charged particles crossing the double layer can be cations or anions. In the case of cathodic polarization, the electrons pile up on the surface, and, as a result, there is an activation energy buildup resulting in an increased double layer. This causes the potential to shift in the anodic direction. The energy barrier can be increased or reduced by applying a potential. This permits changing reaction rates or even directions. If the reaction rate proceeds at a rate faster than the limiting current density for the cathodic reaction, the metal ion concentration in the diffusion layer goes to zero.

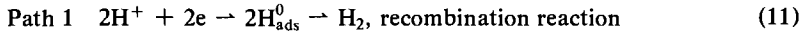
Overpotential is a necessary concomitant to the passage of a net current density across any interface. Reactions differ only in the magnitude of overpotential associated with a particular current density. For a hydrogen overpotential, for example, there could be a high or low overpotential, which indicates the difficulty or ease in the kinetics of the hydrogen evolution. For hydrogen embrittlement, it is important to look at the electrode kinetics of the hydrogen evolution reaction and see how the steps in the reaction can lead to hydrogen entry into metal. The three mechanisms of the hydrogen evolution reaction are listed in Eqs 8, 9, and 10. After the electrochemical



discharge step, the newly formed hydrogen atoms are adsorbed on the surface. The majority of these hydrogen atoms combine to form hydrogen molecules and harmlessly form bubbles of hydrogen gas. A small percentage, however, may enter the metal as hydrogen atoms. It is precisely these atoms of hydrogen that cause embrittlement of metal.

The kinetics of the hydrogen evolution reaction has been studied by many workers, and several excellent reviews are available [11,16,21-24]. According to the work of many electrochemists, in particular, Frumkin, Conway, and Parsons, only two reaction paths are regarded as likely. Common to both these reaction paths is the description of how hydrogen is captured at the electrode surface. In acidic solutions, hydrogen ions are reduced to form neutral hydrogen atoms (Eq 8). It must be understood that the discharge reaction will not proceed unless hydrogen ions are available. Water is an ever present source of hydrogen. In alkaline solutions, there is a reduction of water molecules. The discharge of water molecules also yields adsorbed hydrogen atoms.

The two principle paths for the hydrogen evolution reaction are shown in Eqs 11 and 12. With these two



paths, there are three possible steps (see Eqs 8, 9, and 10), and one, in principle, can be called the rate-determining step. The rate-determining step is the slowest reaction in the process which controls the overall rate. The total rate equation for any electrochemical reaction is

$$i = i_0 \left\{ \left[\exp \frac{-zF\alpha|\eta|}{RT} \right] - \exp \left[\frac{zF(1-\alpha)|\eta|}{RT} \right] \right\} \quad (13)$$

The surface adsorption of atomic hydrogen on the metallic substrate is important in the diffusion process. Any cathodic reaction involving the evolution of hydrogen gas need not be 100% effective. Some fraction of the hydrogen may permeate into the metal. As previously mentioned, it is this small fraction of hydrogen which, after entering the metal lattice, contributes to the insidious embrittlement phenomenon in metals. Thus, a knowledge of the extent of hydrogen coverage on a metal and the variation of that coverage with potential is of considerable importance in assessing the rate of entry of hydrogen into a metal during cathodic polarization.

The form of the Langmuir adsorption isotherm applicable to the kinetics of dissociative chemisorption is [23]

$$\frac{\Theta}{1 - \Theta} = la_p \quad (14)$$

where

Θ = the fraction of surface coverage,
 l = standard free energy of adsorption, and
 a_p = the activity of the adsorbing gas.

In order to apply the Langmuir adsorption isotherm to the hydrogen evolution reaction on a metal in aqueous acidic solutions, the sequential reaction of Eqs 8, 9, and 10 are assumed. Let the velocities of the forward reactions in Eqs 8, 9, and 10 be I_8 , I_9 , and I_{10} , respectively, and the velocities of the reverse reactions be I_{-8} , I_{-9} , and I_{-10} . If one of the just-cited reactions is rate controlling, that is, slowest, the fast reaction will be in equilibrium. The kinetic equations for Reactions 8, 9, and 10 are as follows

$$I_8 = FK_8 a_{\text{H}^+} (i - \Theta) \exp \left[\frac{-\alpha F \eta}{RT} \right]; \quad I_{-8} = FK_{-8} \Theta \exp \left[\frac{(1-\alpha) F \eta}{RT} \right] \quad (15)$$

$$I_9 = K_9 (\Theta)^2, \quad I_{-9} = K_{-9} (1 - \Theta)^2 - P_{\text{H}_2} \quad (16)$$

$$I_{10} = FK_{10} a_{\text{H}^+} \Theta \exp \left[\frac{-\alpha F \eta}{RT} \right]; \quad I_{-10} = FK_{-10} (1 - \Theta) P_{\text{H}_2} \exp \left[\frac{(1-\alpha) F \eta}{RT} \right] \quad (17)$$

where

I = reaction rate, Amps,
 Θ = hydrogen coverage,
 K = reaction rate constant,
 η = activation overpotential ($E - E_r$),
 T = absolute temperature, K,

24 HYDROGEN EMBRITTLEMENT

a_{H^+} = activity of hydrogen ion, and
 P_{H_2} = H_2 gas pressure, atm.

Assume Reaction 10 to be rate controlling and Reaction 8 to be in equilibrium, that is, a condition of fast discharge and slow electrochemical desorption. Equating the forward and backward reaction rates of Eq 10, we have

$$K_8 a_{H^+} (1 - \Theta) \exp\left[\frac{-\alpha F \eta}{RT}\right] = K_{-8} \Theta \exp\left[\frac{(1 - \alpha) F \eta}{RT}\right] \quad (18)$$

when

$$\frac{\Theta}{(1 - \Theta)} = \frac{K_8}{K_{-8}} a_{H^+} \exp\left[\frac{-\eta F}{RT}\right] \quad (19)$$

$\Theta \ll 1$; $(1 - \Theta) \rightarrow 1$; so that for small Θ (low hydrogen coverage) Eq 19 may be written

$$\Theta = \frac{K_8}{K_{-8}} a_{H^+} \exp\left[\frac{-\eta F}{RT}\right] \quad (20)$$

When $\Theta \cong 1$, $(1 - \Theta) \rightarrow 0$, so that for large Θ (almost complete coverage) Eq 19 becomes

$$(1 - \Theta) = \frac{K_{-8}}{K_8 a_{H^+}} \exp\left[\frac{\eta F}{RT}\right] \quad (21)$$

For conditions where $\Theta \ll 1$, Eq 20 is substituted for Θ in the rate equation for the controlling reaction, that is, Eq 17, forward, to give

$$I_{10} = FK_{10} \frac{K_8}{K_{-8}} a_{H^+}^2 \exp\left[\frac{-\eta F(1 + \alpha)}{RT}\right] \quad (22)$$

The relationship between the cathodic current (Reaction Rate 10) and the overpotential for the fast discharge-slow desorption mechanism for small hydrogen coverages ($\Theta \ll 1$) is extracted from Eq 22 as

$$\frac{d\eta}{d \ln I_{10}} = - \frac{1}{(1 + \alpha)} \frac{RT}{F} \quad (23)$$

For conditions of high coverage, $\Theta \cong 1$, the rate controlling reaction (forward direction) becomes

$$I_{10} = FK_{10} a_{H^+} \exp\left[\frac{-\alpha F \eta}{RT}\right] \quad (24)$$

Now the relationship between the current and overpotential for $\Theta \cong 1$, obeying the fast discharge-slow desorption mechanism, is

$$\frac{d\eta}{d \ln I_{10}} = - \frac{RT}{\alpha F} = \beta, \quad \text{the Tafel slope} \quad (25)$$

Similar treatments to obtain the theoretical Tafel slopes of other possible sequential reactions were made and are given in Table 2.

It is observed that the full rate equation is actually the Tafel equation of activation polarization. Using kinetic theory, it can be shown that when the surface of an electrode is covered with newly discharged hydrogen atoms, the slope of the E versus $\log i$ curve is 120 mV/decade, that is, $\beta = 0.120$ V/decade of current; further $\beta = RT/\alpha F$, where $T = 25^\circ\text{C}$, $\alpha = 1/2$, and $F = \text{Faraday's constant}$. Therefore, rearranging Eq 4 and substituting for $\alpha F/RT = \beta$, one obtains the familiar Tafel equation, Eq 5. From this relationship, it can be seen that the smaller the i_0 , the larger the overpotential is required to obtain the same applied i . This is shown in Fig. 3. Thus, it is realized that cathodic polarization (η versus $\log i$ plot) of the hydrogen evolution reaction can be used as a diagnostic criterion to determine the sequential mechanisms operating at the surface.

Hydrogen Diffusion in Metals

After hydrogen is discharged as atomic hydrogen, it becomes adsorbed on the metal surface. It has been shown that surface metal oxides tend to act as barriers to hydrogen entry [35]. When it is absorbed, it goes into the dissolved state by jumping into the interstitial spaces beneath the first atomic layer. From this dissolved state, hydrogen diffuses into the bulk and its rate is proportional to hydrogen coverage, Θ , at the surface. Dissolved hydrogen usually remains in the interstitial spaces available in the lattice unless larger spaces, such as atomic vacancies, are available. The diffusion of hydrogen in the metal is the slowest step in the permeation process. This has been shown by Devanathan and Stachurski [36] and by Beck et al. [37].

Electrochemical Permeation

Most of the recent hydrogen permeation studies in the literature have been carried out by the electrolytic charging method. This technique, developed by Devanathan and Stachurski at the University of Pennsylvania, has become a widely accepted method [38-40]. This method has

TABLE 2—*Hydrogen evolution reaction mechanisms and their corresponding current-potential relationships.*

Mechanism	Tafel Slope, β at 25°C for $\alpha = 1/2$ V/Decade of Current	Hydrogen Coverage, Θ
Fast discharge	0.04	≈ 1
Slow desorption		
Fast discharge	0.12	≈ 1
Slow desorption		
Fast desorption	0.04	≈ 1
Slow discharge		
Fast discharge	0.03	$\ll 1$
Slow combination		
Fast combination	0.12	$\ll 1$
Slow discharge	0.12	≈ 1
Coupled discharge and combination	0.12	1
Coupled discharge and desorption	0.12	1

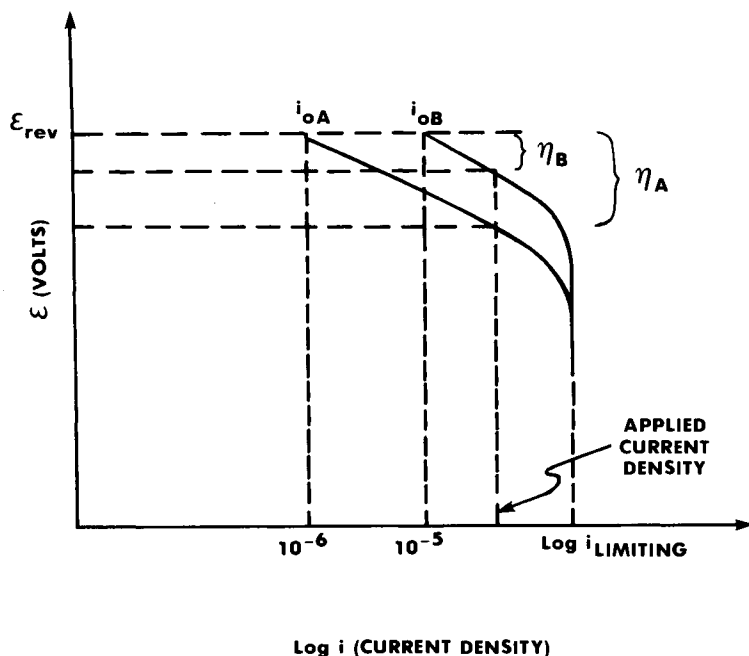
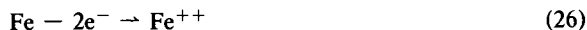


FIG. 3—The effect of i_o on the polarization of the hydrogen evolution reaction at a cathode.

been described by others in a number of publications [40–42]. An applied use of this system is the so-called barnacle electrode [7]. This method essentially employs one half of the permeation cell. It has been developed to measure the mobile, diffusible, hydrogen in high-strength steel parts and is being used to correlate hydrogen concentrations with delayed failure of high-strength steels. The barnacle electrode, as a test method, is described later in this article. It should be noted that both the barnacle electrode and the electrochemical permeation technique rely on the ingress and emergence of hydrogen atoms at unfiled metallic surfaces. Thus, they are only useful on oxide free (nonpassive) metals and alloys. Further, since these methods rely on the transport of atomic hydrogen through the lattice, alloys that form hydrides and irreversible traps, are not recommended for study with these methods.

Hydrogen in Crack Tips

It has been mentioned that electrolytic hydrogen enters a metal when a cathodic process is dominant, for example, electroplating and cathodic polarization. Since corrosion is an electrochemical process consisting of both anodic and cathodic reactions, electrolytic hydrogen is produced in occluded regions in both acidic and neutral solutions [22,26]. This has been shown by Vetter and Strehblow [27] and Pickering [28]. Since an electron is given up in an anodic reaction, an electron must be accepted in a corresponding cathodic reaction. For example, the corrosion on the surface of iron or steel is governed by the following anodic reaction:



The cathodic reaction in acidic solutions is Eq 8. This produces hydrogen which can cause embrittlement. For neutral solutions, the cathodic reaction is as follows

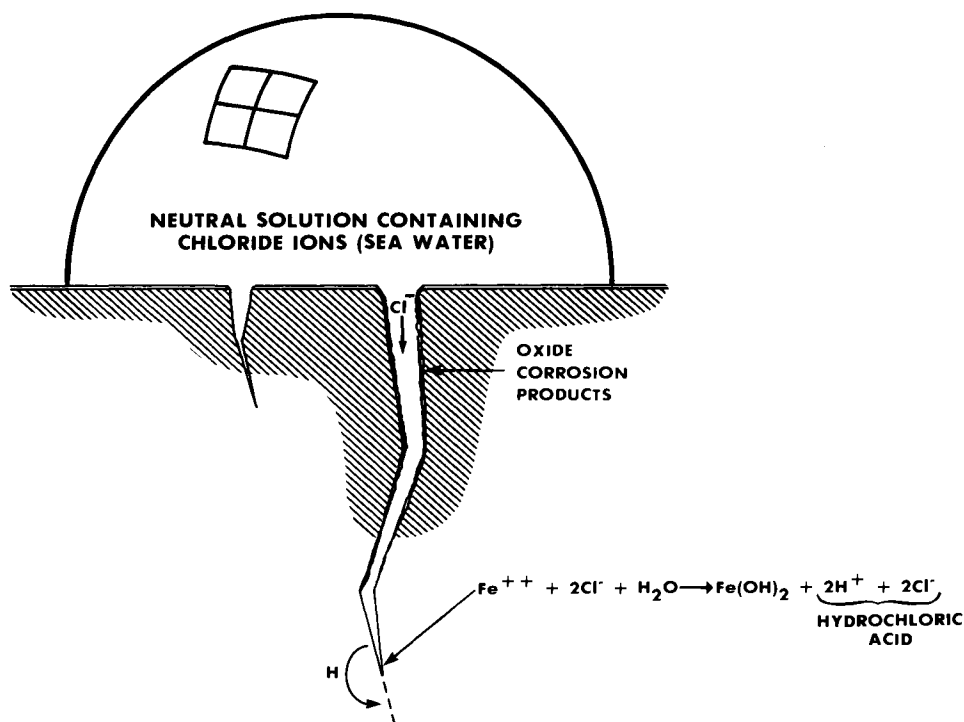
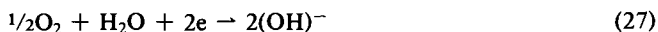


FIG. 4—Chemistry and pH changes in a crack (occluded region) growing in salt water.

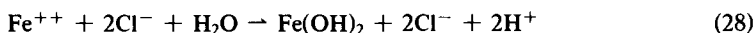


Thus, one would assume the production of hydrogen cannot occur in neutral or alkaline solutions. This is not the case. If there is an occluded area, that is, a pit, crevice, or crack, hydrogen ions can be produced and then discharged. In crevice corrosion, due to the geometry of the metal, for example, in crevices and corners, the solution is prevented from being mixed and causes local buildup of reaction products. This buildup increases the aggressiveness of the local solution and leads to nonuniform corrosion. Quantitative modeling of crevice corrosion has been described elsewhere [29]. Pitting is similar to the conditions for crevice corrosion. Mathematical models of pit growth are given elsewhere by other authors (Vetter and Strehblow [27], Galvele [30]).

It was shown experimentally [27,31–33] that the environment which exists inside a pit, crack, or a crevice differs from the main solution. It has been reported that in a bulk solution of 3.5 weight % sodium chloride (NaCl), the electrolyte acidity in a growing crack may be increased. For aluminum alloys and steels, the pH can be decreased to 3.5. For titanium alloys, the pH has been observed to decrease to 1.7 [34]. This local buildup of acidity is due to the hydrolysis of the reaction products. This occurrence provides favorable conditions for hydrogen absorption. This is especially true on a small area of a freshly corroding metal surface not covered with a protective oxide film [16].

The pH decrease and other processes which occur can be explained with the use of Fig. 4. Figure 4 depicts a growing crack or pit in a neutral solution containing chloride ions. At the tip of a crack, as it grows, Fe^{++} ions are formed. This area becomes electropositive. Thus, in order

to maintain electroneutrality, Cl^- ions rush downward to the tip. The following reaction then takes place at the base of the crack or pit.



Thus, hydrochloric acid is being formed at the base of the crack or pit. As this process continues, the value of the pH within the pit decreases as the pit grows. This creates a situation where hydrogen is easily pumped into the tip of a growing crack, pit, or crevice. It is therefore, important to assess the ability of hydrogen to diffuse into the metal. Again, it is emphasized that it is this diffusible hydrogen in the metallic lattice that causes embrittlement and, hence, catastrophic failures.

The electrochemical permeation technique provides a controlled source and sink for hydrogen permeating through a metal foil. As shown in Fig. 5, the cathode anode sides of the singular metal foil are individually connected with a counter electrode, reference electrode, power supply, and measuring instrumentation. The potentiostat is employed to maintain a sufficient anodic potential in order to electrochemically oxidize the hydrogen which emerges through the foil on the extraction side. The current supplied by the potentiostat for this oxidation is a direct measure of the instantaneous flux of hydrogen in the metal just at the exit, extraction side, and is given by Fick's first law of diffusion

$$\frac{J}{ZF} = -D \left(\frac{dC}{dX} \right)_{X=L} \quad (29)$$

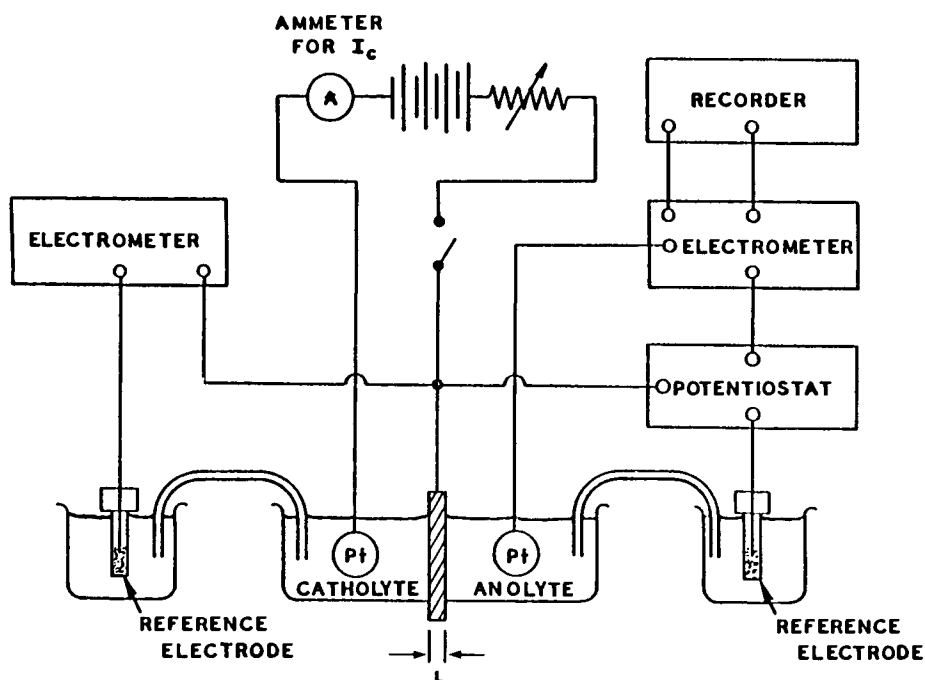


FIG. 5—Schematic of electrochemical permeation cell and circuit diagram.

where

Z = number of electrons transferred,

J = flux atoms/m² · s,

X = distance from cathode interface, m, and

L = thickness of sheet foil, m.

Since currents as low as 10^{-7} A/cm² can be measured, one can determine hydrogen fluxes as small as 10^{-12} g of hydrogen atoms/c³. If one knows the flux, J , and diffusivity, D , of hydrogen and the thickness of the foil, L , the solubility C_0 can then be determined. Although the method to determine C_0 is simple and direct, the successful determination of C_0 can only be associated with a linear gradient of absorbed hydrogen throughout the membrane (see Fig. 6, Curve A).

Mathematics of the Hydrogen Permeation Techniques

The diffusion experiment is represented by the following conditions: a metallic foil of thickness, L , a concentration gradient represented by C_0 on one side of the membrane, that is, at $x = 0$ and C_L on the other side, that is, at $x = L$ (see Fig. 6). At the input side, $x = 0$, the concentration is finite, whereas at $x = L$, it is equal to zero. These boundary conditions are maintained

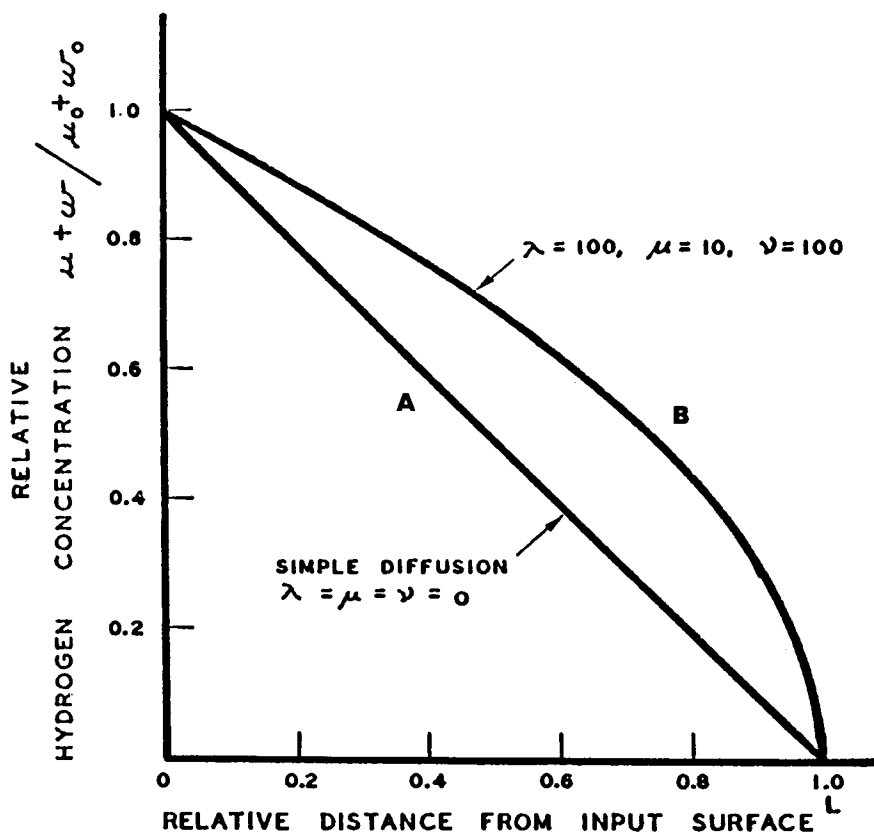


FIG. 6—Steady state concentration profiles for simple diffusion and diffusion with reversible trapping.

electrochemically. The overall problem may be represented by Fick's second law for constant D as

$$\frac{d^2c}{dx^2} - \left(\frac{1}{D}\right) \frac{dc}{dt} = 0 \quad (30)$$

where

D = diffusion coefficient,
 c = concentration, and
 t = time.

The initial and boundary conditions pertaining to the electrochemical experiment are

$$c = C_0; \quad x = 0; \quad t \geq 0 \quad (31)$$

$$c = 0; \quad x = L; \quad t \geq 0 \quad (32)$$

$$c = 0; \quad 0 < X < L; \quad t < 0 \quad (33)$$

The method of solution to Eq 30 is according to McBreen et al. [40]. They utilized Fick's first law, Eq 29, where J = steady state flux of hydrogen, and an operational (Laplace) solution to Eq 30 to define the hydrogen concentration contour within the thickness of the metal. The solution is as follows

$$\frac{J_t}{J_\infty} = \frac{2}{\pi^{1/2}} \cdot \frac{1}{\tau^{1/2}} \sum_{N=0}^{\infty} (-1)^n \exp \left[\frac{-(2n+1)^2}{4\tau} \right] \quad (34)$$

where $\tau = Dt/L^2$, a dimensionless parameter. The first term solution gives results valid up to about 95% attainment of the steady state permeation. A corresponding Fourier solution of Eq 30 with boundary conditions given by Eqs 31, 32, and 33 is valid at longer times

$$\frac{J_t}{J_\infty} = 1 + 2 \sum_{N=1}^{\infty} \cos N\pi \exp \left[\frac{-DN^2\pi^2t^2}{L^2} \right] \quad (35)$$

Computer (machine) programs for these equations have been given by Caskey and Pillinger [43]. Laplace, Eq 34, and Fourier, Eq 35, solutions are plotted against τ in Fig. 7. For the region $\tau < 0.14$, the Laplace solution is invalid. For $\tau > 0.3$, the Fourier solution is valid. There is a good agreement between the two solutions in the range $0.14 < \tau < 0.3$. From these two solutions, it is evident that the Laplace transform method gives a solution which can be used in its simplified first term form to define short time diffusion behavior, and the Fourier solution to define diffusion behavior at long times, for example, $\tau > 0.4$.

Deviations from Simple Diffusion Behavior

An inspection of the literature on the diffusion of hydrogen through metals shows a large amount of disagreement. This is particularly true of iron. The reported literature values of diffusivity of hydrogen in iron and ferritic steels, for example, vary over four orders of magnitude at low temperatures [44]. This lack of agreement for the low-temperature diffusivity of hydro-

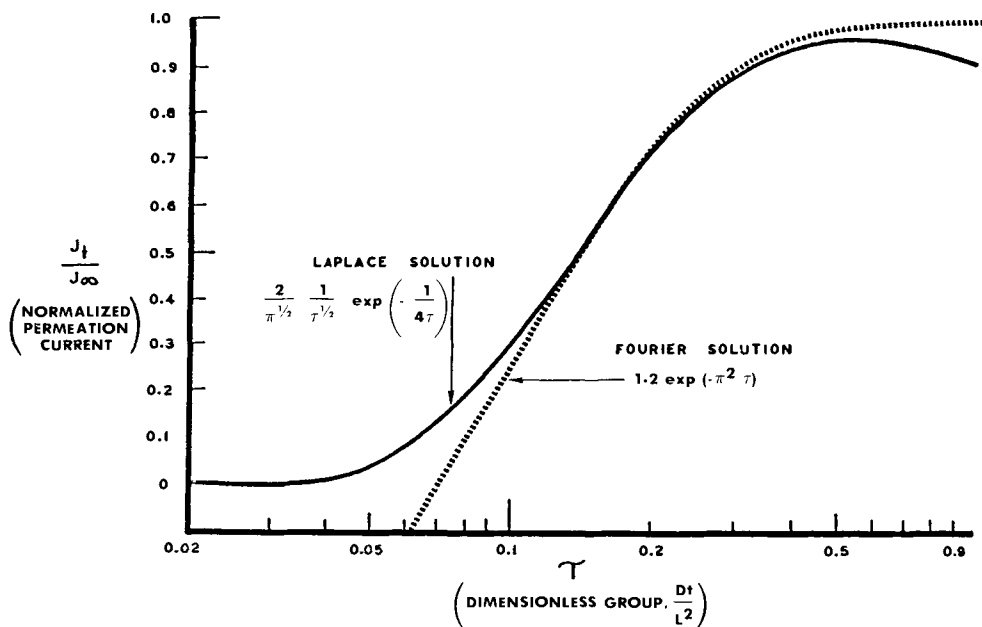


FIG. 7—Laplace and Fourier solutions to Fick's second law (Eq 30).

gen through iron is indicative of the inaccuracies and inadequacies in the experimental methods. These methods were, for the most part, manometric, that is, pressure measuring. The electrochemical permeation technique herein described has done much to restore accuracy and reproducibility to ambient temperature hydrogen measurements. The pioneering effort by Devanathan and Stachurski spawned a number of electrochemical hydrogen permeation studies with varying electrochemical and mechanical conditions through various metals and alloys and established the electrochemical technique as the most sensitive for measuring hydrogen permeation through metals [38,45–48].

Barring surface control of the diffusion experiment, the deviation from simple diffusion behavior of hydrogen in metals, even using the electrochemical method, is indicative of a structure sensitive interaction. This behavior can be rationalized as being caused by buildup of the hydrogen, that is, concentration dependent diffusivity, or trapping, delaying of the hydrogen at fixed states within the metal.

Darken and Smith were the first to suggest that dissolved hydrogen is impeded in its diffusion by lattice imperfections or other microstructural features [49]. This can be observed in Fig. 6, which shows the normalized concentration profiles for simple diffusion and for diffusion with trapping (Curve B). For simple diffusion through a foil with a constant hydrogen concentration at the input side and a zero concentration at the exist side, a straight line concentration gradient through the thickness exists at a steady state. Concentration profiles of steady state permeation conditions with λ , μ , and γ , trapping parameters have been defined by McNabb and Foster [50] and later derived and calculated by Caskey and Pillinger [43]. The calculations determine concentrations of hydrogen retained in both the interstitial state and in traps, as a function of the distance through the thickness of a foil. They essentially describe the rates at which hydrogen atoms are captured and released from the traps. It should be noted that curve B of Figure 7 has nonzero values for λ , μ , and γ .

Other than impeding diffusion, these traps may contain a certain critical concentration of hydrogen molecules which, with sufficient pressure, cause a crack or blister to be formed. Another problem may occur if thick foils are used and the metal under investigation has a low diffusivity for hydrogen. In this case, a steady diffusion gradient throughout the foil may require prolonged times. Table 3 gives the maximum recommended thickness of metal foil to use when the hydrogen diffusivity in the metal has a particular value. From these data, matching the known diffusivity with the stated foil thickness provides a steady state permeation rate which is achieved in about 2 min after the initiation of a charging current [24].

It is emphasized that the electrochemical permeation technique is only valid for determining hydrogen diffusivities through metals when simple diffusion prevails, that is, no trapping or concentration dependence occurs.

Summary

With regard to electrolytic hydrogen in metals, it can be stated that:

1. The electrochemical discharge of hydrogen ions at a metallic surface is a common method of hydrogen entry into metals.
2. Electrochemical hydrogen discharge can occur during electroplating, electromachining, pickling and cleaning, and corrosion.
3. The polarization of the electrochemical discharge and recombination reactions causes an increase in the probability of hydrogen entry and, hence, embrittlement of the metal.
4. Seemingly, innocuous electrolytes (neutral pH) such as salt water can act as powerful sources of hydrogen when the electrolyte is occluded in crevices such as faying surfaces, pits, or cracks.
5. The transport of hydrogen in the metallic lattice can be monitored most easily by the electrochemical hydrogen permeation technique when the host metal does not form hydrides or protective surface oxide films.
6. The electrochemical hydrogen measuring system called the "barnacle electrode" is a diagnostic tool to detect the presence and severity of mobile hydrogen in steel structures.

Acknowledgments

The helpful discussions and administrative aid provided by my colleague, Richard Paciej, are gratefully acknowledged.

TABLE 3—Maximum recommended thicknesses of metal foil to use for a particular D value and a 2 min steady state permeation time [24].

D , m^2/s	L , m
10^{-8}	0.1×10^{-2}
10^{-9}	0.03×10^{-2}
10^{-10}	0.01×10^{-2}
10^{-11}	0.003×10^{-2}

References

- [1] Cailletet, L., *Compte Rendu*, Vol. 58, 1864, p. 327.
- [2] Bodenstein, M., *Zeitschrift für Electrochemie*, Vol. 28, 1922, p. 517.
- [3] Birnbaum, H. K. in *Environment-Sensitive Fracture of Engineering Materials*, Z. A. Foroulis, Ed., American Institute of Mining, Metallurgical, and Petroleum Engineers, Warrendale, PA, 1979, pp. 326-357.
- [4] Tetelman, A. S. in *The Fracture of Engineering Metals*, Wiley, New York, July 1967.
- [5] Thompson, A. W. in *Environment-Sensitive Fracture of Engineering Materials*, Z. A. Foroulis, Ed., American Institute of Mining, Metallurgical, and Petroleum Engineers, Warrendale, PA, 1979, pp. 379-410.
- [6] Beck, W., Jankowsky, E. J., and Fischer, P., "Hydrogen Stress Cracking of High Strength Steel," Technical Report NADC-MA-7140, Naval Air Development Center, Warminster, PA, Dec. 1971.
- [7] DeLuccia, J. J. and Berman, D. A., "An Electrochemical Technique to Measure Diffusible Hydrogen in Metals (Barnacle Electrode)," *Electrochemical Corrosion Testing, ASTM STP 727*, F. Mansfeld and U. Bertocci, Eds., American Society for Testing and Materials, Philadelphia, 1981, pp. 256-273.
- [8] Barth, C. F., Steigerwald, E. A., and Troiano, A. R., *Corrosion*, Vol. 25, No. 9, September 1969, pp. 353-358.
- [9] Groeneveld, P. T., Fletcher, E. E., and Elsea, A. R., "A Study of Hydrogen Embrittlement of Various Alloys," Contract Number NAS8-20029, Columbus Laboratories, Columbus, OH, 23 June 1966.
- [10] Smith, D. P., *Hydrogen in Metals*, University of Chicago Press, Chicago, IL, 1948.
- [11] *Comprehensive Treatise of Electrochemistry*, Vol. 4., J. O'M. Bockris, R. E. Conway, E. Yeager, and R. E. White, Eds., Plenum Press, New York, 1981, p. 422.
- [12] Kargol, J. A. and Paul, L. D., in *Current Solutions to Hydrogen Problems in Steels*, C. G. Interrante and G. M. Pressouyre, Eds., American Society for Metals, Metals Park, OH, November 1982.
- [13] Nanis, L., "Fundamental Corrosion Studies: Hydrogen Embrittlement," Technical Report UPH2-001, University of Pennsylvania, Philadelphia, PA, October 1969.
- [14] *Hydrogen Embrittlement in Metal Finishing*, H. J. Reed, Ed., Reinhold Publishing Co., New York, 1961.
- [15] Zapffe, C. A. and Maslem, M. E., *Plating*, Vol. 37, No. 4, 1950, p. 366.
- [16] Bockris, J. O'M. and Reddy, A. K. N., *Modern Electrochemistry*, Vol. 2, Plenum Press, New York, 1970.
- [17] Bard, A. J. and Faulkner, L. R., *Electrochemical Methods*, John Wiley, New York, 1980.
- [18] Gileadi, E., Kirova-Eisner, E., and Penciner, J., *Interfacial Electrochemistry*, Addison-Wesley, Reading, MA, 1975.
- [19] Ives, O. J. G. and Janz, G. J., *Reference Electrodes*, Academic Press, New York, 1961.
- [20] Gerischer, H., *Analytical Chemistry*, Vol. 31, No. 1, January 1959, pp. 33-39.
- [21] Vetter, K. J., *Electrochemical Kinetics*, Academic Press, New York, 1961.
- [22] Bockris, J. O. M., McBreen, J., and Nanis, L., *Journal of the Electrochemical Society*, Vol. 112, No. 9, October 1965, pp. 1025-1031.
- [23] Conway, B. E., *Theory and Principles of Electrode Processes*, Ronald Press Co., New York, 1965.
- [24] McBreen, J. and Genshaw, M. A. in *Fundamental Aspects of Stress Corrosion Cracking*, R. W. Staehle, A. J. Forty, and D. Van Rooyen, Eds., National Association of Corrosion Engineers, September 1967, p. 51.
- [25] Beck, W., Glass, A. L., and Taylor, E., *Journal of the Electrochemical Society*, Vol. 112, No. 1, 1965, p. 53.
- [26] Pickering, H. W., *Journal of the Electrochemical Society*, Vol. 119, 1972.
- [27] Vetter, K. J. and Strehblow, H. H. in *Localized Corrosion*, R. W. Staehle, Ed., National Association of Corrosion Engineers, Houston, TX, 1974.
- [28] Pickering, H. W., *Journal of the Electrochemical Society*, Vol. 119, 1972, p. 1287.
- [29] Sutari, D. W. and Alkine, R. C., Paper 238 presented at the Electrochemical Society Meeting, Los Angeles, CA, October 1979.
- [30] Galvele, J. R., *Journal of the Electrochemical Society*, Vol. 123, No. 4, April 1976, pp. 464-474.
- [31] Smith, J. A., Peterson, M. H., and Brown, B. F., *Corrosion*, Vol. 26, 1970, p. 539.
- [32] Sandoz, G., Puju, C. T., and Brown, B. F., *Corrosion Science*, Vol. 10, p. 839, 1970.
- [33] Wilde, B. E. and Williams, E., *Electrochimica Acta*, Vol. 16, 1971, p. 1971.
- [34] Brown, B. F., Fuju, G. T., and Dahlberg, E. P., *Journal of the Electrochemical Society*, Vol. 116, 1969, p. 218.
- [35] Beck, T. R., North Atlantic Treaty Organization, Conference on the Theory of SCC in Alloys, Brussels, 1971, p. 68.
- [36] Devanathan, M. A. V. and Stachurski, Z., *Procedures of the Royal Society*, Vol. 290A, 1965, p. 220.

- [37] Beck, W., Bockris, J. O'M., McBreen, J., and Nanis, L., *Procedures of the Royal Society*, Vol. 290A, 1965, p. 220.
- [38] DeLuccia, J. J., "Electrolytic Hydrogen in Beta-Ti," Report No. NADC-76207-30, Naval Air Development Center, Warminster, PA, 1976.
- [39] Saito, Y. and Nobe, K., Abstract No. 126, in *Extended Abstracts of the Fall Meeting*, Electrochemical Society, Atlanta, October 1977.
- [40] McBreen, J., Nanis, L., and Beck, W., *Journal of the Electrochemical Society*, 1966, p. 1218.
- [41] Gileadi, E., Fullenwider, M., and Bockris, J. O'M., *Journal of the Electrochemical Society*, Vol. 113, 1966, p. 928.
- [42] Bockris, J. O'M., Beck, W., and Genshaw, M. A., *Acta Metallurgica*, Vol. 19, 1971, p. 1209.
- [43] Caskey, G. R., Jr. and Pillinger, W. L., *Metallurgical Transactions*, Vol. 6A, 1975, p. 467.
- [44] Oriani, R., "Fundamental Aspects of SCC," Proceedings of Conference at Ohio State University, National Association of Corrosion Engineers, Houston, TX, 1969, p. 41.
- [45] Rieche, E., Schambil, F., and Bobmenkamp in *Hydrogen Effects in Metals*, I. M. Bernstein and A. W. Thompson, Eds., American Institute of Mining, Metallurgical, and Petroleum Engineers, Warrendale, PA, 1981, p. 97.
- [46] Zamanzadek, M., Allam, A., Pickering, H. W., and Hubler, G. K., *Journal of the Electrochemical Society*, 1980, Vol. 127, pp. 1688-1693.
- [47] Driver, R., *Journal of the Electrochemical Society*, Vol. 128, November 1981, pp. 2367-2369.
- [48] Pickering, H. W. and Zamanzadek, M., in *Hydrogen Effects in Metals*, I. M. Bernstein and A. W. Thompson, Eds., American Institute of Mining, Metallurgical, and Petroleum Engineers, Warrendale, PA, 1981, p. 143.
- [49] Darken, L. S. and Smith, R. P., *Corrosion*, Vol. 5, No. 1, 1949.
- [50] McNabb, A. and Foster, P. K., *Transactions of AIME (TMS)*, Vol. 227, 1963, p. 618.

Section 2: Current Standards and Projections

Hydrogen Embrittlement Coverage by U.S. Government Standardization Documents

REFERENCE: Clegg, E. T., "Hydrogen Embrittlement Coverage by U.S. Government Standardization Documents," *Hydrogen Embrittlement: Prevention and Control*, ASTM STP 962, L. Raymond, Ed., American Society for Testing and Materials, Philadelphia, 1988, pp. 37-45.

ABSTRACT: This paper covers the Defense Specifications and Standards Program (DSSP). It describes the Department of Defense (DoD) standardization organization, discusses types of standardization documents, defines standardization terms, and covers requirements and test methods for hydrogen embrittlement in defense standardization documents. The DSSP is administered by the Deputy Under Secretary of Defense for Research and Engineering through the Defense Materials Specification and Standards Office (DMSSO). Authority is delegated by the DMSSO to Army, Navy, Air Force, and Defense Logistics Agency Departmental Standardization Offices (DEPSOs) for portions of the DSSP program. These DEPSOs further delegate responsibility among the forty plus standardization offices located at military installations. The Army Materials Technology Laboratory (AMTL) is one of these standardization offices.

The coverage of hydrogen embrittlement by DoD standardization documents is also discussed. The requirement section of specifications states the required hydrogen embrittlement relief treatment, and the quality assurance section describes the test methods to determine if embrittlement relief treatment has been successful.

KEY WORDS: DoD standardization, hydrogen embrittlement, stress corrosion, hardness, tensile strength, plating, hydrogen-stress cracking, brittle failure, atomic hydrogen, ferrous metals

Background, Defense Standardization Program

In 1952, the DoD Standardization and Specification Program was established. Statutory requirements call for standardization of items, materials, and engineering practices within the Department of Defense (DoD). Basic instructions regarding DoD standardization are contained in Department of Defense Directive 4120.3-M "Defense Standardization and Specification Program Manual" [1].

The primary objective of the program is to ensure that the best material standardization is achieved during the design, development, and acquisition process. The program includes a broad range of engineering and management practices described in such documents as specification, standards, drawings, data item descriptions, purchase descriptions, and commercial item descriptions.

Specifications and standards have been divided into federal supply classes (FSC) and standardization areas (AREA). Federal supply classes, which mainly cover products, are the responsibility of the assignee activity. Standardization areas, which mainly cover processes and procedures, are the responsibility of the lead service activity. Standardization documents for metallic finishes are included in standardization areas. Management responsibility for these FSCs and AREAs is delegated by the Defense Product Standards Office (DPSO) to the military

¹Chemist, Army Materials Technology Laboratory, Watertown, MA 02172-0001.

departments and defense agencies. These departments further delegate the responsibility for conducting the work to lower level commands.

The responsibility of the assignee/lead service activity is to analyze, plan, and ensure the best DoD standardization of the class or area. With the exception of Military Specifications MIL-C-46110B, "Coating Compound, Oxide Black," and MIL-P-50002B, Phosphate Coating Compounds for Phosphating Ferrous Metals," all metal finishing standardization documents are in the MFFP (Metal Finishes and Finishing Processes and Procedures) area. The agency having lead service responsibility for the MFFP AREA is the Army Materials Technology Laboratory at Watertown, MA.

A specification for metal finishing is a document which specifies values for all the important properties of the finish and gives limits of variability and methods for determining these values. In designing an adequate metal finish, quality assurances and realistic accept/reject criteria must be established.

Specifications and standards preparation is performed by a "preparing activity" appointed by the "assignee/lead service activity." The responsibility of the preparing activity is to develop, maintain, and coordinate individual Defense Standardization Program documents and to ensure that they meet specific requirements. Associated with assignee/lead service activities and preparing activities are several other activities. These include "participating," "custodians," "review," "user," and "agents" that assist in the preparation of standardization documents.

The participating activity is responsible for all the documents in a particular class or area in their own department or agency. The custodian is the activity responsible for the coordination of an individual specification or standard within its own department or agency. The review activity has a technical interest in the standardization document and actively participates in the coordination process. The user, whose interest is primarily in the use of the document, makes necessary comments through a review activity. An agent prepares standardization documents under the authority of a preparing activity.

A simplified organization chart, showing the DoD standardization organization is given in Fig. 1.

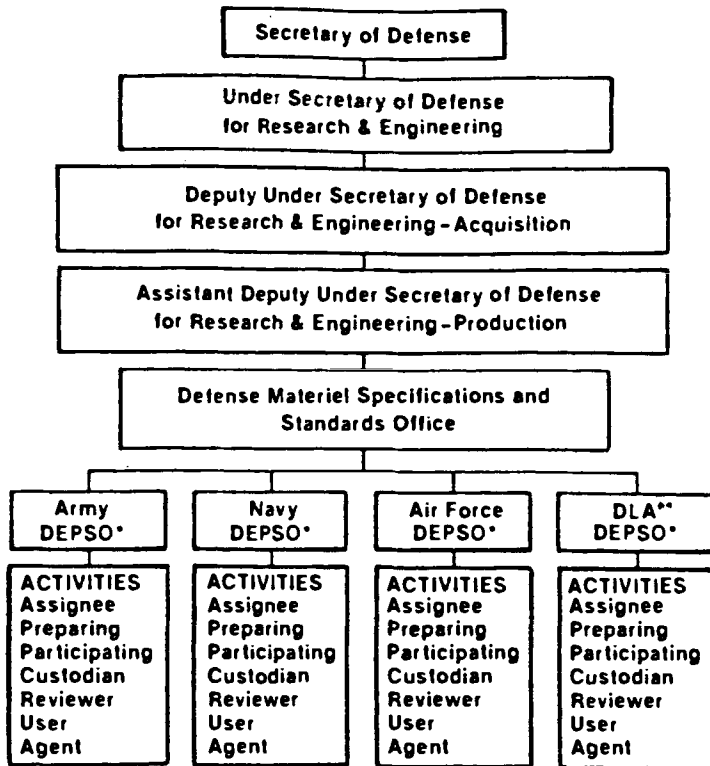
The maintenance of standardization documents extends from publication to cancellation. Periodic revisions, including amendments and notices, occur as a result of procurement need, corrections, and updates, as well as changes in policy. Current policies and regulations require that each active document must be evaluated every five years. The action resulting from this review will be either a validation, a revision, an amendment, or a cancellation.

Department of Defense requirements for repetitively procured products are described in specifications, while services, practices, processes, and data are usually described in standards. Another DoD standardization type of publication entitled, "Handbook," contains standard procedural, technical, engineering, or design information and data relating to the material and associated processes, practices, and methods covered by the Defense Specification and Standards Program. Military specifications are written to cover products or processes used exclusively by the military. Federal specifications are required if these products or processes are used by one or more non-DoD government agencies [2].

Coverage of Hydrogen Embrittlement by Government Documents

The rest of this article will be devoted to the coverage of hydrogen embrittlement by government specifications standards and handbooks. Before proceeding to specific requirements and test methods as found in specifications and standards, a description of hydrogen embrittlement as found in military handbooks is now given [3].

"When atomic hydrogen enters high strength steel (and certain other high strength alloys), it may cause any of several undesirable events to occur. If large quantities of hydrogen are introduced, there may be a general loss in ductility or, if the hydrogen accumulates in certain localized areas, internal



*DEPSO: Departmental Standardization Office

**DLA: Defense Logistics Agency

FIG. 1—DoD standardization organization chart.

burst or blisters may be produced. Under certain circumstances, hydrogen may react with the alloy to produce catastrophic brittle failures at applied stresses far below the yield strength or the nominal design strength for the alloy. These phenomena are collectively referred to as hydrogen embrittlement. However, only the latter, that is, the hydrogen induced brittle failure is of primary concern in the plating and coating of high strength steels. Since this phenomenon often happens in materials that exhibit no significant loss in ductility (as measured by a conventional tensile test), it is sometimes referred to as hydrogen induced delayed brittle failure or hydrogen stress cracking. The term 'hydrogen embrittlement' as used herein will refer to phenomenon associated with hydrogen induced or hydrogen stress failure."

Hydrogen-stress cracking is defined as the failure of a metal as the result of the combined action of stress and the penetration of hydrogen into the metal. The term "hydrogen embrittlement" is frequently used in the literature. However, in its strictest sense hydrogen embrittlement denotes a loss in ductility of a metal as the result of hydrogen penetration. The source of hydrogen may be a chemical process, for example, picklings, or it may be a by-product produced at the metal surface during electroplating. Hydrogen can also be introduced during fabricating or cleaning processes or it may be picked up from the service environment as a result of cathodic protection reaction or corrosion reaction. Thus, any process that presents atomic hydrogen to steel, whether by thermally activated dissociation of the hydrogen gas molecules, electrochemical reaction, or chemical reaction, is capable of introducing sufficient hydrogen to

cause failure. Unless such processes are avoided or the hydrogen introduced is removed from the high-strength steels before permanent damage occurs, the potential exists for failure of these materials in service.

As with stress-corrosion cracking, hydrogen-stress cracking leads usually to brittle failure, and the metals commonly involved are medium- or high-strength steels, and possibly titanium alloys. The stresses may be residual, applied, or a combination of these and are usually nonfluctuating. Under a high-tensile stress the path of failure can be either inter- or transgranular, and it is often difficult to distinguish between hydrogen-stress cracking and stress-corrosion cracking. Frequently a metallographic examination is required to definitely establish which one of these two types of corrosion attack was the cause of failure. As a rule of thumb, however, if specific corrosidents are involved for a given metal, then hydrogen-stress cracking can be suspected. Of course, a knowledge of prior treatments, such as coating by electrolytic means, can serve to reinforce the judgment.

Hydrogen-stress cracking is generally considered to be restricted to the medium- and high-strength steels, steels heat treated to a hardness of 22 Rockwell C or greater, and some of the titanium alloys. At normal temperature the hydrogen atoms are absorbed into the metal and diffuse through the grains, tending to collect at inclusions or imperfections in the crystal lattice. The conjoint action of a tensile stress then favors transgranular cracking. On the other hand, at elevated temperature the absorbed hydrogen tends to collect at the grain boundaries, and intergranular cracking will result.

The problem of hydrogen embrittlement of high-strength steels and alloys is of considerable concern to aerospace, aircraft, and other industries, where components fabricated from high-strength materials are electroplated to provide protection against corrosion, increased wear resistance, or some other desirable surface quality. The application of the electrodeposited coatings can make the part susceptible to hydrogen embrittlement failure, because hydrogen is often introduced during cleanings, pickling, activating, and plating operations.

The susceptibility to hydrogen embrittlement increases with the hardness of the steel. Apparently, the concentration of hydrogen required to cause brittle fracture decreases with increasing ultimate strength of the steel. Certain hardening constituents such as carbon also increase susceptibility. In general, steel parts having a hardness of Rockwell C40 or higher are subject to hydrogen embrittlement to a degree that warrants relief treatment.

Results of many comprehensive studies on cleaning and plating operations have shown that most high-strength steels were embrittled to various degrees by almost all of the common electroplating processes including chromium, cadmium, zinc, nickel, lead, copper, and silver. These studies also show that the amount of hydrogen entering steel specimens during certain electroplating processes may be as great as that introduced during deliberate severe cathodic charging and that more hydrogen is sometimes introduced during pickling or cathodic cleaning than during the actual electroplating operations.

Furthermore, these studies showed that baking treatments to remove hydrogen from plated parts often were not effective in eliminating delayed failure. Also, the sustained load test employing notched specimens was shown to be the most sensitive of the many methods used to evaluate the embrittling tendencies of cleaning, pickling, and electroplating procedures.

Chemicals present in the environment can have an advantageous or detrimental effect with respect to hydrogen-stress cracking, depending upon whether or not the ingress of hydrogen atoms (or possible portions) is facilitated. For example, sodium chromate inhibits the absorption of hydrogen, while sodium disilicate promotes absorption. Some sulfur and arsenic compounds and phosphorous also promote the uptake of hydrogen and are referred to as "poisons" [4].

Failures of steel by hydrogen embrittlement have long plagued the petroleum industry. Steels having a yield strength in excess of 621 MPa (90 000 psi) exposed in environments containing hydrogen sulfide (H_2S), moisture, and sometimes CO_2 , will fail under engineering applied stresses with evidence of brittle fracture. A piece of steel tubing, exposed to such an environ-

ment, showed on superficial examinations no evidence of corrosion, but an examination of the inner surface under low-power magnification revealed a fine network of cracks. Upon sectioning it was found that many of these cracks extended up to halfway through the tube wall. This was a typical case of sulfide cracking or hydrogen cracking. The hydrogen sulfide in the presence of moisture is believed to react with the steel to form atomic hydrogen at the surface, while the sulfide ion present "poison" at the surface of the steel so that some of the hydrogen atoms diffuse into the steel (rather than combining to form molecular hydrogen which does not penetrate steel).

As just discussed, hydrogen embrittlement of hardened plated steel parts intended for resilient or high-stress service can be a serious problem. No visual or chemical inspection method to reveal this defect is known. Designers are, therefore, cautioned to avoid the use of hardened ferrous alloys requiring plating whenever possible. When this set is not feasible, steels employed should be of the lowest carbon content and lowest hardness which will provide the necessary mechanical performance of the part. The microstructure of such steels should be essentially tempered martensite. The use of sharp bends in the part should be avoided, particularly if the part is to be hardened after forming. Plating baths and preplate cleaning processes should be adjusted and operated in a mode designed to prevent excessive hydrogen embrittlement. Oxide and scale removing should be accomplished by tumbling or other mechanical means whenever possible. A brief dip in an acid containing an inhibitor may be used if necessary. Cleaning should be accomplished by means of soaking or anodic treatment in alkaline cleaner.

Hydrogen Embrittlement Relief Requirements

The requirements for hydrogen embrittlement relief in QQ-P-416 are typical of the requirement in most government standardization documents. This requirement states that all steel parts having a hardness of Rockwell C40 and higher shall be baked at a minimum of $191^{\circ} \pm 14^{\circ}\text{C}$ ($375^{\circ} \pm 25^{\circ}\text{F}$) for 3 h or more within 4 h after plating. (For high-strength materials it may be beneficial to extend the baking time to 23 h). Plated springs and other parts subject to flexure shall not be flexed prior to hydrogen embrittlement relief treatment. When tested, baked parts shall not crack or fail by fracture. Specifications having similar requirements include QQ-C-320B, QQ-N-290A, MIL-P-25209, and MIL-C-14550B.

Some variations of the just-stated requirements are as follows:

1. MIL-S-5002C states that baking shall not be less than 3 h and applies to parts which are subject to static loads or designed for limited life under dynamic loads or combinations thereof.
2. MIL-P-23408B calls for baking at $168^{\circ} \pm 6^{\circ}\text{C}$ ($335^{\circ} \pm 10^{\circ}\text{F}$) for 3 h or more within 8 h after plating.
3. MIL-G-45204C requires baking within 1 h after plating.
4. MIL-P-81728A calls for baking at $171^{\circ} \pm 6^{\circ}\text{C}$ ($340^{\circ} \pm 10^{\circ}\text{F}$).
5. MIL-C-26074B calls for baking at 177°C (350°F).
6. MIL-C-13924C states that steel parts having an ultimate tensile strength of 200 000 psi (1379 MPa) or above shall be baked at $191^{\circ} \pm 14^{\circ}\text{C}$ ($375^{\circ} \pm 25^{\circ}\text{F}$) for 3 h or more.

MIL-STD-186D(MI) states that steels of Rockwell hardness C40 or over, including carbonized and steel surfaces hardened by using other methods, shall be either sand, abrasive grit, steel shot, grit, or glass bead blasted for rust or scale removal. Acid pickling or other hydrogen-producing processes shall not be used. Parts which cannot be thoroughly cleaned to insure removal of plating solution shall be vacuum coated with cadmium. Vacuum-deposited cadmium shall be used for high hardness steels subject to the deleterious effects of hydrogen embrittlement.

MIL-STD-808A(USAF) states that where chemical cleaning methods are used, the materials shall not result in any attack of the surface, either pitting or intergranular. Daily determination

for this behavior shall be made using a microscopic method with examination at a magnification which will clearly establish the condition.

MIL-S-5002C states that unless otherwise specified, to assure continuous control of the process to prevent detrimental hydrogen embrittlement during production, the satisfactory behavior of specimens shall be determined once each month or more frequently if required by the procuring activity. If evidence of hydrogen embrittlement of specimens or parts [less than 1655 MPa (240 000 psi)] is shown, the use of the process shall be discontinued until the process conditions are corrected.

Hydrogen embrittlement relief treatment for graphite-coated parts is given by DoD-P-16232F. This document states that phosphated steel parts shall be heated at 98° to 107°C (210° to 225°F) for 8 h or at room temperature for 120 h. In some cases 4 h at 163° ± 14°C (325° ± 25°F) has been approved.

The recently revised TT-C-490 (Revision C) states that parts having a hardness of Rockwell C40 or greater shall be heat treated after phosphating for 8 h at 99° to 107°C (210° to 225°F) or must be held for 240 h at room temperature to relieve any embrittlement due to hydrogen. This specification also states that parts having a hardness of Rockwell C48 or higher shall not be subject to phosphating.

Test Methods

Test methods used to determine if these requirements have been effective are discussed as follows:

According to MIL-C-13924C samples shall be selected at random from each inspection lot in accordance with MIL-STD-105, Inspection Level S-1 and Acceptable Quality Level (AQL) equal to 1.0% defective. Another sampling procedure is prescribed in QQ-S-365D, which states that a random sample of four plated parts or articles shall be taken from each lot for each destructive test or separately plated specimens shall be prepared to represent each lot. If the number of articles in the lot is four or less, the number of articles in the sample shall be specified by the procuring activity. Failure of one or more of the test specimens shall reject the lot.

QQ-P-416 states that separate specimens shall be prepared when the plated articles are of such form, shape, size, and value as to prohibit use thereof, or are not readily adaptable to testing or when destructive tests of small lot sizes are required. These separate specimens shall be plated concurrently with the articles represented. They shall be of basic metal equivalent to that of the article represented. "Equivalent" basic metal includes chemical composition, grade, condition, and finish of surface prior to plating. For example, a cold-rolled steel surface should not be used to represent a hot-rolled steel surface. Due to the impracticality of forging or casting separate test specimens, hot-rolled steel specimens may be used to represent forged and cast steel articles. The separate specimen may also be cut from scrap castings when ferrous alloy castings are being plated. These separate specimens shall be introduced into a lot at regular intervals prior to cleaning operations, preliminary to plating, and shall not be separated therefrom until after completion of plating. Conditions affecting the plating of specimens, including the spacing, plating media, residual air pressure, temperature, etc. in respect to other objects being plated, shall correspond as nearly as possible to those affecting the significant surfaces of the articles represented.

MIL-C-26074B states that sample parts such as spring pins, lock rings, etc. which are installed in holes or on rods shall be similarly assembled using the applicable parts specifications or drawings tolerances which impose the maximum sustained tensile stress on the coated parts. The parts shall be held under the specified load at 20° ± 1°C (70° ± 2°F) for at least 200 h and then examined for cracks.

Sample parts such as pressure containers, fasteners, springs, etc., which in use are subjected to a sustained static tensile load in excess of 25% of the basic material specification minimum

tensile yield strength, shall be subjected to a sustained tensile load equal to 75% of the basic material specification minimum tensile yield strength. Parts which require special fixtures or extreme loads to comply with the just-cited requirements need not be tested as specified, unless they are subjected in use to a sustained static tensile load in excess of 50% of the basic material specification minimum tensile yield strength. Parts which require fixtures or extreme loads to comply with the just-cited requirements and in use are subjected to a sustained static tensile load between 25 and 50% of the basic material specification minimum tensile yield strength may be represented by separate specimens.

As mentioned previously, four specimens shall be prepared to represent each lot. Specimen configuration shall be in accordance with Fig. 8 of ASTM Methods of Tension Testing of Metallic Materials [Metric] (E 8M-84) for rounded specimens. These specimens shall be of alloy steel 4340 conforming to ASTM Specification for Alloy Steel Bars Subject to End-Quench Hardenability Requirements [A 304-79 (1985)] (MIL-P-81728A) and shall have a 60° V-notch located approximately at the center of the gage length. The cross-section area at the root of the vee shall be approximately equal to half the area of the full cross section of the specimen's reduced section. The vee shall have a 0.010 ± 0.0005 -in. radius of curvature at the basis of the notch. The axis of the round notched specimen (load direction) shall be perpendicular to the short transverse grain load direction. These specimens shall be of the same chemical composition (alloy) as the parts represented and shall have been heat treated to the same hardness requirement. Specimens representing surface hardened parts shall be subjected to a sustained static tensile load not less than 20% of the load at which an uncoated specimen will break. The parts or samples shall be held under the specified load at $20^\circ \pm 1^\circ\text{C}$ ($70^\circ \pm 2^\circ\text{F}$) for at least 200 h and examined for cracks.

Inspection of parts for cracks in the bases metal and the coating shall be in accordance with MIL-I-6868 using the fluorescent magnetic particle method. The lot shall be rejected if any coated part develops cracks.

Conclusion

In conclusion, it should be mentioned that considerable research effort has been expended by the U.S. Government and the electroplating and aerospace industries in developing and evaluating nonembrittling or less embrittling electroplating processes, especially processes for electroplating cadmium. As a result, several cadmium electroplating procedures have been developed which are reported to be nonhydrogen or less hydrogen embrittling. To a lesser degree, research has also been carried out to develop nonembrittling or less embrittling procedures for cleaning, pickling, or activating metals, particularly by the use of inhibited acid pickling baths.

Practical steps to minimize hydrogen embrittlement include:

1. Minimize the use of hydrogen-producing treatments. This may be accomplished as follows:

- a. Avoid cathodic cleaning, pickling, or activation treatments when possible by use of alkaline soak cleaning, anodic alkaline cleaning, and anodic etching or electropolishing.
- b. Use vapor degreasing or solvent cleaning to remove the bulk of grease, oil, and other contaminants before cleaning in aqueous solutions.
- c. Use mechanical means (such as tumbling, sand or grit blasting, vapor blasting, etc.) for oxide and scale removal, rather than pickling, when possible.
- d. Use inhibited acid pickling baths. The inhibitors either cut down on the amount of metal dissolved (and thereby reduce the amount of hydrogen generated) or they can change conditions at the surface so that less of the hydrogen generated enters the metal.

2. Employ electroplating or coating techniques that avoid or minimize hydrogen embrittlement as follows:

- a. Use vacuum coating techniques, for example, substitute vacuum-evaporated cadmium coatings for electroplated cadmium.
 - b. Use organic coatings, rather than electroplated metals.
 - c. Use low embrittling versions of electroplating processes such as special bath compositions and operating conditions which result in either a lower pickup of hydrogen or in a deposit that allows easier removal of the absorbed hydrogen during the baking treatment.
3. Use appropriate heat treatment to provide hydrogen embrittlement relief.

APPENDIX

List of Standardization Documents Reviewed

Specifications

<i>Document Number</i>	<i>Title</i>
QQ-C-320B	Chromium Plating (Electrodeposited)
QQ-N-290A	Nickel Plating (Electrodeposited)
QQ-P-416C	Plating, Cadmium (Electrodeposited)
QQ-S-365C	Silver Plating, Electrodeposited, General Requirements for
TT-C-490B	Cleaning Methods and Pretreatment of Ferrous Surfaces for Organic Coatings
MIL-S-5002C	Surface Treatments and Inorganic Coatings on Weapon Systems
MIL-L-13808B(MR)	Lead Plating (Electrodeposited)
MIL-C-13924C	Coating, Oxide, Black for Ferrous Metals
MIL-F-14072C(ER)	Finishes for Ground Electronic Equipment
MIL-C-14538C	Chromium Plating, Black (Electrodeposited)
MIL-C-14550B	Copper Plating (Electrodeposited)
DoD-P-16232F	Phosphate Coatings, Heavy, Manganese or Zinc Base (for Ferrous Metals)
MIL-P-23408B	Plating: Tin Cadmium (Electrodeposited)
MIL-C-26074B	Coatings, Electroless Nickel, Requirements for
MIL-G-45204C	Gold Plating, Electrodeposited
MIL-P-45209B	Palladium Plating, Electrodeposited
MIL-L-46064A	Lead-Tin Alloy Coating, Electrodeposited
MIL-R-46085B	Rhodium Plating, Electrodeposited
MIL-H-55392A(EL)	Nickel-Carbon, Porous Electrodeposited for Camouflage
MIL-C-81562B	Coating, Cadmium, Tin-Cadmium, and Zinc (Mechanically Deposited)
MIL-P-81728A	Plating Tin-Lead (Electrodeposited)
MIL-C-81740(AS)	Coatings, Aluminium and Aluminium Alloys (Metallic Compound Decomposition)
MIL-C-81769	Chemical Milling of Metals, Specification for
MIL-C-83488A	Powder, Plasma Spray
MIL-C-85455	Chromium Molybdenum Plating (Electrodeposited)
MIL-C-87115	Coating, Immersion, Zinc Flake/Chromate Dispersion

Standards

MIL-STD-171D	Finishing of Metal and Wood Surfaces
MIL-STD-868A(USAF)	Nickel Plating, Low Embrittlement, Electrodeposition
MIL-STD-870A(USAF)	Cadmium Plating, Low Embrittlement, Electrodeposition
MIL-STD-1500A (USAF)	Cadmium-Titanium Plating, Low Embrittlement, Electrodeposition

MIL-STD-1501B(USAF)	Chromium Plating, Low Embrittlement, Electrodeposition
DoD-STD-2182(SH)	Engineering Chromium Plating (Electrodeposited) for Repair of Shafting (Metric)

Handbooks

MIL-HDBK-132A	Protective Finishes for Metal and Wood Surfaces
MIL-HDBK-205	Phosphating and Black Oxide Coating of Ferrous Metals
MIL-HDBK-729	Corrosion and Corrosion Prevention of Metals

References

- [1] Department of Defense Directive 4120.3-M, Aug. 1978.
- [2] Burgess, M. T. and Clegg, E. T., "ASTM and the DoD," *Adhesives Age*, February 1984.
- [3] *Protective Finishes for Metal and Wood Surfaces*, Military Handbook 132, Naval Publications and Forms Center, Philadelphia, PA, 9 May 1984.
- [4] Godard, H. P. in *NACE Basic Corrosion Course*, Chapter 8: "Localized Corrosion," National Association of Corrosion Engineers, Houston, TX, 1970.

Other ASTM Committees and ISO Committees Involved in Hydrogen Embrittlement Test Methods

REFERENCE: Grobin, A. W., "Other ASTM Committees and ISO Committees Involved in Hydrogen Embrittlement Test Methods," *Hydrogen Embrittlement: Prevention and Control*, ASTM STP 962, L. Raymond, Ed., American Society for Testing and Materials, Philadelphia, 1988, pp. 46-54.

ABSTRACT: Current standards documentation, concerned with the testing or prevention of hydrogen embrittlement, under development by other ASTM committees and by International Standards Organization (ISO) committees is briefly described.

KEY WORDS: hydrogen embrittlement, standards, ASTM committees

This presentation is the liaison report from ASTM Committee B08 on Metallic and Inorganic Coatings to ASTM Committee F07.04 on Hydrogen Embrittlement. Committee B08 has been actively cooperating with Committee F07.04 in the standardization of hydrogen embrittlement tests and avoidance procedures. The purpose of this formal presentation of the liaison report is to inform others of the activities presently underway and to invite those who are interested to join these activities.

Committee B08 has two subcommittees involved with hydrogen embrittlement. Subcommittee B08.02 on Substrate Preparation, Section 14, is concerned with embrittlement avoidance procedures in the metallic coating processes. Section 15 is concerned with shot peening. Subcommittee B08.10 on Test Methods, Section 08, is concerned with testing for embrittlement in plated articles and in methods for evaluating hydrogen charging characteristics of plating solutions as well as the effectiveness of avoidance treatments as performed in the plating shop.

In addition to these direct activities, Committee B08 prepares standards on low embrittlement processes such as mechanical plating, vacuum deposited coatings, and ion vapor deposited coatings. The committee also administers the U.S. Technical Advisory Group (TAG) for the International Standards Organization Technical Committee 107 (ISO/TC 107) on Metallic and Non-Organic Coatings. ISO/TC 107, Subcommittee 3 (SC 3), Working Group 3 (WG 3) is concerned with preparing draft proposals for hydrogen embrittlement avoidance and testing methods. These proposals, after consideration by the subcommittee and member bodies of ISO, will become international standards. Lastly, Committee B08 maintains a liaison with ASTM Committee F16 on Fasteners. This committee is concerned with embrittlement testing of fasteners covered by the committee's specifications.

ASTM B08.02.14 has completed a subcommittee ballot of two new documents, "Standard Practice for Stress Relief Heat Treatment of Steels Prior to Electroplating, Conversion Coating, Autocatalytic Processes and Chemical Treatment" and "Standard Practice for Embrittlement

¹International Business Machines, Poughkeepsie, NY 12602.

Relief Heat Treatment of Steels and Alloys After Electroplating and Autocatalytic Plating Processes" (see Appendix).

Two identically worded documents, with minor title differences, have also been balloted in ISO/TC 107/SC 3/WG 3. The comments obtained from each of these committees will be cross submitted in order to keep the documents as closely aligned as possible.

After revision of the Shot Peening document balloted in ASTM B08.02.15, the US TAG for ISO/TC 107 intends to propose that document as a new work item for ISO/TC 107/SC 3/WG 3. Again the objective will be to keep the ASTM and ISO documents as closely aligned as possible.

ASTM B08.10.08 is currently balloting "Standard Method of Test for Residual Embrittlement in Metallic Coated Externally Threaded Articles, Fasteners and Rod Inclined Wedge Method" (see Appendix). An identically worded document has just been balloted in ISO/TC 107/SC 3/WG 3. Again the comments of each group will be cross submitted.

ASTM B08.10.08 is also working on a notched spring test method for evaluating hydrogen embrittlement in the electroplating shop. The committee is attempting to formulate a round-robin testing plan before proceeding further.

Committee F16 has balloted a mechanical test for embrittlement to be incorporated into a revision of ASTM Method for Conducting Tests to Determine the Mechanical Properties of Externally and Internally Threaded Fasteners, Washers, and Rivets (F 606-85a).

APPENDIX

This draft document is being developed by Committee B8 on Metallic and Inorganic Coatings. It has no official status within ASTM.

ASTM Subcommittee B08.02.14

Draft Number: 2nd

**Draft Practice for
Embrittlement Relief Heat Treatment of Steels and Alloys After Electroplating and Autocatalytic Plating Processes**

1. Introduction

When atomic hydrogen enters steel and certain other alloys, it can cause loss of ductility or load carrying ability or cracking (usually as submicroscopic cracks), or catastrophic brittle failures at applied stresses well below the yield strength or even the normal design strength for the alloys. This phenomenon often occurs in alloys that show no significant loss in ductility, when measured by conventional tensile tests, and is frequently referred to as hydrogen induced delayed brittle failure, hydrogen stress cracking or hydrogen embrittlement. The hydrogen can be introduced during fabrication, cleaning, pickling, phosphating, electroplating, autocatalytic processes and in the service environment as a result of cathodic protection reactions or corrosion reactions.

2. Scope

This practice establishes a procedure for reducing susceptibility or degree of susceptibility to hydrogen embrittlement or degradation which may arise in the finishing processes. The heat treatment does not guarantee complete freedom from the adverse effects of hydrogen degradation.

3. Applicable Documents

ASTM B 242 Standard Practice for Preparation of High-Carbon Steel for Electroplating

ASTM B 322 Standard Practice for Cleaning Metals Prior to Electroplating

ASTM B 374 Standard Definitions of Terms Relating to Electroplating

ASTM E 44 Standard Definitions of Terms Relating to Heat Treatment of Metals

4. Significance and Use

The heat treatment procedure established herein has been shown to be effective in returning embrittled parts to their previous non-embrittled condition. This heat-treatment procedure is used after plating operations but prior to any secondary conversion coating operation.

5. General

Heat treatment shall be performed on plated metals to

reduce the risk of hydrogen embrittlement. In all cases, the duration of heat treatment shall commence from the time at which the whole of each part attains the specified temperature.

Parts made from steel with actual tensile strengths greater than or equal to 1000 MPa (corresponding hardness values 300 HV, 303 HB or 31 HRC) and surface hardened parts will require heat treatment. Preparation involving cathodic treatments in alkaline or acid solutions shall be avoided. Additionally, the selection of electroplating solutions with high cathodic efficiencies is recommended for steel components with tensile strengths greater than 1400 MPa (corresponding hardness values 425 HV, 401 HB or 43 HRC).

Note: The use of inhibitors in acid pickling baths does not necessarily guarantee avoidance of hydrogen embrittlement.

6. Categorization of Steels

With the exception of surface hardened parts the heat treatment conditions shall be selected on the basis of actual tensile strength. When only the minimum tensile strength is specified or if the tensile strength is not known, the heat treatment condition shall be selected by relating known or measured hardness values to equivalent tensile strengths. This information shall be supplied by the purchaser.

Steels which have been wholly or partly surface hardened shall be considered as being in the category appropriate to the hardness of the surface layer.

7. Heat Treatment after Processing

7.1 The heat treatment shall commence as soon as possible, but not later than 1 hour after plating and before commencement of any grinding or other mechanical operation. For zinc and cadmium plated items, heat treatment shall be carried out before chromate treatment.

7.2 For high strength steels, the following conditions (Table 1 and Figure 1 are mandatory. For steels of actual tensile strength less than 1000 MPa, heat treatment after plating is not mandatory.

Actual Tensile Strength (MPa)	Temperature (° C)	Time (hours)
1000-1100	190-220	minimum 8
1101-1200	190-220	minimum 10
1201-1300	190-220	minimum 12
1301-1400	190-220	minimum 14
1401-1500	190-220	minimum 16
1501-1600	190-229	minimum 18
1601-1700	190-220	minimum 20
1701-1800	190-220	minimum 22

Table 1. Baking Requirements

7.3 If threads or sharp notches exist or parts are greater than 25mm thick, then for cadmium and zinc plated items heat treatment shall be carried out immediately after electroplating for a minimum period of 24 hours.

7.4 Minimum duration of heat treatment for steels of actual tensile strength above 1800 can be selected in accordance with Figure 1, i. e.:

$$t = m \sigma + c$$

where t = minimum duration in hours,

σ = actual tensile strength,

$$m = 0.02$$

$$c = -12$$

7.5 Plated steel items having surface hardened areas and through hardened or bearing steels, which would suffer an unacceptable reduction in hardness by treatment in accordance with Table 1 and Fig 1 shall be heat treated at a lower temperature, but at not less than 130° C for a minimum period of 8 hours. For

zinc and cadmium plated items, the minimum period shall be 16 hours below 1401 MPa and 22 hours for and above 1401-1800 MPa tensile strength.

7.6 For items after chromium plating, the following treatment (Table 2 and Figure 1) shall commence as soon as possible but not later than 1 hour after electroplating and before commencement of any grinding or other mechanical operation. For steels of actual tensile strength less than 1000 MPa, heat treatment is not mandatory.

7.7 Minimum duration of heat treatment for peened steels items of actual tensile strength above 1800 can be selected in accordance with Figure 1, i. e.:

$$t = m \sigma + c$$

where t = minimum duration in hours;

σ = actual tensile strength,

$$m = 0.02$$

$$c = -12$$

7.8 Chromium plated steel items having surface hardened areas and through hardened or bearing steels which would suffer an acceptable reduction in hardness by treatment in accordance with Table 2 shall be heat treated at a lower temperature but at not less than 130° C for a minimum period of 16 hours below 1400 MPa and 24 hours for and above 1400 MPa tensile strength.

Note: This treatment will reduce the hardness of the chromium deposit. It shall not be applied to steels that may be adversely affected by heat treatment at this temperature and the lower temperature range shall be applied. For tempered steels, items shall not be heat treated above a temperature which shall be 50° C below the tempering temperature.

Actual Tensile Strength (MPa)	Peened items		Unpeened items	
	Temperature (° C)	Time (Hours)	Temperature (Note 2) (° C)	Time (Hours)
1000-1100	190-220	min 8	440-480	min 1
1100-1200	190-220	min 10	440-480	min 1
1201-1300	190-220	min 12	440-480	min 1
1301-1400	190-220	min 14	440-480	min 1
1401-1500	190-220	min 16	440-480	min 1
1501-1600	190-220	min 18	440-480	min 1
1601-1700	190-220	min 20	440-480	min 1
1701-1800	190-220	min 22	440-480	min 1

Table 2. Baking Requirements After Chromium Electroplating

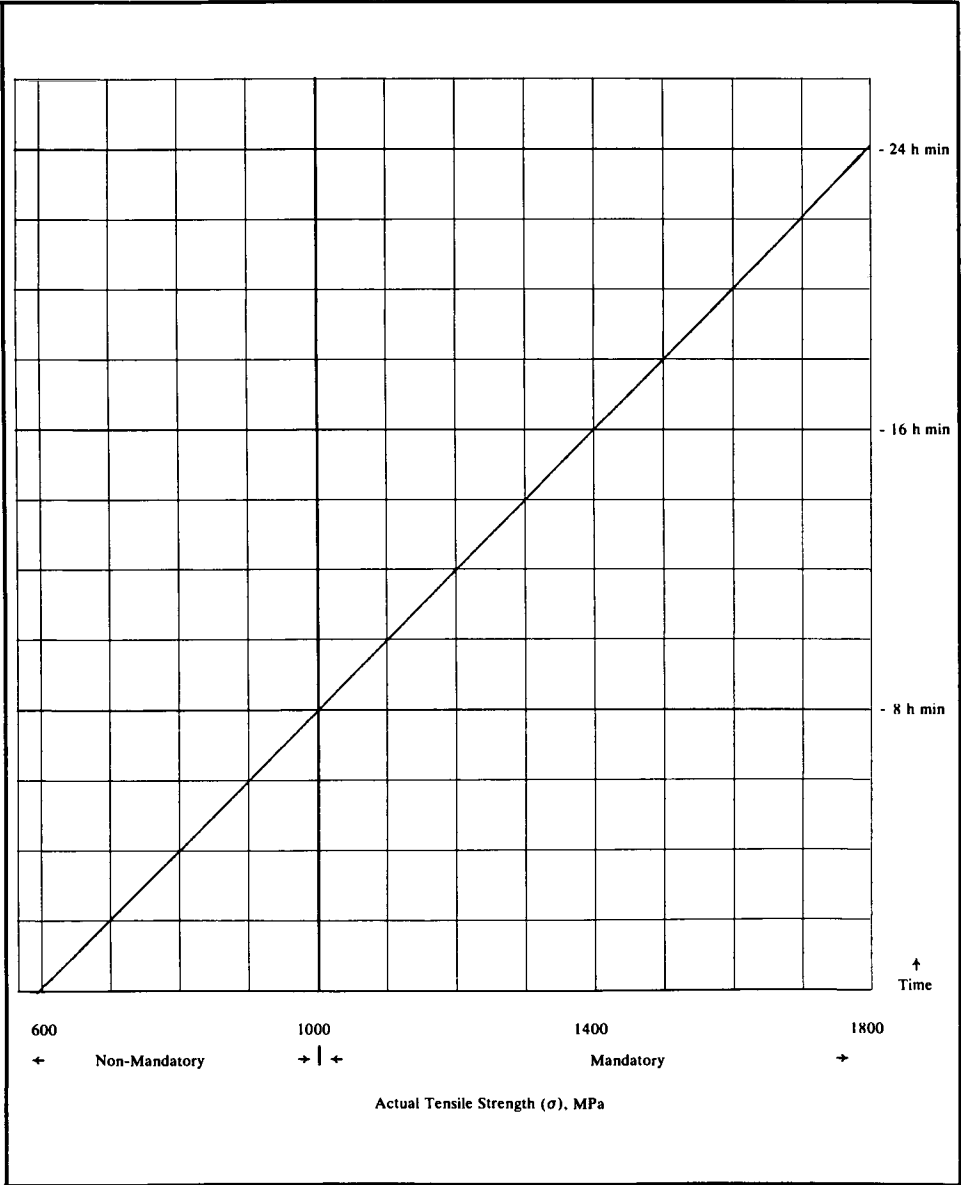


Figure 1. Time - Tensile Strength Relationship at 190 - 230° C

This draft document is being developed by Committee B8 on Metallic and Inorganic Coatings. It has no official status within ASTM.

ASTM Subcommittee B08.02.14

Draft Number: 2nd

Draft Practice for

Stress Relief Heat Treatment of Steels Prior to Electroplating, Conversion Coating, Autocatalytic Processes and Chemical Treatment

1. Abstract

When atomic hydrogen enters steels and certain other alloys, it can cause loss of ductility or load carrying ability or cracking (usually as submicroscopic cracks), or catastrophic brittle failures at applied stresses well below the yield strength or even the normal design strength for the alloys. This phenomenon often occurs in alloys that show no significant loss in ductility, when measured by conventional tensile tests, and is frequently referred to as hydrogen-induced delayed brittle failure, hydrogen stress cracking or hydrogen embrittlement. The hydrogen can be introduced during fabrication, cleaning, pickling, phosphating, electroplating, autocatalytic processes and in the service environment as a result of cathodic protection reactions or corrosion reactions. Parts that have been machined, ground, cold-formed, or cold-straightened subsequent to heat treatment are especially susceptible to hydrogen embrittlement damage.

2. Scope

This practice establishes a procedure for reducing susceptibility or degree of susceptibility to hydrogen embrittlement or degradation which may arise in electroplating, autocatalytic plating, chemical conversion coating and phosphating, and the associated pretreatment processes.

3. Applicable Documents

ASTM B 242 Standard Practice for Preparation of High-Carbon Steel for Electroplating

ASTM B 322 Standard Practice for Cleaning Metals Prior to Electroplating

ASTM B 374 Standard Definitions of Terms Relating to Electroplating

ASTM E 44 Standard Definitions of Terms Relating to Heat Treatment of Metals

4. Significance and Use

The heat treatment procedure established herein has been shown to be effective in reducing the susceptibility of steel parts of tensile strength 1000 MPa or greater that have been machined, ground, cold-formed, or cold-straightened subsequent to heat treatment. This heat-treatment procedure is used prior

to any operation capable of hydrogen charging the parts such as the cleaning procedures prior to electroplating, autocatalytic plating, and other chemical coating operations.

5. General

Heat treatment shall be performed on basis metals to reduce the risk of hydrogen embrittlement. In all cases, the duration of heat treatment shall commence from the time at which the whole of each part attains the specified temperature.

Parts made from steel with actual tensile strengths greater than or equal to 1000 MPa (corresponding hardness values 300 HV, 303 HB or 31 HRC) and surface hardened parts will require heat treatment. Preparation involving cathodic treatments in alkaline or acid solutions with high cathodic efficiencies is recommended for steel components with tensile strengths greater than 1400 MPa (corresponding hardness values 425 HV, 401 HB or 43 HRC).

Note: The use of inhibitors in acid pickling baths does not necessarily guarantee avoidance of hydrogen embrittlement.

6. Categorization of Steels

With the exception of surface-hardened parts the heat treatment conditions shall be selected on the basis of actual tensile strength. When only the minimum tensile strength is specified or if the tensile strength is not known, the heat treatment condition shall be selected by relating known or measured hardness values to equivalent actual tensile strengths. This information shall be supplied by the purchaser.

Steels which have been wholly or partly surface hardened shall be considered as being in the Category appropriate to the hardness of the surface layer.

7. Stress Relief

7.1 For high strength steels, the following conditions are mandatory. For steels of actual tensile strength less than 1000 MPa, stress relief treatment is not mandatory. The heat treatment shall be carried out before commencement of any preparation or cleaning treatment using aqueous solutions, or before any treatment liable to cause embrittlement.

Actual Tensile Strength (Rm) MPa	Temperature ° C	Time h
1000 to 1400	200-230	Minimum 3
1401 to 1800	200-230	Minimum 18
over 1800	200-230	Minimum 24

Table 1. Stress Relief Requirements for High Strength Steels

7.2 Suitable combinations of shorter time at appropriate higher temperatures may be used if they have shown not to be detrimental. For tempered steels, items shall not be heated above a temperature which shall be at least 50° C below the tempering temperature.

7.3 If stress relief is given after shot peening or other cold working processes to introduce beneficial compressive stresses, the temperature shall not exceed 230° C.

7.4 Where the temperatures in Table 1 are likely to alter the previous heat treatment conditions, stress relief at lower temperatures for longer times may be employed.

7.5 Items having surface hardened areas which would suffer an unacceptable reduction in hardness by treatment in accordance with Table 1 shall be heat-treated at a lower temperature but not less than 130° C for a minimum period of 8 hours.

This draft document is being developed by Committee B8 on Metallic and Inorganic Coatings. It has no official status within ASTM.

ASTM Subcommittee B08.10.08

Draft Number: 3rd

Draft Method of Test for

Residual Embrittlement in Metallic Coated Externally Threaded Articles, Fasteners and Rod Inclined Wedge Method

1. Introduction

When atomic hydrogen enters steels and certain other alloys, it can cause loss of ductility or load carrying ability or cracking (usually as submicroscopic cracks), or catastrophic brittle failures at applied stresses well below the yield strength or even the normal design strength for the alloys. This phenomenon often occurs in alloys that show no significant loss in ductility, when measured by conventional tensile tests, and is frequently referred to as hydrogen-induced delayed brittle failure, hydrogen stress cracking or hydrogen embrittlement. The hydrogen can be introduced during fabrication, cleaning, pickling, phosphating, electroplating, autocatalytic processes and in the service environment as a result of cathodic protection reactions or corrosion reactions.

2. Scope

This test determines, on a statistical basis, the probability of the existence of hydrogen embrittlement or degradation in; 1. a lot of barrel electroplated, autocatalytic plated, phosphated, or chemically processed threaded articles or fasteners; 2. a lot of rack plated threaded articles, fasteners or rod. This test is applicable to threaded articles, fasteners and rod made from steel with an actual tensile strength greater than or equal to 1000 MPa (corresponding hardness values 300 HV, 303 HB or 31 HRC) or surface hardened threaded articles, fasteners or rod.

Note: *The use of inhibitors in acid pickling baths does not necessarily guarantee avoidance of hydrogen embrittlement.*

3. Applicable Documents

MIL-STD-105 Sampling Procedures and Tables for Inspection by Attributes

ASTM B602 Method of Attribute Sampling of Electrodeposited Coatings and Related Finishes

ASTM B697 Guidelines for Selection of Sampling Plans for Inspection of Electrodeposited Coatings and Related Finishes

ASTM F436 Specification for Hardened Steel Washers

ASTM F606 Method for Conducting Tests to Determine the Mechanical Properties of Externally and Internally Threaded Fasteners, Washers, and Rivets

4. Terminology

The degree to which parts within a plated lot can be embrittled can vary over a wide range. The degree of embrittlement is a function of the concentration of hydrogen in the individual parts in the lot, measured in ppm, and in particular that portion of the hydrogen that is mobile or free to migrate to areas of high stress concentration.

For the purposes of this test, embrittlement is categorized into three types;

Gross embrittlement, where parts fracture immediately or up to 48 hours after tensioning.

Marginal embrittlement, where parts fracture from 49 hours up to 96 hours after tensioning.

Delayed embrittlement, where parts fracture at 97 hours up to 200 hours after tensioning.

5. Safety Precautions

This standard may involve hazardous materials, operations, and equipment. This standard does not purport to address all of the safety problems associated with its use. It is the responsibility of whosoever uses this standard to consult and establish appropriate safety and health practices and determine the applicability of regulatory limitations prior to use.

(See Paragraph 9.)

6. Summary of Method

The threaded articles, fasteners or rod are subjected to stress by tensioning with a mating nut after insertion through a clearance hole in a hardened rectangular wedge of steel. The upper surface of the wedge is ground at an angle to the lower surface. The mating nut is tensioned by any means capable of measuring tensile load. The torque method described in paragraph 10.1 is one such method. If the torque method of tightening is used, the fasteners are torqued to the desired value and then held for the minimum specified hours and then checked to determine if the initial torque has been maintained. Following this they are examined for embrittlement failures such as missing heads and transverse cracks.

Note: *Increasing the applied torque a small percentage as a "safety factor" is not recommended.*

7. Significance and Use

This test has two main functions: first, when used with a statistical sampling plan it can be used for lot acceptance or rejection; and second as a control test to determine the effectiveness of the various processing steps including pre and post baking treatments to reduce the mobile hydrogen in the articles, fasteners or rod.

8. Apparatus

The basic test fixture shall comprise a hardened wedge, one or more filler plates, and a hardened washer. The hole in each shall be as close to the major diameter of the threaded article, fastener or rod being tested as practical. Excess clearance space may cause the fastener to tilt in the hole and can result in failure at a lower torque value.

A fixture with multiple holes has been found useful for multiple or repetitive testing. The fixture can be readily made from a rectangular piece of an air hardening grade of steel with one face ground to to the appropriate wedge angle and hardened to RC 60.

8.1 Wedge

The wedge shall have an angle as specified in Table 1. The other dimensions and properties shall be as specified in ASTM F606.

8.2 Filler Plate

The filler plate(s) shall be steel and have a thickness such that, after installation and tightening, a minimum of three full threads of the test fastener will be engaged and no more than 5 full threads will extend beyond the nut.

8.3 Washer

The hardened washer shall be in conformance with ASTM F436.

9. Caution

Caution should be taken when applying this test. The heads of embrittled articles, fasteners or rod may suddenly break-off and become flying projectiles capable of causing serious injury or blinding. This hazard can occur as long as 200 hours after the test has started.

10. Torquing Device

If the torque method of tightening is used, the tightening torque shall be determined using a load measuring device capable of measuring the actual tension induced in the article, fastener, or rod as the item is tightened.

10.1 Torque Determination

Three items from the test lot shall be selected at random. Each shall be assembled into the load measuring device, mated with a nut, and the nut tightened until a load equal to 75 % of the specified

minimum ultimate tensile strength of the item is induced. The torque required to induce this load shall be measured and the arithmetic average of the three measured torques shall be the tightening torque.

11. Procedure

11.1 Test Item Placement

Place the test items in the *clearance* holes with the heads positioned against the angle of the wedge. In the case of items without heads, studs or threaded rod one end shall be nutted and tested as the head. When the items are threaded with different pitch threads the finer thread shall be treated as the head. Nut the free end of the items and run them up finger tight.

11.2 Torque Application

Clamp the wedge device with the nutted ends facing up in a securely attached vice. Using a calibrated torque tool tighten the nuts to the desired torque and record the values. The wedge should be removed from the vice and left undisturbed for 96 hours.

12. Evaluation

12.1 Cracks, Separated Heads and Breakage

After the specified holding period is complete examine each item for failures such as cracks, separated heads and breakage. Use finger pressure to check each head for breakage.

12.2 Relaxed Torque

Replace the wedge in the vice and carefully turn each mating nut, with the torque tool, in the *on* direction until a forward angular motion, after break loose, is noticeable. Record the torque value at break loose and compare it with the initially recorded torque. Torque relaxation greater than 10% shall be recorded as failure. Remove the nuts and examine the items for transverse cracks which shall also be recorded as failure.

13. Sampling Plan

The document specifying this standard shall specify an AQL level and sampling plan to be used. Guidance in the selection of sampling plans is provided in ASTM B 697. Widely used sampling plans are provided in ASTM B 602 and MIL-STD-105.

14. Precision

The precision of this test method is in process of being determined. Initial test results indicate that a minimum sample size of 30 pieces is necessary to assure freedom from embrittlement.

15. Bias

The bias has not been determined.

Nominal Size of Threaded Article	Articles with Unthreaded Lengths Less than 2D	Articles with Unthreaded Lengths 2D and Longer
2 mm to 6 mm	6	6
1/16 to 1/4 inch	6	6
6 mm to 18 mm	4	6
1/4 to 3/4 inch	4	6
over 18 mm to 38 mm	0	4
over 3/4 to 1-1/2 inch	0	4

Table 1. Wedge Angle Selection

Specifications for Hydrogen Control Testing of Materials

REFERENCE: Coates, D. J., “Specifications for Hydrogen Control Testing of Materials,” *Hydrogen Embrittlement: Prevention and Control*, ASTM STP 962, L. Raymond, Ed., American Society for Testing and Materials, Philadelphia, 1988, pp. 55–59.

ABSTRACT: This paper discusses and outlines some of the test methods incorporated into specifications for hydrogen control published by various organizations (other than U.S. Government standards). The specifications addressed are published by the Society of Automotive Engineers (SAE), the American Welding Society (AWS), and the National Association of Corrosion Engineers (NACE). Some discussion of the applicability and limitations of each test method is included.

KEY WORDS: hydrogen embrittlement, aircraft maintenance, chemicals, fasteners, welding, sulfide stress cracking

The use of U.S. Government standards [military (MIL) standards and federal (FED) standards] and ASTM standards in hydrogen embrittlement testing has gained widespread application and utilization. Some of these standards are discussed in detail by other authors in this book.

However, hydrogen-induced damage is an insidious and widespread problem that can manifest in a number of forms, not all of which are covered by the just-mentioned standards. To this end, a number of professional societies have developed specific techniques and test methods for the monitoring and control of hydrogen-induced failures of materials. This paper will outline and discuss some of these test methods and their applications as specified by the Society of Automotive Engineers (SAE), the Industrial Fasteners Institute (IFI), the American Welding Society (AWS), and the National Association of Corrosion Engineers (NACE).

The Society of Automotive Engineers/Aerospace Material Specifications

The Society of Automotive Engineers' (SAE) Cooperative Engineering Program has produced a series of aerospace material specifications (AMS). Included in these are a number of specifications for plating steels and requirements for post-plate baking. In these specifications, the requirements for testing plated specimens are generally provided by reference to appropriate ASTM specifications.

One SAE specification that concerns assessment of materials in terms of hydrogen embrittlement is the Aerospace Recommended Practice (ARP) 1525, entitled “Hydrogen Embrittlement Effect of Metals by Aircraft Maintenance Chemicals—Mechanical Test Methods.” This recommended practice “defines a procedure for evaluating the hydrogen generating potential of fluids used for aircraft maintenance.” The testing specified in ARP 1525 is similar to, and based upon, ASTM Method for Mechanical Hydrogen Embrittlement Testing of Plating Processes

¹Formerly, associate consulting engineer, L. Raymond & Associates, Irvine, CA 92714. (Presently, principal engineer, GE-Nuclear Energy, San Jose, CA 95125.)

and Aircraft Maintenance Chemicals (F 519-77). Testing is specified for three types of specimens fabricated from AISI 4340 low-alloy steel with the precaution that any aircraft maintenance fluid found to be nonembrittling to the AISI 4340 low-alloy steel cannot be assumed to be nonembrittling to other types of steel.

Three types of specimen geometries are included:

Type 1a—Notched round bars, stressed in tension under constant load (similar to Type 1a—ASTM F 519).

Type 1b—Notched round bars, loaded in bending with loaded bars (similar to Type 1c—ASTM F 519).

Type 2—Unnotched ring specimens, loaded in bending with displacement bars (similar to Type 2a—ASTM F 519).

The sensitivity to hydrogen embrittlement of the heats of steel used for the specimens is established by plating the heat-treated specimens [1793 to 1931 MPa (260 to 280 ksi) ultimate tensile strength (UTS)] under specified conditions, with and without post-plate baking and testing these specimens.

Testing is conducted on the appropriate specimens:

Type 1a specimens are loaded to 45% of the notch tensile strength and left in the test solution for a period of 150 h or until failure (whichever is shorter).

Type 1b specimens are loaded to 45% of the notch bend strength and left in the test solution for a period of 150 h or until failure (whichever is shorter).

Type 2 specimens are loaded by insertion of an oversize stressing bar into an O-ring specimen. The ring specimens are subsequently immersed in the test solution and left for 150 h or until failure (whichever is shorter).

A minimum of three specimens are tested, and if two or more fracture during the specified time, the solution is considered to have excessive embrittling characteristics.

The test method specified in ART 1525 utilizes specimens that have known (or determined) susceptibility to hydrogen embrittlement. The testing is designed to assess the aggressiveness of the environment (cleaning solutions) that aircraft hardware might be subjected to relative to hydrogen embrittlement, rather than to assess the materials for use in the hardware itself. The test results will only indicate the *relative* aggressiveness in terms of the hydrogen embrittlement-inducing nature of the solution(s) under test. This specification does not, however, give any definitive data on which to assess the propensity for hydrogen embrittlement failure of service components where alloys, heat-treat conditions, stress levels, and geometries may be radically different from the test coupons utilized.

The Industrial Fasteners Institute (IFI)

Fasteners manufactured from high-strength, low-alloy steels and other alloys are susceptible to hydrogen embrittlement failure during service under sustained loading. The source of the hydrogen may be external, as a by-product of corrosion reactions occurring at the fastener surface, or may be internal, originating during electroplating of the fasteners to increase their corrosion resistance. Hydrogen that evolved as a by-product of the electroplating process is absorbed by the steel and must be removed by baking, following the plating process, in order to eliminate the potential for subsequent hydrogen-induced failure (hydrogen embrittlement). IFI, recognizing this source of potential problems, included in their Standard IFI-113 on "Steel Self-Drilling Tapping Screws" a hydrogen embrittlement test procedure as part of the quality control requirements of these components.

The objective of this standard is "to insure that self-drilling tapping screws . . . shall drill a hole and form or cut mating threads in materials into which they are driven, without deforming their own thread and without breaking during assembly." The standard includes requirements

on material (killed steel wire containing 0.13 to 0.27% carbon and 0.64 to 1.71% manganese), case hardening heat treatment, and finish (plain or coated). One requirement is that "Electroplated screws shall be baked for a minimum of one hour within the temperature range 375–450°F [190 to 230°C] as soon as practicable after plating to avoid hydrogen embrittlement." Hydrogen embrittlement testing requirements are specified for cadmium and zinc electroplated screws. The hydrogen embrittlement tests, as detailed in Section 3.9 of IFI-113, are as follows:

Sample screws shall drill their own hole and form a thread in a steel test plate with a thickness equal to the maximum specified for the applicable screw type and size. . . . The head of the screw shall be seated against one or more ANSI B27.2 Standard Plain Washer, Type B, Narrow Series or an equivalent spacer and tightened with a torque equal to the hydrogen embrittlement torque specified. . . . The assembly shall remain in this tightened state for 24 hours. The original hydrogen embrittlement torque shall then be reapplied following which the screw shall be removed.

No requirements in terms of the relationship between the torque applied and the resultant tensile stress induced in the fasteners are directly stated, although this is implied by different torque requirements specified for cadmium-plated screws versus zinc-plated screws. Variations in coefficients of friction between the screw and the test plate during assembly will result in variations in the resultant tensile loading of the fasteners induced by torsionally applied load. Also, no relationship between the applied tensile loading of the screws and their yield strength or ultimate strength are specified. Thus, there are no requirements on loading that would allow direct comparison of results between fasteners manufactured from different materials or having different coatings.

The test method outlined in IFI-113 is intended for, and limited to, testing of plated fasteners to ensure that a large proportion of the residual hydrogen from the electroplating process has been removed, thus reducing the likelihood of hydrogen embrittlement failure. It must be recognized and appreciated that this test technique does not address the susceptibility of the fasteners to hydrogen embrittlement from "in-service" corrosion attack, say, and cannot therefore be used as a guarantee against subsequent hydrogen embrittlement failure of fasteners. Furthermore, for the reasons just stated, the test method is not designed for, nor should it be utilized for, a quantitative evaluation of hydrogen removal or hydrogen embrittlement susceptibility for fasteners manufactured from different alloys or treated to different strength levels. This method is strictly a pass/fail quality control technique to ensure that post-electroplating baking has been performed.

American Welding Society

During welding of steels, hydrogen may be picked up by the weld pool (from electrodes, fluxes, shielding gases, etc.), which may then cause subsequent failure (by hydrogen-induced cracking) of the weld or parent metal. The American Welding Society (AWS) has recently produced a standard, AWS A4.3, entitled "Standard Procedures for Determination of Diffusible Hydrogen Content of Martensitic, Bainitic and Ferritic Weld Metal Produced by Arc Welding."

The standard describes a standard weld test assembly, a standard method of specimen preparation, and two standard methods of analysis for determination of diffusible hydrogen from martensitic, bainitic, and ferritic weld metals.

The intent of the standard is that "it be used as the standard test method for classification purposes to be referenced in individual filler metal specifications. . . ." In addition, the standard is intended for use for "Quality Conformance testing of arc welding electrodes, fluxes and gases."

The test materials used are nonrimming steel of Grade ASTM A 36 [ASTM Specification for Structural Steel (A 36/A 36M-84a)] or SAE 1020. The material is first heat treated for 1 h (minimum) in air, vacuum, or gas at 400 to 650°C (750 to 1200°F) to remove any hydrogen. Four weld test assemblies are prepared and welded with no alteration of weld parameter set-

tings. Each weld test assembly is released from a copper clamping fixture and quenched into iced water within 5 s of extinguishing the arc. It is then stored in a low temperature liquid bath [-60°C (-76°F) or lower]. The specimens are then cleaned and the weld tabs broken off.

The diffusible hydrogen within the specimen is then collected and measured (or at least 90% of the total diffusible hydrogen is). Two methods of measurement may be used: (a) a mercury-filled eudiometer or (b) a gas chromatograph. The minimum hydrogen diffusion time (for either method) is 72 h at 45°C (113°F) or 6 h at 150°C (302°F). The hydrogen volume, converted to standard temperature and pressure, is then normalized to obtain the diffusable hydrogen value in mL/100 g of deposited metal. The average of the four nominally identical specimens is calculated.

The test technique provides a relative measure of hydrogen pickup during a welding process. It does not directly assess the propensity for hydrogen-induced failures of the weld or parent metal due to this pickup or the effectiveness of any post-weld treatments in reducing this propensity. The method is strictly a quality control method for classification of filler metals in terms of the induced hydrogen levels in the finished welds.

National Association of Corrosion Engineers

The National Association of Corrosion Engineers (NACE), as their name implies, are concerned primarily with corrosion of materials in its many aspects. In terms of hydrogen-induced failure of materials, the Association has produced a number of standards concerning materials requirements (MR) and test methods (TM) for sulfide stress cracking of materials used primarily in oil field equipment. This is due to the long-recognized problem of sulfide stress cracking (SSC) failures of metals exposed to hydrogen sulfide containing oil field environments. SSC failures are generally thought to result from a hydrogen embrittlement mechanism. The presence of hydrogen sulfide tends to cause hydrogen ions (produced from corrosion or cathodic charging at the metals surface) to enter the metal rather than combine into hydrogen gas molecules.

NACE has produced a Test Method, TM-01-77, for "Testing of Metals for Resistance to Sulfide Stress Cracking at Ambient Temperatures." The test procedure is summarized as follows:

Stressed specimens are immersed in acidified sodium chloride solution saturated with hydrogen sulfide at ambient pressure and temperature. Applied stresses at convenient increments of the yield strength can be used to obtain sulfide stress cracking data. Time-to-failure at a fixed stress is an important parameter for experimental correlation purposes. A 30-day test period is considered sufficient to reveal failure in materials susceptible to sulfide stress cracking. In borderline cases, longer test periods may be desirable.

The tension specimen dimensions are specified, and tension testing is performed to determine base metal properties (yield strength, ultimate strength, percent elongation, reduction of area). Tension testing is subsequently performed with constant load or sustained load devices at varying load levels and the time(s) to failure noted. The results are reported in tabular and/or graphical plots of applied stress versus time to failure.

As of May 1985, the testing document is undergoing extensive revision to include the use of C-ring specimens and double-cantilever beam (DCB) fracture mechanics specimens.

The objective of the test method is to facilitate conformity in testing so that data accumulated from different sources may be compared on an equal basis. Evaluation of the data in terms of the suitability of a given alloy in a given in-service environment, stress level, and geometry is not specified and remains a matter for the individual user or other specific groups and situations.

Summary

This discussion has outlined the status of hydrogen control testing as specified by a number of professional societies today. As can be seen from this brief survey, the testing of materials for hydrogen-induced degradation involves a wide variety of considerations and test methods. Further discussion of the application of some of these test methods and some of the problems encountered can be found in other papers in this book.

Testing of specimens utilizing the standardized test methods must be done with a basic understanding of the applicability of the test results to "in-service" situations and limitations of the test method chosen. It is encouraging to note that many of the specifications are under constant review and update; however, examination of the various specifications highlights a need for increased agreement on standardizations between the various societies. Hopefully, symposia and other meetings will encourage closer agreement and ultimately aid practicing engineers in their interpretation and use of test data to eliminate hydrogen-induced failures in the field.

Accelerated Acceptance Testing for Hydrogen Embrittlement Control

REFERENCE: Dreher, R. V., "Accelerated Acceptance Testing for Hydrogen Embrittlement Control," *Hydrogen Embrittlement: Prevention and Control*. ASTM STP 962, L. Raymond, Ed., American Society for Testing and Materials, Philadelphia, 1988, pp. 60-67.

ABSTRACT: A recent military hardware development program at Kaiser Electroprecision required the use of 220 ksi, 4330 V steel for a light weight, high reliability aircraft hydraulic component. The need for stringent control and prevention of hydrogen embrittlement was identified as a major program responsibility since both chrome and electroless nickel plating were employed in these components. An effort to use existing military procedures to set up a hydrogen embrittlement (HEM) test program to pull plated tension specimens was met with much frustration. It was found that a time-consuming 200-h pull test was specified in most cases for HEM tension specimens. The procedures were also found to contain a torturous and somewhat ambiguous path of logic upon which the requirements and methods regarding pull specimens were delineated.

The problem was handled in part by instituting an accelerated acceptance method for testing HEM specimens. This method involved pulling a single HEM tension bar, representing each lot of plated parts, in a seven-step load test to fracture over an 8-h period. The loads were based on a percentage of the predetermined fracture load, and each load state was held for 1 h. This technique enabled a relatively quick verification of the absence of embrittlement in the parts. It also provided the assurance that parts could be moved to subsequent processing without waiting the two- to five-week period often associated with the "standard" 200-h tests.

KEY WORDS: hydrogen embrittlement test, 8-hour test, stepped loading test

A military hardware development program conducted in 1984 at Kaiser Electroprecision required the use of a high-strength, high-fracture toughness steel for an aircraft hydraulic system component. Type 4330 V steel, heat treated to an ultimate strength of 1517 MPa (220 ksi), was selected. The component required both corrosion protection and an internal wear surface for piston seals. Electroless nickel per MIL-C-20674 was selected for internal corrosion protection, and thin-dense chrome was chosen as a wear material and was plated on top of the electroless nickel. The selection of these materials and plating processes and the requirement for high reliability dictated the need for stringent control and prevention of hydrogen embrittlement. A 23-h, minimum, bake cycle at 196°C (375°F) was performed immediately after each plating process.

Review of Applicable Specifications

A review of applicable military and testing society standards was made to establish a clear and cost-effective approach towards meeting the responsibility of the control of hydrogen embrittlement. Included in this review were the following plating and test specifications:

¹Manager—Project Engineering, Kaiser Electroprecision, Irvine, CA 92691.

1. MIL-C-26074B Coatings, Electroless Nickel.
2. MIL-C-23422 Chromium Plating, Electrodeposited.
3. QQ-C-320 Chromium Plating, Electrodeposited.
4. ASTM F 519 Method for Mechanical Hydrogen Embrittlement Testing of Plating Processes and Aircraft Maintenance Chemicals (F 519-77).
5. RYY 03-006 (Kaiser) Electrolyzing Process Specification.

The review of these specifications revealed that there were numerous and often conflicting test/control methods for hydrogen embrittlement assessment. In addition, as shown in Exhibit A and Exhibit B, some of the requirements were duplicated (almost, but not quite, verbatim) between some of the specifications, but the text arrangement made this fact almost indistinguishable until after several readings of each specification were made and careful comparisons were done. Even at that, the criteria for requiring any embrittlement testing at all was not uniform among the documents. In addition, the criteria for the load to be applied to the specimen varied from either 75% of the base material yield strength to 75% of the ultimate notched tensile strength. This comparison of specifications and their salient features is summarized in Table 1.

The 200-h Problem

One item that was common to all the specifications was the requirement to pull bars for at least 200 h. This requirement was seen to be very troublesome since it was apparent that the time that lapsed between completion of the plating process and the "proof" that the parts were free of hydrogen embrittlement could be very long. Discussions with various people in the aircraft industry who did plating and testing on-site and other independent testing laboratories revealed that, in practice, it could take several weeks to get test results. This is in spite of the fact that the "200-h" test itself, if run continuously for 200 h, should theoretically take only about nine to ten calendar days.

In practice, there are delays between the completion of a plating process, the transfer of the test bars to the test lab, and often the availability of the proper test machines. These delays can amount to several working days, and, coupled with the time it takes to do the actual test and report the results, the total time can amount to two to four weeks or even longer.

In the meantime, further processing of the components must be carried on at risk. It has been reported that some major aircraft components had completed fabrication and were ready for installation when it was finally reported that the test bars failed the embrittlement tests and the components had to be withdrawn from assembly.

In such cases the costs are high and the consequences are bleak. If embrittlement is detected after plating, the usual and most simple recourse is to rebake the components in an attempt to drive out entrapped hydrogen. This remedy can only be effective if very little time (the subject of much industry debate) has passed since the plating process was completed and if no degradation has occurred. Expensive parts may have to be sacrificed to internal metallographic inspection to verify the absence of irreparable embrittlement damage. And, finally, parts worth thousands of dollars may have to be scrapped and serious schedule delays may be incurred. In a fast-paced hardware intensive program, these results can be disastrous!

A Solution

Consultation with the company's metallurgist resulted in a unique solution to this problem [1]. An 8-h, stepped loading test using standard ASTM E 8 [ASTM Methods of Tension Testing of Metallic Materials (E 8-85)] round notched tension bars according to ASTM F 519 was recommended. The stepped loading test was based on the tests performed by Traiono [2], which are shown in Fig. 1.

EXHIBIT A

EXTRACT FROM MIL-C-26074B 1971

COATINGS, ELECTROLESS NICKEL, REQUIREMENTS FOR

(Extract, para. 4.5.4, Embrittlement Relief)

- b. Sample parts such as pressure containers, fasteners, springs, etc., selected in accordance with 4.4.3, which in use are subjected to a sustained static tensile load in excess of 25 percent of the basis material specification minimum tensile yield strength shall be subjected to a sustained tensile load equal to 75 percent of the basis material specification minimum tensile yield strength. Parts which require special fixtures or extreme loads to comply with the above requirements need not be tested. Parts which are specified, unless in use they are subjected to a sustained static tensile load in excess of 50 percent of the basis material specification minimum tensile yield strength. Parts which require fixtures or extreme loads to comply with the above requirements and in use are subjected to a sustained static tensile load between 25 percent and 50 percent of the basis material specification minimum tensile yield strength may be represented by separate specimens. Four specimens shall be prepared to represent each lot. The configuration shall be in accordance with Figure 8 of ASTM E 8 for rounded specimens. Specimens shall have a 60-degree U-notch located approximately at the center of the gage length. The cross section area at the root of the vee shall be approximately equal to half the area of the full cross section area of the specimen's reduced section. The vee shall have a 0.010 ± 0.0005 inch radius of curvature at the basis of the notch. The axis of the round notched specimen (load direction) shall be perpendicular to the short transverse grain load direction. These specimens shall be of the same chemical composition (alloy) as the parts represented, shall have been heat treated to the parts which they represent through the entire coating process, including all precoat and postcoat procedures. Specimens representing surface hardened parts shall be subjected to a sustained static tensile load not less than 20 percent of the load at which an uncoated specimen will break. The parts or samples shall be held under the specified load (see 6.2) at $70^{\circ} \pm 2^{\circ}\text{F}$ ($2^{\circ} \pm 1^{\circ}\text{C}$) for at least 200 hours, unless otherwise specified, and then examined for cracks.

The parts or samples shall be held under the specified load (see 6.1) at $70^{\circ} \pm 2^{\circ}\text{F}$ ($2^{\circ} \pm 1^{\circ}\text{C}$) for at least 200 hours, unless otherwise specified, and then examined for cracks.

EXHIBIT B

EXTRACT FROM MIL-C-23422 1978

CHROMIUM PLATING, ELECTRODEPOSITED

(Extract, para. 4.4.5, Embrittlement Relief)

- 4.4.5.1.2 Pressure containers, fasteners, springs, etc. Sample parts such as pressure containers, fasteners, springs, etc., selected in accordance with 4.3.3, which in use are subjected to a sustained static tensile load in excess of 25 percent of the base material specification minimum yield strength and all threaded fasteners shall be subjected to a sustained tensile load equal to 75 percent of the base material specification minimum yield strength. The minimum cross sectional area shall be used for calculating tensile load to be applied to the parts being plated.
- (a) Parts which require special fixtures or extreme loads to comply with the above requirements need not be tested as specified, unless, in use they are subjected to a sustained static tensile load in excess of 50 percent of the base material specification minimum yield strength.
- (1) Parts which require fixtures or extreme loads to comply with the above requirements, and in use are subjected to a sustained static tensile load between 25 percent and 50 percent of the base material specification minimum yield strength, may be represented by separate specimens.
- (2) Four specimens shall be prepared to represent each lot.
- (3) The configuration shall be in accordance with Figure 8 of ASTM E 8 with a 0.020 inch deep notch in the center of the gage length with a radius of 0.020 +/- 0.0005 inch and angle of 60 degrees. These specimens shall be a base metal of the same composition, shall have been heat treated to the same hardness requirement, shall have been plated at the same time as the parts they represent, and shall be furnished to the plating contractor by the component fabricator.
- (b) Specimens representing surface hardened parts shall be subjected to a sustained static tensile load not less than 20 percent of the load at which an unplated specimen will break.
- (c) The parts or samples shall be held under the load at room temperature for at least 200 hours, unless otherwise specified, and then examined for cracks.

TABLE 1—Summary of selected specifications for embrittlement control and testing of plating solutions.

Specification	Number of Bars	Bar Material/ Processing	Bar Configuration	End Item Criteria for Use of HEM Testing	Test Duration, h	Test Load
MIL-C-26074 Electroless Nickel Coatings	4	Same as end item	ASTM E 8 (Notched) ^{a,b}	HRC 40 or above	200	75% of base material yield
MIL-C-23422 Electrodeposited Chrome Plating	4	Same as end item	ASTM E 8 (Notched) ^{a,b}	Loaded to 25% of base material yield	200	75% of base material yield
QQ-C-320 Electrodeposited Chrome Plating	5	Equivalent basis material	ASTM E 8 (Notched) ^a	240 ksi ^c ultimate tensile	200	75% of ultimate notch tensile
ASTM F 519	4	AISI Air Melt 4340 at 260 to 280 ksi	Notched Bars, Rings, Bending Bars	User/customer discretion	200	75% of notched ultimate tensile
Kaiser RYY 3-006	N/S	AISI 4340 at 260 to 280 ksi	N/S	220 ksi ultimate tensile	200	75% of ultimate notched tensile

NOTE: N/S = Not specified.

^aNotch details in main specification.

^bRefer to Exhibit A and Exhibit B.

^c1 ksi = 6.895 MPa.

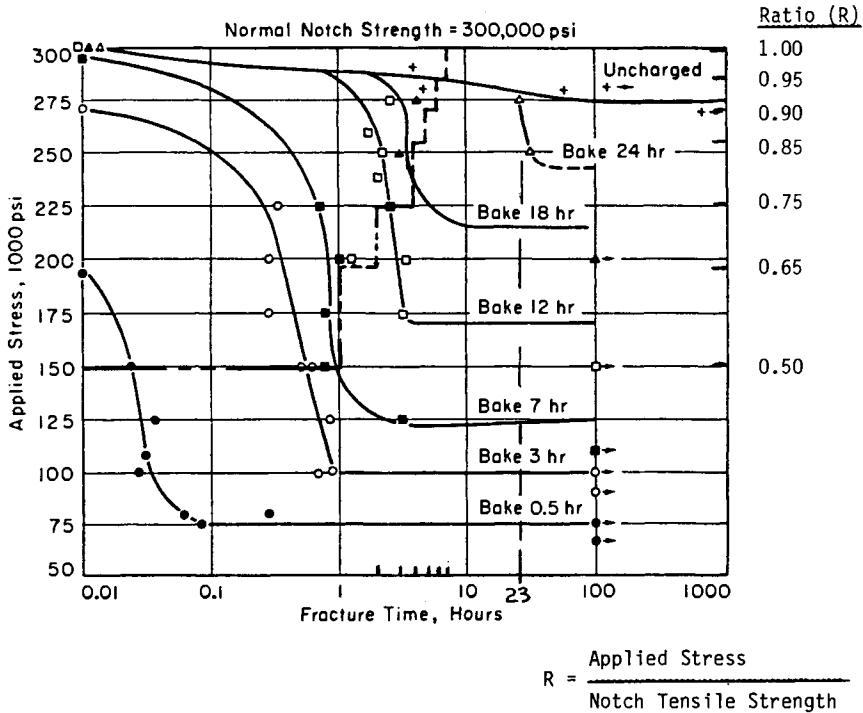


FIG. 1—Sustained load failure curves for various hydrogen concentrations obtained by baking different times at 149°C (300°F). Sharp-notch specimens, 230 000 psi strength level, after Traiono [2]. (Contributed by L. Raymond & Associates, Mettek Laboratories.)

The test plan was devised to maximize the confidence level of the test results while attempting to perform the test from practical considerations in an 8-h shift or normal work day. Figure 1 shows that an 8-h sustained load test at 0.95 notched tensile strength (NTS) would produce the desired results, but would produce a condition where the test results would not discriminate the cause of fracture between an overload due to dimensional and loading variations or failure due to hydrogen embrittlement (HEM). Therefore, a step load test was chosen to discriminate between the two failure mechanisms and also to establish a relative degree of HEM.

The step loads were at essentially 50, 65, 75, 85, 90, and 95% increments prior to loading to ultimate or fracture as shown in Fig. 1. The interpretation of test results was that if failure occurred at the low end, a serious problem existed; if failure occurred at the high end, some residual hydrogen existed; if no failure occurred during the entire 8-h test, then no residual hydrogen was present. If failures occurred near 0.95 NTS, a scanning electron microscope (SEM) examination could be used as a referee inspection for incipient HEM.

It was anticipated that the acceptance level compatible with the standard 200-h 0.75 NTS sustained load test would be established, but, as shown by the test results, neither the standard nor the 8-h tests exhibited failure. To the extent that both tests established that detrimental levels of hydrogen were not present, they were consistent; but an equivalent acceptable level on the 8-h step load test was not established in this program and should be the direction of future efforts.

Test Program

The stepped loading tests adopted by Kaiser are outlined in Table 2. A baseline fracture load (the ultimate notched tensile strength) was established by pulling three unplated sample bars from a lot of 200 tension specimens. All test bars were run through each plating process with the actual parts and were identified by individual serial number with the applicable lot of parts. These test bars were fabricated from 4330 V and were heat treated to 1517 MPa (220 ksi)² ultimate strength. The 8-h tests were run in parallel with standard 200-h tests on separate bars which were pulled at 75% of the base material yield strength. The loads in the stepped load test were selected to represent the more critical stress states which would reveal embrittlement, if it existed. Seven load steps were selected, with the first six load steps required to be held for 1 h each. The seventh and final load step was a pull to fracture. The criteria for acceptability was that fracture had to occur within 2% of the baseline fracture load.

By selecting these load steps, the test lab could complete the embrittlement test in one day. The purchase order to the plater and the test lab required that the 8-h test be commenced within 48 h, maximum, after plating, pending availability of the proper stress-rupture machine. Any failure outside of the prescribed limits was to be reported immediately to the project office.

A summary of the test results for the development program is given in Table 3. Several test bars were run with each plated lot of components. Bars were selected from each lot³ and some were submitted for the 8-h test, while others, taken from the same lot, were selected for the 200-h test. No embrittlement was evidenced by any of the tests. Some of the bars that were taken to fracture were examined by SEM, and the absence of any embrittlement was confirmed.

It can be seen from the summary of elapsed time from completion of plating to the completion of testing that the "8-h" test results were available considerably sooner than the "200-h" test results. Most importantly, this approach permits release of components for further processing or use without the threat of subsequent need for recall.

Recommendations

Kaiser's experience with hydrogen embrittlement testing and controls, outlined only in part in this presentation, indicates that both the military and industry would benefit from consideration of the following recommendations:

TABLE 2—Load steps—incremental loading HEM notched bars.

% of Baseline Fracture Load	TESTING	
	Test Duration, h	
50	1	
65	1	
75	1	
85	1	
90	1	
95	1	
Pull to fracture	. . .	

NOTE: *Acceptance Criteria:* No fracture at any load less than 2% of baseline fracture load.

²Original measurements were made in English units (1 ksi = 6.895 MPa).

³A lot consisted of eight to ten parts.

TABLE 3—Summary of HEM tension testing.

Bar Identification	Bar Type	Bar Diameter, in	Test Load, lb	Fracture Load, lb	Elapsed Time—Plating Completion to HEM Test Completion, Days
BASELINE (UNPLATED)					
Baseline	E 8-Smooth	0.250	N/A	11450	N/A
Baseline	E 8-Smooth	0.250	N/A	11450	N/A
Baseline	E 8-Notched	0.250 ^{a,b}	N/A	15900	N/A
200-H SUSTAINED LOAD (75% OF BASE MATERIAL YIELD)					
C	E 8-Notched	0.250 ^a	7043 ^c	No fracture	18
D	E 8-Notched	0.250	7043	No fracture	18
G1	E 8-Notched	0.250	7043	No fracture	47
H2	E 8-Notched	0.250	7043	No fracture	47
I2	E 8-Notched	0.250	7043	No fracture	22
8-H INCREMENTAL LOAD					
A	E 8-Notched	0.250 ^a	Incremental	15520	1
B	E 8-Notched	0.250	Incremental	15630	1
H1	E 8-Notched	0.250	Incremental	15800	6
I3	E 8-Notched	0.250	Incremental	16050	22

NOTE: N/A = not applicable.

^aDiameter at base of notch.

^b1 in. = 2.54 cm.

^c1 lbf = 4.448 N.

1. Both military and testing society documents should adapt a more uniform and consolidated approach to requirements which govern hydrogen embrittlement testing.

2. Government and industry should promote test programs and/or studies which explore alternatives to the time consuming and cumbersome "200-h tension test," such as the 8-h "quick test."

3. An acceptance level for the 8-h step load test equivalent to the 200-h (0.75 NTS) sustained load test should be established.

References

- [1] Raymond, L., Principal Consultant with L. Raymond and Associates, Inc. (Mettek Labs).
- [2] Troiano, A. R., "Delayed Failure of High Strength Steels," *Corrosion*, April 1959.

Assessment of the Degree of Hydrogen Embrittlement Produced in High-Strength 4340 Steel by Plating-and-Baking Processes Using Slow Strain Rate Testing

REFERENCE: Pollock, W. J., "Assessment of the Degree of Hydrogen Embrittlement Produced in High-Strength 4340 Steel by Plating-and-Baking Processes Using Slow Strain Rate Testing," *Hydrogen Embrittlement: Prevention and Control*, ASTM STP 962, L. Raymond, Ed., American Society for Testing and Materials, Philadelphia, 1988, pp. 68-80.

ABSTRACT: The degree of hydrogen embrittlement produced in high-strength 4340 steel by various cadmium, cadmium-titanium, and nickel plating-and-baking procedures is assessed from fracture stress values obtained during slow strain rate tests using notched tension specimens. At low crosshead displacement rates, the slow strain rate method is capable of quantifying the degree of embrittlement produced by a variety of low-embrittlement, plating-and-baking procedures and is more sensitive than conventional test methods defined in standard specifications. The advantages of using a slow strain rate method as a viable alternative to existing standard methods for assessment of the degree of hydrogen embrittlement in plated-and-baked, high-strength steel are discussed.

KEY WORDS: low-alloy steel, high-strength steel, hydrogen embrittlement, strain rate, plating, cadmium coatings, nickel coatings

In another paper in this publication [1], a slow strain rate test method was used to quantify the degree of hydrogen embrittlement produced in plated high-strength 4340 steel notched tension specimens during exposure to paint strippers. The severity of the test method was inversely proportional to the rate of loading, and at low crosshead displacement rates, small amounts of embrittlement could be readily quantified. Furthermore, the results of multiple slow strain rate tests conducted at a crosshead displacement rate of 2×10^{-4} mm/s revealed that a minimum mean fracture stress could be correlated with the pass/fail criterion for acceptability of paint strippers using standard notched C-ring tests [2].

The ready applicability of the slow strain rate method to assess the degree of hydrogen embrittlement produced by paint strippers in high-strength 4340 steel suggests that a similar approach might be successful in the assessment of plating-and-baking procedures. Slow strain rate methods are used in the present work to determine the degree of embrittlement produced in high-strength 4340 steel by various cadmium (Cd), cadmium-titanium (Cd-Ti), and electroless nickel (Ni) plating-and-baking procedures. The possibility of using the results of slow strain rate tests as criteria for acceptance or rejection of a given plating process is discussed.

¹Principal research scientist, Aeronautical Research Laboratory, Defence Science and Technology Organisation, Department of Defence, Melbourne, Australia.

Experimental Procedures

The 9.5-mm round aircraft quality 4340 steel bar used in the present work complied with the MIL-S-5000E specification [3] and had a composition (weight %) of 0.43 carbon, 0.85 chromium, 0.84 manganese, 0.25 molybdenum, 1.78 nickel, 0.29 silicon, 0.009 sulfur, <0.01 phosphorus, <0.05 aluminum, with the remainder iron. Notched tension specimens were identical to those used in a previous work [1] and complied with the reduced load requirements for the Type 1a tension specimen detailed in ASTM Method for Mechanical Hydrogen Embrittlement Testing of Plating Processes and Aircraft Maintenance Chemicals (F 519-77) [2]. The outer shank diameter of the 100-mm-long specimen was 7.30 mm with a reduction in diameter to 4.50 mm in the vicinity of the notch. The diameter across the notch and notch radius were 3.20 and 0.15 mm, respectively, to give a notch stress concentration factor of 3.1. The notch was prepared by low-stress grinding after heat treatment, which involved austenitizing at 815°C/1 h in salt, oil quenching to 40 to 60°C, followed by double tempering at 260°C/1 h with air cooling to 20°C between tempers.

Notched tension specimens were given the following plating, baking, and passivation treatments:

1. *Porous Cd plating*: specimens were plated to a thickness of 10 to 15 μm in low embrittlement Cd plating baths in accordance with Qantas Processing Specification P65 [4] and Hawker de Havilland Process Specification HPS 1.03.00 [5]. Both these specifications include baking at 190°C/23 h within 4 h of the plating treatment followed by chromate passivation. Details of bath composition and plating current density are given in Table 1. The HPS 1.03.00 specification meets the hydrogen embrittlement requirements outlined in the U.S. specifications MIL-STD-1870A [6] and DPS 9.28 [7], whereas the Qantas P65 specification meets the intent of the specifications BAC 5718 [8], DPS 9.28, QQ-P-416 [9], and AMS2401C [10].

2. *Nonporous Cd plating*: specimens were vat plated to a thickness of 10 to 15 μm in accordance with the U.K. Ministry of Aviation Specification DTD904C [11] in a Cd plating bath containing brighteners (Table 1). Plated specimens were subsequently baked at 190°C for various times.

3. *Brush Cd plating*: specimens were degreased, anodically etched, and plated to a thickness of 10 to 15 μm using Selectron LHE (SPS-5070) Cd plating solution. The specimens were not baked after plating, and several were subsequently given a chromate passivation treatment.

4. *Cd-Ti plating*: specimens were plated to a thickness of 12 to 15 μm in accordance with the BAC 5804 specification [12]. All specimens were baked at 190°C/12 h after plating and a number of these were subsequently chromate passivated.

5. *Electroless Ni plating*: specimens were plated to a thickness of 30 to 40 μm in accordance with the U.S. Military Specification MIL-C-26074B [13]. In these tests, specimens were shot peened, given a vapor degrease, an anodic alkaline clean, and a Ni chloride strike before plating

TABLE 1—Details of Cd plating baths.

	QANTAS P65 [4]	HPS 1.03.00 [5]	DTD 904C [11]
Cd, g/L	49 to 56	21 to 24	14 to 17
NaCN, g/L	67.5 to 112	90 to 120	56 to 63
NaOH, g/L	26 to 37.5	11 to 24	11 to 14
Na ₂ CO ₃ , g/L	60	0 to 37	...
Temperature, °C	20 to 30	21 to 27	15 to 35
Current Density, mA/cm ²	50 to 80	60 to 70	7 to 10
Added brighteners	Nil	Nil	Yes
Embrittling tendency	Low	Low	High

for 2 h at 90°C in an acidic (pH 4 to 5) plating bath. The effects of chemically stripping the Ni plate, replating with Ni, and baking at 190 and 340°C were investigated.

Bare steel specimens were cathodically charged in 4% sulphuric acid plus 50 mg/L sodium arsenite at 8 mA/cm² for various periods of time. This treatment is known to induce severe embrittlement in high-strength steels [14] and provides a basis for assessing the degree of embrittlement produced by the various plating-and-baking procedures.

All specimens were loaded to failure in air in a 20-kN motor-driven tension testing machine which had a variety of gears enabling tests to be conducted over a range of crosshead displacement rates varying from 10⁻² to 10⁻⁶ mm/s. Fracture stress was calculated from the failure load and used to estimate the degree of embrittlement in specimens by comparison with the unembrittled fracture stress obtained by testing bare steel specimens in laboratory air at the same crosshead displacement rate. All tests with Cd and Cd-Ti plated specimens were conducted in duplicate and mean fracture stress values calculated. In all other tests, fracture stress values of individual tests are displayed and no attempt is made to quantify the scatter in the results. This aspect of the problem has been discussed in another paper in this publication [1].

Fracture surfaces of all broken specimens and the structure of the various Cd coatings were studied by optical and scanning electron microscopy.

Results

The fracture stress of unembrittled notched bare steel specimens tested in air was independent of crosshead displacement rate over the range 2×10^{-3} to 2×10^{-6} mm/s. Tests with 21 specimens taken from several specimen batches, heat treated at different times, produced a mean fracture stress value of 2456 MN/m² with a standard deviation of 52 MN/m². The fracture mode of bare steel specimens was transgranular microvoid coalescence.

Severely embrittled 4340 steel specimens failed at low fracture stresses when tested at a crosshead displacement rate of 2×10^{-4} mm/s (Fig. 1). Cathodic charging in 4% sulphuric acid

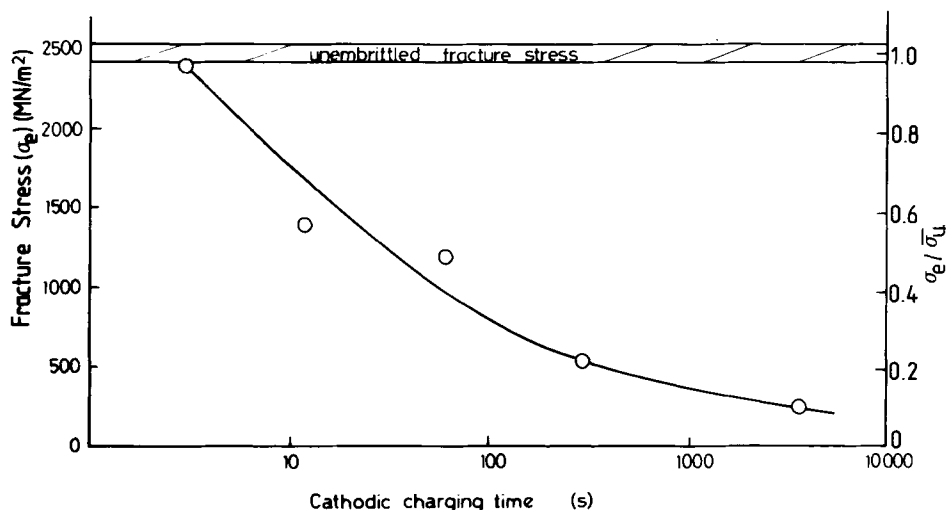


FIG. 1—Fracture stress (σ_c) and fracture stress ratio (σ_c/σ_u) of bare 4340 steel notched tension specimens tested in air at a crosshead displacement rate of 2×10^{-4} mm/s after cathodic charging in 4% sulphuric acid plus 50 mg/L sodium arsenite at 8 mA/cm² for various periods of time, where σ_u is the mean unembrittled fracture stress.

plus 50 mg/L sodium arsenite for just 1 h resulted in a reduction in fracture stress by a factor of 10 from 2456 to 220 MN/m². Sufficient hydrogen was absorbed during the first 20 s to reduce the fracture stress by 50%. All embrittled specimens showed evidence of intergranular cracking with the proportion increasing in specimens that failed at lower fracture stresses.

Slow strain rate testing of Cd plated-and-baked tension specimens in air produced a wide range of mean fracture stresses (Fig. 2). Lowest fracture stresses were obtained with specimens given the bright Cd plating treatment followed by baking at 190°C/23 h. The degree of embrittlement was only partially reduced by baking at 190°C/100 h. It was necessary to conduct tests at a crosshead displacement rate of 2×10^{-6} mm/s to compare the degree of embrittlement produced by porous Cd and Cd-Ti plating after baking at 190°C. Cd-Ti plating-and-baking produced the least amount of embrittlement in 4340 steel, and mean fracture stresses of passivated and unpassivated specimens were similar. In contrast, mean fracture stresses of passivated porous Cd plated-and-baked specimens were lower than in unpassivated specimens.

All brush Cd-plated specimens tested in air at a crosshead displacement rate of 2×10^{-4} mm/s showed no reduction in fracture stress when compared with the results of unembrittled bare steel specimens (Fig. 3). Considerable scatter in fracture stress values were obtained with both unpassivated and chromate passivated specimens when tested at lower crosshead displacement rates.

Application of the electroless Ni-plating treatment (without subsequent baking) to a notched tension specimen resulted in a fracture stress of 1490 MN/m² when tested at a crosshead displacement rate of 2×10^{-4} mm/s (Fig. 4). Low fracture stresses were obtained after Ni plating, stripping, and replating. Further tests with specimens subsequently baked at 190°C/3 h after the double plating treatment resulted in fracture at 2300 MN/m². Identification of a small area

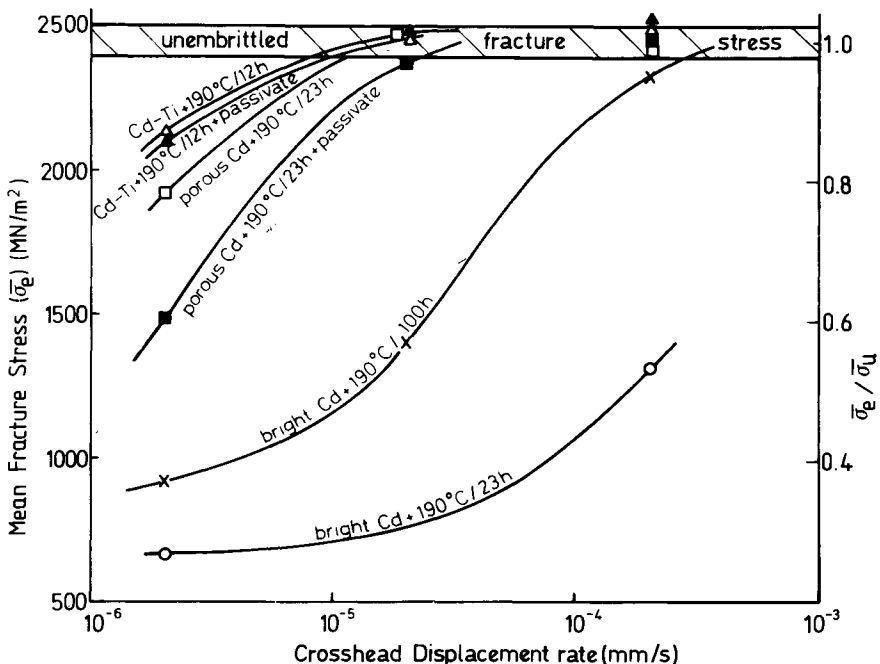


FIG. 2.—Mean fracture stress ($\bar{\sigma}_e$) and mean fracture stress ratio ($\bar{\sigma}_e/\bar{\sigma}_u$) of Cd and Cd-Ti plated-and-baked 4340 steel notched tension specimens tested in air at various crosshead displacement rates.

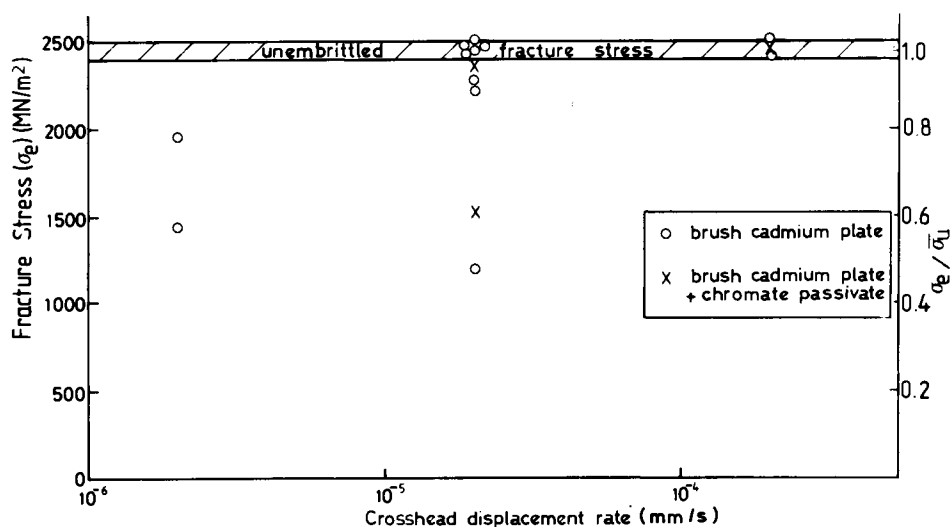


FIG. 3—Fracture stress (σ_f) and fracture stress ratio ($\sigma_f/\bar{\sigma}_u$) of brush Cd plated 4340 steel notched tension specimens tested in air at various crosshead displacement rates.

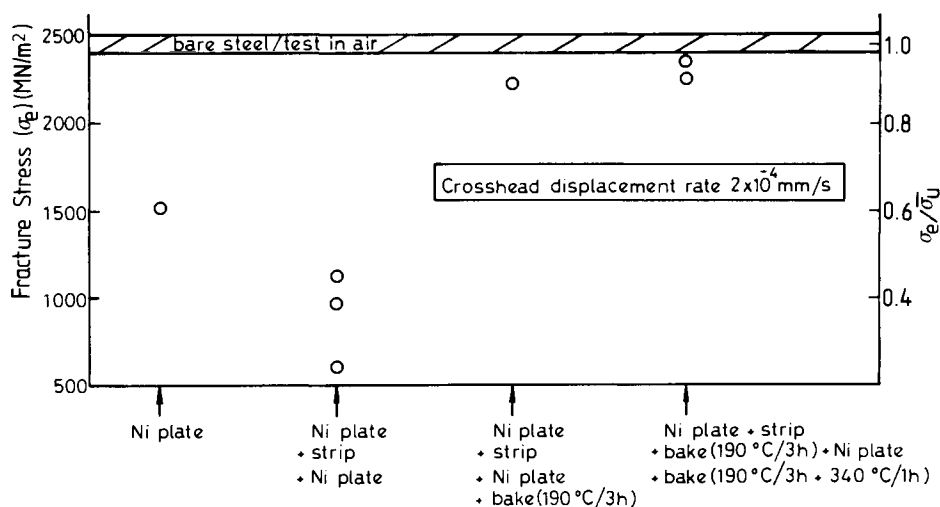


FIG. 4—Fracture stress (σ_f) and fracture stress ratio ($\sigma_f/\bar{\sigma}_u$) of electroless Ni plated 4340 steel notched tension specimens tested in air at a crosshead displacement rate of 2×10^{-4} mm/s.

of intergranular fracture confirmed that sufficient hydrogen was present to initiate premature failure (Fig. 5). A specimen given the previous plating-and-baking treatment followed by further baking at 340°C/1 h failed at 2330 MN/m². Since no intergranular fracture could be found, it is claimed that the degree of hydrogen embrittlement was minimal and that the steel had been softened by tempering.

Examination of all plated specimens revealed that the degree of coating porosity increased in the order: electroless Ni < bright Cd < brush Cd < porous Cd < Cd-Ti (Fig. 6). Coatings

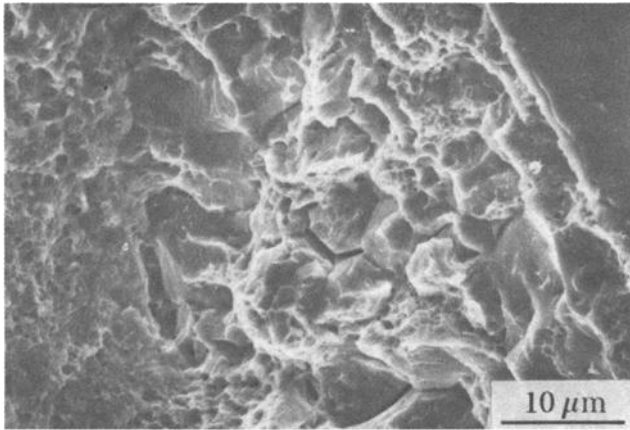


FIG. 5—Intergranular fracture initiation site of 4340 steel notched tension specimen that had been Ni plated, stripped, replated, baked in air at 190°C/3 h and tested in air at a crosshead displacement rate of 2×10^{-4} mm/s.

displaying the greatest porosity were associated with plating-and-baking treatments that produced the least amount of embrittlement in 4340 steel. This trend was also apparent with brush Cd-plated specimens in tests conducted at a crosshead displacement rate of 2×10^{-5} mm/s (Figs. 6d and 6e).

Discussion

Before comparison of the embrittling tendencies of the various plating procedures can be made, it is crucial to establish that the 4340 bare steel specimens are free from any measurable amount of hydrogen embrittlement. The constant fracture stresses obtained by testing a large number of bare steel specimens in air over the range of crosshead displacement rates from 2×10^{-3} to 2×10^{-6} mm/s confirm that any residual embrittlement of the 4340 steel is not detectable.

Assessment of the various plating/baking treatments is made by comparison of fracture stresses in tests conducted at the same crosshead displacement rate. Experiments conducted at a crosshead displacement rate of 2×10^{-6} mm/s constitute a very severe test, and traces of embrittlement are detectable. Tests conducted at a crosshead displacement rate of 2×10^{-5} mm/s are less severe, whereas treatments producing a large reduction in fracture stress from the unembrittled value of 2456 MN/m² in tests conducted at a crosshead displacement rate of 2×10^{-4} mm/s indicate a significant degree of embrittlement (Fig. 1).

The various plating/baking treatments can now be graded in order of increasing tendency to cause hydrogen embrittlement of the steel (Table 2). Although the Cd-Ti plating-and-baking procedure produced the least amount of embrittlement, it is known that this bath is difficult to control, and significant embrittlement of steel has been reported after plating in contaminated baths and when the plating current density is varied from recommended values [15,16]. The high porosity of the Cd-Ti coating allows hydrogen to escape rapidly from the steel during baking, thereby explaining the lower degree of embrittlement of plated specimens after baking for only 12 h compared with 23 h for Cd plated-and-baked specimens.

Cd-plated components are frequently given a chromate conversion coating to provide additional corrosion protection from the effects of deleterious aqueous environments. The coating is applied by immersion of plated specimens in a pH 1 to 2 chromate solution for a period of 30 to

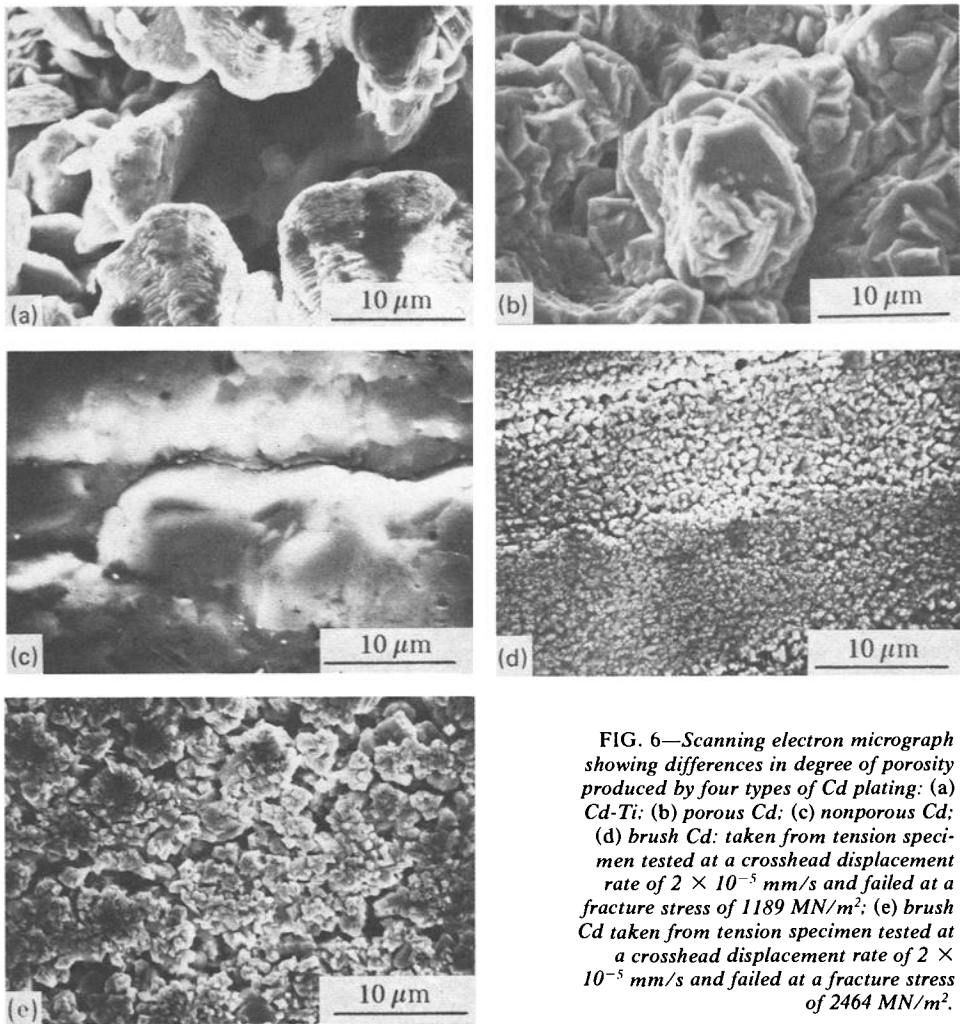


FIG. 6—Scanning electron micrograph showing differences in degree of porosity produced by four types of Cd plating: (a) Cd-Ti; (b) porous Cd; (c) nonporous Cd; (d) brush Cd: taken from tension specimen tested at a crosshead displacement rate of 2×10^{-5} mm/s and failed at a fracture stress of 1189 MN/m²; (e) brush Cd taken from tension specimen tested at a crosshead displacement rate of 2×10^{-5} mm/s and failed at a fracture stress of 2464 MN/m².

TABLE 2—Tendency for plating/baking treatments to cause hydrogen embrittlement of high-strength 4340 steel.

increasing tendency to cause hydrogen embrittlement ↓	Type of Coating	Passivation	Baking Temperature, °C	Baking Time, h
	Cd-Ti	No	190	12
	Cd-Ti	Yes	190	12
	Porous Cd	No	190	23
	Porous Cd	Yes	190	23
	Brush Cd	Yes	Nil	Nil
	Bright Cd	No	190	100
	Electroless Ni	No	190	3
	Electroless Ni	No	Nil	Nil
	Bright Cd	No	190	23

60 s followed by washing and drying. It is important to establish whether the high acidity of the plating bath can cause significant embrittlement in the steel. The present results confirm a slight increase in the degree of embrittlement in passivated porous Cd plated-and-baked specimens, but, surprisingly, this effect is absent in passivated Cd-Ti plated-and-baked specimens (Fig. 2), possibly due to the presence of titanium in the plate acting as a getter for small amounts of hydrogen generated during exposure to the passivating solution [17].

The addition of brightening agents to Cd plating baths results in lower porosity coatings that prevent the escape of hydrogen from the steel substrate during subsequent baking [18, 19]. This interpretation is supported by the results of slow strain rate tests with nonporous Cd-plated specimens where prolonged baking (100 h) at 190°C does not reduce the degree of embrittlement to levels comparable with porous Cd-plated specimens baked at 190°C/23 h and is in agreement with similar work undertaken using constant load and Barnacle electrode tests [19].

Repair of Cd plated-and-baked steel components suffering minor damage is often carried out by brush plating. Special plating solutions have been developed to minimize the degree of hydrogen absorption during brush plating to such an extent that subsequent baking is not required [20–22]. The current tests were designed to quantify the degree of embrittlement in high-strength 4340 steel caused by brush Cd plating so that comparisons could be made with the degree of embrittlement produced by standard plating-and-baking procedures for porous and nonporous Cd. Despite the considerable scatter in fracture stress values obtained in tests conducted at a crosshead displacement rate of 2×10^{-5} mm/s, the degree of embrittlement produced by brush Cd plating lies between the values obtained for specimens given the nonporous and porous plating-and-baking treatments (Figs. 2 and 3). Scanning electron microscopy of various brush Cd deposits reveals an inverse relationship between the grain size of the Cd deposit and the degree of embrittlement in the plated specimen (Figs. 6d and 6e), and hence this criterion could be used to check that excessive embrittlement of the steel has not occurred. Similar trends have been observed with the Lawrence hydrogen detection gage during bulk Cd plating in which more hydrogen is generated during bright nonporous Cd plating than in low-embrittlement porous plating [18]. Although the reasons for the variability in brush cadmium plate porosity are not apparent at present, further work should be devoted to assessment of cleaning procedures since certain contaminants are known to reduce the grain size of Cd deposits [18].

The present results establish that the slow strain rate method can provide a quantitative measure of the degree of embrittlement in high-strength 4340 steel. It is believed that the slow strain rate method can also be used to define an acceptable level of embrittlement for qualification of plating-and-baking treatments. This question was recently addressed [1] in work which equated a minimum mean fracture stress in multiple slow strain tests with the pass/fail criterion for acceptance of paint strippers as defined in standard specifications for hydrogen embrittlement tests using notched C-rings. The pass/fail criterion in these standard tests [1] corresponded to a mean fracture stress within the range 1700 to 1850 MN/m² obtained from slow strain rate tests conducted at a crosshead displacement rate of 2×10^{-4} mm/s. Standard specifications for hydrogen embrittlement testing of plating-and-baking treatments are more severe than for testing paint strippers [2], and taking previous results into account [1], a possible mean fracture stress for acceptance of plating-and-baking treatments is estimated to be approximately 1900 to 2000 MN/m² at a crosshead displacement rate of 2×10^{-4} mm/s. If this estimate is used to reassess the various treatments discussed in the present paper, then cathodic charging in 4% sulphuric acid plus 50 mg/L sodium arsenite for periods >10 s, nonporous Cd plating-and-baking at 190°C/23 h, and electroless Ni plating without baking would be considered unacceptable for application on high-strength 4340 steel. The acceptability of all the other plating-and-baking procedures discussed corroborates all previous experience with these coatings.

Examination of the large number of specifications for plating reveals that many types of specimen are used to assess the degree of hydrogen embrittlement in steel (Table 3). These include notched tension, notched bend, notched C-ring, and smooth O-ring. Furthermore, variation in

TABLE 3—Summary of tests designed to assess the degree of hydrogen embrittlement of high-strength 4340 steel produced by various plating/baking treatments as defined in U.S. standard specifications.

Specification	Plating Process	Specimen Geometry	Stress Concentration Factor	Type of Loading	Applied Stress, % NTS	Maximum Test Time, h	No. specimens, Bath qualification	Frequency of Subsequent Tests
MIL-S-5002 [23]	Inorganic coatings	NT	3.9	CL	75	200	16	4/NS
BAC-5718 [8]	Cd	NT	3.1	CL	75	200	2	2/45 days
AMS 2401C [10]	Cd	NT	3.6	CL	75	200	4	4/NS
QQ-P-416C [9]	Cd	NT	3.9	CL	75	200	4	4/month
MIL STD-870A [6]	Cd	NT	3.9	CL	75	200	16	2/month
ASTM F 519-77(1a) [2]	Cd	NT	3.1	CD	75	200	3	...
ASTM F 519-77(1b)	Cd	NT	2.8	CD	75	200	3	...
ASTM F 519-77	Cd	NB	3.9	CD	75	200	3	...
ASTM F 519-77	Cd	N, C-ring	4	CD	75	200	3	...
ASTM F 519-77	Cd	S, O-ring	...	CD	92(UTS)	200	3	...
DPS 9.28 [7]	Cd	S, O-ring	...	CD	92(UTS)	168	4	4/NS
BAC 5804 [12]	Cd-Ti	NT	3.1	CL	75	150	2	2/week
AMS 2419A [24]	Cd-Ti	Use	ASTM F 519-77	Specification	75	200	3	3/NS
MIL STD-1500A [25]	Cd-Ti	NT	3.9	CL	75	200	4	2/month
MIL-C-26074B [13]	Electroless Ni	NT	3.9	CL	20	200	4	4/NS

NOTE: NT = notched tensile; N, C-ring = notched C-ring; CL = constant load; NS = not specified; NB = notched bend; S, O-ring = smooth O-ring; CD = constant displacement; UTS = Ultimate tensile strength; NTS = notch tensile strength.

geometry of notched tension specimens leads to values of notch stress concentration factor ranging from 2.8 to 3.9 [1,26]. The time to failure of sharply notched embrittled tension steel specimens, loaded to the same percentage value of the unembrittled fracture stress, has been shown to decrease with increase in notch stress concentration factor [27]. Significantly smaller times to failure have also been recorded during constant load tests with chromium-plated notched C-rings compared with notched tension specimens [28]. These results demonstrate that the severity of test method depends on both the type of specimen and geometry of the notch. It is therefore quite possible that the outcome of a pass/fail standard test to assess a plating-and-baking treatment, where specimens are loaded to 75% of the unembrittled fracture stress and held for 200 h, may depend on the type of specimen used. The degree of test severity associated with each specimen type could be determined by equating the pass/fail condition defined in standard specifications with a minimum mean fracture stress determined from several slow strain rate tests. If such a relationship can be established, then slow strain rate tests could be used to perform hydrogen embrittlement tests with any degree of test severity by merely altering the minimum acceptable mean fracture stress or by choosing an appropriate crosshead displacement rate.

The degree of scatter in fracture stresses determined from multiple slow strain rate tests should also provide useful information concerning the performance of particular plating baths. Plating baths that perform consistently over a period of time should produce constant values of mean fracture stress and standard deviation. Any sudden increase in the standard deviation, even in the absence of a change in mean fracture stress, could signify a decrease in the reliability of the plating bath. This parameter could therefore have particular significance in assessment of plating baths on a regular basis. Adoption of these guidelines could lead to a fixed number of specimens being required to assess the degree of hydrogen embrittlement produced by plating-and-baking treatments. At present, hydrogen embrittlement test methods defined in standard plating specifications insist on a minimum number of specimens that can vary from 2 to 16 (Table 3). Furthermore, with a maximum test time of 2.5 h, slow strain rate tests could be used to assess plating baths on a daily or even more regular basis compared with a minimum period of 8 to 9 days for conventional methods detailed in current standard specifications (Table 3).

Further analysis of plating specifications relating to porous Cd, brush Cd, Cd-Ti, and electroless Ni reveals little agreement concerning the maximum strength level of steel that is allowable without obtaining specific approval of the procuring authority (Table 4). Although most specifications quote a maximum ultimate strength level within the range 1380 to 1930 MN/m² (200 to 280 ksi), a few do not specify an upper limit (Table 4). This lack of agreement suggests that little consensus has been reached concerning acceptable risk factors associated with the use of plated-and-baked, high-strength steel components. The present experiments were conducted using 4340 steel heat treated to an ultimate tensile strength of 1845 MN/m² (267 ksi) and which is known to be particularly susceptible to hydrogen embrittlement. Consequently, plating-and-baking treatments that produce minimal hydrogen embrittlement in 4340 steel should be acceptable for application on comparable low-alloy steels of similar or lower strength level. Decisions to use steel of strength level 1792 to 1930 MN/m² (260 to 280 ksi) in the manufacture of plated-and-baked components are based on the assumption that no additional hydrogen will enter the steel during maintenance and subsequent service. The possibility must always be considered since previous work has shown that exposure of plated specimens to deleterious paint strippers [1] and aqueous environments [33] can readily provide additional sources of hydrogen. The situation would become even more critical in cases where plating and baking produce a finite but insufficient degree of embrittlement to cause failure in tests conducted in accordance with standard specifications. Such a case is identified in the present work where electroless Ni plating is followed by stripping, replating, and baking at 190°C/3 h (Fig. 4). It is claimed that slow strain rate tests will identify this situation and provide engineers with sufficient information to make a definitive decision concerning the acceptability of a particular plating-and-baking treatment.

TABLE 4—*Details of maximum allowable strength levels and baking procedures for plating high-strength, low-alloy steels with Cd, Cd-Ti, and Ni as defined in standard specifications.*

Specification	Plating Treatment	Max Strength Level, MN/m ² (ksi)	Baking Temperature, °C	Minimum Baking Time, h
MIL-S-5000C [23]	Surface treatments/coatings	1379 (200)	190	3
BAC 5718 [8]	Cd	1654 (240)	190	23 ^a
AMS 2401C [10]	Cd	1793 (260)	190	23 ^a
QQ-P-416 [9]	Cd	1654 (240)	190	23
HPS 1.03.00 [5]	Cd	N/S	200	24 ^a
DPS 9.28 [7]	Cd	N/S	149 to 200	23 ^a
NAS 672 [29]	Cd	1517 (220)	190	23
ASTM A 165-80 [30]	Cd	N/S	150 to 205	1 to 5 ^a
MIL STD-870A [6]	Cd	1654 (240)	190	23
BAC 5804 [12]	Cd-Ti	N/S	190	12
AMS 2419 A [24]	Cd-Ti	N/S	190	23 ^a
MIL STD-1500A [25]	Cd-Ti	1654 (240)	190	12
MIL-C-26074B [13]	Electroless Ni	1517 (220)	177	3
AMS 2404C [31]	Electroless Ni	N/S	190	3
ASTM-B-733-84 [32]	Electroless Ni	N/S	190	23 ^a
DPS 9.89 [20]	Brush Cd LHE	1654 (240)	Nil	
		1654 (240)	190	3
BAC 5854 [21]	Brush Cd LHE	N/S	Nil (< 12 in. ²)	
MIL STD 865 [22]	Brush Cd LHE	1930 (280)	Nil	

NOTE: N/S = not specified; LHE = low hydrogen embrittlement.

^aMinimum baking time depends on strength level.

The large number of specifications devised to assess the degree of hydrogen embrittlement in plated high-strength steel highlights the overall lack of consensus in determining the optimum method to accomplish this task. This aspect of the problem has been highlighted in the U.K. Defence Standard 03-4/Issue 2, which states in part [34] "Methods whereby aqueous protective treatments can be applied without some risk of harmful effects e.g. embrittlement or poor adhesion, are not yet established with certainty." It is claimed in this document that insufficient work has been done to develop a satisfactory standard method that can reliably predict the safe behavior of high-strength steel components to the effects of hydrogen embrittlement. It is hoped that the approach taken in the present work will go some way to solving this problem and to provide some meaningful basis for future evaluation of the degree of hydrogen embrittlement in high-strength steel.

Conclusions

The results of strain rate tests using notched tension specimens provide a quantitative estimate of the degree of hydrogen embrittlement produced in 4340 steel by plating-and-baking treatments. The versatility of the technique combined with the simplicity of the assessment method provide remedies for many of the limitations and inconsistencies apparent in existing specifications for assessment of the degree of hydrogen embrittlement in plated high-strength steels. Some of these advantages include:

1. Slow strain rate tests can be accomplished using notched tension specimens that comply with the reduced load requirements of an existing specification (ASTM F 519-77).
2. Slow strain rate tests with notched specimens utilize the fracture stress as a simple parameter for assessing the degree of embrittlement.

3. For multiple tests undertaken at a constant crosshead displacement rate, a minimum mean fracture stress can be specified for acceptance of a given plating-and-baking process.

4. Information relating to the continued reliability of plating baths could be derived from both the mean fracture stress and standard deviation obtained from a continuing series of multiple slow strain rate tests.

5. The slow strain rate technique could be used to quantify the relative severity of the test procedures outlined in the various standard specifications.

6. Slow strain rate tests conducted at a crosshead displacement rate of 2×10^{-4} mm/s can be completed within 2.5 h compared with 200 h for conventional tests defined in standard specifications.

7. Quantitative comparison of plating-and-baking treatments producing low levels of hydrogen embrittlement in 4340 steel can be made by undertaking slow strain rate tests at low crosshead displacement rates (10^{-5} to 10^{-6} mm/s).

It is believed that these advantages provide strong evidence for adoption of the slow strain rate method as a viable standard method for assessment of the degree of hydrogen embrittlement in plated-and-baked, high-strength steel. It is also hoped that the information provided by this type of test will help to increase awareness and understanding of the many dangers associated with the use of high-strength steel in a large load-bearing structure.

Acknowledgments

The author wishes to acknowledge P. G. Bushell for assistance with the experimental program and to the Australian Government Aircraft Factories, Hawker de Havilland Australia P/L, Qantas Airlines, Ansett Airlines, and Asko Processing Inc., Seattle for permission to use their plating facilities.

References

- [1] Pollock, W. J. and Grey, C., "Assessment of the Degree of Hydrogen Embrittlement Produced in Plated High-Strength 4340 Steel by Paint Strippers Using Slow Strain Rate Testing," this publication.
- [2] American National Standard ANSI/ASTM F 519-77 (1977), Method for Mechanical Hydrogen Embrittlement Testing of Plating Processes and Aircraft Maintenance Chemicals.
- [3] American Military Specification MIL-S-5000E (Nov. 1982) for Steel, Chrome-Nickel-Molybdenum (E4340) Bars, and Reforging Stock.
- [4] Qantas Process Specification P65 (1981), Low Hydrogen Embrittlement Cd Plate of High Heat Treat Steels.
- [5] Hawker de Havilland, Australia, Process Specification HPS 1.03.00 (1981), Cd Plating (Electrodeposited).
- [6] U.S. Military Standard MIL-STD-870A (USAF) (Aug. 1978), Cd Plating, Low Embrittlement, Electrodeposition.
- [7] Douglas Aircraft Co., Process Engineering Order DPS.9.28 (1973), Special Cd Plating for High Strength Steels.
- [8] Boeing Aircraft Co., Process Specification BAC 5718, Rev F (1976), Low Hydrogen Embrittlement Cd Plating.
- [9] Federal Specification QQ-P-416C (Aug. 1979), Plating, Cd (Electrodeposited).
- [10] Aerospace Material Specification AMS2401C (1978), Cd Plating-Low Hydrogen Content Deposit.
- [11] U.K. Ministry of Aviation Specification DTD 904C (May 1963), Cd Plating.
- [12] Boeing Aircraft Co., Process Specification BAC 5804 (April 1981), Low Hydrogen Embrittlement Cd-Ti Alloy Plating.
- [13] American Military Specification MIL-C-26074B (May 1971), Requirements for Electroless Ni Coatings.
- [14] Groeneveld, T. P. and Elsea, A. R. in *Hydrogen Embrittlement Testing, ASTM STP 543*, American Society for Testing and Materials, Philadelphia, 1974, pp. 11-19.
- [15] Altura, D. and Mansfield, F., *Corrosion*, Vol. 31, 1975, pp. 234-236.
- [16] Short, R., Boeing Test Report T6-2404, 1962, Boeing Airplane Co., Washington, DC.

- [17] Kudryavtsev, V. N., Lyakhov, B. F., Anufriev, N. G., Bagnev, S. P., and Pedan, K. S., *Protection of Metals*. Vol. 14, 1978, pp. 552-559.
- [18] Lawrence, S. C. in *Hydrogen Embrittlement Testing*. ASTM STP 543, American Society for Testing and Materials, Philadelphia, 1974, pp. 83-105.
- [19] Berman, D. A., *Materials Performance*. Vol. 24, Nov. 1985, pp. 36-41.
- [20] Douglas Aircraft Co., Process Engineering Order DPS 9.89, Rev G (Sept. 1977), Brush Plating.
- [21] Boeing Aircraft Co., Process Specification BAC 5854 (June 1982), Low Hydrogen Embrittlement Stylus Cd Plating.
- [22] U.S. Military Standard MIL-STD-865A (USAF) (April 1976), Selective (Brush Plating), Electrodeposition.
- [23] American Military Specification MIL-S-5002C (July 1971) for Surface Treatments and Inorganic Coatings for Metal Surfaces of Weapon Systems.
- [24] Aerospace Material Specifications AMS2419A (1979), Cd-Ti Plating.
- [25] U.S. Military Standard MIL-STD-1500A (USAF) (Jan. 1983), Cd-Ti Plating, Low Embrittlement, Electrodeposition.
- [26] Petersen, R. E., *Stress Concentration Factors*. R. E. Wiley and Sons, New York, 1974, Figs. 30,31.
- [27] Troiano, A. R., *Corrosion*, Vol. 15, 1959, pp. 207t-212t.
- [28] Williams, F. S., Beck, W., and Jankowsky, E. J., *Proceedings*, Vol. 60, 1960, ASTM, Philadelphia, pp. 1192-1202.
- [29] National Aerospace Standard NAS 672 (June 1981), Plating, High Strength Steels, Cd.
- [30] American National Standard ANSI/ASTM A 165-80 (Aug. 1980), Specification for Electrodeposited Coatings of Cadmium on Steel.
- [31] Aerospace Material Specification AMS 2404C (July 1984), Electroless Ni Plating.
- [32] American National Standard ANSI/ASTM B 733-84 (May 1984), Specification for Autocatalytic Nickel-Phosphorus Coating on Metals.
- [33] Pollock, W. J. and Hinton, B. R. W., "Hydrogen Embrittlement of Plated High-Strength 4340 Steel by Galvanic Corrosion," to be published in *Galvanic Corrosion*. ASTM STP 978, 1988.
- [34] U.K. Ministry of Defence Standard 03-04/Issue 2 (March 1977), "The Pre-Treatment and Protection of Steel Parts of Specified Maximum Tensile Strengths Exceeding 1450 N/mm²."

Panel Discussion: Sections 1 and 2¹

This panel discussion was held to discuss the content of papers reproduced in Sections 1 and 2 of this book. The discussion is presented in its original form and was not peer reviewed.

The moderator was Carlo Sonnino, Emerson Electric Co., St. Louis, MO. Panel members were: Lou Raymond, L. Raymond & Associates, Irvine, CA; John J. DeLuccia, Naval Air Development Center, Warminster, PA; Edward T. Clegg, Army Materials Technology Laboratory, Watertown, MA; Allen W. Grobin, International Business Machines, Poughkeepsie, NY; David J. Coates, L. Raymond & Associates, Irvine, CA; and Robert V. Dreher, Kaiser Electro-precision, Irvine, CA.

Participants were Rudy Frictioni, LECO Corp., St. Joseph, MI; Dale McIntyre, Cortest Labs, Inc., Cypress, TX; and C. G. Interrante, National Bureau of Standards, Gaithersburg, MD.

Discussion

Sonnino: Please give a short summary of your presentation prior to opening the discussion to the floor.

Raymond: As Chairman of F07.04, my paper summarizes existing standards and ones currently under consideration. I tried to project the future direction of standards, which is toward test methods that incorporate fracture mechanics analysis. Being able to quantify resistance to hydrogen embrittlement with the threshold stress intensity parameter would permit use in either design analysis or in specifying the level of nondestructive inspection. Such an approach would put us in a life prediction mode as far as a structure being exposed to a potential hydrogen embrittling environment.

DeLuccia: My talk attempted to give an overview of the effects of hydrogen that could be introduced electrolytically or electrochemically into engineering materials. I looked at some of the basic aspects of the hydrogen entry, looked at some of the electrochemical parameters to find certain things, described a few tests, one of which was the electrochemical permeation test that is a research tool and is very, very useful in determining such things as the diffusivity of hydrogen. It is important to know diffusivity in order to know how long you must bake and how long you must consider the hydrogen in your metal.

Another technique that I talked about is the electrochemical technique based on one half of the permeation experiment, and that is the Barnacle Electrode. The electrochemical Barnacle Electrode is a technique that can be used as a diagnostic tool that measures the amount of mobile hydrogen in parts. It can also be used as a quality assurance tool in plating lines of landing gear manufactured instead of waiting the 200 hours that was mentioned this morning. If you could adequately take some barnacle readings in one half hour, you might be able to determine whether you have pumped too much hydrogen in your part in the plating process, so I think that it has two uses: (1) a diagnostic tool for failure analysis; and (2) as a quality assurance tool.

Clegg: My presentation was in two parts, one part covering the Department of Defense speci-

¹This section represents the interaction of the presenters and the participants in response to the technical content of the various papers. The sessions were taped and written copies of the discussions sent to each participant for comments and/or corrections. It is hoped that by including these sections, the reader will be able to better understand the controversial aspects of these presentations.

fications and standardization organization and the other part covering the DOD standardization coverage of hydrogen embrittlement documents. I suggested at the end of the talk that much could be done to improve the DOD coverage of hydrogen embrittlement. This could be accomplished by the adoption of nongovernment documents such as ASTM F 519, which is referenced in documents for aircraft cleaning compounds.

Grobin: My talk this morning was on other ASTM committees doing work in the area of hydrogen embrittlement and international committees doing work on hydrogen embrittlement. I am acting with two hats as Chairman of the ASTM Liason Committee to F07.04 and as the Convener of ISO TC.107, Subcommittee 3, Working Group 3, on hydrogen embrittlement, avoidance treatments, and test methods.

Coates: I gave a presentation on some of the test methods used by professional societies other than ASTM, and how they approach hydrogen embrittlement or hydrogen failure of materials. I included discussion of current specifications of the National Association of Corrosion Engineers and the American Welding Society, what their specifications entail, and some recent developments. The presentation was in the form of an overview of the current procedures and specifications utilized by these societies, without going into any rigorous or critical assessment of the test procedures therein.

Dreher: I am a program manager at Kaiser Aerospace in Irvine. This morning I shared with you the experience that we went through, some of the trauma that we went through, in trying to use existing military specifications as well as societies' specifications, to update and supplement our own in-house proprietary specifications in an effort to set up a hydrogen embrittlement control program. We did advocate the shortening of the standard 200-h test with an innovative 8-h step load test that we recommend be further examined to perhaps shorten up the cycle of the time between when plating is completed and the time you know that you have not embrittled your parts.

Sonnino: Thank you, gentlemen. We will now allow questions from the floor.

Fricioni: Where can we obtain a source for military specifications and standards?

Clegg: Military specifications and standards may be obtained from The Naval Publications and Forms Center, 5801 Taber Ave., Philadelphia, PA 19120. Standardization documents in the MFFP area may be obtained separately at a cost of about \$13.00.

Raymond: Can anodic polarization prior to plating inhibit hydrogen embrittlement by restricting/modifying entrance of hydrogen?

DeLuccia: Yes, if the anodic polarization results in a passive oxide film. You can anodically polarize certain metals and never form a passive oxide film. If the metal is capable of forming that passive oxide film, yes you then will have a barrier to the entrance of hydrogen, and subsequent cathodic polarization will not cause the hydrogen to enter the metal.

Raymond: Based on your presentation, did you suggest that cathodic overprotection of a system for corrosion protection, for example zinc on steel, can generate conditions for hydrogen embrittlement?

DeLuccia: Yes, I did suggest that, and yes it is true that if you cathodically protect a steel structure, you can inadvertently cause hydrogen to enter that steel structure. This is probably not very important in low-strength steel structures, such as ocean-going ships and things of that nature, plain old ordinary steel. However, as the strength level of the steel increases and you are becoming more susceptible to hydrogen embrittlement, then your cathodic protection could be important from the standpoint of causing embrittlement. I think this is perhaps on the horizon for our navy ships, which are going to higher and higher strength steels in their submarine hull program. Did that answer your question?

Raymond: I want to restate the fact that I was focusing on the word overprotection. In other words, would there be systems where, if you used sacrificial cadmium, it would provide protection from corrosion. You might not have a problem with hydrogen embrittlement, but if you wanted to protect with a greater potential such as with zinc, you would now have a hydrogen embrittlement problem. This is what I meant by the term overprotection.

DeLuccia: That may or may not be true. If you are below that line that I showed on the Pourbaix diagram and you are capable of generating hydrogen, then I think it does not matter whether you are generating it from zinc or generating it from aluminum. I think what matters is the susceptibility of your underlying steel. If it is very high-strength steel, it is only going to take a very small amount of hydrogen because it has become embrittled. I think that Dr. Berman found that you can actually embrittle certain high-strength steels with fractional parts per million of hydrogen in the steel. In fact, I think he talked in parts per billion. Here again, I think it is not so much the potential difference, but as long as you are below that line in the Pourbaix diagram, it is really the susceptibility of your underlying steel.

Sonnino: I have a remark confirming what you are saying. We did some work with 300M steel that was vacuum plated with aluminum. The original aluminum vacuum plating was very porous, and instead of protecting the steel from corrosion and also from embrittlement, we embrittled the 300M parts because of overprotection because of the large anodic-cathodic surface ratio of the vacuum deposit of aluminum with high porosities. So it is a direct confirmation that an overprotection can cause hydrogen embrittlement if it is not taken care of very, very carefully.

Grobin: In mild steels, plated with zinc for example, that are inadequately proportioned in thickness, you can have what we call today "postplating" hydrogen embrittlement due to the anodic protection of the steel by the zinc and the using up of the zinc, whereby hydrogen is now created at the interface of the remaining zinc and steel, and hydrogen gets into the part and it cracks some five to six years after it has been plated and put into service.

DeLuccia: To parenthetically add to that I would say that is probably the case if your environment is acidic and your cathodic reaction is the reduction of hydrogen. I could see that happening very easily.

Raymond: I would like to emphasize the importance of consolidating the different standards on hydrogen embrittlement testing because, as we heard from Bob Dreher, the interpretation or use of some standards causes damage to hardware rather than to establish quality, as was the original intent.

The problem seems to focus on testing actual hardware to insure freedom from hydrogen embrittlement. Standards, including the MIL and FED standards, are vague, specifically with regard to load or stress level. The plating standards call for loads of 50% of the design yield. For a 240 ksi steel, a load is calculated that produces a stress of about 120 ksi, which is then sustained for 20 h. If no failure, the part is assumed free of embrittlement.

What was found to occur was that parts failed in 210, 212 h, etc., or slightly beyond the 200 h go-no-go criterion. One could only conclude that the 200 h represented consumption of over 90% of the total life of the part instead of establishing the integrity of the part as was intended. If the test would have been stopped after 200 h and put into service, the disastrous consequences are apparent.

The reason for this situation is that the coupon tests are conducted at 75% of the *notched* tensile strength or, in the case of the 240 ksi steel, 75% of 350 ksi or about 260 ksi, which is slightly more than the smooth bar tensile strength. For a notched tensile bar, 120 ksi represents the gray region or threshold region below which no failures occur. In reality, significant scatter or spread in data occurs in this region, which was the same stress level of the parts. Therefore, I strongly advocate stressing parts to at least 75% of their breaking load, which is a way of taking into account the geometry of the part. Pieces will have to be sacrificed in many cases because the parts will be considered to be destructively tested because of the high stress level. For nondestructive testing of each part for reuse in service, a specific proof test logic for each piece of hardware based on fracture mechanics will have to be established.

Sonnino: Why 200-h tests for electroless nickel when the plated steel must be baked at 650°F?

Dreher: Well, unless I am misinterpreting the specification, there are at least three categories of Class 2 coatings. One is for materials below Rockwell C 40 (HRC 40), the other is for materi-

als above HRC 40, and then there is another category which talks about the high Vickers hardness. First of all, in our material, the 4330 V is only tempered at 550°F so we couldn't heat it to 650°F, and secondly, we did not care about the hardness of the nickel. All we wanted was corrosion protection, and I think the legality of this specification is such that it is not mandatory to bake at 650°F, that is only if you want 700 Vickers hardness, and we did not.

Sonnino: There are several revisions of the military specification, and I think the last revision made the baking mandatory for all types of deposits. Evidently, there is something here that I also found in the latest edition, to bake at 650°F, and that means that you are practically tempering the material in the brittle range, so somebody has to take a closer look.

Dreher: We looked at whether we are tempering in the so-called blue brittle range. We are not.

Sonnino: The brittle range is normally 400 and 700 °F.

McIntyre: Do you have data to compare to the 200 test results with the 8-h step load test results for materials that did show embrittlement?

Dreher: I am glad to say no. We did not have anything that was embrittled, and in our modest little program in our six months, our crash effort to get through the prototype hardware program, we did not take any steps to purposely diffuse hydrogen into bars to compare the validity between the 8-h test and 200-h test, but that is what I would like to see done. Somebody should do it on purpose and make a systematic comparison, but, no, we did not have any embrittled parts on any embrittlement specimens.

Grobin: I want to go back to the question on electroless nickel. I want to point out that Committee B08 has just issued a brand new specification on electroless nickel and has reviewed much of the heat treatment and hardness data in earlier standards, both the military, other industry standards, and ASTM practices, and as revised it is based on better information than was available in the past. I believe that document has been submitted to the Department of Defense. There is a lot of controversy as to what these various heat treatment data represent. But one thing is certain, electroless nickel can be hardened at a lower temperature with a longer bake so that if you question reaching a hardness with the electroless nickel and exceeding the tempering temperature of the steel, let the tempering temperature of the steel dictate the heat treatment and just bake it for a longer period of time and you will achieve the same hardness.

Dreher: It is clear that the industry and the customer may be best and more quickly served if the plating houses would do their own specimen testing on site. How can this approach best be implemented in industry? Through ASTM or by end users?

Grobin: It is going to take a concerted effort, and certainly by efforts through the utilization of ASTM standards and specifications. The plater will attest that he will perform the entire specification, which says that he is ready to do those tests. Now, a lot of this test equipment is extremely expensive. The cost will have to be added to the cost of the plating. I know that in the case of my own company we prefer to have the plater do the testing in his own plating shop. We will help him with unusual test equipment and get him trained to use it, because as part of the bottom line it is much cheaper, much more efficient, and we do not have delays for critical parts because the testing is done where it should be, at the end of the plating line.

We cannot expect the plating shops to suddenly pick up and buy a lot of expensive equipment or to bring in the people to run this equipment if there is not a concerted effort on the part of the buyers of plating to support their effort. I think that perhaps a conference of this type should be organized in the near future. Perhaps we ought to involve the American Electroplaters Society and the National Association of Metal Finishers and the various industry groups to see what can be practically done. Because certainly we are in a war for quality. This type of testing represents quality and a lot of dollars. It represents avoiding a tremendous amount of wasted time. Certainly we can improve our whole national economic picture by being more efficient at doing this job, and I suggest that perhaps this is the time that we should start making our way towards a more efficient method of production. That means a revolution in the plating shops by giving

them the responsibility for testing, which I personally believe they rightfully should have. Then let's do it.

Raymond: I totally support your position. I think that is the way to go, but I think the one problem with that has been the contractor's avoiding the use of self-loading frames instead of using creep frames. When we went through a round-robin when we first drafted F 519 and we compared the self-loading bent beam test to the notched tensile sustained load test. The results were every bit as good, if not better, relative to scatter from the self-loading bent beam test results that we had. It was through a subsequent ASM questionnaire that we found that 95% of the people were still using the sustained load notched tensile test demanding a 12 000 to 18 000 capacity creep frame.

That is where problems occur with being able to conduct test results within the desired time frame because of the limited availability of the test machines. There has been a tremendous reluctance on the part of industry to go to the self-loading frames and I for one don't understand because the C-ring has had good results and is reproducible and has been around a long time. The same thing can be said of the bent beam, which has been developed by Lockheed and used for a long time. The precision reproducibility has been excellent. More was gained from controlling the manufacturing of the notch detail by using crush grinding and spending time on detailing the notch. Better reproducibility was obtained by the notch detail than by adjusting the loads, whether they used a bent beam test with the small specimen self-loading type system or whether they used a large creep frame that required direct tensile loads on the notched tensile coupons.

Section 3: Hydrogen in Steel and Titanium

Opening Remarks

The introduction of hydrogen in molten metal sampling was discussed. Areas of concern were the introduction of hydrogen in quenching the pin sample and the formation of condensation as the pin sample was taken from the liquid temperatures to the ambient temperatures of sample preparation.

Comparison testing of water quenching and liquid nitrogen storage to direct liquid nitrogen quenching has not indicated any hydrogen introduction due to water quenching. Tests performed on the formation of condensation as the sample is taken to room temperature indicates condensation to be a source to be careful of. Rinsing the sample in freon as part of the final sample preparation stages appears to remove the condensate formation.

The introduction of hydrogen through cadmium plating processes was discussed to assist in developing a means of control. Tests performed on pieces using a 15-s plate time followed by a several minute delay time where the pieces are removed from the plating bath then another 15-s plate period. The process was repeated until the desired plate thickness was achieved. This process has been successful in reducing the hydrogen introduction. Precautions in plating include accurate monitoring and control over the plating baths and materials.

General discussions were conducted on hydrogen activity through the various work stages and the effects of temperature and environment that contribute to hydrogen introduction and evolution.

Rudy Fricioni,

LECO Corp., St. Josephs, MI; chairman,
Section 3.

Electrochemical Sensor for the Determination of Hydrogen in Metals by Potential Measurements

REFERENCE: Mackor, A., de Kreuk, C. Wim, and Schoonman, J., "Electrochemical Sensor for the Determination of Hydrogen in Metals by Potential Measurements," *Hydrogen Embrittlement: Prevention and Control*, ASTM STP 962, L. Raymond, Ed., American Society for Testing and Materials, Philadelphia, 1988, pp. 90-97.

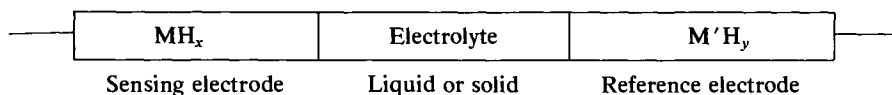
ABSTRACT: An electrochemical sensor is described for the nondestructive determination of the activity of mobile elemental hydrogen in a wide range of metals, like steel and palladium. The sensor is based on the principle of a concentration cell. In this cell one of the electrodes is either the sample metal to be investigated or an ultrathin palladium layer in direct contact with the sample, acting as a sensing electrode. The other electrode functions as the reference, for which we have used palladium hydride or molybdenum bronze. The electrolyte is a liquid or preferably solid proton conductor. A version, using molybdenum bronze and thin palladium film (20 nm) electrodes and hydrogen uranyl phosphate tetrahydrate, has been found to be especially valuable because of its selectivity and long-term stability.

Various metal samples from research and industry have been investigated to yield significant potential differences between samples containing (mobile) hydrogen and those which were low in hydrogen content. The qualitative and quantitative information from these hydrogen measurements may be used for many purposes provided that suitable calibration procedures are carried out.

KEY WORDS: electrochemical sensor, mobile elemental hydrogen, potential measurements, concentration cell, palladium (hydride) and bronze electrodes, steel, metals

In 1982, Schoonman, Franceschetti, and Hanneken [1] reported on an electrochemical sensor for the determination of local hydrogen concentration (activity) in a metal, based on work at Utrecht State University. They showed that by potential measurements hydrogen activities a_H can be determined in palladium wire that is nonuniformly loaded with hydrogen. Other samples investigated were pressed pellets of zirconium (Zr) powder and crystalline and amorphous samples of intermetallic compounds like $Ni_{64}Zr_{36}H_x$.

This sensor is based on the principle of a concentration cell of the type



¹Project leader, (photo) electrochemistry, and electrochemist, respectively, Institute of Applied Chemistry TNO, P.O. Box 108, 3700 AC Zeist, The Netherlands.

²Professor of inorganic chemistry, Laboratory of Inorganic and Physical Chemistry, Delft University of Technology, P.O. Box 5045, 2600 GA Delft, The Netherlands.

in which two different or equal metals are brought into contact with a liquid or preferably a solid electrolyte to give an asymmetrical (M,M') or symmetrical (M,M) cell, respectively. The solid electrolyte is hydrogen uranylphosphate tetrahydrate (HUP), a well-known solid proton-conductor [4,12]. At both interfaces $\text{MH}_x|\text{electrolyte}$ and $\text{M}'\text{H}_y|\text{electrolyte}$, an elemental hydrogen $\text{H}_{\text{el}}/\text{hydrogen ion}$ equilibrium is established, which leads to a potential difference between the electrodes, according to the Nernst equation:

$$\Delta E = \Delta E_0 + \frac{RT}{nF} \log \frac{a(\text{H}_{\text{el}}' \text{ sample})}{a(\text{H}_{\text{el}}' \text{ standard})}$$

Here, n denotes the number of electrons involved in the redox process $\text{H}_{\text{el}}/\text{H}^+$. For a symmetrical cell, $\text{M} = \text{M}'$, the potential difference under standard conditions $\Delta E_0 = 0$.

These results were carried further by Franceschetti and Hanneken et al. [2,3] and by Schoonman and Mackor et al. [4], aiming at monitoring interstitial and solar hydrogen and its electrotransport in metals or intermetallic compounds. Current research by Schoonman et al. is directed towards improved solid electrolytes which permit hydrogen determination at elevated temperatures and a better understanding of the interfacial phenomena in the sensor, while TNO has been developing the solid-state sensor further for practical use [5]. Shortly afterwards, the same invention was published by Lyon and Fray [6]. Simultaneously, the use of a symmetrical cell concept with HUP and palladium powder electrodes for hydrogen gas measurements was described by Lundsgaard et al. [7].

With respect to sensor response to different hydrogen-containing environments, it was found for gaseous hydrogen that n in the Nernst equation amounts to 2, thereby yielding a 30-mV potential difference per decade of difference in hydrogen pressure at ambient temperature. For elemental hydrogen in metals, we expect the value 1 for n , hence a response of 60 mV/decade of hydrogen activity. So far, this has not been confirmed experimentally due to the absence of suitable calibration materials.

In the field of measurement of (mobile) hydrogen activity in metals, the development which is closest to our sensor is that of electrochemical sensors, which are based on electrochemical permeation of hydrogen through metal foils and oxidation of the extracted hydrogen to give a hydrogen oxidation current. So-called "barnacle electrodes" [8,9] and "hydrogen patch cells" [10] are based on this concept, which was introduced by Devanathan and Stachurski [11]. A principal difference between these sensors and the present concept is that by measuring currents, one is consuming hydrogen in the metal sample under investigation, thereby changing the hydrogen distribution in the material. This is a dynamic method and therefore, the diffusion coefficient of hydrogen in the metal needs to be known. Our potential measurements do not seriously perturb the hydrogen distribution in the sample. For measurements under equilibrium one does not need to know the diffusion behavior.

The present paper reports the preliminary results of an evaluation and development program for the solid-state sensor.

Experimental Procedure

A series of prototype sensors were fabricated by pressing HUP powder [12] to give HUP disks (diameter 5 mm; thickness 1 mm). These disks were similarly pressed together with powdered molybdenum bronze on one side. This bronze was prepared by reduction of MoO_3 with zinc in hydrochloric acid to give a composition $\text{H}_{0.34}\text{MoO}_3$, as determined by X-ray diffraction [13]. The thus-obtained half-cell was mounted in an $\alpha\text{-Al}_2\text{O}_3$ (corundum) cylinder with bare HUP at the outside (Fig. 1). Before mounting, two gold strips were painted on the in- and outside of the cylinder, and they were baked at 800°C to ensure a stable contact with the electrodes. The

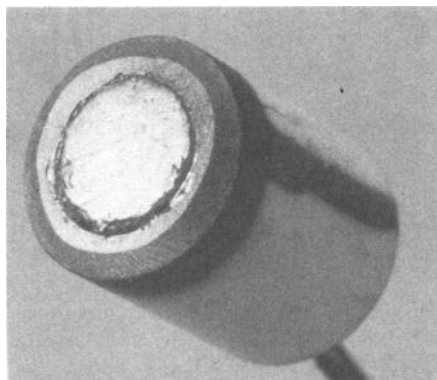


FIG. 1—Solid-state hydrogen sensor, comprising a 20-nm Pd film as the sensing electrode on a HUP disk and a $H_{0.34}MoO_3$ reference electrode mounted in a corundum cylinder (external diameter 8 mm).

outside of the HUP disk was sputtered with a 20-nm layer of palladium in an Edwards vacuum sputter-coater type S 150B. A contact wire was connected via silver epoxy resin with the reference electrode.

Results and Discussion

Palladium

The initial experiments [1] were carried out with a HCl/KCl (pH 2.2) liquid electrolyte or with a pressed disk in probes as depicted in Fig. 2, however, without the palladium sensing layer.

The reference electrode was a palladium (Pd) wire that had been brought into contact with hydrogen at atmospheric pressure for several days. This electrode was immersed (liquid electrolyte) or firmly pressed against the HUP disk. A palladium wire (length 10 cm) was inserted about halfway into a locally melted glass wall, which after cooling was kept in a hydrogen atmosphere on one side and in air on the other. The open-circuit voltage of the cell Pd(H)/Electrolyte/PdH_x was measured as a function of position along the Pd sample wire directly after removal of the hydrogen atmosphere. The results are given in Fig. 3. They show a clear transition between the hydrogen-containing zone (right side) and the hydrogen-free zone, corresponding to a potential difference of about 600 mV (aqueous electrolyte) and 400 mV (solid electrolyte), respectively.

Steel

In principle one can use the same sensor concept for the measurement of mobile hydrogen in steel and other nonnoble metal samples. As an example, we find considerable potential differences between freshly prepared steel weldments used as sensing electrodes and those weldments which had undergone a heat treatment at 300°C. However, it was realized that corrosion processes and oxidic layer formation on these metal samples may considerably influence the result of the measurement. In order to obtain unambiguous results, we decided to introduce an intermediate palladium (or palladium-silver alloy) layer as sensing electrode between the metal sample and the electrolyte. The two configurations are presented in Fig. 2. Palladium, having a high

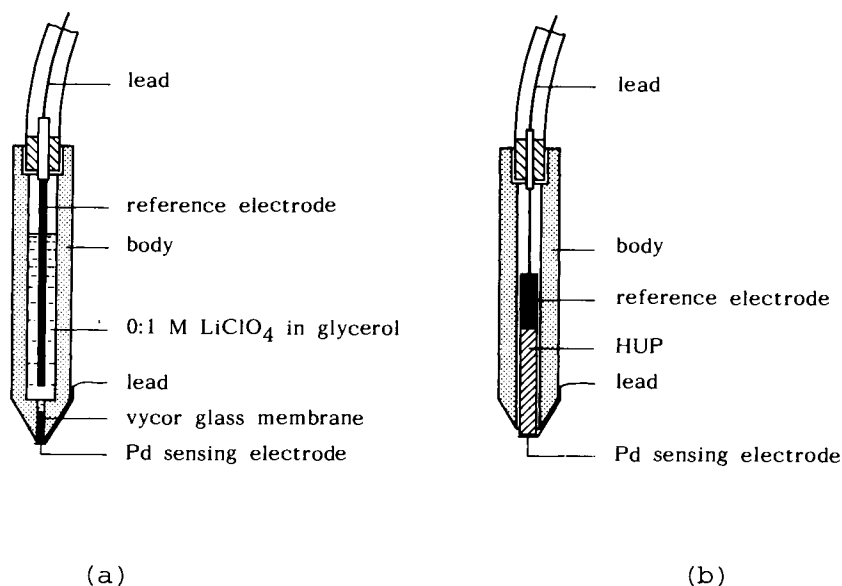


FIG. 2—Hydrogen activity probe: (a) PdH_x /aqueous proton conductor; (b) PdH_x /solid proton conductor.

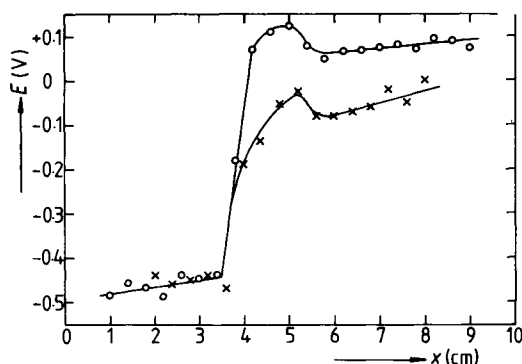


FIG. 3—Hydrogen activity profile in a Pd wire as monitored with the aqueous electrolyte probe (OOO) and the solid electrolyte probe (XXX).

affinity towards hydrogen, will absorb hydrogen from the sample until an equilibrium is reached, in which the concentrations of hydrogen in the palladium-sensing electrode and in the metal sample are related. Hence, we now have two kinds of problems to solve. The first is of a kinetic nature, caused by the fact that two surfaces (metal and palladium) with a certain roughness will have a limited number of contact points and consequently hydrogen equilibration may be a slow process. We have observed that hydrogen transfer is strongly accelerated if glycerine is used as a contact liquid between the two surfaces. The mechanism of action of this contact liquid is not quite clear, but we note that glycerine is a very poor solvent for molecular hydrogen. It is conceivable that glycerine influences one or more of the following processes: (1) release of hydrogen atoms from the bulk of the metal to the surface as adsorbed atoms; (2) recombination

of hydrogen atoms to give hydrogen molecules; (3) release of hydrogen molecules from the surface; (4) transport from the metal to palladium or the dissociation and absorption processes on palladium. In principle it is also conceivable that hydrogen atoms are transported through the liquid. We exclude galvanic processes between the metal sample and palladium through the glycerine electrolyte because of the large numbers of internal direct contacts between the two metals. Some less-polar liquids having a higher solubility for H_2 (polyglycols, paraffin oil) are considerably less effective in hydrogen transfer.

The second problem relates to the thickness of the palladium layer and has two effects:

1. *The diffusion time of hydrogen* from the incoming side of the layer to the electrolyte side. This is illustrated in Fig. 4, where the response time is presented for three liquid electrolyte probes, each provided with a palladium layer of a certain thickness (100 μm , 25 μm , and 20 nm), which are placed on a piece of hydrogenated palladium.

The response time of, for example, 1 h for a palladium foil may not be important for certain applications, like the continuous monitoring of pipeline corrosion, but it certainly is a serious constraint for on-the-spot measurements of larger series, like the testing of fresh weldments.

2. *Dilution of hydrogen* by the volume of the sensing palladium electrode may lead to a depletion of hydrogen in the metal sample and hence to a measured hydrogen activity which is lower than the initial activity. Also, it may take a longer time for the sensor to equilibrate, since the hydrogen will be extracted from a greater part of the sample than with a very thin film and diffusion will take place in it.

The second problem has been resolved by taking an ultrathin palladium layer of 20 nm, sputtered onto a vycor glass support (liquid electrolyte) or directly onto the solid electrolyte HUP (Fig. 2).

In this way a number of solid state hydrogen probes were manufactured, and they were calibrated against hydrogen gas in three percentages, diluted with nitrogen (Fig. 5).

Figure 5 exhibits two features: all sensors have a probe response of 29.5 mV/decade of hydrogen concentration. However, the intercept is considerably different for each sensor. We are inclined to believe that the preparation procedure for reduced MoO_3 does not yield a homogeneous product. However, for a proper functioning and calibration of the hydrogen sensor, these differences are not relevant.

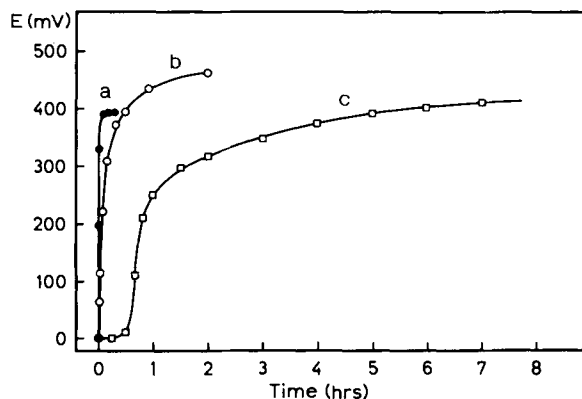


FIG. 4—Response time of three liquid electrolyte probes provided with a palladium layer and placed on a sample of PdH_x . Thickness of Pd layer: a = 20 nm; b = 25 μm ; c = 100 μm .

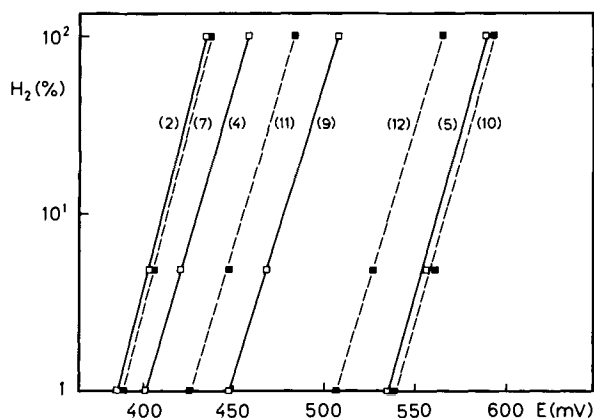


FIG. 5—Potential given by several solid state hydrogen probes versus hydrogen concentration in H_2/N_2 mixtures. Reference electrode: $H_{0.34}MoO_3$. Sensing electrode: Pd (20 nm). Response time < 10 min.

We used samples of steel 37 to test some effects on its hydrogen contents. A steel sample was electrochemically charged with circa 30 ppm of hydrogen, and a sensor with the thin palladium film (20 nm) was applied. A rapid probe response was observed (Fig. 6a). The same steel sample was then depleted in hydrogen by a thermal treatment at 300°C for 15 min. Interestingly, the potential of the Pd film changed considerably over a period of 1 h, indicating the formation and/or uptake of hydrogen by the steel sample over that period.

In Fig. 6b', we have plotted the sensor response of the steel 37 sample after the heat treatment on a longer time scale (hours). It seems that some equilibrium position is slowly reached.

The discharge of hydrogen from a sensor after removing it from the steel sample of Fig. 6a in air is a rather slow process, as shown in Fig. 6c. This discharge may be speeded up, for example, by making contact with a palladium foil, which is depleted in hydrogen.

Conclusion

In the foregoing we have described a novel electrochemical sensor for determining hydrogen activity in metals and in gases, which is based on the measurement of potential differences with respect to a reference metal hydride. The described method, using a thin palladium (or palladium-silver) film as the sensing electrode, leaves the hydrogen distribution in the test sample largely as it is. With a palladium film one also avoids other sources of potential differences than arising from differences in hydrogen activity. Thus, the sensor may be used for the determination of local hydrogen activity in a metal sample. Also, it opens the possibility for scanning the surface of the sample metal, preferably with a miniaturized version of the sensor.

For this purpose it is necessary to carry out calibration procedures, thereby relating hydrogen activities with sensor responses for each of the metals to be tested. The method may find ample use in metallurgical research, provided that the data mentioned above will be made available and also by giving the sensor sufficient robustness. For rapid and routine analysis of hydrogen activity, data processing is also necessary. The temperature stability of the tetrahydrate of hydrogen uranyl phosphate limits the continuous use of the present sensor to temperatures below 40°C.

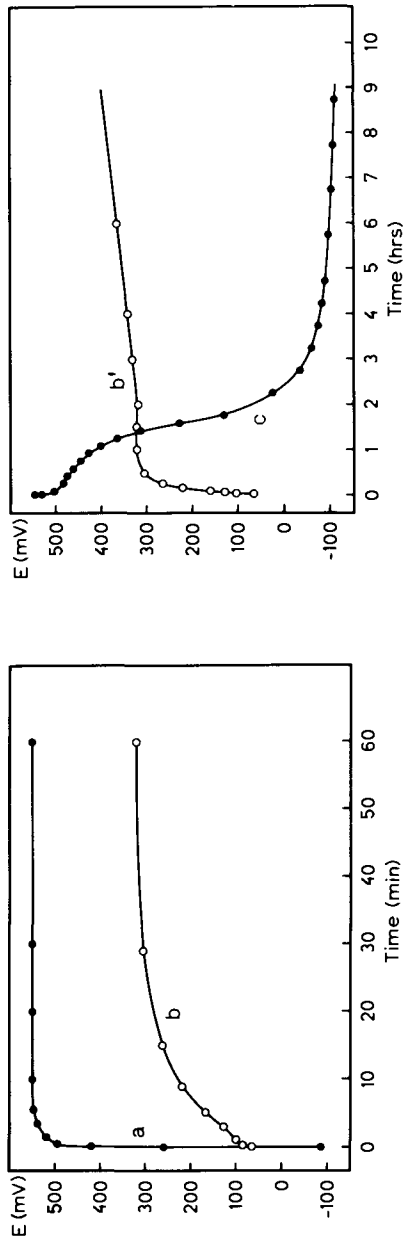


FIG. 6—Solid state probe response on steel 37: (a) after electrochemical charging with circa 30 ppm of hydrogen; (b) after a heat treatment at 300°C for 15 min; (b') as (b), but on a different time scale; (c) relaxation of the probe after removing it from the sample, as in (a).

Acknowledgment

The authors are grateful to H. S. Kiliaan of the Solid State Department, Physics Laboratory of Utrecht University for preparing the sample of H_xMoO_3 .

References

- [1] Schoonman, J., Franceschetti, D. R., and Hanneken, J. W., *Berichte der Bunsengesellschaft für physikalische Chemie*, Vol. 86, 1982, pp. 701-703.
- [2] Franceschetti, D. R., Shefsky, S. I., and Hanneken, J. W., *International Advances in Nondestructive Testing*, Vol. 10, 1984, pp. 101-114.
- [3] Hanneken, J. W., Franceschetti, D. R., and Loftin, R. B., "Nondestructive Determination of Local Hydrogen Concentration in Metals," to be published.
- [4] Kiliaan, H. S., Wilt, H. M. de, Schoonman, J., Kreuk, C. W. de, and Mackor, A., "The Proton-Conducting Solid Electrolytes HUP and Nafion in (Photo)-Electrochemical Cells," presented at Fourth EUCHEM Conference in Solid State Chemistry and Electrochemistry, Oxford, 19-23 March 1984.
- [5] TNO has filed patent applications in the Netherlands (8 June 1982) at the European Patent Office and in the U.S., for example, J. Schoonman, C. W. de Kreuk, and A. Mackor, U.S. patent application 501,854 (7 June 1983).
- [6] Lyon, S. B. and Fray, D. J., *Solid State Ionics*, Vols. 9-10, 1983, pp. 1295-1298.
- [7] Lundsgaard, J. S., Malling, J., and Berchall, M. L. S., *Solid State Ionics*, Vol. 7, 1982, pp. 53-56.
- [8] De Luccia, J. J. and Berman, D. A., "An Electrochemical Technique to Measure Diffusible Hydrogen in Metals (Barnacle Electrode)," *Electrochemical Corrosion Testing, ASTM STP 727*, F. Mansfeld and U. Bertocci, Eds., American Society for Testing and Materials, Philadelphia, 1981, pp. 256-273.
- [9] Mansfeld, F., Jeanjaquet, S., and Roe, D. K., *Materials Performance*, Vol. 21, 1982, pp. 35-38.
- [10] Martin, R. L. and French, E. C., Petrolite Corp., U.S. Patent No. 4,065,373, 27 Dec. 1977.
- [11] Devanathan, M. A. V., Stachurski, Z., and Beck, W., *Journal of the Electrochemical Society*, Vol. 110, 1963, pp. 886-890.
- [12] Howe, A. T. and Shilton, M. G., *Journal of Solid State Chemistry*, Vol. 28, 1979, pp. 345-361.
- [13] Glenser, O. and Lutz, G., *Zeitschrift für Anorganische und Allgemeine Chemie*, Vol. 264, 1951, pp. 17-33.

The Barnacle Electrode Method to Determine Diffusible Hydrogen in Steels

REFERENCE: Berman, D. A. and Agarwala, V. S., "The Barnacle Electrode Method to Determine Diffusible Hydrogen in Steels," *Hydrogen Embrittlement: Prevention and Control*, ASTM STP 962, L. Raymond, Ed., American Society for Testing and Materials, Philadelphia, 1988, pp. 98-104.

ABSTRACT: An electrochemical method to determine diffusible hydrogen in steels is described. It is a simple but very sensitive device which is capable of measuring hydrogen concentrations of less than 1 weight ppm. The method makes use of nickel/nickel oxide as a polarizing electrode, which is coupled to a hydrogen-containing steel part. The hydrogen is oxidized at the specimen surface, and the current measured is related to the hydrogen concentration. The method demonstrates a high precision in the measurements. It is shown that the measured hydrogen concentration resulting from cadmium plating is a function of specimen bulk. Results from experiments with plated/baked/stressed 300M steel are reviewed.

KEY WORDS: hydrogen embrittlement, diffusible hydrogen, hydrogen determination, hydrogen permeation, barnacle electrode, cadmium plating, high-strength steels

The phenomenon of hydrogen embrittlement (HE) is well known and studied, as indicated by the number of symposia devoted to the subject [1-3]. The problem of HE is especially severe with high-strength steels, which become more susceptible with increasing strength. Though many mechanisms as to how hydrogen causes embrittlement have been proposed [4] and may be operative, the diffusion of atomic hydrogen to produce local damaging effects must always be considered.

The sources of hydrogen can include corrosion or processing, such as electroplating. Protons from aqueous media can be reduced at the metal's surface to form atomic and then molecular hydrogen. However, some of the atomic hydrogen can also enter the metal and diffuse along stress and concentration gradients to produce embrittlement. A knowledge of the diffusible hydrogen concentration should be of great help in determining whether or not a material will be susceptible to embrittlement. To obtain this information, an electrochemical cell called the barnacle electrode (BE) was developed.

The electrochemical permeation method [5,6], in which hydrogen is produced on one side of a metallic membrane and oxidized on the other side after it diffuses through, has made it possible to measure very low hydrogen levels. The BE system [7,8] is an adaptation of this method, in which only the exit side is used. It is capable of measuring less than 1 weight ppm of diffusible hydrogen in steels [8].

In the BE method, the hydrogen-containing steel part is coupled to a nickel/nickel oxide electrode in an alkaline electrolyte. This galvanic coupling polarizes the steel to a potential at which hydrogen is oxidized at the surface as it diffuses out. The oxidation current can then be

¹Research chemist and materials technical specialist, respectively, Aero Materials Division, Naval Air Development Center, Warminster, PA 18974.

related to the hydrogen concentration in the metal by the first term solution to Fick's second law [8,9].

$$J_t/F = C_o(D/\pi t)^{1/2} \quad (1)$$

where

- J_t = oxidation current density at Time t ,
- C_o = concentration of hydrogen in the metal,
- D = diffusivity of hydrogen in the metal, and
- F = Faraday constant.

Using a hydrogen diffusivity of 2.5×10^{-7} cm²/s in Eq 1, a 30-min current density measurement of 0.50 μ A/cm² corresponds to a hydrogen concentration of 0.10 ppm. Details of this calculation have been given elsewhere [8]. It has been determined that a 30-min reading leads to better precision because the rate of change of the current is almost insignificant at this time.

There are some limitations to the use of Eq 1 [8], which will be discussed in following paragraphs. However, once BE measurements have been correlated with mechanical testing, such as sustained load, these BE measurements can be used directly as the criterion for susceptibility (for a given alloy and heat treatment) without regard to the actual hydrogen concentration.

The BE method has been applied to a variety of problems to determine diffusible hydrogen concentrations and to relate these values to embrittlement susceptibility. In previous work, it was shown that: (1) the hydrogen concentration of a high-strength steel could be related to working load, and that a threshold curve (fail/not fail) could be developed [8]; (2) the loss of hydrogen with time from a thick steel weldment could be ascertained [8]; (3) the efficiency of baking cadmium-plated steels could be evaluated [10]; and (4) the changes in hydrogen concentration after constant load testing could be detected [10].

In this paper, further results on the determination of hydrogen in cadmium-plated steel will be given, which will illustrate the precision and sensitivity of the method. Also, details not discussed in previous papers [8,10] will be given.

Experimental

The BE system consists of an electrochemical cell and a current measuring circuit. A drawing of the cell is shown in Fig. 1. The gasket seat is an improvement in the design which prevents deformation of the gasket when the cell is tightened up. The gasket dimension shown in Fig. 1 defines a solution contact area of 1.0 cm when the parts are clamped to the specimen (the anode). The nickel/nickel oxide electrode is inserted into the cavity, which is filled with 0.2 *M* sodium hydroxide solution. The measurement of current is made using the voltage drop across a resistor [8] or by using a current follower circuit [11]. The output is monitored with a strip chart recorder. Because the current is very high at the start of the measurement, it is not recorded for the first 10 min.

The verification of the contact area can be made by clamping the cell together with a piece of aluminum foil between the gasket and a specimen (or other flat material) and filling the cavity with 0.2 *M* sodium hydroxide (NaOH). After about 15 min, the foil will be sufficiently etched so that the area can be determined and examined for roundness and absence of crevices. The occurrence of a crevice would lead to extraneous corrosion currents which will be an added factor in the BE measurement.

Since the nickel/nickel oxide electrode will depolarize with use, it must be recharged. This is done by charging it at 5 to 10 mA/cm² for 1/2 h using a platinum cathode in 0.2 *M* NaOH.

Experiments were run to determine the amount of hydrogen taken up during electroplating using 35 by 75 mm coupons of 300M steel, heat-treated to the 1900 to 2100 MPa (280 to 300 ksi) strength level. The coupons were 2, 4, or 6 mm thick. They were cadmium electroplated in

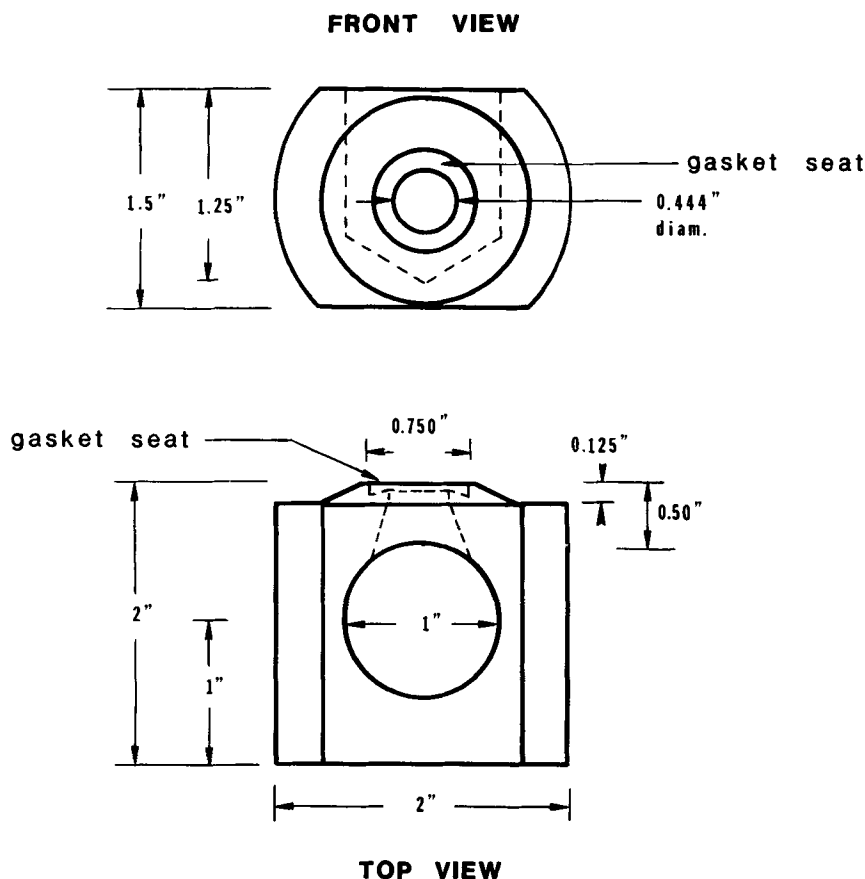


FIG. 1—Drawing of the BE cell.

batches of nine specimens each to a thickness of approximately $15\text{ }\mu\text{m}$ (0.0005 in.) from a cyanide bath containing brighteners and baked at 190°C (375°F). Each batch contained three specimens of each thickness (2, 4, or 6 mm), one for each baking time (0, 24, and 48 h), arranged randomly in the plating rack. The cadmium was removed by swabbing the area to be measured with ammonium nitrate solution and by abrading lightly with Scotch-Brite. The time required to remove the plating and set up the cell for the measurement was controlled to less than 10 min. Two measurements were made on each specimen, and the average 30-min reading was used as the reported value. Background measurements were made on either unplated or plated and stripped specimens. These were kept over a desiccant for at least two weeks before measuring. Further procedural details can be found elsewhere [8].

Results and Discussion

Current Density Versus Hydrogen Concentration

As stated earlier, there are limitations to the use of Eq 1 for calculating the hydrogen concentration from the extraction current density. It has been shown [8] that this relationship holds for relatively high hydrogen concentrations, such as those obtained by cathodic charging or plating.

However, certain assumptions have been made [8,9] concerning boundary conditions in the derivation of Eq 1. Also, it is assumed in Eq 1 that all the current is due to the oxidation of hydrogen. This is a good approximation at relatively high hydrogen concentrations because contributions due to oxidation or passivation of the steel are relatively small and can be neglected. At low values, however, these contributions become significant and must be considered. From Eq 1, a plot of $\log J$ versus $\log t$ gives a straight line of slope $-1/2$ for the hydrogen oxidation reaction. The passivating reaction, on the other hand, has been shown to exhibit a slope of -1 [12].

If the just-cited assumptions are valid, the log-log slope for the BE measurement should be $-1/2$. As can be seen in Table 1, this is not always the case. The slopes for the unbaked specimens do adhere to Eq 1, but become steeper for lower levels of hydrogen (longer baking times), indicating a greater contribution from the passivating (or other) reaction. In actual practice, therefore, it can be seen that the slope of the extraction curve is a function of the hydrogen concentration, varying from -0.5 for the plated and unbaked condition to -0.8 for the background. Therefore, it is not possible to calculate the hydrogen concentration using Eq 1 with any degree of accuracy except in the case of relatively high values. This does not mean, however, that the method is not applicable at low hydrogen concentrations; to the contrary, it has been shown [8,10] that the BE measurement (current density) does give good correlations with mechanical (embrittlement) tests for very low hydrogen concentrations (<0.1 ppm). Therefore, in this paper, the terms, "30-min reading" and "hydrogen concentration" are used interchangeably.

Hydrogen Concentration and Specimen Thickness

When measuring hydrogen in plated laboratory specimens which are small and thin, the question of relevance to large parts often arises. In order to correlate the BE measurements with specimen bulk, three thicknesses of 300M steel coupons were plated under the same conditions. Since the surface area does not change significantly with a change in thickness, the total amount of hydrogen taken up will be essentially constant. The volume, on the other hand, will change significantly, resulting in a similar change in hydrogen concentration. Hence, the hydrogen concentration should be inversely proportional to the thickness.

The average BE measurements, after plating, for three specimens of each thickness is given in the first column of Table 2. It can be seen that the hydrogen concentration (current density) falls off with thickness as expected. Because both the area and volume change with thickness in these specimens, a more exact comparison of these results is shown in Fig. 2 in which the average current densities from Column 1 of Table 2 are plotted against the volume to area ratio. The good agreement shows that comparisons can be made between thin and thick specimens. It

TABLE 1—Log-log slopes of BE extraction curves as a function of the hydrogen concentration.

Baking Time, h ^b	BE Measurement ^a	
	$\mu\text{A}/\text{cm}^2$	Slope
0	0.60	0.52
48	0.45	0.63
72	0.42	0.67
96	0.38	0.67

^aAverage of four specimens each. Background values average $0.35 \mu\text{A}/\text{cm}^2$ with a slope of -0.82 .

^bBaking temperature, 190°C .

TABLE 2—*Hydrogen concentration of cadmium-plated 300M steel coupons as a function of specimen thickness and baking time at 190°C.*

Baking Time, h	0		24		48	
Thickness, mm	Hydrogen Concentration, $\mu\text{A}/\text{cm}^2$ ^a					
	\bar{X}	s	\bar{X}	s	\bar{X}	s
2	0.65	0.025	0.56	0.048	0.46	0.070
4	0.55	0.033	0.52	0.059	0.44	0.062
6	0.47	0.103	0.48	0.042	0.43	0.046

^a \bar{X} and s are three-specimen averages and standard deviations, respectively.

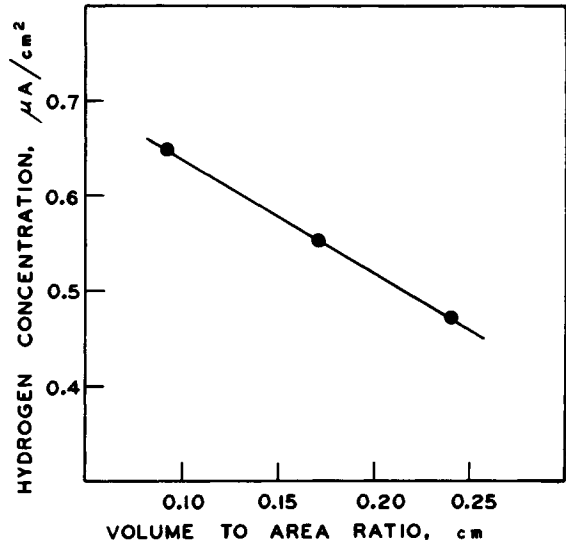


FIG. 2—*The BE determination as a function of specimen bulk for cadmium-plated 300M steel coupons, 2, 4, and 6 mm thick.*

should also be noted that this experiment confirms that the electrochemical measurement is that of a bulk, rather than just a surface property, and that it is related to the hydrogen concentration.

The results of the hydrogen measurements for the baked specimens are also shown in Table 2. After the 48-h bake, all were at about the same level, far from completely baked out. As was reported earlier [10], over 100 h of baking would be needed due to the barrier effect of the cadmium plate.

It is apparent from the data in Table 2 that, for both the unbaked and baked specimens, the reproducibility among specimens having the same treatment is very good, as evidenced by the standard deviations.

Sensitivity

Two examples with 300M steel from previous work will illustrate the sensitivity of the method. Results from a study of the effect of short baking on cadmium-plated coupons are

given in Table 3 [10]. An increase in hydrogen concentration is seen after baking for 2 h, presumably because some of the hydrogen which was codeposited with the cadmium is preferentially driven into the steel during baking. This subject is currently under further investigation. In another experiment in which cadmium-plated specimens were subjected to sustained-load testing [10], an increase in hydrogen concentration is seen after stressing (Table 4). Again, the hydrogen can be assumed to come from the cadmium. In both of these studies, either the changes were small or the hydrogen concentrations were near the background levels. In spite of these limitations, the differences in the average values were shown to be statistically significant at the 95% confidence level [10]. Again, the reproducibility (standard deviation) was very good.

Conclusions

It has been shown that the BE method is a simple, precise, and sensitive way to determine diffusible hydrogen in steels and can be used for a variety of problems. Once correlations with mechanical tests have been made, the rapid BE method using coupons can be used in place of time-consuming mechanical tests using tension specimens, thus reducing testing time and costs.

The method is applicable to quality control in processing, or to detect changes in hydrogen content in service, especially to high-strength, low-alloy steels which have relatively high hydrogen diffusivities and low background currents.

TABLE 3—*Hydrogen concentrations of cadmium-plated 300M steel coupons upon short baking at 190°C.*

Baking Time, h	Hydrogen Concentration, $\mu\text{A}/\text{cm}^2$ ^a	
	Avg	Standard Deviation
0	0.43	0.031
1	0.43	0.063
2	0.53	0.029
4	0.52	0.039

^aFour specimens each.

TABLE 4—*Effect of stressing on the hydrogen concentration of cadmium-plated 300M steel tension specimens.*

Baking Time, h ^a	72		96	
	Hydrogen Concentration, $\mu\text{A}/\text{cm}^2$			
	Avg	Standard Deviation	Avg	Standard Deviation
Unstressed ^b	0.42	0.073	0.38	0.037
Stressed ^c	0.52	0.070	0.44	0.056

^aBaking temperature, 190°C.

^bFour specimens each.

^cSix specimens each.

In studies with cadmium-plated 300M steel, it has been shown that: (1) the BE measurement correlates well with a hydrogen distribution throughout the specimen and is not just a surface effect; (2) long baking is needed to remove all the hydrogen; and (3) tensile stress causes an increase in hydrogen concentration.

A modification of the barnacle electrode method in which the specimen is immersed instead of being clamped has also been reported [13]. This adaptation would be especially suitable for small parts such as fasteners. In this case it would be advisable to use a cylindrical nickel/nickel oxide electrode. Though the mathematics of diffusion would differ from that cited, the empirical treatment would be the same.

Acknowledgments

The authors thank L. Biggs and P. Sabatini for their able assistance, W. Worden for making the cell, and J. J. De Luccia for helpful suggestions.

References

- [1] *Hydrogen Embrittlement Testing*, ASTM STP 543, Raymond, L., Ed., American Society for Testing and Materials, Philadelphia, 1974.
- [2] *Hydrogen Effects in Metals*, Bernstein, I. M. and Thompson, A. W., Eds., The Metallurgical Society of AIME, Warrendale, PA, 1981.
- [3] *Current Solutions to Hydrogen Problems in Steels*, Interrante, C. G. and Pressouyre, G. M., Eds., American Society for Metals, Metals Park, OH, 1982.
- [4] Interrante, C. G. in *Current Solutions to Hydrogen Problems in Steels*, American Society for Metals, Metals Park, OH, 1982, pp. 3-17.
- [5] Devanathan, M. A. V. and Stachurski, Z., *Proceedings of the Royal Society*, Vol. A270, 1962, pp. 90-102.
- [6] Devanathan, M. A. V., Stachurski, Z., and Beck, W., *Journal of the Electrochemical Society*, Vol. 110, 1963, pp. 886-891.
- [7] Berman, D. A., Beck, W. and DeLuccia, J. J. in *Hydrogen in Metals*, I. M. Bernstein, and A. W. Thompson, Eds., American Society for Metals, Metals Park, OH, 1974, pp. 595-607.
- [8] DeLuccia, J. J. and Berman, D. A. in *Electrochemical Corrosion Testing*, ASTM STP 727, F. Mansfeld and U. Bertocci, Eds., American Society for Testing and Materials, Philadelphia, 1981, pp. 256-273.
- [9] Bockris, J. O'M., Genshaw, M. A., and Fullenwider, M., *Electrochimica Acta*, Vol. 15, 1970, pp. 47-60.
- [10] Berman, D. A., *Materials Performance*, Nov. 1985, pp. 36-41.
- [11] Mansfeld, F., Jeanjaquet, S. and Roe, D. K., *Materials Performance*, Feb. 1982, pp. 35-38.
- [12] Jones, D. A. and Greene, N. D., *Corrosion*, Vol. 22, 1966, pp. 198-205.
- [13] Savage, W. F. and Nippes, E. F., "Development and Qualification of Methods for the Determination of Diffusible Hydrogen Content in Weldments," Interim Technical Report, 1 July 1977 to 30 June 1980, Office of Naval Research Contract No. N00014-75-C-0944, NR 031-780, Rensselaer Polytechnic Institute, Troy, NY, 1980.

The Development of an In-Situ Sensor for Measuring the Hydrogen Content of Liquid Iron

REFERENCE: Ohtsubo, T., Kawase, H., and Yamazaki, S., "The Development of an In-Situ Sensor for Measuring the Hydrogen Content of Liquid Iron," *Hydrogen Embrittlement: Prevention and Control*, ASTM STP 962, L. Raymond, Ed., American Society for Testing and Materials, Philadelphia, 1988, pp. 105-116.

ABSTRACT: For in-situ measurement of the hydrogen content of liquid iron, a new inert gas probe technique has been developed which consists of injection of inert gas into molten iron through a nozzle, collection of the ascending bubbles in which hydrogen partial pressure is in equilibrium with the iron, instantaneous determination of hydrogen concentration in the gas using a mass spectrometer, and conversion of the concentration to hydrogen content in iron by Sievert's law. The experimental result is in good agreement with the theoretically calculated hydrogen content. Response is quite rapid (~1.5 min). The efficiency of hydrogen recovery by a bubble is affected by the bubble size, the hydrogen concentration, and the ascending distance. The bubble size is determined by the flow rate and the nozzle size.

KEY WORDS: hydrogen, measurement, iron, steel, molten metal, chemical analysis, in-situ measurement

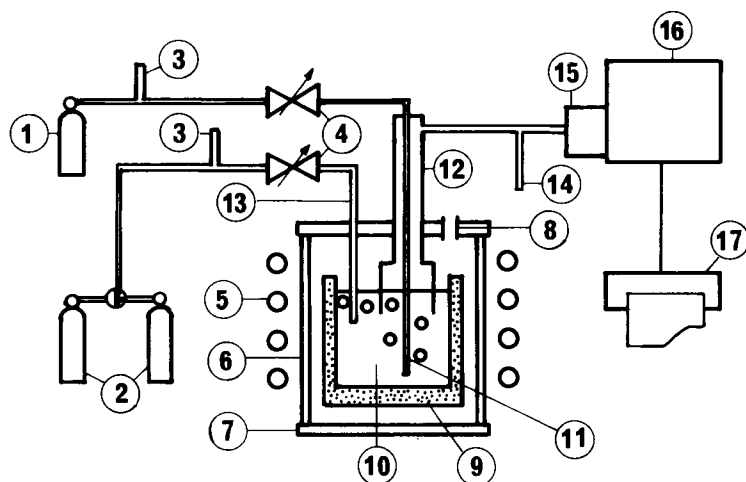
In the steel industry, the recent development of the direct rolling process—without cooling and reheating—of continuously cast iron [1,2] and the accelerated cooling process after controlled rolling for thick plates [3,4] has decreased the chances for removing hydrogen from the cast iron and the plates before and after rolling. A degassing system in the steelmaking process is, therefore, essential for these processes to prevent hydrogen-caused ultrasonic testing (UST) defects in as-rolled products. The need for the in-situ determination of hydrogen in molten steel has become urgent in order to make it possible to carry out the degassing operation at the optimum condition. The conventional method, which consists of sampling with a quartz tube [5], quenching in water, cutting, grinding, and fusion followed by thermal conductivity detector (TCD) determination [6], takes more than 10 min after sampling; moreover, it has been pointed out that the result obtained by this method is not very accurate because of hydrogen escape during and after sampling. The purpose of the present paper is to develop a method for in-situ measurement of hydrogen in molten iron and steel.

Experimental Apparatus and Procedure

Determination of Gas Concentration

The experimental apparatus is shown in Fig. 1. Nine hundred grams of pure iron (O: ~160 ppm, C: 80 ppm, N: ~40 ppm, and B: 1 ppm) in an alumina crucible [inner diameter (ID)

¹Chief researcher, senior researcher, and chemist, respectively, Nippon Steel Corp., R & D Labs, Kawasaki-City, Japan, 210.



1. Ar, 2. blowing gas, 3. flowmeter, 4. flow valve, 5. induction furnace, 6. quartz tube, 7. jacket, 8. gas outlet, 9. crucible, 10. molten iron, 11. nozzle, 12. collector, 13. nozzle, 14. bypass, 15. capillary, 16. mass analyzer, 17. recorder

FIG. 1—Experimental apparatus.

45 mm] was melted in a quartz tube with an induction furnace (8 kVA), and the hydrogen content was kept at a constant level by blowing Ar/H₂ mixture gases (1.05% H₂, 1.05% N₂, 1% He, balance Ar and 2.12% H₂, 5.25% N₂, 1% He, balance Ar) at a rate of 1200 N cm³/min through a high purity alumina tube (immersion depth: 10 mm). A gas probe consists of an argon (Ar) carrier gas injection nozzle (Type A: outer diameter (OD) 6 mm, ID 1.2 mm; Type B: OD 2 mm, ID 1.2 mm, high purity alumina), a gas collector (Fig. 2) made of boron nitride (OD 25 mm, ID 20 mm, and 600 mm in length), and a metal cap with a gas outlet, connected to each other by means of a Viton o-ring at the top of the collector. Boron nitride (BN) was selected after preliminary tests on gas-tight and antiheat shock properties, and high-purity alumina was used only for a small section part because of its poor antiheat shock property. The probe was immersed in the molten iron (immersion depth: 40 mm for nozzle, 5 mm for collector), and pure Ar carrier gas was injected at a rate of 50 to 200 N cm³/min. The collected gas in the collector was taken out through a copper tube (ID 2 mm, length = 5 m), and a portion of the gas (approximately 2 mL/min) was analyzed by a quadrupole mass spectrometer (vacuum: 10⁻⁶ torr). Whenever helium (He) was detected in the gas, the result was rejected because it has no solubil-

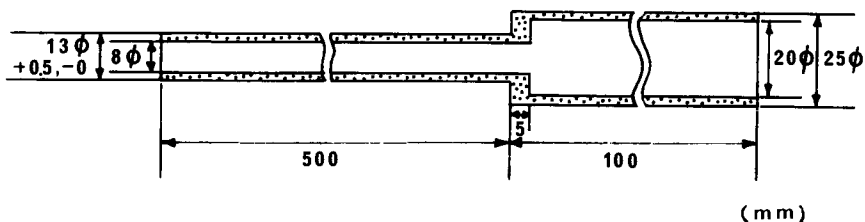


FIG. 2—Gas collector.

ity in iron and the detection of He suggests a shortcut from the blowing gas to the carrier gas. The calibration was made using the Ar/H₂/N₂ mixture gases, and the time-dependent drift in the sensitivity of the mass spectrometer was cancelled by monitoring the peak intensity of neon (Ne), which was always introduced to the spectrometer through a constant leak.

Determination of Bubble Size

The frequency of the bubble formation was determined using the apparatus shown in Fig. 3 in order to obtain the size of the bubble for the discussion of degassing kinetics. The flow rate of the carrier gas was determined by a mass flow meter which was previously calibrated with a soap solution flow meter. The frequency of the pressure change in the gas line was measured by means of a crystal earphone whose output (> 10 mV) was recorded by an oscillograph. The Ar gas was injected to the molten iron heated at 1600°C (nozzle Type A or B) at a rate of 15 to 500 N cm³/min without preheating.

Results and Discussion

Blank test

In order to investigate the possible interference from permeation of gases through the collector wall at high temperature (approximately 1600°C), the normal gas collector was replaced with a blank collector whose bottom was sealed by a BN plate with the same thickness as the wall. The blank collector was immersed into molten iron (flow rate: 200 N cm³/min for the Ar carrier and 1200 N cm³/min for Ar/2.12% H₂/5.25% N₂ mixture gas). The hydrogen content in the Ar carrier gas taken from the immersed blank collector was determined as $8.2 \times 10^{-3}\%$. Thus the blank value, including permeated hydrogen, if any, was negligibly small compared with the hydrogen content in the injected-and-collected gas (more than 0.2%), as shown later.

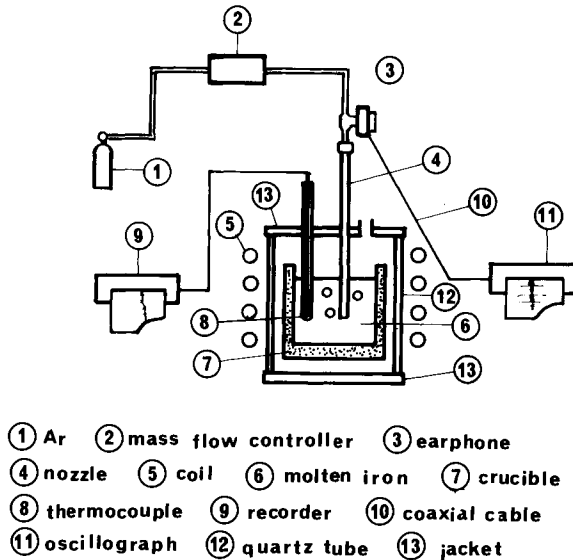


FIG. 3—Apparatus for the determination of the frequency of bubble formation.

Nitrogen Determination

Figure 4 shows the changes of the nitrogen content [obtained from the peak intensity at mass-to-charge ratio (m/e) = 14 for N_2^{2+}] and the carbon monoxide (calculated from the peak intensity at m/e = 28 for CO^+ and N_2^+ , and that at m/e = 14 for N_2^{2+}) as compared to the change of the nitrogen content in the blowing gas (1.05 to 5.25 and to 1.05% again). For this experiment, a Type A nozzle was used for the carrier gas injection.

From the figure the following is obvious:

1. No relationship is observed between the nitrogen content of the blowing gas and that of the collected carrier gas, and the latter decreases when the flow rate of the carrier gas is increased and increases when the flow rate decreased.
2. A remarkable amount of carbon monoxide is detected, but this amount decreases consistently according to the bubbling time, indifferent of the flow rate.

The extensively increased nitrogen content of the collected carrier gas is attributed to the decomposition of BN caused by bubbling in molten iron. This is supported by the facts that the boron content in the iron sample increased from 0 to 0.3% and that the wall of the collector made of BN was eroded at the immersion end. If we assume that this erosion occurs depending on the flow rate of the blowing gas (this flow rate is greater than that of the carrier gas), the change of the nitrogen content according to the flow rate change of the carrier gas can be explained as a dilution effect. And the analytical time lag is estimated as 1.5 to 2 min from the time between the flow rate change and the observed content change. The independence of the nitrogen content of the collected carrier gas on that of the blowing gas proves that no short-circuit gas flow occurred owing to the He detection-and-reject system.

The carbon monoxide is attributed to oxygen (approx. 160 ppm) and carbon (80 ppm) in the original iron (C content after blowing: 20 ppm). The reason why the flow rate dependence was not found is not clear.

Hydrogen Determination

The hydrogen content of blowing gas was changed from 1.05 to 2.12 and to 1.05% again by switching the source gas valve, and the change of the hydrogen content in the injected-and-

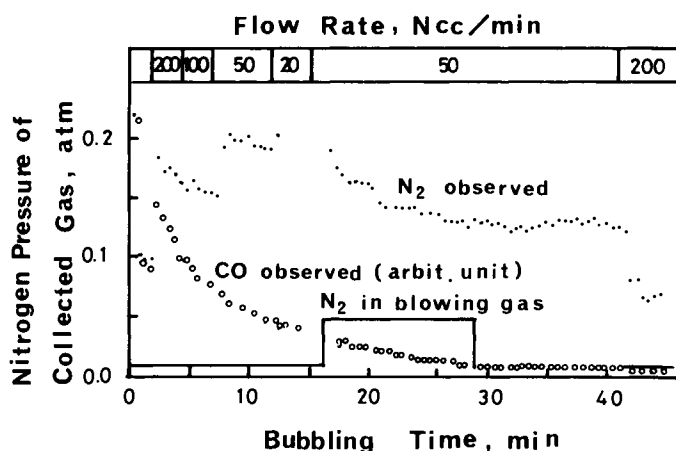


FIG. 4—Time-dependent change of nitrogen pressure in injected-and-collected gas in comparison with blowing gas change.

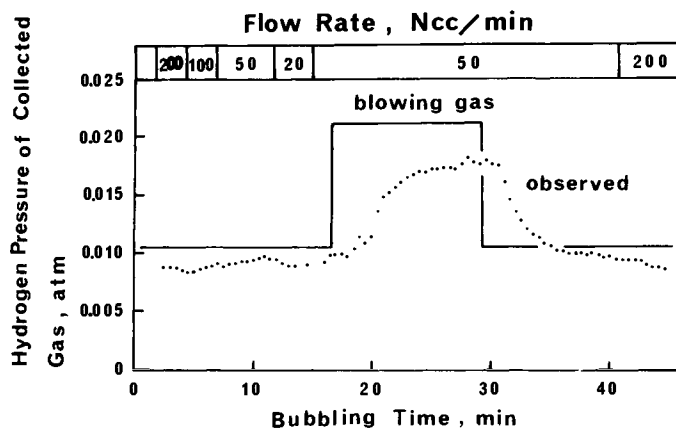


FIG. 5—Time-dependent change of hydrogen pressure in injected-and-collected gas in comparison with reference to blowing gas change.

collected Ar carrier gas was determined continuously. From the result (Fig. 5) the following can be pointed out:

1. The hydrogen pressure of the collected gas changes according to that of the blowing gas. Therefore, this technique can be used as an analytical means.
2. The analytical time lag is estimated as about 1.5 min from the time differences at increasing and decreasing points.
3. The change of hydrogen pressure of the collected gas is not so sharp as that of blowing gas. This may be attributed to the time required for the equilibrium and also to the time required for the changeover of the gas within the collector. This point will be discussed later in more detail.
4. The effect of the flow rate of the carrier gas is small. This is explained mainly by the fact that the hydrogen transfer rate is high enough for the flow rate range and that the flow rate of the blowing gas ($1200 \text{ N cm}^3/\text{min}$) is high enough to recover most of the hydrogen amount which is removed by the carrier gas (50 to $200 \text{ N cm}^3/\text{min}$).
5. The hydrogen pressure of the collected gas changes in proportion to that of the blowing gas; however, the former is not exactly equal to the latter. This point will also be discussed later.

Regarding the time lag, the capacity of the collector and the copper tube is 25 cm^3 and 15 cm^3 , respectively, and the flow rate at the end of the copper tube was measured as approximately $30 \text{ N cm}^3/\text{min}$ when the injection flow rate was greater than $50 \text{ N cm}^3/\text{min}$, the balance overflowing from the collector. The calculated delivery time ($25 + 15/30 = 1.3$) is nearly equal to the observed time lag; therefore, the time lag is attributed to the transfer time to the analyzer through the copper tube. The time lag can be optimized in consideration of the diameter (conductance) of the tube and the volume in it.

Results of the several experiments using different flow rates are shown in Fig. 6. The abscissa at the top of the figure is given in hydrogen content (ppm) of iron calculated by Sievert's equation

$$[H] = K\sqrt{P_{H_2}} \quad (1)$$

$$\log K = -1900/T - 1.577 \text{ [Ref 7]} \quad (2)$$

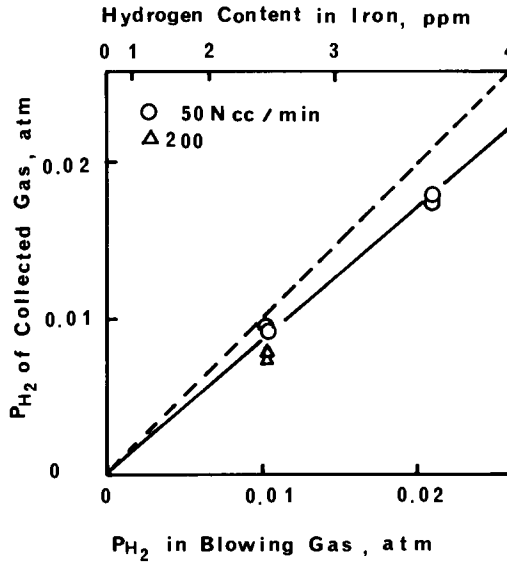


FIG. 6—Relationship of hydrogen pressure of blowing gas and injected-and-collected gas.

where

- [H] = hydrogen solubility in iron, %,
 P_{H_2} = hydrogen partial pressure in gas phase, atm,
 K = equilibrium constant, % · atm^{-1/2}, and
 T = temperature of molten iron, Kelvin.

A good relationship between the hydrogen content in the blowing gas and that in the collected gas is found over the range from 0 to 2% in gas (0 to 4 ppm in iron). A small difference caused by the difference of the flow rate is observed. The flow rate is considered to determine the size and number of ascending bubbles, thus the transfer rate to a bubble and the total removal rate of hydrogen.

Determination of Bubble Size

The bubble size (at the surface of liquid) can be determined by the frequency of the bubble formation and the flow rate using the following equation:

$$d_B = \left(\frac{6V_B}{\pi} \right)^{1/3}$$

$$= \left(\frac{6V_g}{\pi f} \right)^{1/3} \quad (3)$$

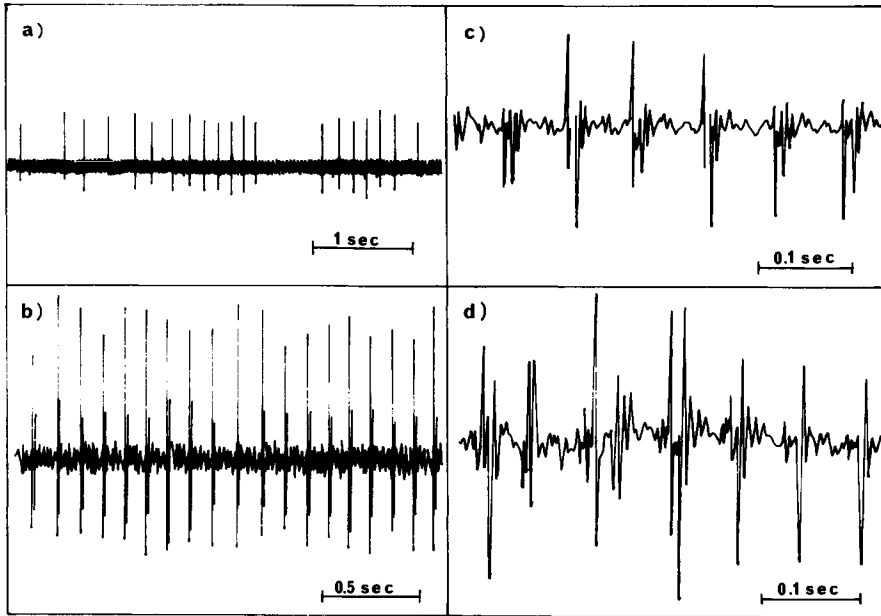
where

- d_B = diameter of gas bubble, cm,
 f = frequency of bubble formation,
 V_B = volume of gas bubble, cm³, and
 V_g = gas flow rate, cm³/s.

Some examples of the frequency determination are shown in Fig. 7. By Nozzle A, when the flow rate is low (a) the bubble formation occurs irregularly but cyclically and regularly at the flow rate greater than 40 N cm³/min (b, c, and d). And by Nozzle B, the critical flow rate is 100 N cm³/min. The frequency at the regular bubble formation is approximately 10 to 20 Hz. The diameter of the bubble was calculated based on the experimental results obtained by a nozzle facing downward (Fig. 8). In the lower flow rate range, the average of the measured frequencies was used. According to the figure, by Nozzle A the diameter is constant (= 1 cm) if the flow rate is smaller than 50 N cm³/min (≈ 5 cm³/s at 1600°C), but it gradually increases when the flow rate is increased and Nozzle B is slightly effective in making smaller bubbles for the flow rate range lower than 200 N cm³/min. For comparison, the theoretical lines calculated from Eq 4, obtained [8] and verified for mercury and liquid silver [9], and Eq 5, obtained for molten iron [10], both using a nozzle facing downward, are shown in the figure.

$$d_B = \left[\frac{3\sigma d_{no}}{\rho g} + \left(\frac{9\sigma^2 d_{no}^2}{\rho^2 g^2} + \frac{10 V_g^2 d_{no}}{g} \right)^{1/2} \right]^{1/3} \quad (4)$$

$$d_B = \left\{ \left(\frac{6\sigma d_{no}}{\rho g} \right)^2 + [0.54(V_g d_{no}^{0.5})^{0.289}]^6 \right\}^{1/6} \quad (5)$$



a) $V_g = 16.7 \text{ Ncc/min} = 1.90 \text{ cc/sec}$ (at 1600°C)

b) $V_g = 46.7 \text{ Ncc/min} = 5.34 \text{ cc/sec}$ (at 1600°C)

c) $V_g = 182 \text{ Ncc/min} = 20.8 \text{ cc/sec}$ (at 1600°C)

d) $V_g = 364 \text{ Ncc/min} = 41.6 \text{ cc/sec}$ (at 1600°C)

FIG. 7—Frequency determination of bubble formation.

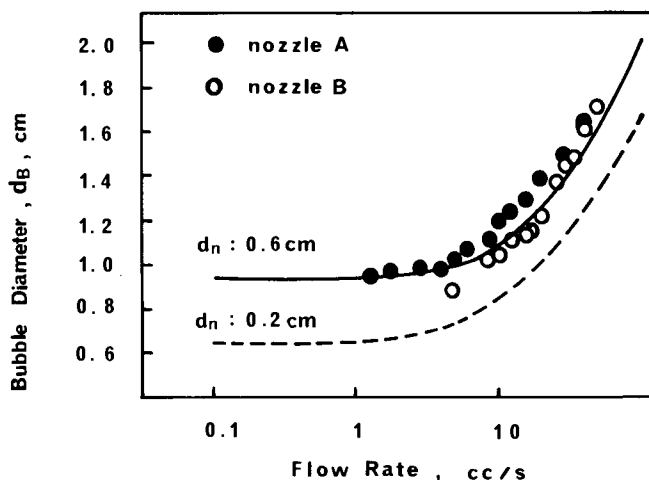


FIG. 8—Relationship between flow rate and bubble diameter.

where

σ = surface tension, dyne/cm,
 d_{no} = outer diameter of nozzle, cm,
 ρ = density of liquid, g/cm³, and
 g = constant of gravitation, cm/s².

In calculation, the following values were used as constants:

$\rho = 7.17 \text{ g/cm}^3$ [11],
 $\sigma = 1600 \text{ dyne/cm}$ (at O = 50 ppm) [12],
 $d_{no} = 0.6 \text{ cm}$ for Nozzle A, and
 $d_{no} = 0.2 \text{ cm}$ for Nozzle B.

The result calculated by Eq 5 is almost equal to that of Eq 4; therefore, only two lines are shown in Fig. 8. From the figure, it is clear that the size of the bubble is 1.0 to 1.8 cm, and for the practical flow rate range (60 ~ 300 N cm³/min) it is nearly equal to 1 cm and the variation is small; the experimental results by Nozzle A nearly fit the calculated line while the results by Nozzle B do not. Although this result suggests that for the downward facing nozzle the reduction of the outer diameter is not so effective in making smaller bubbles as in the case of the upward facing nozzle, but this is not conclusive at this stage because the vibration of the nozzles was observed during argon bubbling using both Nozzle A and Nozzle B.

Kinetics of Degassing Reaction

In general, the degassing reaction by inert gas is controlled by one or two of the following three rate determining steps [13, 14]:

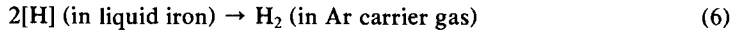
1. Liquid phase mass transfer at the liquid-gas interface.
2. Chemical reaction (formation of hydrogen molecule) at the interface.
3. Gas phase mass transfer at the interface.

The rate of the dehydrogenation from molten iron by inert gas bubbles has not been studied. Pehlke and Bement [15] studied the dehydrogenation from molten aluminum by Ar injection,

but detailed theoretical discussion was not made. Mori et al. [13] made a study on the rate of oxygen removal from molten silver by inert gas flushing from a nozzle immersed facing upward, the dimension of the nozzle and the immersion depth being similar to those of the present study. According to their conclusion, the rate data were consistent with the model describing the liquid-phase mass transfer during the bubble formation at the nozzle and the bubble ascent in the melt. Ban-ya et al. [14] studied the rate of hydrogen desorption from the liquid iron surface by the carrier gas method using Ar. According to them the rate of hydrogen desorption is controlled by the liquid-phase mass transfer at the liquid-gas interface.

It would be reasonable to assume that the rate determining step of the dehydrogenation in the present study is also the liquid-phase mass transfer based on the just-mentioned studies.

For the dehydrogenation reaction (Eq 6) at the free surface of metal, controlled by the liquid-phase mass transfer, the rate is shown by Eq 7



$$-\frac{dn_{\text{H}}}{dt} = S k_L (C_B - C_S) \quad (7)$$

where

- n_{H} = amount of removed hydrogen atom, mol,
- t = reaction time, s,
- S = area of reaction interface, cm^2 ,
- k_L = mass transfer coefficient, cm/s ,
- C_B = hydrogen content of bulk iron, mol/cm^3 , and
- C_S = hydrogen content of iron layer at interface, mol/cm^3 .

Further, according to Mori et al.'s mathematical derivation [13] for deoxidation by a single ascending bubble, the rate for dehydrogenation by a single ascending bubble is shown by Eq 8

$$-\frac{dn_{\text{H}_2}}{dx} = \frac{2(D_L \pi)^{1/2}}{(0.5g)^{1/4}} \cdot \frac{\rho}{100 M_{\text{H}_2}} \cdot d_B^{5/4} ([\text{H}] - [\text{H}]_e) \quad (8)$$

where

- n_{H_2} = amount of removed hydrogen molecule in bubble, mol,
- x = ascent distance of bubble from nozzle tip, cm,
- D_L = diffusivity in liquid phase, cm^2/s ,
- g = constant of gravitation, cm/s^2 ,
- ρ = density of liquid, g/cm^3 ,
- M_{H_2} = molecular weight of hydrogen, g/mol ,
- d_B = diameter of bubble, cm,
- $[\text{H}]$ = hydrogen concentration in liquid iron, wt%, and
- $[\text{H}]_e$ = hydrogen concentration in liquid iron in equilibrium with hydrogen partial pressure in bubble, wt%.

Here, $[\text{H}]_e$ and the partial hydrogen pressure in an ascending bubble at ascent Distance x are shown as follows

$$[\text{H}]_e = K \left\{ P_o + \frac{\rho g(h-x)}{1.013 \times 10^6} \right\} \cdot \frac{n_{\text{H}_2}}{n_{\text{Ar}} + n_{\text{H}_2}} \quad (9)$$

$$P_{H_2} = \left\{ P_o + \frac{\rho g(h-x)}{1.013 \times 10^6} \right\} \cdot \frac{n_{H_2}}{n_{Ar} + n_{H_2}} \quad (10)$$

where

P_o = atmospheric pressure, atm,

h = immersion depth, cm, and

n_{Ar} = amount of removed argon, mol.

The relation between P_{H_2} and x was obtained from Eqs 8, 9, and 10 using a numerical calculation by the Runge-Kutta-Gill method, and constants $D_L = 1.05 \times 10^{-3}$ cm²/s at 1600°C [16], $\rho = 8.17$ g/cm³ at 1600°C [11], and $k = 0.00256$ wt% at 1600°C [7].

Based on the just-cited calculation, the efficiency of dehydrogenation is given as follows

$$f_H = \frac{P_{H_2}}{P_{H_{2i}}} = \frac{\left\{ P_o + \frac{\rho g(h-x)}{1.013 \times 10^6} \right\} \frac{n_{H_2}}{n_{Ar} + n_{H_2}}}{[H]^2/K^2} \quad (11)$$

where $P_{H_{2i}}$ = hydrogen partial pressure in blowing gas, atm.

In Fig. 9 the relationship between the ascent distance x and the dehydrogenation efficiency f_H is shown for various hydrogen concentrations ($[H] = 2, 6,$ and 10 ppm), various bubble sizes ($d_B = 1.0$ and 1.5 cm), and immersion depth $h = 4$ cm. From the figure it is evident that all of the three parameters influence the efficiency. The bubble size in the practical flow rate range is approximately 1 cm as just shown; so, referring to the solid lines, very high efficiency (95%) can be expected for iron containing 10 ppm of hydrogen if the ascending distance is set as 4 cm. The

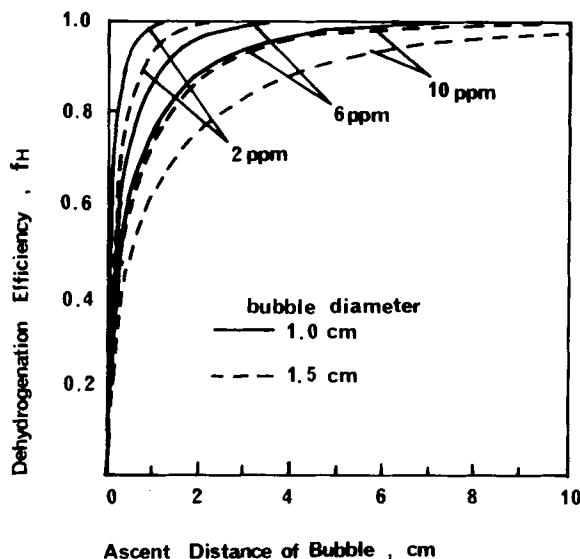


FIG. 9—Relationship between bubble ascent distance and dehydrogenation efficiency.

hydrogen content which was tested experimentally by the present study is not so high as the contents used for the calculation, but within the limit the test results show very high efficiency and good agreement with the calculated results and support the assumption that the rate-determining process is the mass transfer in liquid phase at the interface on which the calculation was made.

The comparison was also made (Fig. 10) for the hydrogen decrease in the collected carrier gas when the hydrogen concentration in the blowing gas was changed from 2.12 to 1.05% (experimental conditions: weight of iron = 900 g, immersion depth = 4 cm, ascending distance = 4 cm, Nozzle A, $d_{no} = 0.6$ cm, flow rate of carrier gas = 50 N cm³/min). In drawing the calculated results, the analytical time lag (from collector to detection) of 1.5 min (found in Fig. 5) was taken into consideration. It is clear that the hydrogen concentration in the collected carrier gas changes quickly, corresponding to the blowing gas change, and the decrease of the concentration is similar to the calculated line. The slight difference of [H] between observed and calculated is found again but is consistent with Fig. 6. This incomplete recovery is attributed to:

1. Incomplete supply of hydrogen to molten iron because of insufficiently high flow rate ($1200/200 = 6$) and of insufficiently deep immersion ($h = 1$ cm).
2. Overflowing of the carrier gas from the collector and removing hydrogen from the iron surrounding the collector. In the practical application, the former can be neglected and the latter can be solved by the improvement of the collector design and the optimization of the tube diameter.

Conclusion

In order to determine in situ the hydrogen content in molten iron, a new inert gas probe technique has been developed which consists of injection of carrier gas into molten iron through

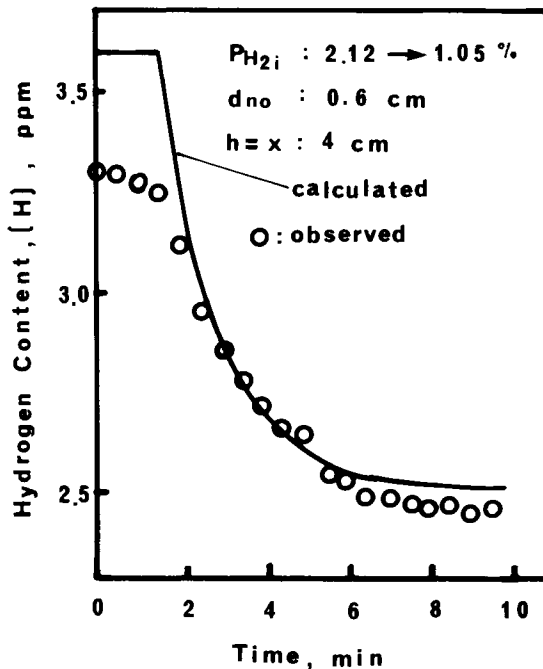


FIG. 10—Hydrogen content change after blowing gas change.

an immersed small nozzle, collection of the gas at the surface of iron by an immersed gas collector, and instantaneous determination of hydrogen content in the gas by means of a gas analyzer. Based on the experiments the following results were obtained:

1. The in situ determination of hydrogen in molten iron is possible by the present method.
2. The rate determining step of the dehydrogenation is the mass transfer process in liquid phase at the interface, but the transfer of hydrogen from iron to a bubble is so rapid that hydrogen concentration in the bubble at the surface is almost equal to the equilibrium value when the carrier gas is injected at the depth of 40 mm and the carrier gas flow rate is about 50 N cm³/min.
3. The hydrogen concentration in molten iron can be obtained from the hydrogen concentration in the collected carrier gas using Sievert's law.
4. The analytical time lag is mainly caused by the gas transfer through a small tube from the collector to the analyzer. By the present apparatus it was approximately 1.5 min, but it can be improved by optimization of the tube diameter.
5. The flow rate and the diameter of the nozzle affect slightly the size of the gas bubble. Higher recovery is obtained with smaller bubbles.

References

- [1] Takemura, Y., Mizoguchi, S., Tsubakibara, O., Kuwabara, T., and Saito, M., *Seitetsu Kenkyu*, No. 310, Dec. 1982, p. 251.
- [2] Tsubakibara, O., Kusano, A., Terada, T., Yamamoto, T., Sirabe, K., and Ohashi, W., *Tetsu-to-Hagane*, Vol. 71, No. 3, 1985, p. 425.
- [3] Matsuda, H., Onoe, Y., Moriyama, K., and Sekine, H., *Seitetsu Kenkyu*, No. 310, Dec. 1982, p. 277.
- [4] Kunioka, K., *Tetsu-to-Hagane*, Vol. 71, No. 3, 1985, p. 513.
- [5] Shigematsu, H. and Yoshida, S., Trans. Japan Institute for Metals, Vol. 24, 1960, p. 359.
- [6] Shanahan, C. E. A. and Cooke, C. F., *Journal of the Iron and Steel Institute*, Vol. 190, 1958, p. 381.
- [7] Ban-ya, S. and Fuwa, T., *Tetsu-to-Hagane*, Vol. 60, 1974, p. 1299.
- [8] Mersmann, A., *V.D.I. Forschungsheft*, Vol. 26B, No. 491, 1962, p. 1.
- [9] Sano, M. and Mori, K., *Tetsu-to-Hagane*, Vol. 60, No. 3, 1974, p. 348.
- [10] Sano, M., Mori, K., and Sato, T., *Tetsu-to-Hagane*, Vol. 63, No. 14, 1977, p. 2308.
- [11] Ogino, K., Adachi, A., and Noshiro, K., *Tetsu-to-Hagane*, Vol. 59, 1973, p. 1237.
- [12] Ogino, K., Noshiro, K., and Koshida, S., *Tetsu-to-Hagane*, Vol. 59, 1973, p. 1380.
- [13] Mori, K., Sano, M., and Hoshino, H., *Tetsu-to-Hagane*, Vol. 61, 1975, p. 182.
- [14] Ban-ya, S., Mori, K., and Tanabe, Y., *Tetsu-to-Hagane*, Vol. 66, 1960, p. 1494.
- [15] Pehlke, R. D. and Bement, A. L., *Transactions of the Metallurgical Society of AIME*, Vol. 224, 1962, p. 1237.
- [16] Bester, H. and Lange, K. W., *Archiv für Eisenhüttenwesen*, Vol. 48, 1977, p. 487.

A Study of the Effect of Voids on Hydrogen Diffusion Through Electroslag Refined Steel

REFERENCE: Wang, M. and Shewmon, P. G., "A Study of the Effect of Voids on Hydrogen Diffusion Through Electroslag Refined Steel," *Hydrogen Embrittlement: Prevention and Control*. ASTM STP 962. L. Raymond, Ed., American Society for Testing and Materials, Philadelphia, 1988, pp. 117-124.

ABSTRACT: Disk-shaped thin specimens made of electroslag refined (ESR) carbon steel were treated with hydrogen at 758 kPa (450 psi) at 600°C for 120, 240, or 432 h to produce microvoids (from methane bubbles) with a diameter of about 0.1 μm and a volume fraction up to 0.2%. Using the two-step replica technique, the size and density of voids were measured. The hydrogen diffusion coefficients of these specimens were determined by an electrochemical permeation method. Different charging current densities were used. The microvoids serve as traps for hydrogen as indicated by the hydrogen diffusion coefficient decreasing as the current density and the void density increased.

KEY WORDS: diffusion, hydrogen, voids, carbon steel, permeability, electrochemistry

Permeation of hydrogen through metals and the concomitant effects on the properties of metals have been the subject of much interesting research. Since Darken and Smith [1] first recognized the essential role of trapping in hydrogen transport in steels, a number of papers related to trapping have been published, leading to rapid progress in this area.

Microvoids are one type of trapping site. But microvoids in body-centered cubic (bcc) metals have not been so easy to observe. Only a few papers have discussed the effect of microvoids on trapping. Boniszewski and Moreton [2] showed that microvoids produced at inclusions in rimming steel by plastic deformation in tension retarded the hydrogen evolution at room temperature, but did not retain hydrogen in the steel permanently. Evans and Rollason [3,4] found a correlation between the volume of microvoids introduced by cold-working and the effective diffusion coefficient of hydrogen in experimental low-carbon steels and free-cutting steel. They showed that trapping was reversible because all entrapped hydrogen desorbed at room temperature. Ellerbrock et al. [5] analyzed the observations on room temperature hydrogen degassing as previously published by a number of investigators. They were able to adequately fit the data by calculating the rate of detrapping of hydrogen from microvoids. Allen-Booth and Hewitt [6] also proposed a model of hydrogen diffusion in iron and steel based upon the assumption of an equilibrium between interstitial hydrogen and hydrogen present as molecular gas in microvoids. Kumnick and Johnson [7] found traps remaining in deformed Armco iron after a recrystallization anneal and suggested that this was due to microvoids, though they could not observe them under the microscope. According to the analysis of Johnson et al. [8], the concentration of molecular hydrogen trapped in pores increases without limit as the lattice concentration C_L increases. Thus, for pores, the effective hydrogen diffusivity decreases as lattice concentration

¹Department of Metallurgical Engineering, Ohio State University, Columbus, OH 43210.

increases. However, the previous work on void trapping did not allow the determination of the dependence of D_{eff} on C_L .

Although in all these papers microvoids were considered to trap hydrogen, the nature of microvoids as trapping sites was still not clear; that is, their binding energy, density, and saturability are not known. In this work the microvoids are produced by hydrogen attack; therefore, the density of microvoids can be varied and controlled. An attempt is made to understand the nature of microvoids from the analysis of the permeation experiment.

Experiment

Specimen Preparation

The composition of the steel used is given in Table 1. Strips of electroslog refined (ESR) steel [thickness = 2.5 mm (0.1 in.)] were cold-rolled to 0.5 mm (0.020 in.) thickness. Round specimens of 2.54 cm (1 in.) diameter were cut from these cold-rolled strips. Then these round specimens were annealed in a tube furnace at 900°C for 1 h in a hydrogen atmosphere. The grain size was ASTM No. 9. After annealing, some specimens were treated with hydrogen at 600°C and 758 kPa (450 psi) for 120, 240, or 432 h. The microvoid density was measured using the two-steps replica technique. For each sample, over 150 fields of view were observed and the number of microvoids counted. Then the average size and density of microvoids were calculated as shown in Table 2.

Permeation Method

All experiments were carried out using an electrochemical cell. Hydrogen was introduced by cathodic charging on the one side of the round specimen while a potentiationstat maintained an anodic potential on the other side high enough to oxidize all the arriving hydrogen atoms. The current flowing in the anodic side of the cell was a direct measure of hydrogen atoms traversing the specimen. Before each experimental run with the steel, a sample of pure iron was run to check the system and procedure. These repeated runs agreed to within 10%. Three runs were made on each steel specimen and the average reported.

TABLE 1—*Composition of the steel.*^a

C	Mn	Si	S	P	Cr	Ni	Cu	Mo	Al	V
0.29	1.04	0.21	0.003	0.014	0.13	0.18	0.24	0.05	0.005	0.002

^a The steel was electroslog refined.

TABLE 2—*Parameters of microvoids in specimens after hydrogen attack.*

HA Time, h	Radius of Microvoid, μm	Volume Density, μm^3	Volume Fracture of Voids, 10^{-5}
0	0.066	0.0049	6.5
120	0.170	0.0170	34
240	0.180	0.0300	72
432	0.220	0.0600	264

After heat treatment the specimens were mechanically and chemically polished to a mirror-like finish and palladium-plated on the anodic surface to prevent iron oxidation. Then the sample was assembled into the cell. The solution on the cathodic side was borate buffer solution ($\text{pH} = 8.45$) and on the anodic side was 0.1 N sodium hydroxide (NaOH). A few specimens with different thickness were prepared to determine the thickness dependence of permeation.

The charging current density was varied from 1.34 to 10 mA/cm^2 . A sequence of transients was made at several temperatures between 25 and 72°C.

Results and Discussion

It is well known that to measure permeation any surface effect (rate control) must be eliminated. The best test of this is the measurement of the steady-state flux as a function of the thickness [9]. The good fit to a linear relation found in Fig. 1 is clear evidence that volume diffusion controls the rate in these experiments. Figure 2 also indicates freedom from the surface control [10].

Permeability values are not influenced by trapping since the permeability is a steady-state characteristic of the material. After hydrogen attack the specimens have a higher trap density and a longer time lag in permeation transient measurements, but the steady-state flux of all

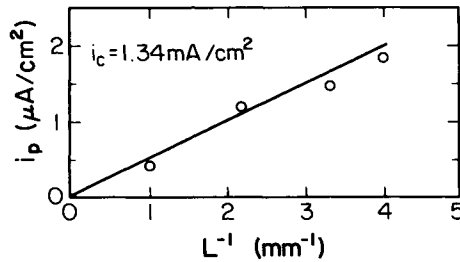


FIG. 1—Permeation current i_p of specimens after 432 h HA as a function of reciprocal thickness L^{-1} .

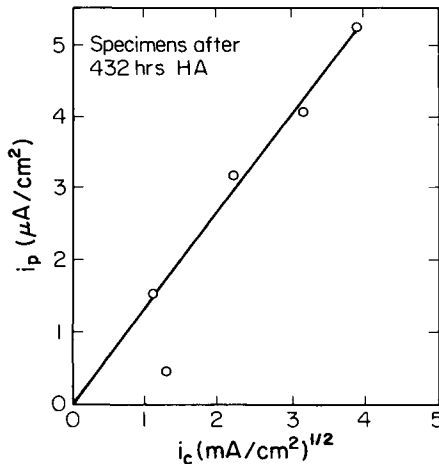


FIG. 2—Variation of the permeation current i_p with the square root of the current density i_c .

specimens was identical within experimental error. An activation energy for permeation of ESR steel was determined from measurements of the steady-state flux as a function of temperature (Fig. 3). The value of 35 ± 2 kJ/mol is what one would expect from the sum of activation energies from self-diffusion (6.5 to 7.0 kJ/mol) and the heat for solution of molecular hydrogen gas from the bubbles into the metal (26.1 kJ/mol) [15].

The effective diffusivity, D_{eff} , was determined by the time-lag method, which is related to the time lag, t_L , for hydrogen to appear at the exit surface by the equation

$$D_{\text{eff}} = L^2/6t_L$$

where L is the thickness of the specimen.

The values of D_{eff} found for the various samples are shown in Fig. 4. The diffusivity of the specimen after 432 h hydrogen attack (HA) is consistently lower than that of the annealed specimen. This shows that the microvoids form important trapping sites in the steel.

Figure 5 shows typical buildup and decay transients. The buildup and decay transients of specimens after 432 h of HA are slower than those of annealed specimens. This can be explained by microvoid trapping. By definition, a trap is a site where hydrogen atoms are preferentially attached. The presence of such traps can retard the movement of hydrogen atoms through the metal. As the density of traps increases, the number of atoms captured by traps also increases. This suggests that the buildup transient curve should be shifted to long times as the density of traps increases. The observed shifting of the buildup transient in Fig. 5 is exactly in this direction. In the specimens subjected to HA for 432 h, the density of microvoids is about 50 times the density of annealed specimens (see Table 2). It is microvoids that cause the shifting of the buildup transient. The same reasoning can be used for decay transients. When charging is interrupted, both lattice dissolved and trapped hydrogen have to be taken out. The trapped volume increases with the density of microvoids. Therefore, the decay transient of specimens after 432 h of exposure takes a longer time than does the decay transient of annealed specimens.

Trapping phenomena may be well characterized by the dependence of D_{eff} on the lattice concentration of hydrogen. Several workers have shown [7,10-12] that D_{eff} of deformed iron increases at higher hydrogen concentration, as would be expected for saturable traps. However, our results show the opposite. Figure 6 shows plots of D_{eff} against the volume density of micro-

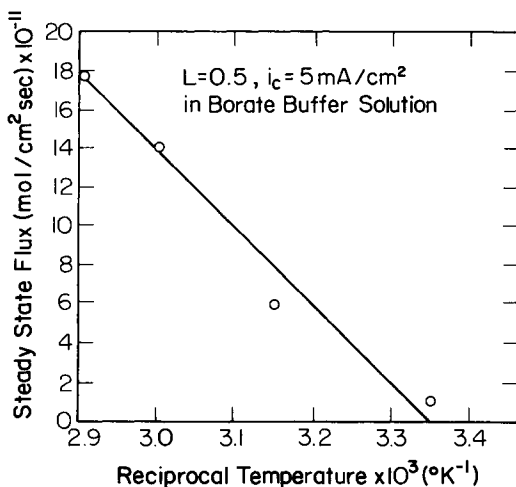


FIG. 3—Steady-state flux as a function of reciprocal temperature.

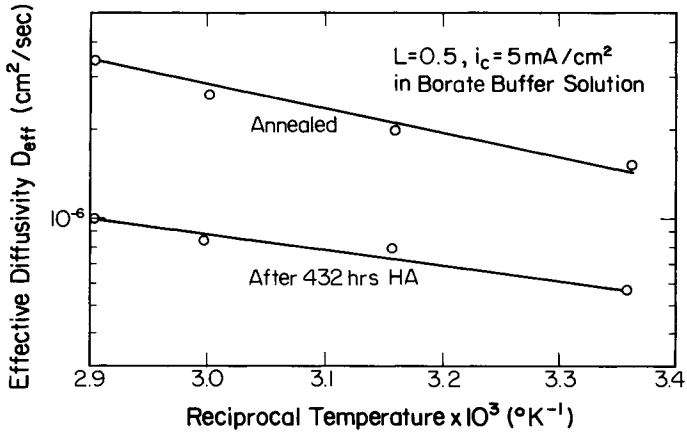


FIG. 4—Effective diffusivity as a function of reciprocal temperature.

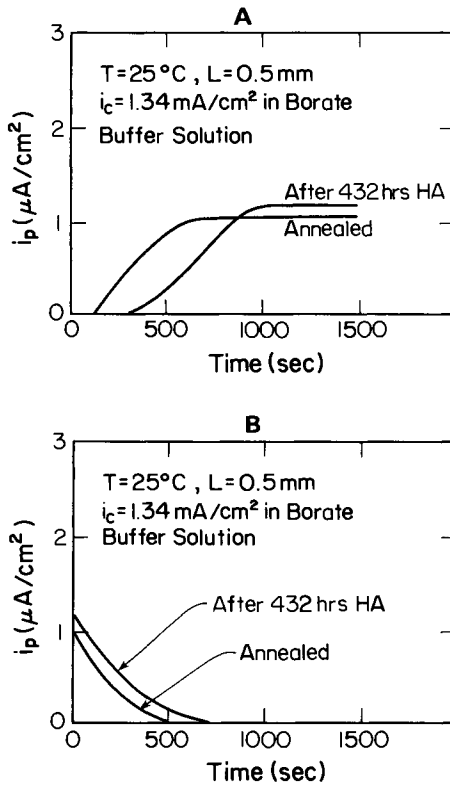


FIG. 5—Typical permeation curves: (A) buildup transient; (B) decay transient.

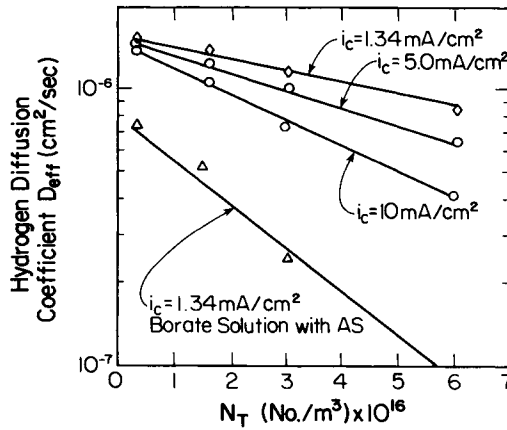


FIG. 6—Linear relationship of hydrogen diffusion coefficient and density of microvoids.

voids at different charging current density. It is clear that the greater the microvoids volume or the larger the charging current density, the lower the effective diffusivity described in Figs. 6 and 7. This is what would be expected for nonsaturable traps such as voids.

In order to increase the concentration of hydrogen in the metal still more, arsenic trioxide was added to the borate buffer solution to a concentration of 10^{-5} g-atom/L. This increased the steady-state flux, but the effective diffusivity of specimens decreased. For example, the effective diffusivity of the specimen after 432 h HA decreased by one order of magnitude (see Fig. 6), and there were no cracks in the specimen. Thus, D_{eff} decreased because of trapping.

The concentration dependence of the diffusivity had been analyzed as mentioned before [8]. For nonsaturable traps, the lattice concentration C_L is related to the trap concentration C_T by the equation

$$C_T = k C_L^m \quad m = 1, 2, 3 \quad (1)$$

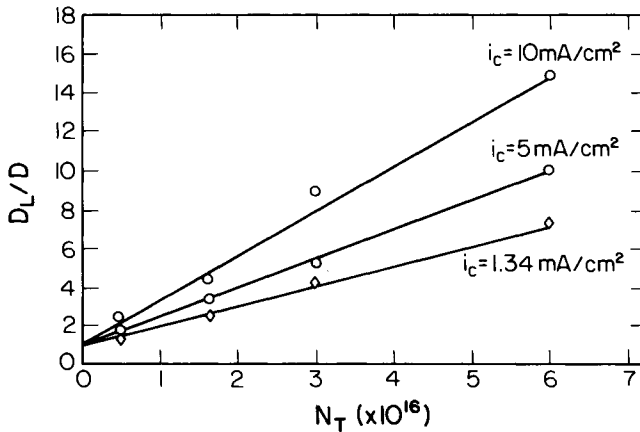


FIG. 7—Linear relationship between P_0/P and the density of microvoids.

where $m = 2$ for the trapping of hydrogen as molecules in voids. Correspondingly, the effective diffusivity becomes

$$D_{\text{eff}} = D_L(1 + mkC_L^{m-1})^{-1} \quad (2)$$

For $m = 2$, D_{eff} decreases as C_L increases, so our results are in agreement with the presence of nonsaturable traps.

At 1.34 mA/cm² charging current density (i_c), the results were reproducible for all specimens to well within experimental error. But when i_c was increased, buildup for the second transient was faster than the first. The more the microvoid volume, the bigger the difference. With saturable traps the deeper irreversible traps should be responsible for the first buildup transient and the reversible traps for the later buildup transient [13, 14].

However the same trap can be either "reversible" or "irreversible" depending on the rate of release from the traps. To demonstrate this and to estimate the release rate for hydrogen from the voids, the following test was conducted. The specimen which had undergone 240 h of hydrogen attack was charged, then charging was stopped for 7 or 21 h, and charging commenced again. The results are shown in Table 3. After 21 h the value of D_{eff} was returned to its original value, while after only 7.5 h the traps were still largely saturated and D_{eff} was close to that of a trap-free lattice.

The effective diffusivity of hydrogen in iron with a density of traps N_T is related to lattice diffusivity

$$\frac{D_L}{D_{\text{eff}}} = 1 + \frac{k}{P} N_T$$

Since D_L for ESR steel without traps is not known, it is assumed that the high order buildup transient of the annealed specimen can be considered as D_L where $D_L = 6 \times 10^{-6}$ cm²/s. The linear relationship between D_L/D and N_T also was observed, as is shown by Fig. 7.

Acknowledgment

This work was supported by the Department of Material Research, BES, U.S. Department of Energy. It was greatly aided by the kind assistance of Prof. S. Smialowska, in those laboratory the measurements of D_{eff} were made, and by the continued assistance of Dr. T. A. Parthasarathy.

Conclusion

The effect of microvoids produced by hydrogen attack on the permeation behavior of hydrogen through 0.2% carbon ESR steel is observed. Microvoids trap the hydrogen, but do not retain hydrogen permanently. As would be expected for bubble traps, the diffusivity decreases with increasing hydrogen concentration and with increasing volume of microvoids.

TABLE 3—Decharging effect of diffusion coefficient.

Procedure	Density	Charging Current D_{eff} , cm ² /s
1. First charging	10 mA/cm ²	8.0×10^{-7}
2. Charging after 7.5 h, hold at $i = 0$	10 mA/cm ²	1.1×10^{-6}
3. Charging after 21 h, hold at $i = 0$	10 mA/cm ²	8.5×10^{-7}

References

- [1] Darken, L. S. and Smith, R. P., *Corrosion*, Vol. 5, 1949, p. 1.
- [2] Boniszewski, T. and Moreton, J., *British Welding Journal*, June 1967, p. 1141.
- [3] Evans, G. M. and Rollason, E. C., *Journal of the Iron and Steel Institute*, Vol. 207, 1969, p. 1484.
- [4] Evans, G. M. and Rollason, E. C., *Journal of the Iron and Steel Institute*, Vol. 207, 1969, p. 1591.
- [5] Ellerbrock, Von H.-G., Vibrans, G., and Stuwe, H.-P., *Acta Metallurgica*, Vol. 20, 1972, p. 53.
- [6] Allen-Booth, D. M. and Hewitt, J., *Acta Metallurgica*, Vol. 22, 1974, p. 171.
- [7] Kumnick, A. J. and Johnson, H. H., *Metallurgical Transactions*, Vol. 5A, May 1974, p. 1199.
- [8] Johnson, H. H., Quick, N., and Kumnick, A. J., *Scripta Metallurgica*, Vol. 13, 1979, p. 67.
- [9] Bernstein, I. M. and Thompson, A. W., *Proceedings*, 3rd International Conference on the Effect of Hydrogen on the Behavior of Materials, I. M. Bernstein and A. W. Thompson, Eds., Metallurgical Society of AIME, Warrendale, OH, 1981.
- [10] Choo, W. Y. and Lee, J. Y., *Metallurgical Transactions*, Vol. 13A, 1982, p. 135.
- [11] Kumnick, A. J. and Johnson, H. H., *Acta Metallurgica*, Vol. 28, 1980, p. 33.
- [12] Nanis, L. N. and Namboodhiri, T. K. G., *Acta Metallurgica*, Vol. 21, 1973, p. 663.
- [13] Pressouyre, G. M. and Bernstein, I. M., *Metallurgica Transactions*, Vol. 9A, 1978, p. 1571.
- [14] Mezzanotte, D. A., *Metallurgical Transactions*, Vol. 13A, 1982, p. 1181.
- [15] Hirth, J. P., *Metallurgical Transactions*, Vol. 11A, 1980, p. 861.

Panel Discussion: Section 3¹

The moderator was Rudy Fricioni, LECO, St. Josephs, MI. Panel members were: Nancy Stecyk, Timken Co., Canton, OH; Takashi Ohtsubo, Nippon Steel Corp., Kawasaki-City, Japan; David A. Berman, Naval Air Development Center, Warminster, PA; and Adri Mackor, TNO, Zeist, Netherlands.

Participants were: Francois Faure, FRAMATOME, Paris; Alan Grobin, IBM, Poughkeepsie, NY; John J. DeLuccia, Naval Air Development Center, Warminster, PA; and W. Chionis, Parker Hannifin Corp., Irvine, CA.

Discussion

Berman: First, does the steel come in contact with water during quenching?

Fricioni: Yes.

Berman: And does that result in hydrogen entering?

Stecyk: No. If your steel pin is solid, it does not.

Berman: There is contact, so therefore there is going to be a reaction between the water and the hydrogen.

Stecyk: The first reaction is the shock of the quartz fracturing in the water. I believe the quartz shatters almost immediately. As soon as the quartz shatters, you take the pin out of the water. While it is cooling, however, I suppose that is a possibility.

Berman: Then you cool the steel with liquid nitrogen. When you take it out of the nitrogen, it is cold and you get condensate on it. It then has to be warmed up to temperature to do your analysis. Is this correct?

Stecyk: We rinse the sample after it breaks. It does frost up, yes. We give it two successive, one-second-in-and-out rinses in methanol, and then two rinses in freon. Freon, of course, does not have any hydrogen in it. These rinses are at room temperature.

Berman: But doesn't the evaporation cool the sample and again get the moisture on it?

Stecyk: No, we have not seen this occur.

Fricioni: We are only measuring hydrogen now. We are not measuring the water.

Berman: Yes, but water introduces hydrogen. That is what I am getting at.

Stecyk: Once again, if your sample is solid . . . and there again, this is where operator training is tremendously important.

Berman: Of course, you are reproducing the same thing. But I am just wondering if possibly the analysis that you are doing is not really a true analysis, but rather an analysis of other hydrogen that you might have put into it—because you do have a small sample.

Fricioni: We have performed a direct liquid nitrogen quench. The reaction is somewhat violent, but we have not seen any difference between our results with liquid nitrogen and our results with water.

¹This section represents the interaction of the presenters and the participants in response to the technical content of the various papers. The sessions were taped and written copies of the discussions sent to each participant for comments and/or corrections. It is hoped that by including these sections, the reader will be able to better understand the controversial aspects of these presentations. This panel discussion was held to discuss the content of papers reproduced in Section 3 of this book. The discussion is presented in its original form and was not peer reviewed.

Berman: I would like to mention one other point. If you are not doing this type of analysis, but instead want to determine total hydrogen in small samples—say you have a material which you want to cut up and throw into an analyzer—you have the same problem: are you really measuring the hydrogen that was originally present in the samples, or are you introducing hydrogen to them?

Fricioni: Dr. Ohtsubo, didn't you do some work in which you heated the sample before placing it in the analyzer?

Ohtsubo: I would like to make one important point. The solubility of hydrogen is very great. We have performed some tests using sodium chloride and have found that condensation does form when the sample is taken out of the liquid nitrogen. This moisture can be reduced and detected as hydrogen in the analysis.

Fricioni: Regarding condensation, I think both you and Dr. Endo did some work using a graphite crucible. You would take the sample and heat it, thereby picking up the water moisture but not the hydrogen. You would drop it down in the hot bath and pick up the other portion. So there is a way to get around it. If you are using a graphite reaction, the moisture reduction is very pronounced. With the quartz reaction, you do not have this reaction.

Mackor: In my presentation, I showed a slide with the results of some experiments I did with "steel 37." There was one interesting point relevant to this discussion: when we annealed the sample at 300° for 15 min, we found a very low hydrogen activity, but interestingly, in the coming hours the hydrogen activity increased. This could have been due to a reaction between water vapor and the corroded material on the outside. I think we are able to measure accurately the hydrogen activity in this type of sample. We could do this, for instance, by cooling the sample and the nitrogen, excluding all water molecules, and see how it would look then.

Fricioni: Again, you have to be careful that you do not have any reaction of moisture in the gas. That is what you are really picking back up in the sample.

Mackor: You can use essentially water-free nitrogen gas. We have a lot of experience with that.

Fricioni: The only way you can determine whether or not it is water free is to put a piece of iron in your reaction chamber and pass the gas over the iron.

Mackor: The problem is that you cannot use copper for that.

Fricioni: Yes, you can. Copper will not do anything for the water, but it will for gas. That is a good way to check your gasses out. Put a 10- or 15-g metal pin in the reaction chamber. That will tell you whether or not you have removed all the water from the gas.

Faure: Some two or three years ago, we performed some experiments on welds to see how fast they needed to be quenched after welding to avoid any hydrogen loss before specimen analysis. We waited for different periods of time from a few seconds up to a few hours between the moment we completed the weld and the moment we quenched the specimen. The specimens were quenched first in water and then in liquid nitrogen. We found that it took 3 to 5 min before any hydrogen loss could be detected. When we waited longer than that to quench the specimen, we saw a decrease in the apparent hydrogen determination. I think we have a similar problem when measuring in steel.

Grobin: Have you ever tried some of the old techniques of avoiding hydrogen embrittlement when using your Barnacle electrode? I notice that you mention seeing an increase in hydrogen after testing. Let me explain. What we used to do in the past (about 35 years ago) when we encountered hydrogen embrittlement. We would plate the part for about 15 s, and then remove the object from the plating bath and bake it for 4 h. Then we would put the part back in the bath and continue to plate it. We rarely ran into hydrogen embrittlement problems after that treatment. I suspect we were taking advantage of some electrochemical effect and discharging the hydrogen on the small amount of cadmium that was initially deposited. I was going to suggest that this is something you might want to investigate with your Barnacle electrode.

Berman: John and I reported some work of that type in the first paper we published together, which we presented at the ASM meeting at Seven Springs in 1973. But our initial plating was

not for 15 s; we put on two mils, baked the material, and then followed with a finish to five mils. And we saw no improvement. In between, of course, there was cleaning, which perhaps took off some of the thickness because it had been baked. Other people, too, I think, have shown that it does not seem to work.

Grobin: Two mils is quite a thick coating. It was probably a complete diffusion barrier.

Berman: Well, actually, on the first baking it seemed to get rid of some of it, but then replating showed that the barrier wasn't really there.

Grobin: I suggest that you might want to experiment with the following procedure: plate for 15 s, bake, then continue the plating to final thickness, and then do your work. Have you used this with platings other than cadmium, such as zinc or nickel?

Berman: No, not in my work.

Grobin: That would be interesting because today cadmium is rarely plated; zinc is the predominant plating in the United States, as far as tonnage of plating, and nickel is the second most prevalent.

Berman: I don't think we use zinc in the Navy. Do we John?

DeLuccia: No, we don't. We use a lot of cadmium.

Berman: There is one little problem: you have to take the plate off to make your measurements, but you have to take it off with something that will not reintroduce hydrogen. That is one reason why I have not done it with chromium; chromium plating is hard and rather difficult to remove, and it tends to crack, allowing hydrogen to escape.

Grobin: You can remove nickel anodiolyin sodium nitrate, and zinc with sodium hydroxide. Concerning the ASTM B08 specifications, which you made reference to, all the hydrogen embrittlement relief treatments are being changed; the new specifications are much more rigorous. The baking temperatures are slightly higher and baking periods longer. My last point concerns the cadmium plating bath you are using. I would suggest that impurities in the cadmium oxide which is used to make up the bath will effect the properties of the plate, so I think that cadmium oxide should be carefully specified along with all the other materials used in the cadmium plating process. The B08 Committee does not specify processes for that reason. We specify end-point requirements of the plating because sometimes very minor impurities can affect the properties of the plating.

Berman: That could be. But to my knowledge, we are using reagent grade chemicals.

Grobin: Reagent grade can vary in some of the impurities. Minor differences within a specified grade of cadmium oxide could have an impact.

Berman: I haven't checked what chemicals are used to make up the baths. Of course, what we are interested in is what is happening in industry: if hydrogen is picked up, how is it measured? In the work that I have been doing, I have not been concerned, per se, with improving the bath or doing anything with it.

Grobin: I am not suggesting that you improve it. I am just saying that you ought to look carefully at the chemicals and determine what impurities they contain.

Chionis: Dr. Berman, when the Barnacle electrode is being used, is the rubber gasket subject to chemical decomposition from the environment inside the electrode?

Berman: We are using silicone rubber gaskets, and as far as I can tell, there is no change in them under reasonable conditions; we can use them for quite a while. If you check periodically to see that you are getting a nice circle, you can be reasonably certain you have a good gasket there. I have described that in some of my work, including the paper I wrote for this symposium. I have not, however, checked the rubber itself for degradation.

Chionis: My concern was that if the rubber itself were decomposing in some way, that decomposition might alter the hydrogen concentration value.

Berman: I don't think that is happening, because if it were, you wouldn't get the reproducibility. There is good reproduction even when the same gasket is used throughout a series of measurements.

Summary: Section 3

Electrochemical Sensor for the Determination of Hydrogen in Metals by Potential Methods

This method employs a three-part electrode consisting of palladium hydride as a reference electrode, a solid proton conducting electrolyte (hydrogen uranyl phosphate tetrahydrate), and a thin layer of palladium sputtered over the end of the electrolyte.

The determination of hydrogen is based on the increase of voltage from the electrode when the electrode is in contact with the sample material through a contact liquid. The localized hydrogen content is calculated by finding the net voltage increase attributable to hydrogen activity.

The electrochemical sensor offers long-term stability from a few minutes to a few months. The method has been applied to hydrogen problems in the petrochemical, welding, and galvanic industries.

The Barnacle Electrode Method to Determine Diffusible Hydrogen in Steel

The Barnacle Electrode Method is an adaptation of the electrochemical permeation method for hydrogen diffusion. In this method the sample material is the anode of the circuit, the cathode is a nickel, nickel oxide plate enclosed in a chamber filled with a 0.2 *M* sodium hydroxide solution. Mobile hydrogen leaving the surface of the sample is converted to moisture by the sodium hydroxide at the nickel, nickel oxide electrode interface. The hydrogen in the form of water causes a current shift in the electrode relative to the surface mobile hydrogen concentration.

The analysis method is a qualitative method with applications for monitoring hydrogen uptake in material processing or corrosion.

Determination of Hydrogen Content in Molten Steel Using an Inert Gas Bubbling Probe

The Inert Gas Bubbling Method for determining hydrogen offers an on-line determination directly from the molten bath. Experimental data has been accumulated by bubbling argon, nitrogen, and hydrogen mixtures at set flow rates through a precisely sized nozzle immersed at a precise depth into 900 g of molten iron. The gas bubble collector was immersed above the nozzle. Nozzle size, gas flow rate, and positioning of the nozzle and collector tube are extremely important to this method. The gas bubbles were sensed by a mass spectrometer. The experimental data was obtained by calculating the frequency of hydrogen bubble formation using Sieverts law. There was a good correlation of the determined hydrogen contents to the theoretical injected volumes.

A Study of the Effect of Voids on the Hydrogen Diffusion Through ESR Steel

Samples of ESR steel were annealed at 900°C for 1 h. After annealing, the grain size was determined to be 9 ASMS. The samples were then attacked with hydrogen at 600°C for time periods ranging from 120 to 432 h. Afterward the samples were polished and micrographically examined.

By this method it was possible to count the number of voids in the samples and determine the average size of the voids. The volume of the voids was calculated based on the average size. The

diffusion of hydrogen and the level of hydrogen contained in the voids was measured electrochemically and correlated to the theoretical volume. Through this study it was found that microvoids will retard the evolution of hydrogen but hydrogen is not permanently retained in microvoids. The diffusivity of hydrogen is relative to microvoid volume. As microvoid volume increases, the diffusion rate decreases.

The Simultaneous Determination of Diffused and Residual Hydrogen

Comparison studies of sampling with a dual-chambered metal sampler, a diffused hydrogen sample carrier, and standard hydrogen studies have been made. Correlative data are obtained using any of the three sampling methods.

Though values accumulated with all three sampling methods are correlative, sampling and sample handling with the metal tube sampler is not totally foolproof. Strict guidelines for sampling immersion time and sampler stripping procedures must be followed. Either of the dual hydrogen sampling methods used appears to provide a more consistent and less tedious method of hydrogen sampling and sample handling than the present standard method.

Rudy Fricioni,

LECO Corp., St. Josephs, MI; chairman, Section 3.

Section 4: Relative Susceptibility

Overview: Section 4

Test Methods for Ranking Relative Susceptibility of Alloys to Hydrogen Damage

Can any short-term test method be trusted to predict 20+ years of service damage in a hydrogen environment? Is it better to accelerate such tests by raising the hostility of the environment out of all recognition to reality, or increasing the stress intensity beyond any reasonable engineering level? How does one rate test methods for their balance between cost-effectiveness and predictive power? These are the sort of questions we must consider.

A low-alloy steel for landing gears, with hardness of HRC 55, a submarine hull steel of HRC 34, and a pipeline steel of HRB 85 have little in common despite their small differences in composition. Strength, toughness, and fabricability are so far apart that calling all three members the same alloy family is more confusing than useful.

If there is a common factor among the three alloys cited, it is their susceptibility to hydrogen-induced cracking. All three alloy types suffer from different manifestations of the problem within their particular application and environment.

Consider the range of hydrogen-induced cracking mechanisms in low-alloy steels:

Hardness Range	Mechanism	Test Methods
HRC 38 to 55	H ₂ embrittlement	ASTM F 519
HRC 32	Stress corrosion	ASTM G 44
HRC 22	Sulfide stress cracking	NACE TM-01-77
Any	Step-wise cracking	NACE TM-02-84

Within the broad bands of hardness suggested above, there are still variations in relative resistance due to a complex interaction of composition and thermal history. The standard test methods listed above were developed to rank and sort materials within their alloy classes in relationship to particular applications and possible fracture mechanisms.

Given the vast difference in hydrogen availability between an electrolytic plating operation and 20 years' service in an H₂S-bearing gas pipeline, no universal test method for hydrogen cracking seems feasible. The challenge materials engineers face is to develop cost-effective test methods with the broadest possible applicability to different alloys being considered for a given environment.

Dale R. McIntyre

Cortest Laboratories, Inc., Cypress, TX;
chairman, Section 4.

Sensitivity of Steels to Degradation in Gaseous Hydrogen

REFERENCE: Cialone, H. J. and Holbrook, J. H., "Sensitivity of Steels to Degradation in Gaseous Hydrogen," *Hydrogen Embrittlement: Prevention and Control*, ASTM STP 962, L. Raymond, Ed., American Society for Testing and Materials, Philadelphia, 1988, pp. 134-152.

ABSTRACT: Sensitivity of API-5L X42 and X70 line-pipe steels to hydrogen degradation of fracture properties has been studied under a variety of loading conditions. Hydrogen-enhanced crack growth under fatigue and static loading was evaluated in numerous hydrogen-rich gas mixtures. Under cyclic loading, hydrogen accelerated fatigue-crack growth, depending on frequency, stress ratio, stress-intensity range, and composition of the gas mixture in the environment. Under static load, subcritical-crack growth has been shown to occur in high-strength steels, in weld heat-affected zones, and in steel heat treated to simulate local hard regions in pipeline steels. *J*-integral fracture-toughness experiments have shown that hydrogen reduces the fracture toughness J_{IC} , and, in steels that undergo subcritical-crack growth, reduces the tearing resistance, dJ/da . A relationship between hydrogen-accelerated fatigue-crack growth and hydrogen-induced reductions in fracture toughness is presented. The reduction or elimination of hydrogen-degradation effects by the presence of certain inhibitor gases, such as oxygen (O_2), carbon monoxide (CO), or sulfur dioxide (SO_2), also is discussed.

KEY WORDS: steel, hydrogen degradation, gaseous hydrogen, fatigue-crack growth, fracture toughness, inhibitors

There are many service conditions in which structural components are exposed to gaseous hydrogen and in so being may undergo degradation of their properties. One such situation may be the future transmission of high-pressure hydrogen or synthetic natural gas through steel pipelines. This application would utilize existing natural gas pipelines to transport the gas from the producers to the distributors. Thus, it is necessary to evaluate the sensitivity of pipeline steels to degradation of their properties by gaseous hydrogen and to determine methods, such as the addition of inhibitor gases, to minimize degradation in practice.

Historically, problems related to hydrogen embrittlement primarily have involved delayed failure of high-strength steels [1-4]. Such steels are susceptible to sustained-load, subcritical-crack growth when exposed to hydrogen. Laboratory studies have indicated that under conditions of sustained load, steels with yield strengths below about 580 MPa (85 ksi) are essentially immune to embrittlement [5], and almost all pipeline steels have yield strengths below that value. However, more recent studies have shown that moderate-strength steels also may suffer degradation of their properties under severe environmental conditions [1,6].

Other studies indicate that for a given fugacity of hydrogen, the extent of degradation is greater when the steel is deformed in the presence of hydrogen than when the loading and the exposure to hydrogen are sequential [7]. In addition, cyclic loading in a hydrogen environment appears to make steels of all strength levels susceptible to hydrogen degradation [6,8-10]. In pipelines, cyclic loading arises from daily pressure fluctuations of approximately 10% of the

¹Senior research scientist and section manager, respectively, Physical Metallurgy Section, Battelle, Columbus Division, Columbus, OH 43201-2693.

nominal pressure as well as from less frequent depressurization/repressurization cycles that result from forced on scheduled shutdowns and subsequent startups. Daily pressure fluctuations may be more pronounced when hydrogen-rich gases are being transported because the higher compressibility of hydrogen relative to natural gas may make it more difficult and expensive to maintain the higher throughput pressures that will be required. Moreover, pipelines may have local regions, such as weld heat-affected zones or hard spots, which are more sensitive to degradation than the bulk of the pipeline. When steels with strength levels and microstructures similar to those of local hard regions are exposed to hydrogen, they are susceptible to various forms of delayed failure including sustained-load, subcritical-crack growth. In view of the potential for subcritical-crack growth at local susceptible regions and the possibility of enhanced fatigue-crack growth throughout the pipe, it is important to evaluate the sensitivity of pipeline steels to degradation of their properties by gaseous hydrogen at high pressure.

Gaseous hydrogen may degrade various properties of moderate-strength steels, such as smooth-bar tensile ductility, notched-bar tensile strength and ductility, fatigue life, fatigue-crack-growth rate, and fracture properties, to varying degrees. These effects depend on various factors, such as the hydrogen pressure and purity, the loading rate, the composition and microstructure of the steel, and the test temperature. Steels with yield strengths ranging from 200 to 580 MPa (30 to 85 ksi) have been shown to suffer significant ductility loss in smooth-bar and notched-bar tests, exhibiting losses in reduction of area as high as 50 to 60% in smooth bars and 70 to 80% in notched bars [11]. Losses in notched-bar tensile strength up to 25% also have been reported. However, subcritical-crack growth has not been observed in steels in this strength range, even though losses in fracture toughness have been measured using *J*-integral techniques [12].

The properties of moderate-strength steels that appear to be most affected by gaseous hydrogen are fatigue life and fatigue-crack-growth rate. Losses in fatigue life of 90% typically are reported when a stress raiser such as a notch is present [10,13–15]. Increases in fatigue-crack-growth rate in excess of 10 times also have been observed, and in some cases the crack-growth rate in hydrogen may be over 100 times faster than that in a reference environment [6,8–10,16–18]. Hydrogen effects on fatigue properties are influenced by many factors, including stress concentration; stress ratio, R ($R = K_{\min}/K_{\max}$); cyclic frequency; partial pressure of hydrogen; test temperature; and the presence of other gases.

In general, the extent of fatigue-crack-growth acceleration by hydrogen increases with decreasing frequency [10,19], although there is some experimental evidence that at very low frequency, approaching static conditions, the magnitude of acceleration decreases substantially [20,21]. The pressure dependence of hydrogen-accelerated, fatigue-crack growth follows approximately a cube-root-pressure relation [22]. Most hydrogen effects exhibit a maximum embrittlement temperature, which for steels is in the neighborhood of room temperature [23,24]. Fortunately, gaseous-hydrogen effects are very sensitive to the presence of other gas species, such as oxygen, which appear to eliminate the effects of hydrogen on crack growth in steels [6,25]. This paper describes studies of the effects of hydrogen and hydrogen-rich gases on line-pipe steels representing typical base metals, weld heat-affected zones, and hard spots, under test conditions that were intended to accentuate the degradation.

Experimental Procedures

Materials Studied

Specimens were prepared from two joints of API-5L line pipe, Grades X42 [290 MPa (42 ksi) specified minimum yield strength] and X70 [483 MPa (70 ksi) specified minimum yield strength]. The chemical compositions of the pipes are presented in Table 1. The X42 steel had a banded microstructure that consisted of ferrite and pearlite and contained numerous elongated

TABLE 1—Chemical compositions of pipe steels.

API-5LX Pipe Grade	Content, weight %											
	C	Mn	P	S	Si	Ni	Cr	Mo	Al	Cb	Cu	Sn
X42	0.26	0.82	0.020	0.026	0.014	0.016	0.038	0.010	0.004	0.000	0.022	0.005
X70	0.09	1.50	0.008	0.006	0.31	0.084	0.13	0.31	0.42	0.028	0.31	0.010

manganese-sulfide inclusions, typical of hot-rolled steels. The X70 steel was a controlled-rolled steel microalloyed with niobium and molybdenum and having a microstructure that consisted of polygonal ferrite intermixed with a constituent consisting of acicular ferrite and blocky islands of martensite/retained austenite. The electric-resistance-welded X42 pipe was 30.5 cm (12 in.) in diameter with a 0.95 cm (0.375-in.)-thick wall. The double-submerged-arc-welded X70 pipe was 101.6 cm (40 in.) in diameter with a 1.52 cm (0.6-in.)-thick wall.

Standard 1/2T compact-tension specimens with a thickness of 0.635 or 1.27 cm (0.25 or 0.5 in., respectively), depending on the pipe wall thickness, were prepared from the pipes and oriented for axial crack growth. Thus, the cracks grew parallel to the pipe length and the rolling direction of the original plate. In all cases, the specimens were prepared without flattening the pipe.

Specimens were prepared from the base metal of both pipes in the as-received condition. In addition, specimens were prepared from the weld region of the X42 pipe, with notches located in the weld heat-affected zone. Also, specimens were machined from a portion of the X42 pipe that had been austenitized and water quenched to simulate hard spots, which occasionally have been found in some older pipes. Table 2 presents tensile properties for base-metal specimens that were tested in air and in hydrogen.

Test Procedures

Fatigue-crack-growth tests and J -integral fracture-toughness tests were performed in stainless steel autoclaves that were equipped with stainless steel load linkage and U-cup Teflon sliding seals, and which were mounted on servohydraulic test frames. The fatigue-crack-growth

TABLE 2—Smooth-bar tensile properties of pipe steels.^a

API-5LX Pipe Grade	Test Environment	0.2% Offset Yield Strength, MPa (ksi)	Ultimate Tensile Strength, MPa (ksi)	Percent Elongation in 1 in.	Percent Reduction of Area
AXIAL (LONGITUDINAL) ORIENTATION					
X42	Air	366 (53)	511 (74)	21	56
	6.9 MPa H ₂	331 (48)	483 (70)	20	44
X70	Air	584 (85)	669 (97)	20	57
	6.9 MPa H ₂	548 (79)	659 (95)	20	47
TRANSVERSE ORIENTATION					
X42	Air	311 (45)	490 (71)	21	52
	6.9 MPa H ₂	338 (49)	476 (69)	19	41
X70	Air	613 (89)	702 (102)	19	53
	6.9 MPa H ₂	593 (86)	686 (99)	15	38

^aTests were conducted at an engineering-strain rate of 10^{-4} s⁻¹.

tests were conducted with base-metal specimens only, and in accordance with ASTM Test Method for Constant-Load-Amplitude Fatigue Crack Growth Rates Above 10^{-8} m/Cycle (E 647-83). The fracture-toughness tests were conducted with all materials, and in accordance with ASTM Test Method for J_{IC} , a Measure of Fracture Toughness (E 813-81). Experiments in all environments were performed at a total pressure of 6.9 MPa (1000 psi) to allow comparisons to be made without the complication of considering the effects of the hydrostatic hydrogen pressure on crack growth. An additional nonstandard test was performed with some of the fracture specimens to determine whether hydrogen would promote subcritical-crack growth in those materials.

Fatigue-crack-growth experiments were conducted under load control at stress ratios from 0.1 to 0.8, with a sinusoidal waveform at cyclic frequencies from 0.1 to 10 Hz. All fatigue-crack-growth experiments were conducted to fracture. Most experiments in hydrogen were performed at a frequency of 1 Hz; little difference was observed between crack-growth rates in hydrogen at 1 Hz and 0.1 Hz. The acceleration of fatigue-crack-growth rate in hydrogen did, however, diminish somewhat at 10 Hz. Experiments in nitrogen were performed at 5 Hz.

Crack length was monitored with foil gages that were applied to the surfaces of the specimens and which provide an indirect method of making d-c electric-potential-drop measurements of the crack length at the surface of the specimen. Because the crack front was nearly straight through the thickness during the fatigue experiments, crack-length measurements made with the foil gages were in good agreement with post-test measurements on the fracture surfaces using an optical comparator. Crack length and number-of-cycles data were recorded automatically by computer at intervals that decreased with increasing crack length. The crack-growth rate, da/dN , was determined by fitting a quadratic equation to three points on the crack length versus number of cycles record and determining the derivative of the equation at the middle point.

Fracture-toughness experiments were performed with specimens that were similar to those used for the fatigue-crack-growth experiments, except that the fracture-toughness specimens were prepared with machined steps for load-line-displacement measurements and had deeper notches. Crack length was monitored directly using a d-c electric-potential-drop technique. The specimens were fatigue precracked in the test environment and then loaded in load-line-displacement control at displacement rates of 2.5×10^{-7} and 2.5×10^{-6} m/s (10^{-5} and 10^{-4} in./s, respectively) to provide data for the estimation of the J -resistance curves. No differences were observed between results obtained at these two displacement rates. The final crack length was marked by fatigue loading at the completion of the test, and the specimen then was broken apart.

Subcritical-crack-growth experiments were performed with the same type of specimen that was used for the fracture-toughness experiments. After fatigue precracking in the environment, the specimen was loaded to a fixed displacement and the load and crack length were monitored for a period of at least 1 h. This procedure was used instead of an actual sustained-load approach because more information could be obtained in displacement control; under fixed load the stress intensity increases with increasing crack length and rapid, unstable fracture would occur as soon as subcritical-crack growth initiated. The initial displacement was selected on the basis of the point in the fracture-toughness experiments at which crack initiation was observed.

Typically, specimens that did not exhibit subcritical-crack growth displayed a drop in load of approximately 5% due to plastic-relaxation processes at the crack tip. This plastic deformation produced an apparent increment in crack length, based on electric-potential drop, of approximately 0.025 cm (0.01 in.). If significant load decrease (typically 15% or greater) or crack growth [0.127 cm (0.05 in.) or more] over the amount that would represent crack-tip relaxation was not observed in the 1-h period, the displacement was increased approximately 0.0025 cm (0.001 in.) and maintained for 1 h. This procedure was repeated until subcritical-crack growth was detected or until at least three trials had been made. In some cases, specimens exhibited subcritical-crack growth in a hydrogen-rich environment but did not exhibit subcritical-crack

growth in the reference nitrogen or methane environment, or in a hydrogen environment containing an inhibiting gas. When this was observed, the reference or inhibited environment was removed from the autoclave and replaced with the embrittling (hydrogen-rich) environment to determine whether this observation was a result of specimen-to-specimen variations in susceptibility to subcritical-crack growth. At the completion of the experiments, the final crack length was marked by fatigue cracking to failure.

Test Environments

Six gas compositions were used to evaluate the sensitivity of these materials to hydrogen degradation in transmission of hydrogen or hydrogen-rich gases; these are described in Table 3. To study the case of transmission of pure hydrogen, experiments were performed in 6.9-MPa (1000-psi) hydrogen and in 6.9-MPa (1000-psi) nitrogen for reference data. The effectiveness of several additive gases in inhibiting the degrading effects of hydrogen was studied by adding up to 2% by volume of those gases to the hydrogen. To study the situation of transmission of hydrogen-rich gases such as synthetic natural gas, four other environments were used: (1) 100% methane (designated M), to provide baseline data; (2) 60% (by volume) hydrogen and 40% methane (MH), to represent the most embrittling condition; (3) 60% hydrogen, 24% carbon monoxide; and 16% methane (MHC), to study the inhibiting effects of carbon monoxide; and (4) 60% hydrogen, 24% carbon monoxide, 10% carbon dioxide, 6% methane, and 100% relative humidity (MHCC), to represent a potential synthetic natural gas environment with all major constituents present.

Results

Fatigue-Crack-Growth Experiments

The effects of hydrogen on fatigue-crack growth are shown in Figs. 1 through 4. Those figures present fatigue-crack-growth rates versus stress-intensity amplitude, ΔK , for the X42 and X70 base metals in 6.9-MPa (1000-psi) hydrogen and in 6.9-MPa (1000-psi) nitrogen. Figures 1 and 2 show the effect of hydrogen on fatigue-crack-growth rates in the X42 and X70 steels, respectively, at low stress ratio. In general, the magnitude of the acceleration increased with increasing ΔK . Large accelerations were observed for both steels, although the magnitude of the acceleration was greater for the X42 steel, for which crack-growth rates in hydrogen were as much as 150 times greater than those in nitrogen at the same value of ΔK .

Figures 1, 3, and 4 illustrate the influence of stress ratio, R , on the acceleration by hydrogen of fatigue-crack-growth rate in the X42 steel. Those figures show that the acceleration of Stage II crack growth decreased with increasing R . Similar behavior was observed with the X70 steel.

TABLE 3—Description of test environments.

Environment Designation	Composition, volume % ^a
H ₂	≥ 99.999 hydrogen
N ₂	≥ 99.99 nitrogen
M	≥ 99.99 methane
MH	60 hydrogen, 40 methane
MHC	60 hydrogen, 24 carbon monoxide, 16 methane
MHCC	60 hydrogen, 24 carbon monoxide, 10 carbon dioxide, 6 methane ^b

^aTotal pressure = 6.9 MPa.

^bPlus 100% relative humidity.

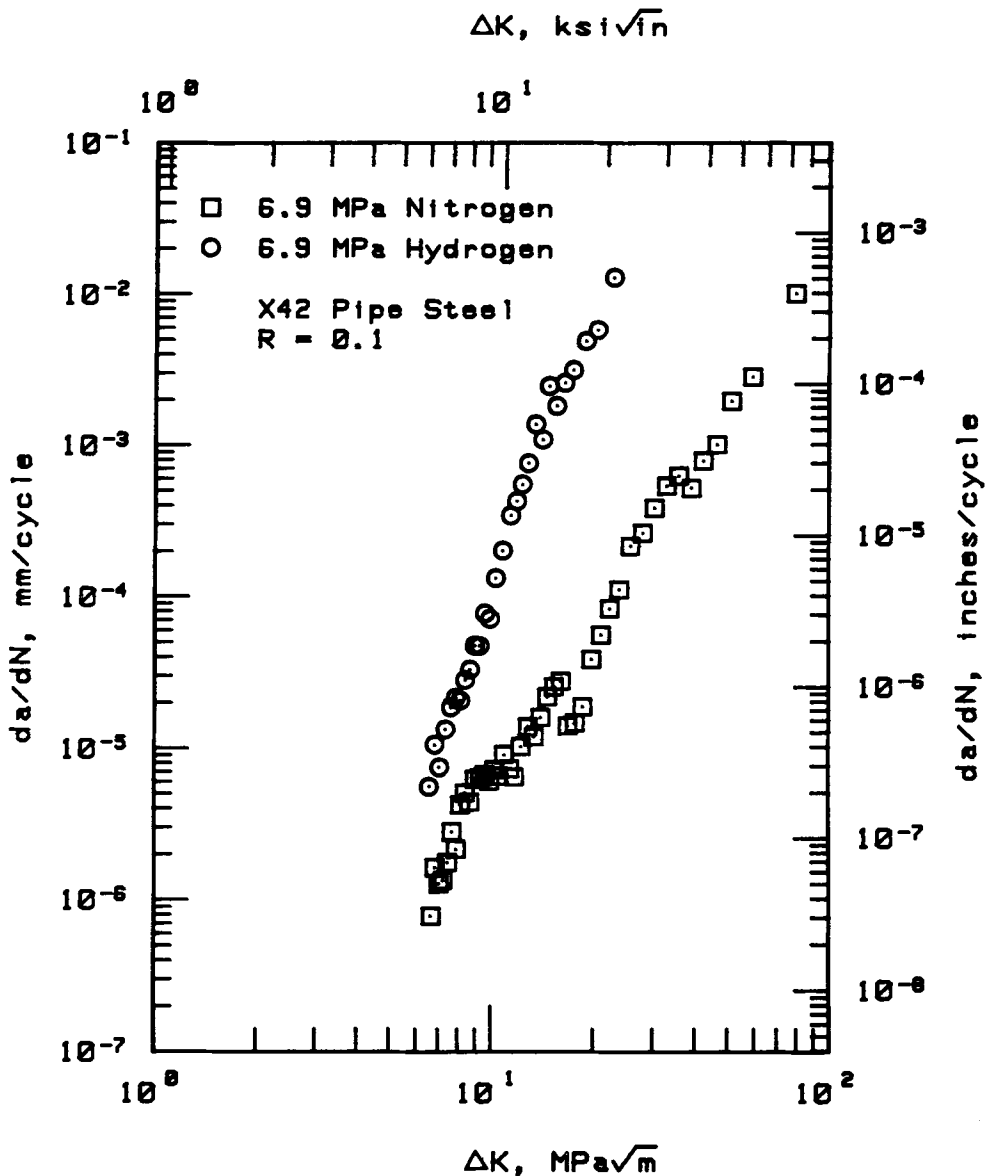


FIG. 1—Fatigue-crack-growth rates for X42 pipe steel in 6.9-MPa (1000-psi) hydrogen and in 6.9-MPa (1000-psi) nitrogen at $R = 0.1$.

The manner in which the decrease in acceleration of Stage II crack growth occurs is reflected in Fig. 4. For $R < 0.5$, the figure shows that the fatigue-crack-growth rate in nitrogen increased with increasing R , but the crack-growth rate in hydrogen remained essentially independent of R . Thus, the acceleration decreased with increasing R . However, for $R > 0.5$, the crack-growth rate in hydrogen increased with increasing R , and the rate of increase was greater than that in nitrogen. The reason for this divergence is shown in Fig. 3, which presents crack-growth data for the X42 steel at $R = 0.8$, and shows that hydrogen promoted the onset of Stage III crack

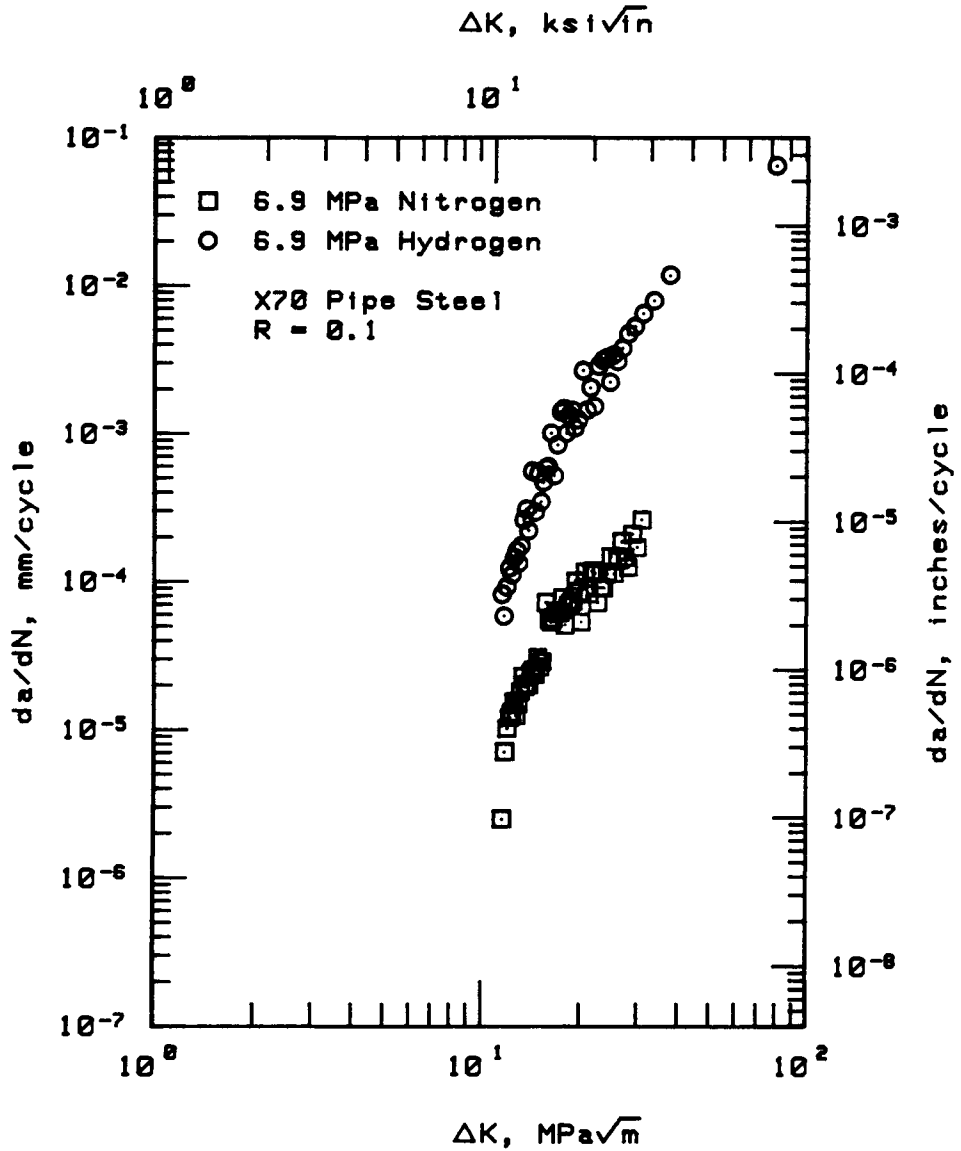


FIG. 2—Fatigue-crack-growth rates for X70 pipe steel in 6.9-MPa (1000-psi) hydrogen and in 6.9-MPa (1000-psi) nitrogen at $R = 0.1$.

growth. Thus, although at high stress ratio hydrogen did not accelerate Stage II crack growth substantially, premature Stage III crack growth (that is, at lower ΔK than in nitrogen) was promoted by hydrogen. This behavior presumably is a result of the higher K_{\max} values that are encountered at higher stress ratios, because $\Delta K = (1 - R) K_{\max}$, and may be related to reductions in fracture toughness.

The inhibiting effects of several gas additives on fatigue-crack-growth acceleration in the X42 steel are shown in Figs. 5 through 8. The lines in each of those figures represent the crack-growth rates in nitrogen and hydrogen, which were presented in Figs. 1 and 3. At $R = 0.1$,

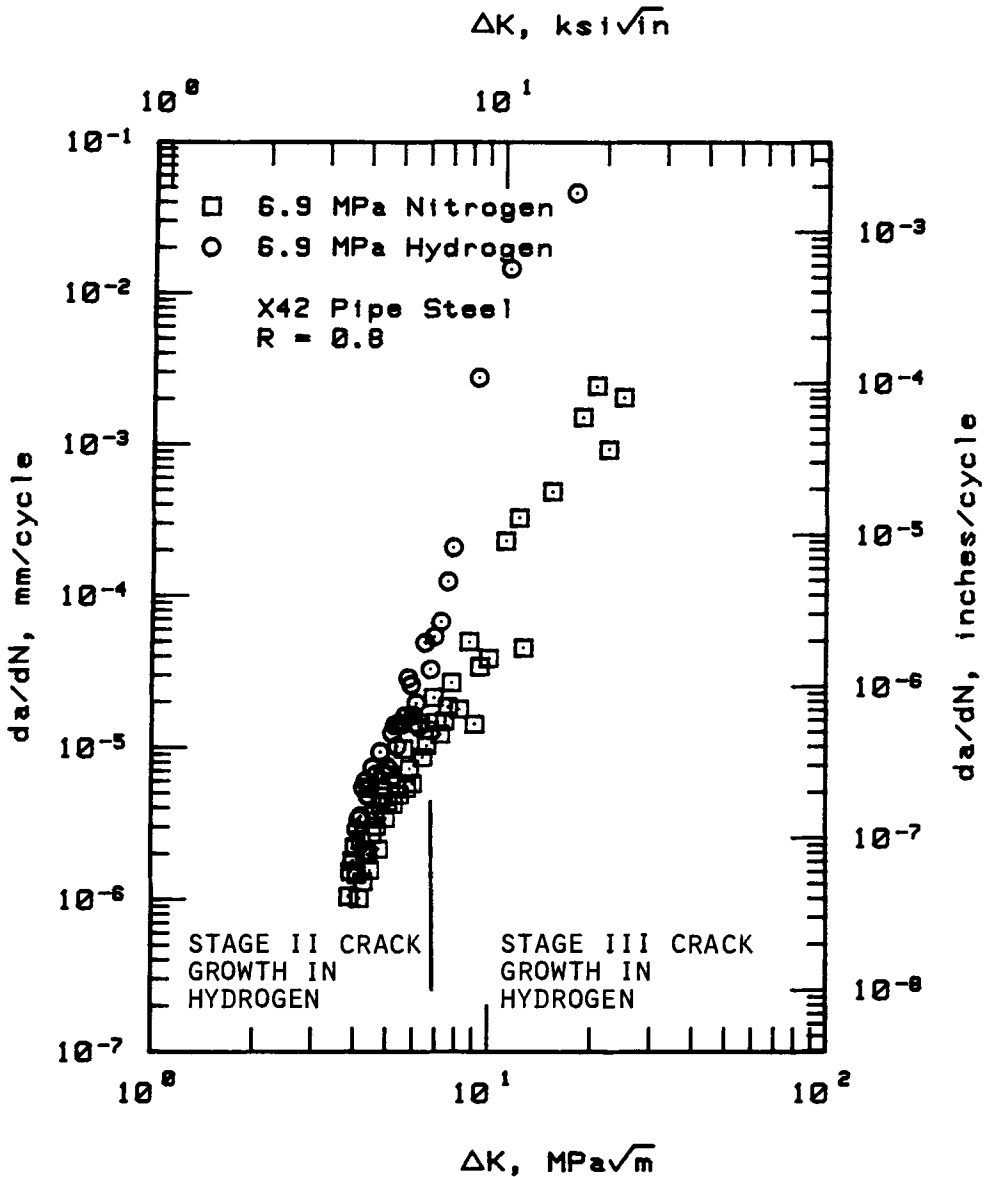


FIG. 3—Fatigue-crack-growth rates for X42 pipe steel in 6.9-MPa (1000-psi) hydrogen and in 6.9-MPa (1000-psi) nitrogen at $R = 0.8$.

additions of small concentrations of oxygen or sulfur dioxide to the hydrogen provided complete inhibition of acceleration, and nearly complete inhibition was achieved with carbon monoxide. Figure 8 illustrates that complete inhibition of premature Stage III crack growth also can be achieved, at least with oxygen. The mechanism of inhibition is not fully understood in detail, however it is believed to involve preferential adsorption of the inhibitor species on the surface of the metal.

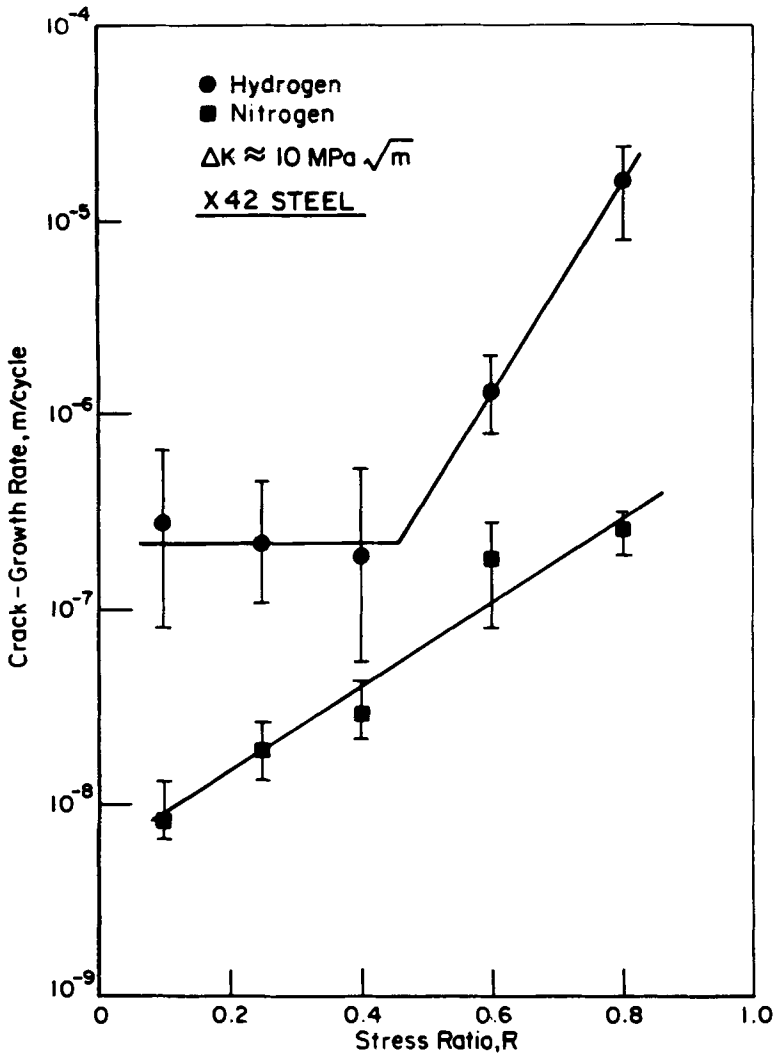
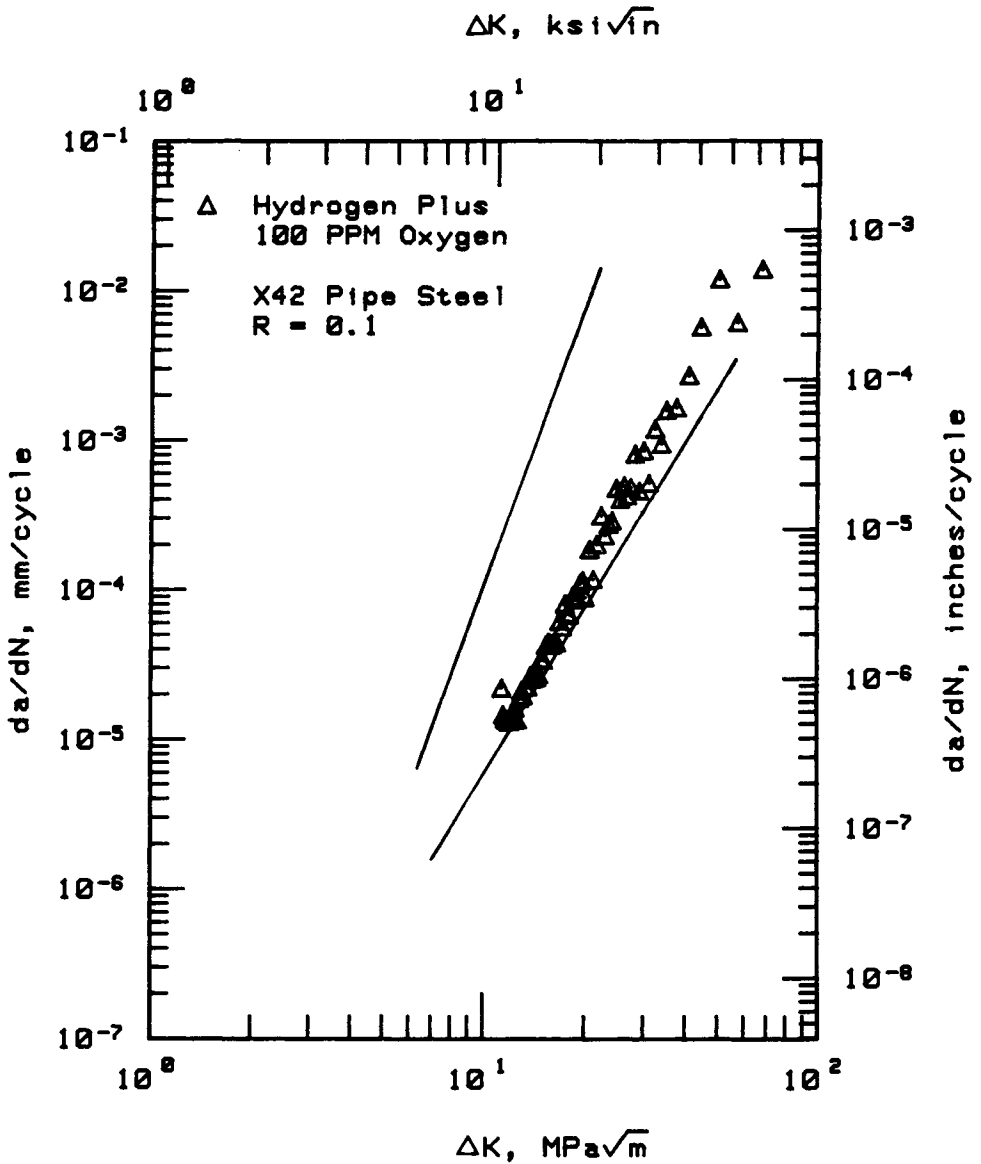


FIG. 4—Fatigue-crack-growth rate for X42 pipe steel as a function of stress ratio.

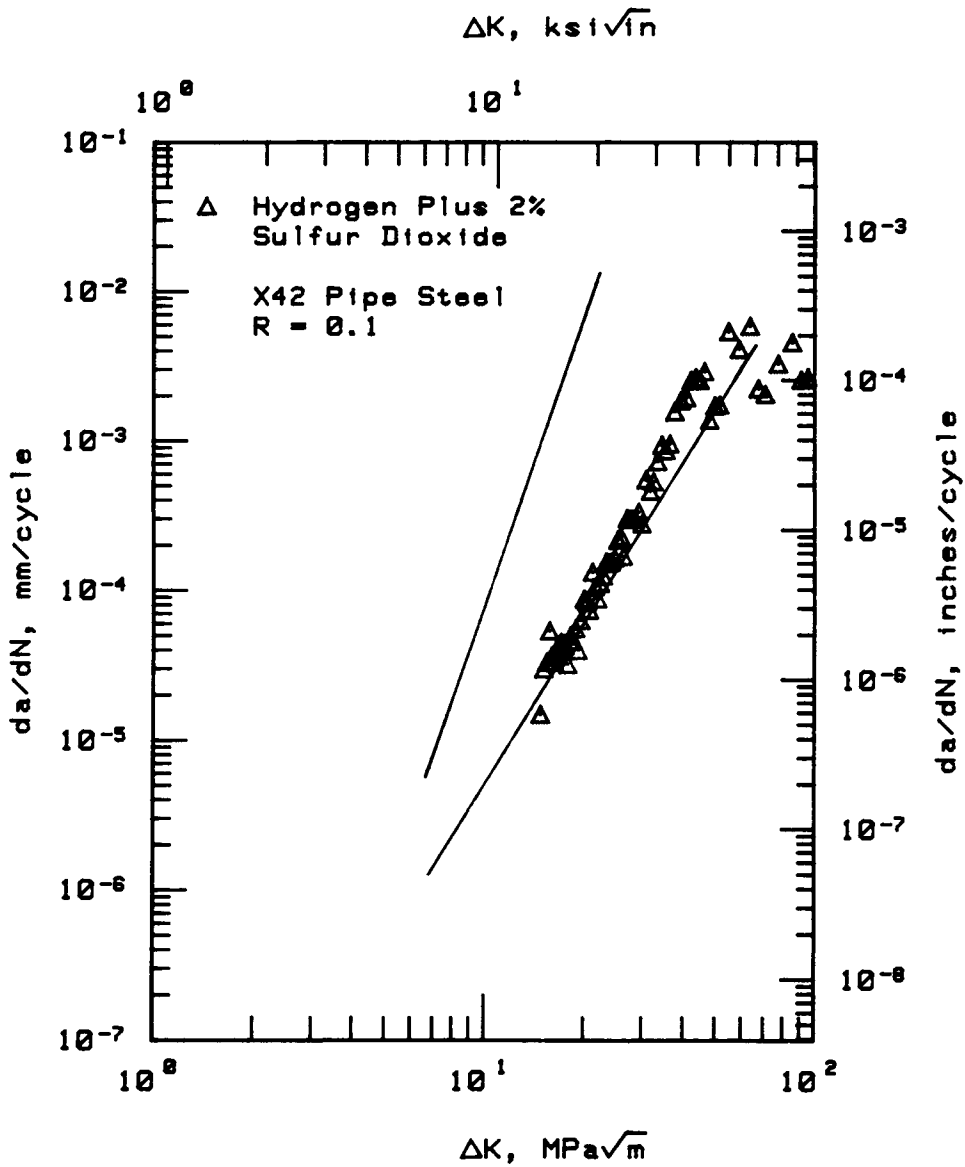
Fracture-Toughness Experiments

Figure 9 presents J -resistance curves for the X42 steel in hydrogen and nitrogen. The fracture-toughness data are summarized in Table 4, which presents J_{Ic} and dJ/da -values for each material and environment. For all of the materials, hydrogen, either pure or mixed with methane, substantially reduced the elastic-plastic fracture toughness, J_{Ic} , although the tearing resistance, dJ/da , was reduced significantly only in the case of the X70 steel and the simulated hard spots in the hardened X42 steel. In the cases in which the environment contained carbon monoxide (CO), the effect of hydrogen was almost completely inhibited. It is interesting to note that for the X70 steel and the heat-treated X42 steel, the J_{Ic} and dJ/da -values were higher in the MHC and MHCC environments than in methane. This observation suggests that methane reduced toughness moderately, which is supported by comparing the J_{Ic} and dJ/da data for the



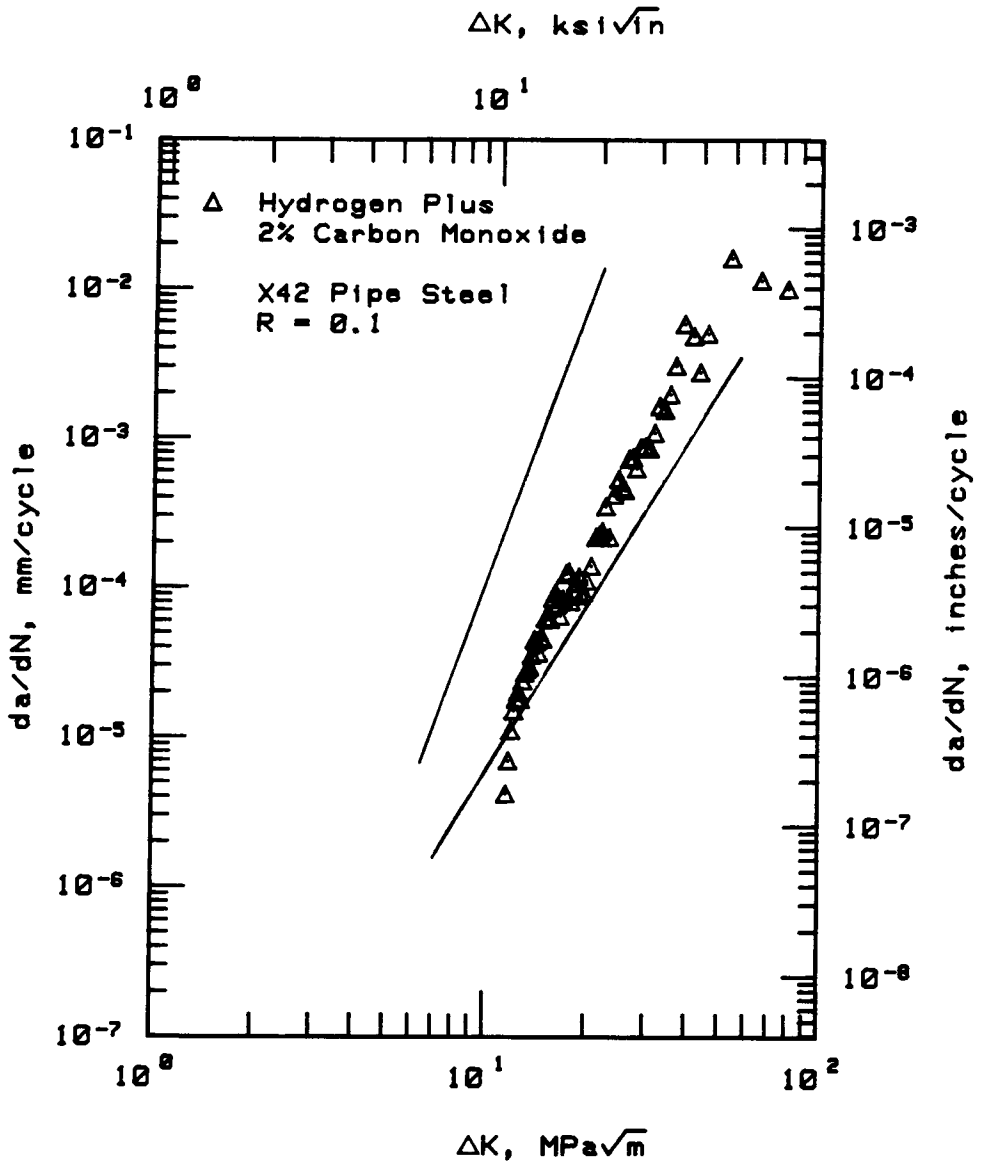
Solid lines represent hydrogen (upper line)
and nitrogen (lower line) data.

FIG. 5—Fatigue-crack-growth behavior for X42 pipe steel with oxygen addition to hydrogen at R = 0.1.



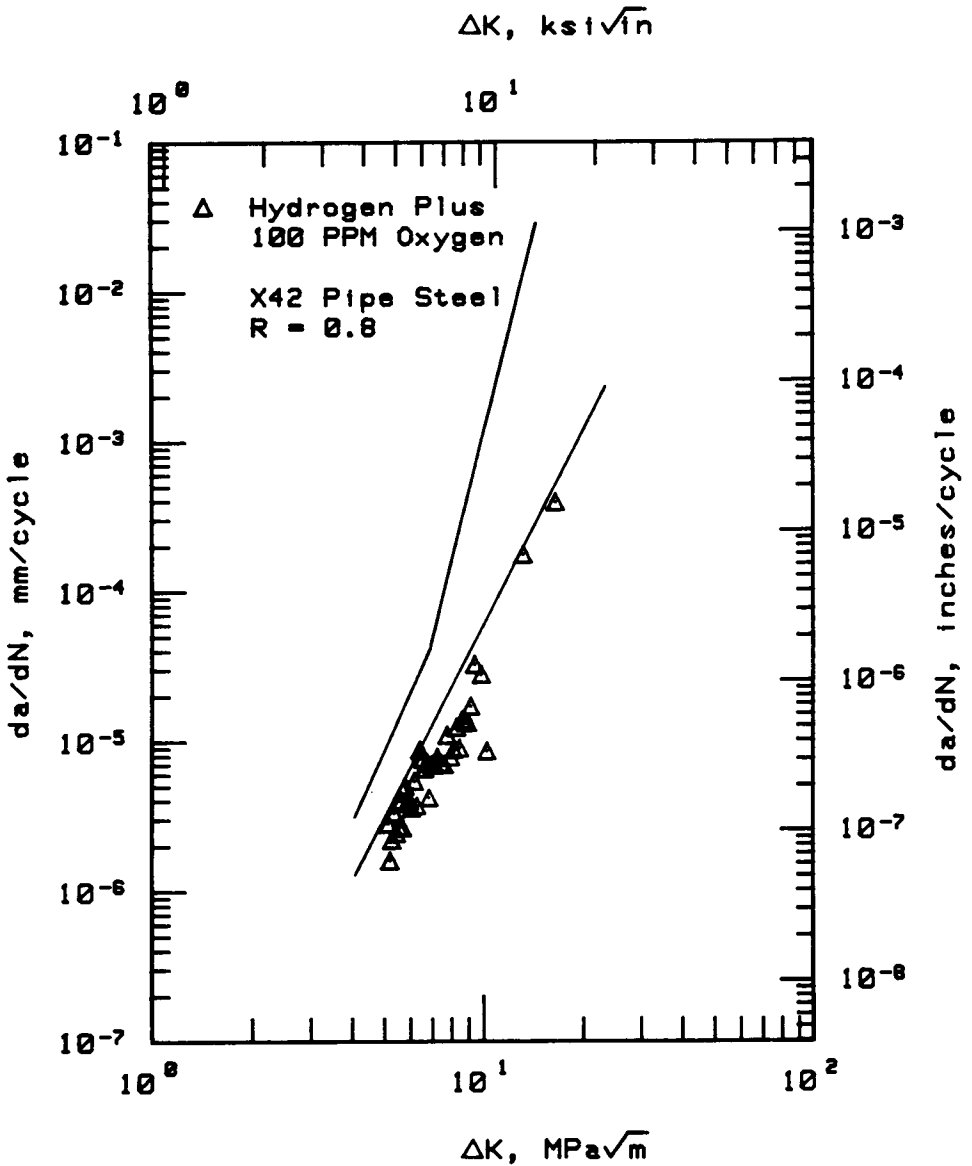
Solid lines represent hydrogen (upper line)
and nitrogen (lower line) data.

FIG. 6—Fatigue-crack-growth behavior for X42 pipe steel with sulfur dioxide addition to hydrogen at R = 0.1.



Solid lines represent hydrogen (upper line) and nitrogen (lower line) data.

FIG. 7—Fatigue-crack-growth behavior for X42 pipe steel with carbon monoxide addition to hydrogen at R = 0.1.



Solid lines represent hydrogen (upper line)
and nitrogen (lower line) data.

FIG. 8—Fatigue-crack-growth behavior for X42 pipe steel with oxygen addition to hydrogen at $R = 0.8$.

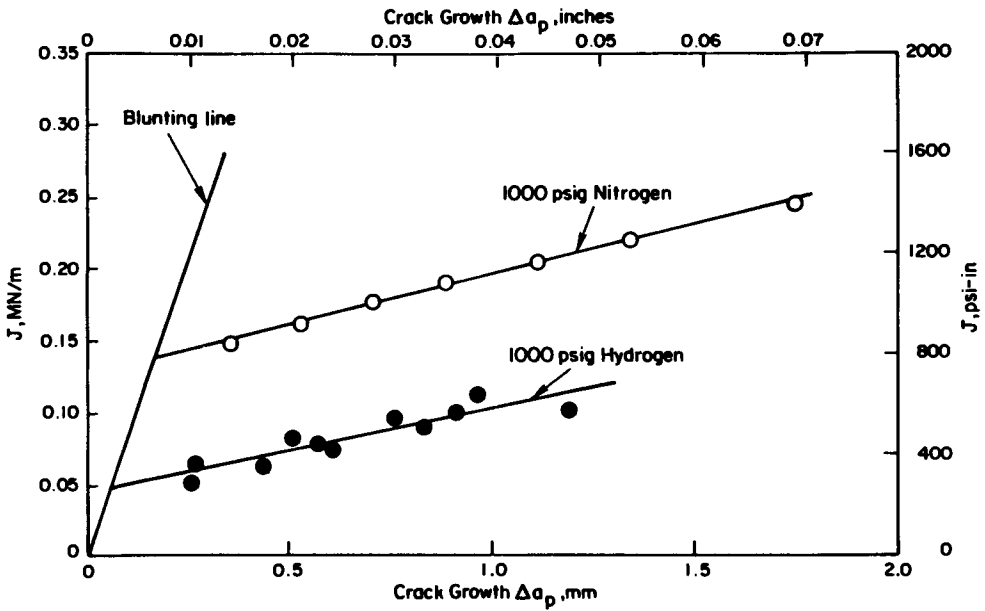


FIG. 9—J-resistance curves for X42 steel base metal tested in 6.9-MPa (1000-psi) hydrogen and in 6.9-MPa (1000-psi) nitrogen.

TABLE 4—Summary of fracture-toughness data from J-integral tests.

Steel Identification	J_{Ic} , MN/m						dJ/da , MN/m ²					
	M	MH	MHC	MHCC	N ₂	H ₂	M	MH	MHC	MHCC	N ₂	H ₂
X42	0.13	...	0.14	0.05	82	...	70	63
X70	0.20	0.03	0.23	0.22	0.17	0.04	152	40	207	179	251	23
X42-HAZ	0.02	0.01	97	69
Hardened X42	0.02	0.01	0.03	0.03	14	3.5	18	21

^aExperiments were not performed in this environment.

X70 steel in nitrogen and in the MHC environment. Thus, the properties measured in hydrogen or in the MH environment should logically be compared with the properties measured in nitrogen or in the MHC or MHCC environments, rather than methane, to infer the effects of hydrogen on these properties. This comparison is made in Table 5.

Subcritical-Crack-Growth Experiments

Subcritical-crack-growth experiments were conducted with the X70 steel, the HAZ of the X42 steel, and the hardened X42 steel in various environments. Figure 10 presents load-versus-time and crack-length-versus-time data at two fixed load-line displacements for the heat-treated X42 steel. This figure shows the difference in the behavior that was observed when subcritical-crack growth occurred and when crack-tip relaxation occurred but there was no subcritical-crack growth.

TABLE 5—Reductions in fracture-toughness properties by hydrogen.

Hydrogen Environment ^a	Percentage Reduction in Property ^b			
	X42	X70	X42-Heated Affected Zone	Hardened X42
REDUCTION IN J_{Ic}				
H ₂	63	81	50	... ^c
MH	... ^c	85	... ^c	67
REDUCTION IN dJ/da				
H ₂	17	89	29	... ^c
MH	... ^c	81	... ^c	82

^aThe partial pressure of hydrogen was 6.9 MPa in H₂ and 4.1 MPa in MH.

^bRelative to N₂, MHC, and MHCC.

^cExperiments were not performed in this environment.

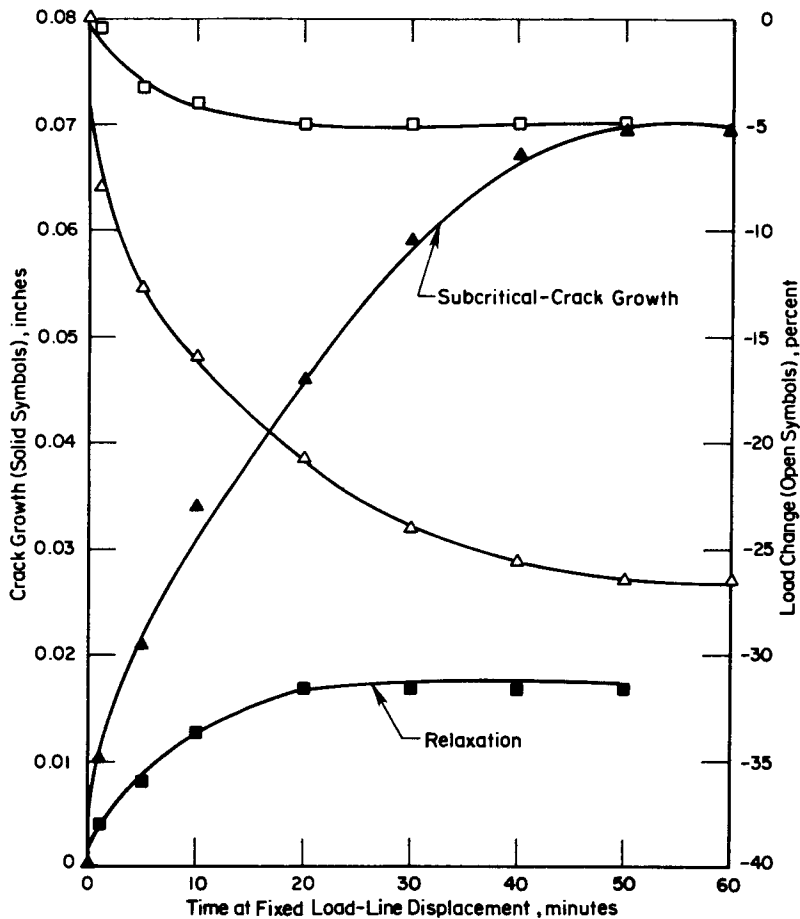


FIG. 10—Load-change and crack-growth behavior exhibited by hardened X42 steel in MH environment during crack-tip relaxation (square symbols) and during subcritical-crack growth (triangles).

The observations of subcritical-crack growth are summarized in Table 6, which indicates that the only material that exhibited subcritical-crack growth was the portion of the X42 steel pipe that was hardened. This was one of the two materials in which hydrogen induced a reduction in the tearing resistance dJ/da in the fracture-toughness tests. For that material, the CO that was present in the MHC and MHCC environments completely inhibited subcritical-crack growth; the reduction in dJ/da by hydrogen also was inhibited in these environments. In those subcritical-crack growth experiments, after three hold periods at fixed displacement, the inhibited environment was removed, and the test vessel was evacuated and purged and then backfilled with the MH environment. In both cases, subcritical-crack growth was detected in the MH environment. This observation indicates that the inhibition of subcritical-crack growth by CO was real and not an anomaly resulting from the use of an unusually resistant specimen.

Discussion and Conclusions

Gaseous hydrogen has been shown to degrade various crack-growth-resistance properties in moderate-strength line pipe steels, depending on the type of loading. Until recently, steels of such low-strength level were thought to be practically immune to hydrogen degradation. However, when cyclic loads were applied, hydrogen increased the Stage II fatigue-crack-growth rate. Crack-growth rates as much as 150 times greater than those with comparable loading in nitrogen were observed in X42 steel tested at $R = 0.1$ in hydrogen at a pressure of 6.9 MPa. This effect may have been a result of cyclic work hardening locally increasing the crack-tip sensitivity to hydrogen degradation. Crack-growth acceleration by hydrogen was inhibited completely by 100 ppm oxygen and nearly completely by 2% CO or 2% sulfur dioxide (SO₂). These inhibitors block hydrogen access to the steel by preferential adsorption and can displace any hydrogen that is already adsorbed on the surface if a sufficiently high concentration of inhibitor is present [26].

At higher stress ratios, hydrogen had little or no effect on Stage II fatigue-crack growth, but it promoted Stage III fatigue-crack growth at lower values of ΔK than occurred in nitrogen. Fracture occurred shortly after the initiation of Stage III crack growth. The transition to Stage III crack growth may be related to the value of the maximum stress intensity, K_{max} , which suggests that hydrogen also influences the fracture toughness of these moderate-strength materials. This, in fact, was shown by the J -resistance curves.

Hydrogen, either pure or in a mixture with methane, reduced the fracture toughness, J_{Ic} , by the amounts shown in Table 5. Thus, resistance to initiation of ductile cracking was reduced by hydrogen. This reduction is consistent with the acceleration of crack growth in the fatigue-crack-growth tests, which at higher values of K_{max} occurred by a premature transition to Stage III crack growth. Crack growth under those conditions can be viewed as a series of ductile-

TABLE 6—Summary of observations in subcritical-crack-growth experiments.

Steel Identification	Subcritical-Crack Growth Detected ?				
	Hardness	MH	MHC	MHCC	H ₂
X70	98 HRB	No	No	No	... ^a
X42-HAZ	99 HRB	... ^a	... ^a	... ^a	No
Hardened X42	38 HRC	Yes	No	No ^b	... ^a

NOTE: HRB = Rockwell Hardness "B"; HRC = Rockwell Hardness "C."

^aExperiments were not performed in this environment.

^bWhen the test environment was replaced with MH, subcritical-crack growth was detected.

crack-initiation events that are facilitated by hydrogen. However, the mechanism by which hydrogen enhances ductile-crack initiation is not understood at this time. As shown in Fig. 8 and Table 5, these events can be inhibited by adding oxygen, carbon monoxide, or possibly other gases to the hydrogen or hydrogen/methane environment. Again, preferential adsorption of the inhibitor on the steel blocks access of hydrogen to the steel.

The tearing resistance, dJ/da , was reduced significantly only for the X70 steel and the simulated hard spots in the X42 steel. The hardened X42 steel also was the only material that exhibited subcritical-crack growth in an uninhibited hydrogen-rich environment. The substantial reduction in J_{Ic} for the other materials evidently was not sufficient to cause significant time-dependent crack growth to occur. It is possible that limited crack initiation and growth did occur in those specimens, but that the tearing resistance was sufficiently high that further crack growth could not occur without increasing the applied J integral. This apparently was the case for the X70 steel, even though the tearing resistance was reduced by hydrogen. Thus, it appears that there may be a connection between the extent to which hydrogen reduces the tearing resistance of a material and the material's sensitivity to subcritical-crack growth in a hydrogen environment. This connection, and possible correlations between reduced fracture-toughness parameters and enhanced fatigue-crack growth, should be verified and studied further with other materials. One possible application of such correlations would be to develop the J -integral test as a standardized procedure for screening materials for their resistance to enhanced fatigue-crack growth and subcritical-crack growth in hydrogen or other aggressive environments.

Acknowledgments

The portions of this work dealing with hydrogen degradation in the transmission of synthetic natural gas (experiments in the M, MH, MHC, and MHCC environments) were supported by the American Gas Association under the supervision of the NG-18 Line Pipe Research Committee. The remaining portions of the work described were supported by Brookhaven National Laboratory under Contract 55072-S. We also wish to thank G. T. Wall and M. Oliver for their technical support in performing these experiments.

References

- [1] Groeneveld, T. P. and Elsea, A. R. in *Hydrogen in Metals*, I. M. Bernstein and A. W. Thompson, Eds., American Society for Metals, Metals Park, Ohio, 1974, pp. 727-738.
- [2] Fessler, R. R., Groeneveld, T. P., and Elsea, A. R. in *Stress Corrosion Cracking and Hydrogen Embrittlement of Iron Base Alloys*, Proceedings of Conference at Unieux-Firminy, France, 12-16 June 1973, National Association of Corrosion Engineers, Houston, TX, 1977, pp. 135-146.
- [3] Laws, J. S., Frick, V., and McConnell, J., "Hydrogen Gas Pressure Vessel Problems in the M-1 Facilities," NASA Report CR-1305, National Aeronautics and Space Administration, Washington, DC, March 1969.
- [4] Robinson, S. L., *Industrial Heating*, November 1978, pp. 23-26.
- [5] Loginow, A. W. and Phelps, E. H., *ASME Journal of Engineering for Industry*, February 1975, p. 274.
- [6] Nelson, H. G. in *Effect of Hydrogen on Behavior of Materials*, A. W. Thompson and I. M. Bernstein, Eds., The Metallurgical Society of AIME, New York, 1976, pp. 602-611.
- [7] Jewett, R. P., Walter, R. J., Chandler, W. T., and Frohberg, R. P., "Hydrogen Environment Embrittlement of Metals," NASA Report CR-2163, National Aeronautics and Space Administration, Washington, DC, March 1973.
- [8] Cialone, H. J. and Holbrook, J. H., *Metallurgical Transactions Annual*, Vol. 16A, January 1985, pp. 115-122.
- [9] Wachob, H. F. and Nelson, H. G. in *Hydrogen Effects in Metals*, I. M. Bernstein and A. W. Thompson, Eds., The Metallurgical Society of AIME, New York, 1981, pp. 703-710.
- [10] Walter, R. J. and Chandler, W. T. in *Effect of Hydrogen on Behavior of Materials*, A. W. Thompson and I. M. Bernstein, Eds., The Metallurgical Society of AIME, New York, 1976, pp. 273-286.
- [11] Walter, R. J. and Chandler, W. T., "Effects of High-Pressure Hydrogen on Metals at Ambient Tem-

- perature," Technical Report R-7780-1, 2, 3, Rocketdyne, Division of North American Rockwell Corp., Canoga Park, CA, February 1969.
- [12] Robinson, S. L. and Stoltz, R. E. in *Hydrogen Effects in Metals*, I. M. Bernstein and A. W. Thompson, Eds., The Metallurgical Society of AIME, New York, 1981, pp. 987-995.
 - [13] Kesten, M. and Windgassen, K.-F. in *Hydrogen Effects in Metals*, I. M. Bernstein and A. W. Thompson, Eds., The Metallurgical Society of AIME, New York, 1981, pp. 1017-1024.
 - [14] Kesten, M. and Windgassen, K.-F. in *Current Solutions to Hydrogen Problems*, C. G. Interrante and G. M. Pressouyre, Eds., American Society for Metals, Metals Park, OH, 1982, pp. 389-393.
 - [15] Cialone, H. J. and Holbrook, J. H., "Effects of SNG/Hydrogen Gas Mixtures on High Pressure Pipelines," AGA Report L51473, American Gas Association, Arlington, VA, February 1985.
 - [16] Frandsen, J. D. and Marcus, H. L. *Metallurgical Transactions Annual*, Vol. 8A, February 1977, pp. 265-272.
 - [17] Clark, W. G., Jr. in *Hydrogen in Metals*, I. M. Bernstein and A. W. Thompson, Eds., American Society for Metals, Metals Park, OH, 1974, pp. 149-164.
 - [18] Lynch, S. P. and Ryan, N. E., *Proceedings, Second International Congress on Hydrogen in Metals*, Paper No. 3D12, Paris, 1977, Pergamon Press, New York, 1977.
 - [19] Walter, R. J. and Chandler, W. T., Technical Report RSS-8601, Rocketdyne, Division of North American Rockwell Corp., Canoga Park, CA.
 - [20] Stewart, A. T. in *Mechanisms of Environmentally Sensitive Cracking of Materials*, Proceedings of International Conference, Guilford, April 1977, The Metals Society, London, 1977, p. 400.
 - [21] Smith, P. and Stewart, A. T., *Metal Science*, Vol. 13, 1979, pp. 429.
 - [22] Holbrook, J. H., Cialone, H. J., Mayfield, M. E., and Scott, P. M., "The Effect of Hydrogen on Low-Cycle-Fatigue Life and Subcritical-Crack Growth in Pipeline Steels," Brookhaven Report BNL 35589, Brookhaven National Laboratory, Upton, New York, 1982.
 - [23] Hoffman, W. and Rauls, W., *Welding Journal Research Supplement*, Vol. 44, 1965, pp. 225s-230s.
 - [24] Bowker, P. and Hardie, D., *Metal Science*, July 1979, pp. 432-436.
 - [25] Cialone, H. J., Scott, P. M., Holbrook, J. H., Sieradzki, K., and Bandyopadhyay, N. in *Hydrogen Energy Progress V*, T. N. Veziroglu and J. B. Taylor, Eds., Pergamon Press, New York, 1984, Vol. 4, pp. 1855-1867.
 - [26] Holbrook, J. H., Collings, E. W., Cialone, H. J., and Drauglis, E. J., "Hydrogen Degradation of Pipeline Steels," report to Brookhaven National Laboratory, Upton, New York, under Contract 550722-S, 11 March 1986.

DISCUSSION

Interrante: Is oxygen beneficial in blocking hydrogen entry into steel?

Cialone: John DeLuccia indicated that oxide films are very beneficial in the sense of blocking hydrogen entry into steel. In the case of oxygen as an inhibitor, that is something that is easy to envision happening. In the case of CO as an inhibitor, we are not sure whether it is the formation of an oxide film or carbon deposition possibly forming an intermetallic at the surface, which causes inhibition. This is one of the phenomena that we are studying now with the application of surface science techniques, but we really do not know what the fundamental processes are. It looks as though inhibition can occur with any gas that will deposit carbon, oxygen, or sulfur on the surface, provided that it does not generate additional hydrogen, as H_2S does. Gases that do not generate hydrogen but deposit one of those three elements on the surface appear to be very good inhibitors.

Interrante: The other point to mention on that question is this. For the behaviors that you studied, you are always creating new surfaces (the fatigue case and the case of the elastic-plastic tests involving J-measurements) and it is then that it becomes important to have an adsorbate to cover the surface of the newly created metal or fresh surface. This is much more important for your tests than it would be in any static test.

Cialone: In a static test, presumably there would be some mill scale on the pipe surface, or some oxide that formed on the specimen, and maybe the steel would be more resistant than with

a steadily deforming surface. There is a question whether the entry of hydrogen is blocked forever or just slowed down, and we do not know the answer. A long-term test would have to be performed to get that answer.

Interrante: It is really interesting to see your results and to contrast them with the early studies like those conducted by Hoffman. The nature of his work is identical to yours—and yours is the next generation. I am really delighted to see what you have done.

Cialone: I appreciate your comments.

Mackor: Would it not be easy to assume that the first step in hydrogen embrittlement is the hydrogen adsorption and that you have active sites on the surface of your steel on which hydrogen is adsorbed. In the presence of CO this compound of course is preferentially absorbed to the steel so it prevents the hydrogen from entering the steel? Would not that be an easy type explanation for what you observe as inhibition?

Cialone: Yes, but our surface science studies indicate that it is not just CO sitting on the surface as CO. There is a dissociative adsorption process and what happens after it dissociates is unclear at this time, but what you say is true in general. We are creating preferential sites. We are forcing fresh metal surface to be formed, and we are measuring the resistance of the material to this process. If we can give something else a chance to adsorb preferentially to the hydrogen, then we can block the hydrogen out.

Mackor: It seems completely logical to assume that CO and oxygen are preferentially adsorbed to the steel.

Cialone: On the basis that they perform well as inhibitors or on some other basis?

Mackor: On the basis of chemical intuition and knowledge. I expect that for instance CO is much more strongly adsorbed onto iron than H_2 . This is a thing related to catalysis. You have to talk to catalysis people about adsorption of these gases to the surface of your steel.

McIntyre: When you see the accelerated crack growth in the hydrogen environments, what kind of shift in fracture mode do you see on the SEM?

Cialone: In the near threshold range at low values of delta K, we see a tendency towards intergranular crack growth and, through etching studies, have determined that the intergranular crack growth occurs between ferrite grains, at least in the X-42 steel, which has a microstructure consisting of bands of ferrite and pearlite. We had expected the pearlite to be more severely affected than the ferrite, but were surprised to find that the crack growth favored the ferrite-ferrite grain boundaries. At high delta K, we did not see as distinctive a difference in fracture mode, but there was always a tendency for less deformation on the surface of the specimens fractured in hydrogen.

The Present Status of the Disk Pressure Test for Hydrogen Embrittlement

REFERENCE: Fidelle, J.-P., "The Present Status of the Disk Pressure Test for Hydrogen Embrittlement," *Hydrogen Embrittlement: Prevention and Control*, ASTM STP 962, L. Raymond, Ed., American Society for Testing and Materials, Philadelphia, 1988, pp. 153-172.

ABSTRACT: This paper is an update of an enormous amount of work done since STP 543. Accept/reject criteria are illustrated as well as numerous parameters examined such as: (1) strain rate, (2) interfacial and geometrical factors, (3) metallurgical factors, and prior embrittlement from other sources or combined mechanisms, for example, gaseous hydrogen embrittlement on previously embrittled titanium or steel.

Applications to sustained load, rising load, cyclic loads and small alternating loads on sustained loads are illustrated.

A large amount of new test results on a variety of material is presented, including welded Inconel 718.

KEY WORDS: disk pressure test, internal hydrogen embrittlement, gaseous hydrogen embrittlement, high-strength steels, precious metals

Background and Scope of the Present Survey

The issue of hydrogen effects on metals has been frequently clouded by a lack of common understanding of the vernacular. This is why the definitions pertinent to the Disk Pressure Test (DPT) have been addressed.

During this test, disks clamped in a cell (Fig. 1) are stressed by fluid pressures applied on one or both sides until disk pressures (P upstream, P downstream) increase continuously (dynamic test) or stepwise, be maintained constant (static, delayed failure tests), or become cycled.

Fluids can be liquids, gases (for example, molecular hydrogen), or mixtures; they can be neutral (for example, helium) or aggressive and hence decrease the rupture pressures, the times to failure, and the number of cycles to failure during fatigue tests, or degrade the macroscopic and microscopic appearances of the ruptures.

The technique, its successive developments, and its achievements have already been described by a number of papers since 1969 [1-25], including its first comprehensive publication in English as ASTM STP 543 [7,8], as film [26], and as a book [27].

Therefore, we shall focus on new results. Easily available data only will be pinpointed except in the few instances where data have to be corrected or can be presented in a more striking manner.

New data include:

1. Those obtained by an enlargement of the DPT experimental range between -196 and $+1000^{\circ}\text{C}$, at strain rates between 0.2 and $2 \times 10^{-8}\text{s}^{-1}$ ($50\,000$ to $0.005\text{ bar} \cdot \text{mn}^{-1}$) at frequencies between 0.1 to 0.005 Hz during low-cycle fatigue [22].
2. The generalization of a criterion for acceptance or rejection of material-environment or internal hydrogen concentration-material couples.

¹Service Metalurgie, CEA, PV 12, Burge Res' Le' Chotel, France 91680.

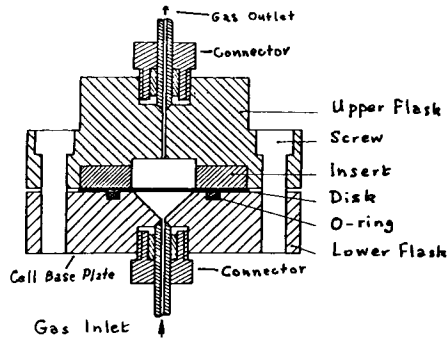


FIG. 1—The basic DPT cell (BF-58).

The Pressure Deflection Curves [10,29,21,22]

They consist of two types (Fig. 2). Type 1 is typical of a material with a small work-hardening coefficient, at odds with Type 2. But in both instances, the pressure at the onset of localized plastic flow is small compared with the rupture pressure under neutral gas. This emphasis on the plastic regions is a most interesting feature because hydrogen embrittlement (HE) precisely decreases the ability of materials to resist by plastic deformation growth and propagation and defects.

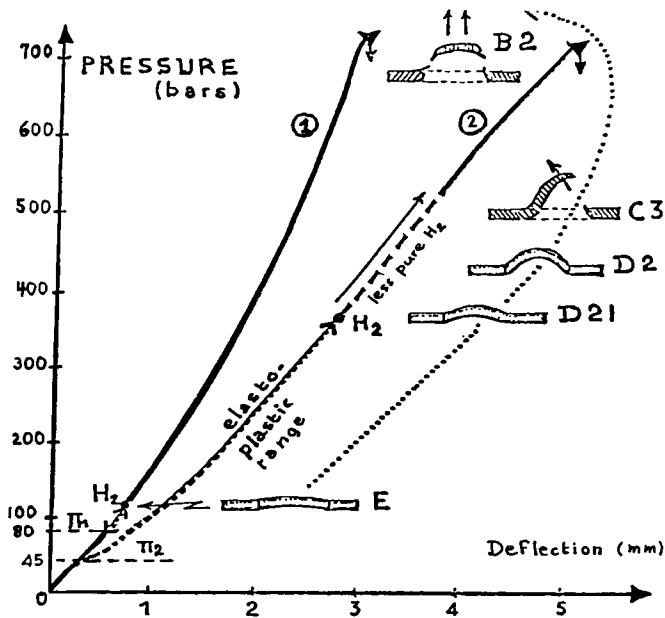


FIG. 2—The two typical pressure-deflection curves with hydrogen gas are supplied by this 35 NiCrMo 16 martensitic steel heat treated to: ① 1900 MPa; ② to 1050 MPa. Typical rupture aspects of the disk are drawn to illustrate change in shape of the disk with increased pressure.

It is noteworthy that hydrogen gas (H_2) does not change the shape of the pressure-deflection curve. It is simply interrupted earlier, much earlier in the case of higher strength material. The pressure-deflection curve is only modified in peculiar cases, for example, materials previously charged to very high hydrogen (H) contents such as Beta III titanium alloy [11] or able to absorb large amounts of hydrogen during their deformation in the presence of this gas, such as palladium (Pd).

Reasons for the Disk Pressure Test's Very High Sensitivity [10, 12, 22, 23]

In Fig. 2, one also sees that, under the effect of pressure, disks increasingly evolve to domes, that is, to a geometry increasingly resistant to the effect of pressure. Then, besides the effect on a given geometry, hydrogen also prevents the disk evolution towards a geometry more resistant to the effect of pressure.

This can be easily confirmed by preforming disks under helium pressure.

After the helium is removed, the rupture pressure under hydrogen (P_H) exceeds the normal rupture pressure under hydrogen of the disk with no prior deformation (Fig. 3).

Stress triaxiality and inhomogeneity of deformation are known to enhance sensitivity to embrittlement.

A finite-element analysis has shown that a triaxial stress state builds up at the anchorage at the very beginning of the test (Fig. 4). As soon as it is exceeded, a notch-like plastic enclave in tension appears at the anchorage.

Its growth will cause a sweep of the material by the displacement of the elastoplastic interface, a continuous generator of mobile dislocation able to foster localized hydrogen absorption and segregation to the critical zones of the material.

Some of the most important rupture aspects are either ductile rupture under an increasing helium pressure, where necking occurs at the anchorage and produces outstripping of the central cap or intergranular brittle cracking at the anchorage due to the simultaneous presence upstream of hydrogenated fluid and an increasing helium pressure.

Let us consider Fig. 5, the strains in a 35 NiCrMo 16 high-strength steel disk under pressures of 100 and 650 bars, which are close to the rupture pressures under hydrogen and helium, respectively.

Because of the clamping of the disk, the tangential strain always remains low even when pressure increases. On the other hand, the absolute values of the deformations according to depth ϵ_r , and the radial deformations become very high at the anchorage. There the disk stretches and gets thinner, both favorable to the hydrogen absorption in the relatively narrow zone deformed in such a way.

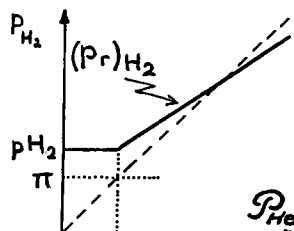


FIG. 3—Effect of the prestress under helium pressure on the rupture pressure during a following hydrogen test.

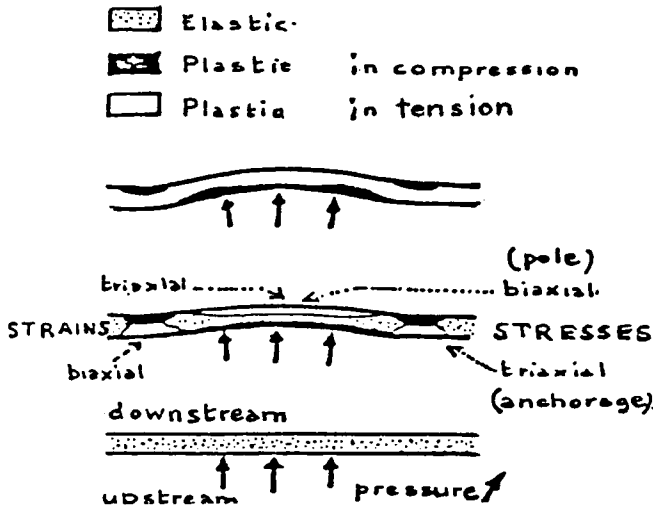


FIG. 4—Stresses and strains in a pressurized embedded disk; evolution of the plastic regions in compression and tension as pressure grows.

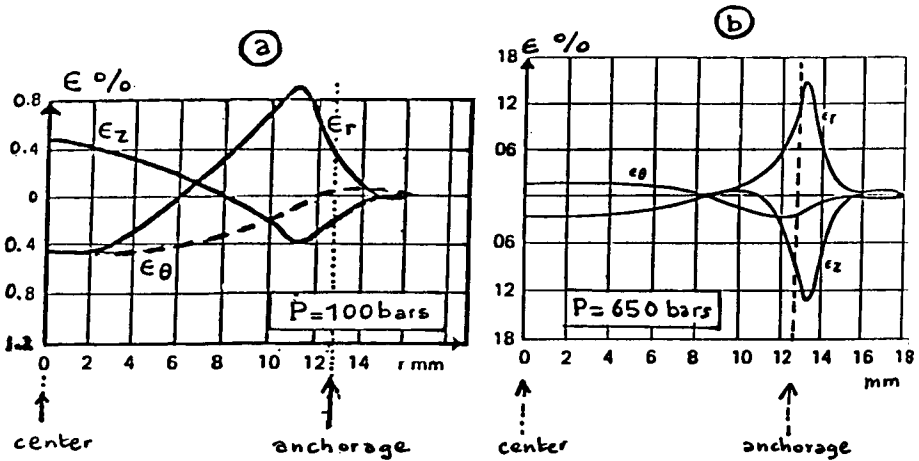


FIG. 5—Distribution of strains ϵ_θ , ϵ_r , ϵ_z on the upstream face of a disk as a function of the applied pressure.

Influence of Strain Rate—Relationship Between Dynamic Static Tests and Low-Cycle Fatigue Static

Rupture pressures are designated P_r in a general way, P_H for ruptures under hydrogen gas, P_{He} for ruptures under helium of uncharged specimens, P_{HeC} for ruptures helium-charged specimens, etc.

There are three ways to plot these parameters as a function of time or increased pressure rate $\Delta P/\Delta t$, the compared interests of which will be discussed later.

Influence of Hydrogen on the Rupture Pressures During Strain Rate Testing, Relationship with Delayed Failure

When disks are deformed under hydrogen or under helium after hydrogen charging, the rupture pressures P_H or P_{He} are lower than P_{He} , but in a few instances, such as titanium alloys, a beneficial effect of hydrogen can prevail before helium eventually appears.

On a classical $P_r = f \log(t)$ diagram, one sees that materials become embrittled faster if the following conditions (A) and (B) are fulfilled or at least one has a dominant influence:

- (A) High hydrogen diffusivity = D_H .
- (B) High sensitivity to hydrogen embrittlement.

This is illustrated by Fig. 6a, which shows the isotopic effect on 35Ni-Cr-Mo 16 high-strength steel and the effect of temperature on D_H at three temperatures where condition (B) is approximately the same.

On Fig. 6b appears the dominating influence of hydrogen embrittlement sensitivity for the same steel heat treated to two different strength levels where, however, hydrogen diffusivities are approximately the same.

Figure 6c compares two platinum alloys, one with moderate conditions A and B (Phynox).

Figure 6d deals with three different austenitic stainless steels on a pressure vs $\log(t)$ diagram. Although D_H are practically the same for an unstrained metastable 302L, a stable 316L, and a hardened stable A286, some hydrogen effect appears on 316L, but it appears at a higher loading ratio ($\Delta p/\Delta t$) for hardened A286 because it is more sensitive to hydrogen gaseous embrittlement and much higher rates for metastable 302L because straining induces a partial transformation of austenite to martensitic phases more sensitive to hydrogen embrittlement and where D_H is also larger than in austenite: Cases (a) and (b).

In Fig. 6e, in a very similar way to stress corrosion cracking (SCC), a significant recovery of hydrogen embrittlement takes place at low strain rates because the generation rate of oxide-free clean surfaces by plastic deformation ceases to be high enough to prevent their passivation by the oxygen impurities present in hydrogen. The odd consequence is that hydrogen embrittlement may be better observed at higher loading ratios than those where it would be larger if the repassivation effect were not present. Such an effect has already been observed in the cases of Ta, Nb, and Nb alloy wires, according to Refs 28 and 29, and Ta and Nb disks, according to Ref. 30.

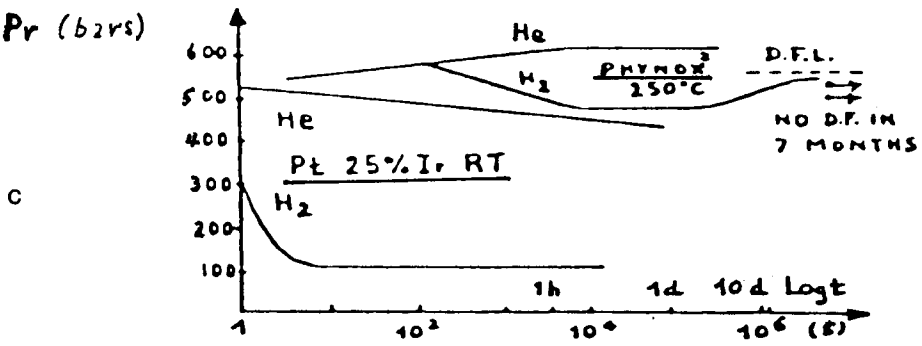
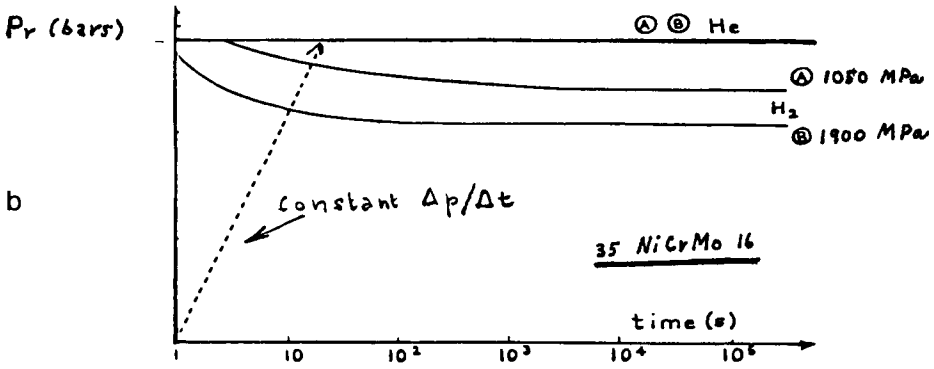
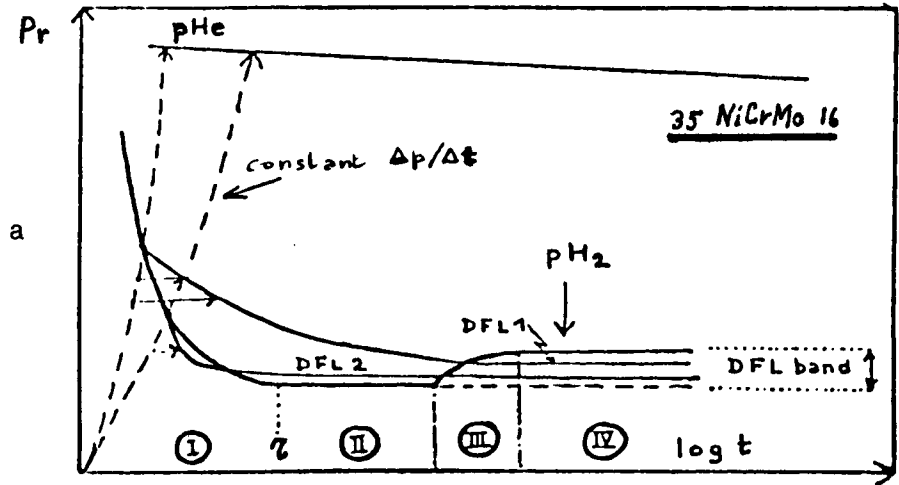
Earlier work has shown that the Delayed Failure Limit (DFL) was close but never lower than Plateau II of the P_H minimum observed on steels, Co alloys, Mn 12% Ni alloy, etc. On the other hand, in the case of materials very sensitive to surface poisoning by impurities of hydrogen, such as O_2 , the DFL is not expected to be close to P_H minima values obtained during strain rate test, but rather to rise up to the values, unless the experiments are conducted with special care.

Internal Hydrogen Embrittlement

The DPT has been used in a number of instances for internal hydrogen embrittlement studies on disks charged cathodically or during plating [2, 7, 10, 13] but more frequently thermally charged in case a too low D_H at room temperatures would not ensure a homogeneous charging.

Materials include Ti40 [10], Ti-5Al-2.5 Sn [18], Ti-12Mo-Zr-Sn (Beta III) [27] Ti alloys, U alloys such as U 0.2% V [19] Inconel 718, A286 hardened austenitic stainless steel [4, 7], AISI 326 (IN 744) (austenitic + martensitic) stainless steel and a variety of nonaustenitic steels such as 20 CrNiMo 10, A508, etc., 35 NiCrMo 16 [7] and 350 Maraging steels and other alloys as shown in Figs. 7 and 8.

At p/Ar, between 15 and 200 bars/mn and between S and 800 bars/mn hydrogen embrittlement at slow strain rates due to dissolved hydrogen take place in thermally charged Beta III Ti alloys, respectively, to 1800 and 3000 ppm hydrogen. In the second instance, above 800 bars/



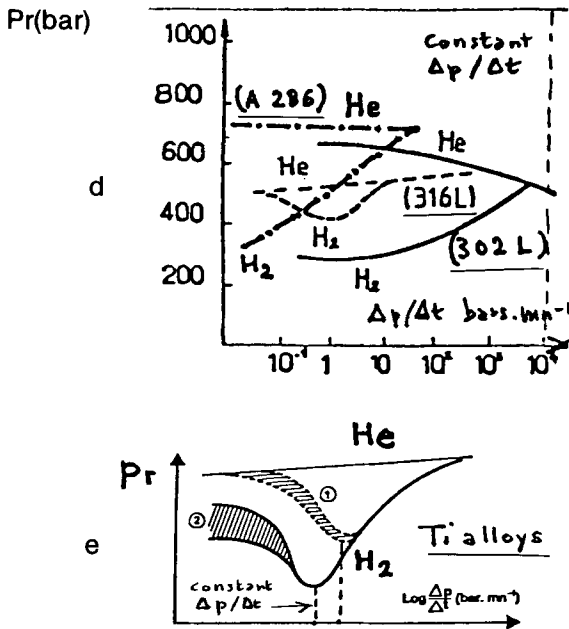


FIG. 6—(a) 35 NiCrMo 16 high-strength steel. Conditions A and B are fulfilled. (b) Influence of test time P of 35 NiCrMo 16. $Q + T$ 2 times at: (A) 650°C , $TS = 1050$ MPa; (B) 230°C , $TS = 1900$ MPa. (c) Influence of test time on hydrogen gas embrittlement of two platinum face centered cubic alloys: (1) Phynox = moderate condition: (A) and (B); (2) platinum alloy with very low Pt: 75% platinum and 25% iridium at room temperature. (d) Case of three austenite stainless steels with same D_H but different helium susceptibilities. Condition (B) dominates plus additional effect of (A) for 302L (after Ref 24). (e) Influence of pressure increase rate and gas purity ② purer than ①. DFL is the delayed failure limit.

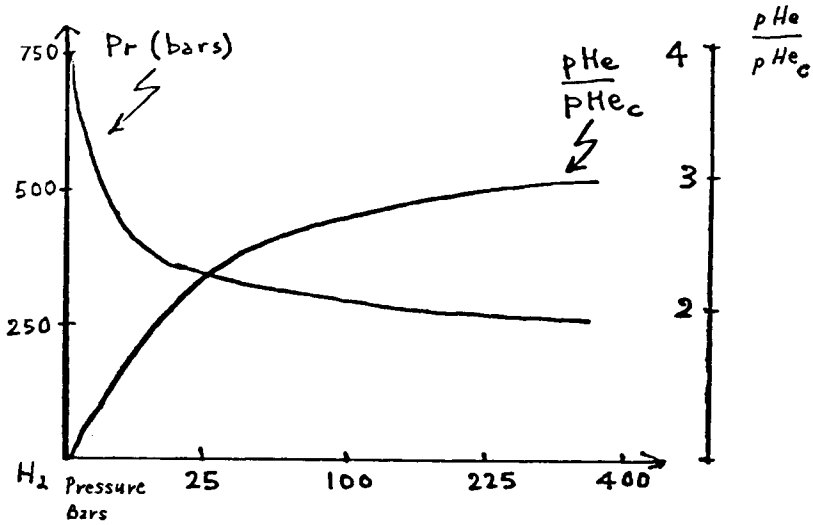


FIG. 7—This figure shows the influence of hydrogen contents absorbed of hydrogen pressures during the aging treatment, 3h at 520°C, of Phynox face-centered cubic Co alloy.

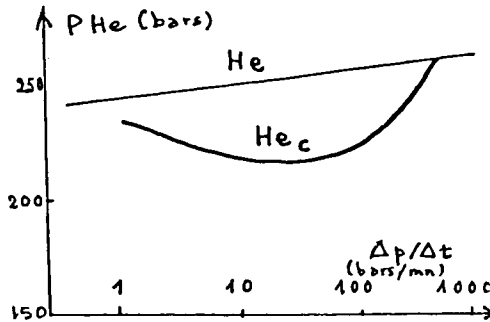


FIG. 8—Diagram on internal hydrogen embrittlement of diametrically welded 304L disks (charged to 20 ppm) similar to the one for gaseous hydrogen embrittlement of 316L (see Fig. 6d).

mn P_{He} decreases rapidly due to the Kolachev effect [13] appearance of high hydride embrittlement. (See Fig. 9.)

The Kolachev effect is already indicated on the right of the 1800-ppm curve and a rapid drop of p_{He} has also been noted above 150 bars/mn⁻¹ for Ti-40 charged up to 1100-ppm hydrogen (mostly as hydrides) [11].

However, in these instances, the DPT sensitivity to the effects of hydrogen at high pressure is clearly not so good as that of an impact test. Therefore, in order to increase the versatility of the DPT, it is desirable:

1. To concretize a project based on the principle of a "gas gun" in order to achieve a quite significantly higher, yet reliable loading rate.

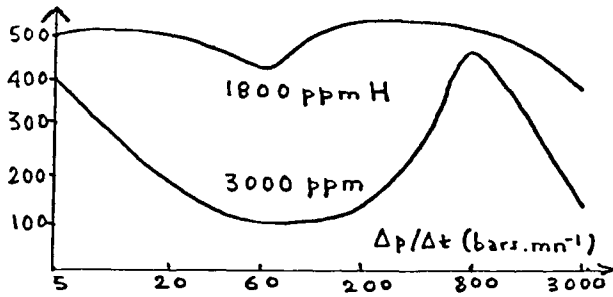


FIG. 9—Internal hydrogen embrittlement due to dissolved hydrogen at low and high strain rates in a thermally charged Beta III Ti alloy.

2. To use disks with a center prismatic notch, the efficiency of which has already been seen earlier in studies of low-temperature embrittlement on 1018°C steel [27] and hydrogen pressure on the hydrogen gaseous embrittlement of 27 CrMo 12 steel used for mechanical reactors [21].

Low-Cycle Fatigue (LCF)

Alternatively reversed LCF experiments have been conducted by applying successively sustained pressures and alternative pressures on a clamped disk [15].

LCF is a cumulative process of plastic deformation on a microscopic scale. Accordingly, this can be affected by hydrogen above the endurance limit and can decrease the number of cycles to rupture as compared with helium, but no hydrogen effects have to be expected where fatigue no longer takes place. This is why, after a number of experiments on 35 NiCrMo 16 high-strength steel, we had hypothesized in 1977 that the endurance limit should be the same for helium and hydrogen [15].

Experiments carried out recently in our laboratory by Sella and Bonnereau on X 50 CrMoV 5 (H 11) medium-strength steel and cold-worked (austenitic + martensitic) 304L have confirmed this hypothesis.

Advantages and Inconveniences of the Different Diagrams

1. $P_r = f(\log p/t)$ easily allows comparison of the rupture pressures P_{He} , P_H , or P_{He} at the same loading rate to obtain the P_{He}/P_H ratios (Fig. 6d, 6e; Fig. 8, 9).

2. $P_r = f(\log t)$. Here the above determination is less easy, but Delayed Failure and LCF curves can be easily plotted on this diagram and compared to strain rate test curves, which is not possible in Case 1 (Fig. 6a, 6b; Fig. 10).

3. $\log P_r = f(\log t)$ (Fig. 6c). Here the upper part of the diagram is compressed, which sometimes can be a disadvantage, but it includes the advantages of the other two diagrams: loading rate curves there appear as lines with different slopes instead of verticals as in Case 1.

Influence of Other Testing Variables

Instances of Environmental Variables

1. *Hydrogen pressure* studies have already been carried out on several alloys: HS 35 NiCrMo 16 steel [1]; martensitic 4330 steel heat treated to HS, MS, and LS levels [8, 9]; 9% Ni cryogenic steel; and aged Inconel 718, for which results will be presented later.

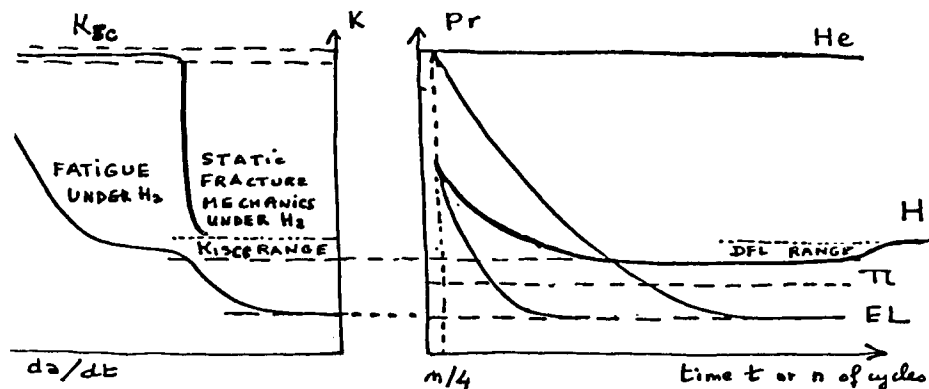


FIG. 10—Comparison on diagram (b) of strain rate test, delayed fracture, and LCF curves and to a fracture mechanics diagram (a).

In Fig. 11 Am 355 precipitation-hardened martensitic stainless steel appears as extremely sensitive to hydrogen embrittlement, even more than most low- or medium-alloyed martensitic steels with almost a double yield strength. Accordingly, it remains considerably embrittled even under low hydrogen partial pressures.

2. *H purity.* The presence of traces of oxygen reduces considerably or even suppresses hydrogen gaseous embrittlement of materials very sensitive to its contamination such as Nb, Ta, and Ti alloys [12, 27]. But it also significantly influences steels [31].

3. *Low and Elevated Temperatures.* Physical hydrogen embrittlement (not CH_4 embrittlement) of 20 CrNiMo 10 martensitic steel exists above 600°C . For TZM Mo alloy [22] and Haynes 188 FCC Co alloy [15], the limits (if any) are above 800 and 1000°C , respectively. Hydrogen gaseous embrittlement of 35 NCD 16 martensitic steel exists at least between -145 and $+300^\circ\text{C}$ [7]. (See Fig. 12.)

Figure 13 shows that hydrogen gaseous embrittlement exists at temperatures very close to liquid N_2 temperature.

The need for slower and slower tests as temperature decreases, as well as the rate of surface reactions and diffusion, adds the problem of very long tests at low temperatures to the already existing problem of such tests at room temperature.

Since hydrogen gaseous embrittlement also appears dependent on pressure, it might well be that liquid N_2 temperature is not the limit for hydrogen gaseous embrittlement as temperature decreases.

Interfacial and Geometrical Factors

Among them several have been studied previously in earlier papers:

1. Surface condition and surface treatments [2, 7, 8, 27]. Additionally a polishing bath was found to suppress hydrogen gaseous embrittlement of Ti-6Al-4V during strain rate test.

2. Notches can enormously increase hydrogen gaseous embrittlement as seen in a case without special care, processed 27 CrMo 12 MSS, even under a pressure of 200 bars, that of a commercial cylinder [27].

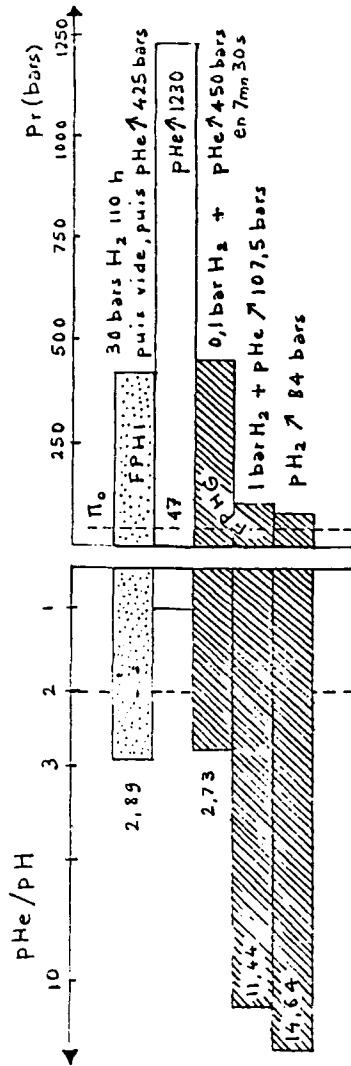


FIG. 11—Internal hydrogen embrittlement and hydrogen gaseous embrittlement of AM 355 PH martensitic stainless steel.

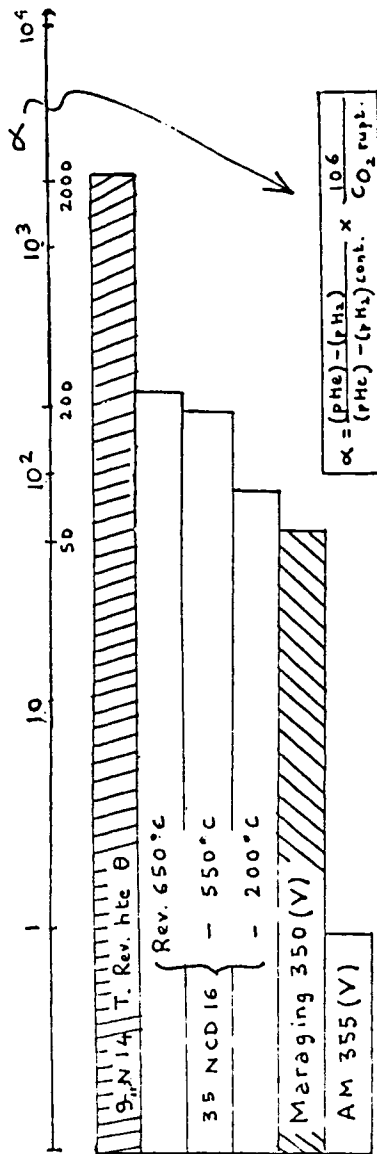


FIG. 12.—Confirms the inhibiting effect of oxygen, but for a given proportion of oxygen the effect is the largest for the least hydrogen embrittlement sensitive and decreases by steel strength level.

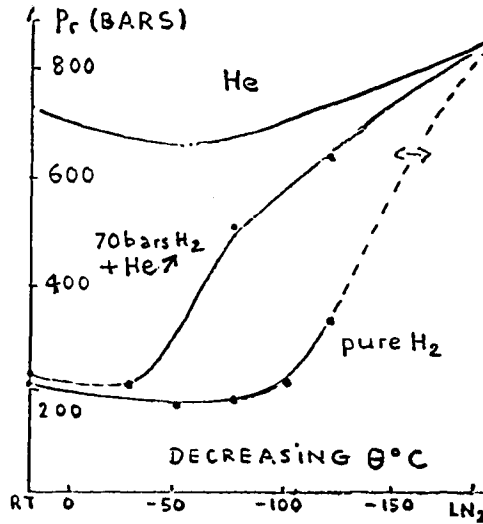


FIG. 13—Hydrogen gaseous embrittlement of a 9% Ni cryogenic steel at low temperatures. (We thank Dr. Martin Kesten of Messer Griesheim Co. in Dusseldorf for the supply of the steel and permission to publish the results.)

Instances of Metallurgical Factors

There are many metallurgical variables, the influence of which are so interrelated that they can hardly be isolated, for example, mechanical properties and heat treatments. They may also appear differently according to circumstances, for example, the sensitivity to hydrogen embrittlement of the crystallographic structure according to the nature of the base metal.

Many have already been considered in the general literature, including the literature on the DPT such as the influences of phase transformations, welding, sensitization treatments, thermomechanical treatments, texture, etc. Therefore, we shall now only focus on two aspects which are especially important for the two highlights of this paper. (See Fig. 14).

1. *Influence of cold work.* We have seen earlier, in Fig. 3, the beneficial effect of a cold work according to the directions to be strained in service.

In a different situation, cold work can be detrimental. Here cold work also decreases hydrogen embrittlement but at the expense of a severe loss of ductility even in the hydrogen absence.

2. Various factors related to the nature of the base metal, crystallographic or microscopic structure, and materials processing are presented in Fig. 15.

Comparison Between Various Sources of IHE and EHE.

Figure 16 shows how the DPT can be used to make quantitative comparison between various sources of the internal hydrogen embrittlement and environmental hydrogen embrittlement, although the ductility is low because of P_{He} .

Miscellaneous

The DPT has also been successfully used for investigation of other environmental effects such as:

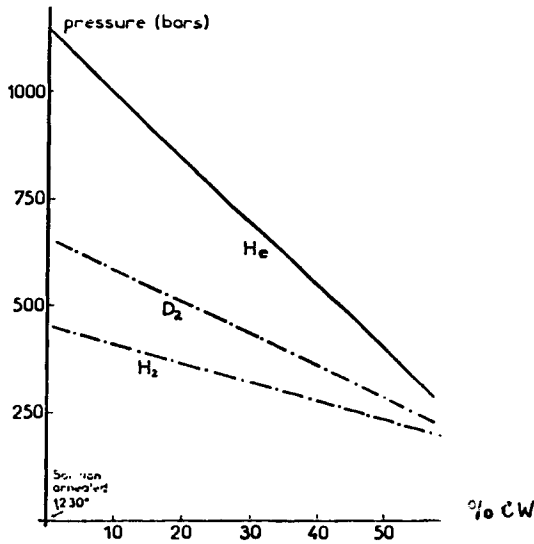


FIG. 14—Influence of %cw: $(t_o - t_f \times 100)$ on P_H , P_{H_2} , pD of Haynes 25 Co alloy disks.

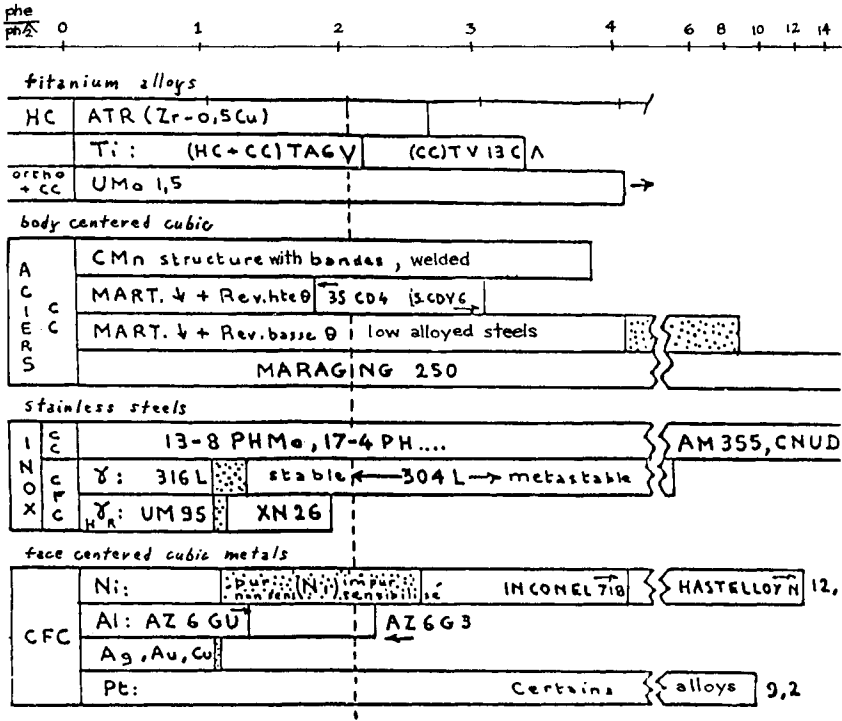


FIG. 15—Comparison of hydrogen gaseous embrittlement for various alloy systems, structures, and conditions.

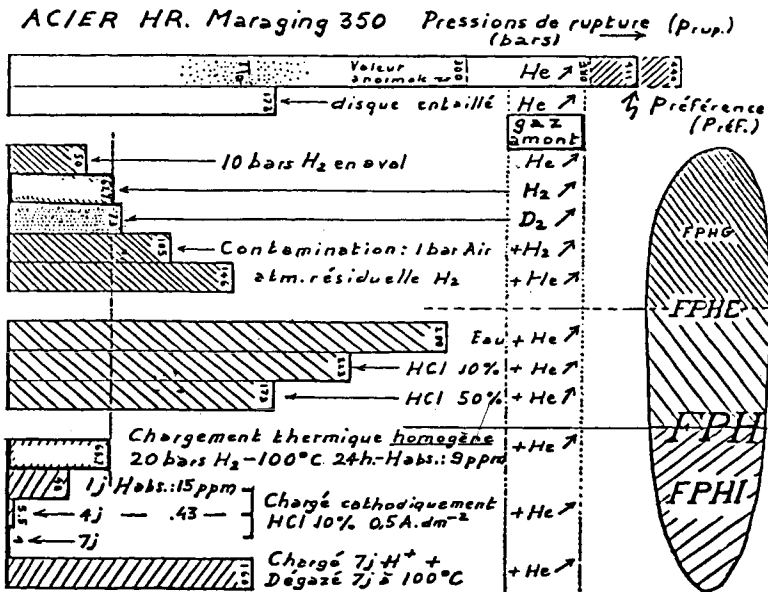


FIG. 16—Comparison of a variety of sources for the embrittlement of a 350 Maraging steel.

1. Embrittlement of U 0.2 wt% V uranium alloy in ethylic alcohol, degreasing, machining fluids [32].
2. Instances of stress corrosion cracking of steels and U 10% Mo uranium alloy exposed to moist air on one side and/or wet compressed gases on the other side [22,27] SCD of steels in liquid NH.
3. General corrosion by hydrogen or D of rare earths such as Y or U alloys such as U 0.2 wt% and U 1.5 wt% Mo, with or without the accelerating effect of pressure-generated stresses [33].
4. Permeability to hydrogen isotopes [34,35] and research of coatings proposed to delay and decrease hydrogen entry and embrittlement.

Similarities of the case of hydrogen blisters and disk tests have already been pointed out earlier [21,25]. Development of these comparisons, extended to the case of "raised blisters" found by Shewmon [36] during the hydrogen attack and methane in C steels, should logically be beneficial and allow a better understanding of these cases of hydrogen reaction embrittlement.

Acceptance or Rejection Criteria for H-Materials Couples

Case of Gaseous Hydrogen Embrittlement

In the case of gaseous hydrogen embrittlement, for many materials it has been possible to compare the laboratory results obtained on reference material or sampled-out accidented structures to the behavior of real structures: no accidents after many years or accidents at an early stage of service life, sometimes even on starting the equipment. Hence, it has been possible to find out that the ratio $P_{He}/P_H = 2$ was a landmark, separating materials for which hydrogen embrittlement alone could be the cause of failure from those for which hydrogen alone would not be the only cause of failure [25].

Accordingly the criterion

$$P_{He}/P_H \text{ unambiguously } < 2$$

is a quality criterion for a material in a given environment. If the mean ratio would be lower than 2 but with a scatter exceeding 2, the criterion would not be fulfilled.

Of course, if the material changes, ages, or if the environment is modified, becomes more or less aggressive, the ratio has to be reassessed.

Figure 17 provides the case of a welded Inconel 718, which could not have been safely operated in the presence of high pressure hydrogen, but could be operated safely under a pressure of only 4 bar.

Limits and Complements of the Criterion

Such a criterion cannot prevent any error involved in the ruin of a structure. It is a quality factory applicable to:

1. A given material in a specified environment.
2. A given environment for a specified material.
3. A tolerable amount of hydrogen in a given material.

But it has not been questioned in the case of things like poor design, misuse of the equipment, inadequate sampling of specimens, etc., and generally in those cases where hydrogen embrittlement is not the primary cause of rupture but only a contributing factor.

The tests on cold-worked HS 25 Co have shown that, as the hardening of the material exhausts ductility, P_{He}/P_H decreases from 2.52 to 1; because P_{He} has decreased, too, and even under helium rupture is brittle now. This indicates that such a criterion as P_{He}/P_H can be used only if the classical mechanical properties, and especially ductility, are at first hand satisfactory.

The DPT has generated another criterion, useful in the absence of confirmed knowledge on the classical mechanical properties. This criterion (P_{He} unambiguously > 5) ensures that the

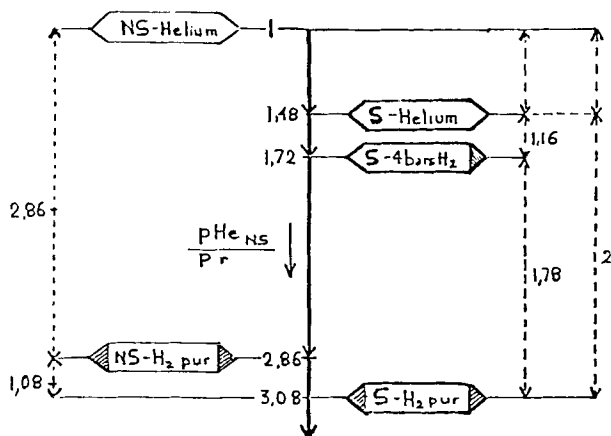


FIG. 17—Single or combined effects of a welding technique and of hydrogen gaseous embrittlement due to different H_2 pressures, in the case of an age-hardened Inconel 718. S = welded; NS = not welded; pur = purified.

material has sufficient ductility. Of course, this criterion can be adapted to other environments than helium in which a contemplated material has to be operated. For instance, it has been found that Beta III Ti alloy could be operated in ordinary purity hydrogen but not in purified hydrogen.

Depending on materials, one or the other of the two criteria (a) $p_{\text{He}}/p_{\text{H}} < 2$ by decreasing pressure of helium and (b) $P_{\text{He}}/P_{\text{H}} > 5$ is the most severe, generally (a) for steels and (b) for Ti alloys.

In general, safety will demand to abide by the more severe one.

Extension to Other Media and Internal Embrittlements

We have shown that, generally, hydrogen had only a negligible effect on the loading rate curves. Therefore, the just-mentioned criterion is applicable to other media provided that they do not change the shape of the stress strain curves and have as a main effect their premature interruption.

It is also applicable to internal embrittlement, provided these main conditions are fulfilled and that the stress strain curves can be drawn under the conditions of best sensitivity to the adverse phenomenon.

Conclusions

1. The application range of the DPT and therefore its industrial and scientific interest have been expanded considerably. But it remains to extend the strain rate range beyond the lowest and the highest rates existing presently.

2. The DPT has made it possible to significantly improve the relationship existing among various effects of hydrogen, some apparently different at first glance.

3. Comparison of hydrogen gaseous embrittlement tests and service behavior of a large variety of materials and industrial equipments has made it possible to specify acceptance criteria for industrial service, which, provided the shape of the stress strain curves is not significantly affected, can be expanded to internal hydrogen embrittlement, hydrogen embrittlement by other fluids than hydrogen, the selection of candidate materials in specified media or candidate media to environ-specified materials.

4. From the tests on a large number of metal systems, a theory of hydrogen embrittlement has been derived which accounts for the behavior of metals and alloys embrittled by dissolved hydrogen and/or which specifically form solid hydrides by a direct reaction with hydrogen.

This theory, supplemented by the other factors we have presented, can contribute to predict which new or hitherto untested material may be affected in some capacity.

References

- [1] Fidelle, J. P., Allemand, L. R., Roux, C., and Rapin, M., "Essai rapide de fragilisation de disques métalliques par l'hydrogène sous pression," Colloque *L'hydrogène dans les métaux* 1967, J. P. Fidelle, M. Rapin, Eds., CEA, Paris, 1969, pp. 131-172.
- [2] Fidelle, J. P., Deloron, J. M., Roux, C., and Rapin, M., "Protection des aciers 35 NCD 16 et maraging contre l'action de l'hydrogène comprimé," *Métall. Constr. Mécan.*, Vol. 101, 1969, pp. 341-349.
- [3] Poirier, J., Fidelle, J. P., and Roux, C., "Essai mécanique pour zones soudées et cordons de soudure," Congr. Internat. Soudage et fusion par faisceaux d'électrons, Paris, 1970, Interbus Paris, 1971, pp. 529-543.
- [4] Legrand, J., Caput, C., Couderc, C., Broudeur, R., and Fidelle, J. P., "Contribution à l'étude de la fragilisation par l'hydrogène d'un acier austénitique stable," Xè. J. Aciers Spéciaux, Nantes (13.5.71) *Mem. Sc. Rev. Mét.*, Vol. 68, 1971, pp. 861-869.
- [5] Fidelle, J. P., Legrand, J., and Couderc, C., "A Fractographic Study of Hydrogen Gas Embrittlement in Steels," Paper F-7, AIME Fall Meeting, Detroit, Oct. 1971.
- [6] Legrand, J., Couderc, C., and Fidelle, J. P., "Examen microfractographique de disques en acier 20

- CND 10 fragilisés par traitement thermique et par l'hydrogène sous pression," Congr. Internat. L'hydrogène dans les métaux, Chatenay-Malabry, 1972, pp. 316-318.
- [7] Fidelle, J. P., Broudeur, R., Pirrovani, C., and Roux, C., "Disk Pressure Technique," symposium on Hydrogen Embrittlement Testing, Los Angeles, June 1972, L. Raymond, Ed., *ASTM STP 543*, 1974, pp. 34-47.
 - [8] Fidelle, J. P., Bernardi, R., Broudeur, R., Roux, C., and Rapin, M., "Disk Pressure Testing of Hydrogen Environment Embrittlement," *ASTM STP 543*, pp. 221-253.
 - [9] Fidelle, J. P., Arnould-Laurent, R., Roux, C., and Lacombe, P., "Fragilisation par l'hydrogène interne et externe," 17^{ème} Coll. Métallurgie Fracteurs mécaniques et métallurgiques de la rupture, notamment dans l'industrie nucléaire, Saclay, Juin 1974, INSTN, Saclay, 1975, pp. 437-518.
 - [10] Fidelle, J. P., Broudeur, R., and Roux, C., "Les essais de disques sous pressions, Colloque d'Ivry" Les essais de disques sous pression, 29/5/1985, J. P. Fidelle, Ed., CEA, Paris, 1975, pp. 5-48.
 - [11] Clauss, A., Criqui, B., and Fidelle, J. P., "Application des essais de disques à l'étude de l'influence de l'hydrogène interne et externe sur le comportement mécanique du titane et de ses alliages," *Ibid 10*, pp. 56-84.
 - [12] Fidelle, J. P., Broudeur, R., and Roux, C., "Hydrogen Gas Embrittlement Under the Influence of Strain Rate, Temperature and Thickness Effects. Relationship with delayed failure," Conference Effect of Hydrogen on Behavior of Materials, Jackson Lake, WY, 1975, A. W. Thompson, I. M. Bernstein, Eds., AIME, Detroit, 1976, pp. 507-514.
 - [13] Criqui, B., Fidelle, J. P., and Clauss, A., (a) Effects of Internal and External Hydrogen on Mechanical Properties of Beta III Titanium Alloy Sheet, *Ibid 46*, pp. 91-101; (b) Effets de l'hydrogène interne et externe sur les propriétés mécaniques de tôles en alliage de titane Béta III, 4^{ème} J. Etude du titane et de ses alliages Nantes (2-3/5/1976), pp. 54-85.
 - [14] Fidelle, J. P., "Hydrogen Gas Embrittlement," *J. Internat. d'étude sur l'hydrogène et ses perspectives*, Tome III Liège, 1976, pp. 204-207.
 - [15] Fidelle, J. P., Criqui, B., Arnould-Laurent, R., and Broudeur, R., "Nature, importance, caractères de la fragilisation par l'hydrogène externe (FPHE)," Congr. Internat. L'hydrogène dans les métaux, Châtenay-Malabry, Juin 1977, Article 3D1.
 - [16] Raharinaivo, A., Broudeur, R., and Fidelle, J. P., "Fragilisation par l'hydrogène des aciers de précontrainte," *Ibid 15*, Article 3E6.
 - [17] Fidelle, J. P. and Tison, P., "On H Gas Entry and Embrittlement at RT. Importance of Dislocations," Conf. Environmental degradation of engineering materials, Virginia Tech., Blacksburg, VA (10-12/10/1977), M. R. Louthan and R. P. McNitt, Eds., Virginia Tech. Press, 1977, pp. 495-499.
 - [18] Gesthaz, J. M., Fidelle, J. P., and Clauss, A., "Influence de l'hydrogène interne sur le comportement mécanique de l'alliage de titane TA 5 E. Sème," *J. Etude du titane et de ses alliages Nantes*, 28-29/11/1978.
 - [19] Arnould-Laurent, R. and Fidelle, J. P., "Influence de l'hydrogène sur le comportement des métaux. V—Fragilisation par l'hydrogène et fissuration par corrosion sous contrainte de l'alliage uranium—vanadium à 0,2% en poids—Rapport," CEA-R-4983, Août, 1979.
 - [20] Clermont, R., Ovejero-García, J., Chene, J., Aucouturier, M., Pirrovani, C., Tison, P., and Fidelle, J. P., "Microstructural Localization of Hydrogen Introduced Under Pressure in Steels," Internat. Congr. Hydrogen in metals, Minakami, 1979, Proc. JIMIS-2 Jap. Inst. Metals, Sendai, Japan, 1980, pp. 233-236.
 - [21] Fidelle, J. P., Arnould-Laurent, R., and Pressouyre, G., "Investigation of Hydrogen Embrittlement with Disc Pressure Tests," *Ibid 20*, pp. 505-508.
 - [22] Arnould-Laurent, R. and Fidelle, J. P., "The Disk Pressure Test. A Powerful Investigation Method," Poster Internat. Congr. on Fracture ICF 5, Cannes, 30/3 to 3/4/1981, Tirages disponibles au CEA, Paris.
 - [23] Fidelle, J. P. and Arnould-Laurent, R., "The Embedded Disk Pressure Test (DPT): A Sensitive Technique to Investigate Materials Embrittlement," Advanced Research Institute Atomistics of Fracture, San Bastiano/Calcatoggio, Mai 1981, Plenum Press, New York, 1983.
 - [24] Azou, P. F. and Fidelle, J. P., "Fragilisation par l'hydrogène gazeux d'aciers inoxydables" Article G7, 731-736, Congrès Internat. L'Hydrogène Dans Les Métaux. Châtenay-Malabry, 7 to 11/6/1982.
 - [25] Fidelle, J. P., "On Disk Pressure Selection of Materials and Hydrogen Environments," Congress on Current Solutions to Hydrogen Problems in Steels, Washington, DC, 7-11/11/1982.
 - [26] "Défi à l'hydrogène," CEA, 1969, 16mm Son optique 18mm, en version anglo-saxonne: "Hydrogen Challenge."
 - [27] "Les essais de disques sous pression," Ivry, J. P. Fidelle, Ed., CEA, Paris, 1975.
 - [28] Clauss, A., "Comportement des métaux du sous-groupe Va (V, Nb, Ta) en atmosphère d'hydrogène à la température ambiante," Colloque *L'hydrogène dans les Métaux* 1967, J. P. Fidelle and M. Rapin, Eds., CEA, 1969, pp. 280-304.
 - [29] Hechelski, R., Fidelle, J. P., and Clauss, A., "Hydrogen Gas Embrittlement (HGE) of Niobium alloys," Communication G 10. Intern. Congr. on H and Materials, 1982, p. 749.

- [30] Speitling, A. and Vibrans, G., "Druckversuch zur Prüfung der Wasserstoff Versprödung von Metallen," 1984, à paraître dans Z. F. Werkstofftechnik.
- [31] Bretin, L. and Toitot, M., "What the Metallurgist Can Anticipate from the Disk Pressure Tests," Ivory Conference on The Disk Pressure Tests, J. P. Fidelle, Ed., CEA, Fr., 1975, pp. 49-55.
- [32] Arnould-Laurent, R., Jouve, G., and Fidelle, J. P., "Contribution of Hydrogen Embrittlement to Stress Corrosion Cracking of U 0.2.% V Uranium alloy—Mechanisms of Environment Sensitive Cracking of Materials," University of Surrey, Guildford, GB, 1977, P. R. Swann, F. P. Ford, and A. R. C. Westwood, Eds., The Metals Soc., Great Britain, 1978, pp. 531-537.
- [33] Poirier, J., Thèse Dr. Ing. Univ. Louis Pasteur—Strasbourg, 1969.
- [34] Tison, P. and Fidelle, J. P., (a) Etude des phénomènes qui, avec la diffusion, peuvent contrôler la perméabilité des métaux à l'hydrogène et à ses isotopes, Note CEA-N-2231 (Oct. 1981), (b) Investigation of Phenomena which, with Diffusion, Can Control Metals Permeability to H Isotopes," European contribution to the 3rd workshop INTOR meeting on fusion reactor technology EURFUBRU/XII—2/81/EDV/70 Group D Tritium—AIEA Vienna, Dec. 1981, CEE, Bruxelles, Belgium.
- [35] Tison, P. and Fidelle, J. P., "Some H Isotopes Interactions to be Accounted for INTOR Technology," INTOR meeting on fusion reactor technology, Vienna, Austria, 1982.
- [36] Shewmon, P. G., *Hydrogen effects in metals* I. M. Bernstein and A. W. Thompson, Eds., AIME, New York, 1981.

Bibliography

- Barthelemy, H. and Pressouyre, G., "Hydrogen Gas Embrittlement of Steels," synthesis of a subtask of the CEC hydrogen energy programme (1975-1983), 1985.
- Fidelle, J. P., "Influence de l'hydrogene sur le comportement des metaux: III (N) 'Suggestions pour la reconstruction de la courbe $da/dt = f(K)$ dans le cas d'éprouvettes de tenacité insuffisamment imprégnées en hydrogene," Centre d'Etudes Nucleaires de Bruyeres-le-Chatel, March 1986.
- Habashi, M., Huwart, P., Fidelle, J. P., and Galland, J., "Plastic Zone Size Evolution at Fatigue Crack Tip with Microstructural and Hydrogenated Effects in Austenitic Stainless Steels," 1986.
- Huwart, P., Habashi, M., Fidelle, J. P., Garnier, P., and Galland, J., "Propriétés Mécaniques d'Aciers Inoxydables Austénitiques Stable (ZXNCTD 26-15) et Instable (Z2CN 18-10), Role des Traitements Thermiques et de l'Hydrogene Cathodique," 7th International Conference of the Strength of Metals and Alloys, Concordia University, Montreal, Quebec, Canada, (12-16 Aug. 1985).
- Philippe, M. J., Lemoisson, P., Hocheid, B., and Fidelle, J. P., "Effet d'une predeformation sur l'aptitude a la deformation en expansion biaxiale du zirconium," from *Matériaux et Techniques*, Jan. 1985.
- Speitling, A. and Vibrans, G., "Druckversuch an Scheiben zur Prüfung der Wasserstoffversprödung von Metallen (Disk Pressure Testing of Hydrogen Embrittlement), 1985.

DISCUSSION

DeLuccia: Dr. Fidelle, in your experiment with Beta-3 titanium, did you see a lot of plastic deformation in the disk and did you fracture it to rupture?

Fidelle: Yes, we would observe the plastic deformation and we would observe the rupture.

DeLuccia: So you did see lots of plastic deformation. It did not fracture in a very brittle fashion then. Is that correct?

Fidelle: It depends on the heat treatment and the amount of cold work and the amount of oxygen and the amount of hydrogen and the way hydrogen has been introduced.

DeLuccia: I was more interested in the high hydrogen content of the Beta-3. Did that have deformation to your recollection?

Fidelle: Something which is surprising is that, if you introduce hydrogen thermally during the heat treatment, at first it makes the material better. It increases ductility and yield strength and only after hydrogen range embrittlement appears. There are materials for which hydrogen embrittlement appears at the lowest contents and materials which are improved in a similar range before embrittlement appears.

DeLuccia: Again, I have done some work with Beta-3, looking at the electrolytic hydrogen introduced into that alloy. It is a body centered cubic alloy and does not form hydrides, so it acts very much like iron or steel. This was my finding with Beta-3. I was just wondering what you found.

Fidelle: If you go above 7000 ppm, you can make hydrides.

DeLuccia: Yes. Maybe very, very high amounts of hydrogen.

Fidelle: But, this is typically the case of materials where you can have high strain rate embrittlement due to hydrogen in solution.

Screening Tests for Hydrogen Stress Cracking Susceptibility

REFERENCE: Crumly, W. R., "Screening Tests for Hydrogen Stress Cracking Susceptibility," *Hydrogen Embrittlement: Prevention and Control*, ASTM STP 962, L. Raymond, Ed., American Society for Testing and Materials, Philadelphia, 1988, pp. 173-177.

ABSTRACT: A need for a rapid, inexpensive test method for determining K_{Isc} is shown. Two test methods, focusing on hydrogen stress cracking of steel, are described: (1) a test using machined, side-grooved, Charpy specimens step-loaded and held at each step under deflection controlled conditions, and (2) a slow strain rate tension test. Examples of the use of step-load test methods are presented showing excellent correlation of results between the test methods and other test methods up to a value of K_{Isc} less than 0.1 ultimate tensile strength (UTS). The utility of the test method as a screening test and inexpensive estimate for K_{Isc} in steels is demonstrated. It is recommended that ASTM Subcommittee F07.04 on Hydrogen Embrittlement consider standardization of this test method. The slow strain rate tension test is also examined for the use above 0.1 UTS, and a method for analyzing the test results in terms of K_{Isc} is presented. Both test methods are conducted under potentiostatic control in a hydrogen-producing aqueous environment.

KEY WORDS: hydrogen stress cracking, slow strain rate testing, rising step load testing, K_{Isc} estimation

Failure mode analysis is used in design based on fracture toughness, K_{Ic} [1]. Subcritical crack growth by fatigue is well enough understood so that useful safe-life predictions can be made. However, design for the control of stress corrosion cracking (SCC) is presently restricted to relative ranking of materials to select the best material. It is not used as a quantitative design consideration, although a critical stress intensity, K_{Isc} , is often measured. For the purposes of this paper, the K_{Isc} designation will be maintained, although the tests are converted in a hydrogen-producing aqueous environment and a hydrogen stress cracking (HSC) designation would be more appropriate.

Background

The majority of stress corrosion testing performed today is for specific applications, such as acceptance quality control of fasteners, platings, baths, etc. Typical tests load a part or a notched specimen to high stress levels (75% of the notched breaking load) and monitor time [2]. Such tests rank a material or process against a benchmark such as a 200-h acceptance limit, but do not provide quantitative data that can be used in design.

The critical threshold stress intensity, K_{Isc} , has been established as a material parameter and can be used in design for stress corrosion control. Use of K_{Isc} in design is limited due primarily to the methods used to measure K_{Isc} . Only two test methods are generally recognized to measure K_{Isc} , one using the wedge opening load (WOL) specimen and the other using the cantilever beam (CB) specimen. Both methods are long duration, typically a few hundred to a few thousand hours, depending on the material and environment.

¹Senior staff engineer, Hughes Aircraft Co., Electron Dynamics Division, Torrance, CA.

It would be extremely valuable to be able to estimate K_{Isc} from a short-duration inexpensive test. This paper will report on the successful use of such a test, the step-load bend test, which correlates well with K_{Isc} for steels where K_{Isc} /Ultimate tensile strength (UTS) is less than 0.1 $m^{1/2}$ (0.7 in.^{1/2}). This paper will also report on a slow strain rate tension test where K_{Isc} /UTS is greater than 0.1.

Step-Load Bend Specimen Test Method

A machined, side-grooved, Charpy-sized specimen is exposed to hydrogen and tested by sequentially loading the specimen in bending to loads corresponding to 50, 65, 75, 80, 85, 90, and 95% of breaking load that is determined by monotonically loading another specimen in air to failure. The specimen is held at each load under deflection controlled conditions for 1 h. Cracking is detected by the unloading of the specimen that occurs at one of the load steps when cracking occurs. Hydrogen is generated at the surface of the specimen by potentiostatic means.

The test method measures the stress intensity at crack initiation under deflection controlled conditions. Under these conditions, crack initiation can be measured by monitoring the load. Due to the large value of the modulus of elasticity of steel (200 GPa), a very small crack extension causes a measurable drop in load, so that crack initiation can be readily determined. This method can be compared to the cantilever beam test method, which is load controlled. A large amount of crack extension must take place before deflection of the beam is noticeable. The only way to determine the crack initiation load is to wait for a sufficient amount of time for a crack to grow to a detectable size.

Examples of Use of Step-Load Test Method

Screening Test

The test was originally developed [3] as a screening test to evaluate weld parameters used to weld HY steels. K_{Isc} was subsequently measured for some of the more promising candidate welds using WOL and CB specimens. Figure 1 shows the excellent correlation to K_{Isc} measured by the step-load method. The success of the method allowed an extensive matrix of additional weld parameters to be screened, while reducing the number of full-scale K_{Isc} tests required.

Preliminary Evaluation

In another application, Type 4340 steel produced by two different methods, electroslog remelted (ESR) and vacuum arc remelted (VAR), were compared for SCC resistance.

Machined, side-grooved, Charpy-sized specimens were prepared for the steels tempered to two hardness levels, 43 Rockwell Hardness—C scale (HRC) [1.38 GPa (200 ksi) UTS] and 53 HRC [1.79 GPa (260 ksi) UTS]. After the K_{Isc} test, that depends on crack initiation, K_{Ic} measurements were also made on the same sample using the now precracked Charpy-sized specimens. For the lower hardness, a plasticity correction (crack opening displacement) was used to estimate the toughness.

Table 1 shows the results of the K_{Ic} and K_{Isc} tests for the two materials. While both materials had the same strength and toughness, steel made using the VAR process showed a significant advantage in SCC resistance.

Slow Strain Rate Tension Test

For many steels, the restriction of K_{Isc} /UTS < 0.1 will not apply. However, there is a large class of materials where K_{Isc} is larger than 0.1 UTS. For example, a low-carbon steel that is commonly used for land construction was being considered for maritime use. The application

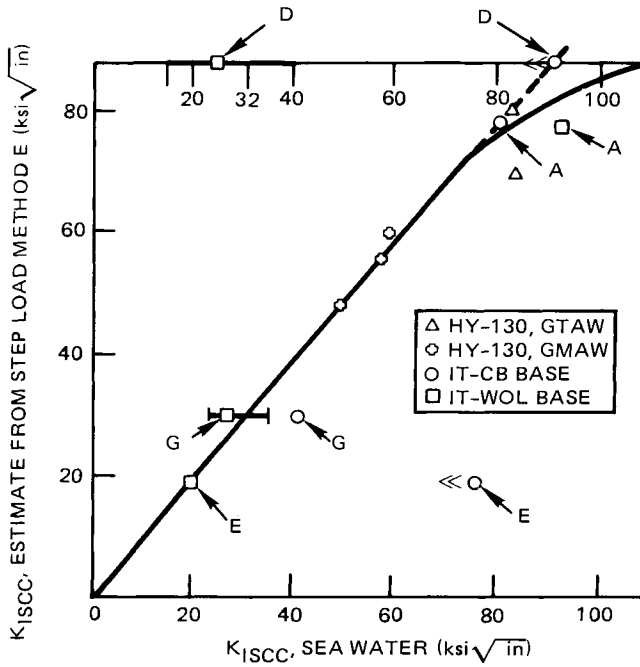


FIG. 1—Correlation between threshold stress intensity measured by step-load test method and $K_{I SCC}$ measured by cantilever beam or WOL specimen methods for HY steels: HY80, HY130, and HY180.

TABLE 1—Estimate of $K_{I SCC}$ using step-load test method for 4340 ESR and VAR steels heat-treated to 43 HRC [138 MPa (200 ksi) UTS] and 53 HRC [179 MPa (250 ksi) UTS].

Type	43 HRC		53 HRC	
	$K_{I SCC}$	$K_{I c}$	$K_{I SCC}$	$K_{I c}$
VAR	43	130	15	62
ESR	29	130	10	62

did not warrant the expense of full-scale $K_{I SCC}$ testing, but some confidence in the material's suitability for use was desired.

Example of Use of Slow Strain Rate Test Method

The steel was initially tested in a 3.5% sodium chloride (NaCl) solution at -1.2 V referenced to a standard calomel electrode by the step-load method. No SCC or HSC was detected, indicating that $K_{I SCC}$ was greater than 0.7 UTS. The UTS for this material was 620 to 690 MPa (90 to 100 ksi), so $K_{I SCC}$ was greater than $66 \text{ MPa} \cdot \text{m}^{1/2}$ (60 ksi).

Since the step-load bend testing did not detect any susceptibility to HSC, slow strain rate tension tests were performed in the same environment to see if the steel had any susceptibility to HSC.

Background

Slow strain rate tension testing in SCC environments is becoming a well-established method for relative ranking of materials for resistance to SCC [4]. Figure 2 shows the slow strain rate test results of this program for a steel in air and under hydrogen-SCC conditions. The major difference seen is in the shape of the curve after UTS was achieved. Fracture strain is much reduced under SCC conditions, and it is generally felt that the most sensitive parameter to monitor in slow strain rate tension testing is reduction in area (RA), which is a measure of true strain at fracture. Examination of the slow strain rate tensile curves, Fig. 2, shows significant effects of the environment. The engineering strain to fracture is obviously effected by HSC. The RA was similarly effected, degrading from 0.70 to 0.38 when tested in the environment. In this case, an estimate of K_{Isc} greater than (60 ksi) from the step-load test was sufficient to qualify the material. However, the slow strain rate tensile data indicated some variation in sensitivity to SCC.

Method of Analysis

In an effort to determine the margin available, a K_{Ic} correlation from tensile data is available and the same calculation was used to estimate K_{Isc} from the slow strain tensile data shown in Fig. 2. Table 2 lists the results of the K_{Isc} correlation from slow strain rate tensile data shown in Fig. 2. The K_{Isc} estimate for the base metal of $68 \text{ MPa} \cdot \text{m}^{1/2}$ (62 ksi) is consistent with the step-load bend test results, and the use of slow strain rate tensile data to estimate from tensile ductility estimate of K_{Ic} shows promise.

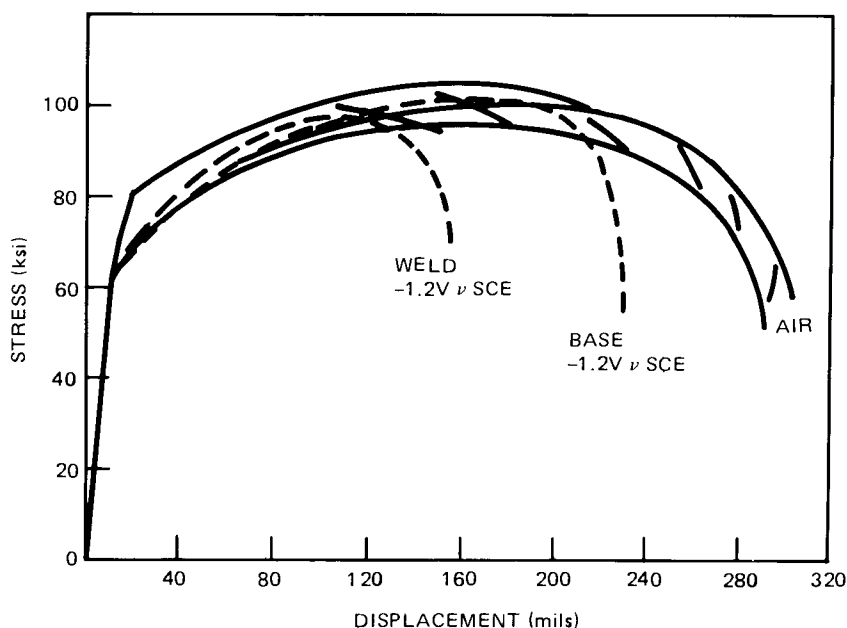


FIG. 2—Slow strain rate tensile curves for low-carbon steel in air and in SCC environment.

TABLE 2— K_{Ic}/K_{Isc} estimates from slow strain rate tensile curves shown in Fig. 2.

	SCC ductility analysis	
	K_{Ic} (MPa), Air	K_{Ic} (MPa), HSC
Base metal	231 (254 MPa · m ^{1/2})	91 (100 MPa · m ^{1/2})
Weld metal	229 (252 MPa · m ^{1/2})	62 (68 MPa · m ^{1/2})

Summary

Two methods have been examined as rapid, inexpensive tests for estimating K_{Isc} in steels:

1. The step-load bend test has been successfully used as: (a) a screening test to evaluate weld parameters for welding HY steels; (b) a method for evaluating ESR and VAR 4340 steel when K_{Isc} is less than 0.1 UTS.
2. The slow strain rate tension test was used in estimating K_{Isc} in low-strength steels with high SCC resistance, when $K_{Isc} > 0.1$ UTS.

Conclusions

At present, the only material parameter that can be used in design for SCC control is K_{Isc} , and its use is restricted primarily by expense and duration of the required testing. It is clear that the step-load bend test is a rapid and inexpensive test that can be used to estimate K_{Isc} , provided that K_{Isc} is less than 0.1 UTS.

In this paper, the step-load bend test method has been used to estimate K_{Isc} for high-strength steels [Type 4340 heat treated to 1.79 GPa (260 ksi) UTS] and low-strength steels (HY80, HY100, and HY130) where K_{Isc} measurements by WOL and CB specimens were also available. The threshold stress intensity estimated by the step-load test method verified the initial long-term K_{Isc} tests.

In this paper, the slow strain rate tension test discriminated between the susceptibility of weld and basic methods for K_{Isc} greater than 0.1 UTS.

ASTM Subcommittee F07.04 on Hydrogen Embrittlement should consider elevating the step-load bend test to a standard for measuring K_{Isc} in steel.

References

- [1] ASTM Test Method for Plane-Strain Fracture Toughness of Metallic Materials (E 399-83), in *Fracture Toughness Testing and Its Applications*, ASTM STP 381, ASTM, Philadelphia, 1984.
- [2] 1985 Annual Book of ASTM Standards, Vol. 02.05, 15.03, ASTM F 519-77, Method for Mechanical Hydrogen Embrittlement Testing of Plating Processes and Aircraft Maintenance Chemicals, ASTM, Philadelphia.
- [3] Raymond, L. and Crumly, W. R., "Accelerated Low-Cost Test Method for Measuring the Susceptibility of HY-Steels to Hydrogen Embrittlement, in *Proceedings*, First International Conference on Current Solutions to Hydrogen Problems in Steel, Washington, DC, Nov. 1982, American Society for Metals, Metals Park, OH.
- [4] *Stress Corrosion Cracking—The Slow Strain Rate Technique*, ASTM STP 665, ASTM, Philadelphia, 1979.

Ranking Materials for Extreme Sour Gas Service Using the Slow Strain Rate Method

REFERENCE: McIntyre, D. R., "Ranking Materials for Extreme Sour Gas Service Using the Slow Strain Rate Method," *Hydrogen Embrittlement: Prevention and Control, ASTM STP 962*, L. Raymond, Ed., American Society for Testing and Materials, Philadelphia, 1988, pp. 178-189.

ABSTRACT: Equipment for use in sour gas wells is exposed to high-chloride brines saturated with hydrogen sulfide (H_2S) and carbon dioxide (CO_2) at temperatures up to $260^\circ C$ ($500^\circ F$). Both hydrogen-induced cracking and stress corrosion cracking are possible. However, traditional methods for testing environmental cracking resistance, such as the National Association of Corrosion Engineers (NACE) tension test or the magnesium chloride ($MgCl_2$) test, have limited applicability to this service. The slow strain rate method overcomes many of the disadvantages of more traditional test methods, while posing some unique questions of its own. Apparatus and procedure are described. The theoretical interaction between slowly rising dynamic strain and hydrogen-related cracking is discussed. Selection of appropriate strain rate and sample size will be described. The possible evaluation criteria will be compared, including: time to failure, percent reduction in area, loss of ductile fracture surface area, and the appearance of secondary cracking. Certain ambiguous features in the transition zones between cracking and noncracking environments will be described. The strengths of the method (rapidity, positive results) will be balanced and compared with its limits of use.

KEY WORDS: hydrogen embrittlement, sulfide stress cracking, test methods, strain rate effects, low-alloy steels, corrosion-resistant alloys

Hydrogen sulfide (H_2S) is a common component in subterranean hydrocarbon reservoirs. It is extremely toxic, corrosive when wet, and flammable. Consequently, materials which cannot resist environmental cracking in H_2S ("sour" service) find only limited application for oil and gas production or refining equipment.

H_2S promotes hydrogen embrittlement at low temperatures [below approximately $93.3^\circ C$ ($200^\circ F$)]. Compared with other hydrogen environments such as molecular hydrogen gas, H_2S environments produce environmental crack growth at lower stress intensities and higher crack growth rates (Fig. 1). In addition, H_2S causes environmental cracking at higher temperatures on many alloy systems due, apparently, to an anodic stress corrosion cracking (SCC) mechanism.

The potency of sour environments varies widely depending on environmental factors such as acid gas partial pressure and water chemistry. Metallurgical variables including microstructure, trace element content, and strengthening treatments can render materials susceptible or immune to H_2S cracking.

Consequently, there is a need for test methods to rank environments for their tendency to cause sulfide stress cracking (SSC) and for methods to rate the relative susceptibility of materials to SSC.

¹Cortest Laboratories, Inc., Cypress, TX 77429.

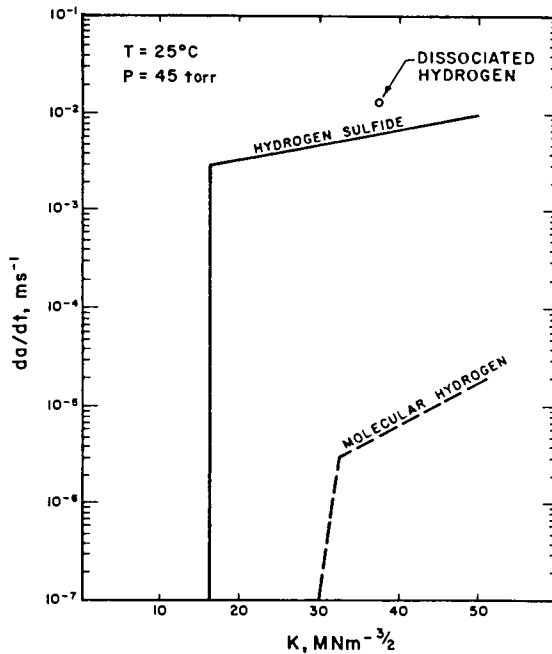


FIG. 1—Sustained load crack propagation rates in 4130 steel tested in three different hydrogen-containing environments [8].

Historically the oil and gas companies have ranked the SSC susceptibility of carbon steels and low-alloy steels with the National Association of Corrosion Engineers (NACE) tension test, a method using statically loaded direct tension specimens to determine the material's SSC threshold stress [1].

Precision and interlaboratory repeatability with the NACE tension test have been good. However, three problems have surfaced with its use. First, the test requires 30 days to complete. Consequently its use as a quality control requirement causes delays in shipping and using sour service materials. Second, the test is not directly applicable to the new generation of corrosion-resistant alloys being applied or considered for extreme sour service.

Third, the NACE tension test environment, which involves exposure to an ambient temperature acidified sodium chloride (NaCl) solution saturated with H_2S , is considerably more aggressive than many actual production environments with regard to its tendency to promote hydrogen embrittlement. However, because of the relatively low temperature, it is considerably less aggressive than many actual production environments with regard to anodic SCC. Thus, there are difficulties in relating NACE tension test results to actual service conditions.

To overcome these problems, the slow strain rate test method has been proposed for characterizing sour service environments and ranking materials for H_2S service.

The speed and environmental versatility of the slow strain rate method recommend it for the tasks just described. However, the method was first developed for characterizing environments for their tendency to promote anodic SCC [2]. It was not meant for ranking materials or for investigating hydrogen service.

Therefore, an inquiry into the method's fundamental applicability and practical utility for ranking materials for H_2S service is appropriate.

Experimental Procedure

The slow strain rate test involves applying a steadily rising tensile load to a specimen of the test material while that specimen is exposed to the test environment. The rate of loading is constant (at least up to the onset of necking) and slow enough to allow corrosion and absorption processes to interact with material freshly exposed to the environment by the process of plastic deformation.

The test is run until the specimen fractures. Fracture mode and measures of ductility are then compared with a specimen fractured in an inert environment.

Necessary equipment for the slow strain rate test, therefore, involves:

1. A loading mechanism capable of controlling the elongation of the specimen at rates between 1×10^{-4} and $1 \times 10^{-7} \text{ s}^{-1}$.
2. Specimens removed from the material of interest.
3. An environmental chamber in which solution chemistry, gas composition, pressure, temperature, and electrochemical potential can be controlled to simulate anticipated service conditions while permitting mechanical access to the specimen for the loading frame.

Conduct of a slow strain rate test for environmental cracking proceeds as follows:

1. Based on prior experience, select a strain rate for the test series.
2. Perform a tension test in an inert environment (air, inert gas, or nonreactive heat transfer oil) on the material of interest at the selected strain rate. Determine total time to failure, final diameter, ultimate load, and fracture load.
3. Load the specimen into the environmental chamber and simulate the desired environment by adding test solution and atmosphere and adjusting temperature, pressure, and electrochemical potential.
4. While the specimen is exposed to the test environment, perform a tension test at the strain rate selected. Determine time to failure, final diameter, ultimate load, and fracture load.
5. Remove the fractured specimen from the test environment and examine it for evidence of environmental cracking under an optical microscope at $\times 20$ or greater. Note any evidence of environmental crack growth on the primary fracture surface or secondary cracking along the gage length.
6. Compare the fracture appearance and measures of ductility obtained in the inert environment to those obtained in the test environment.

Selection of necessary test parameters is now discussed.

Selection of Strain Rates

Many early investigators commented on the profound reduction in tensile strength which occurs in notched specimens in hydrogen environments [3]. The effect is now believed to be two-fold: stress concentration and localized plasticity from the notch geometry, as well as a locally low strain rate due to the constraint of the notch.

The effect of slow strain rate on increasing the severity of hydrogen damage has since been confirmed by a number of investigators [4,5]. In general the effect of decreasing strain rate was described by Kim and Wilde [6] (Fig. 2).

Unlike anodic SCC, which may show a minimum in strain rate effects, below and above which maximum susceptibility is not observed, hydrogen embrittlement produces a gradually increasing loss of ductility as the strain rate is slowed below some threshold value.

Consequently, the slow strain rate test may be regarded as being more convenient for hydrogen-induced environmental cracking studies than for anodic stress cracking. When anodic stress corrosion is the concern, the question of critical strain rate effects always arises and often

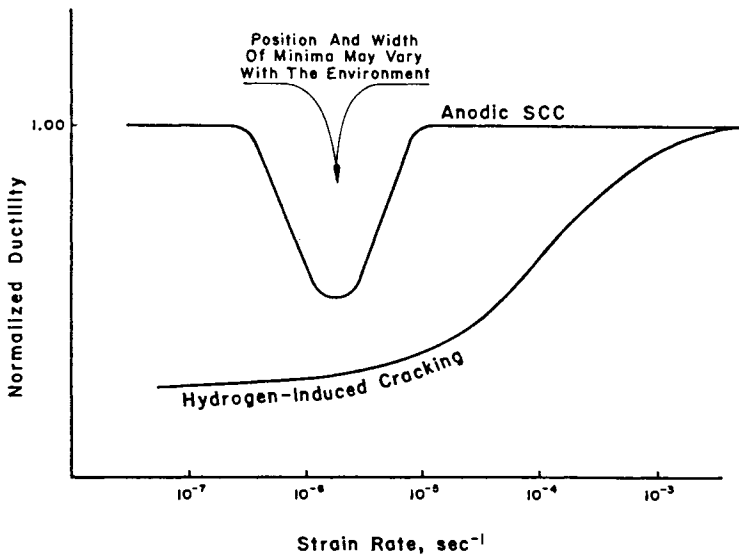


FIG. 2—Schematic showing effect of strain rate on tension test results in anodic SCC or hydrogen-induced cracking. After Kim and Wilde [6].

consumes a significant portion of the time and effort put into the program. Hydrogen-induced phenomena, however, such as SSC, show strong ductility losses across much wider ranges of strain rate.

The slow strain rate test is normally continued until fracture unless crack growth rates are to be obtained. The resulting plastic deformation can produce pronounced ductility loss in many carbon and low-alloy steels which historically do not show problems in sour service at more realistic stress levels. Slower strain rates tend to magnify this effect, leading to poor differentiation between acceptable and unacceptable materials (Fig. 3). Thus, for carbon and alloy steels a relatively rapid strain rate (approximately 1×10^{-5} in./in./s) would appear to be a good compromise for H_2S environments, giving a consistent embrittling effect and yet producing useful differentiation between less sensitive and highly susceptible materials.

More highly alloyed corrosion-resistant materials are typically tested at slower strain rates than low-alloy steels. A strain rate of 4×10^{-6} s brings out both anodic stress cracking and hydrogen-induced crack growth in many stainless steels and nickel-based alloys.

Specimen Size and Type

Round tension specimens without notches are most commonly used for slow strain rate (SSR) tests in H_2S environments. Repeatability reportedly suffers when specimens of rectangular cross section are employed [9].

Heavy cold work on the exposed specimen gage length may obscure the test results and must be avoided. A machined surface with a 32-rms surface finish or better is typically specified.

Specimen diameter will affect time to failure (Figs. 4 and 5). An environmental crack propagating at a given rate will bring a smaller diameter specimen to its fracture load faster than a larger diameter specimen; simply, each unit length of crack growth severs a greater percentage of the remaining ligament. Test results should only be compared between specimens of the same diameter. Although this would seem an obvious point, it is not required in some of the materials

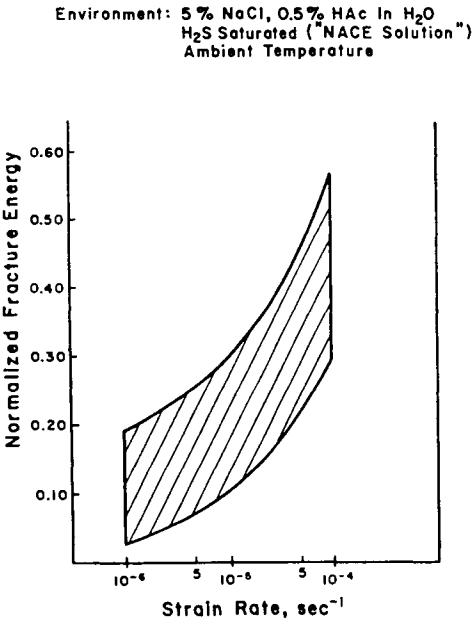


FIG. 3—Strain rate effects in SSR tests in NACE solution. Data are from ten heats of OCTG low-alloy steel, yield strength 80 to 110 ksi [7].

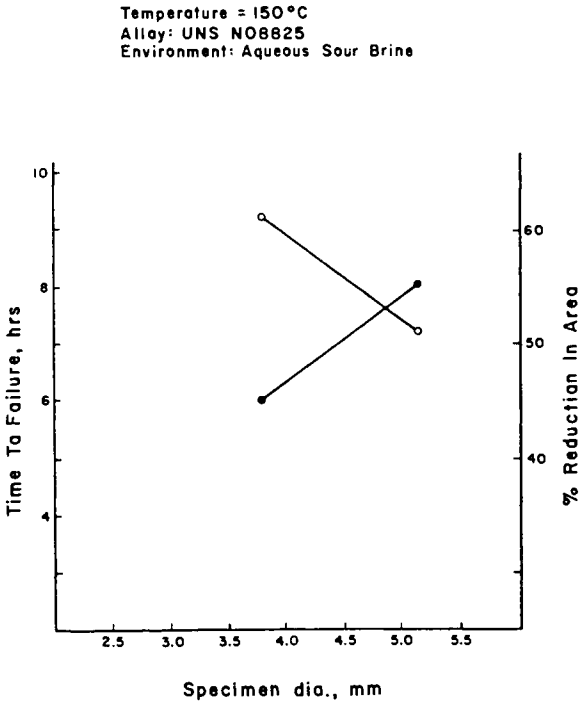


FIG. 4—Section size effects in SSR testing in H₂S environments. NOTE: Solid points show time to failure. Open points show reduction in area.

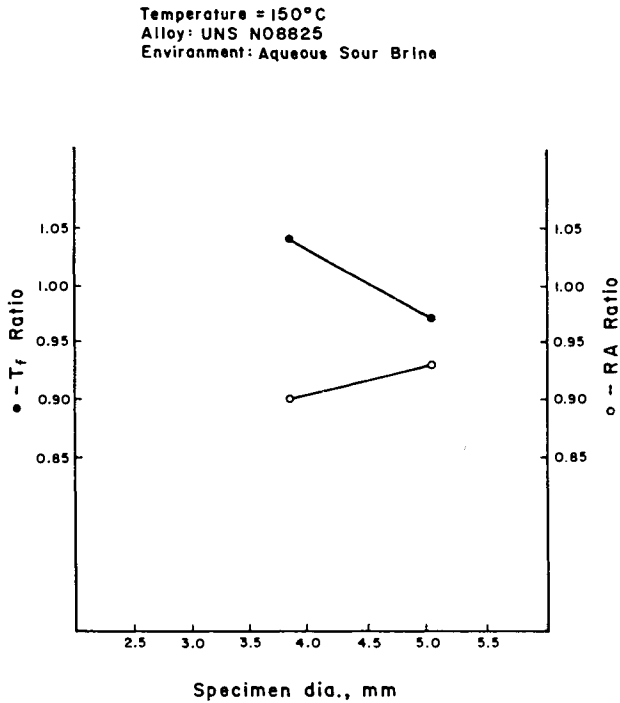


FIG. 5—Section size effect versus T_f and RA ratio, test environment versus inert environment.

specifications which call for slow strain rate testing. Thus, a supplier whose material fails a minimum elongation requirement with one gage diameter might retest and pass the specification with a larger gage diameter.

Load Train

Single specimen load trains are preferred. On machines with multiple specimens on the same load train, loading spikes may occur when one specimen fractures, causing "sympathy failures" on other specimens.

Electrically driven ground ball screw loading rams are preferred because of their low-speed control capabilities. Servohydraulic loading rams have been widely used for slow strain rate testing with good results in some systems. However, servohydraulic machines may have reproducibility problems at low (less than 10^{-5} s) strain rates.

When a specimen is loaded in a slow strain rate test, a small component of the measured elongation is due to elastic deformation of the load frame. Thus, two load frames of different compliance might give slightly different total elongation on specimens with the same actual elongation (Fig. 6).

Once plastic deformation begins, it can safely be assumed that virtually all the elongation in the load train takes place in the specimen's gage section. Thus, the effect of load frame stiffness can be eliminated by reporting plastic elongation only rather than total elongation.

Crosshead speed must be established accurately if time to failure, or total elongation derived from time to failure, is used as an acceptance criterion. Crosshead speed should be established as a function of motor speed controller setting each time the strain rate is changed, using the

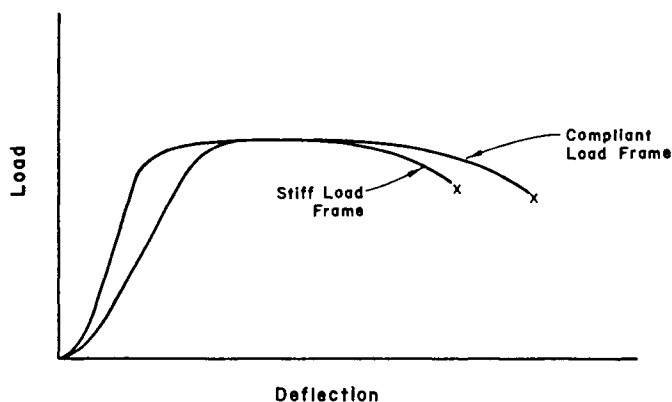


FIG. 6—Apparent difference in time to failure with the same plastic elongation, due to differences in load frame stiffness.

deflection of a dial indicator over a period of at least 2 h. The difference between 3.5 and 4×10^{-6} s is small compared to the range of possible strain rate effects. However, such a difference will result in a 14% decrease in time to failure. Such a difference might be significant in relationship to specification minimums.

Applications

For H_2S service, there are three basic applications for SSC tests of any sort:

1. Materials qualification testing.
2. Determination of critical temperature ranges for cracking.
3. Determination of the optimum combination of strength and SSC resistance.

Materials Qualification Testing

The quality assurance function involves comparing materials of differing compositions or processing history to materials whose sour service resistance is known. This is very much a materials ranking task. For example, Fig. 7 shows slow strain rate test results for three corrosion-resistant alloys in a simulated produced brine with high H_2S and carbon dioxide (CO_2) pressure. The proposed proprietary alloy would have resistance comparable to Alloy UNS N08825 at room temperature. At higher temperature it could be expected to perform somewhat better than Alloy N08825 but considerably worse than Alloy N10276. Thus, the new material might be substituted for Alloy N08825 but not for N10276.

Critical Cracking Temperature Determination

Both hydrogen-induced cracking and anodic SCC frequently manifest specific temperature ranges below or above which the phenomena do not occur in service.

These temperature limits are of great practical interest to sour well designers. Although the gas composition stays more or less constant down the depth of the well, the temperature varies continuously with depth. Identifying safe and dangerous temperature zones thus allows the designer to match the material's resistance to local conditions most cost effectively.

Figure 8 presents a graph of slow strain rate test results for Alloy UNS N08825 in an H_2S environment. Cracking resistance is excellent up to $150^\circ C$. However, a severe drop in resistance

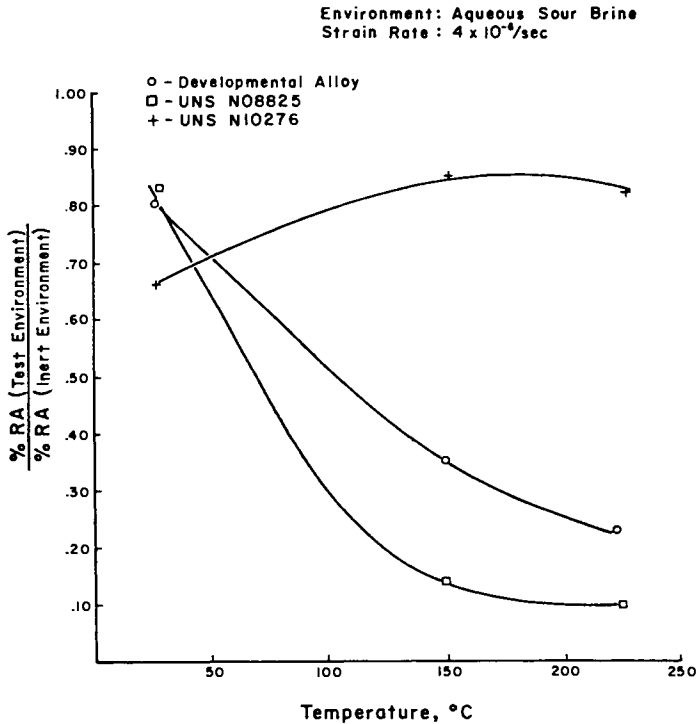


FIG. 7—Ranking corrosion-resistant alloys with the slow strain rate test.

occurs at 175°C, corresponding to the onset of pitting in this alloy. These data correspond very well with autoclave tests of C-rings and double cantilever beams (DCBs), and with field experience with this alloy.

Comparing Materials With Different Strength Levels

Ranking of alloys with different compositions is best done at similar strength levels since prior thermomechanical processing can profoundly affect the cracking resistance of an alloy. Even with similar strength levels, direct measures of ductility (elongation or reduction in area) should not be compared between materials. Rather the ratio of properties in the test and the inert environment is the only proper comparison between different alloy compositions because these ratios factor out any basic differences in mechanical ductility and toughness.

For a given composition, however, the slow strain rate test is a useful method for rapid ranking of strengthening treatments or thermal cycles with regard to their effect on SSC resistance. Effects of cold working, quenching and tempering, and precipitation hardening show up clearly with the slow strain rate test and correlate well with service experience.

Possible Ambiguities

Slow strain rate testing was originally seen as a go/no-go test that would give a positive answer as to whether environmental cracking might occur with a given combination of material and environment. By and large this has proven to be the case. However, there are occasions when test results are not so clear cut.

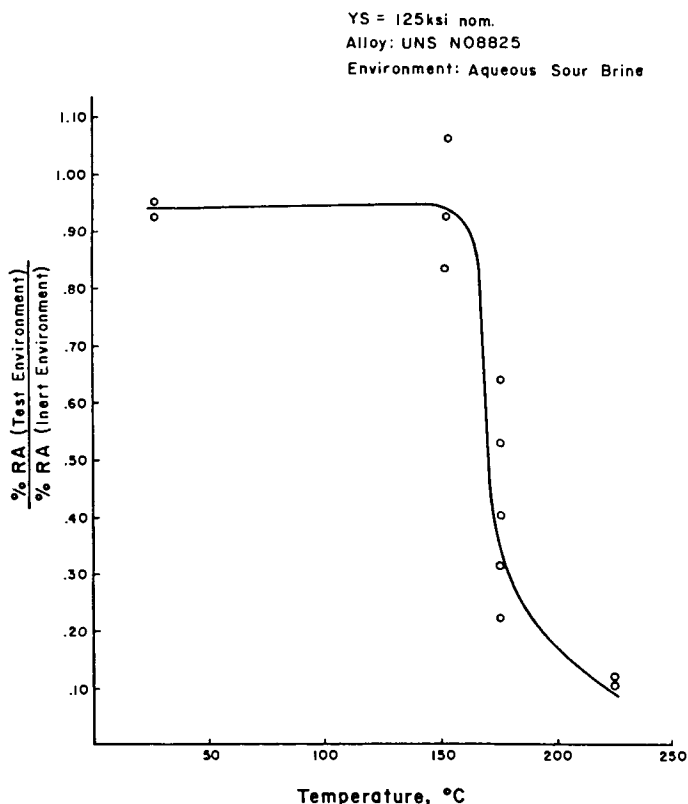


FIG. 8—Determination of critical cracking temperature with the slow strain rate test.

Some specifications for slow strain rate testing rely heavily on the measures of ductility to define the test results. This arises from a natural desire to quantify the severity of the attack. However, there are mechanisms by which measures of ductility are reduced without the onset of environmental cracking.

General corrosion can reduce the total elongation and time to failure (although not usually the reduction in area) simply because the load-bearing area is being reduced by general thinning or pitting. Severe pitting can both reduce cross-sectional area and create mechanical notches which accelerate simple overload of the specimen.

More subtle are hydrogen's interactions with the ductile fracture process. High hydrogen fugacities can interact with dislocation motion and reduce plasticity in alloys which show no evidence of apparent environmental crack growth. Figure 9 presents data obtained on slow strain rate tests of two alloys in a simulated down-hole environment with H_2S , CO_2 , and brine. No SCC was observed on any of these specimens, and the fracture surfaces were entirely ductile rupture. However, ductility losses of up to 35% (reduction in area ratio of 0.65) were recorded.

Classical severe environmental cracking manifests itself with obvious brittle fracture zones on the final fracture surface and secondary cracking in the gage section (Fig. 10).

There are cases, however, when environmentally induced brittle fracture can coexist with substantial ductility in the slow strain rate test.

Some observers speculate that the appearance of shallow secondary cracks only at the extremes of the necked region signals a material which is susceptible to environmental cracking

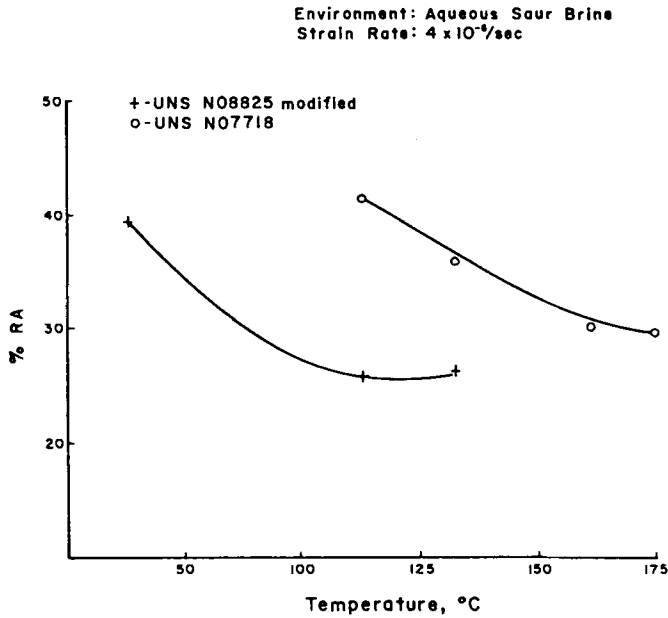


FIG. 9—Ductility loss without brittle crack growth.

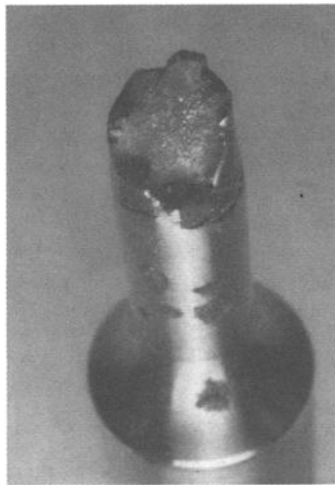


FIG. 10—Severe sulfide stress in the SSR test, manifested by brittle fracture zones on the final fracture and secondary cracking in the gage length.

only after cold working or plastic flow. Since such behavior usually occurs only on relatively low-strength materials which have, historically, cracked in service only when cold-worked or welded without stress relief, this theory seems logical. However, additional experience with matching slow strain rate test results of such low-strength alloys with service history will be necessary before the general applicability of such a criterion is established.

Summary

Slow strain rate testing permits relatively rapid ranking of sour service materials in realistic simulations of anticipated service conditions. The method is more versatile than traditional ranking methods in that corrosion-resistant alloys can be evaluated as well as low-alloy steels. Critical service parameters (temperature, yield strength) can be determined as well as relative susceptibility.

Specifications which require slow strain rate testing for sour service materials qualifications should also specify the following experimental parameters:

1. Strain rate ($\pm 2\%$).
2. Specimen diameter.
3. Temperature.
4. Pressure.
5. Deaeration practice.
6. Electrical isolation of the specimen.
7. Evaluation method.

Evaluation based solely on time to failure is subject to more experimental error than final reduction in area. The ratio of ductility (as measured by either elongation, time to failure, or percent reduction in area) in the test environment versus ductility in an inert environment is more meaningful than the measures of ductility per se.

Slow strain rate test results for candidate materials for sour service generally manifest five classes of behavior:

Category 1—Immunity. No evidence of environmental crack growth on microscopic examination. Ductility ratios equal or exceed 0.9.

Category 2—Practically Immune. No evidence of environmental crack growth on microscopic examination. Ductility ratios reduced to 0.65 to 0.9. (See text for discussion on possible ambiguities.)

Category 3—Mildly Susceptible in Extreme Conditions. Shallow secondary cracking only in the necked region of the gage section. Ductility ratios of 0.75 to 0.95.

Category 4—Moderately Susceptible. Environmentally induced brittle fracture on the final fracture surface. Secondary cracking in the gage section and necked region. Ductility ratios between 0.5 and 0.75.

Category 5—Susceptible. Environmentally induced brittle fracture predominates on the final fracture surface. Extensive secondary cracking on gage length which may extend down into the fillets. Necking limited or eliminated. Ductility ratios less than 0.5.

This separation makes maximum use of the slow strain rate method's rapid screening capabilities. Category 1 and 2 materials have not historically shown environmental cracking problems in sour service. Threshold stress determination may be in order for Category 3 materials, which have been known to give good service in the solution-annealed or stress-relieved conditions. Longer-term testing, threshold stress, or K_{Isc} determination are in order before using Category 4 materials in sour service. Category 5 materials may be severely affected by service in sour environments; isolation from the H_2S or preventive measures should be evaluated.

References

- [1] "Testing of Metals for Resistance to Sulfide Stress Cracking at Ambient Temperature," NACE TM-01-77, National Association of Corrosion Engineers, Houston, TX.
- [2] Parkins, R. N. in *Fundamental Aspects of Stress Corrosion Cracking*, R. W. Staehle and A. J. Forty, Eds., National Association of Corrosion Engineers, Houston, TX.
- [3] Troiano, A. R., "The Role of Hydrogen and Other Interstitials in the Mechanical Behaviors of Metals," Campbell Memorial Lecture, American Society for Metals, Metals Park, OH, 1959.

- [4] Fidelle, J. P. and Broudeur, R., "Hydrogen Gas Embrittlement under the Influence of Strain Rate, Temperature and Thickness: Relationship with Delayed Failure," in *Effects of Hydrogen on Behaviour of Materials*, American Institute of Mining, Metallurgical, and Petroleum Engineers, New York, NY, 1976, pp. 507-517.
- [5] Williams, D. N., "The Hydrogen Embrittlement of Ti Alloys," *Journal of the Institute of Metals*, Vol. 91, 1962-63, pp. 147.
- [6] Kim, C. D. and Wilde, B. E., "A Review of the Constant Strain Rate Stress Corrosion Cracking Test," in *Stress Corrosion Cracking—The Slow Strain-Rate Technique*, ASTM STP 665, Philadelphia, pp. 97-112.
- [7] Nippon Steel Corp., "Slow Extension Rate Test (SERT) in Evaluating Sulphide Stress Cracking of High Strength Steels for Oil Field Applications," 15 Dec. 1978.
- [8] Franson, J. D. and Marcus, H. L., "Crack Growth and Fracture in Gaseous Hydrogen," in *Effect of Hydrogen on Behaviour of Materials*, American Institute of Mining, Metallurgical, and Petroleum Engineers, New York, NY, pp. 233-245.
- [9] Farrow, K. et al., "Effect of Anhydrous NH_3 Composition on Its Ability to Cause SCC in Steels," *B. Corros, J.*, 1981, Vol. 16, No. 1, pp. 11-19.

A Bent Beam Test Method for Hydrogen Sulfide Stress Corrosion Cracking Resistance

REFERENCE: Cox, D. O., "A Bent Beam Test Method for Hydrogen Sulfide Stress Corrosion Cracking Resistance," *Hydrogen Embrittlement: Prevention and Control*, ASTM STP 962, L. Raymond, Ed., American Society for Testing and Materials, Philadelphia, 1988, pp. 190–199.

ABSTRACT: Brittle fracture due to hydrogen sulfide exposure of high-strength, low-alloy steel has been recognized for many years. A relatively simple testing procedure used to estimate and rank a material's resistance to hydrogen sulfide stress corrosion cracking is described. This test gives quantitative data regarding relative susceptibility after a relatively short testing period. Field testing is also possible.

Development of the testing procedure is reviewed. The test uses the concept of a "threshold stress," which is established on a statistical basis for each material or environment under consideration. Results are presented where the test procedure has been used to establish behavior of Grade 9Q thick wall castings [ASTM Specification for Steel Castings Suitable for Pressure Service (A 487/A 487M-84)] fabricated using argon-oxygen deoxidation (AOD) and air-melted materials having niobium and/or molybdenum additions.

One disadvantage of the method is the fact that the test procedure has never been truly standardized. It is hoped that this paper will generate interest in the bent beam method and lead to the development of a standard testing procedure.

KEY WORDS: hydrogen embrittlement, stress corrosion cracking, hydrogen sulfide, environmental cracking, steel castings

Brittle fracture due to hydrogen sulfide exposure of high-strength, low-alloy steel used in the oil field has been recognized for many years [1]. Such failures can result in serious economic losses as well as increased risk to oil field personnel. For this reason, numerous testing procedures have been employed to estimate material resistance to hydrogen sulfide stress corrosion cracking. One method, incorporating a tension specimen, has been standardized by the National Association of Corrosion Engineers (NACE) as TM-01-77. Another test method developed in the late 1950s by engineers at Shell Oil Co. is still used today. It is commonly called the Shell Bent Beam Test and incorporates a small bar specimen loaded in three-point bending.

Test Method

Background

Shell engineers [2] wanted a quantitative test for measuring the relative susceptibility of alloys to hydrogen sulfide (H₂S) stress corrosion cracking—a test procedure which could be used as a method for ranking various materials available for use in sour environments. In addition, they

¹Principal engineer, Failure Analysis Associates, Los Angeles, CA 90025.

sought a testing procedure which could be used to study the effect various metallurgical or environmental variables have on H_2S stress corrosion behavior.

It was felt that the testing procedure should meet the following requirements:

1. The test method must measure relative susceptibility of various alloys to H_2S stress corrosion cracking.
2. The testing method should be such that testing could be completed within a definite time period.
3. The data developed from the test method should be quantitative rather than qualitative in nature.
4. The environment used for testing should be as similar as possible to the expected service environment.
5. The procedure and testing equipment would be such that the loads or strains used during testing could be accurately and precisely measured and could be varied over a wide range.
6. Multiple testing should be easily done at a relatively low cost.
7. The specimen and method should be designed so that field testing would also be a realistic possibility.

A test meeting these requirements maximizes the usefulness of information obtained and gives design engineers a realistic method for selection of materials to be used in H_2S .

It was recognized that various factors influence resistance to H_2S cracking, the most obvious being alloy composition and hardness. Severity of the chemical environment encountered during service is also an important variable, as are times and temperature of exposure. Another significant factor in stress corrosion behavior is the nature and magnitude of stress imposed.

Having established the test requirements and recognized the variables which influence a material's behavior, it is apparent that a realistic test procedure requires compromise. It is also evident that the test procedure must account for the statistical nature of stress corrosion behavior. In addition, correlation between laboratory test results and in-field service must be established.

The test developed uses the concept of a "threshold stress," which is established on a statistical basis for each material under investigation. The basic assumption inherent to the test procedure is that this threshold stress, determined during laboratory testing for a finite period of time, varies among materials in the same way as the relative susceptibility to H_2S stress corrosion cracking in actual field service. Furthermore, it is assumed that the relative order of resistance to H_2S stress corrosion does not change as the severity of the field environment decreases or increases relative to the laboratory test conditions (provided the active species in the environment do not change). Time has shown that these two basic assumptions are quite reasonable; laboratory and field behavior do correlate quite well [1,3].

As mentioned, stress corrosion behavior is statistical in nature. Thus, it would be difficult to determine a quantitative threshold stress above which all specimens crack and below which none crack because the statistics of failure would necessitate many tests. To avoid this problem, the bent beam test determines the stress or strain at which the failure (cracking) rate for a material is 50%. This "50% threshold" or critical stress, S_c , is just as useful for *comparing* material behavior as a true "threshold" (for example, as obtained from NACE TM-01-77 testing) and simplifies the testing procedures and analysis.

Thus, the bent beam test method yields a quantitative result by establishing the stress (or strain) at which the probability of failure is one half when a material is exposed for a given period of time to a laboratory H_2S environment.

Testing Procedure

The method uses a standard beam specimen loaded in three-point bending. The specimen configuration is shown in Fig. 1. The beams are 6.99 cm (2.75 in.) in length with a nominal

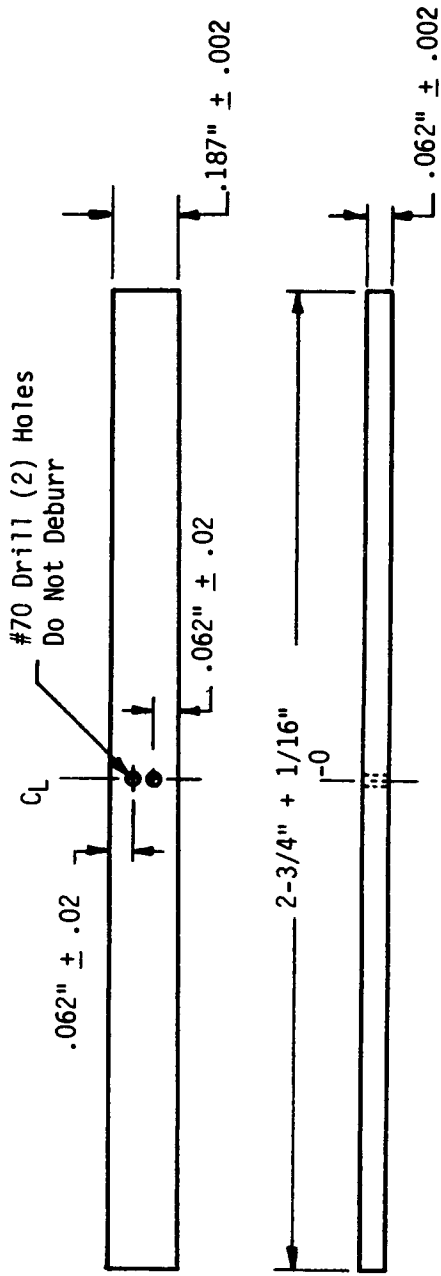


FIG. 1—Bent beam test specimen.

thickness of 0.15 cm (0.062 in.). To increase the severity of the stress or strain and insure that failure occurs at the center of the beam, two small holes are drilled through the specimen. The holes also produce a triaxial stress state (plane strain conditions) at the failure location.

Details of specimen preparation are important and should be consistent from sample to sample to insure that comparison of results will be meaningful. The machining must be done carefully to insure that no overheating takes place. Specimens are surface ground to final dimensions, with the last two passes during this process removing only 0.0013 cm (0.0005 in.) of material to reduce the possibility of material residual stress. They are finally hand ground using 180-grit silicon carbide paper such that the scratches remaining on the surface are aligned parallel to the long axis of the specimen. The specimens are rinsed in acetone and stored in a desiccator until testing.

The specimens are loaded in three-point bending using a jig design as shown in Fig. 2. The jig is made of stainless steel, and the specimen is insulated from the jig using glass tubing around the supporting bolts and a glass bead between the specimen and the loading screw at the center of the jig.

A fixed displacement loading condition is employed. The deflection corresponding to the desired outer fiber stress or strain is calculated using the standard beam formula

$$\delta = \frac{\epsilon L^2}{6t} \quad (1)$$

where

- δ = the beam deflection,
- ϵ = the specimen strain,
- L = the support span, and
- t = the specimen thickness.

The stress or strain is a nominal value, as no allowance is made for yielding or the stress concentration effect of the holes. A deflection gage is used to accurately set the desired specimen displacement.

A 0.05% acetic acid distilled water solution is used as the testing environment. The specimen jigs are immersed in this solution and the containment vessel is sealed. The solution is purged for 30 min using nitrogen gas to remove dissolved oxygen from the system. H_2S gas is then bubbled through the solution for 1 h to obtain saturation. H_2S gas is subsequently bubbled for 30 min every 24 h to insure that saturated conditions are maintained.

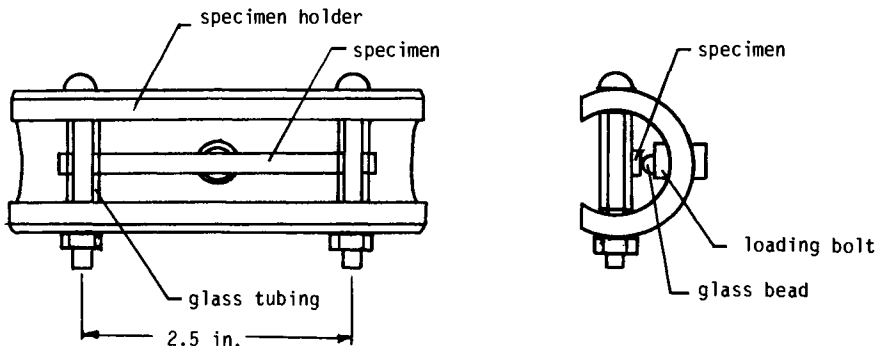


FIG. 2—Test jig showing specimen in place.

The initial pH of the test solution was reported in the original paper by Fraser et al. to be approximately 3 [2]. It was then reported that during the first few days the pH of the solution would increase to approximately 4 and then remain constant for the remainder of the test period. There has been some suggestion that the pH of the testing solution may vary significantly depending upon the size of the test vessel and the method used to insure hydrogen sulfide saturation².

The procedure used to establish the critical strain, $(S_c)_s$, incorporates the following equation (see Table 1)

$$(S_c)_s = \frac{\Sigma \epsilon + B \Sigma T}{n} \quad (2)$$

where

- ϵ = nominal outer fiber strain (cm./cm. $\times 10^3$),
- B = empirical constant = 0.07,
- T = test result = +1 no failure
= -1 failure, and
- n = total number of specimens.

The test data used in calculating the tentative $(S_c)_s$ must have strain values which do not vary more than $\pm 0.07 \times 10^{-3}$ cm/cm from the calculated strain corresponding to $(S_c)_s$. The just-cited equation is based on the statistical method of probit analysis.

While Eq 2 is based on strain, the "50% threshold" or critical stress, S_c , is reported in 10 000 psi

$$S_c = \frac{(S_c)_s E}{10\,000} \quad (3)$$

TABLE 1—Procedure to determine S_c .

1. Test one specimen	<div style="display: flex; align-items: center;"> <div style="flex: 1; border-left: 1px solid black; margin-left: 10px; position: relative;"> <div style="position: absolute; top: -10px; left: 0; right: 0; border-bottom: 1px solid black;"></div> </div> <div style="flex: 1; padding-left: 10px;"> <p>Failure—decrease strain 0.5×10^{-3} in./in.^a</p> <p>No Failure—increase strain 0.5×10^{-3} in./in.</p> </div> </div>
2. Specimen at strain halfway between failed and unfailed values.	
3. Calculate tentative $(S_c)_s$ value.	
4. Test four specimens at strain increments 0.1×10^{-3} in./in. with the refined tentative $(S_c)_s$ in middle of strain range.	
5. Calculate refined tentative $(S_c)_s$ value.	
6. Test four specimens at strain increments of 0.05×10^{-3} in./in. with the refined tentative $(S_c)_s$ in middle of strain range.	
7. Calculate S_c value.	

^aOne inch = 2.54 cm.

²Private communication, Jose R. Canal, NL Shaffer, Houston, TX.

where E is the elastic modulus for the material. Over the years, experience has shown that materials which have an S_c above 10 (100 000 psi or 689 MPa) usually show satisfactory service in H_2S environments [1,3].

It has been found that 80% of the specimens which will fail during the standard 30-day test period do so within the first three days of testing, and 98.5% fail within the first three weeks [2]. Thus, to save time, initial testing can be limited to a few days and a tentative S_c calculated. As one obtains a better estimate for S_c , the standard test period of 30 days is used. At completion of the 30-day period, the specimens are removed from the test fixtures and bent approximately 30° to determine if any incipient cracking is present. If a specimen is found to contain any macroscopic cracks, the specimen is considered to have failed the test.

Test Limitations

The bent beam test at its current stage of development has many advantages, the major ones being simplicity and the fact that testing is completed within a fixed period of time. The method can easily be used as a screening criterion in comparing various alternative materials for a given application. The data are quantitative and the procedure allows for multiple and field testing.

While the method and resulting data are quite useful, the limitation of the procedure must also be kept in perspective. It should be remembered that the calculated S_c represents a stress level at which half of the specimens fail. In addition, since the specimen is relatively small and is loaded in three-point bending, the actual volume of material tested is relatively small.

Perhaps the greatest disadvantage of the bent beam test at the present time is the fact that the test method has not been truly standardized. Laboratories use slightly different procedures, and recent work and discussion have shown that minor variations may significantly affect the results of the testing program. For example, the pH of the test solution may vary significantly depending upon how often H_2S gas is introduced to the fluid and the size of the containment vessel which is used for testing.² Such variations may significantly affect the S_c value obtained from the testing.

Current and future efforts by ASTM Standards Committees and other interested parties should address these problems in an effort to establish a truly standard testing procedure. At the present time, one should be cautious when comparing data developed in different laboratories. The specific test procedures used by the different laboratories should be obtained to insure that test results can be compared on a realistic basis.

Testing of Thick Wall Castings

As part of an ongoing program [4,5], bent beam testing has been used to investigate the effect of alloy additions and casting process on the H_2S stress corrosion resistance of large low-alloy steel castings used for blowout preventers (BOPs). Specific to the work reported here, testing has been done to establish the effect molybdenum and niobium additions have on behavior of ASTM A 487 Grade 9Q material. The effect of an AOD (argon-oxygen deoxidation) casting process, which reduces the sulfur content relative to air-melted material, has also been investigated.

Four materials, described in Table 2, have been tested. Samples of the four materials were received as trepanned plugs, approximately 5.1 cm (2 in.) in diameter and 38.1 cm (15 in.) in length, removed from production castings. The samples were taken from the casting such that the long dimension of the trepanned samples represents the thickness of the casting wall. Since variations in composition and response to heat treatment are expected through the wall thickness, material from three regions of the trepanned sample were tested: inside, center, and outside.

Bent beam specimens were machined from each region and tested in the fashion previously described. The containment vessels for this testing were 1200 mL capacity and held four speci-

TABLE 2—The four thick wall casting materials tested.

Material	Chemistry, Weight %										Yield Strength, ksi ^a		Ultimate Strength, ksi ^a		Reduction in Area, %	
	C	Mn	Mo	P	S	Si	Cr	Cu	Ni	Nb	Location		Location		Location	
											Inside	Center	Outside	Inside	Center	Outside
Air-melted, Mo modified, A 487 9Q	0.22	0.91	0.77	0.013	0.006	0.57	1.04	0.13	0.19	0	75	71	85	96	97	105
Air-melted, Mo and Nb modified, A 487 9Q	0.20	0.88	0.78	0.012	0.004	0.52	0.99	0.11	0.21	0.022	63	64	83	91	92	105
AOD, Mo-modified, A 487 9Q	0.19	0.92	0.89	0.027	0.008	0.49	0.94	0.18	0.13	0	88	89	93	108	109	110
AOD, Mo and Nb modified, A 487 9Q	0.19	0.93	0.80	0.017	0.005	0.53	0.88	0.16	0.08	0.032	88	72	82	109	98	104
ASTM A 487 9Q requirements	0.33 max	0.60 to 1.00	0.15 to 0.30	0.04 max	0.045 max	0.80 max	0.75 to 1.10	0.50 max	0.50 max	85 min	...	105 min	...	35

^aConversion factor: 1 ksi = 6.894 757 E + 06 Pa.

mens and approximately 1000 mL of the acetic acid solution. The test solution was resaturated by bubbling H_2S gas through the solution for 30 min every 24 h.

The test results are summarized in Table 3. As can be seen, all materials tested had S_c values greater than 10, the standard criterion for acceptance in H_2S -containing environments.

The ASTM A 487 material containing molybdenum and niobium additions produced using the AOD melting practice showed the best resistance to H_2S environments. However, there were significant S_c variations with location for this casting, with the center of the wall showing significantly higher cracking resistance. Metallographic examination of material from the three regions showed the microstructure at the center wall location had a significantly different appearance from those of the inner and outer wall [4]. This may explain why the measured S_c is significantly better. Additional work is required to substantiate this preliminary observation.

Discussion

Over the years, the bent beam test originally proposed and developed by engineers at Shell Oil Co. has been a useful tool in establishing the relative susceptibility of various material to H_2S stress corrosion cracking. The method has also been used to determine the effects environment, alloy composition, and actual field conditions have on stress corrosion resistance.

The use of thick wall castings, rather than more expensive forging for pressure control equipment, is being investigated using the bent beam test method. From the work completed to date, it is apparent that minor chemical modifications of standard low-alloy steel casting compositions may lead to a material which is as resistant to H_2S stress corrosion cracking as the more expensive forgings currently used for BOPs. Further testing is required to more precisely define alloy composition, casting method, heat treatment procedures, and microstructure, which will result in optimum properties for these thick wall castings. It is expected that the bent beam testing method will be used extensively during the subsequent testing program.

Additional efforts are required by both industry and standard developing agencies such as ASTM to truly standardize the bent beam test method. This will insure that test results obtained in various laboratories throughout the world can be realistically compared and used by design engineers to select materials which will insure reliable operation in environments where hydrogen embrittlement or stress corrosion cracking may be a problem.

TABLE 3—Thick wall casting bent beam test results.

Material	Location	Rockwell B Scale Hardness		$S_c (\times 10^{-4} \text{ psi}^a)$
		Average	Range	
Air melted, Mo modified, ASTM A 487 9Q	Inside	90	89 to 90	13.4
	Center	91	89 to 95	13.1
	Outside	97	94 to 99	11.0
Air melted, Mo and Nb modified, ASTM A 487 9Q	Inside	92	90 to 95	12.4
	Center	88	86 to 89	14.1
	Outside	98	97 to 98	12.7
AOD, Mo modified, ASTM A 487 9Q	Inside	96	91 to 98	10.8
	Center	93	91 to 94	13.1
	Outside	97	92 to 99	13.0
AOD, Mo and Nb modified, ASTM A 487 9Q	Inside	94	90 to 96	12.0
	Center	90	89 to 91	18.7
	Outside	96	95 to 97	15.1

^aConversion factor: 1 psi = 6.894 757 E + 3. Pa.

Acknowledgments

The author wishes to gratefully acknowledge J. R. Canal, Shaffer/NL Industries, Inc., who supplied funding and materials for testing, and Craig V. Smith, who capably performed the testing and assisted with the analysis.

References

- [1] "H₂S Corrosion in Oil and Gas Production—A Compilation of Classic Papers," Tuttle, R. N. and Kane, R. D., Eds., National Association of Corrosion Engineers, Houston, TX, 1981.
- [2] Fraser, J. P., Eldredge, G. G., and Treseder, R. S., "Laboratory and Field Methods for Quantitative Study of Sulfide Corrosion Cracking," *Corrosion*, Vol. 14, 1958, pp. 517t-523t.
- [3] Fraser, J. P. and Eldredge, G. G., "Influence of Metallurgical Variables on Resistance of Steels to Sulfide Corrosion Cracking," *Corrosion*, Vol. 14, 1958, pp. 524t-530t.
- [4] Canal, J. R. and Singh, G., "Development of Sulfide Stress Cracking Resistance Material for Heavy Wall Castings," Paper F80-2, The Metallurgical Society of AIME, Warrendale, PA, 1980.
- [5] Cox, D. O., "The Shell Bent Beam Test and its Application to Thick Wall Castings," Proceedings of the NL Shaffer 1981 H₂S Symposium, J. R. Canal, Ed., NL Shaffer/NL Industries, Houston, TX, pp. 68-79.

DISCUSSION

McIntyre: Dr. Cox, what is your opinion on using the bent beam test for evaluating corrosion-resistant alloys such as stainless and nickel base alloys?

Cox: It has been done. I think it is a valid way to go, but again here you have to make sure that you define environments in a similar fashion as others using the same method. It has been used for chlorides on stainless steels and that type of thing, but again you have got to have a standard method.

McIntyre: Dr. Cox, the primary complaint I hear about this test or this sort of test for use as a quality control or quality assurance measure is the long time required to do the testing. What are your thoughts on ways to accelerate the tests so that you might get the results and derive in essence, say, in one or two days instead of four consecutive five-day or ten-day test periods?

Cox: I am not certain how much you can accelerate it. You can try and increase the severity of the environment in some way. I really think it is going to be difficult to decrease the time period. As I did show, though, most failures occur early on in the test period and there may be a way around the longer time by eliminating the last two or three weeks. I do not think you can go much less than a week or week and a half. That is for sure.

Berman: You indicated a concentration of acetic acid in your test method, 5 mL of glacial acetic and 1000 mL of water; in other words, you made up 1005 mL of solution? As a chemist, I am very sensitive to things like this because metallurgists are sometimes careless in their definitions of concentration, because you run into things like 50% nitric acid, while I look in the book and see nitric acid concentrated 28% or something like that so I assume they mean one to one, but it is not defined that way. I just wanted to make sure that is what you want, and do other people realize that or do they just make up a liter of solution?

Cox: I think that most people have been doing it like you say. We are not interested in getting an exact liter of solution; we are more interested in getting the concentration that we want. We add 5 mL acetic acid to the 1000 mL of water, for a total volume of 1005 mL.

McIntyre: Let me add a comment to that. The reason or the rationale for putting the acetic acid in is that, normally in oil and gas environments, you have significant amounts of CO_2 and H_2S dissolving into any liquid that forms, either as condensate or as produced brine. The effect of those acid gases dissolving into the liquid is to drop the pH. As it happens in high-pressure situations, it is to a level right near pH of 3, so the acetic acid addition gives you the pH drop without adding inorganic anions which could affect the corrosion mechanism.

Selection of Petroleum Industry Materials Through Use of Environmental Cracking Tests

REFERENCE: Ciaraldi, S. W., "Selection of Petroleum Industry Materials Through Use of Environmental Cracking Tests," *Hydrogen Embrittlement: Prevention and Control*, ASTM STP 962, L. Raymond, Ed., American Society for Testing and Materials, Philadelphia, 1988, pp. 200-213.

ABSTRACT: Four environmental cracking problems experienced by the petroleum industry are described. These problems warrant the use of laboratory environmental cracking tests as an aid to materials selection. Test methods used at the Amoco Research Center include tensile-type (static load and slow strain rate), U-bend, bent-beam, and fracture mechanics techniques. Choice of method is shown to depend upon service conditions, alloy system, and product form. Typical test results for carbon and low-alloy steels, stainless steels, and nickel-base alloys are presented. In particular, methods of utilizing test results to provide specific materials selections are described.

KEY WORDS: stress corrosion, hydrogen embrittlement, sulfide stress cracking, polythionic acid, test methods

Environmental cracking (hydrogen embrittlement and stress-corrosion cracking) is a major problem experienced by the petroleum industry. It affects all major sectors of the industry, including refining, gas/oil production, and chemical processing operations. Indeed, a recent in-house survey of several years of failure analyses revealed hydrogen embrittlement (HE) and stress-corrosion cracking (SCC) to be the major causes of materials failures, accounting for over 50%.² Since the oil industry is heavily capital-equipment intensive, the failures represent major losses of funds. Additionally, because systems containing large quantities of explosive and/or toxic substances are involved, worker and environmental safety must be maximized by preventing serious failures.

Because of these economic and safety concerns, environmental cracking tests are often used by the petroleum industry as an aid to materials selection. A variety of test methods are available, and there is often only limited agreement on optimum techniques. Realistically, each test method has strengths and weaknesses, and it appears that no single method is best suited to all environmental cracking systems and alloys. Often, more than one technique is used for a single environment-alloy combination.

Table 1 lists some characteristics of four important environmental cracking problems encountered by Amoco and the oil industry. The problems include polythionic acid SCC, sour gas cracking, chloride SCC, and amine SCC. Each environmental cracking problem is briefly described and common test techniques discussed. Generic test results are presented and methodologies for materials selection based on the result suggested. It is shown that for these four SCC systems, service temperature can play a key role in materials selection.

¹Corrosion specialist, Research Department, Amoco Corp., Amoco Research Center, P.O. Box 400, Naperville, IL 60566.

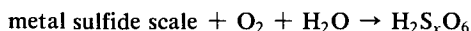
²Johnson, J. M., Amoco Corp., Naperville, IL, private communications.

TABLE 1—Some important petroleum industry environmental cracking problems.

Type	Industrial Sector	Alloys	Typical Environment
Polythionic acid SCC	Refining	Austenitic stainless steels, nickel-base alloys	Aqueous H ₂ S, O ₂ , SO ₂ , S
Sour gas cracking	Gas processing	High-strength steels, stainless steels, nickel-base alloys	H ₂ S, CO ₂ -containing brines
Chloride SCC	Refining	Austenitic stainless steels, nickel-base alloys	Elevated temperature aqueous chlorides
Amine SCC	Chemical processing	Carbon-steels	Elevated temperature aqueous amines
	Refining		
	Gas processing		

Polythionic Acid SCC

Polythionic acids occur in refinery systems by reaction of metal sulfide scales with water and oxygen, as



where x ranges from 3 to 5 [1]. In refinery equipment, polythionic acids may form during down-times. Affected equipment include flare tips, furnace tubes, catalyst transfer lines, and valves involved in desulfurizer, reformer, and hydrocracker processes.

Austenitic stainless steels and nickel-base alloys are attacked by polythionic acids in the form of intergranular SCC. Cracking requires the presence of a sensitized structure produced by grain boundary chromium-carbide precipitation, as well as appropriate environment. Sensitization results from welding or by service in the sensitization range, 425 to 825°C (800 to 1520°F) [2]. Low-carbon (L) stainless steel grades are not totally immune and often high-temperature strength requirements dictate use of higher carbon (H) steels and alloys.

Because polythionic acid SCC requires a sensitized microstructure, recent laboratory work has focused on defining compositional, processing, and operating parameters that promote sensitization.³ Table 2 summarizes alloys and conditions currently being investigated for resistance to polythionic acid SCC. The number of factors studied requires that a large quantity of specimens be tested.

TABLE 2—Alloys investigated for resistance to polythionic acid SCC [4].

Type	Grades	Conditions
Austenitic stainless steels	304H	Solution annealed; stabilized and TIG welded; stabilized, TIG welded, and restabilized; furnace sensitized
	321H	
	347	
	347H	
Nickel-base	Incoloy 800H ^a	Solution annealed, TIG welded, furnace sensitized
	Incoloy 825 ^a	
	Inconel 601 ^a	
	Inconel 625 ^a	

^aTrademark, Huntington Alloys, Inc.

³Beggs, D. V., Amoco Corp., Naperville, IL, private communications.

ASTM has standardized several tests for detecting sensitization and evaluating polythionic acid SCC susceptibility. These include ASTM Practices for Detecting Susceptibility to Intergranular Attack in Austenitic Stainless Steels (A 262-85a) and ASTM Recommended Practice for Determining the Susceptibility of Stainless Steels and Related Nickel-Chromium-Iron Alloys to Stress Corrosion Cracking in Polythionic Acids [G 35-73 (1982)]. Common practice is to expose specimens to the selected test solutions at ambient temperature for several weeks in sealed glass kettles. U-bend SCC specimens assembled onto alloy racks, as shown in Fig. 1, are generally used. Welds in the specimens are located at the region of maximum bending stress. Results obtained, Fig. 2, are of the failure/no-failure type. This limited degree of test sophistication is sufficient to identify the influences of variables of interest. Although the tests are cost-effective, lack of consistent failure/no-failure results requires that multiple specimens be tested under identical conditions. This lack of repeatability is thought to be associated with both variable U-bend stress levels and the preparation of aqueous test solutions.

Sour Gas Cracking

Gas and oil production from sour (containing hydrogen sulfide) formations can result in sour gas cracking of down-hole tubulars, instrumentation, workover tools, wellhead components, and gathering lines. Such wells can be highly aggressive when saturated brines are produced under high partial pressures of hydrogen sulfide and carbon dioxide. Bottom-hole temperatures to 230°C (450°F) and total pressures to 140 MN/m² (20 000 psi) are not uncommon. Conditions can be made more severe during formation acidizing operations, when concentrated acid solutions are introduced down-hole. Sour gas cracking can also be a problem in refining and gas plant operations.

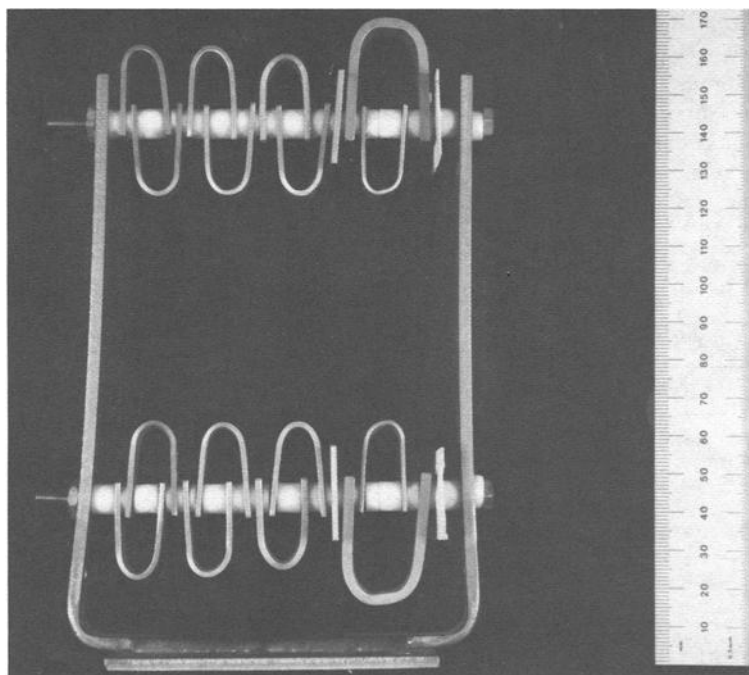


FIG. 1—Rack of welded U-bend specimens used for polythionic acid SCC evaluation of stainless steels and nickel-base alloys.

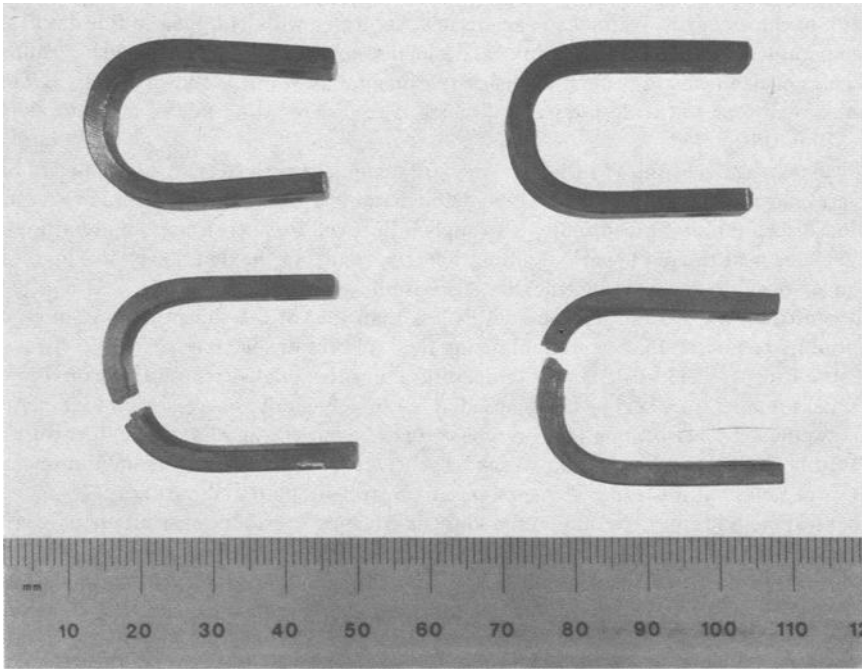


FIG. 2—Typical results of polythionic acid SCC tests. Results are of the failure/no-failure type.

Table 3 lists some characteristics of sour gas cracking. As noted, two apparently distinct cracking mechanisms, hydrogen embrittlement and chloride-induced SCC, can be encountered. Under appropriate conditions, a wide range of steels and alloys can be susceptible to cracking.

The hydrogen embrittlement form of sour gas cracking, often termed sulfide stress cracking (SSC), has received considerable attention. This is because the great majority of wells are completed with high-strength carbon and low-alloy steel tubulars. Laboratory SSC testing has been standardized by the National Association of Corrosion Engineers (NACE) in "Testing of Materials for Resistance to Sulfide Stress-cracking at Ambient Temperature" (TM-01-77). The TM-01-77 test is performed by exposing round tension specimens to an aqueous solution containing

TABLE 3—Some characteristics of sour gas cracking.

SCC Mechanism	Most Common Temperature Regime	Susceptible Alloys
Hydrogen embrittlement	Ambient	Carbon-steels, low-alloy steels, martensitic stainless steels, precipitation hardening stainless steels, duplex stainless steels, nickel-base alloys
Chloride SCC	Elevated	Precipitation hardening stainless steels, duplex stainless steels, austenitic stainless steels, nickel-base alloys

5% sodium chloride (NaCl) and 0.5% acetic acid, saturated with hydrogen sulfide gas at ambient temperature and pressure. Specimens are loaded to various stress levels using calibrated proof rings or dead-weight testers. A basic experimental assembly is shown in Fig. 3. Time to failure is monitored until 720 h duration, which is considered a no failure if failure does not occur within this period.

Typical test results by the TM-01-77 method for a high-strength steel are illustrated in Fig. 4. In general, an SSC threshold stress can be defined and is used as the predominant measure of cracking susceptibility. Susceptibility is strongly influenced by steel strength and hardness. By testing a steel heat treated to various strength levels, results of the type shown in Fig. 5 can be developed. A sharp increase in cracking susceptibility with increased hardness is often observed. Restricting a steel to hardness levels less than that of the sharp increase in cracking susceptibility has been effective in minimizing field failures in sour service.

Because hydrogen embrittlement is temperature sensitive, high-strength steels unacceptable for ambient temperature service can be used at lower well depths where elevated temperatures are maintained. By performing tension-type or bent-beam tests in elevated temperature solutions, results of the type shown in Fig. 6 can be generated. With these results, minimum acceptable service temperatures can be selected based on steel strength and hardness.

Other test methods for determining the sour gas cracking resistance of steels are used. NACE is currently attempting standardization of these methods. The techniques vary mainly by specimen type, a few of which are shown in Fig. 7, including double cantilever beam, bent beam, smooth tensile, and C-ring. Note that for tubular goods, cracking orientation changes with specimen type. Cracking susceptibility can vary extensively with orientation [3]. Down-hole tubulars are generally more highly stressed axially due to string weight. For this reason, tests producing cracking transverse to the longitudinal tubular axis (that is, tensile and bent beam) are generally preferred.

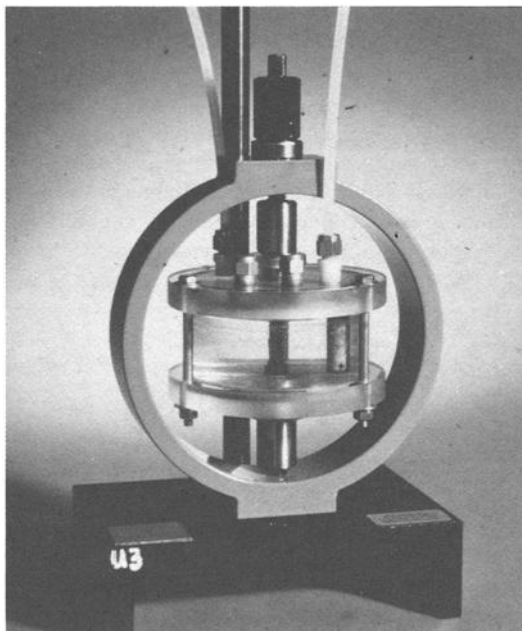


FIG. 3—Proof-ring, NACE TM-01-77 test assembly for sour gas cracking evaluation of high-strength steels.

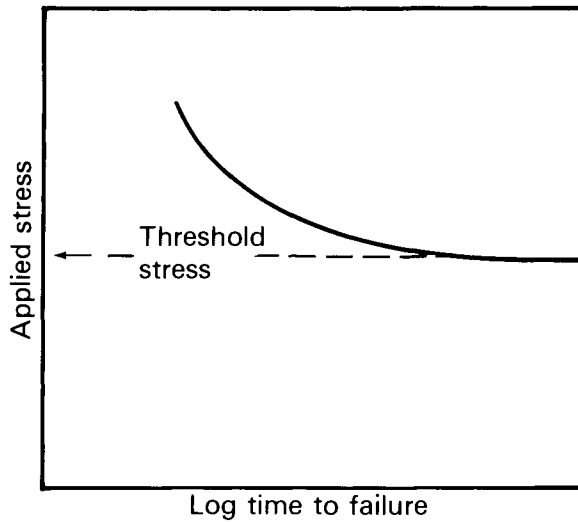


FIG. 4—Typical results of NACE TM-01-77 tests for a high-strength steel. Threshold stress is obtained as indicated and is the primary measure of cracking resistance.

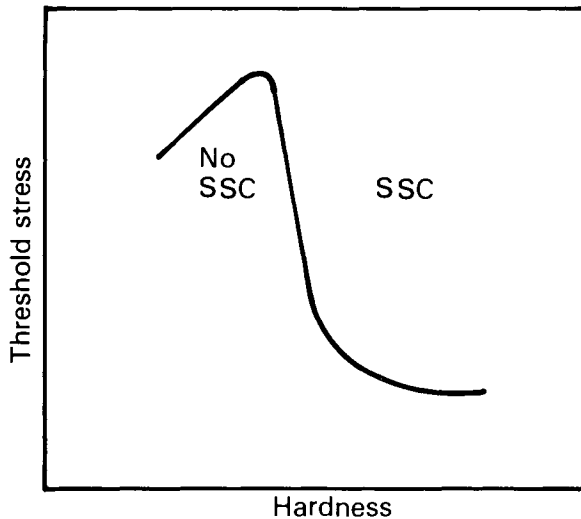


FIG. 5—Sour gas cracking threshold stress variation with hardness for a high-strength steel. Maximum sour service hardness can be selected as that just prior to the large increase in cracking susceptibility.

General corrosion in aggressive gas and oil wells is most frequently controlled by down-hole inhibitor additions. However, increased use of stainless and nickel-base alloys to control corrosion has occurred in recent years. In most cases, the alloys are used in the cold-drawn or cold-pilgered condition, so that required high-strength levels are obtained. Thus, depending upon alloy and environmental conditions, chloride-induced SCC, enhanced by the presence of hydrogen sulfide, is possible.

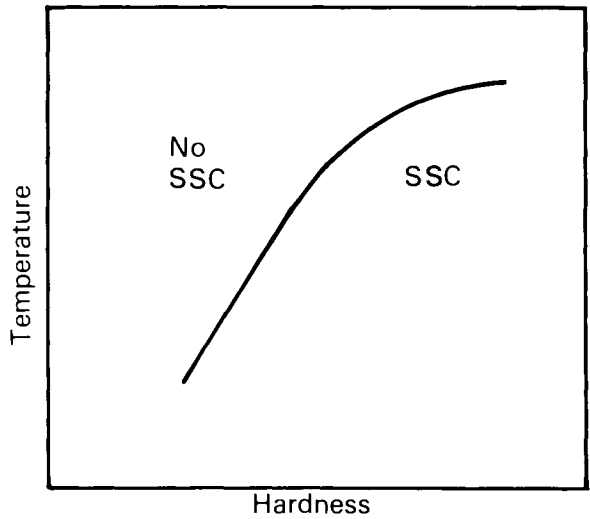


FIG. 6—Results of elevated temperature sour gas cracking tests for high-strength steels. Minimum no-SSC service temperature can be selected based on steel hardness.

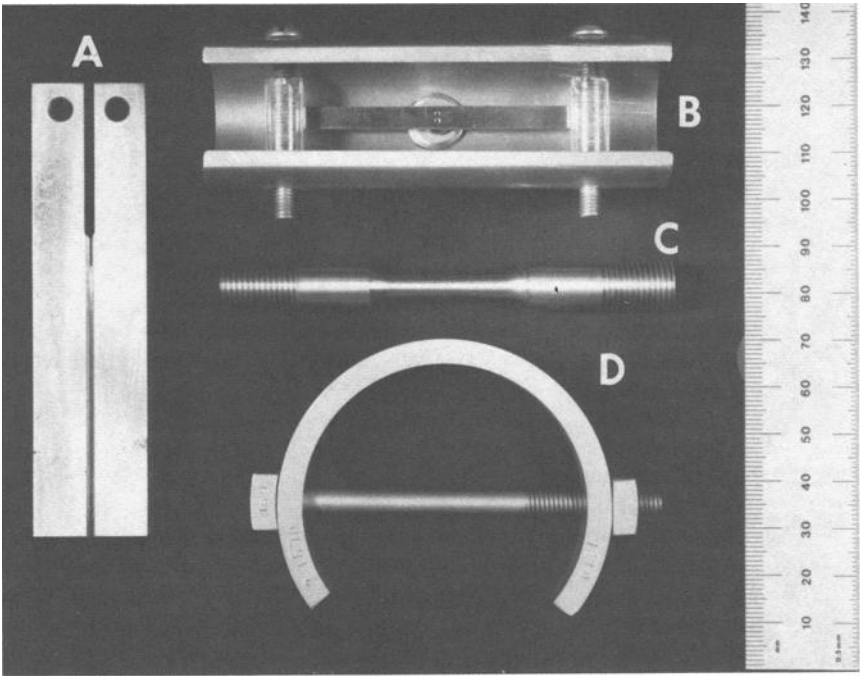


FIG. 7—Specimen types for sour gas cracking evaluations include: (A) DCB, (B) bent-beam, (C) TM-01-77 tensile, and (D) C-ring.

Laboratory evaluation of alloy resistance to the chloride-induced form of sour gas cracking is generally performed by specimen exposure to test solutions in pressurized autoclaves, an example of which is shown in Fig. 8. Although a variety of specimen types can be used, interest in fatigue precracked double cantilever beam (DCB) specimens is growing. This is because crack initiation stages for other specimen types can be substantial for corrosion-resistant alloys, resulting in lack of repeatability and the need for long test durations [4].

Examples of alloy DCB specimens before and after autoclave SCC testing are shown in Fig. 9. DCB specimens produce cracking in the most susceptible direction for cold-worked tubulars. Use of wedge loading and curved specimens obtained full wall from tubulars is common. Specimens are generally side-grooved 20 to 25% on both sides to prevent extensive crack branching. By testing DCB specimens at various temperatures, results of the type shown in Fig. 10 can be generated. Based upon temperature and alloy nickel content, three distinct regions of SCC susceptibility can be defined. No growth of the fatigue precrack by SCC is observed for highly resistant alloys. When SCC does occur, threshold stress intensity for SCC arrest can be determined and compared to a fracture mechanics calculated acceptable minimum value. This stress intensity will depend on yield strength, applied stress, and anticipated flaw size and geometry. Based upon this value, SCC results can be separated into unacceptable and fracture mechanics acceptable regions.

At lower temperatures, fracture mechanics acceptable results have not been observed often. Therefore, no growth of the fatigue precrack by SCC is an appropriate materials selection criterion. If bottom-hole or maximum service temperatures are known, the minimum nickel content to resist SCC can be selected. Note that at higher temperatures, the fracture mechanics accept-

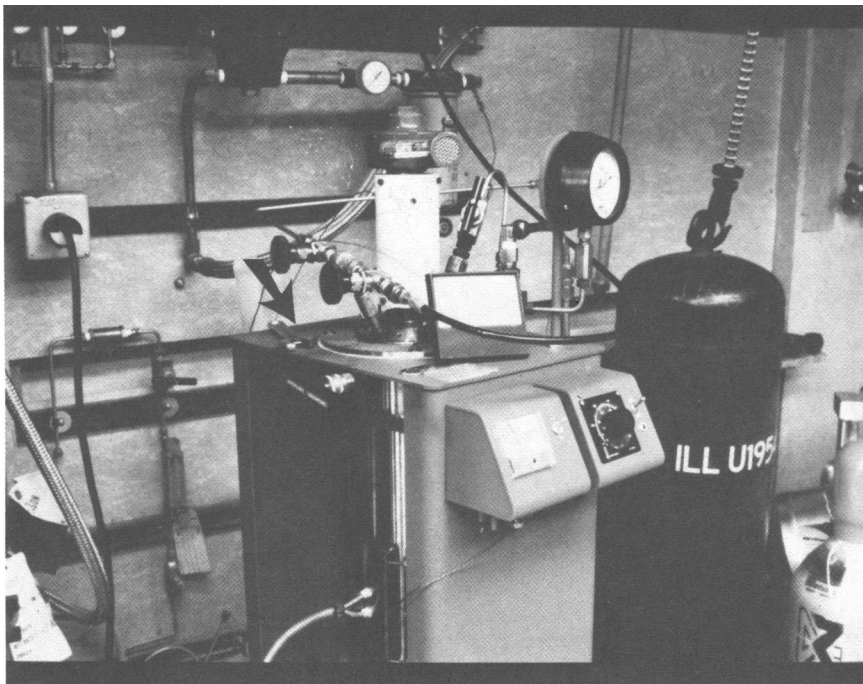


FIG. 8—Autoclave for performing elevated temperature/pressure sour gas cracking tests of stainless steels and nickel-base alloys.

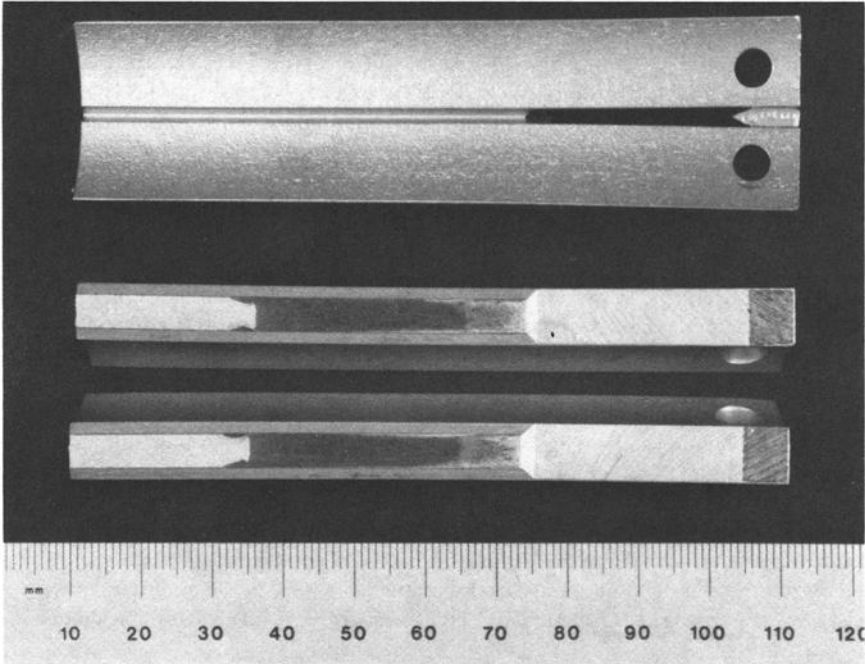


FIG. 9—Wedge-loaded, fatigue precracked DCB specimens for sour gas cracking tests of alloys. Note that specimens are curved because they were obtained full wall from alloy tubulars. Specimens are heavily side-grooved to prevent crack branching. Fractured specimen shows typical SCC arrest.

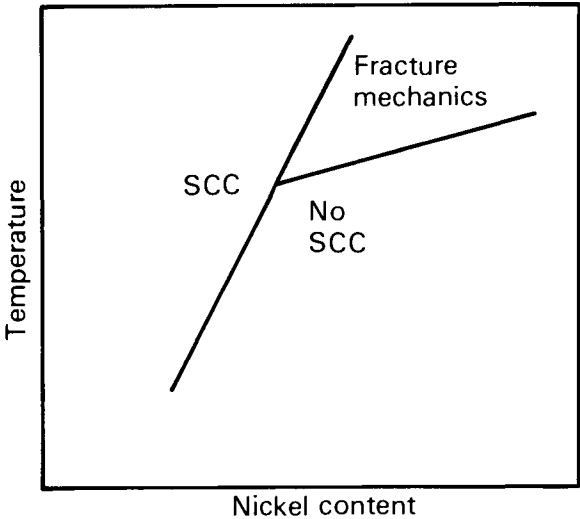


FIG. 10—Typical results of sour gas cracking tests of stainless steels and nickel-base alloys. At lower temperatures, an SCC/no-SCC criterion for alloy nickel content selection is appropriate. At higher temperatures, a fracture mechanics acceptable region can be defined within the SCC range.

able region of Fig. 10 becomes significant. Use of fracture mechanics for higher service temperature alloy selection results in lower alloy expense than selection by the no-SCC criterion.

Other specimen types used for sour gas, chloride-induced SCC evaluation of alloys include U-bends, bent beams, and C-rings. These methods suffer from the crack initiation problems mentioned previously. A test method also gaining interest for this evaluation is the slow strain rate technique (SSRT). Use of this method for chloride-induced SCC evaluation is described in following paragraphs.

Chloride SCC

Chloride-induced SCC of austenitic stainless steels can be a problem in refinery and chemical processing operations. Failures have occurred in a variety of equipment, including heat exchangers, columns, piping, pumps, valves, expansion joints, bolting, and steam tracing. In the past, chloride SCC problems have often dictated replacement with titanium components, at greatly increased expense. The development of duplex stainless steels and higher nickel austenitic alloys with improved SCC resistance now offers alternatives to titanium. However, the SCC resistance of these newer alloys has not been fully quantified.

U-bend and tension-type specimens have been used frequently for chloride-induced SCC evaluations. Unfortunately, lack of repeatability of SCC initiation is a major deficiency of these methods. SSRT testing and use of fracture mechanics techniques have largely overcome this difficulty.

An example of an SSRT system is shown in Fig. 11. SCC resistance is measured by slowly straining tension-type specimens of the type shown in Fig. 12(B). Environments for SCC evaluation are generally elevated temperature brines. The test system shown in Fig. 11 also allows effects of applied potential to be evaluated. Although much of this testing is new, results of the

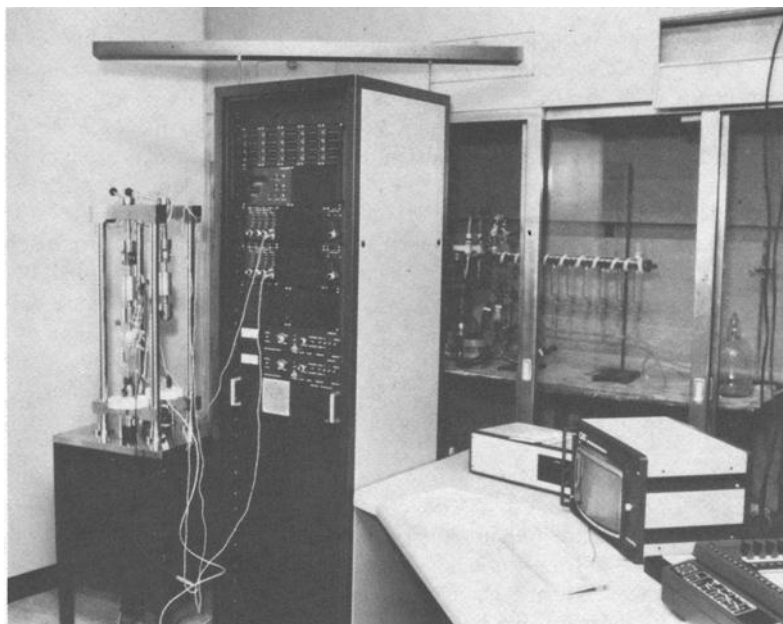


FIG. 11—Slow-strain-rate testing machine used for chloride-induced SCC evaluation of austenitic stainless steels.

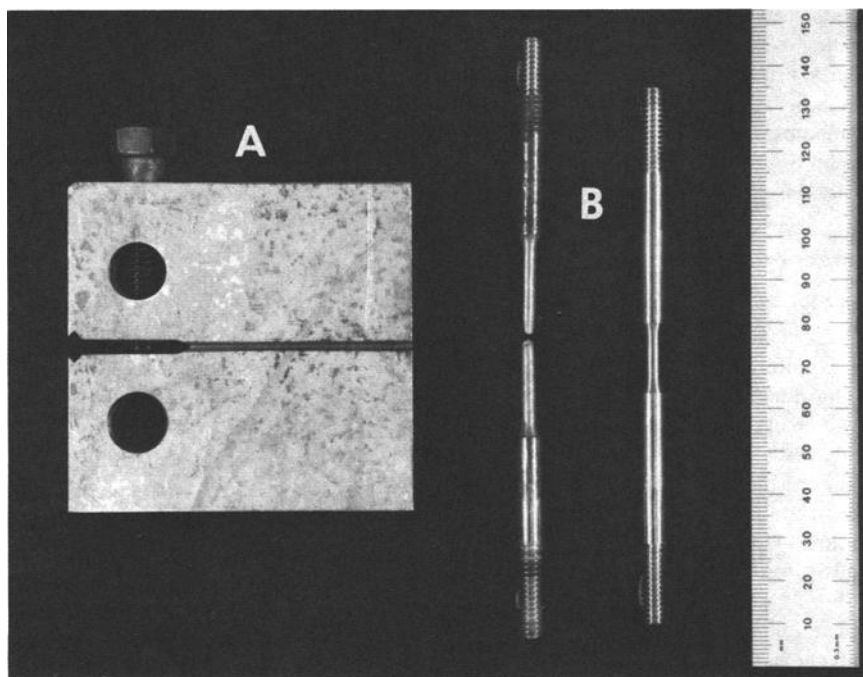


FIG. 12—Compact tension specimens (A) and slow-strain-rate tension specimens (B) used for chloride-induced SCC evaluation of austenitic stainless steels. Similar specimens have been used to investigate amine SCC of carbon steels.

type shown in Fig. 13 are being generated. With test temperature as the major experimental variable, the region of SCC susceptibility can be defined. Therefore, for a given alloy, maximum service temperature to resist SCC can be selected.

Also shown in Fig. 12(A) is a fatigue precracked, bolt-loaded, compact tension (CT) specimen used for chloride SCC evaluation of austenitic stainless steels. Application of DCB specimens to this testing is generally impractical due to the low-strength level of the alloys. The long arms of DCB specimens result in plastic deformation of low yield-strength alloys at low deflections, limiting the maximum obtainable applied stress intensity. Increased arm height and decreased arm length of CT specimens allows higher stress intensities to be obtained. By testing at various temperatures in brine solutions, results of the type shown in Fig. 14 are anticipated.⁴ Again, maximum temperature for no SCC of a given alloy can be defined. Use of threshold stress intensity data for materials selection within the SCC range is possible. The CT test method does have the disadvantage that thick specimens are required to obtain plane strain conditions. Because of this limitation, use of J -integral SCC tests is being considered [5].

Amine SCC

Aqueous amine solutions are used in refinery and gas plant operations to strip hydrogen sulfide and/or carbon dioxide from gaseous process streams. Equipment used for this function include columns, piping, and heat exchangers. In most cases, this equipment is fabricated from plain carbon steels. Industry practice has generally been to postweld heat treat welds in equipment operating above 66°C (150°F) to prevent amine SCC. However, throughout the refining

⁴Kaley, L. C., Amoco Corp., Naperville, IL, private communications.

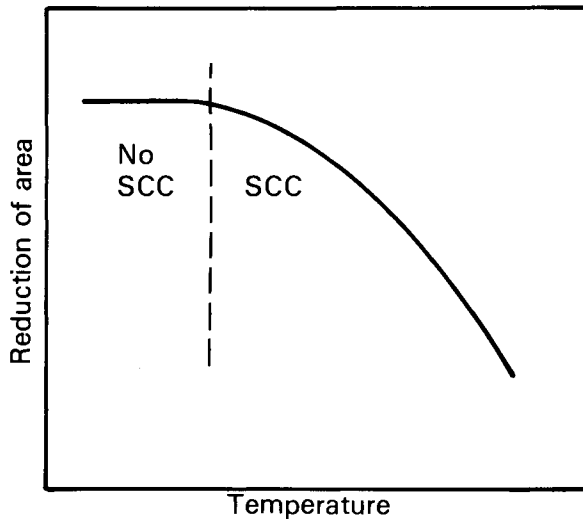


FIG. 13—Test result type anticipated for chloride SCC of austenitic stainless steels by slow-strain-rate techniques. The maximum no-SCC temperature for a given alloy can be determined.

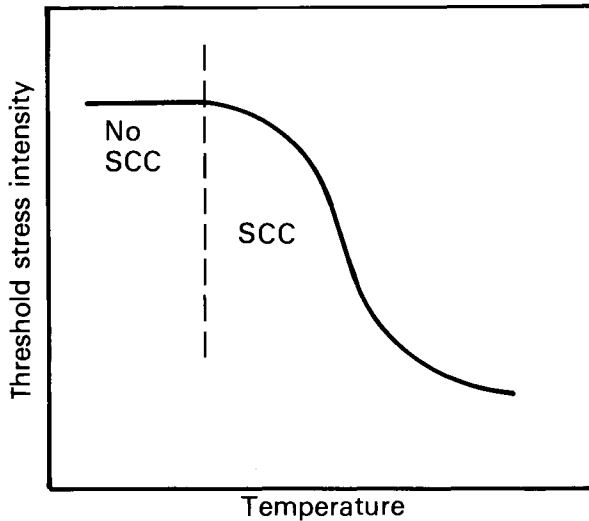


FIG. 14—Typical test results being generated for chloride SCC of austenitic stainless steels through use of bolt-loaded compact tension specimens. Maximum no-SCC service temperature can be selected. Fracture mechanics analyses can be applied within the SCC range.

industry, failures have recently occurred in components operating at temperatures as low as 50°C (120°F). Amine SCC is typically intergranular in carbon steels, with monoethylamine solutions apparently the most aggressive.

Some difficulty has occurred in reproducing amine SCC in the laboratory. Test methods that have been used include U-bend, tensile-type (including notched specimens), and precracked

CT techniques. No SCC has been obtained by these methods. Currently, the most promising technique for amine SCC evaluation is the SSRT method. Initial results indicate that there is a fairly narrow applied potential range in which SCC is obtained.⁴ However, even within this range, only limited SCC has occurred. Field amine SCC failures are known to generally require long incubation times, so that use of smooth SSRT specimens may be a problem. Perhaps this problem may be compensated for by appropriate strain-rate selection or by step loading. Equipment is currently being assembled for J -integral amine SCC tests. Polarization of specimens will probably be required. It is hoped that the use of dynamically strained, precracked specimens will result in more extensive SCC in laboratory tests.

Conclusions

Environmental cracking continues to be a problem in the petroleum industry and dictates the need for laboratory testing. However, no single test technique appears optimum for all environmental cracking systems. U-bend and statically loaded tension-type SCC tests are sufficient to produce meaningful results for polythionic acid SCC and sour gas cracking of steels. However, more sophisticated SSRT and fracture mechanics methods are being used for sour gas cracking of alloys, chloride-induced SCC, and amine SCC evaluations. In these latter stress-corrosion systems, crack initiation can have poor reproducibility within a limited test duration. Dynamic strain and use of precracked specimens enhance SCC initiation, allowing test results to be obtained within practical time frames.

References

- [1] Ahmed, S., Mehta, M. L., Saraf, S. K., and Saraswat, I. P., *Corrosion*, Vol. 37, No. 7, July 1981, p. 412.
- [2] *Guidelines for Control of Stress-Corrosion Cracking of Nickel-Bearing Stainless Steels, and Nickel-Base Alloys*, MTI Manual No. 1, Materials Technology Institute, Columbus, OH, June 1979, p. 31.
- [3] Ciaraldi, S. W., "Anisotropy of Sulfide Stress Cracking in C-90 Grade Oil Country Tubular Goods," paper presented at the 23rd Mechanical Working and Steel Processing Conference, Iron and Steel Society of AIME, Pittsburgh, PA, October 1981, American Institute of Mining, Metallurgical, and Petroleum Engineers, New York.
- [4] Ciaraldi, S. W., "Application of a Double Cantilever Beam Specimen to the Stress-Corrosion Evaluation of High-Alloy Production Tubulars," paper No. 162 presented at Corrosion/83, NACE, Anaheim, CA, April 1983, National Association of Corrosion Engineers, Houston, TX.
- [5] Abramson, G., Evans, J. T., and Parkins, R. N., "Investigation of Stress Corrosion Crack Growth in Mg Alloys Using J -Integral Estimations," paper presented at Corrosion/84, NACE, Boston, MA, April 1984, National Association of Corrosion Engineers, Houston, TX.

DISCUSSION

DeLuccia: I am fascinated with your last topic of the amines, of not being able to reproduce cracking in the laboratory. Amines are sometimes used as corrosion inhibitors, so that if your mechanism is in fact stress corrosion cracking, you might not see cracking in the laboratory. Are you faithfully reproducing the environment in a laboratory that is causing the cracking in the field?

Ciaraldi: We have obtained amine solutions and water from our Texas City Refinery. Since they are actually from the plant, we know that they cause cracking because we have cracked refinery piping from the same solutions.

DeLuccia: What is the pH of this water?

Ciaraldi: The pH is around 10 or 11, pretty high. Usually we use monoethanolamine and it is usually about a 25% solution of amine to water.

DeLuccia: Could be that down deep the pH is lower and you are getting hydrogen? That is just a guess.

Ciaraldi: That is a possibility, except that there has been some work done in amine cracking. Parkins has evidently done some proprietary work for Exxon, so that information is not available. He apparently was able to get cracking and from what we know about it, it definitely appears to be an anodic type of stress corrosion cracking because you get the temperature effect of increased temperature and more cracking. We have also seen that in one of our gas plants in Egypt where they were operating with DEA, diethanol amine, but at much higher temperatures, 250 to 260°F. They had cracking failures in that case in a period of about six months. We could probably go to higher temperatures and maybe get cracking. We are trying to work below the boiling point so that we can test within a glass vessel.

Section 5: Hydrogen in Welding

Overview: Section 5

Hydrogen in Ferritic Arc Welding

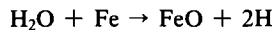
Hydrogen, regardless of the form it takes, is potentially dangerous if introduced in the vicinity of the welding arc. Once a hydrogen-bearing substance enters the energetic milieu of the welding arc it can be converted into monatomic hydrogen (H) which is sufficiently small to pass through the interstices of the iron lattice and therefore be dissolved in the weld pool. Diatomic hydrogen (H₂) cannot be dissolved in the molten weld pool because the hydrogen molecule is too large to pass freely through the matrix structure of steel.

Upon solidification of the weld pool, the once high solubility of hydrogen in iron is drastically reduced. Hydrogen will be rejected at the solid-liquid interface from the supersaturated liquid, which in turn may result in blowholes, porosity, etc. The remainder of the hydrogen will form a supersaturated solid solution with iron. The hydrogen, which is much more soluble in austenite than ferrite, will diffuse rapidly upon further cooling of the solid weld metal. Some diffuses to the air, some into voids and other into the surrounding base material. At some time after the austenite to ferrite transformation, the hydrogen which remains in the weld metal or surrounding material, combined with residual stresses from welding and a susceptible microstructure,¹ can result in cold cracks.

There are several ways to control the resulting microstructures in the weld zone. Preheating and heat input manipulation are the primary means. In either case the objective is to reduce the cooling rate in order to avoid the formation of martensite. By avoiding a martensitic microstructure the chances of cold cracking are greatly reduced.

In recent years, the welding industry has had much success in reducing the number of cracking incidents related to hydrogen with the development of low hydrogen consumables. But still, hydrogen continues to pose a cracking threat due to the hydrogen which is available in so many aspects of welding.

Water is the major contributor of hydrogen during welding. When water vapor is present with molten steel, it is believed that the reaction to form monatomic hydrogen is as follows:



As a result, a potential cracking situation develops. Water may be introduced to the vicinity of the arc as moisture on the weld joint, moisture in the shielding gas, or moisture from the surrounding atmosphere. But by far, the largest contributor of water is the flux or coating related with the flux-assisted processes (SMAW, SAW, FCAW, etc.). The moisture may be combined or held mechanically in a flux or coating. Mechanically held moisture is that which is held in voids either between flux particles or in flux particles. Combined moisture is that which is an inherent part of the crystalline structure. The moisture which is held mechanically is driven off much more easily than the combined moisture. Therefore, the heating of the electrode during welding is sufficient to drive off most of the mechanically held moisture while the combined moisture is much more stable and thus enters the arc, which in turn becomes monatomic hydrogen upon reactions with the weld pool.

¹A susceptible microstructure is generally one which is martensitic. Whether or not the original baseplate is martensitic, it is possible to produce this susceptible martensitic structure in the heat-affected areas of the baseplate as a result of the thermal cycling during welding.

Most of the hydrogen which originates as moisture is associated with the flux assisted processes, but many other factors also contribute to the formation of monatomic hydrogen which are present in all arc welding processes. The base metal and filler metal are likely to contain hydrogen unless vacuum melting techniques were employed during productions. Ferro-alloys which are used in flux coatings also contain measurable amounts of hydrogen. Oil, grease, paint or any substance containing hydrocarbons also present the potential for monatomic hydrogen to be introduced into the weld pool.

Another major contributor to hydrogen which is often overlooked is rust. Rust, which is iron-hydroxide rather than iron-oxide, contains water which is a potential contributor to the hydrogen content of the weld zone. Ordinary preheat temperatures are not sufficient to cause the breakdown of iron-hydroxide into iron-oxide and water. Therefore, the water present in the iron-hydroxide stands a good chance of entering the weld pool and being further reduced to monatomic hydrogen, which in turn poses a cracking threat.

There are many techniques and an abundance of data which evaluate the effects of hydrogen on the cracking susceptibility of steels. There are also many techniques for determining the sources of, and measuring the amount of, hydrogen in a weld. The results vary from technique to technique, but there is good agreement among investigators on the trends of the results.

The following section on hydrogen in ferritic arc welding deals with various test methods for predicting hydrogen levels and hydrogen-embrittled material behavior during ferritic arc welding.

In some cases, authors present data which correlates the amount of potential hydrogen with actual results obtained in specific weldability tests. In other cases, the authors discuss how changing testing conditions can alter the results of a particular test.

Particular attention should be paid to the procedures and variables involved in predicting hydrogen behavior during welding in order to appreciate and understand the validity of the data obtained by any of the various test methods. For it is this understanding which leads to the development of better testing techniques, further comprehension of hydrogen behavior, and ultimately the prevention of hydrogen cracking during welding.

Joseph Blackburn,

David Taylor Naval Ship R & D, Annapolis,
MD; chairman, Section 5.

G rard M. Pressouyre,¹ Veronique Lemoine,²
Daniel J. M. Dubois,³ Jean-Baptiste Leblond,⁴
Patrick R. Saillard,⁵ and Francois M. Faure⁶

In Situ Measurement of Hydrogen in Weld Heat Affected Zones Thru Mass Spectrometry and Computer Analysis

REFERENCE: Pressouyre, G. M., Lemoine, V., Dubois, D. J. M., Leblond, J.-B., Saillard, P. R., and Faure, F. M., "In Situ Measurement of Hydrogen in Weld Heat Affected Zones Thru Mass Spectrometry and Computer Analysis," *Hydrogen Embrittlement: Prevention and Control*, ASTM STP 962, L. Raymond, Ed., American Society for Testing and Materials, Philadelphia, 1988, pp. 219-237.

ABSTRACT: This paper proposes a new mass spectrometry technique to measure hydrogen evolution in the heat affected zone (HAZ) of a welded material *while* welding. Square block specimens are used, with a small-diameter hole drilled parallel to the surface to be overlaid at such a depth that the hole will be seated in the future HAZ. This hole is connected to a mass spectrometer that will detect hydrogen evolution in the HAZ during welding; also recorded are the evolutions of temperature in the HAZ and bead deposit advance. Parallel to such experiments, hydrogen diffusion and solubility characteristics have been determined versus temperature using mass spectrometry on base metal and HAZ microstructures.

Results show that hydrogen evolves in the HAZ during welding with characteristic humps and maxima, which may be attributed to variations in diffusion coefficients with temperature and phase changes in the HAZ. These observations were confirmed by computer modelling. Thus, this technique, together with the numerical simulation, is powerful in qualitatively and/or quantitatively evaluating various welding parameters such as: nature of the welding material, the welding process, preheating, and postheating.

KEY WORDS: hydrogen, low-alloy steel, welding, HAZ, diffusion, mass spectrometer, numerical simulation

Cold cracking, that is, cracking due to hydrogen either in the weld metal or the heat affected zone (HAZ) of a welded material, is a well-known phenomenon that has been of concern to welders for years. This paper deals with HAZ cold cracking.

The mechanism invoked is that of an oversaturation of the HAZ by hydrogen brought in from the weld deposit. This oversaturation is provoked by phase changes of the HAZ and rapid cool-

¹Senior research metallurgist, division head, Center for Materials Research, Creusot-Loire Industrie, 71208 Le Creusot, France.

²Research metallurgist, Center for Materials Research, Creusot-Loire Industrie, 71208 Le Creusot, France.

³Head of Research and Development Section, Centre de Calcul, Division des Fabrications, Framatome, 71380 Saint-Marcel, France.

⁴Scientific advisor, Centre de Calcul, Division des Fabrications, Framatome, 71380 Saint-Marcel, France.

⁵Development engineer, Centre de Calcul, Division des Fabrications, Framatome, 71380 Saint-Marcel, France.

⁶Consulting materials engineer, Materials Dept., Framatome, 92084 Paris La Defense, France.

ing rates during which hydrogen has little time to degas. Thus, hydrogen activity in the HAZ is relieved, among other ways, by trapping on various sites of the HAZ microstructure where cracks may nucleate once a critical trapped hydrogen concentration is reached (see paper by Pressouyre and Faure in this publication). Crack nucleation is even more favored by the fact that the “as-welded” HAZ microstructure is very sensitive to hydrogen embrittlement (HE) and that large transformations and cooling stresses exist. The understanding of this phenomenon requires the knowledge of the hydrogen concentration in the HAZ and its position versus critical concentrations for crack nucleation.

The measure of the quantity of hydrogen brought by a given process into the HAZ has been made so far, to the best of our knowledge, through indirect methods.

For instance, hydrogen may be conventionally analyzed from the deposited metal after welding; it is then common practice to say that the higher this hydrogen content, the more hydrogen that will enter the HAZ. A disadvantage of this method is that the actual HAZ content remains unknown; furthermore, different electrode materials with the same initial hydrogen content do not lead to the same HAZ hydrogen content (because the equilibria between “deposit and HAZ” may be different).

Another method consists of analyzing hydrogen from an extracted specimen of the HAZ after welding is completed [1]. This method also offers disadvantages: (1) hydrogen will be lost while extracting a sample from the HAZ; (2) the motion of hydrogen *during* welding remains unknown.

Among the rare attempts to measure hydrogen evolution in HAZ while welding, Howden [2] used mercury manometers that recorded hydrogen permeating through a flat specimen, the top of which was fused using a weld arc with a varying hydrogen atmosphere. This paper proposes a very accurate method to measure “in situ” the hydrogen flux in the HAZ, namely mass spectrometry. Concomittant diffusion characteristics and computer simulations will also be provided.

Experimental

Material

The base metal for all experiments was a A508 Class 3-type steel with a chemical composition as shown in Table 1. This steel is quenched and tempered.

Welding Procedure

The austenitic stainless steel weld overlay was deposited with shielded metal arc welding using a 309L-type stick electrode (4 mm diameter). Use of such an electrode is typical for first layers welded on ferritic base metal so as to overcome the dilution effect; in the present study the same electrode was kept for all experiments to ensure consistency in the amount of hydrogen in the deposited metal. Prior to welding, the electrodes were first dried according to manufacturer specifications (baking for 1 h at 300°C) and then rehumidified at 20°C in 90% humidity (holding time between 48 and 96 h). Previous studies [12] had shown that this treatment yielded reproducible high hydrogen contents in the welds.

TABLE 1—Chemical composition of A508 Class A steel, 10⁻³ weight %.

C	S	P	Si	Mn	Ni	Cr	Mo
165	10	9	220	1350	710	240	510

Welding parameters were: 30 ± 2 V, 140 ± 10 A, with a travel speed ranging between 0.43 and 0.56 cm/s (that is, nominal values of 30 ± 5 cm/min).

More specific details for each set of experiments are given in Table 2.

Prior to welding, all base metal specimens were thoroughly degassed by heating them at 600°C for several days while connected to the mass spectrometer to ensure that hydrogen fluxes observed during welding were actually brought in by the bead deposit and were not due mainly to residual hydrogen.



Test Specimens and Experimental Setup

For in situ measurement of hydrogen pickup in HAZ while welding, square block specimens such as those in Fig. 1 were used. A small diameter hole was drilled parallel to the surface to be overlaid at such a depth that the hole should be seated in the future HAZ (1.5 to 2 mm depth). This "hydrogen pickup" hole was connected to the mass spectrometer through a stainless tube welded on the block side. Two other holes (1.5 mm in diameter) were drilled on both sides of the "hydrogen pickup" hole, but perpendicular to it; the bottom of these holes was at the same depth as the axis of the "hydrogen pickup" hole. The holes contained a bottom spot welded thermocouple for recording the temperature at that depth as bead deposit progresses (Fig. 1). Bead deposit was made perpendicular to the "hydrogen pickup" hole and went over the thermocouple hole bottoms.

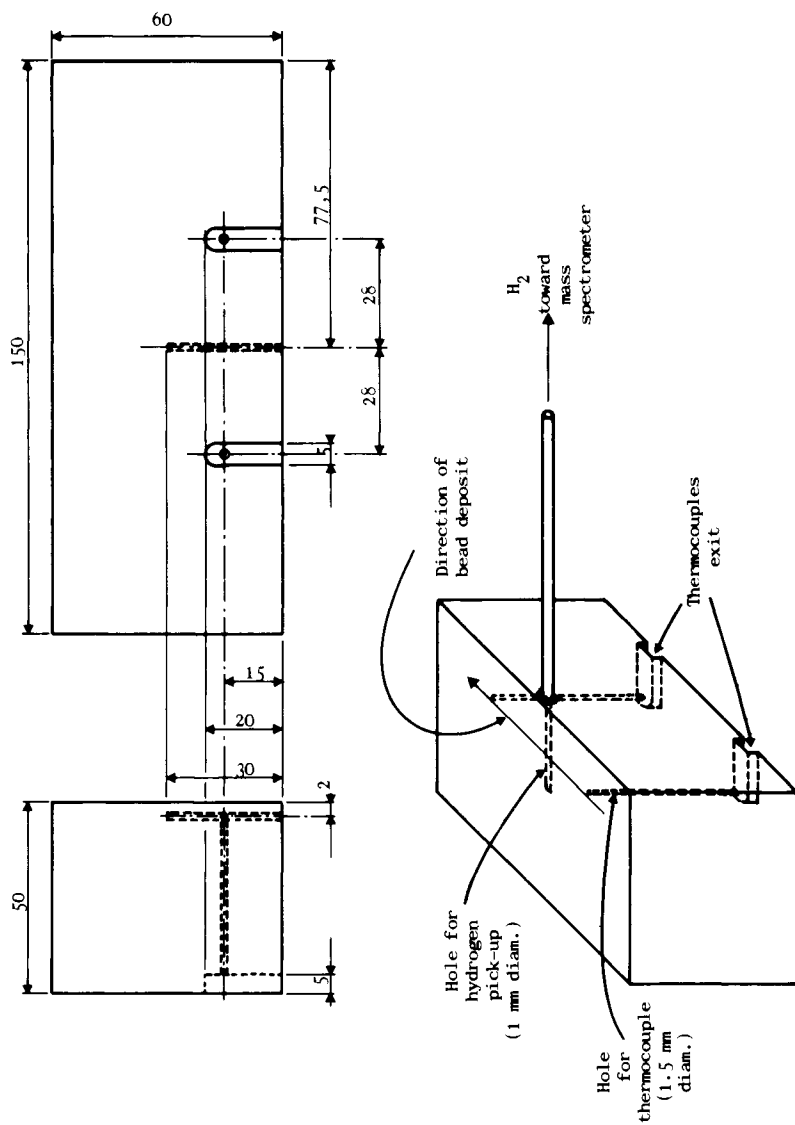
Prior to welding, the "hydrogen pickup" hole and connecting tubes were thoroughly degreased and degassed using the turbomolecular pumping and were then pumped through the mass spectrometer pumping system (diffusion pumps).

The mass spectrometer was a Kenos Analysis spectrometer equipped with a quadrupole probe and a gold ion source; all amplification and detection was centered around hydrogen mass (Mass 1 and 2). The final vacuum in the system was around 10^{-8} millibars. Prior to the start of the experiment, a complete spectrum of possible residual elements in the remaining atmosphere was made to check the quality of the vacuum; also, the spectrometer was calibrated upon a hydrogen standard source [Vacuum Instrument Corp., 3.2×10^{-6} cm³/s of hydrogen gas (H₂) at 20°C] via bypass tubing. When welding proceeded, a multiple entry recorder printed the evolution of the hydrogen flux (that is, through the maxima of hydrogen peaks scanned by the spectrometer), as well as the evolution of temperature from thermocouples, and the advance of bead deposit.

TABLE 2—Welding sequences, thermal conditions, and hydrogen level for each experiment.

Experiment	Preheating	Postheating and Soaking	Hydrogen Level in Deposited Metal, cm ³ /100 g ^a
Single bead	None	None	15 to 19
Two beads side by side	None	None	≈ 17
			
Single bead	175°C	27 h at 175°C + 4 h at 250°C	16 to 18
Two beads side by side + one on top			
			
1st	175°C	Keep at 175°C before 2nd bead	17 to 19
2nd	175°C	20 h at 175°C + 4 h at 250°C	17 to 19
3rd	None	None	≈ 19

^aTechnique used for hydrogen level determination is fully described in Ref 12.



Aside from the welding experiments, the mass spectrometer was also used to compute the diffusion and solubility characteristics of the base material and its HAZ through conventional permeation experiments [11]. The aim of these experiments was to obtain data to be used in the numerical simulation of the welding experiment. For this, a disk-shaped specimen (46 mm diameter exposed to hydrogen, thickness 1 to 5 mm for temperatures $< 400^{\circ}\text{C}$, or 48 mm diameter and 10 mm thickness above 400°C up to 800°C) was placed between two autoclaves, one containing the hydrogen pressure (1 to 2 bars pure H_2), the other being in vacuum and connected to the mass spectrometer. The seal between disks and autoclaves was made by diffusion (aluminum) gaskets below 400°C , and by austenitic stainless electrode filling above 400°C . Thus, hydrogen permeates from the hydrogen autoclave through the disk to the autoclave under vacuum and is detected by the mass spectrometer. Prior to starting a permeation experiment, the superficial oxide layers on the input side of the disk were taken off by several consecutive hydrogen pressurizations of the input side, followed by vacuum extraction at 300°C . Deoxidation was considered completed when the permeating hydrogen flux stayed at a maximum. Then, all permeations at various temperatures could be started (the "hydrogen" autoclave never contained air between permeations). Following each permeation, a calibration of the spectrometer was made using the standard hydrogen source. The complete experimental setup is shown in Fig. 2.

Results

Determination of Diffusion and Permeability Characteristics Versus Temperature

Both base metal and a simulated HAZ of the A508 Class 3 steel of this study have been characterized. The simulated HAZ was obtained by austenitizing disk specimens at 1200°C for 20 s and quenching them in large buckets of water at room temperature (20 to 25°C). This was done before machining the specimens to their final thicknesses. At all temperatures, several permeation and degassing experiments were performed (degassing being obtained by placing the input side in vacuum). At higher temperatures, experiments were conducted for both increasing and decreasing temperatures. Metallurgical structures at a given temperature are not the same when heating up or cooling down from 1200°C and also depend upon heating or cooling rates when working above the steel transformation range (for A508 Class 3, $\text{AC1} \approx 710^{\circ}\text{C}$, and $\text{AC3} \approx 830^{\circ}\text{C}$).

Figures 3 and 4 summarize diffusion and permeability (diffusivity times solubility) data, respectively. The diffusion coefficients given here are computed according to the "time-lag" method (see Ref 4, for instance). Several remarks are in order:

1. Diffusion coefficients from degassing curves are usually higher than those from permeation curves. This is to be related to trapping.
2. The Arrhenius straight line law ($\log D = a/T + b$) breaks down at temperatures below 100°C . This can also be attributed to trapping [more active at temperatures close to room temperature (see, for example, Ref 5)].
3. Diffusion coefficients in the HAZ are lower than in base metal, below 200°C . This also is due to more trapping in the HAZ than in base metal because of finer and more numerous carbides as well as more obstacles to diffusion (for example, interstitial carbon atoms) in the HAZ.
4. A sharp drop in the diffusion coefficient is obviously obtained when structure transforms to austenite (data point at 880°C) or is mixed (ferrite + austenite).
5. Identical remarks are valid for permeability data on Fig. 4 concerning HAZ versus base metal and phase changes. Note that permeability at 880°C was not obtained due to standard source disfunctioning on this permeation.

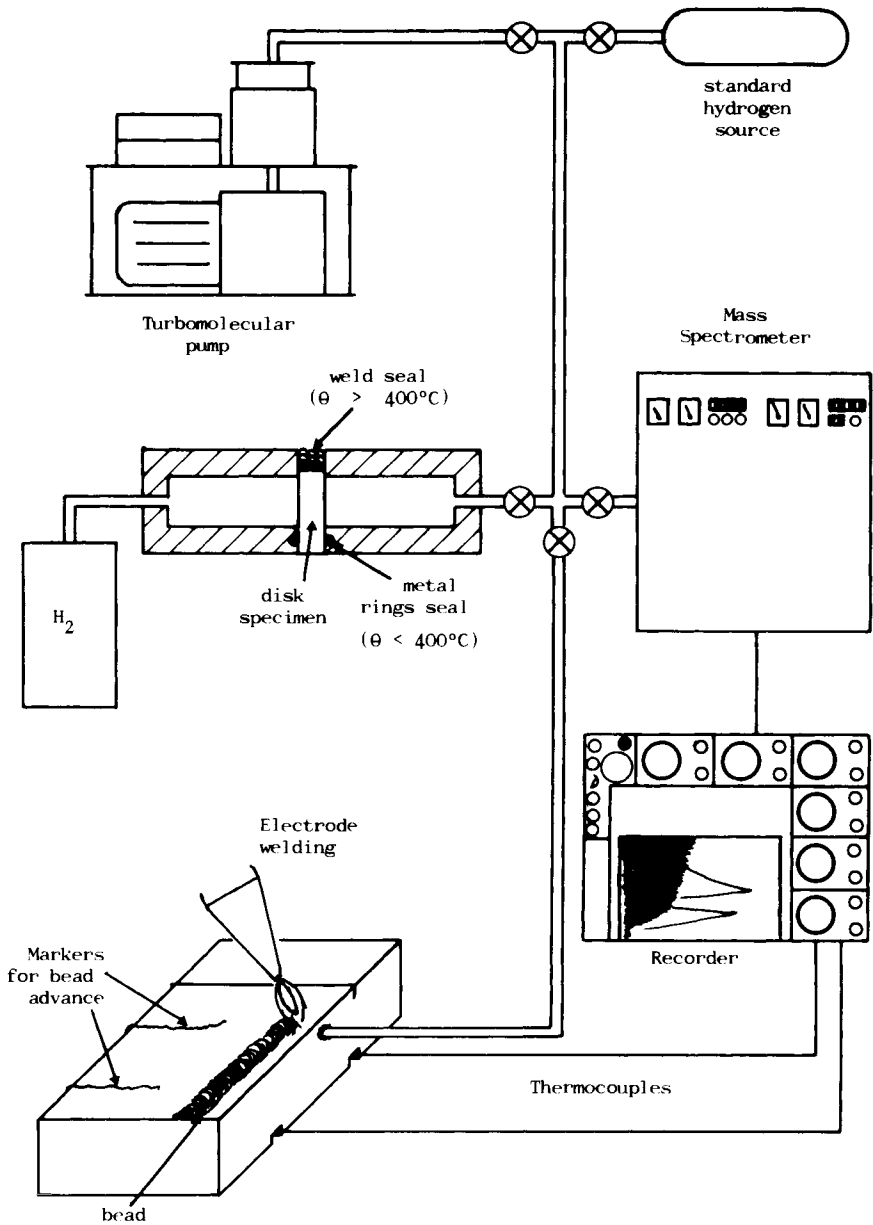
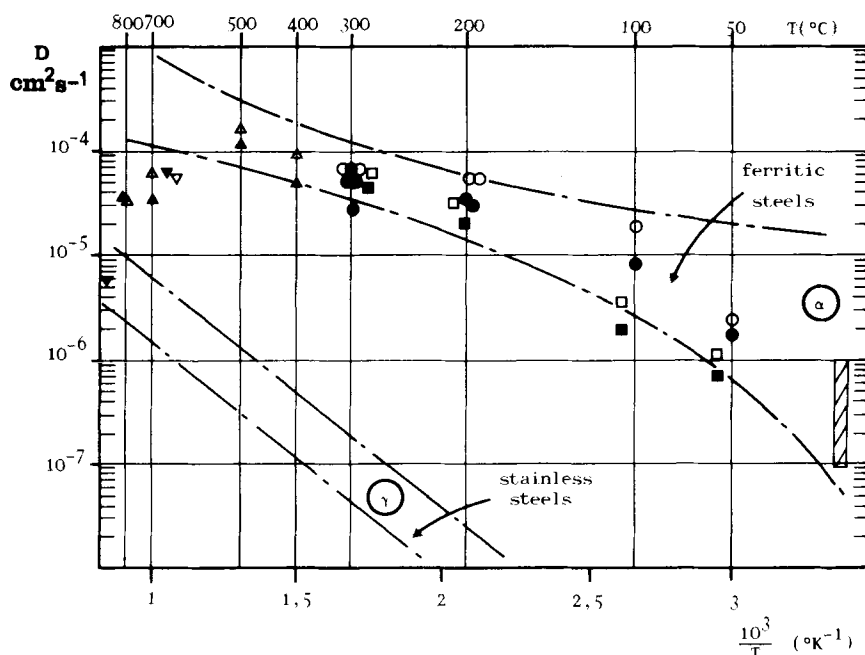


FIG. 2—Schematic of experimental setup.

In Situ Measure of Hydrogen Flux in HAZ While Welding

Several experiments were performed, using one or several beads, without or with preheating and/or postheating. Welding procedures were previously described.

The evolution of hydrogen flux and temperature in the HAZ while welding is shown in Fig. 5 in the case of one bead (stainless A309L), without pre- or postheating, along with the location of holes in the HAZ. Several facts are remarkable:



Permeation	Degassing	Type of Experiment	Metal
■	□	$\theta < 400^{\circ}\text{C}$	HAZ
●	○	$\theta < 400^{\circ}\text{C}$	Base
▲	Δ	$\theta > 400^{\circ}\text{C}$ Decreasing θ	Base
▼	▽	$\theta > 400^{\circ}\text{C}$ Increasing θ	Base

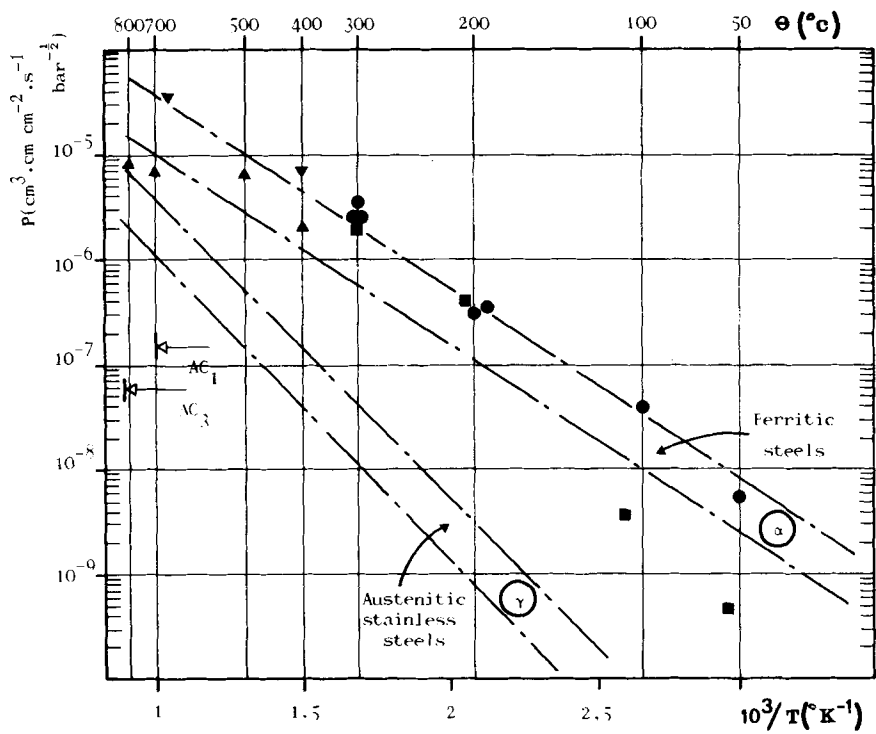
▨ : room temperature diffusivity on base A508 Cl.3 steel obtained from electrochemical permeation.

FIG. 3—Diffusion data using mass spectrometry. Scatter bands are from Ref 3.

1. Arrival of hydrogen in the "pickup" hole is extremely rapid, although the hole is 0.4 to 1.6 mm below the lower part of fused metal.

2. A hump (maximum followed by a minimum) happens at a particular temperature followed by a second flux increase.

3. Maximum temperature recorded by thermocouples is around 720°C ; however, the metallographic cross section (Fig. 6) shows that the bottom of the thermocouple hole is somewhat



Permeation or degassing	Type of Experiment	Metal
■	$\theta < 400^{\circ}\text{C}$	HAZ
●	$\theta < 400^{\circ}\text{C}$	Base
▲	$\theta > 400^{\circ}\text{C}$ Decreasing θ	Base
▼	$\theta > 400^{\circ}\text{C}$ Increasing θ	Base

FIG. 4—Permeability data using mass spectrometry. Scatter bands are from Ref 4.

lower than the hydrogen pickup hole axis (2.6 mm from the lower part of the fused metal). Hence, temperature at the hydrogen pickup hole is higher than recorded by the thermocouples. Nevertheless, the recording of the temperature evolution, as well as the depth of the various holes, will allow the computation of the temperature gradient in the HAZ. From this first gross computation, it seems that: (1) the heating rate is too fast for the $\alpha \rightarrow \gamma$ phase transformation to be noted on the hydrogen flux evolution; (2) the hump appears when the γ -HAZ cools down, while the second flux increase will later on be attributed to and simulated as the $\gamma \rightarrow \alpha$ (bainitic/martensitic) transformation).

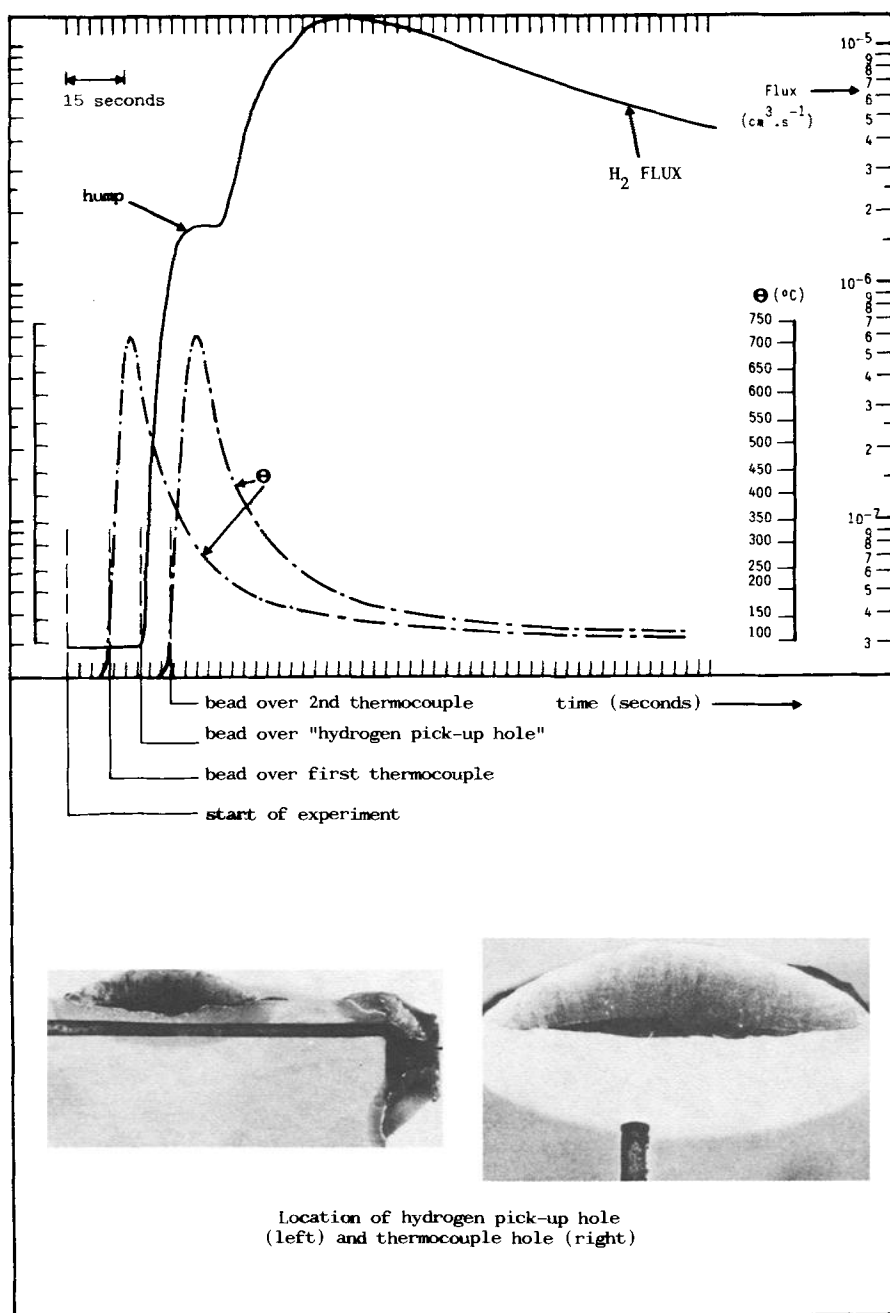


FIG. 5—Evolution of hydrogen and temperature in HAZ during one bead deposit (Stainless A309L). No PPH.

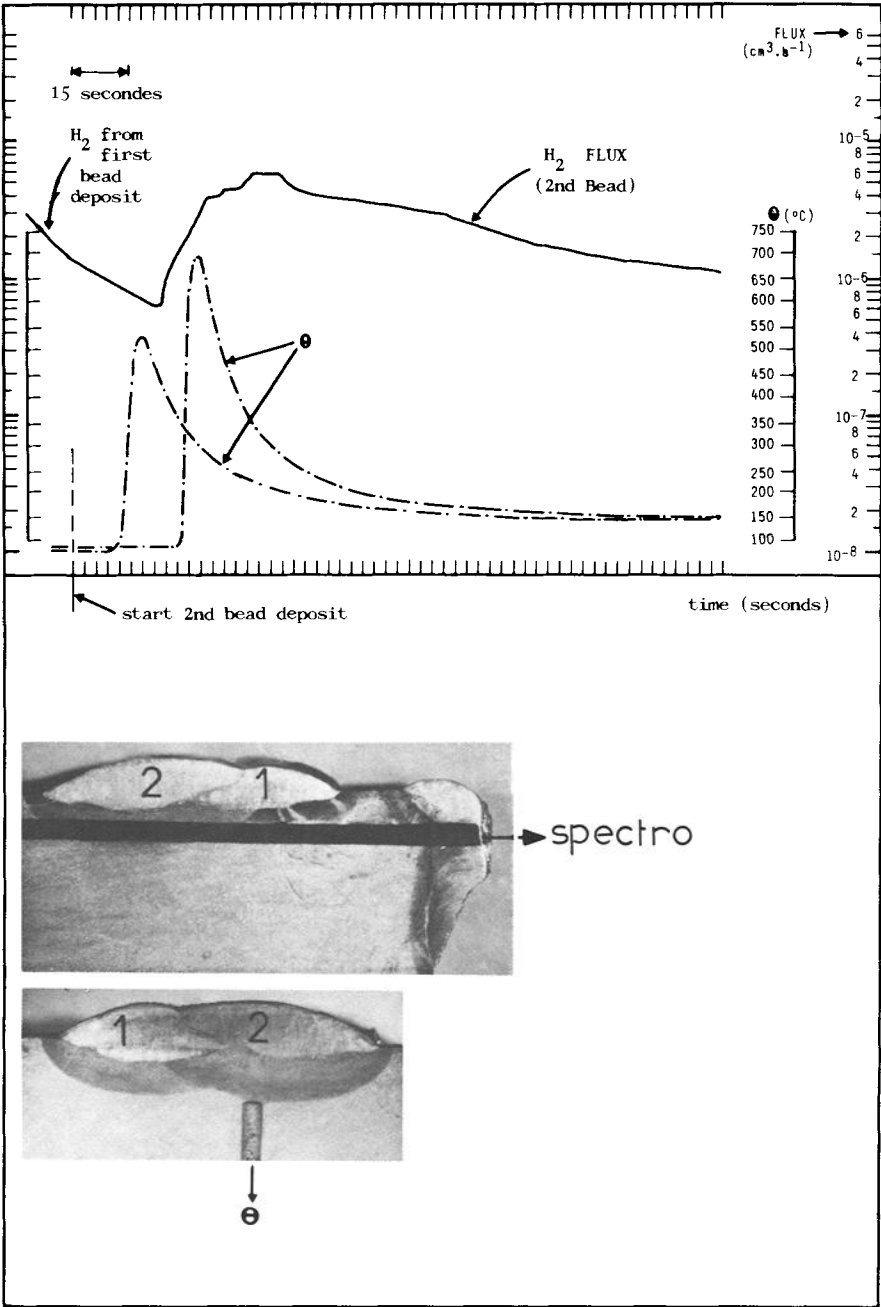


FIG. 6—Evolution of hydrogen and temperature in HAZ during a second bead deposit (Stainless A309L). No PPH.

4. The hydrogen flux quickly reaches a maximum (≈ 1 min), that is, 400 times higher than the "background" hydrogen flux. One hour after welding, the hydrogen flux was around $6.5 \times 10^{-8} \text{ cm}^3/\text{s}$ (not shown on Fig. 5).

The same experiment as just cited has been performed (that is, no pre- or postheating), but with two beads deposited side by side. The results are given in Fig. 6. The evolution of temperature is different from one thermocouple to another. This is due to the fact that one of the thermocouples was welded too far from the hole bottom; nevertheless, knowing its position in the hole makes it possible to get a close estimate of the temperature at the hydrogen pickup hole. Temperatures reached are somewhat lower than for the first experiment, due to the greater depth of the thermocouple holes. This experiment shows that:

1. A hump still exists with the second bead, although not as high as for the first.
2. The maximum hydrogen flux is not as high for the second bead as for the first (same as Fig. 6) since the second bead is deposited partly on top of the first, that is, further from the hydrogen collecting hole.
3. The hydrogen flux decreases after the second bead more slowly than after the first.

The third experiment consisted of a single bead deposited, but with a pre- and postheating (PPH) (preheat for 1 h at 175°C , postheat at 175°C for 27.5 h followed by soaking at 250°C for 4 h). Comparing this result with that of a single bead without PPH leads to the following remarks (Fig. 7):

1. With PPH the hump seems somewhat more marked, although it appears at the same flux height (around $2 \times 10^{-6} \text{ cm}^3 \cdot \text{s}^{-1}$) with or without PPH.
2. The maximum happens at the same value with or without PPH.
3. The effect of postheating is felt essentially after the maximum, that is, when the HAZ degasses. Indeed, degassing lasts for a much longer time when postheating is performed (for example, with no PPH the flux is $6.5 \times 10^{-8} \text{ cm}^3 \cdot \text{s}^{-1}$ after 1 h, and $1.3 \times 10^{-6} \text{ cm}^3/\text{s}^{-1}$ with PPH). This may mean that postheating is effective in "degassing" hydrogen (that is, hydrogen from HAZ degasses outside or into deeper zones of the base metal; the hole here also "pumps" some hydrogen).
4. The effect of the soaking treatment at 250°C is hardly seen since the specimen's relatively small volume had been kept for a number of hours at 175°C . The effect would certainly be quite different on a bulkier industrial component (where typical thicknesses range between 100 and 200 mm) on which many layers are deposited, resulting in more hydrogen buildup and slower degassing.

Note: The change of hydrogen degassing rate observed during postheating at 175°C about 5 h after welding was not explained and might be due to experimental problems in the thermal regulation.

Finally, the fourth experiment consisted in depositing three beads, the first two side by side and the third on top in between, with PPH. Fig. 8 summarizes the results for the first and third beads. The evolution of the hydrogen flux picked up by the hole for the first bead is similar to what was observed before, with the difference that hump and maximum heights are higher. This is due to the hydrogen pickup hole being located much closer to the fused metal (0.2 mm at the closest). The third bead still induces variations of the hydrogen flux in the HAZ, with a lessened hump and a much lower maximum ($4 \times 10^{-7} \text{ cm}^3/\text{s}^{-1}$ as compared to $\approx 3 \times 10^{-5} \text{ cm}^3/\text{s}^{-1}$ for the first bead). This is remarkable, as this bead is now quite far from the hole (2 mm) and is separated from the HAZ by austenitic stainless steel.

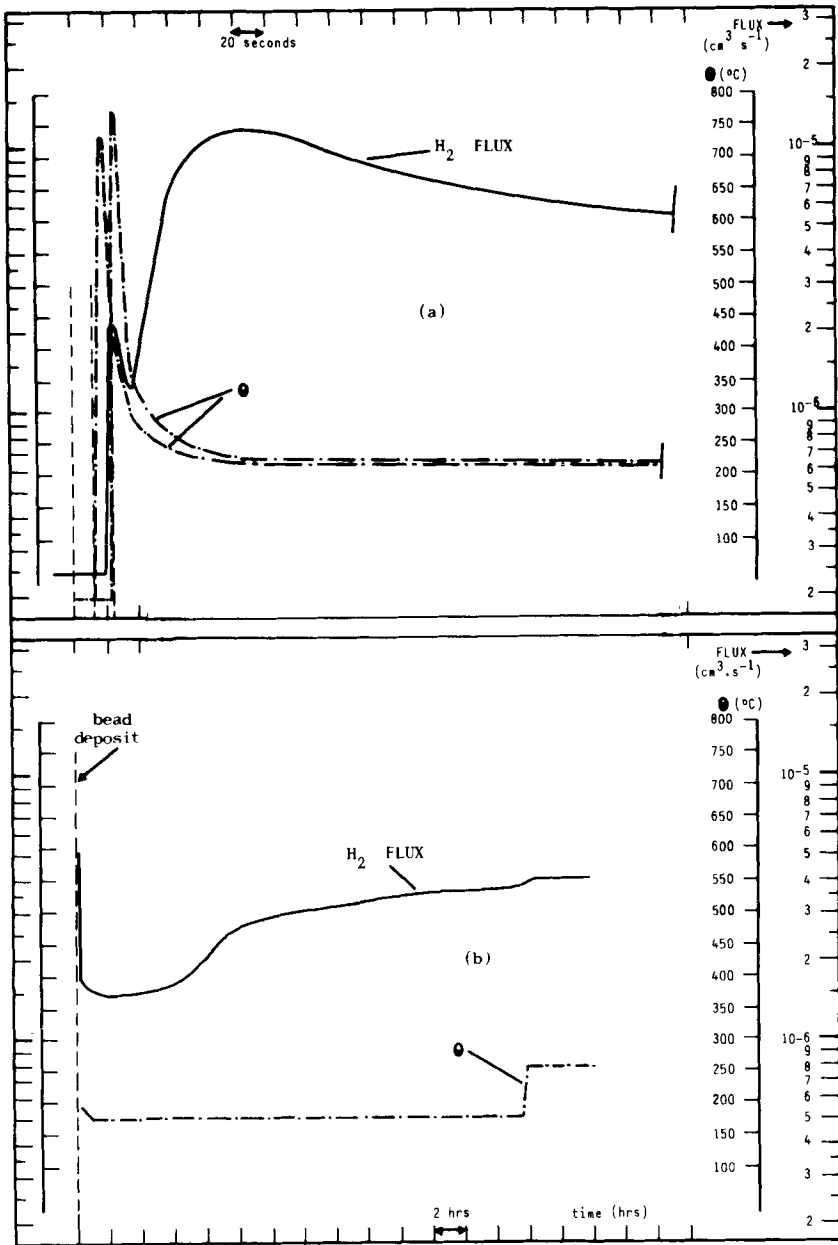


FIG. 7—(a) Hydrogen motion in HAZ during first instants of bead deposit with PPH. (b) Effect of post-heating on hydrogen in HAZ (see text) (Bead A309L).

In fact, these variations do not mean that hydrogen diffuses from the third bead to the HAZ: they arise primarily from the variations of the diffusion coefficient due to the welding thermal cycle and from a new hydrogen transfer from the first and second beads to the HAZ induced by the high temperatures attained.

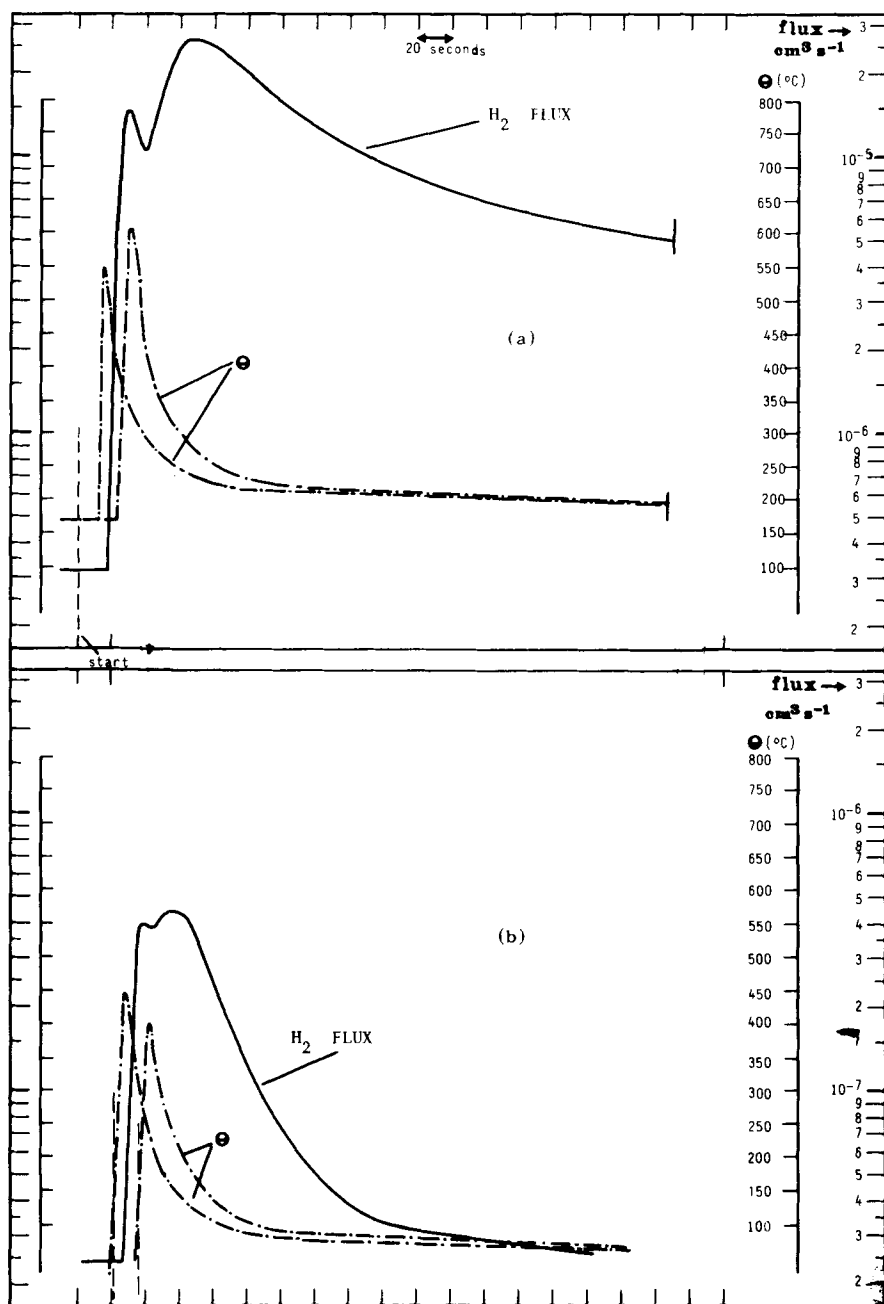


FIG. 8—(a) Evolution of hydrogen in HAZ with first bead deposit (see text, Bead A309L). (b) Evolution of hydrogen in HAZ with third bead deposit on top of first two beads. Both (a) and (b) are with PPH.

Computer Analysis

Background

The objective of the computer analysis is twofold:

1. First, to qualify the numerical simulation of hydrogen diffusion during welding operations (which at the present time is the only way to obtain the concentration as a function of position and time) by comparing experimental and computed fluxes.
2. Second, to quantitatively demonstrate that the second increase of the flux, after the hump, is due to the structural transformation which occurs during cooling, as just outlined.

The hydrogen motions are described by a modified 2nd Fick's law, which has been implemented in a diffusion modulus of the Titus finite-element programme:

$$\partial n / \partial t = \nabla [DS \nabla (n/S)]$$

where

- n = the concentration of mobile hydrogen,
- D = the diffusion coefficient,
- S = the solubility, and
- $P = D \cdot S$ the permeability.

A more complete description of the mathematical model is given in Ref 6.

As P and S are strongly dependent on temperature and metallurgical phases, it is necessary to compute the temperature distribution first, then the metallurgical phases (using a model described in Ref 7) before studying hydrogen motion.

Diffusion Characteristics

The permeability and solubility in the alpha phase of the base metal and in the HAZ have been deduced from the permeation experiments just described and are as follows:

$$P = 6.82 \exp(-4601.6/T) \text{ ppm} \cdot \text{mm}^2 \cdot \text{s}^{-1} \cdot (\text{bar})^{-1/2} \text{ for both materials}$$

$$S = 42.44 \exp(-2613/T) \text{ ppm} \cdot (\text{bar})^{-1/2} \text{ for temperatures} > 100^\circ\text{C}$$

$$S = 0.0723 \exp(-222.4/T) \text{ for temperatures} < 100^\circ\text{C}$$

for the base metal.

$$S = 42.44 \exp(-2613/T) \text{ ppm} \cdot (\text{bar})^{-1/2} \text{ for temperatures} > 200^\circ\text{C}$$

$$S = 0.329 \exp(-372/T) \text{ for temperatures} < 200^\circ\text{C}$$

for the HAZ.

The permeability and solubility in the stainless steel (ss309L) have been taken from Refs 8 and 9 and are as follows

$$P = 7.945 \exp(-7178.4/T) \text{ ppm} \cdot \text{mm}^2 \cdot \text{s}^{-1} \cdot (\text{bar})^{-1/2}$$

$$S = 40.718 \exp(-972.4/T) \text{ ppm} \cdot (\text{bar})^{-1/2}$$

The diffusion coefficient of the γ phase of the A508 Class 3 steel has been measured at one temperature only, and its permeability has not been measured. For this reason, the values used in the present simulation for the γ phase of the A508 Class 3 steel have been deduced from a fitting of the experimental and computed fluxes from the time period when the HAZ is austenitic, starting with those given by Geller and Sun [10] for pure iron (this will be commented upon further). The final values are as follows

$$P = 7.276 \exp(-5740.7/T) \text{ ppm} \cdot \text{mm}^2 \cdot \text{s}^{-1} \cdot (\text{bar})^{-1/2}$$

$$S = 42.7 \exp(-2713.6/T) \text{ ppm} \cdot (\text{bar})^{-1/2}$$

Numerical Simulation

The numerical simulation is concerned with Experiment No. 1 (one layer deposition without preheating).

The 2D mesh used in the calculation is parallel to the welding direction and is plotted in Fig. 9. The weld deposit is modeled by a parallelepipedic element having the same volume as that of the actual deposit. The penetration is equal to the average experimental penetration.

For the thermal simulation, it is imposed that the weld pool stays at liquid metal temperature for a length of time determined from experimental data (welding speed and length of the weld pool).

The computed and measured thermal histories are compared in Fig. 10 for the first thermocouple. The agreement is very good above 300°C. The discrepancy observed for lower temperatures does not affect the analysis since experimental and computed hydrogen fluxes will be compared mainly for higher temperatures.

The numerical simulation of the metallurgical structure yields a martensitic structure all around the hole, which is in complete agreement with hardness measurements.

The computed evolution of the hydrogen flux is plotted in Fig. 11; the flux is obtained by multiplying the 2D-computed flux by the width of the weld, assuming therefore that the hydrogen flux is independent of the z coordinate over a distance equal to the weld width. The evolution of the hydrogen flux is easily explained as follows:

1. Flux onset as the deposit reaches the region above the hole.
2. Hump decrease resulting from a decrease in the diffusion coefficient (due to the temperature decrease).
3. Steep flux increase due to the increase in the diffusion coefficient resulting from the gamma-alpha transformation (notice that the flux increase does not mean that the concentration gradient changes but that it reflects the variation in the diffusion coefficients only).
4. Final decline due to both decreasing diffusion coefficients (decreasing temperatures) and decreasing concentrations.

Preliminary calculations were performed using for the gamma phase of the base metal data measured by Geller and Sun [10] for pure iron. The experimental hump could not be obtained; in fact, the flux decreased rapidly during this period of time due to a diffusion coefficient depending too much on temperature. The initial value of the activation energy (9946 cal/mole) had to be replaced by 6025 cal/mole to reproduce the hump.

The numerical values of the flux on the hump and at the maximum are of the same magnitude as those actually measured. The difference of about 30% in fluxes is not surprising. The flux is proportional to the diffusion coefficient whose values are measured with a greater uncertainty.

The time-shift observed for the maximum flux indicates that the computed martensitic transformation does not occur exactly at the same time as in the experiment (since the second in-

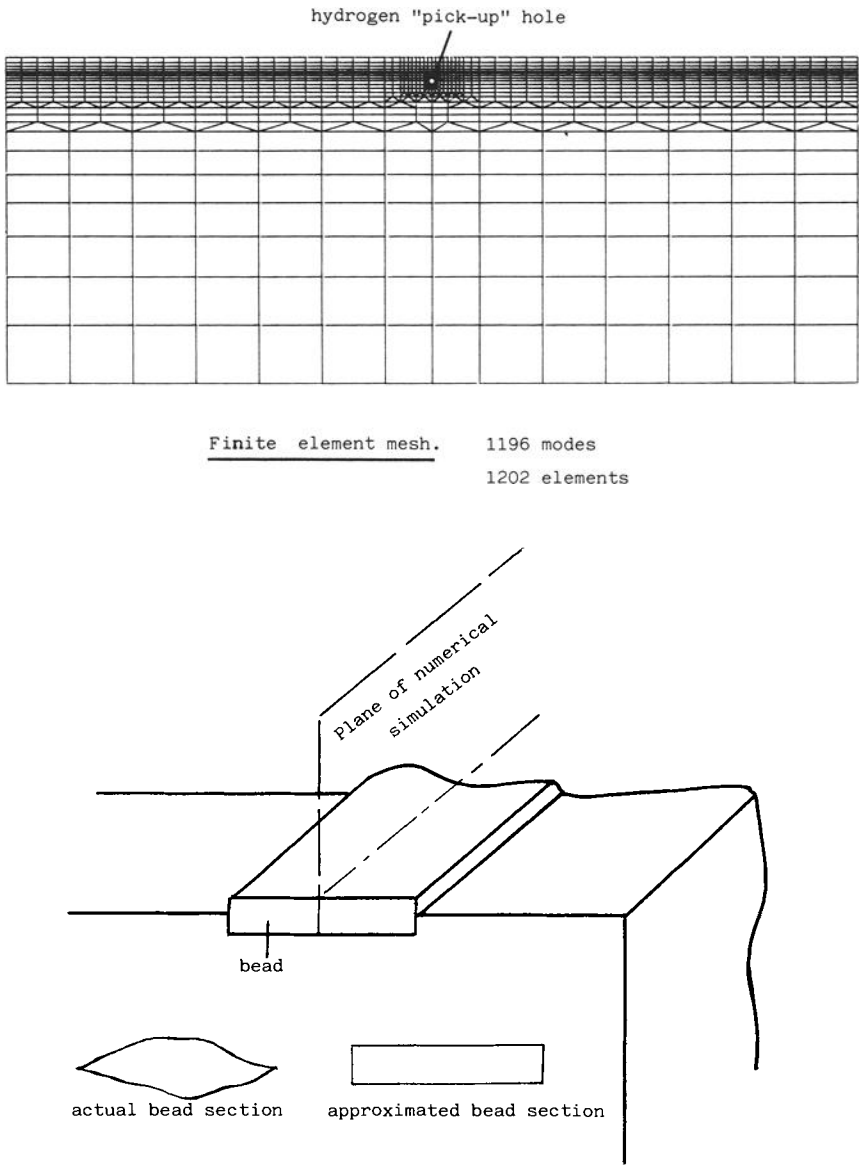
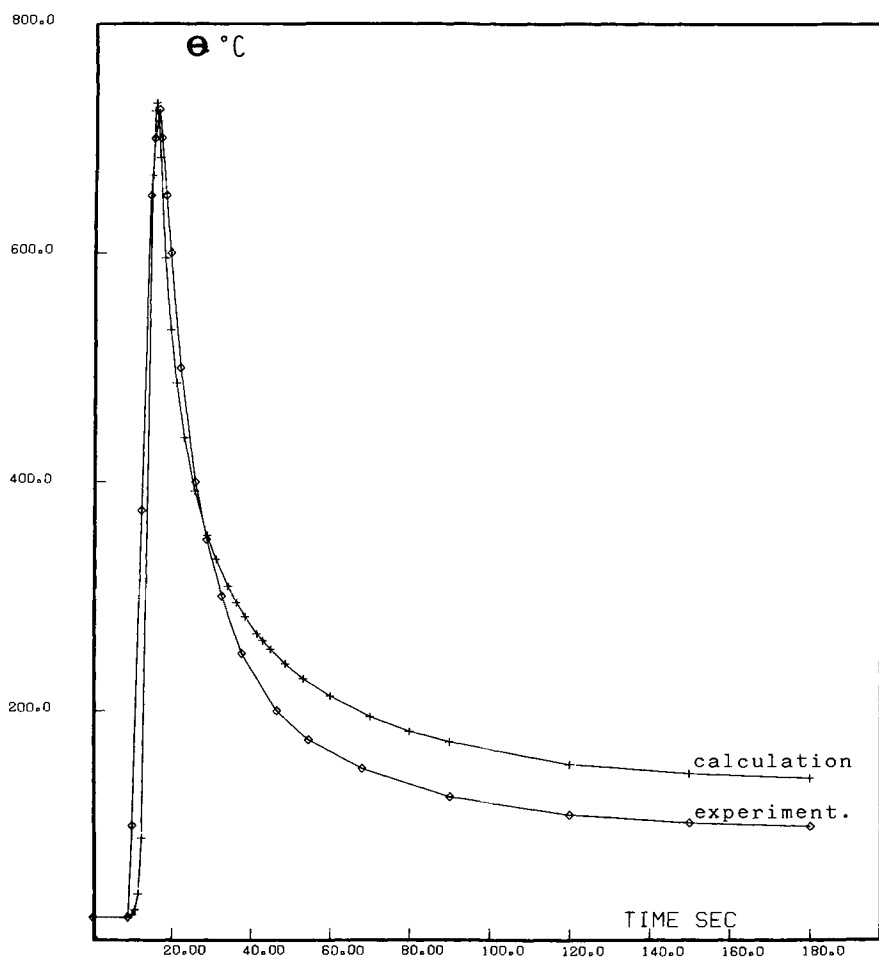


FIG. 9—2D Mesh for numerical simulation in the case of one bead deposit.

crease of the flux coincides with the occurrence of this transformation) and consequently that the computed temperatures are not quite precise. Since the thermal calculation has been adjusted by comparison with thermocouple measurements, a possible explanation would be that the actual position of the thermocouple does not coincide exactly with the one assumed in the numerical simulation. A 0.5-mm depth-shift can induce a 200°C error in the numerical simulation and result in a 20-s time-shift for the beginning of the martensitic transformation and therefore in the second increase of the flux. This discrepancy is also certainly influenced by the



DEPTH 3.4 MM

FIG. 10—Computed and measured temperatures at Thermocouple No. 1.

averaging effect of the 2D model in which the weld pool is schematized by a parallelepiped (uniform width and depth).

Conclusions

This paper presents a new mass spectrometry technique that allows one to measure the evolution of hydrogen in the HAZ of a material *during welding*. Thus, the hydrogen flux is seen to evolve with humps and maxima that correspond to variations in diffusion coefficients and concentration gradients with temperature and phase changes:

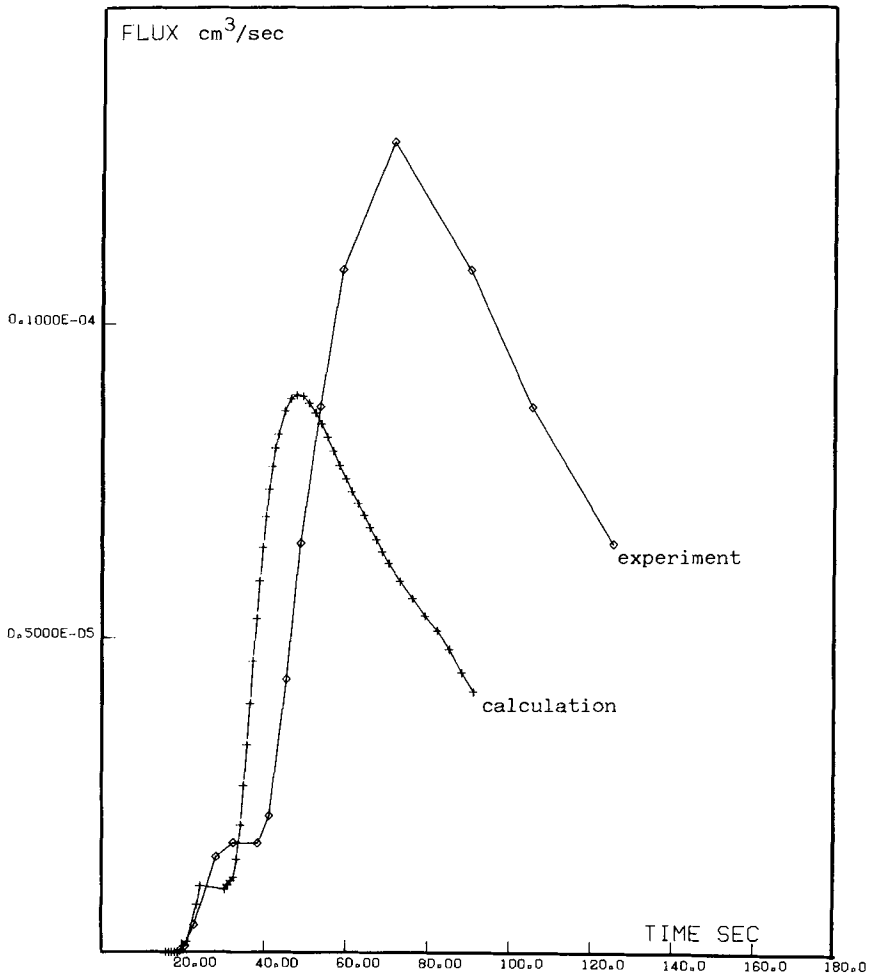


FIG. 11—Computed and measured hydrogen fluxes.

1. The hydrogen flux first increases while hydrogen is coming in from the bead deposit to the γ -phase HAZ.
2. The flux then decreases due to a decrease in the diffusion coefficient with decreasing temperature of the γ -phase HAZ.
3. The flux rapidly increases again with the sharp increase in the diffusion coefficient when the γ -phase HAZ transforms to α -phase.
4. The flux decreases again after having reached a maximum, as temperature continues to fall (that is, when diffusion coefficients and concentration gradients keep decreasing).
5. Quantitatively it has been shown possible to computer simulate such evolutions by using permeation and diffusion characteristics evaluated through mass spectrometry permeation experiments on disk-shaped specimens. Thus, one may know at any time during welding the hydrogen concentrations in HAZ and compare it to critical values for crack initiation (for instance, see Ref 11).

6. Qualitatively this technique is powerful in understanding the mechanism of cold cracking and therefore in optimizing methods used for its prevention.

Acknowledgments

Part of this work was sponsored by the French Ministry of Research and Technology under Contract MAT-P-113/81 P.0714.

References

- [1] Kasatkin, B. S. et al., *Awt Swarka*, Vol. 12, 1973, p. 63.
- [2] Howden, D. G., *Welding Research Supplement*, Vol. 103, 1982, p. 108 S.
- [3] Tison, P. et al., *2nd International Congress on Hydrogen in Metals*, Communication 14A, Ecole Centrale, Paris, 1977.
- [4] Crank, J., *Mathematics of Diffusion*, Clarendon Press, Oxford, England, 1956.
- [5] Pressouyre, G. M., *Metallurgical Transactions*, Vol. 10A, 1979, p. 1571, and Vol. 14A, 1983, p. 2189.
- [6] Leblond, J. B. and Dubois D., *Acta Metallurgica*, Vol. 31, No. 10, 1983, p. 1459-1478.
- [7] Leblond, J. B. and Devaux, J., *Acta Metallurgica*, Vol. 32, No. 1, 1984, p. 137.
- [8] Sakai, T. et al., in *Proceedings of First International Conference on Current Solutions to Hydrogen Problems in Steels*, C. G. Interrante and G. M. Pressouyre, Eds., American Society for Metals, Metals Park, OH, 1982, p. 340.
- [9] Kinoshita, K. et al., in *Proceedings of First International Conference on Current Solutions to Hydrogen Problems in Steels*, C. G. Interrante and G. M. Pressouyre, Eds., American Society for Metals, Metals Park, OH, 1982, p. 369.
- [10] Geller, W. and Sun, T. H., *Archiv für Eisenhüttenwesen*, Vol. 21, 1950, p. 423.
- [11] Pressouyre, G. M. and Faure, F., this publication.
- [12] Faure, F. et al., *First International Conference on Current Solutions to Hydrogen Problems in Steels*, C. G. Interrante and G. M. Pressouyre, Eds., Washington, DC, American Society for Metals, Metals Park, OH, 1982.

Testing of Welding Electrodes for Diffusible Hydrogen and Coating Moisture

REFERENCE: Siewert, T. A., "Testing of Welding Electrodes for Diffusible Hydrogen and Coating Moisture," *Hydrogen Embrittlement: Prevention and Control*, ASTM STP 962, L. Raymond, Ed., American Society for Testing and Materials, Philadelphia, 1988, pp. 238-246.

ABSTRACT: For the last 35 years the American welding industry has placed limits on electrode coating moisture to control the hydrogen content of shielded metal arc (SMA) welds in order to minimize weld cracking in steels. Within the past several years, however, various tests have been proposed or developed for the direct measurement of diffusible hydrogen in welds. This report compares many of these tests with each other and with the coating moisture test.

The methods of measuring diffusible hydrogen that were compared were the International Institute of Welding (IIW) test (collection over mercury), the American Bureau of Shipping test (collection over glycerin), collection over silicone oil, a gas chromatographic technique, and several variations of the above. The gas chromatographic technique produced results that agreed within 15% with the IIW method, while the other test methods produced results that were often 50% smaller than the IIW value. The lower values were attributed to solubility of hydrogen in the collection media. It was therefore concluded that these two methods also produced the most reliable measure of the diffusible hydrogen content. The coating moisture was measured in the electrodes used and had a poor correlation with the diffusible hydrogen content.

KEY WORDS: coating moisture, diffusible hydrogen, gas chromatograph, glycerin, hydrogen, mercury, shielded metal arc welding, welding electrodes

For the past 35 years, the American welding industry has placed limits on shielded metal arc (SMA) electrode coating moisture to control the risk of cracking due to diffusible hydrogen in steel weldments [1]. Diffusible hydrogen is that portion of hydrogen not locked in traps within the weld metal and which is, therefore, free to migrate within the metal lattice. After welding, it tends to collect in lattice defects and cause cracking in susceptible materials, particularly in the heat-affected zone (HAZ) of steel welds. The procedures and criteria for moisture measurement have remained virtually unchanged [2]. However, this test was recently found to have deficiencies for certain applications:

1. The test was specifically designed for SMA electrodes. If modified for use with other welding processes, the results cannot be meaningfully compared.
2. Coating moisture is only an indirect measure of the diffusible hydrogen level that will be produced in the weld, which is the actual cause of hydrogen cracking. For accurate prediction of the cracking tendency in welds containing hydrogen near the critical cracking level, a direct measurement of the diffusible hydrogen content is necessary. However, for electrodes that produce welds with diffusible hydrogen levels that are far below the critical level, coating moisture might continue to be an acceptable screening test.

¹Metallurgist, National Bureau of Standards, Fracture and Deformation Division, Boulder, CO 80303.

3. The accuracy of the coating moisture test is questionable. The uncertainty in the measurement may not be evident when the moisture is controlled near the 0.4% coating moisture level but may be very important if the moisture must be controlled below the 0.10% coating moisture level [3]. Since the coating moisture content at which hydrogen cracking occurs generally decreases with the weld strength, application of this test to high-strength steel welds is of questionable reliability in protecting the welds from hydrogen cracking. For this reason, recent Navy specifications for the high-strength grades HY-80 and HY-100 require a direct measure of the diffusible hydrogen level in the weld [4].

These three deficiencies have stimulated the search for a direct test for diffusible hydrogen, especially at low concentrations. This report compares various candidate diffusible hydrogen test methods.

This work extended over a period of several years, during which many different methods were evaluated and compared with either the American Bureau of Shipping (ABS) glycerin test or the International Institute of Welding (IIW) test. The IIW test, which involves collection over mercury, is believed to produce the most accurate results, although the use of mercury has restricted its wide acceptance. The ABS test was chosen initially as the standard against which these other tests were compared. As its inaccuracies became obvious, the IIW test replaced it as the standard. As a result, some methods and modifications were not directly compared with both tests. Thus, the results are discussed in two sets: ABS versus others, and IIW versus others.

Procedure

Test Materials

The welding electrodes used in these tests all had low-hydrogen coatings (AWS Type XX18) and were primarily Type 7018. They were obtained from various manufacturers. Some tests were performed with electrodes that were produced in 1978 and which did not have "moisture-resistant" coatings which are now widely available on low-hydrogen electrodes. Two techniques were used to obtain a range of coating moisture contents for this study: rehydration of the electrodes in a humidity cabinet, and heating high-moisture newly manufactured (unbaked) electrodes to temperatures lower than those experienced in a production bake cycle. Each set of coating moisture and diffusible hydrogen tests was welded with a single lot of electrodes so the measured values could be compared with each other.

The diffusible hydrogen specimens were machined from ASTM Specification for Structural Steel (A 36/A 36M-84a), a nonrimming-quality mild steel plate with a carbon content below 0.26%.

Coating Moisture Test

Detailed descriptions of the procedures for collecting and measuring SMA electrode coating specimens for moisture determination have been reported elsewhere [3]. The key steps are removal of the electrode coating without contamination (skin oil, dirt, or moisture) and rapid transfer to a hermetically sealed container until analysis. The analysis consists of collecting, in a perchlorate drying tube, the moisture evolved when a weighed specimen is placed in a 982°C (1800°F) dry-oxygen-purged oven. The weight of the expelled moisture is used to calculate the weight percent moisture in the specimen.

Diffusible Hydrogen Specimen Preparation

Two types of specimens and the following orientations were used: the IIW specimen, which was 10 mm thick by 15 mm wide by 7.5 mm long, and the ABS specimen, which was 12 mm

thick by 25 mm wide by 125 mm long. The IIW specimens were welded four at a time with the bead on the face, which is 15 mm wide, and with the weld in the 7.5-mm direction [5]. Run-on and run-off tabs were used to eliminate the effects of the arc start and stop regions. The ABS specimens were welded with the bead on the face, which is 25 mm wide, and with the weld in the 125-mm direction [6]. Most were welded without run-on or run-off tabs. Four specimens were welded sequentially so all diffusible hydrogen results could be compared as the average of four determinations on individual hydrogen specimens. In certain tests, 6-mm-thick ABS specimens were used instead of the 12-mm-thick specimens.

All diffusible hydrogen tests included the welding of a single SMA stringer bead centered on the width of the specimen using 4 mm-(5/32-in.)-diameter electrodes at 185 A [7]. They were welded using the same power supply and welder to minimize variations in arc length and arc voltage. The travel speed was kept near 0.25 cm/s (6 in./min) to control the weld-to-test piece weight ratio, the amount of electrode used, the dilution by the test piece, and the time to complete the weld. Within 5 s of the completion of welding, the specimens were quenched in ice water. Within 60 s, the specimens were cleaned of slag and dried. The welded specimens were then placed in the test containers (specified for each method) for the collection of the hydrogen. If a container was not available, the specimen was stored in liquid nitrogen for up to eight days.

After the hydrogen had diffused from the specimens and had been measured, the specimens were removed and weighed to find the weight of the deposited weld. This weight was used to determine the diffusible hydrogen content in units of mL of hydrogen per 100 g of deposited metal.

Diffusible Hydrogen Tests

Six types of diffusible hydrogen tests were used:

1. *IIW Test* [6]. This test method, where the specimens are submerged for 72 h in mercury at room temperature during the hydrogen evolution, is widely used in Europe. The data included in this report were obtained from 7.5 by 10 by 15-mm specimens. A simplified version of this test has recently been proposed [8].

2. *ABS Test* [5,9,10]. This method, commonly used by ship classification societies, uses the 12 by 25 by 125-mm specimen, which is submerged for 48 h in glycerin at 45°C during the hydrogen evolution. A 6-mm-thick ABS specimen and the IIW specimen were also evaluated with this technique. These modified tests are identified as glycerin tests since they no longer follow the ABS requirements.

3. *Teapot Test* [11]. This method, developed in Japan, uses the ABS specimen, which is submerged for 72 h in glycerin at 45°C. The specimen is enclosed in a glass container with a manometer to measure the volume expansion due to dissolution of hydrogen gas in the glycerin.

4. *Silicone Oil Test* [12]. This method, which uses silicone oil instead of glycerin as the working fluid and gas seal, was originally proposed for use with the IIW specimen but was used with the ABS specimen in this report. The hydrogen was measured after 48 h at 45°C.

5. *Gas Chromatograph Test* [13]. This method, gaining in favor since it is an automated technique, involves collection of hydrogen in a sealed cannister. At the end of 48 h at 45°C, the cannister atmosphere is sent through a gas chromatograph for quantitative measurement.

Results and Discussion

Coating Moisture Versus Hydrogen

Coating moisture tests were performed concurrently with certain ABS and IIW diffusible hydrogen tests. The results are listed in Table 1 and plotted as coating moisture versus diffusible hydrogen in Fig. 1. The ABS test data exhibit a fairly linear trend with coating moisture, up to

TABLE 1—Results of concurrent coating moisture and diffusible hydrogen tests on various SMA electrodes.

Coating Moisture, %	Diffusible Hydrogen, mL/100 g		Exposed to Humidity (X)
	ABS	IIW	
0.08	1.3
0.09	1.9	5.5	...
0.12	4
0.13	1
0.13	4
0.14	2.7	6.9	...
0.15	3.6	6.8	...
0.15	2.5	6	X
0.15	2.2	...	X
0.17	4
0.18	4
0.19	3.3	9.2	...
0.19	3.2	...	X
0.21	4
0.22	3.8	8.9	...
0.24	6
0.28	4.3	...	X
0.29	6
0.47	10	20	...
0.48	9.5	...	X
0.74	12	18	...

about 0.5% moisture. A single value at 0.75% moisture indicates that further increases in coating moisture may have a smaller effect on the diffusible hydrogen. This is expected since the strongest bonding sites in the coating would accept the coating moisture first. Subsequent absorption of moisture would go to lower energy sites. These lower energy sites would also lose their moisture more easily as the electrode becomes hot during welding. Moisture lost due to heating of the coating above the arc region would not add to the weld hydrogen, producing the observed trend.

The IIW test data also exhibit a fairly linear trend up to 0.5% coating moisture. However, the slope of the line is less. This indicates a higher hydrogen level for the various coating moisture contents than measured by the ABS test.

Figure 1 includes electrodes with various as-manufactured coating moisture levels and electrodes that have been rehydrated through exposure to a humid environment (typically 80% relative humidity and 27°C) for up to 24 h. These two forms of coating moisture are thought to have differing effects on the hydrogen level [14, 15]. The as-manufactured coating moisture is thought to be tightly bound within the coating matrix. As such, it is released as the coating decomposes at the arc, and dissociated hydrogen is dissolved in the weld deposit. The rehydrated coating moisture is much more weakly bound, and much of the moisture is released as the coating is heated by the current flowing through the electrode core wire. Thus, much of this moisture is lost before the arc region and does not enter the molten weld metal.

However, this study found that the hydrogen levels are substantially the same for as-manufactured and rehydrated coating moisture. This effect is attributed to the use of electrodes that were not moisture resistant, that is, the tests were conducted before "moisture-resistant" electrodes were generally available. These older generation electrodes absorbed the moisture more readily and apparently were able to bind the moisture until the coating was decomposed by the

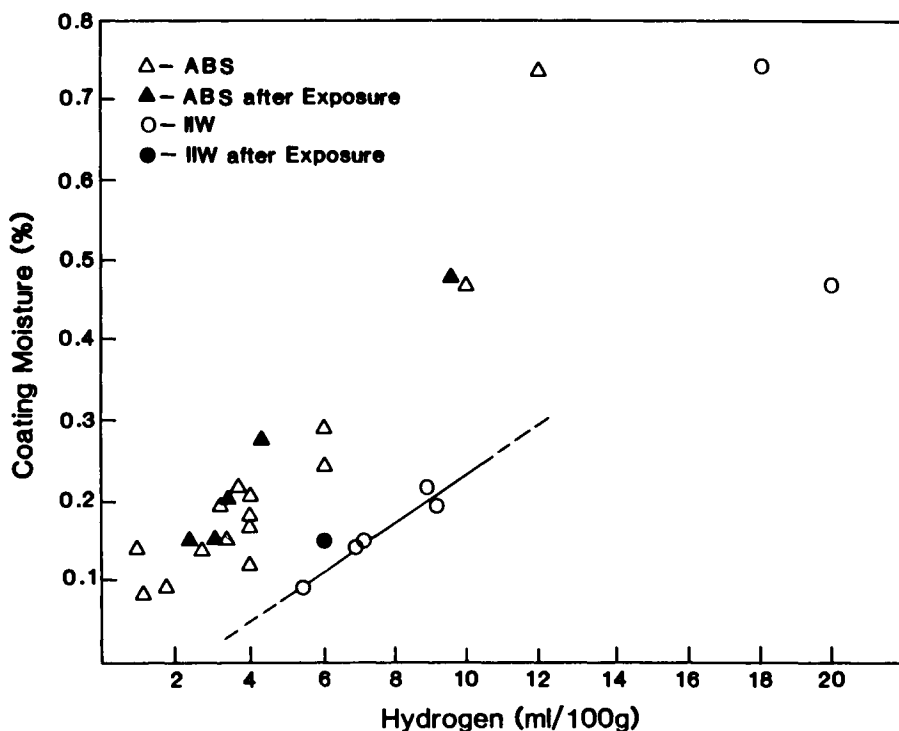


FIG. 1—Coating moisture versus ABS and IIW diffusible hydrogen.

arc. The coating moisture test is, therefore, a poor method to control the deposit hydrogen when there is no specific information on the electrode moisture retention characteristics.

Hydrogen Test Methods

Early in this study, the ABS test was thought to be the best candidate test method and many of the other test methods and test modifications were compared with it in the concurrent tests. Figure 2 is a plot of the hydrogen results (averages of four specimens) using the ABS test method versus the others. A one-to-one correlation line is included. Table 2 contains the same information in tabular form.

The method described as glycerin-IIW specimen was simply the ABS test method with the IIW size specimens and the bath saturated with hydrogen. Saturating the bath with hydrogen by the use of an aquarium diffuser was expected to eliminate loss of hydrogen by dissolution into the glycerin. One test result falls on the correlation line while the other lies above it, near the values of the original IIW test method. The smaller specimen size allows more complete evolution of hydrogen because of a shorter diffusion path to the surfaces and a reduced likelihood of being trapped in an internal defect. However, the much smaller specimen size used with this modified test method may cause increased scatter in the results due to (1) some hydrogen dissolving in the large volume of glycerin and (2) a small weld weight, resulting in a small volume of evolved hydrogen which is difficult to measure.

The method described as glycerin-thin specimen was the standard ABS procedure with a 6-mm-thick specimen. The single result on the figure seems very promising, but because of the

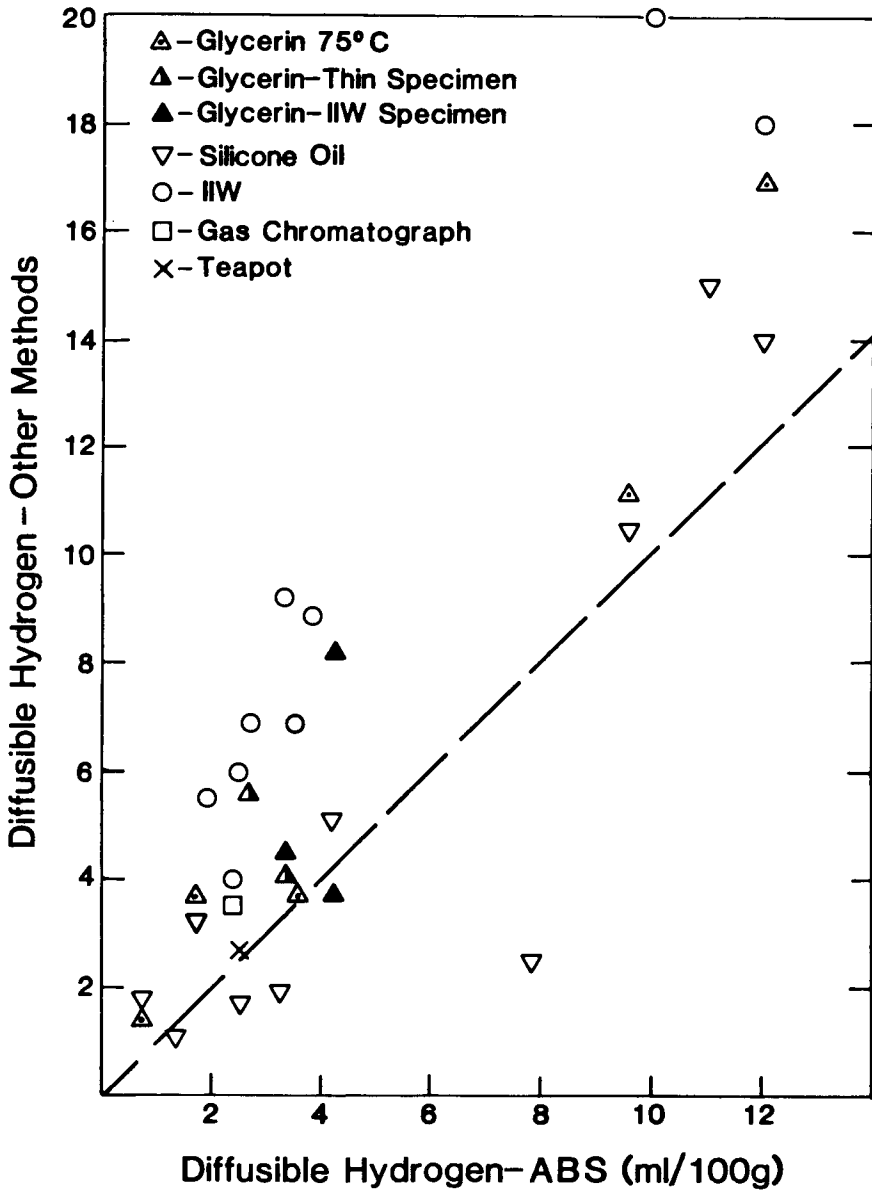


FIG. 2—Diffusible hydrogen—ABS versus other methods.

possibility of hydrogen dissolution, as seen with the other methods using glycerin, no further tests were conducted.

The teapot method incorporated a manometer to measure the glycerin volume expansion due to dissolution. The result with this method lies on the line, indicating that the volume expansion of the glycerin due to hydrogen dissolution had no effect on the calculated diffusible hydrogen value.

TABLE 2—Diffusible deposit hydrogen levels determined by various techniques (mL/100 g).

ABS Test	Glycerin Test, but 75°C	Glycerin, Thin ^a	Glycerin, IIW ^b	Teapot	Silicone Oil	IIW	GC
...	3.5	4
...	8.2	7.6
0.7	1.4	1.8
1.3	1.2
1.9	3.7	3.2	5.5	...
2.4	4	3.6
2.5	2.8	1.7	6	...
2.7	5.6	6.9	...
3.2	1.9
3.3	4.5	9.2	...
3.7	4	6.8	...
3.8	3.7	8.9	...
4.2	8.2
4.2	...	3.7	5.1
7.8	2.5
9.0	9.4	9.8
9.6	11.2	10.5
10	20	...
11	15
12	17	14	18	...

^aABS Test, but 6-mm (0.25-in.)-thick specimen.

^bABS Test, but IIW-size specimen.

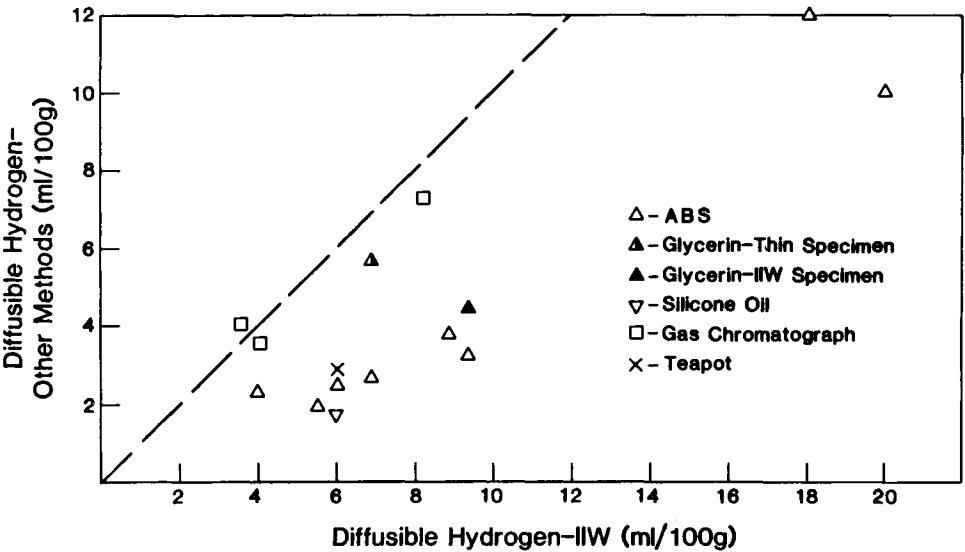


FIG. 3—Diffusible hydrogen—IIW versus other methods.

Some of the silicone oil method determinations are the only values below the one-to-one correlation line. The rest of the silicone oil results lie along the one-to-one correlation line together with the various modifications of the ABS test method.

The tests performed with the IIW method and the single result with the gas chromatography (GC) method are consistently higher than the one-to-one correlation line, indicating a larger value for the diffusible hydrogen content. Figure 3 compares all test methods against the IIW test method. Once again a one-to-one correlation line has been drawn to facilitate the comparison of the methods. This format again confirms that the ABS test method (including modifications) and the silicone oil test method produce values below those of the IIW test method. The lower values indicate that these other methods are not measuring all the hydrogen that is released by the welded specimens. Glycerin has a significant solubility for various gases [16], and it is evident in this figure that modifications (measuring the glycerin volume expansion due to this dissolution, changing the specimen size, or saturating the glycerin with hydrogen before the test) are unable to correct for this solubility. The silicone oil is subject to the same problem. This figure also contains more values for the gas chromatography method. The values are evenly distributed along the one-to-one correlation line, indicating equivalence for these two methods. The choice between the IIW and gas chromatograph methods will be based on the regulatory restrictions on mercury or the cost of a gas chromatograph.

Conclusions

1. Measurements of diffusible hydrogen by gas chromatography and by collection over mercury (IIW method) agreed within 15% for hydrogen contents ranging from 4 to 8 mL/100 g. These methods give the most reliable measurements of diffusible hydrogen.
2. Other test methods, using glycerin or silicone oil for the collection of hydrogen, gave values which were typically about 50% lower than IIW values. This was attributed to the solubility of these media for hydrogen.
3. Measurements of coating moisture had a poor correlation with the diffusible hydrogen content.
4. Rehydrated electrodes produced deposit hydrogen values similar to those of as-manufactured electrodes when both were evaluated at a constant coating moisture content. This unexpected result is attributed to performing the tests with electrodes not of the moisture-resistant type.

Acknowledgments

These tests were performed and reported to the AWS A5 Task Force on Hydrogen while the author was employed by Alloy Rods, Inc. The tests were, with the following exception, performed with the assistance of the technicians at Alloy Rods. The author particularly appreciates the assistance of Damian Kotecki, who performed the Teapot tests on the system at Teledyne McKay. The author appreciates helpful discussions with members of the A5 Task Force on Hydrogen.

References

- [1] Gayley, C. T. and Wooding, W. H., "Determining Total Water Content in Electrode Coatings," *Welding Journal*, Vol. 29, 1950, p. 629.
- [2] "Specification for Low Alloy Steel Covered Arc Welding Electrodes," A5.5-81, American Welding Society, Miami, FL.
- [3] Siewert, T. A., "Moisture in Welding Filler Materials," *Welding Journal*, Vol. 64, 1985, p. 32.
- [4] "Electrodes, Welding, Mineral Covered, Iron-Powder, Low-Hydrogen, Medium High Tensile and Higher Strength," Military Specification MIL-E-22200/10A, Department of the Navy, Washington, DC.

- [5] "Rules and Regulations for the Construction and Classification of Steel Ships," Lloyds Register of Shipping, London, 1970, p. 493.
- [6] "The Determination of the Hydrogen Content of Ferritic Arc Weld Metal," IIW Document No. II-959-81, American Council of the International Institute of Welding, Miami, FL.
- [7] "Standard Procedures for Determination of the Diffusible Hydrogen Content of Ferritic Arc Weld Metal," proposed standard by AWS A5 Task Group on Hydrogen, American Welding Society, Miami, FL, 1983.
- [8] Shutt, R. C. and Fink, D. A., "New Considerations for the Measurement and Understanding of Diffusible Hydrogen in Weld Metal," *Welding Journal*, Vol. 64, 1985, p. 19.
- [9] "Approved Welding Electrodes Wire-Flux and Wire-Gas Combinations," American Bureau of Shipping, New York, 1979, p. 147.
- [10] "Extract from the Rules for the Construction and Classification of Steel Ships," Det. Norske Veritas, Hovik, Norway, 1976, p. 442.
- [11] Kotecki, D., Teledyne McKay, York, PA, correspondence to the A5 Task Force on Hydrogen, 1982.
- [12] Nippes, E. F., Ball, D. J., and Gestal, W. J., Jr., "Determination of Diffusible Hydrogen in Weldments by the RPI Silicone-Oil Extraction Method," *Welding Journal*, 1981, p. 50-S.
- [13] "Method for Measurement of Hydrogen Evolved from Gas Shielded Arc Welds," Draft JIS Standard, IIW Document No. II-A-567-82, American Council of the International Institute of Welding, Miami, FL.
- [14] Evans, G., Oerlikon, Zurich, Switzerland, correspondence to the American Welding Society A5 Task Group on Hydrogen, 1983.
- [15] Hirai, Y., Minakawa, S., and Tsuboi, J., "Prediction of Diffusible Hydrogen Content in Deposited Metals with Basic Type Covered Electrodes," IIW Document II-929-80, American Council of the International Institute of Welding, Miami, FL.
- [16] International Critical Tables of Numerical Data, *Physics, Chemistry and Technology*, McGraw-Hill, New York, 1926, p. 271.

Diffusible Hydrogen Testing by Gas Chromatography

REFERENCE: Quintana, M. A. and Dannecker, J. R., "Diffusible Hydrogen Testing by Gas Chromatography," *Hydrogen Embrittlement: Prevention and Control, ASTM STP 962*, L. Raymond, Ed., American Society for Testing and Materials, Philadelphia, 1988, pp. 247-268.

ABSTRACT: In recent years, there has been a rising interest in diffusible hydrogen testing of steel weld metals. Several test methods have been used with varying degrees of success. The glycerin displacement method, which has been widely used, has been demonstrated to be inaccurate and under certain conditions totally unreliable. Alternative use of mercury as a collection medium provides for reliability in testing but introduces complications associated with the use of a hazardous material. Recently, gas chromatography has been used as a basis for diffusible hydrogen analysis. The method presented in this paper allows for degassing of a welded specimen in a closed chamber and subsequent analysis of the resulting gas mixture by gas chromatography. The method is flexible in that it allows for degassing at several temperatures and allows for analysis of the gas contained without consuming it entirely. The purpose of this paper is to outline the general method and provide experimental and analytical verification of its accuracy. It is discussed in comparison with other methods and equipment in current use, and some examples of its application are presented.

KEY WORDS: diffusible hydrogen, steel, weld, gas chromatography

It is well recognized that hydrogen present as an interstitial impurity has a detrimental effect on the mechanical properties of steels. Frequently, hydrogen uptake during material processing is responsible for this degradation of mechanical properties. During welding, hydrogenous compounds dissociate, producing atomic hydrogen in the arc atmosphere which dissolves in the molten weld pool. Subsequent to solidification, some hydrogen diffuses to free surfaces where it escapes to the atmosphere, while some hydrogen diffuses to other areas of the weldment where it contributes to a deterioration of properties. Consequently, considerable effort has been devoted to the control of the hydrogen potential of welding consumables and processes. This has been achieved, in part, through the careful selection of lubricants for drawing operations and an increased emphasis on cleanliness and control of contaminants. Perhaps the greatest effort has been expended for shielded metal arc welding (SMAW) electrodes where the indirect control of weld metal hydrogen levels has been achieved through minimization of coating moisture levels [1-3]. This approach is reasonable for covered electrodes since the coating moisture does contribute to the hydrogen content of the resulting deposit [3,4]. However, there are limitations. Since the relationship between coating moisture and hydrogen content can vary significantly with electrode type [3], a given coating moisture level can result in a wide range of weld metal hydrogen contents depending upon the coating system. It, therefore, becomes necessary to evaluate the actual hydrogen content of the deposit. When considering a process such as flux cored

¹Senior engineer and senior chemist, respectively, General Dynamics, Electric Boat Division, Groton, CT 06340.

arc welding (FCAW) or gas metal arc welding (GMAW), indirect tests have limited meaning [5], and the hydrogen content of the deposit must be measured directly.

Several tests have been used for the direct measurement of weld metal diffusible hydrogen content. Diffusible hydrogen is that fraction of the total hydrogen content which evolves rapidly from a sample at or near room temperature. The most popular methods involve the use of collecting fluids [6–10]. Welded specimens are allowed to degas in eudiometers filled with collecting fluid. Bubbles form as a result of gas evolution from the specimens and collect in the upper portions of the eudiometers. The volume of gas collected is measured, and the diffusible hydrogen content is reported as the volume of gas collected per unit mass of weld deposit. Some methods use mercury as a collecting fluid, requiring from three to seven days for specimen degassing [6, 10]. Because of the health hazards associated with exposure to mercury, the glycerin test has been widely used in the United States wherein glycerin is used as the collecting fluid [7, 8]. Other collecting fluids which have had limited use include silicone oil [9], distilled water [11], and liquid paraffin [11].

The glycerin test in particular has been demonstrated to be unreliable [12, 13]. Although the test is easily implemented, the gas collected over glycerin has been found to contain gases other than hydrogen [12, 14, 15]. Distilled water, liquid paraffin, and silicone oil suffer from similar problems. Tests utilizing mercury displacement have been shown to be reliable. However, the health hazards associated with mercury use render these tests somewhat unattractive for certain industries. Consequently, recent development efforts have resulted in alternate techniques. One method allows degassing of the specimen in an evacuated chamber. Subsequent displacement with water allows for gravimetric determination of the amount of hydrogen evolved [16]. Other methods have been based on hydrogen detection by gas chromatography [17–19]. One feature common to these methods is the extended period of time required for degassing, typically several days.

In general, there is a need for a test method which will: (1) eliminate the inaccuracies associated with the use of a collecting fluid having high hydrogen solubility, like glycerin [20, 21]; (2) avoid the health hazards associated with the use of mercury; and (3) provide for completion of a test in a reasonable length of time.

The test method presented herein accomplishes these things. Its primary purpose is to accurately measure the amount of hydrogen evolved from a welded specimen without the use of a hazardous material. The test can be accomplished within an 8-h time period. In addition, the method allows the user to repeat analysis on the gas samples for verification and provides some indication of malfunctions which may occur.

Experimental

The method for diffusible hydrogen testing has three parts: (1) specimen preparation and storage, (2) degassing, and (3) analysis. The detailed procedure is based on the American Welding Society (AWS) procedure [22] and is detailed in Appendix 1. A weld deposit is made on a steel specimen. The specimen is allowed to degas in inert atmosphere in a closed test chamber. The hydrogen evolved from the specimen is contained within the test chamber, and the amount of hydrogen is then determined analytically by gas chromatography.

During the course of development, different specimen sizes and configurations were used prior to making a final decision regarding suitable specimen dimensions. This resulted from work conducted by the AWS task group charged to write a diffusible hydrogen test standard. They considered several sizes and configurations before reaching a conclusion. This work was conducted in conjunction with the task group's effort and therefore reflects some of those changes. The original specimen was a 12 by 25 by 127-mm specimen from the glycerin test procedure [8] which included weld starts and stops (Fig. 1a). Finally, the specimen evolved into a three-part assembly having a run-on, a center specimen with dimensions 12 by 25 by 80 mm, and a runoff (Fig. 1c). Only the center specimen is used for diffusible hydrogen deter-

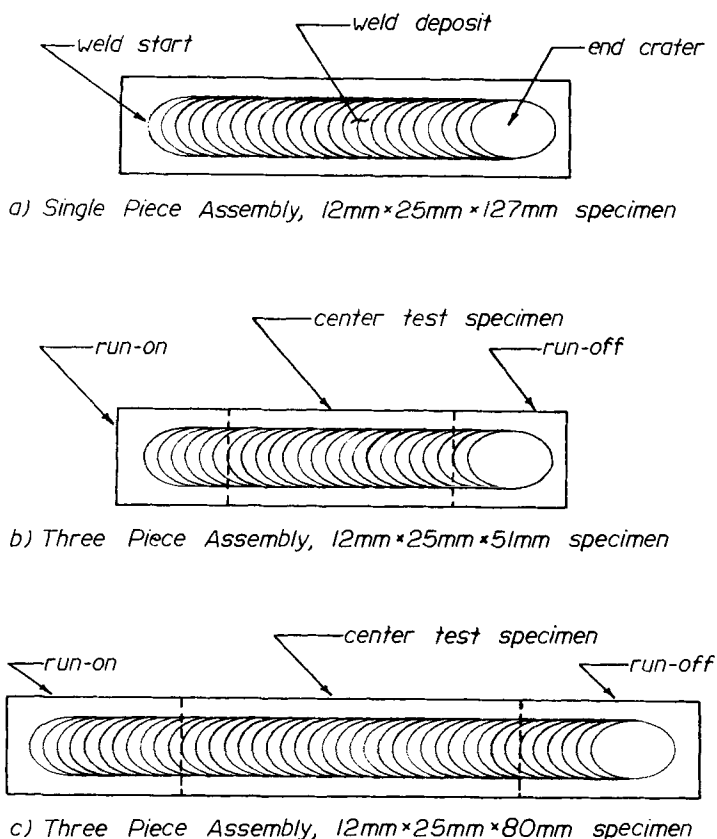
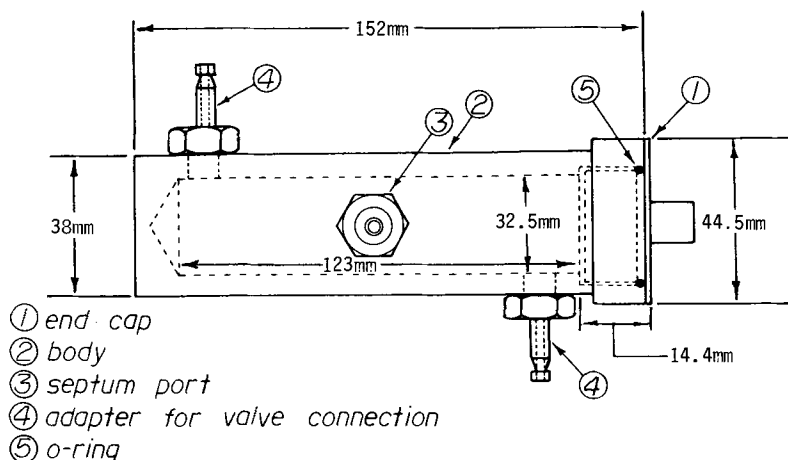


FIG. 1—Test specimens schematic illustrations.

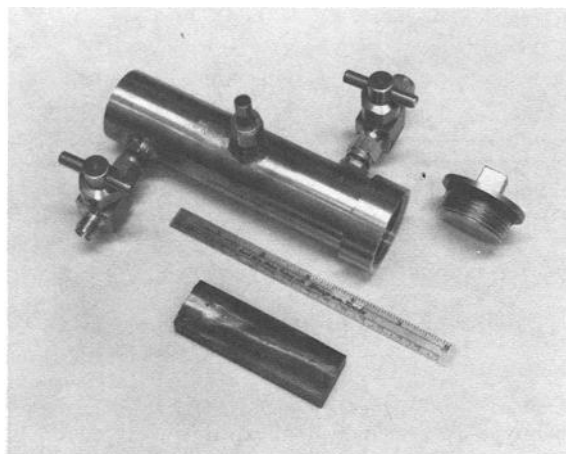
mination. The specimen type used for individual experiments is identified, and the effect of specimen type on the individual test results is discussed.

Test Chamber

The test chamber in current use is illustrated in Fig. 2. This design is the end result of several evolutions. The overall size of the chamber has been minimized for ease of handling and more effective purging. Fittings and valves have been improved to provide for swifter operation and easier maintenance. Because of the relatively low diffusivity of hydrogen in austenitic stainless steel, the main body of the chamber is fabricated of 304 stainless steel round bar. The soft seat plug valves made of 316 stainless steel are connected to the chamber body via 316 stainless steel adapters, 7/16 MS (male, straight thread) by 0.250 tube, which have been welded in place. Soft seat valves were chosen for durability and easy maintenance. Previous experience with metal seat valves resulted in seat deformation and leakage after only a few months of use. The septum port atop the chamber is a 316 stainless steel adapter, 7/16 MS x 0.250 FLRLS (flairless) tube, installed upside down and welded in place. The septum nut and guide are also stainless steel. The septum used is silicone rubber with a Teflon backing. To prevent galling, copper-nickel was chosen for the end cap which forms an O-ring seal with the main body. The O-rings used are butyl rubber, for minimal hydrogen permeability.



a) Schematic Representation



b) Chamber with 80mm Specimen

FIG. 2—Test chamber illustrations.

Gas Analysis

Analysis of the resultant gas mixture is accomplished by gas-solid chromatography [23], the preferred method for rapidly and accurately analyzing volatiles [24]. The volatile material is injected into a column which contains an active solid packing. The carrier gas sweeps this plug of vapor through the column. The crystal structure of the solid packing contains fine pores which are approximately 5×10^{-10} m (5 Å) in diameter. These pores form a series of tunnels throughout the packing. Small molecules pass through these pores rather easily, whereas larger ones pass through with difficulty and therefore more slowly. As a result, separation is due to a sieving effect. Thus the packing is termed molecular sieve. Generally, elution is in order of

increasing molecular size. Also affecting the elution time of each component are the column temperature, carrier gas flow rate, and carrier gas composition. When each of these is held constant, each component travels through the column at its own rate. Upon elution from the column, each component then enters a detecting device which subsequently sends a signal to a computer processor. This processor converts the signal into a series of peaks which are identified and quantitated. This signal appears on a chart (or chromatogram) as a plot of time versus the composition of the carrier gas stream. The time of emergence of a peak, known as retention time, identifies the component. The peak area is directly proportional to the concentration of the component in the mixture.

The operation of the detecting device, known as a thermal conductivity detector, is based on the principle that heat is conducted away from a hot wire by gas passing over it. If the composition of this gas is constant, the amount of heat conducted will also be constant. As the composition changes, the thermal conductivity of the gas changes and the amount of heat lost by the wire also changes. This hot wire, known as a thermistor, forms one leg of a Wheatstone bridge circuit. As the temperature of the thermistor varies, the resistance changes, causing an unbalance in the Wheatstone bridge. The extent of the unbalance is recorded by the computer processor as a peak.

Identifying the compounds of interest in gas chromatography is straight forward and may be accomplished by injecting pure standards of known identity into the gas chromatograph (gc) and comparing their resultant retention times to those of the unknowns. One may be reasonably certain of proper identification of an unknown if its retention time matches that of the standard. The gas sample matrix must not be complex in order to avoid interferences leading to erroneous results. Quantitating the now identified compounds is somewhat more difficult but is again accomplished by injecting standards of known concentration into the instrument and comparing the resultant peak areas to those of the unknowns. With each set of specimens, a gas standard is prepared which is used to calibrate the instrument prior to analysis. This standard is prepared by adding known quantities of the components of interest, 1 mL each of hydrogen and helium with a balance of argon. Hydrogen is added because this is the unknown component in the test chambers after degassing the welded specimen. Helium is added to each test chamber as well as the standard to serve as the internal standard.

The internal standard calculation method results in the greatest potential for precise quantitative results [25]. Because the internal standard is included with each gas sample, anything affecting the sample will also affect the internal standard. To elaborate on the purpose of the internal standard, consider the following example. After degassing and prior to analysis, a leak develops in a specimen test chamber, resulting in a 50% pressure loss. All gas components within this chamber are lost proportionately. Analysis reveals that the amount of helium was reduced to half. It may also be assumed that a proportional amount of hydrogen and argon were lost. Therefore, a correction factor relates the helium peak intensity from the standard to the helium peak intensity from the sample. The computer processor computes this correction factor and applies it to the raw data to report the correct hydrogen volume. The internal standard will similarly correct for other factors which affect all components of the gas mixture proportionately. For example, use of the internal standard corrects for variations in test chamber volume, variations in injection volume, and variations in gas pressure.

Prior to the analysis of the specimen test chamber samples, 100 μL of the standard is analyzed. A minimum of three standard injections are made to verify the precision and accuracy of the standard hydrogen amount. If the standard injections are within ± 0.01 mL of the actual hydrogen volume, analysis of the test chamber samples may proceed. If the difference is greater than 0.01 mL, the computer processor must be recalibrated and the standard reanalyzed. Following the analysis of the samples, the standard must again be analyzed to verify that the calibration is within tolerable limits. If a shift is observed, the instrument must be recalibrated and all samples reanalyzed. Each specimen test chamber is analyzed in triplicate. A sample is withdrawn using a syringe and immediately injected into the gc.

Upon injection, the computer processor is activated. As mentioned previously, the composition of the carrier gas is plotted versus time. Under normal test conditions only two elutants, helium and hydrogen, are present (Fig. 3). Occasionally traces of oxygen and nitrogen also appear. This is caused by the presence of air contamination in the sample. Argon from the specimen test chamber is blanked out by the use of argon as the instrument carrier gas. Following emergence of all peaks of interest, the plot is terminated and the processor prints a report listing all pertinent data including retention times, amounts (in millilitres) of hydrogen and helium, area counts, and integration types. The volume of hydrogen is reported as the average of three such analyses. The amount of hydrogen was then transcribed into a sample log notebook for subsequent data reduction according to the detailed procedure in Appendix 1.

Time/Temperature Determination

To demonstrate the use of the method and to determine appropriate time at temperature for degassing of the specimens, several series of tests were conducted. Welding was accomplished using the mechanized spray GMAW process. The electrodes used were MIL-100S-1 [26] type. All "711" and "D" numbered specimens were fabricated with a 1.6-mm-diameter electrodes under the same welding conditions (26 to 26.5 arc V, 320 to 340 A, 5.1-mm/s travel speed, 21.2-L/min gas flow rate with a 16-mm-diameter gas cup, 13-mm cup to work distance, 16-mm tip to work distance). All "691" numbered specimens were fabricated with a 1.1-mm-diameter electrode under the same welding conditions (27.5 arc V, 260 to 270 A, 4.2-mm/s travel speed, 21.2 L/min gas flow rate with a 16-mm-diameter gas cup, 13-mm cup to work distance, 16-mm tip to work distance).

At any given test temperature, the time required for degassing should be dependent upon the level of hydrogen present. It was, therefore, necessary to evaluate time/temperature relationships for different levels of diffusible hydrogen. Since GMAW is inherently a low hydrogen

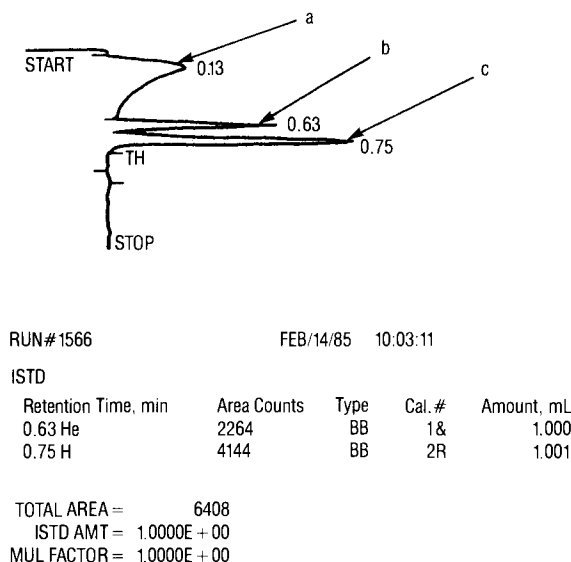


FIG. 3—Chromatograph and report: (a) pressure transient due to injection; (b) helium peak; (c) hydrogen peak.

process, the hydrogen potential of the process was elevated by introducing hydrogen in the shielding gas. Therefore, shielding gas composition was varied as indicated in Table 1.

To determine the time required for degassing at a given test temperature, hydrogen determinations were made for specimens periodically during their degassing period. The first set of tests (711-2-26, 711-2-28, 711-2-29) was conducted at 45°C for a total time of approximately 70 h with single-part test assemblies (see Fig. 1a). This starting point was selected because some electrode specifications require degassing at this temperature [8,27]. In an effort to minimize overall test time, subsequent tests were conducted at elevated temperatures. The second set of tests (711-2-30 thru 711-2-33) was conducted at 100°C for a total test time of approximately 118 h. It was intended to terminate the test within 48 h. However, interference with other work in the laboratory resulted in the unintended extension of the test. The third set of tests (711-110, 711-111, 711-112, 711-117) was also conducted at 100°C. However, these tests were completed in approximately 26 h. It is also important to note that three-part test assemblies were used (see Fig. 1b). The center specimens were 12 by 25 by 51 mm. The overall size of the assembly (run-on, center specimen, runoff) was 12 by 25 by 127 mm, which is the same as the single-part assembly (see Fig. 1a). Essentially, the 51-mm-long center specimen represents the same welded specimen without the weld start and stop. This specimen size was also used for the fourth set of tests (711-120, 711-122, 711-123), which was conducted at 150°C for approximately 8 h. The fifth set of tests (D4, 691-2, 691-6, D6) utilized the final specimen size/configuration (Fig. 1c). The 12 by 25 by 80-mm specimens were welded with varying shielding gas compositions, thereby producing varying diffusible hydrogen levels. Testing was accomplished at 150°C for approximately 10 h. It is recognized that variation of specimen size and configuration can have a significant effect on diffusible hydrogen values. However, because the specimen cross section is held constant, the time/temperature relationship should be unaffected.

Results and Discussion

The test chamber in Fig. 2 is the end result of several design changes. At the beginning of the development effort, requirements for the test chamber were outlined. The inside dimensions were to be as small as practicable for the specimen size used in order to minimize purge times, minimize internal volume to improve analytical accuracy, and provide for ease of handling. As specimen size changed throughout the test effort, the overall dimensions were reduced to correspond with those changes. Placement of the inlet and outlet was to be such as to provide for efficient purges. The end closure design was to provide for gas tight seal under pressure at elevated temperature and for rapid loading of the specimen. Another consideration which became important after extensive testing had been completed concerned valve selection and installation. Ideally valves should have changeable soft seats and should be designed for swift operation. Originally, the valves used were slow acting with metal seats which permanently deformed after extensive operation. Temporary attachment is advantageous to allow for replacement of

TABLE 1—Shielding gas composition.

Composition	Specimen Numbers
1.5% H ₂ , 4.2% CO ₂ , 94.3% Ar	D6
1.0% H ₂ , 4.7% CO ₂ , 94.3% Ar	711-2-26, 711-2-28, 711-2-29, 711-2-30, 711-2-31, 711-2-32, 711-2-33, 711-110, 711-111, 711-112, 711-117, 711-120, 711-122, 711-123
0.6% H ₂ , 5.2% CO ₂ , 94.2% Ar	691-6
5.9% CO ₂ , 94.1% Ar	D4, 691-2

valves when it becomes necessary after extensive use. Further, it was essential to provide for sampling without consuming all of the gas contained within a test chamber. This was important for the purpose of multiple analyses from a single chamber for verification of test results. For this reason, a septum port was provided in the test chamber design for withdrawal of gas samples with a syringe.

There are two options for introducing a gas sample into the gc, by way of injection with a syringe and by way of a gas sampling valve on the instrument. In this case, use of the gas sampling valve would involve direct connection of the test chamber to the gc and introduction of argon flow through the chamber to push the gas mixture to be analyzed into the gc. Once done, any of the initial gas mixture remaining in the chamber would be considerably diluted, making subsequent analysis much more difficult if at all possible. In contrast, withdrawal of gas with a syringe leaves the gas mixture unaltered for subsequent analysis. The test chambers in current use (Fig. 2) incorporate all of these considerations.

In addition, it was essential to ensure that hydrogen contained within the chambers would not escape the system via diffusion through the chamber walls. Consequently, steady state solutions to the diffusion equations were used to estimate this potential loss of hydrogen (Appendix 2a). The simplifying assumption of a steady state condition represents a worse than actual case. It assumes that all of the hydrogen evolved from a specimen is in contact with the inside surface of the chamber for the entire test period. It also assumes steady state diffusion for the entire test period, which is more severe than the actual condition. The actual situation is not this severe since hydrogen evolves gradually and the maximum hydrogen concentration is not reached until near the end of the test period. Even so, the steady state calculations indicate that the estimated loss of hydrogen is less than the level of accuracy for the analytical method used for hydrogen determination. Consequently, diffusional losses have no effect on test results.

The reliability of the analytical method was established by statistical analysis and maintained through strict adherence to modern quality control procedures [28]. These procedures have two primary functions. They act to monitor reliability (accuracy and precision) of the test results reported and to control the quality of these results. This is accomplished by the use of \bar{X} - R control charts (Appendix 3). Ten sets of triplicate determinations of samples containing a known concentration of hydrogen were analyzed under routine daily conditions.

Averages (\bar{X}) and ranges (R) were computed for each set of data. From these values warning and control limits were determined and plotted on \bar{X} - R control charts (Appendix 3). Following the initial construction of these charts, standards were analyzed in triplicate along with each set of specimens. The average and range must fall within the established limits. If, for example, the values obtained from a triplicate analysis were 0.992 mL, 1.003 mL, and 0.988 mL, the average (\bar{X}) and range (R) are 0.994 and 0.015 mL, respectively. The average falls below the lower control limit ($LCL_{\bar{X}}$) indicating an "out of control" condition. By this, one may deduce that the analysis for this set of samples was inaccurate. Furthermore, the range is above the upper control limit (UCL_R). This again indicates an "out of control" condition and shows the results to be imprecise. If either of these two values for a set of analyses are out of control, the results are discarded and the test is repeated. It is preferable that one always stay within the working limits of the control charts.

Upon review of Appendix 3, it is concluded that under routine conditions the test method developed proved to be both highly accurate and precise. Only on 7/7 did the \bar{X} value fall out of the warning limit but did not qualify as "out of control." If the range values were consistently out of control, this would indicate poor reproducibility. Equipment malfunction or poor technique might be the cause. If the \bar{X} values were consistently out of the warning limits, the methodology is suspect and must be reevaluated.

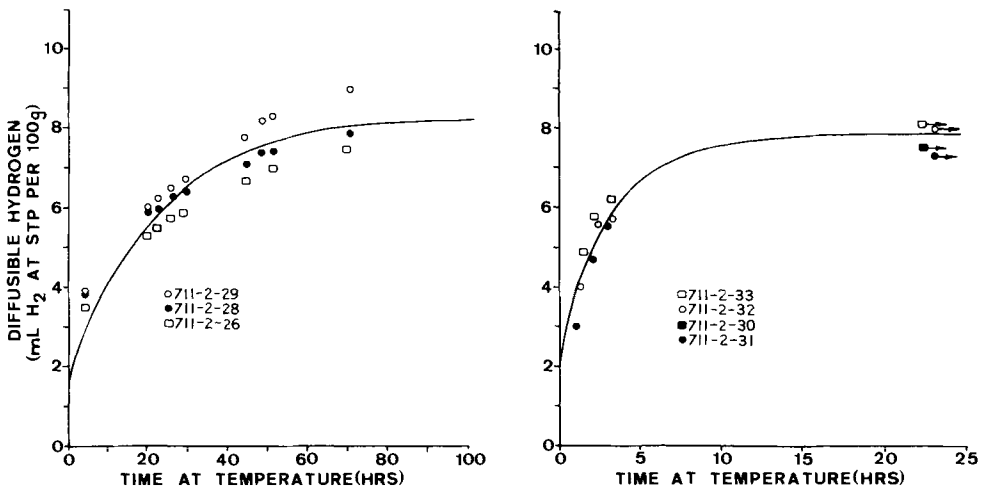
The quality of results is also of major concern. This encompasses the use of standards and reagents of the highest quality. All bottled gasses are "zero" grade, which are certified to be 99.998% pure and have less than 0.5 ppm total hydrocarbons as methane. Occasionally, certified gas mixtures are analyzed as an additional verification that the instrument and method are

functioning properly. These NBS traceable standards are prepared by an outside vendor and are certified to be within $\pm 2\%$ of the actual concentration of the component of interest. In this case it is hydrogen. Instrument maintenance is also important to ensure high quality. Fittings are routinely checked for leaks and are replaced if found faulty. There is also a periodic replacement of the thermal conductivity detector filament. This guarantees a continuation of the highest sensitivity attainable.

An additional test to establish statistical reproducibility was conducted. One laboratory-prepared standard containing 1 mL hydrogen, 1 mL helium and a balance of argon was consecutively sampled and analyzed under routine daily conditions 20 times. For these repetitive analyses the average hydrogen value was 1.002 mL with a standard deviation of 0.0053 mL and a variance of 0.000026 mL². Considering that, under normal conditions of testing, only three analyses are conducted for each test chamber, the level of reproducibility was determined by computing a "confidence interval" [33]. Using a t-distribution and 0.95 level of significance, the "confidence interval" for a sample of three was computed as ± 0.013 mL. In other words, the volume of hydrogen determined by the average of three repetitive analyses is reasonably accurate within about ± 0.01 mL. Therefore, these results should be reported only to the nearest 0.01 mL. This results in diffusible hydrogen values reported to the nearest 0.1 mL H₂ per 100 g.

Since this test method has been shown to accurately determine the quantity of hydrogen, the only remaining problem was to reduce the test time such that chamber loading, degassing, and analysis could be completed within an 8-h shift. Beginning with the 45°C test temperature and the single-part assembly, hydrogen evolution as a function of test time was determined (Fig. 4a). The mL H₂ per 100 g deposit is plotted as a function of test time. Figure 4a shows that, at the hydrogen levels tested, evolution was probably not quite complete at 70 h. Extrapolation of the curve predicts complete evolution at approximately 90 h. Consequently, evolution is about 98% complete at 70 h.

To reduce the test time, test temperature was raised to 100°C. Selection of this temperature was based on previous work with the RPI Silicone Oil Test [9] at 100°C. Single-part assemblies



a) Hydrogen evolution at 45°C(113°F)

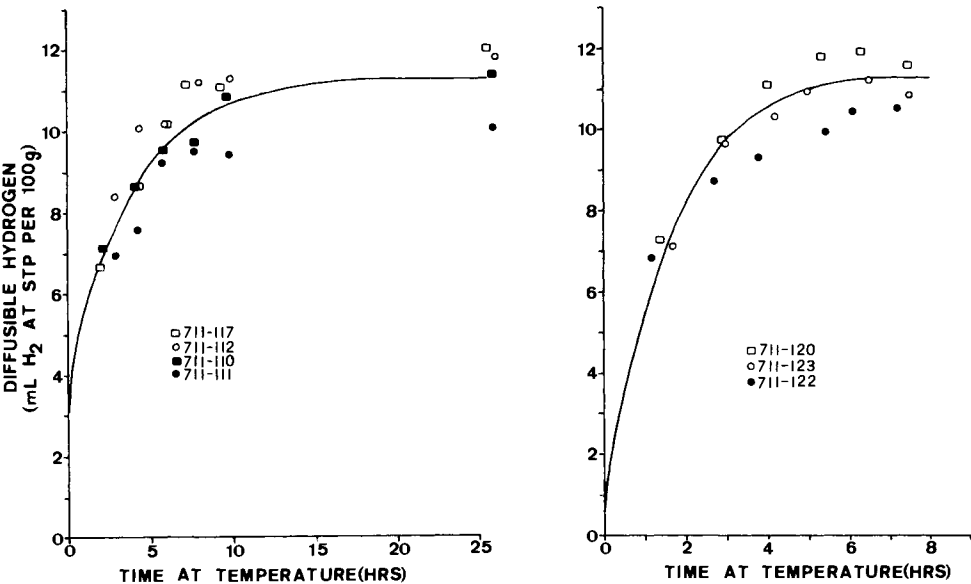
b) Hydrogen evolution at 100°C(212°F)

FIG. 4—Comparison of 45°C and 100°C hydrogen evolution curves, 127-mm specimen (including starts and stops).

were degassed at 100°C (Fig. 4*b*). The precise shape of the curves is subject to some speculation since the end points are off the graph. However, complete evolution is indicated at about 20 h. Specimens from three-part test assemblies (51 mm long) were also tested at 100°C (Fig. 5*a*). Since the cross sections of the single-part assemblies and the three-part assemblies are identical, the rates of hydrogen evolution should be the same at a given test temperature even though the amount of hydrogen per unit weight should be different due to the exclusion of weld starts and stops. Figure 5*a* verifies that evolution is complete at approximately 20 h. Ninety-eight percent completion is expected in 12 to 13 h.

Since a 12-h test is still too lengthy to be completed in a single 8-h shift, a further increase in temperature was required. Given that test times had been determined for two temperatures, the diffusion equations were utilized to predict the final temperature (Appendix 2*b*). It was determined that complete evolution could be achieved in 6 h at a test temperature in the vicinity of 150°C. The results of 150°C degassing of specimens from three-part assemblies (Fig. 1*b*) are presented in Fig. 5*b*. Evolution is virtually complete in 6 h. This time period is sufficient to allow for completion of a test in a single 8-h shift. Specimens can be removed from low temperature storage and loaded at the beginning of the shift, degassed for 6 h, then analyzed at the end of the shift.

After establishing the final set of test conditions at 6 h and 150°C, the specimen size was changed to the 80-mm-long specimen of Fig. 1*c*. This change affects only the specimen length, not the specimen cross section. Consequently, the evolution time at 150°C (302°F) should remain 6 h. Figure 6 verifies this. Figure 6 illustrates hydrogen evolution curves at four levels of diffusible hydrogen. At the high levels (14 mL H₂ per 100 g and 20 mL H₂ per 100 g) the entire 6-h period is required for complete evolution. At the lower levels, a reduced time of 4 h could be used successfully. Using 6 h as a routine test time will provide for proper testing of specimens



a) Hydrogen evolution at 100°C(212°F) b) Hydrogen evolution at 150°C(302°F)

FIG. 5—Comparison of 100°C and 150°C hydrogen evolution curves, 51-mm specimen (excluding starts and stops).

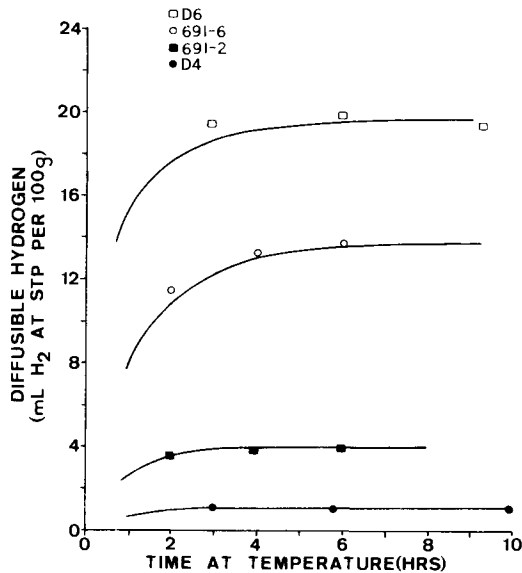


FIG. 6—Hydrogen evolution curves at 150°C (302°F) for various levels of diffusible hydrogen, 80-mm specimen (excluding starts and stops).

having a 12 by 25-mm cross section. If for some reason thicker specimens are used, this test time would have to be reevaluated.

It is noted that all curves presented are "best fit" curves. The evolution of hydrogen from a specimen is expected to behave according to an equation of the form $y = B - \exp(a + bx)$ (Appendix 2b). Regression analysis according to this equation results in the curves shown.

Although the intent of the tests conducted was to establish hydrogen evolution time at a series of temperatures, some discussion of diffusible hydrogen levels can be made. Figures 4 and 5 represent specimens which were fabricated under the same welding conditions with the same gas mixture. It is therefore expected that specimens having the same size/configuration should have the same nominal levels of diffusible hydrogen. The single-part assemblies degassed at 45°C resulted in an average diffusible hydrogen level of 8.1 mL H₂ per 100 g \pm 0.6 mL H₂ per 100 g, while similar assemblies degassed at 100°C resulted in an average diffusible hydrogen level of 7.7 mL H₂ per 100 g \pm 0.3 mL H₂ per 100 g. Using a t-test [33], it was determined that the small difference of 0.4 mL H₂ per 100 g between average values is insignificant. The 45°C test and 100°C test for a common specimen size are statistically equivalent. Similarly, the 51-mm-long specimens degassed at 100°C resulted in the same nominal diffusible hydrogen level as similar specimens degassed at 150°C. The 100°C test is statistically equivalent to the 150°C test.

However, there is a marked difference between 51-mm specimens and 127-mm specimens. At the 100°C test temperature, the average for 127-mm specimens is 7.7 mL H₂ per 100 g, whereas the overall average for the 51-mm specimen is 11.3 mL H₂ per 100 g. This represents a 3.6 mL H₂ per 100 g (42%) difference for specimens welded under the same conditions. The difference is believed to be a direct result of specimen size/configuration changes. As shown in Fig. 1, the 51-mm specimen represents the center portion of the 127-mm specimen without the weld starts and stops. The length of deposit is the same in both cases. It has been shown that the hydrogen volume evolved from the deposit is a minimum at the start and increases toward the end of deposit [34]. In most cases, the high hydrogen level at the end of the deposit is not sufficient to

make up for the low level at the beginning. The result is that the average test result including start and stop is expected to be lower than the average test result for the center section alone. Consequently, the elimination of weld starts and stops for the shorter specimen is considered responsible for a 3.6-mL H₂ per 100-g (42%) increase in average test result. Even though total time required at temperature is unaffected, the apparent level of diffusible hydrogen is affected. Therefore, if the method presented here is to be used to evaluate welding consumables or procedures, consistent specimen size must be used throughout the investigation.

Although the test method presented is somewhat more complex than a fluid displacement method [6-10], it has many attractive features. The inaccuracies inherent in the glycerin test [12-15] have been eliminated. For example, the analysis is unaffected by atmospheric contamination. The elution time for oxygen and nitrogen are greater than for helium and hydrogen and the resulting peaks are clearly separated. Consequently, if some air were present, it would have no effect on the hydrogen analysis for the conditions presented. The accuracy of the method is ensured by the use of standards, which are checked before and after analysis of samples. Furthermore, the ability to perform multiple analyses for a single test chamber provides for verification of test results.

Summary and Conclusions

The use and reliability of the test method have been demonstrated. Reliability has been established and maintained through implementation and consistent use of a quality control system. Accuracy and precision have been established by statistical analysis. A study of evolution time required for a variety of test temperatures has resulted in a significant reduction in overall test time. Since degassing can be completed in 6 h at 150°C, testing of a set of specimens (exclusive of welding) can be accomplished during a normal 8-h work day. It should be noted that the 6-h period is applicable only for the 12 by 25-mm cross section tested. Use of another specimen size/configuration would require a reevaluation of test time. Comparison of the specimen sizes used during this investigation demonstrates that specimen size/configuration can have a significant effect on resultant diffusible hydrogen values. Consequently, when this method is used for evaluation of welding consumables or procedures, an appropriate specimen size/configuration must be used consistently throughout the investigation. The preferred size is the 12 by 25 by 80 mm [22] used in the final series of tests. This specimen size will be used for all subsequent work. It has been demonstrated that variation of test temperature provides for significant reduction of the time required for completion of a test. Also, the hazards associated with the use of mercury are avoided with a chromatographic method.

The objective of this development effort was to develop an accurate diffusible hydrogen test method which could be accomplished within an 8-h time period without the use of a hazardous material. This was successfully accomplished through test chamber design and analytical method development. Once thoroughly developed, the test equipment and method were used to develop time/temperature relationships which resulted in minimization of total test time.

APPENDIX 1

Procedure

1. The weld test assemblies used for this investigation were of two configurations for reasons previously stated.
 - a. Single-part assembly having dimensions 12 by 25 by 127 mm.
 - b. Three-part assembly consisting of a run-on, a center specimen, and a runoff. The center

specimen was finished to dimensions of 12 by 25 by 80 mm. The run-ons and runoffs were finished to dimensions of 12 by 25 by 40 mm.

All parts were cut from 15.9-mm-thick plate, MIL-S-22698A (2, TY3, C1. B), and finished by surface grinding to the dimensions indicated. All parts possessed orthogonal faces.

2. All parts for weld test assemblies were heat treated for 1 h at 625°C to remove any diffusible hydrogen present in the base material.
3. Surface oxide resulting from heat treatment was removed by power wire brushing. Each specimen (excluding run-on and runoff) was uniquely numbered by die stamping. To remove dirt and grease, all parts were scrubbed with a bristle brush and hot soapy water, thoroughly rinsed in hot water, and finally washed down with acetone and dried.

NOTE: A preferred method of cleaning in current use is ultrasonic cleaning in Freon 113 for 30 min. After cleaning, the parts are dried by warming to 100°C for 30 min.

Lint free gloves were worn for specimen handling from this point until completion of welding in order to maintain cleanliness.

4. Numbered specimens were then weighed to the nearest 0.01 g and placed in a desiccator for temporary storage until ready for welding.
5. Welding was accomplished by depositing a single stringer bead along each test assembly.
 - a. In the case of a single-part assembly (Fig. 1a), the specimen was clamped firmly in a copper fixture. Welding progressed from one end of a 25 by 127-mm face to the other without running off the end.
 - b. In the case of the three-part assembly (Figures 1b and c), a run-on, center specimen, and runoff were clamped firmly together in a copper fixture. Welding progressed uninterrupted from the run-on across the center specimen on a 25 by 80-mm face and onto the runoff. Welding was terminated on the runoff such that the trailing edge of the crater was on the runoff but within 25 mm of the trailing edge of the center specimen.

For SMAW tests, a single electrode was used to fabricate a single test assembly. For GMAW tests, all gas lines were purged with dry argon for 30 min prior to the start of welding to remove any residual moisture which might otherwise contribute to the diffusible hydrogen content.

6. Immediately after extinguishing the welding arc, the test assembly was removed from the copper clamping fixture and plunged into an ice water bath. Typically, this was accomplished within 5 s. The assembly was then agitated in the ice water for approximately 20 s after which it was placed in an acetone/dry ice slurry at -78°C.
7. After approximately ten min at low temperature, test assemblies were removed, one at a time, from the acetone/dry ice and cleaned by power wire brushing to remove any adherent slag.
 - a. Single-part test assemblies were immediately replaced in the acetone/dry ice slurry.
 - b. Three-part assemblies were immediately broken apart. Run-on and runoff parts were discarded. Only the center specimens were returned to the acetone/dry ice slurry.

All specimens were fabricated in this way. Degassing was accomplished as follows:

8. Specimens were transported to the testing facility in acetone/dry ice and stored for a maximum of three days until testing could begin.

NOTE: If prolonged storage should become necessary, specimens may be stored at -196°C for a maximum of 21 days. This practice was not employed during the development effort. However, it is in current use.

9. With the test chamber (Fig. 2) uncapped and both valves open, an argon purge was started through the chamber at 12.5 L/min.
10. A cleaned specimen was removed from the low temperature bath, rinsed in acetone to remove any ice which may have formed, and blotted dry with a clean cloth or paper towel. Only one specimen is handled at a time.
11. While still cold, the specimen is placed inside the open test chamber. The cap is tightened and argon purge continued for 30 s. At this point, both valves were closed, outlet first and inlet second. The argon line was then disconnected. The resulting pressure in each chamber

was 170.3 kPa. Test chambers were loaded in this way until either no specimens remained or all available chambers were loaded. Any specimens remaining were stored until test chambers became available again.

12. In addition to the loaded test chambers, a glass 250-mL gas sampling bulb equipped with two Teflon stopcocks and a sideport septum was purged with argon at 12.5 L/min for 30 s. After ensuring elimination of all traces of air, the bulb was pressurized with 170.3-kPa argon. This was performed in conjunction with the purging and pressurization of the sample chambers.
13. Following pressurization, exactly 1 mL of hydrogen was injected into the gas standard bulb. In addition, 1 mL of helium was also added in similar manner to each of the specimen test chambers and the gas standard bulb. This serves as the internal standard. At this time, laboratory temperature and barometric pressure were recorded.
14. All loaded test chambers were then placed in a preheated oven for the designated time at temperature. They were then removed from the oven and cooled. Cooldown was accomplished by placing each chamber in a cold water bath for approximately 5 min.

The amount of hydrogen in each test chamber was determined in millilitres by gas chromatography. The volume of hydrogen for each chamber is reported as the average of triplicate analyses converted to standard temperature and pressure (STP).

15. When the test chambers had cooled to the touch, 100- μ L gas was withdrawn through the side port septum on the test chamber using a 100- μ L gas-tight syringe. It was immediately injected into a gc which had previously been calibrated. A basic gas chromatograph equipped with dual injection ports and a thermal conductivity detector was used. The gc oven temperature was maintained by isothermal heating at 105°C (temperature adjust setting "80"). The detector was set on "low" temperature with "left" polarity. Instrument attenuation was set on "x1." The argon carrier gas was set at 308.2 kPa on the bottle regulator and was allowed to flow continuously through the gc overnight prior to each test. The gc contained two 8-ft. stainless steel columns (3.2 mm O.D. and 2.1 mm I.D.) packed with 60/80 mesh molecular sieve 5A adsorbant (Supelco Inc., Bellefonte, PA).
16. A 3390A integrator (Hewlett Packard) was used to transduce the signal from the detector onto the chromatogram. Immediately after injection, the integrator was activated and began plotting the chromatogram and recorded the injection time. The retention times for each peak as each component eluted from the column were reported as the plot progressed. This computer processor also measured and recorded the area of each peak in relative units. Following the emergence of all peaks of interest, the plot was terminated. The processor then printed a report listing all pertinent data including retention times, amounts (in mL) of hydrogen and helium, area counts, and integration types.
17. The average of three hydrogen determinations for a single chamber is taken as the hydrogen volume for that chamber and is then converted to STP according to:

$$V_{\text{STP}} = \frac{273}{273 + T} \times \frac{P}{760} V_m$$

where

T = laboratory temperature measured at the time of loading, °C,

P = barometric pressure measured at the time of loading, mmHg, and

V_m = measured hydrogen volume, mL.

18. After analysis was completed, specimens were removed from their respective chambers and weighed to the nearest 0.01 g. Deposit weight for each specimen is then determined by difference between initial and final weights.
19. Diffusible hydrogen content for each specimen is calculated, V_{STP} divided by deposit weight.
20. Normally, four specimens consecutively welded under identical conditions constitute a single diffusible hydrogen test.

APPENDIX 2

Diffusion Calculations

a. Estimate of Possible Hydrogen Loss Through Test Chamber Walls

Using the steady state solution to the diffusion equations for a cylinder, the potential loss of hydrogen through diffusion can be estimated. It is noted that use of the steady state case is an oversimplification. However, it is conservative in that it represents a worse-than-actual situation since the system does not start out at steady state. For the purposes of estimate it is considered adequate. The quantity of diffusing species which diffuses through a unit length of cylinder is given as [29]

$$Q = \frac{2\pi Dt(C_1 - C_2)}{\ln(b/a)}$$

where

- D = diffusion coefficient,
- C_1 = concentration of diffusing species at inside wall,
- C_2 = concentration of diffusing species at outside wall,
- a = inside radius,
- b = outside radius, and
- t = time.

Similarly, the ends of the test chamber can be modelled as plane sheets at steady state [29] wherein the quantity of diffusing species which is lost through diffusion per unit area is given as

$$F = Dt(C_1 - C_2)/l$$

where

- l = thickness of the end plate.

The total quantity of diffusing species lost can be approximated by adding

$$QL + FA$$

where

- L = cylinder length, and
- A = end cross-sectional area.

Given the geometry of the test chamber (Fig. 2), QL is approximately 30 times greater than FA . Therefore, the contribution to hydrogen loss through the ends of the test chambers is neglected and the total loss is given by

$$Q' = \frac{2\pi DtL(C_1 - C_2)}{\ln(b/a)} = 5.04 \times 10^2 Dt(C_1 - C_2) \quad (a1)$$

The diffusion coefficient, D , can be determined for different temperatures from the Arrhenius equation

$$D = D_0 \exp(-\Delta H_D/RT)$$

where, for 304 stainless steel,

$$\begin{aligned}
 D_o &= 2.72 \times 10^{-6} \text{ m}^2/\text{s} = 2.72 \times 10^{-2} \text{ cm}^2/\text{s}, [30] \\
 \Delta H_D &= 54\,300 \text{ J/mol}, [30] \\
 R &= 8.314 \text{ J/mol}, \text{ and } [32] \\
 T &= \text{temperature, } ^\circ\text{K}.
 \end{aligned}$$

For the various test temperatures, D is calculated as follows

$$\begin{aligned}
 D(45^\circ\text{C}) &= 3.27 \times 10^{-11} \text{ cm}^2/\text{s} \\
 D(100^\circ\text{C}) &= 6.76 \times 10^{-10} \text{ cm}^2/\text{s} \\
 D(150^\circ\text{C}) &= 5.36 \times 10^{-9} \text{ cm}^2/\text{s}
 \end{aligned} \tag{a2}$$

The concentrations (C_1 , C_2) of diffusing species are related to the hydrogen pressure. This pressure is zero at the outside surface. Therefore, $C_2 = 0$. The volume fraction of hydrogen in the test chambers rarely exceeds 0.006. Given an initial total pressure at time of loading of 24.7 psi ($1.70 \times 10^5 \text{ N/m}^2$) and test temperatures in $^\circ\text{K}$, the hydrogen pressures at each test temperature are determined by

$$p = 0.006(1.70 \times 10^5 \text{ N/m}^2)(T_{\text{test}}/T_{\text{amb}})$$

$(T_{\text{test}}/T_{\text{amb}})$ accounts for total pressure increase \propto temperature increase.

$$\begin{aligned}
 p(45^\circ\text{C}) &= 1.09 \times 10^3 \text{ N/m}^2 \\
 p(100^\circ\text{C}) &= 1.28 \times 10^3 \text{ N/m}^2 \\
 p(150^\circ\text{C}) &= 1.45 \times 10^3 \text{ N/m}^2
 \end{aligned}$$

The concentration of diffusing species at the inside surface is given by

$$\begin{aligned}
 C_1 &= 8.6 \times 10^{-3} p^{1/2} \exp(-9600/RT) \text{ mL H NTP/cm}^3 \quad [31] \\
 &= 7.9 \times 10^{-3} p^{1/2} \exp(-9600/RT) \text{ mL H STP/cm}^3
 \end{aligned}$$

where

$$\begin{aligned}
 p &= \text{hydrogen (H}_2\text{) pressure, N/m}^2, \\
 R &= 8314 \text{ J/kmol, } ^\circ\text{K, and} \\
 T &= \text{temperature, } ^\circ\text{K}.
 \end{aligned}$$

Concentrations are calculated for the test temperatures as

$$\begin{aligned}
 C_1(45^\circ\text{C}) &= 0.26 \text{ mL H STP/cm}^3 \\
 C_1(100^\circ\text{C}) &= 0.28 \text{ mL H STP/cm}^3 \\
 C_1(150^\circ\text{C}) &= 0.30 \text{ mL H STP/cm}^3
 \end{aligned} \tag{a3}$$

Using Eq a1, calculated values (a2) and (a3), and test times

$$\begin{aligned}
 t(45^\circ\text{C}) &= 90 \text{ h} = 3.24 \times 10^5 \text{ s} \\
 t(100^\circ\text{C}) &= 14 \text{ h} = 5.04 \times 10^4 \text{ s} \\
 t(150^\circ\text{C}) &= 6 \text{ h} = 2.16 \times 10^4 \text{ s}
 \end{aligned}$$

the maximum loss of hydrogen can be estimated as

$$Q'(45^{\circ}\text{C}) = 1.4 \times 10^{-3} \text{ mL H STP} = 0.0007 \text{ mL H}_2 \text{ STP}$$

$$Q'(100^{\circ}\text{C}) = 4.8 \times 10^{-3} \text{ mL H STP} = 0.0024 \text{ mL H}_2 \text{ STP}$$

$$Q'(150^{\circ}\text{C}) = 1.8 \times 10^{-2} \text{ mL H STP} = 0.009 \text{ mL H}_2 \text{ STP}$$

In each case, the anticipated loss of hydrogen through diffusion is less than the level of accuracy of the analytical equipment. Therefore, such losses are insignificantly small. It should be noted again that these estimates are extremely conservative and represent a worse than actual case for the test temperatures and times in use.

b. Estimate of Final Test Temperature and Time

The trigonometric series solution for an initial condition being a square wave (sorption method) [29] was used in conjunction with the Arrhenius equation for the diffusion coefficient to predict a new test time based on 45 and 100°C test data. The equation for absorption is written as

$$\bar{c} = c^* - c^* \frac{8}{\pi^2} \sum_{m=0}^{\infty} \frac{1}{(2m+1)^2} \exp[-D(2m+1)^2 \pi^2 t / l^2]$$

where

\bar{c} = concentration of diffusing species in the specimen at time, t ,
 c^* = equilibrium concentration of diffusing species, and
 l = thickness of specimen.

For desorption or degassing, which is the case here, this becomes

$$\bar{c} = c_m + (c_m - c^*) \frac{8}{\pi^2} \sum_{m=0}^{\infty} \frac{1}{(2m+1)^2} \exp[-D(2m+1)^2 \pi^2 t / l^2]$$

where

c_m = initial concentration of diffusing species.

Since $c^* \approx 0 \ll c_m$ and terms for $m > 0$ make a negligible contribution, this reduces to

$$\bar{c} = c_m \frac{8}{\pi^2} \exp\left[-\frac{\pi^2}{l^2} Dt\right] \quad (\text{b1})$$

This can be rewritten in terms of diffusible hydrogen values, H_D , as

$$c_m \propto H_{D\max} \quad \text{and} \quad \bar{c} \propto [H_{D\max} - H_D(t)]$$

$$H_{D\max} - H_D(t) = H_{D\max} \frac{8}{\pi^2} \exp\left[-\frac{\pi^2}{l^2} Dt\right]$$

$$D = -\frac{l^2}{\pi^2 t} \ln\left[\frac{\pi^2}{8} \frac{H_{D\max} - H_D(t)}{H_{D\max}}\right]$$

From Figure 4a for 711-2-28

$$T = 45^{\circ}\text{C}, H_{D\max} \approx 8.0 \text{ mL H}_2/100 \text{ g}$$

$$H_D(27 \text{ h}) = 6.2 \text{ mL H}_2/100 \text{ g}$$

$$D(45^\circ\text{C}) = 0.05 \frac{l^2}{\pi^2} \text{ h}^{-1}$$

Similarly from Fig. 4b for 711-2-33

$$T = 100^\circ\text{C}, H_{D\text{max}} \simeq 8.1 \text{ mL H}_2/100 \text{ g}$$

$$H_D(3.2 \text{ h}) = 6.2 \text{ mL H}_2/100 \text{ g}$$

$$D(100^\circ\text{C}) = 0.39 \frac{l^2}{\pi^2} \text{ h}^{-1}$$

The ratio of diffusion coefficients is therefore

$$\frac{D(100^\circ\text{C})}{D(45^\circ\text{C})} = 7.8$$

From the Arrhenius equation for a temperature dependent diffusion coefficient

$$D = D_0 \exp(-\Delta H_D/RT)$$

$$\frac{D(T_1)}{D(T_2)} = \frac{\exp(-\Delta H_D/RT_1)}{\exp(-\Delta H_D/RT_2)} = \exp\left[\frac{\Delta H_D}{R} \left[\frac{1}{T_2} - \frac{1}{T_1}\right]\right] \quad (\text{b2})$$

Substituting

$$\begin{aligned} \frac{D(100^\circ\text{C})}{D(45^\circ\text{C})} &= 7.8 = \exp\left[\frac{\Delta H_D}{R} \left(\frac{1}{318} - \frac{1}{373}\right)\right] \\ \frac{\Delta H_D}{R} &= \left(\frac{1}{318} - \frac{1}{373}\right)^{-1} \ln 7.8 = 4.43 \times 10^3 \text{ }^\circ\text{K} \end{aligned} \quad (\text{b3})$$

Figures 4b and 5a indicate degassing to be complete in approximately 20 h for 100°C test temperature. Now, it is necessary to find a value of temperature, T , for which

$$c(20 \text{ h}, 100^\circ\text{C}) = c(6 \text{ h}, T)$$

From Eq b1

$$\begin{aligned} \exp\left[-\frac{\pi^2}{l^2} D(100^\circ\text{C}) \cdot 20 \text{ h}\right] &= \exp\left[-\frac{\pi^2}{l^2} D(T) \cdot 6 \text{ h}\right] \\ \frac{D(100^\circ\text{C})}{D(T)} &= \frac{6}{20} = \exp\left[\frac{\Delta H_D}{R} \left(\frac{1}{T} - \frac{1}{373}\right)\right] \end{aligned}$$

From Eq b2

$$\frac{1}{T} = \frac{R}{\Delta H_D} \ln \frac{6}{20} + \frac{1}{373}$$

Substituting from Equation b3

$$\frac{1}{T} = (4.43 \times 10^3)^{-1} \ln \frac{6}{20} + \frac{1}{373}$$

$$T = 415^\circ\text{K} = 142^\circ\text{C}$$

Therefore, a test time of 6 h should be adequate for a test temperature of $\sim 142^\circ\text{C}$. Noting that this is a rough approximation, test temperature was selected at 150°C .

DATA							CALCULATIONS						
DATE	NO.	\bar{x}_1	\bar{x}_2	\bar{x}_3	$\bar{\bar{x}}$	R							
7/7	1	1.004	1.000	1.006	1.003	0.006	$\bar{\bar{R}} = \sum R \div n = 0.004$						
7/11	2	1.000	1.002	0.998	1.000	0.004	$UCL_R = D_4 \times \bar{\bar{R}} = 0.0103$						
7/12	3	0.998	1.000	0.997	0.998	0.003	$UWL_R = 2/3(D_4\bar{\bar{R}} - \bar{\bar{R}}) + \bar{\bar{R}}$						
7/12	4	1.002	0.996	1.002	1.000	0.006	$= 0.0082$						
7/17	5	0.998	0.997	0.995	0.996	0.003	$\bar{\bar{x}} = \sum \bar{x} \div n = 0.999$						
7/23	6	1.000	1.002	1.002	1.001	0.002	$CL_{\bar{x}} = A_2 \times \bar{\bar{x}} = 0.0041$						
7/23	7	0.999	0.996	1.001	0.999	0.005	$WL_{\bar{x}} = 2/3 \times CL_{\bar{x}} = 0.003$						
7/30	8	1.000	0.997	0.998	0.998	0.003	$UCL_{\bar{x}} = \bar{\bar{x}} + CL_{\bar{x}} = 1.003$						
7/30	9	1.000	0.999	0.997	0.999	0.003	$UWL_{\bar{x}} = \bar{\bar{x}} + WL_{\bar{x}} = 1.002$						
10/10	10	1.000	0.995	1.000	0.998	0.005	$LWL_{\bar{x}} = \bar{\bar{x}} - WL_{\bar{x}} = 0.996$						
							$LCL_{\bar{x}} = \bar{\bar{x}} - CL_{\bar{x}} = 0.995$						

Reference value = 1.000

$$\text{TOTALS } \sum \bar{x} = 9.992 \quad \sum R = 0.040$$

\bar{x} = OBSERVED VALUES R = LARGEST-SMALLEST

n = SETS OF VALUES UCL = UPPER CONTROL LIMIT

LCL = LOWER CONTROL UWL = UPPER WARNING LIMIT

LIMIT LWL = LOWER WARNING LIMIT

D_4 = 3.267 FOR $n'=2$: 2.575 FOR $n'=3$

A_2 = 1.880 FOR $n'=2$: 1.023 FOR $n'=3$

n = NUMBER OF VALUES IN THE SET

FIG. 7—Data and calculations for quality control charts.

APPENDIX 3

Statistical Computations

Quality Control Charts

In order to establish the reliability of the analytical method, quality control charts were developed for ten sets of triplicate determinations [28]. Data and calculations for upper and lower control limits and upper and lower warning limits are summarized in Fig. 7.

Quality control charts developed from these data illustrate the control and working limits relative to the test data (Fig. 8).

These charts are used when performing a standard determination. The standard gas mixture is analyzed in triplicate. If the average or range for the three determinations fall outside of the control limits, the analyses are repeated. If the average or range consistently fall outside of the control limits, it is an indication of an equipment malfunction or error in technique.

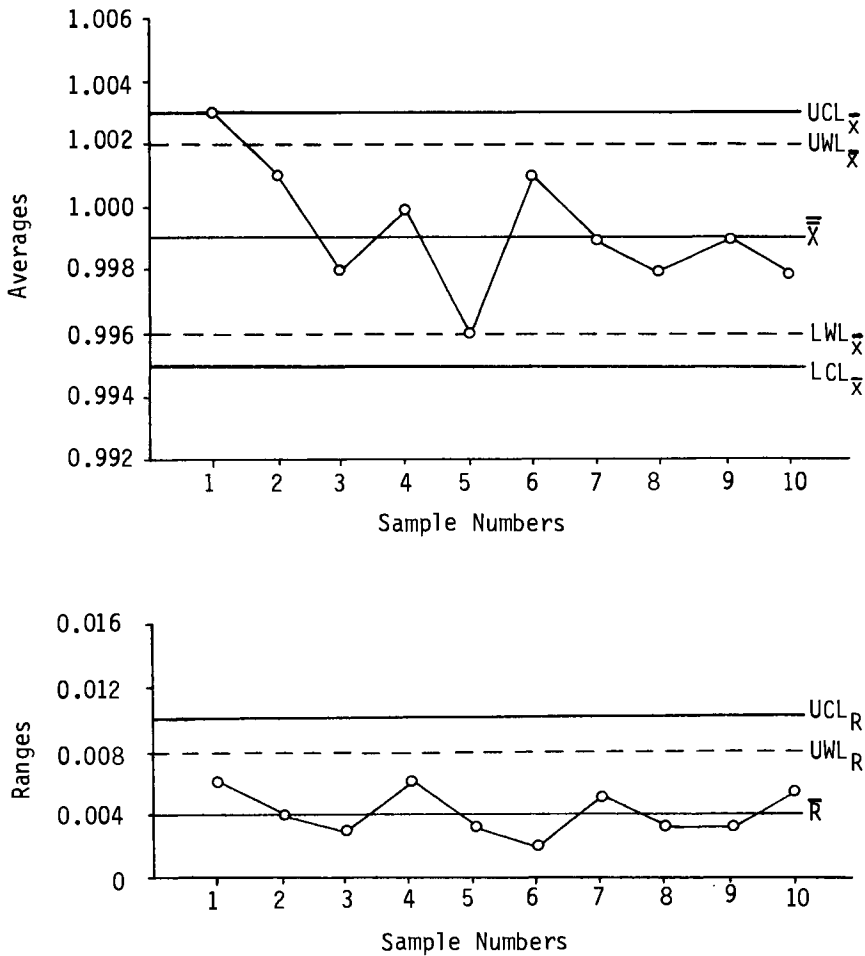


FIG. 8—Quality control charts.

References

- [1] Vialette, "Inspection of Welding Consumables as a Means of Controlling Hydrogen in Deposited Metal," *Current Solutions to Hydrogen Problems in Steels* (Proceedings of the First International Conference), Washington, DC, 1-5 Nov. 1982, American Society for Metals, Metals Park, OH.
- [2] IIW Commission II—Subcommission A, "Recommended Procedure for the Determination of Total Water Contents of Electrode Coatings by Combustion (Potential Hydrogen Contents)," Doc. IIS/IIW-314-68, International Institute of Welding.
- [3] Chew, "Hydrogen Control of Basic-Coated MMA Welding Electrodes—Part III: Relationship Between Coating Moisture and Weld Hydrogen," *Metal Construction*, Vol. 14, No. 7, July 1982.
- [4] Hirai, Minakawa, and Tsuboi, "Prediction of Diffusible Hydrogen Content in Deposited Metals with Basic Type Covered Electrodes," IIW Doc. II-929-80, International Institute of Welding.
- [5] Morton, Parker, and Jenkins, "Welding Institute Recommendations for the Measurement of Potential Hydrogen Levels and Weld Metal Hydrogen Levels in Fusion Welding," Research Report M/61/71, Welding Institute, Hilton Head Island, SC.
- [6] "The Determination of the Hydrogen Content of Ferritic Arc Weld Metal," Document No. II-959-81, International Institute of Welding.
- [7] "Method for Measurement of Hydrogen Evolved from Deposited Metal," Japanese Standard JISZ3113.
- [8] "Military Specification, Electrodes—Welding, Flux-Cored, General Specification for," MIL-S-24403A, dated 12 Dec. 1981.
- [9] Ball, Gestal, and Nippes, "Determination of Diffusible Hydrogen in Weldments by the RPI Silicone-Oil Extraction Method," *Welding Journal*, Vol. 60, No. 3, 1981, pp. 51s-56s.
- [10] Shutt and Fink, "New Considerations for the Measurement and Understanding of Diffusible Hydrogen in Weld Metal," *Welding Journal*, Vol. 64, No. 1, 1985, pp. 19-28.
- [11] Fabling and Chew, "The Performance of Collecting Fluids in Diffusible Hydrogen Analysis," *Welding Research International*, Vol. 3, No. 4, 1973.
- [12] Quintana, "A Critical Evaluation of the Glycerin Test," *Welding Journal*, Vol. 63, No. 5, 1984, pp. 141s-149s.
- [13] Kotecki and LaFave, "AWS A5 Studies of Weld Metal Diffusible Hydrogen," *Welding Journal*, Vol. 64, No. 3, 1985, pp. 31-37.
- [14] Kapinos, et al, "Analysis of the Gas Collected by the Glycerin Method in Investigations into Joints Made with Cellulose Electrodes," *Svar. Proiz.*, 1974, No. 9, pp. 36.
- [15] Tarlinskii, Blekherova, and Kapinos, "Determination of the Fraction of Diffusible Hydrogen in the Composition of the Gas Generated in Welding Cellulose Electrodes," *Svar. Proiz.*, 1978, No. 11, pp. 13-14.
- [16] Schmid and Rodabaugh, "A Water Displacement Method for Measuring Diffusible Hydrogen in Welds," *Welding Journal*, Vol. 59, No. 8, 1980, pp. 217s-225s.
- [17] "Method for Measurement of Hydrogen Evolved from Gas Shielded Arc Welds—Draft JIS Standard," IIW Doc. II-A-567-82, Subcommittee No. 2, Technical Committee, Welding Rod Division, Japan Welding Engineering Society.
- [18] Feichtinger and Marincek, "A Contribution to Behavior and Determination of Hydrogen During and After Welding," *Welding Research International*, Vol. 6, No. 3, 1976.
- [19] Jenkins and Coe, "Hydrogen Analysis at BWRA, Part 3," *BWRA Bulletin*, 1966.
- [20] *Physical Properties of Glycerine and Its Solutions*, Glycerine Producer's Association, New York.
- [21] *International Critical Tables*, National Research Council of U.S., National Academy of Sciences, 1926.
- [22] "Standard Methods for Determination of the Diffusible Hydrogen Content of Martensitic, Bainitic, and Ferritic Weld Metal Produced by Arc Welding," Standard AWS A4.3-86, American Welding Society, Miami, FL.
- [23] Thompson, *Fundamentals of Gas Analysis by Gas Chromatography*, Varian Associates, Walnut Creek, CA, 1977.
- [24] Conn and Stumpf, *Outlines of Biochemistry*, 3rd ed., Appendix 2, John Wiley and Sons, New York, 1972.
- [25] *Operation Manual, Hewlett Packard Reporting Integrator 3390A*, July 1982, 03390-90050, pp. 52.
- [26] "Military Specification, Electrodes and Rods-Welding, Bare, Solid, or Alloyed Cored, Low Alloy Steel," MIL-E-23765/2B, 9 Feb. 1981.
- [27] "Military Specification, Electrodes-Welding, Mineral Covered, Iron-Powder, Low Hydrogen Medium, High Tensile and Higher-Strength Low Alloy Steels," MIL-E-22200/10A, Rev. A., 8 July 1983.
- [28] *Handbook for Analytical Control in Water and Waste Water Laboratories*, EPA-600/4-79-019. U. S. Environmental Protection Agency, Office of Research and Development, Washington, DC, March 1979.
- [29] Crank, *The Mathematics of Diffusion*, 2nd ed., Chapters 4 and 5, Oxford University Press, New York, 1979.

- [30] Quick and Johnson, "Permeation and Diffusion of Hydrogen and Deuterium in 310 Stainless Steel, 472K to 779K," *Metallurgical Transactions A.*, Vol. 10A, January 1979, pp. 67-70.
- [31] Nelson and Stein, "Gas Phase Hydrogen Permeation through Alpha Iron, 4130 Steel, and 304 Stainless Steel from Less than 100°C to near 600°C," NASA Technical Note, NASA TN D-7265, NASA, Washington, DC, April 1973.
- [32] *Handbook of Chemistry and Physics*, 49th Edition, CRC Press, Boca Raton, FL, 1969.
- [33] Dowdy and Wearden, *Statistics for Research*, John Wiley and Sons, New York, 1983.
- [34] Evans and Baach, *Hydrogen in Weld Metal—Reprints from Schweissmitteilungen*, Welding Industries Oerlikon Bühle Ltd., Zurich, Switzerland, pp. 4-14.

Panel Discussion: Gas Chromatography¹

This panel discussion was held to discuss the content of papers reproduced in this section on gas chromatography. The discussion is presented in its original form and was not peer reviewed.

The moderator was C. G. Interrante, National Bureau of Standards, Washington, DC. Panel members were Francois Faure, FRAMATOME, Paris; K. A. Lyttle, Union Carbide Corp., Ashtabula, OH; M. A. Quintana, General Dynamics, Groton, CT; Thomas A. Siewert, National Bureau of Standards, Boulder, CO; Richard Wong, David Taylor Naval Ship R & D Center, Annapolis, MD; and Dawn White, U.S. Army Construction Engineering, Champaign, IL.

Participants were W. Chionis, Parker Hannifin Corp., Irvine, CA; V. S. Agarwala, Naval Air Development Center, Warminster, PA; David Berman, Naval Air Development Center, Warminster, PA; Rudy Frizioni, LECO Corp., St. Joseph, MI; Carl Sonnino, Emerson Electric, St. Louis, MO; Alan Grobin, IBM, Poughkeepsie, NY; T. Ohtsubo, Nippon Steel, Japan; Adri Mackor, TNO Zeist, Netherlands; and Mr. Worth, Armament R & D Center.

Sonnino: After you have evolved the hydrogen or gases in your test cylinder, do you cool the cylinder, or what is the temperature that you have when you extract the gas for the gas chromatography?

Quintana: We do cool the cylinder down, primarily just to ease handling. It is hard to handle something that is 150°C. It is about room temperature when we do the analysis.

Grobin: This is a nontechnical question. It is procedural. Some of this work was done with the American Welding Society. Where will these test methods eventually end up? As American Welding Society Methods or as ASTM Methods?

Quintana: Right now it is an AWS standard test method. Gas chromatography is not new. I have simply presented one application of that analytical technique. LECO right now, I believe, is marketing test equipment that will do essentially the same thing and that also is acceptable within the AWS standard guidelines. There is another unit marketed through Oerlikon in Switzerland, which is basically a Japanese development. I think it was developed at Kobe Steel. This also satisfies the AWS guidelines. Earl Pickering at Combustion Engineering is currently using that and I think Joe Blackburn at Annapolis (DTNSRDC).

Nippon Steel several years ago developed a similar method, which would also fit the guidelines. The important point is that your analytical method be accurate. You have to be able to verify your test results. What is really important is the standardization of the specimen size and preparation.

Grobin: It sounds like we really have an AWS guideline. Do we want to take this up as an ASTM standardization test method and carry it up one step further in the standardization process?

Fricioni: First of all, if it is going to come under ASTM, we have to find out whose jurisdiction it comes under. Total hydrogen in metals is coming under the jurisdiction of E03. Whether this comes under the jurisdiction of F07, we will have to have it defined, the actual determination of hydrogen. I think we are dealing with something different here. We are determining hydrogen in metals, but it would fall in there because of the weld.

¹This section represents the interaction of the presenters and the participants in response to the technical content of the various papers. The sessions were taped and written copies of the discussions sent to each participant for comments and/or corrections. It is hoped that by including these sections, the reader will be able to better understand the controversial aspects of these presentations.

Quintana: Yes, the application is strictly weld metal, and that is something that is new to ASTM as I understand, and I am not sure, administratively, that has all been worked out yet.

Fricioni: Dr. Ohtsubo from Nippon Steel has done some of the work. We have a device of his that has twelve chambers, and it automatically goes in and samples, and you can vary the temperature. We also have the second unit that you can ramp the temperature. You can look at the hydrogen at 300 or 400 on up into 600°F, so when you are looking at techniques, you may be looking at one that you can get the total diffusible hydrogen. The last comment is on your moisture and most of the fellas are saying if you do not take off this loosely bound water, your results are very erratic because you cannot control that amount. If it is water that is tightly bound within the electrode, then I think you start more correlation on that. You have to go back and look at your water determinations. One would not normally subject these electrodes to wet conditions under normal operations.

Ohtsubo: We have been using this technique a couple of years. We fully agree with the previous two presentations. I agree with you 99%, but I have minor comments for the remaining 1%. Regarding the accuracy of the mercury method, when we measure the very low content of hydrogen by the mercury method, we do not get reproducible results. It is said that the hydrogen does not have any solubility in mercury, but the hydrogen is evolved in very fine bubbles and they do not merge with each other making a larger bubble, which can flow up to the surface. The hydrogen stays as a very small bubble, so we cannot measure the volume of the very small content of hydrogen when using mercury.

Interrante: Let me understand that. Would your comment be that hydrogen goes into the mercury, but it cannot rise to the top of the eudiometer?

Quintana: Yes, it cannot completely float up. The bubble remains suspended at low levels.

Ohtsubo: According to your results, you showed only the results to 4 mL per 100 g. Right?

Interrante: To what level? Four ppm. I thought Siewert also had two data points of 11 and 12 ppm. Most of the results were in the range that you stated, four down to two, or less than two, but he had two points in the range of 11 to 12 ppm.

Ohtsubo: When we test around 2 mL, we do not get any reproducible results by the mercury method. This is number 1.

Interrante: You get a lot of scatter.

Ohtsubo: Number 2, you suggested calibration gas by injection to a column directly, but we have a slight difference between the result obtained when you inject into a column directly and that obtained by introducing calibration gas to the collection cell which will be used for the measurement of the test sample because the shape of the peak of the gas chromatograph is different because of the effect of the cell volume.

Quintana: That is why I use an internal standard. That is what the helium is for. Helium is an internal standard. I add helium both to my standard gas mixture, the thing I am going to use to calibrate, and to every test chamber before I put them in the oven, and that compensates for the slight variation in volume from one chamber to another. The computer processor corrects itself. It takes the ratio of the helium peak intensities as a correction factor and applies that to the hydrogen peak ratio. You do the same thing with a strip chart if you do it by hand.

Ohtsubo: I understand. Thank you.

Interrante: Yes, you have another question?

Mackor: I happen to have looked into this question of solubility of hydrogen in various solvents. This solubility decreases when you go from nonpolar to polar solvents. This was published a long time ago in Landolt-Börnstein's physicochemical data. Furthermore, when I think about the release of hydrogen from a weldment, I expect that primarily the hydrogen does not come off as bubbles, but just dissolves in the mercury, because there is local production of hydrogen all over the weldment surface. There are several factors involved. There is the solubility of hydrogen in mercury. This is not the same as the rate of solution. If you presaturate your solution with hydrogen, you may have difficulties in reaching an equilibrium state. It may take days, for instance, to completely saturate your system.

Interrante: You are saying that the process of getting to the saturation point may be extremely slow?

Mackor: Yes. I think it is very difficult to get a completely saturated solution when starting with hydrogen-free mercury and bubbling hydrogen gas through it. There is, of course, some solubility. The second point is that if you release hydrogen molecules from the weldment, you probably end up with a super-saturated solution of hydrogen in mercury and do not get thermodynamic equilibrium. It is probably very difficult by the very nature of the method to get reproducible results, especially if you say low hydrogen concentration. Even in mercury I would expect too little hydrogen coming off. This is what Mr. Ohtsubo settled, probably, and I can completely understand that. So the mercury stays (super) saturated with hydrogen.

Interrante: On the bubble point that you mention, the bubbles actually form on the surface of the specimen before they become big enough to leave the specimen, which sort of indicates that what is happening is hydrogen is leaving the sample and finally becomes an adsorbate, and two of these adsorbates become combined to form H_2 (gaseous hydrogen), and when enough H_2 s cluster to form a large enough bubble for escape through the medium, depending on the density of the medium, the bubble finally then raises up.

Mackor: That is what you see with the naked eye, but at the same time at the places where you do not evolve bubbles at the surface, I am sure you are dissolving the hydrogen locally directly into the mercury. That is unavoidable. Both processes occur at the same time.

Quintana: I think you are right, and I think it is more pronounced when you look at the glycerine and the silicone oil tests, because I do not know whether anyone noticed, but the silicone oil test is run at $100^\circ C$, and supposedly it only takes 2 h. After 2 h, you do not see any more bubbles. But, when you run the same test in a closed chamber in a gas system, it takes 20 h at that temperature. What is happening after 2 h is the gas is not coming off fast enough to make a bubble anymore. It is going into solution.

Interrante: That is true, but another point that might contribute is that the rate of transfer might be encouraged by the alternative medium to the air or argon or whatever. In other words, the solid/liquid transfer might be accelerated compared with the transfer of solid to gas. Having the liquid there may accelerate the surface processes and get rid of the hydrogen on the surface and thereby encourage outgassing more quickly. I am not saying that is the case.

Mackor: We observed that also. That is why we use glycerine as a medium in between the metal sample which we investigate and hydrogen sample.

Interrante: To accelerate the process?

Mackor: I think that is one of the major factors involved. I have finally a suggestion to make. If somebody could add something to the glycerine in order to make it a more polar solvent, something which does not corrode the steel, then you would probably have a better technique.

Interrante: We have one more question before we will have to stop the questions.

Worth: Ms. Quintana, my one thought when you were going over your outgassing procedure in this chamber, after you purged the chamber with the air and then you filled it with argon, whatever gases you were using. Then if you were to evacuate the system partially, my thought is maybe you are looking for a shorter time to reach these higher levels of hydrogen and you had maybe a smaller partial pressure, my idea is a smaller partial pressure of these inert gases during the bakeout, and then later on going back and backfilling with inert gas. Have you tried anything like that, or have you found a shorter time?

Quintana: I tried that in the initial phases of this program. We tried degassing at a variety of pressures and one of those was a slight negative pressure, and it did not affect total test time. What it did do was complicate our analysis because we did not have as much gas to analyze. As I say, we take repeated samples out and inject them, so it helps to have more gas. Unfortunately, at the time we started, these pieces of equipment that are on the market now were not available.

Interrante: We have a final burning question that has to finish it off.

Agarwala: I think I can answer this problem. The way I can is if you put a sample in a vacuum chamber and try to degas it at room temperature or a little higher, you can obtain the same

efficiency of taking the hydrogen out of the steel, so putting lots of pressure will not help in any way in getting more out of it. That is the whole objective here. The question which I had for Ms. Quintana is: You do clean the surface of the weld specimen? Right?

Quintana: Yes.

Agarwala: That is the standard procedure, I believe.

Quintana: The general procedure for the specimen preparation: If you clamp the run-on, the center piece, the run-off together in the fixture which you saw in the previous paper, you deposit a weld bead. Immediately after extinguishing the arc, you remove that three-piece unit from the fixture and you quench it in ice water. You then place it in a low-temperature bath. Typically, what I have been using is acetone and dry ice. After it has been in the low-temperature bath for 10 or 15 min and is now cold, then I take it out, clean it, power wire brush it, break off the starts and stops, and put it back in there until I am ready to test it. When I get ready to test it, I remove it from that low-temperature bath, wash it down in acetone to remove any frost and any residual moisture on the surface, put it into the chamber, and then purge. Does that answer your question?

Agarwala: The following question, which I had was: You came to 100% estimation of hydrogen by limiting the temperature to 150°C, which was about 7 h of time?

Quintana: Six.

Agarwala: I was wondering what the limitation was? Why couldn't you go to the higher temperature and have achieved the objective in a shorter time? As Dr. Berman said yesterday morning, baking out hydrogen is very difficult. We have the MIL specs that tells us to use 3 to 4 h, and he has convinced almost everybody that it does not happen. We don't bake it out. We are talking about low hydrogen. What I am saying, we will remove hydrogen even at room temperature if given enough time.

Quintana: Given enough time, yes.

Agarwala: But when you are talking about a couple of hours or a half an hour, can we do that at 200°C? Did you look at the prospect of it?

Quintana: No, I did not, because my test chamber cannot withstand those temperatures, but LECO and Nippon Steel have done some work at the higher temperatures. Also, I have a rubber septum, which I pierce, and that also limits temperature. I can only go to 300°F and I am right about at the limit for that.

Agarwala: Gas chromatography would probably be a good technique to study that, but I wish we could do it more expeditiously.

Interrante: As a closing remark on that same theme, I would like to ask whether or not the experts feel that, once you have established the specimen shape and the temperature at which you intend to do the extraction, would not a mathematical formulation of the rate at which you approach the asymptote be usable to permit you to use a test in 2 h even though it would normally take 6 h to extract enough. Would 2 h establish the curve for you in a way so you could mathematically predict the end result? Can you do that, Dr. Faure?

Faure: It all depends on what you really want to measure. When doing practical work in welding we differentiate between "diffusible" and "total" hydrogen. That is why the IIW procedure originally recommended diffusible hydrogen collection at a temperature of 20°C, which was then raised to about 50°C. I was concerned when it was said that hydrogen could be collected at 150°C because at that temperature one would also extract part of the trapped hydrogen, but not all. Other procedures are used extensively for measuring total hydrogen, either by completely fusing the sample, and there are a number of apparatus for that, or doing vacuum hot extraction for example at 600°C for ferritic welds or 900°C for austenitic welds. Extraction temperature should be selected depending on the material. If you have strong trapping effects, you may not be measuring the same thing by doing extraction at 40, 150, or at 600°C.

Interrante: In that sense, what he is talking about from a practical point of view is that he believes that hydrogen that is trapped at the lower temperature may never be released at room temperature. You could perhaps argue that, with time, it may become significant, or, with

stress and a triaxial site near that trapped hydrogen, the difference in chemical potential between the low chemical potential at the triaxial stress site and the high chemical potential of the trapped hydrogen may establish enough of a potential difference for the driving force to push you there. I would guess that you could have people argue with you on what is an appropriate temperature, but it is a point that is well taken nevertheless. You should really fix the temperature and, having fixed it, live with it, but realize that you are maybe looking at a different phenomena depending upon the temperature at which you are doing the extraction.

The Effect of Weld Metal Diffusible Hydrogen on the Cracking Susceptibility of HY-80 Steel

REFERENCE: Wong, R. J., "The Effect of Weld Metal Diffusible Hydrogen on the Cracking Susceptibility of HY-80 Steel," *Hydrogen Embrittlement: Prevention and Control*, ASTM STP 962, L. Raymond, Ed., American Society for Testing and Materials, Philadelphia, 1988, pp. 274-286.

ABSTRACT: An investigation was conducted to characterize the influence of welding variables, such as weld metal diffusible hydrogen content, on the hydrogen cracking resistance of HY-80 steel. The moisture pickup characteristics of several shielded metal-arc welding products were measured by the standard combustion technique. The weld metal diffusible hydrogen level corresponding to the electrode coating moisture was measured by gas chromatography.

Implant weldability tests were performed to quantify the cracking resistance of HY-80 steel under different combinations of weld metal diffusible hydrogen level and welding preheat/interpass temperature. Implant lower critical stress values were found to increase with a decrease in weld metal diffusible hydrogen content.

Self-restrained weldability tests (rigidly restrained cracking specimens) were performed at selected conditions determined on the basis of implant testing. The dimensions of rigidly restrained cracking specimens were varied between different tests in order to produce restraint levels that would result in cracking or no cracking situations based on implant lower critical stress values. The results of rigidly restrained cracking tests at reduced preheat temperatures (that is, 0° and 16°C) agreed with anticipated critical stress levels required for cracking as determined by implant lower critical stress values.

KEY WORDS: hydrogen cracking, weldability, weld metal diffusible hydrogen, implant test, welding

Hydrogen cracking in weldments is an insidious problem which may not manifest itself until days after welding is completed. Costly fabrication controls such as minimum welding preheat and interpass temperature, postweld thermal soak, and stringent electrode handling requirements may be imposed in order to avoid hydrogen cracking. This problem is typically more serious with higher strength steels such as the quenched and tempered steels which are often used for high-strength/high-toughness applications.

HY-80 steel is a quenched and tempered high-strength steel (551 MPa yield strength) used in naval ship construction [1]. Most high-strength steels, including HY-80, typically experience hydrogen cracking in the heat affected zone (HAZ). The hardness of the HAZ is often a good indication of the material's resistance to hydrogen cracking. The chemical composition of the base plate strongly influences the HAZ hardness and the options available to improve weldability. For example, Graville and other investigators [2-4] have categorized steels into different groups depending on their carbon and calculated carbon equivalent value. The three regions shown in Fig. 1 exhibit significantly different hardenability curves (Fig. 2). For example, Zone I

¹Metallurgist, David Taylor Naval Ship Research and Development Center, Annapolis, MD 21402-5067.

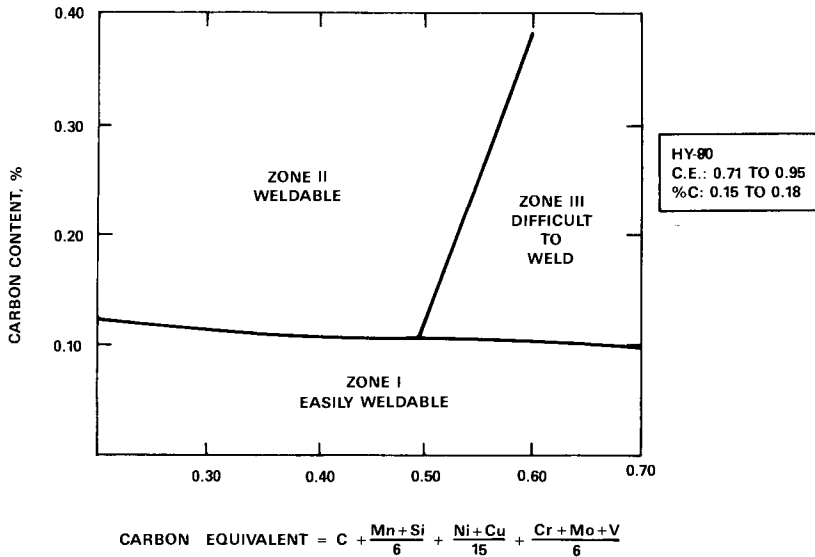


FIG. 1—Carbon-carbon equivalent diagram (from Ref 2).

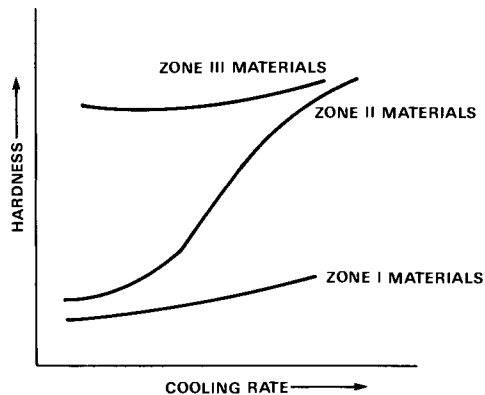


FIG. 2—Hardenability curves for Zone I, II, and III materials.

materials are low-carbon steels which exhibit a rather flat hardenability curve. Consequently, they do not exhibit hard HAZ microstructures with the cooling rates typically experienced during welding. These materials, therefore, exhibit the best resistance to hydrogen cracking in the HAZ. In this situation the weld metal may be the controlling factor in the prevention of hydrogen cracking. The Zone II materials exhibit a steep hardenability curve, and the HAZ hardness can be significantly affected by the range of cooling rates which arise from differences in welding condition. For these materials, hydrogen cracking resistance can be controlled in part by controlling the hardness of the HAZ through the use of appropriate welding parameters (for example, preheat and heat input). HY-80 steel falls into the Zone III region. Characteristic of Zone III materials are moderately high carbon and carbon equivalent values which result in

hard HAZ microstructures during welding. Consequently, HAZ hardness control would not be the primary method to control hydrogen cracking in HY-80 steel.

Analysis of the weldability of HY-80 steel at different preheat/interpass temperatures is therefore reduced to the interdependence between the amount of stress present and the level of hydrogen in the weld. The level of hydrogen in the weld is controlled by the initial amount introduced and the welding interpass temperature, which governs diffusion of hydrogen out of the weld described by Fick's second law [5].

Procedure

In order to provide for a range of weld metal diffusible hydrogen (H_D) levels, shielded metal-arc welding electrodes were used immediately after removal from a preheated holding oven and after exposure in an 80% relative humidity, 27°C environmental chamber for up to 9 h. The three electrodes employed in this investigation included an older MIL-11018 product, a currently available moisture-resistant MIL-11018M product, and a recently developed moisture-resistant MIL-10018M1 product. Moisture pickup characteristics of the electrode coatings were measured by the standard combustion technique [6], with additional procedural controls to minimize moisture loss prior to moisture testing. The gas chromatography technique was employed with the procedures described in Ref 7 to measure the weld metal diffusible hydrogen content of deposited metal after electrode exposure. The specimen blanks used for H_D determination were 40 mm long instead of the 80-mm specimen prescribed in Ref 7 in order to facilitate use of existing equipment.

The hydrogen cracking resistance of HY-80 steel at different H_D levels and preheat/interpass temperatures was measured by a modified implant test, shown schematically in Fig. 3. The test involves inserting (or implanting) the implant specimen through a hole in a 25-mm-thick welding pad (support plate) flush with the top surface of the pad. A 1.8 MJ/m heat input welding bead is then deposited on the welding pad, which fuses the specimen to the welding pad. The welding bead also creates a HAZ in the specimen and introduces a level of hydrogen correspond-

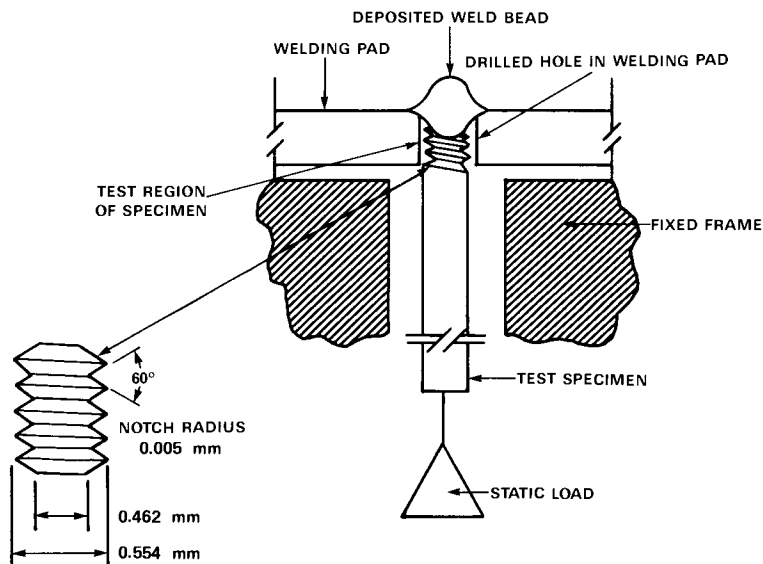


FIG. 3—Schematic illustration of the implant test.

ing to the electrode and electrode exposure condition. The implant specimen is then statically loaded approximately 2 min after welding to a desired stress. If the specimen fractures within 1000 min, the time interval between loading and fracture is recorded by a clock monitoring the test. By conducting this test at different stress levels, one can determine a threshold stress below which fracture does not occur. This value is called the lower critical stress (LCS). The LCS value can be treated as a quantitative measure of the cracking susceptibility. The results of an implant test series can be represented on a graph of applied stress versus time to failure. The LCS value is identified as the highest stress at which failure did not occur.

Welding conditions characterized by implant testing included a low, moderate, and high (that is, 0°, 16°, 52°C) preheat and interpass temperature and various H_D conditions.

The rigidly restrained cracking (RRC) test (Fig. 4) was performed under selected implant test welding conditions in order to correlate implant LCS values with results from a self-restrained weldability test (that is, RRC). The RRC test simulates a butt welding application for a structure in which the development of welding stresses is controlled in part by restraint imposed by the structure being welded. Previous investigators [8,9] have determined that the intensity of restraint (R) developed in an RRC test is proportional to the thickness of the plates (t) and inversely proportional to the unrestrained length of the specimen (L) as described by Eq 1

$$R = \frac{Et}{L} \quad (1)$$

where

E = Young's modulus,

t = thickness of specimen, and

L = unrestrained length (Fig. 4).

For welding stresses (σ) in the elastic region, the average stress is directly proportional to the intensity of restraint (R). The proportionality constant, m , has been found to lie between 0.045 and 0.050 for a variety of steels [8,9]. The resulting average stress (σ) in the RRC specimen can therefore be approximated by Eq 2

$$\sigma = mR \quad (2)$$

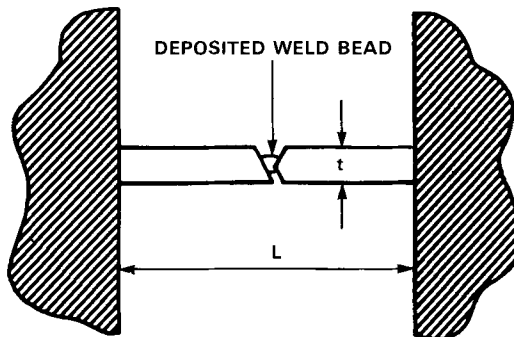


FIG. 4—The rigidly restrained cracking test.

where

- σ = average stress,
- m = proportionality constant (≈ 0.045), and
- R = intensity of restraint.

The RRC specimens evaluated in this study were produced from 1-in.-thick HY-80 steel plate, 6 in. wide and 4 ft long. A portion of each specimen was fillet welded to a 2-in.-thick backing plate. The portion of the specimen not welded to the plate was denoted as the unrestrained gage length L . The welding conditions for the RRC tests consisted of using the MIL-10018M1 electrode after 5 h exposure to 80% relative humidity at 27°C. The tests were performed at three preheat/interpass temperatures: 0°, 16°, and 52°C. The gage length L was different in some of the individual tests in order to change the intensity of restraint. Calculated average stress values from RRC specimens were compared to implant LCS values under similar welding conditions. If the calculated stress in the RRC specimen was above the measured implant LCS value for that condition, cracking in the RRC specimen was expected. Conversely, if the calculated stress in the RRC specimen was below the measured implant LCS value no cracking in the RRC specimen was anticipated.

Experimental Work

Moisture and Hydrogen Analysis

The electrode coating moisture levels of the three electrode products are plotted as a function of exposure time to 80% relative humidity at 27°C in Fig. 5. The older MIL-11018 electrode displayed consistently higher electrode coating moisture values than the other products after identical exposure time. The MIL-11018M and MIL-10018M1 electrodes exhibited similar moisture pickup characteristics.

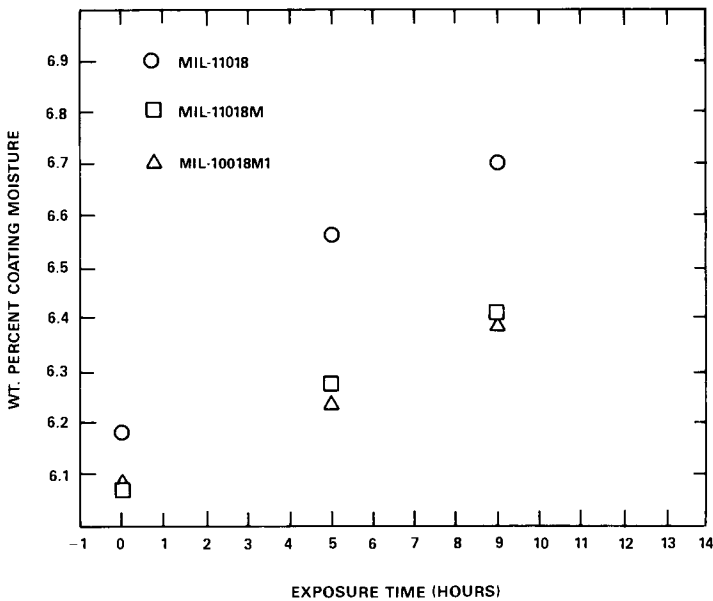


FIG. 5—Moisture pickup characteristics of MIL-11018, MIL-11018M, and MIL-10018M1 electrodes.

Weld metal diffusible hydrogen measurements performed on these electrode products after the 0, 5, and 9-h exposure times indicated an approximately linear increase in H_D with increase in electrode coating moisture. Linear regression analysis of the coating moisture level and corresponding H_D content shown in Fig. 6 yielded the relationship given by Eq 3 with a coefficient of correlation = 0.96

$$H_D = 13.8M + 3.5 \quad (3)$$

where

H_D = deposited weld metal diffusible hydrogen content in mL/100 g as measured by gas chromatography, and

M = electrode coating moisture in weight percent.

Implant Tests

The results of implant testing shown in Fig. 7 indicated that HY-80 steel is somewhat susceptible to hydrogen cracking even with a standard 52°C preheat and interpass temperature when the stress is high enough, even at minimum hydrogen levels. Less stress is required for cracking at higher hydrogen levels (for example, MIL-11018 with 5-h electrode exposure, Fig. 7). At lower preheat temperatures such as 0°C, implant data in Fig. 8 show there was an overall decrease in hydrogen cracking resistance, as indicated by a downward shift in LCS values. Some improvement in cracking resistance was observed when the electrode exposure time was reduced from 9 to 0 h, or when a more moisture-resistant electrode product was used. For example, after the MIL-11018M product was exposed for 5 h, it contained 7.4 mL/100 g of diffusible hydrogen, which corresponded to an LCS value of 290 MPa (Fig. 8). The MIL-10018M1 electrode required a 9-h exposure to reach this hydrogen level and corresponding LCS value as shown in Fig. 9. A slight improvement in LCS value was also observed when the preheat and interpass temperature was increased from 0°C (Fig. 9) to 16°C (Fig. 10).

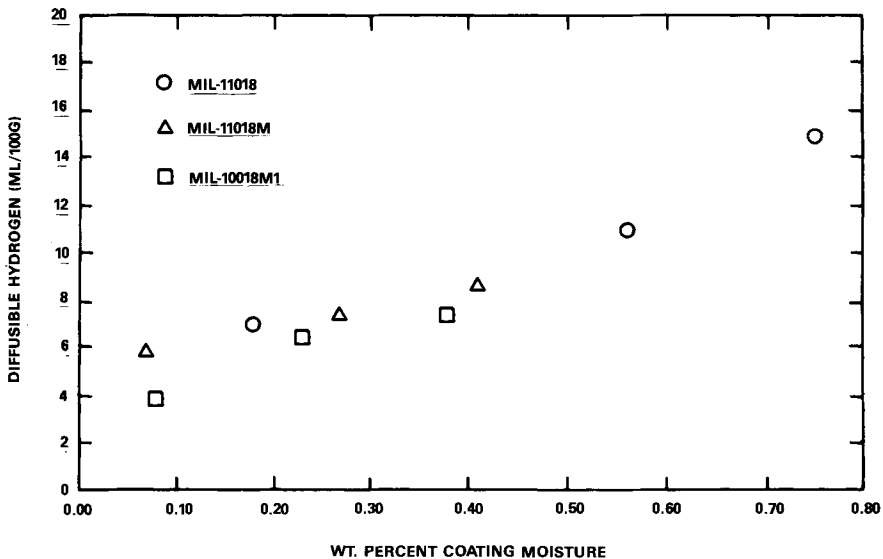


FIG. 6—Electrode coating moisture versus weld metal diffusible hydrogen.

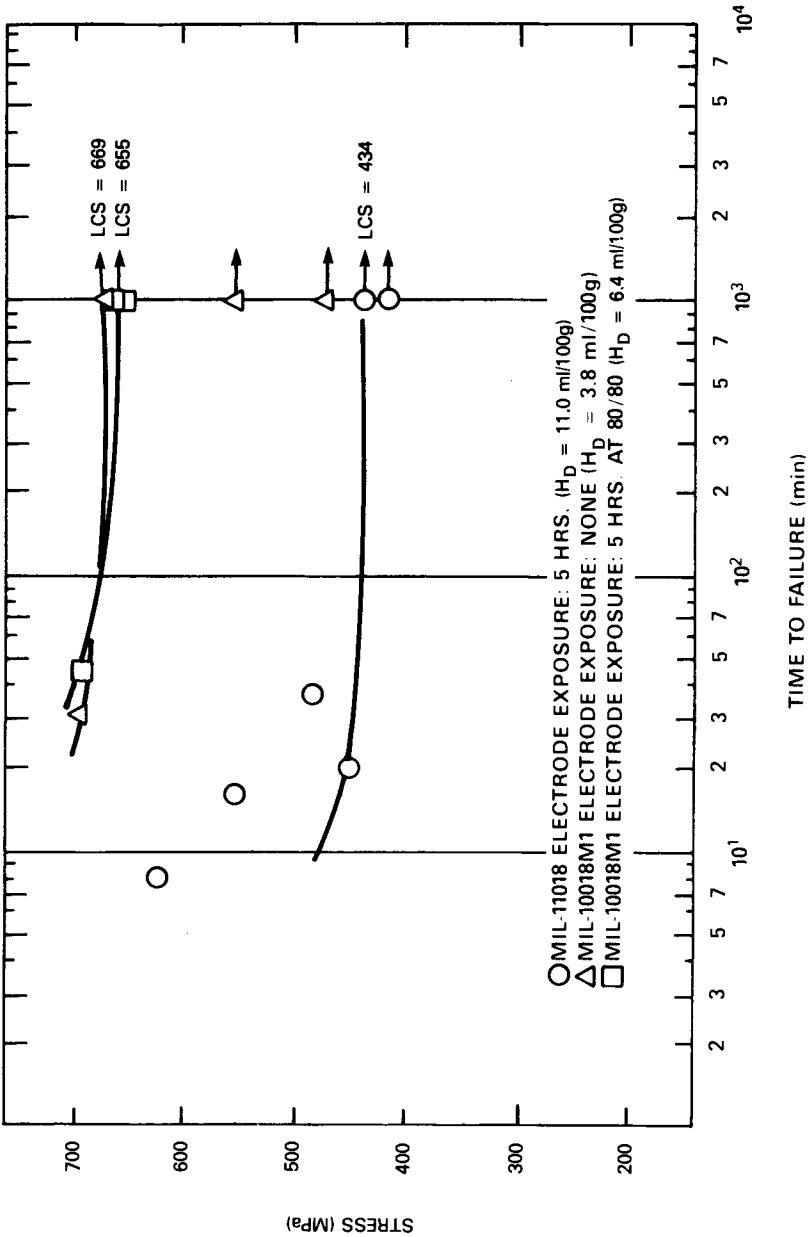


FIG. 7—Implant test results with MIL-11018 and MIL-10018M1 electrodes, 52°C preheat and interpass temperature.

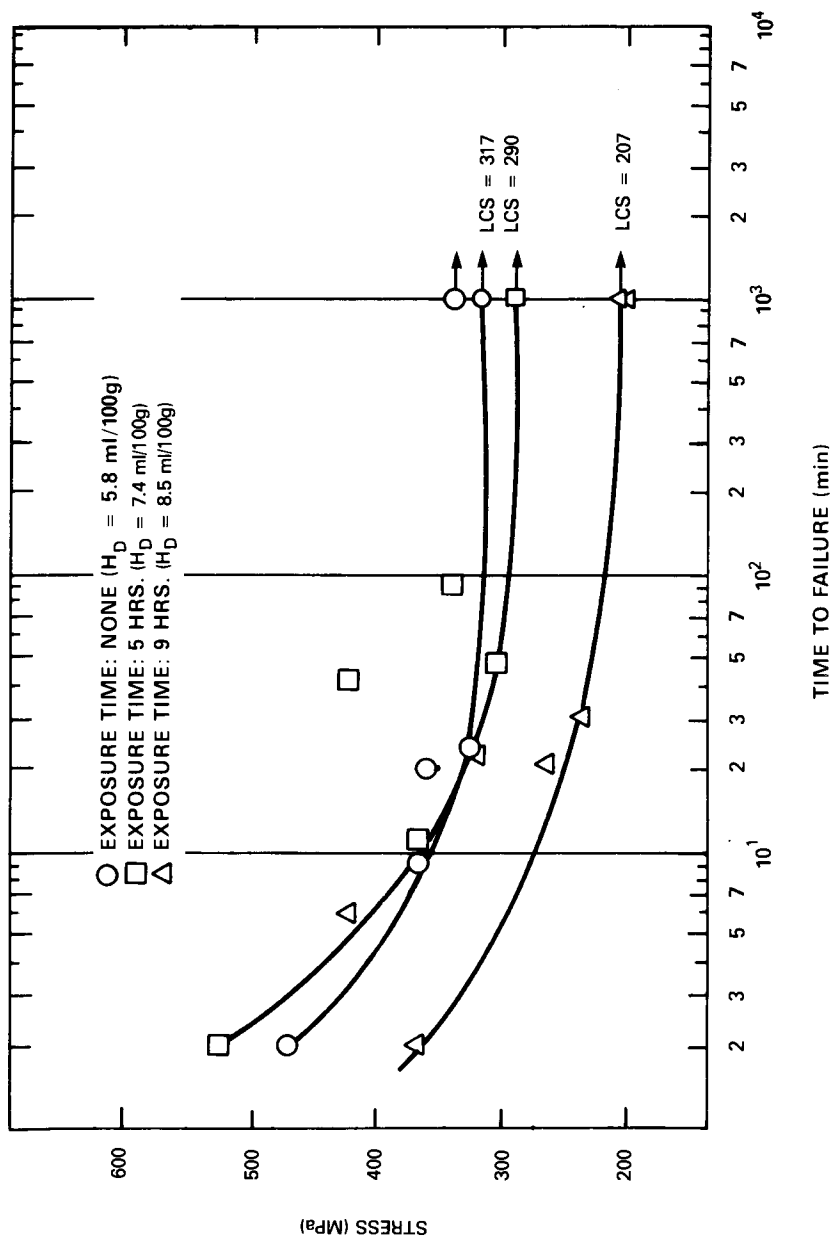


FIG. 8—Implant test results of MIL-11018M electrode under simulated 0°C conditions.

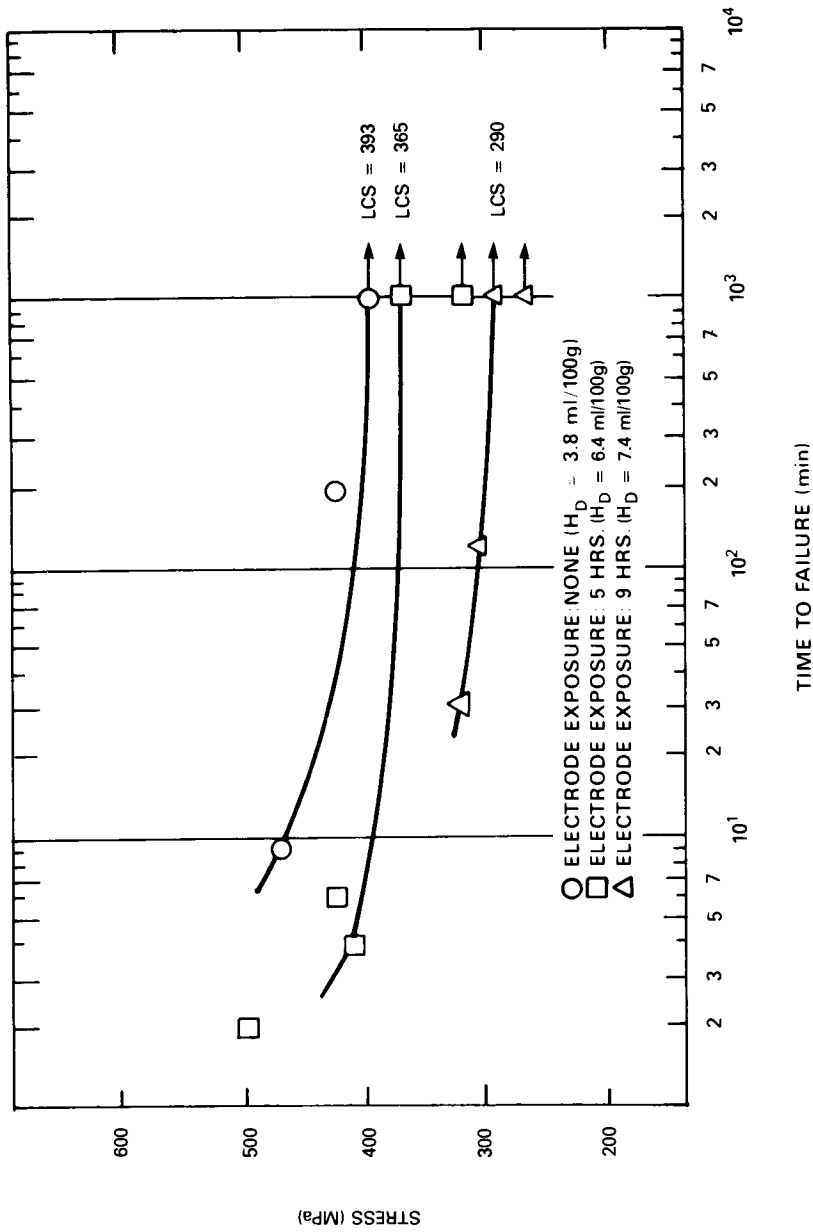


FIG. 9—Implant test results with MIL-10018M1 electrode under simulated 0°C conditions.

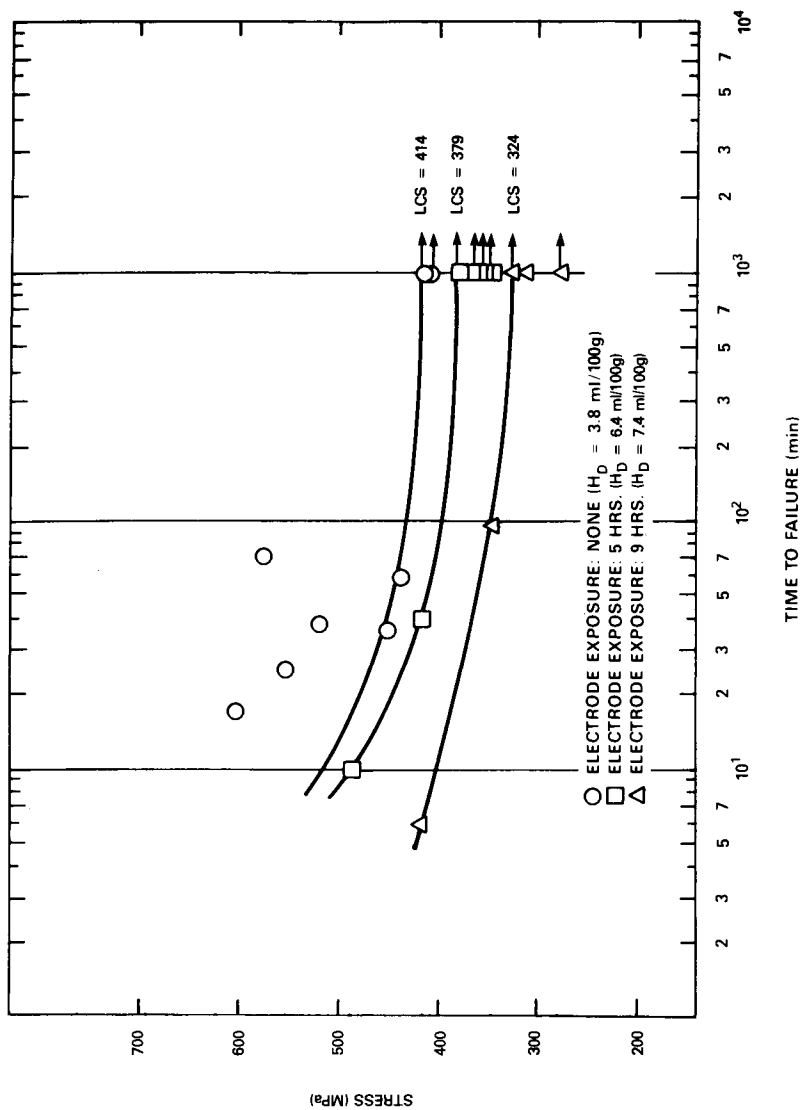


FIG. 10—Implant test results with MIL-10018M1 electrode, 16°C preheat and interpass temperature.

In Fig. 11 the implant LCS values are plotted as a function of H_D for the three preheat/interpass temperatures. The resulting curves illustrate the effect of H_D on implant LCS values. Tolerance for hydrogen is significantly increased by increasing preheat/interpass temperatures.

Rigidly Restrained Cracking Tests

The summary of RRC test conditions and corresponding implant test results are given in Table 1. The occurrence of hydrogen cracking in the RRC specimen was determined by mag-

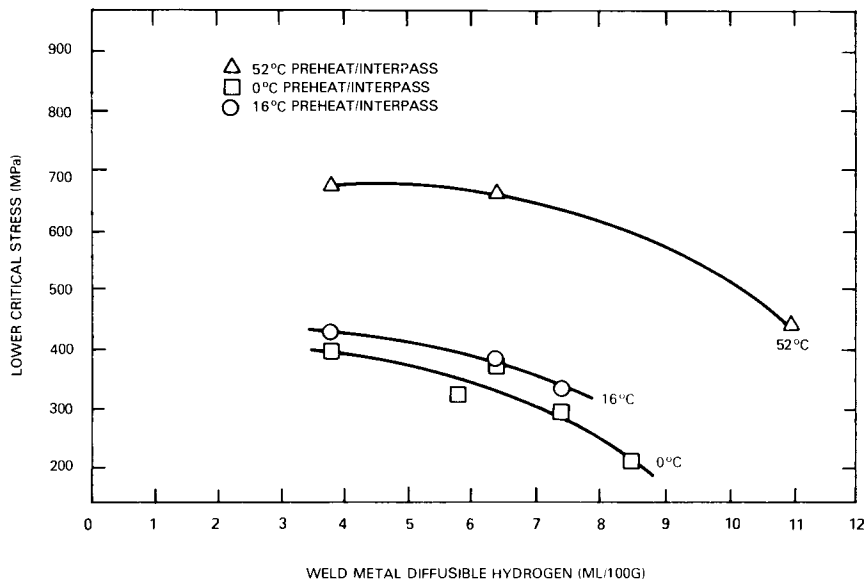


FIG. 11—Effect of weld metal diffusible hydrogen on implant lower critical stress values of HY-80 steel.

TABLE 1—Summary of rigidly restrained cracking test conditions and corresponding implant test results.

RRC Test Conditions		Implant Results MIL-10018M1, 5-h Exposure		
Gage ^a Length L, in.	Calculated Stress ^b , MPa (ksi)	LCS Value, MPa (ksi)	Temperature, °C (°F)	Expected Results of RRC Tests
12	752 (109)	365 (53)	0 (32)	Cracking
18	503 (73)	365 (53)	0 (32)	Cracking
0 ^c	0 (0)	365 (53)	0 (32)	No cracking
18	503 (73)	397 (55)	16 (60)	Cracking
48	186 (27)	397 (55)	16 (60)	No cracking
18	503 (73)	655 (95)	52 (125)	No cracking
12	752 (109)	655 (95)	52 (125)	Cracking

^aL is schematically illustrated in Fig. 4.
^bEqs 1 and 2.
^cUnrestrained plate.

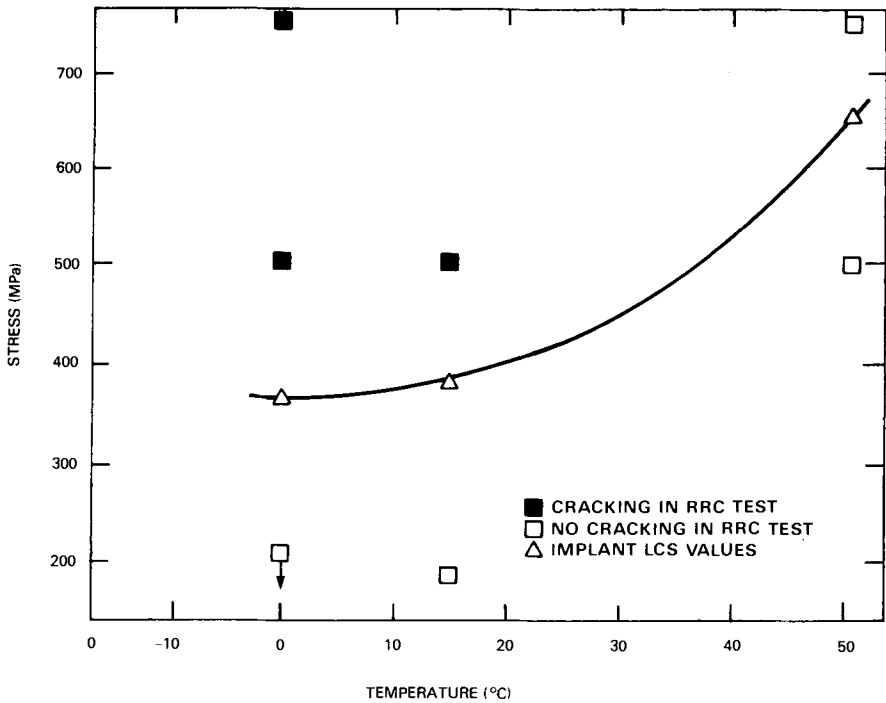


FIG. 12—Results of rigidly restrained cracking specimens and corresponding implant LCS values.

netic particle inspection 48 h after welding, followed by metallographic sectioning to confirm the results. The results of RRC testing shown in Fig. 12 illustrate the correlation between cracking versus no cracking in a self-restrained RRC specimen and the threshold cracking stress measured by implant LCS values. The only condition that did not exhibit hydrogen cracking as expected from implant LCS value was the RRC specimen fabricated with a 12-in. gage length and welded with a 52°C preheat and interpass temperature. One of the possible reasons for this discrepancy was that m of Eq 2 is only constant in the elastic region of stress. Another factor is the combination of slower developing restraint stresses in the RRC specimen in conjunction with the rapid diffusion of hydrogen out of the weld at this elevated preheat temperature, which may have resulted in a less severe test condition than for the implant test.

Conclusions

1. The electrode coating moisture was directly relatable to the resulting weld metal diffusible hydrogen content measured by gas chromatography.
2. Significant improvement in hydrogen cracking was observed by use of a moisture-resistant MIL-11018M or a MIL-10018M1 electrode compared to a nonmoisture-resistant MIL-11018 electrode.
3. The implant test was found to be a useful method for measuring hydrogen cracking resistance and quantifying the factors which contribute to the occurrence of hydrogen cracking in HY-80 steel.

Acknowledgment

The author wishes to acknowledge J. M. Blackburn for the development of moisture and hydrogen measurement procedures employed in this study.

References

- [1] "The Metallurgy and Welding of QT35 and HY-80 Steels," Report Series No. 85300859, The Welding Institute, Hilton Head Island, SC, 1974.
- [2] Graville, B. A., *The Principles of Cold Cracking Control*, Dominion Bridge Co., Ltd., 1975, pp. 119-127.
- [3] Baker, R. G., et al., *Proceedings 2nd Commonwealth Welding Conference*, Institute of Welding, London, 1966, pp. 125-131.
- [4] Rothwell, A. B., "Weldability of HSLA Structural Steels," *Metal Progress*, June 1977, pp. 43-50.
- [5] Bird, B. R., *Transport Phenomenon*, Chap. 19, John Wiley and Sons, New York, 1960.
- [6] "Specification for Covered Carbon Steel Arc Welding Electrodes," ANSI/AWS A5.1-81, American Welding Society, Miami, FL, October 1981.
- [7] "Standard Methods for Determination of the Diffusible Hydrogen Content of Martensitic, Bainitic, and Ferritic Weld Metal Produced by Arc Welding," ANSI/AWS A4.3-86, American Welding Society, Miami, FL, December 1985.
- [8] Suzuki, H., "Cold Cracking and its Prevention in Steel Welding," *Transactions of the Japan Welding Society*, Vol. 9, No. 2, 1978, pp. 2-11.
- [9] Satoh, K. et al., "Japanese Studies on Structural Restraint Severity in Relation to Weld Cracking (Preliminary Report)," *Welding in the World*, Vol. 15, No. 7/8, 1977, pp. 155-189.

In-Process Prediction of the Diffusible Hydrogen Content of Gas Metal Arc Welds

REFERENCE: White, D. R. and Chionis, W. G., "In-Process Prediction of the Diffusible Hydrogen Content of Gas Metal Arc Welds," *Hydrogen Embrittlement: Prevention and Control*, ASTM STP 962, L. Raymond, Ed., American Society for Testing and Materials, Philadelphia, 1988, pp. 287-298.

ABSTRACT: A noncontacting, spectroscopic technique has been developed to measure weld arc composition in real time. Measurements have been made of hydrogen emission line intensity and correlated with weldment hydrogen content as measured using gas chromatography. A model based on Sievert's Law is proposed to explain the relationship between the partial pressure of hydrogen measured in the welding arc and the hydrogen content of the completed weld.

KEY WORDS: diffusible hydrogen, gas metal arc welding, gas chromatology, spectroscopy, hydrogen arc atmosphere

The hydrogen-induced cracking of welds, also known as delayed or cold cracking, is a phenomenon which has been recognized for many years [1-4]. The deleterious effects of hydrogen on weldment mechanical properties have prompted the development of low-hydrogen welding consumables and fabrication practices for the welding of medium- and high-strength steels. However, hydrogen-induced cracking is still a common fabrication difficulty, often as a result of human error in the design process or poor quality control.

As a result, the hydrogen-induced cracking of welds has been studied extensively. The conditions required for its occurrence are well understood [5-7], and much quantitative data exist defining the specific nature of the hydrogen-induced cracking problem in a variety of welding systems. For example, the quantity of diffusible hydrogen which must be present in the joint to produce delayed cracking in welds having a variety of compositions and microstructures has been established [7]. In addition, a great deal of work has been done to correlate the moisture content of welding consumables such as electrode coatings and fluxes with weld hydrogen content. Techniques such as encapsulation [8] have been developed to evaluate the level of organic contamination of filler wires and its effect on the hydrogen potential of the weld. But, although the composition of the weld arc atmosphere has been measured experimentally [2, 9], the experimental difficulties involved appear to have largely discouraged attempts to correlate actual arc hydrogen content with the diffusible hydrogen content of the weld.

The difficulties involved in analyzing the welding arc which have been mentioned can be overcome if a real time, noncontacting method is used to study arc composition. Such a method has been developed [10-12] and in this investigation was used to measure the partial pressure of

¹Applications engineer, MTS Systems Corp., Minneapolis, MN 55424 (formerly, Department of the Army, Construction Engineering Research Laboratory, Champaign, IL).

²Metallurgist, Parker-Britte, 14300 Alton Parkway, Irvine, CA 92718 (formerly, Department of the Army, Construction Engineering Research Laboratory, Champaign, IL).

hydrogen in the arc atmosphere during welding. Using gas chromatography, the hydrogen content of the resulting welds was determined. An expression based on Sievert's law was then developed to predict weld diffusible hydrogen contents from experimentally obtained measurements of weld arc hydrogen concentration.

Background

Spectroscopy has been used to develop the composition of the welding arc. The high excitation energies of the welding arc plasma make emission spectroscopy an attractive method for obtaining quantitative information about the composition of the welding arc. It is particularly suitable because a real time, noncontacting sensor to perform optical spectroscopy on welding arcs can be easily produced. Spectroscopic methods have been used in other studies to measure the temperature of the welding arc [13-16] and to note variations in chromium content during the welding of 18-8 stainless steel [17].

Equipment has been developed to make use of spectroscopic techniques in analyzing the welding arc by the U.S. Army Construction Engineering Research Laboratory (USA-CERL) and the University of Illinois Radio Research Laboratory. The system is a high resolution, microprocessor-controlled spectrograph (Fig. 1). Optical radiation emitted by the welding arc in the visible region of the spectrum is collected by a fiber optic bundle designed to withstand the high temperatures surrounding the welding arc. This bundle terminates at the entrance slit of an Instruments SA spectrograph, which images a flat field spectrum onto a 1024 element linear photodiode array. This array can be scanned through the visible spectrum to obtain 60-nm bandwidth spectral samples with a resolution of 0.05 nm. The photodiode array is interfaced with a high-speed, analog-to-digital converter and an LSI 11/23 microprocessor. Spectroscopic

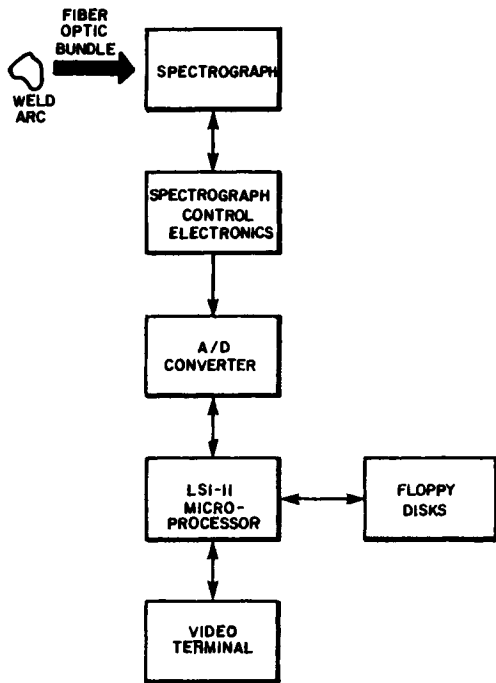


FIG. 1—Block diagram of optical data acquisition system.

data, along with measurements of the arc voltage current and travel speed, can be processed in real time or stored on disks for later analysis [10].

In previous investigation [18], this system was found to be capable of detecting arc blow, loss of or reduction in shielding gas flow, and the local absence of flux in flux-cored arc welding by detecting changes in the intensity of light emitted by the welding arc at appropriate wavelengths. In addition, experiments performed to measure the hydrogen content of the welding arc showed that it is possible to detect and measure hydrogen contents of as low as 0.05% in argon shielding gas and to correlate the relative intensity of a Balmer alpha series hydrogen emission line with the hydrogen content of the weld shielding gas and the occurrence of cracking in test welds [19].

When a spectral sample is taken using this technique, the intensity of an elemental emission line provides semiquantitative data concerning the concentration of that element in the welding arc. This makes use of the same principle that is employed in analytic spectroscopy, where quantitative determinations depend on reasonable linearity of response between analyte element concentration and observed line intensity. Analytical curves are essentially exponential curves in which the so-called linear portion of the curve is the useful range of line intensities. By appropriate choice of analytical lines of varying intensity, several orders of magnitude of analyte concentration can be determined within the linear range of the curve [20].

The same spectroscopic techniques can be applied to weld arc plasma analysis. Unlike the plasmas used in conventional diagnostic spectroscopy, the welding arc is not a steady state system. Therefore, elemental emission line intensities are not independent of arc instabilities or variations in process parameters such as voltage and current. However, these difficulties can be overcome if the intensity of the emission line of the element of interest (in this case hydrogen) is normalized to that of another emission line to determine relative intensity. This is accomplished by determining the area, I_I , under the emission line of the element of interest, the area, I_N , under the emission line to be used for normalizing, and the background intensity level (produced by bias in the photodiode array and any blackbody continuum radiation), I_B . Then an expression of the form

$$I_{REL} = \frac{I_I - I_B}{I_N - I_B}$$

where I_{REL} is the relative intensity of the line of interest is obtained. In these experiments, an argon emission line was used to normalize hydrogen emission line intensities. Although the amount of argon present changes slightly with varying arc hydrogen content, so much argon is present at all times that the intensity of many argon lines (including the line used for normalizing) remains relatively constant with respect to changes in hydrogen concentration. Therefore, the relative intensity of the hydrogen emission line can be expressed as

$$I_{REL}^H = \frac{I_H - I_B}{I_A - I_B}$$

The ability to measure weld arc hydrogen contents in real time suggests that it may also be possible to predict the hydrogen content of a welded joint during processing. A variety of investigators have used Sievert's law to model the absorption of hydrogen by the weld pool. Mallet [2] proposed that this method could be used to predict the hydrogen content of welds made with coated electrodes. He used the composition of the welding arc, as measured by collecting the gases formed during welding in an evacuated chamber, to estimate weld hydrogen content. Salter [21] also found that the absorption of hydrogen during arc welding varies with the square root of the hydrogen partial pressure. Chew [22] used a similar procedure in calculating the

thermodynamic activity of the hydrogen in the shielded metal arc process. Sievert's law states that

$$C = S_H \sqrt{P_{H_2}}$$

where

C = the concentration of hydrogen dissolved in the metal,

S_H = the solubility constant for hydrogen in molten iron at the temperature of the welding arc, and

P_{H_2} = the partial pressure of hydrogen present.

S_H is a known quantity, and the partial pressure of hydrogen can be related to quantities which are measurable spectroscopically, as just discussed. Hence, the objective of these experiments was to determine whether it is possible to predict the hydrogen content of a weld in real time, using Sievert's law, and spectroscopic hydrogen measurements.

Experimental Procedure

In order to accomplish this objective, a relationship between hydrogen emission line intensity and the partial pressure of hydrogen in the arc atmosphere was needed, as well as a relationship between the hydrogen partial pressure in the arc atmosphere and the hydrogen content of the completed weld. To determine the relationship between relative hydrogen emission line intensity data and shield gas (that is arc atmosphere) hydrogen content, spectral data were acquired at various arc hydrogen contents. The shortcomings of the various immersion techniques used to measure the hydrogen content of weld metal are well documented [23,24]. Therefore, gas chromatography was the method selected for measuring the diffusible hydrogen content of test welds. A gas chromatograph and integrator were purchased for this purpose, and stainless steel outgassing chambers were used. The outgassing and analysis procedures used were similar to those described by Quintana [23,25]. The details of the welding and gas chromatographic analysis procedures were as follows.

Gas metal arc welds were made on hydrogen analysis specimens with dimensions of 40 by 23 by 5 mm. The base metal used was Mil SAL 2560 (Table 1), an armor plate steel. Several specimens were placed between run-on and runoff tabs and clamped in copper chill block (Fig. 2). Welds were made at hydrogen concentrations of 0.00, 0.05, 0.10, 0.15, 0.25, 0.30, 0.50, and 1.00% hydrogen mixed in Argon-2% O_2 shielding gas. The welding parameters used were 28 V, 320 A, 10 in./min travel speed. All welds were monitored using the spectroscopic technique described by taking spectral samples with a bandwidth of 60 nm and a center wavelength of 656 nm for each test weld. The hydrogen line located at 656.3 nm was used to monitor arc hydrogen content, and the argon line at 675.2 nm was used to normalize the hydrogen line intensity. The hydrogen line at 656 nm was chosen for analysis for two reasons. First, it is a primary emission line of hydrogen and is of relatively high intensity [26]. Second, its close proximity to the argon line at 675.2 nm simplifies the normalization of hydrogen emission line intensity data for this data acquisition system.

TABLE 1—Composition of MIL-A-46100 armor steel.

C	Mn	P	S	Si	Mo	Cr	Ni
0.27	1.34	0.01	Nominal 0.005	Nominal 0.3	0.58	0.13	0.05

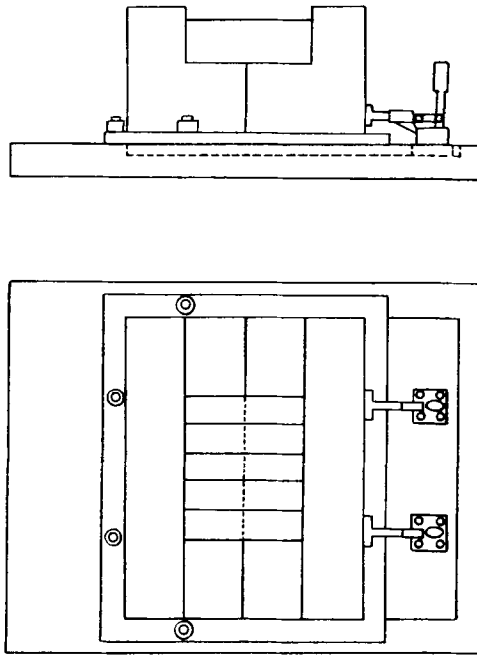


FIG. 2—Copper chill block and specimen geometry.

Immediately after welding, the specimens were quenched in a methanol bath at -30°C . After the specimens were separated from the run-on and runoff tabs and each other, they were placed in liquid nitrogen to prevent premature outgassing. Prior to testing for diffusible hydrogen content, specimens were removed from the liquid nitrogen and subjected to the following cleaning procedure: immersion in a dry ethanol bath followed by immersion in an anhydrous diethyl ether bath finished by drying with a blast of ultra-high-purity (UHP) argon. The time required for the cleaning procedure did not exceed the 60 s specified in the ISO/IIW standard. Specimens were then placed in stainless steel degassing bombs which were purged with UHP argon and injected with a helium standard. The degassing fixtures were then heated at 150°C for a period of 8 h.

After degassing, a sample of the gas in the outgassing fixture was taken and injected through a 4.57 m (15-ft) packed column of Molecular Sieve Type 5A 60/80 and into a Gow-Mac Thermal Equilibrium Gas Chromatograph Model 20-150 using UHP argon as the carrier gas. The output signal was sent to a Hewlett Packard 3380A Integrator (Fig. 3). The results of the integrated area percent calculations were normalized into millilitres hydrogen per 100 g of deposited weld metal at standard temperature and pressure.

Results

Figures 4 and 5 show qualitatively the nature of the change in hydrogen emission line intensity as the hydrogen content in the welding arc is increased. As in previous studies [1, 18, 19], a linear relationship was observed between relative hydrogen emission line intensity and the partial pressure of hydrogen present in the weld shielding gas (Fig. 6). Although it was recognized that the presence of residual lubricants on welding wire could affect the hydrogen content of the arc atmosphere, it was assumed in this investigation that this effect could be neglected. Hence,

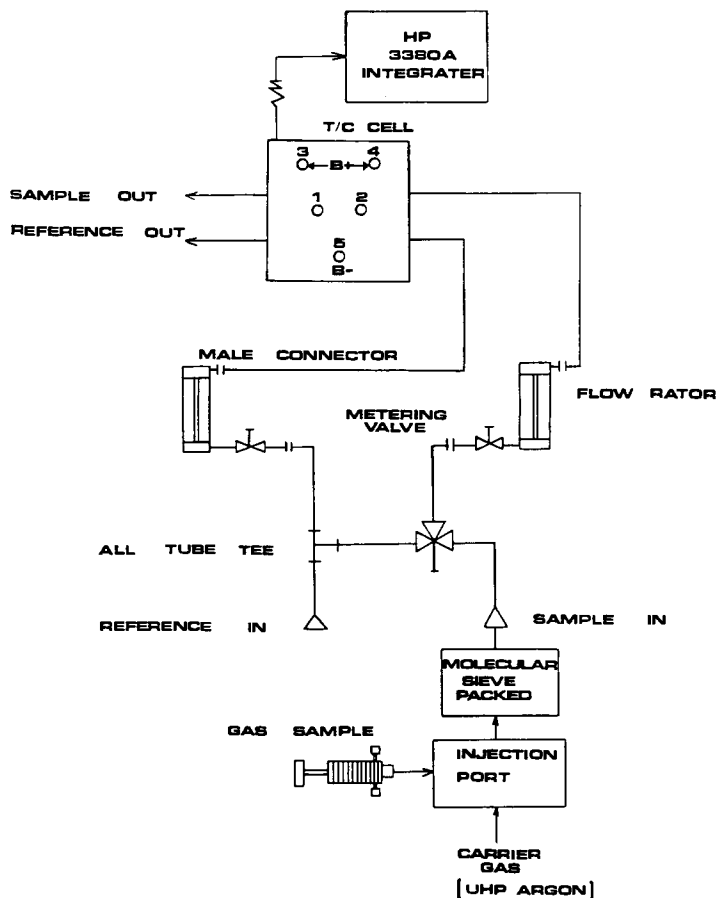


FIG. 3—Schematic of gas chromatograph data acquisition system.

the partial pressure of hydrogen in the shielding gas was equated with the partial pressure of hydrogen in the arc atmosphere. The diffusible hydrogen content of the test weld was observed to increase as the partial pressure of hydrogen in the shielding gas (arc atmosphere) increased (Fig. 7).

Discussion

It has been noted that a number of investigators have proposed that Sievert's law can be used to predict the concentration of hydrogen in a weld if the partial pressure of hydrogen present is known. In one study [2], shielded metal arc welds were made in an evacuated chamber, and the atmosphere was analyzed following welding. When the partial pressure of hydrogen present in the chamber was substituted into Sievert's law, it was found that the weld hydrogen content as measured by cold extraction and vacuum hot extraction quite closely correspond to the predicted value. In a study performed by Salter [21], it was found that weld metal hydrogen content varied with the square root of the partial pressure of the hydrogen content of the cover gas.

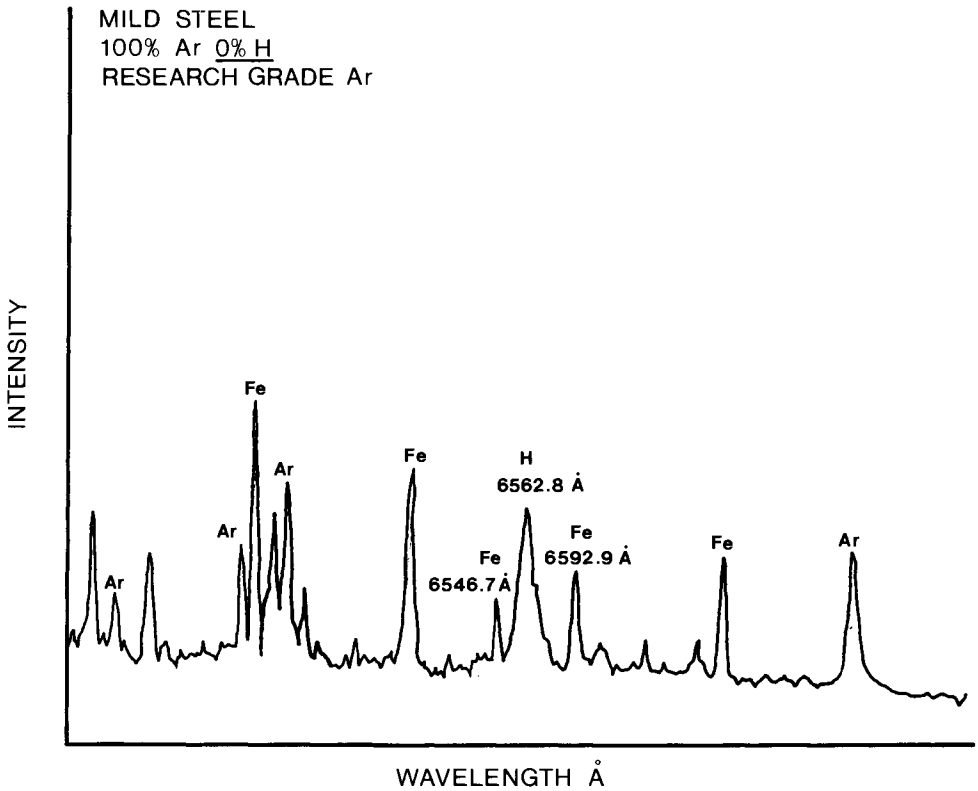


FIG. 4—Intensity of hydrogen line at 6562.8 Å when the hydrogen content of shield gas is nominally zero. Gas metal arc (GMA) weld on mild steel.

In this study, Sievert's law was used in attempting to predict weld hydrogen contents from the partial pressure of hydrogen measured spectroscopically in the welding arc. Sievert's law states that

$$C_H = S_H \sqrt{P_{H_2}} \quad (1)$$

Although the test welds in this study were made under carefully controlled conditions, residual lubricants on the filler metal or moisture on the base metal could have affected the total hydrogen content of the weld. Therefore, the hydrogen content of welds made under nominally clean conditions (no added hydroxen) was measured. The average hydrogen content of such welds was found to be 0.55 mL H_2 /100 g deposited weld metal, which was assumed to be due to the presence of hydrogen in the base metal and residual lubricants on the filler wire. A constant, C_H^0 was assigned this value and added to the original expression, resulting in

$$C_H = C_H^0 + S_H \sqrt{P_{H_2}} \quad (2)$$

Arata et al. [26] used a similar procedure in estimating the hydrogen contents of welds made underwater. The spectroscopic measurements made in this study were performed in order to determine the relationship between the hydrogen content of the arc atmosphere and the relative

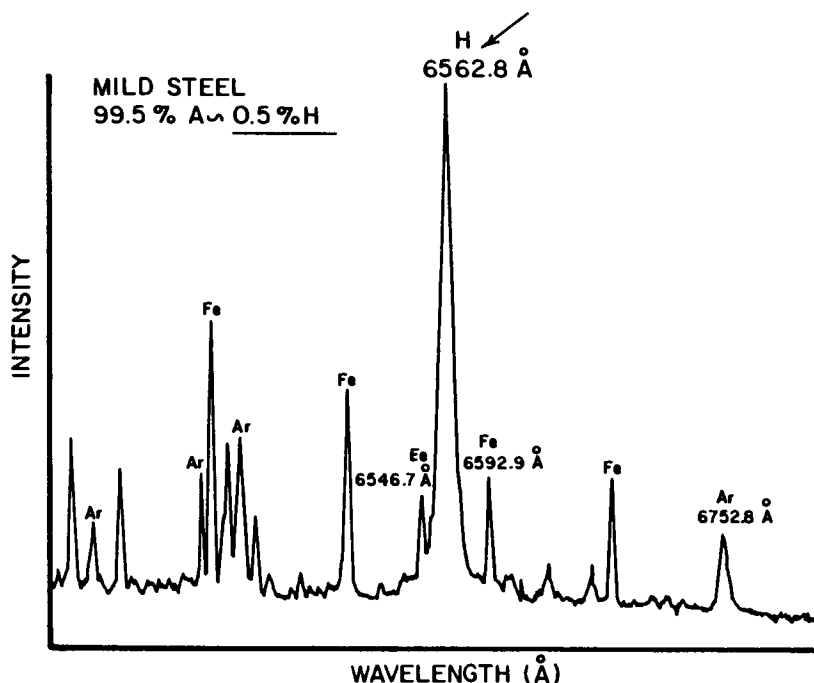


FIG. 5—Intensity of hydrogen line at 6562.8 Å when the hydrogen content of shield gas is 0.5%. GMA weld on mild steel.

intensity of the hydrogen emission line located at 656.3 nm. When the relative intensity of the hydrogen line (normalized to that of the Argon I line located at 696.5 nm) was plotted against shield gas hydrogen partial pressure, the following equation

$$I_{\text{REL}}^{\text{H}} = 287.5(P_{\text{H}_2}) + 0.7 \quad (3)$$

was found to fit the data. When this equation is solved for the partial pressure hydrogen in the arc atmosphere, P_{H_2} , and the result substituted into the modified version of Sievert's law just given, the following expression is obtained

$$C_{\text{H}} = C_{\text{H}}^{\circ} + S_{\text{H}} \left(\frac{I_{\text{REL}} - 0.7}{287.5} \right)^{1/2} \quad (4)$$

C_{H}° was determined to be 0.55 mL H_2 /100 g deposited weld metal, and after an appropriate value was selected for S_{H} , this expression was used to predict weld metal diffusible hydrogen contents.

The solubility of hydrogen in molten iron changes with temperature, and while the exact weld pool temperature is a matter of some dispute, 1650 and 1700°C were selected as the weld pool temperatures for which C_{H} was calculated. Values of S_{H} were found in the literature [27] and substituted into Eq 4. Although hydrogen solubility is also affected by alloy content, as well as temperature, this effect was neglected in the analysis. The results are found in Fig. 8. The predicted and measured values agreed very closely at low hydrogen concentrations, but at shield gas hydrogen partial pressures of greater than 0.005 they begin to deviate significantly.

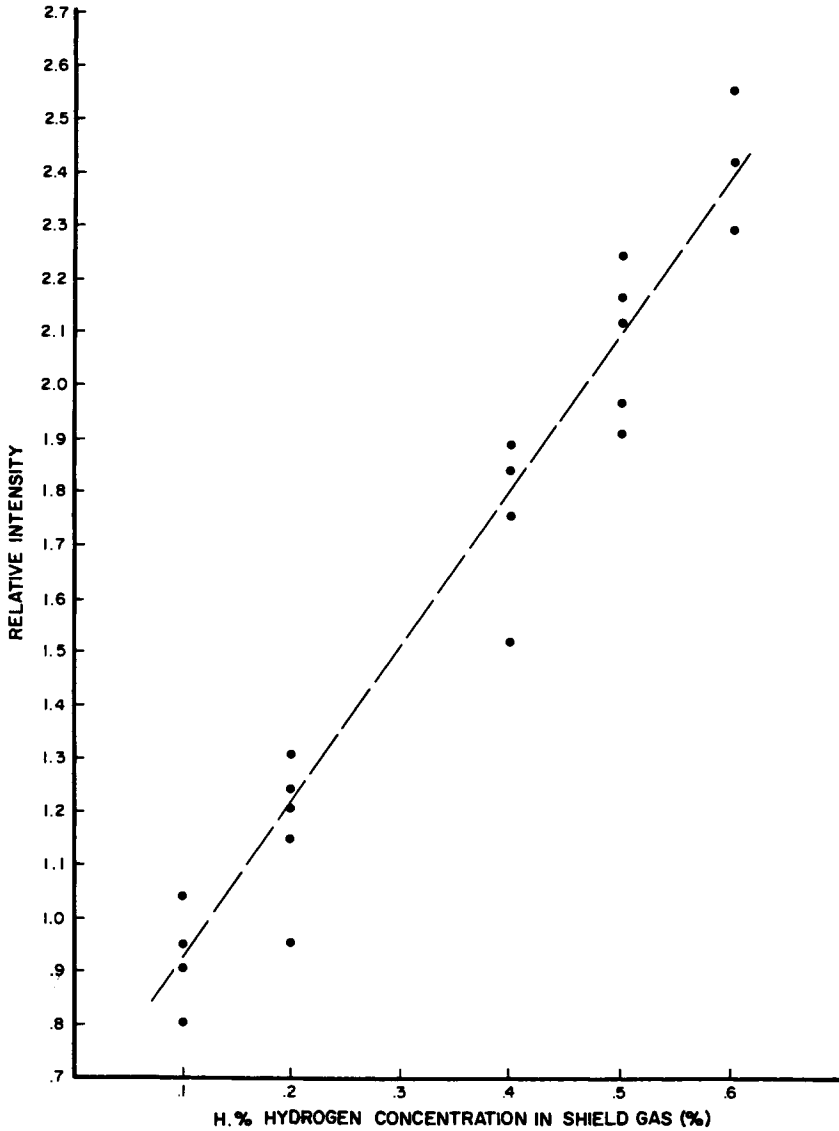


FIG. 6—Percent hydrogen concentration in shielding gas versus relative hydrogen emission line intensity at 6562.8 Å.

There are several possible reasons for this. A very small, nonstandard specimen was used in measurements of weld hydrogen content, therefore, inaccuracies in weld metal hydrogen determinations may be partially responsible. However, an additional explanation for the observed deviation may be an increase in weld pool temperature. As hydrogen is added to the arc atmosphere, an increase in arc temperature occurs particularly near the arc-weld pool interface. In addition, there is a tendency for arc constriction to occur. Thus, weld pool temperature immediately below the hottest part of the welding arc, where the greatest density of hydrogen ions is

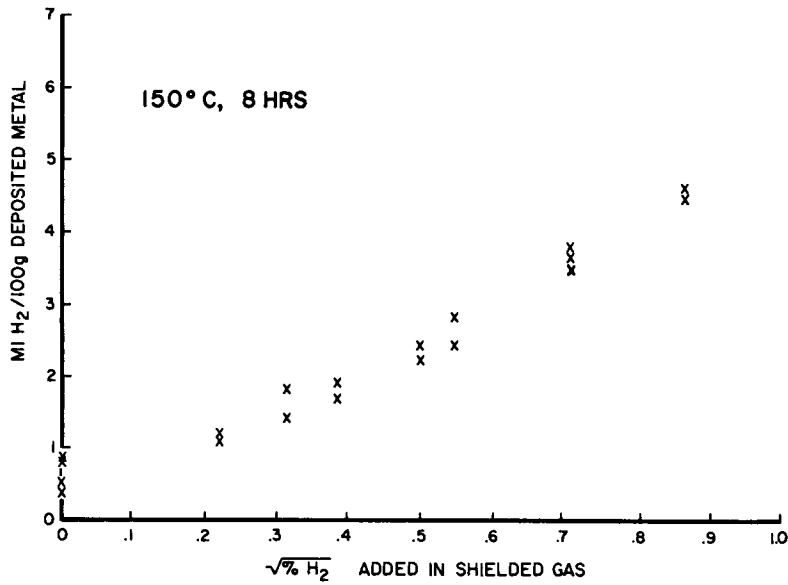


FIG. 7—Partial pressure of hydrogen in shielding gas versus hydrogen content in weldment.

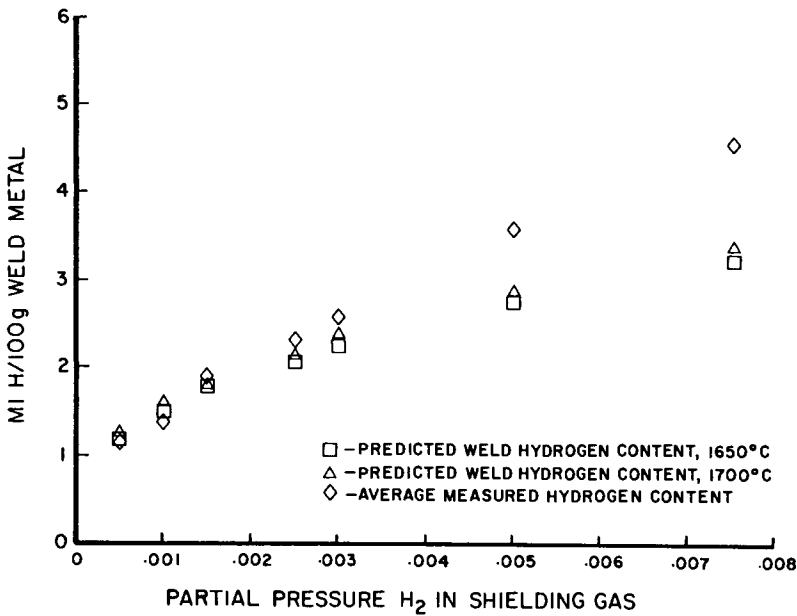


FIG. 8—Shield gas hydrogen partial pressure versus predicted and actual diffusible hydrogen content of weld.

found, may be considerably higher than the average weld pool temperature, with a greatly increased hydrogen solubility resulting.

Some of the observations made by Salter [21] support this hypothesis. He observed that an increase in hydrogen partial pressure did not appreciably increase the size of the "hot zone" in the center of the weld pool, but that it did produce a noticeable increase in the optical intensity of the zone. An increase in the temperature of the hot zone would explain this increase in the brightness of the weld pool region immediately beneath the arc. Although, in measurements of specimen temperature made in the same study, increasing hydrogen partial pressure was found to have a negligible effect on average specimen temperature, the author noted that when the tungsten/tungsten rhenium thermocouple was introduced into this region, it immediately melted.

This indicates that average weld pool temperature does not completely reflect the conditions existing near the hottest part of the welding arc where hydrogen absorption can most readily occur. The solubility of hydrogen in the weld pool increases very rapidly with increasing weld pool temperature. The solubility of hydrogen in iron is approximately 31 mL H_2 per 100 g iron at 1700°C, while at 2300°C it is about 51 mL H_2 /100 g iron. Therefore, the deviations observed at higher shield gas hydrogen contents may be the result of an increased hydrogen solubility as the weld pool temperature increases with increasing hydrogen.

The results of previous experiments [18] indicated that hydrogen-induced cracking results in the material studied when shield gas hydrogen contents exceed approximately 0.2% and at weld diffusible hydrogen contents of 2 ppm (Table 2). Therefore, despite the deviations from predicted behavior noted at higher shield gas hydrogen contents, the capabilities of the current model are sufficient to predict cracking in the highly susceptible steel studied.

Conclusions

1. It is possible to relate the hydrogen content of a gas metal arc (GMA) welding atmosphere to the relative intensity of the hydrogen emission line at 6562 Å.
2. For the armor steel used in this study, Sievert's law and spectroscopic measurements can be used to predict the weld metal hydrogen content as the weld is being made when the hydrogen partial pressure in the arc atmosphere is small.
3. Although actual results deviate considerably from those predicted at higher arc hydrogen concentrations, agreement between theory and experiment is good at hydrogen concentrations sufficient to cause hydrogen-induced cracking in welds in the material studied.

Acknowledgments

This work was performed at the U.S. Army Construction Engineering Research Laboratory. The authors wish to acknowledge the contributions of F. Kisters and T. Hayden to the research work described.

TABLE 2—Results of cruciform tests on armor steel with varying shield gas hydrogen content.

Shield Gas Hydrogen Content	Type of Cracking
0.1%	No cracking
0.2%	Mild weld metal cracking
0.4%	Severe weld metal cracking
0.5%	Weld metal and underbead cracking
0.6%	Weld metal and underbead cracking

References

- [1] Reeve, L., *Welding Journal*, 24 Nov. 1945, pp. 618s-623s.
- [2] Mallett, M. W., *Welding Journal*, Vol. 25, No. 7, 1946, pp. 396s-399s.
- [3] Mallett, M. W. and Rieppel, P. J., *Welding Journal*, Vol. 25, No. 11, 1946, pp. 748s-759s.
- [4] Hopkins, G. L., *Welding Journal*, 1944, Vol. 11, pp. 606s-608s.
- [5] Dorsch, K. E., *W.R.C. Bulletin*, No. 231, October 1977.
- [6] Boniszewski, T. and Watkinson, F., *Metals and Materials*, February 1973, pp. 89-96.
- [7] Coe, F. R., *Welding Steels Without Hydrogen Cracking*, The Welding Institute, Cambridge, England, 1973.
- [8] Coe, F. R., *Metal Construction and British Welding Journal*, February 1969, pp. 108-109.
- [9] Pokhodnya, I. K. and Shvachko, V. I., *Automatic Welding*, 1981, No. 2, pp. 11-13.
- [10] Norris, M. E. and Gardner, C. S., RRL Report 512, University of Illinois, Urbana, IL, 1981.
- [11] Blackmon, D. R., Norris, M. E., Shea, J., Gardner, C. S., and Kearney, F. W., *Proceedings, First International Conference on Current Solutions to Hydrogen Problems in Steels*, Interrante and Res-souyre, Eds., American Society for Metals, Metals Park, OH, 1982.
- [12] Peterson, D. W. and Ransom, P. L., RRL Report 522, University of Illinois, Urbana, IL, 1983.
- [13] Etemadi, K. and Pfender, E., *Review of Scientific Instruments*, Vol. 53, No. 2, 1982, pp. 255-257.
- [14] Kobayashi, M. and Suga, T., *Arc Physics and Weld Pool Behavior*, The Welding Institute, Cambridge, England, 1980.
- [15] Glickstein, S. S., *Arc Physics and Weld Pool Behavior*, The Welding Institute, Cambridge, England, 1980.
- [16] Mills, G. S., *Welding Journal*, Vol. 56, No. 3, 1977, pp. 93s-96s.
- [17] Vinogradov, V. A. et al., *Welding Production*, 1974, Vol. 12, pp. 5-6.
- [18] Blackmon, D. R. and Hock, V. F., *SAMPE Quarterly*, Vol. 15, No. 2, January 1984.
- [19] Shea, J. E. and Gardner, C. S., *Journal of Applied Physics*, Vol. 54, No. 9, 1983, pp. 4928-4938.
- [20] Vogel, R., private communication, 1983.
- [21] Salter, G. R., *British Welding Journal*, Vol. 10, No. 6, June 1963, pp. 316-325.
- [22] Chew, B., *Welding Journal*, Vol. 52, No. 9, September 1973, pp. 386s-391s.
- [23] Quintana, M. A., *Welding Journal*, Vol. 65, No. 5, 1985, p. 141s.
- [24] Sohrman, B., Budgivars, S., Dahlskog, H., Elvander, J., Nilsson, G., *Proceedings, Joining of Metals 2*, Al-Erhayem, Ed., Helsingor, Denmark, April 1984.
- [25] Quintana, M. and Dannecker, J., this publication.
- [26] Arata, Y., Hamasaki, M., and Sakakibara, J., *Transactions, Japan Welding Research Institute*, March 1981.
- [27] Fast, J. D., *Interactions of Metals and Gases, Vol. 1: Thermodynamics and Phase Relations*, Academic Press, New York and London, 1965.

Panel Discussion: Diffusible Hydrogen¹

This panel discussion was held to discuss the content of papers reproduced in this book on diffusible hydrogen. The discussion is presented in its original form and was not peer reviewed.

The moderator was C. G. Interrante, National Bureau of Standards, Washington, DC. Panel members were Francois Faure, FRAMATOME, Paris; K. A. Lyttle, Union Carbide Corp., Ashtabula, OH; M. A. Quintana, General Dynamics, Groton, CT; Thomas A. Siewert, National Bureau of Standards, Boulder, CO; Richard Wong, David Taylor Naval Ship R & D Center, Annapolis, MD; and Dawn White, U.S. Army Construction Engineering, Champaign, IL.

Participants were W. Chionis, Parker Hannifin Corp., Irvine, CA; V.S. Agarwala, Naval Air Development Center, Warminster, PA; David Berman, Naval Air Development Center, Warminster, PA; Rudy Frizioni, LECO Corp., St. Joseph, MI; Carol Sonnino, Emerson Electric, St. Louis, MO; Alan Grobin, IBM, Poughkeepsie, NY; T. Ohtsubo, Nippon Steel, Japan; Adri Mackor, TNO, Zeist, Netherlands; and Mr. Worth, Armament R & D Center.

Faure: This question is addressed to Ms. White. On one of your slides, you showed us some cracking with increased hydrogen level. The cracking occurred in the weld metal before occurring in the heat affected zone, which is not a very usual situation. Could we have more details about the base plate and consumables you have been using? Also, I do not remember quite well what the hydrogen levels were as referred in the usual way of ppm or millilitre per 100 g.

White: First of all, the material we are using was an armor steel. It is a high-strength, fairly low-alloy steel with some chromium and nickel and an E-70-S-3 type filler metal. The amount of hydrogen measured in millilitres per 100 g deposited weld metal is around 2 ppm (when converted to ppm) to cause cracking and that is consistent with what the manufacturer claims. They say that anywhere from 2 to 3 ppm is sufficient to cause cracking in this particular material. It is very susceptible to cracking, having a carbon equivalent of about 0.8.

Chionis: This question is directed toward handling of samples. You said to take samples out from liquid nitrogen, warm them, and dry them. How long are these samples kept under liquid nitrogen conditions before they are tested?

Lyttle: In most instances, not more than several hours at liquid nitrogen temperatures.

Chionis: How much time does it take to warm and clean these specimens?

Lyttle: Basically, within the AWS Standard, there is a fixed amount of time that you are allowed to warm the specimen and then place it in the bath. It is several minutes; I do not remember the actual time. It is fixed in this particular standard to minimize any differences that you might see.

Interrante: Isn't that 60 s? Is anyone sure?

Floor: Confirmed.

Chionis: I take it you used just the AWS cleaning standard?

Faure: Keeping samples in liquid nitrogen till hydrogen analysis is current practice in Europe. It is generally recommended that the specimens should be introduced in the hydrogen analyzer no more than 4 min after being taken out of the liquid nitrogen bath, to avoid any hydrogen loss. All this is well documented in IIW Commissions documents.

¹This section represents the interaction of the presenters and the participants in response to the technical content of the various papers. The sessions were taped and written copies of the discussions sent to each participant for comments and/or corrections. It is hoped that by including these sections, the reader will be able to better understand the controversial aspects of these presentations.

Agarwala: When you thaw the sample from liquid nitrogen temperature, don't you see any adsorption of moisture on it? Or do you do it in a very inert way where there is no humidity? If that is so, the amount of hydrogen you can lose during this warm-up period is significant in my experience, and how do you account for this error in determining total hydrogen when you do that collection over mercury?

Lyttle: Basically, the committee that put the standards together looked at this in fairly great detail, and among the various eight or ten or twelve laboratories that participated in this, they arrived at this as being an acceptable procedure where we can repeat the results. Based on our experience, that is so, and I do not believe that there is significant error introduced because of that.

Agarwala: I understand that, but since I do not understand the standard deviations you had in the results, I am just wondering about the validity of the effects which you indicated. Are they within the spread of that?

Lyttle: In fact, are they the cause of the variable test results?

Agarwala: That is right.

Lyttle: I would think by the fact that we have consistently reproduced the effect that we have seen, the error introduced in the test would be much smaller than some of the differences we have seen.

Agarwala: By the way, what was the standard deviations that you reported, like 1.279, 1.284? I do not personally think there is much difference in there, the total hydrogen values, if the standard deviations are within 20%.

Lyttle: We are drawing conclusions based on differences of one-half millimeter or so; we feel these are significantly different from our work so far.

Interrante: I noted that to maintain constant geometry, you have varied welding parameters other than travel speed. Did these parameters affect the measured diffusible hydrogen content of the bead? What I would have done probably would have been to vary the travel speed so as to maintain constant geometry in the hope that it would be a somewhat innocuous variable to change. I think that you had to vary the voltage.

Lyttle: We were varying the current level for the different wire diameters to get the same deposition rate at a fixed travel speed.

Berman: With all the variables, that looks like a good example of where you can use a statistically designed experiment rather than just using statistics on your results. That is something that we have been doing lately and it helps screen out some of these variables.

Fricioni: Has all the work been done to date on common steel base plates?

Lyttle: Basically, the standard used is what the American Welding Society requires; it is a specific base material and it is a common grade of steel.

Fricioni: How about the different grades of wire?

Lyttle: For example, we were using different grades of wire for our own tests, particularly when we are looking at the surface residual.

Fricioni: What happens when you deviate from the standard?

Lyttle: The standard does not require a specific welding material. That is one of the variables you would look at by running the test. The standard only requires the base plate upon which you weld. For a calibration test, there was a fixed set of parameters, but in this particular instance, we are choosing our parameters independently. The material could be a wire, or could be a flux cored wire or it could be stick electrode or could be a submerged arc weld. The technique is used to try and compare them on some basis.

Section 6: Prevention and Control: Case Histories

Overview: Section 6

The following is an overview of papers concerned with the effects of hydrogen embrittlement on manufactured parts. Some present case histories of embrittled parts while others deal with coatings, shortened destructive testing, and a proof test logic for nondestructive testing.

Since all of the case histories presented here involve parts which were either plated or coated, we devote the beginning of this overview to coatings themselves. Although applied to a product to protect it (for example, to prevent corrosion), many coatings also provide the hydrogen needed to embrittle the parts. Most of today's hardware needs some type of coating protection, making this a large-scale problem. G. T. Murray presents a view of several coatings shown to be very effective in prevention of hydrogen embrittlement in stainless steel as well as a review of current prevention and control methods.

Gerry Voorhis presents a specific example of hydrogen embrittlement caused by coating. The products are high-strength steel artillery submunitions coated with zinc phosphate. Testing for embrittlement was accomplished by stressing ring specimens at 65% of the normal breaking load for 200 h. Relief procedures consisted of thermal bake-out or storage at room temperature.

A more aggressive source of hydrogen embrittlement than zinc phosphating is cadmium plating. Milton Levy and Gordon Bruggeman present a situation dealing with cadmium-plated 4340 steel fasteners used in helicopters. Failure of these parts was determined by a 200-h test and found to be caused by brightener solution additives to the cadmium-plating bath. Filtration of the bath proved successful in rectifying the problem. Suspect parts were relieved by thermal bake-out.

Regardless of the source of the embrittling hydrogen, rejection of large numbers of manufactured parts because of failed test coupons can be costly. Nondestructive tests are needed to salvage good parts from failure-dominated lots. W. E. Krams presents a proof test logic based on fracture mechanics that is designed to provide the required margins of safety and reliability without damaging the hardware.

These papers demonstrate the difficulties with hydrogen embrittlement presently encountered. Protective coatings are the source of hydrogen in many of the current embrittlement situations. Shortened destructive testing and eventually nondestructive testing will afford manufacturers better control in combatting this problem.

Werner Field,

Armament R & O Center; Chairman,
Section 6.

Prevention of Hydrogen Embrittlement by Surface Films

REFERENCE: Murray, G. T., "Prevention of Hydrogen Embrittlement by Surface Films," *Hydrogen Embrittlement: Prevention and Control*, ASTM STP 962, L. Raymond, Ed., American Society for Testing and Materials, Philadelphia, 1988, pp. 304-317.

ABSTRACT: In liquid or gaseous media, certain additives, called inhibitors, can occupy, via a strong binding energy to the base metal, atom sites on the metal surfaces, thus preventing a metal-hydrogen bond and thereby inhibiting the entry of hydrogen into the base metal. For both metallic and nonmetallic solid films, hydrogen entry can be prevented or reduced if the film has a lesser binding energy for hydrogen than the base metal and if a low solubility and/or a low diffusivity for hydrogen. Nonmetallic films appear to be the better films for preventing hydrogen entry and subsequent embrittlement of the base metal.

Data are presented for oxide and nitride films in the 50 to 3000-nm range of thickness. A 50-nm-thick film of sputtered alumina (Al_2O_3) and a 3000-nm-thick, thermally grown oxide film appear to prevent hydrogen embrittlement in the precipitation-hardening stainless steels.

KEY WORDS: hydrogen embrittlement, precipitation hardened, stainless steels, surface films

For purposes of review, it is convenient to classify the effect of surface films into three categories:

1. Those imposed on the metal surface in liquid or gaseous form and in liquid or gaseous media, commonly referred to as inhibitors.
2. Metallic thin films.
3. Nonmetallic thin films.

"Thin" in the context used here could mean coatings from a monolayer of atoms to something on the order of $10^{-6} \mu\text{m}$ in thickness. In other words, we are not discussing paint, spray, or clad coatings and the like where entry of hydrogen is prevented essentially by mechanical screening barriers. The barriers discussed here retard hydrogen entry either through some type of surface adsorption effect or by possessing, as in the case of some solid films, a low diffusivity and/or a low solubility for hydrogen. Solid films can also retard entry by adsorption effects. For the case of solid films where surface adsorption is not a factor, that is, either diffusivity and/or solubility is rate controlling, it is more convenient to deal with permeability which combines both parameters, that is

$$\text{permeability} = \text{diffusivity} \times \text{solubility}$$

Protective solid films can then be selected if both diffusivity and solubility are known. In most published data the experimental parameter that is often measured is permeability itself. One must be sure in such cases that extraneous surface adsorption effects, such as those due to oxides or inhibitors, do not enter the picture.

¹Department head—Metallurgical Engineering Dept., California Polytechnic State University, San Luis Obispo, CA 93407.

Inhibitors

In the study of the effect of additives in the prevention of hydrogen embrittlement, the bond energy of the hydrogen atom to the metal surface and how this bond is affected by additives must be considered. The theories of the surface chemistry for the bonding of gaseous molecules to metal surfaces have been well developed and will be used as a general guide for the understanding of the role of additives. Tompkins [1] has presented a rather clear, concise picture of the surface chemistry involved in the general case. As a gaseous molecule approaches the metal surface it is first physisorbed, a process involving weak van der Waals forces that arise from the interaction of fluctuating dipoles with metal surface atoms. The binding energy here is relatively small, that is, on the order of 20 KJ/mol. Chemisorption occurs when the molecule leaves this physisorbed state and bonds directly to surface atoms by means of a stronger bond, the binding energies varying over a wide range from about 50 to 400 KJ/mol. The lower energy values are often those of the "associative chemisorbed state," where molecules are bound by forces somewhat stronger than those of the ordinary van der Waals type. The higher energies are more often associated with "dissociative chemisorption," where the molecules are dissociated and are bound to the metal surface as atoms and/or radicals of the molecules. This process is favored by the presence of unsaturated metal bonds. It is possible for both associative and dissociative chemisorption to occur in the same metal-gas system, the former being favored at higher temperatures. When dissociative chemisorption occurs, the adsorbed species are referred to as "ad-atoms."

The dissociative chemisorption energy curves for hydrogen on copper are shown in Fig. 1 (from Ref 1; energy units are in KJ/mol).

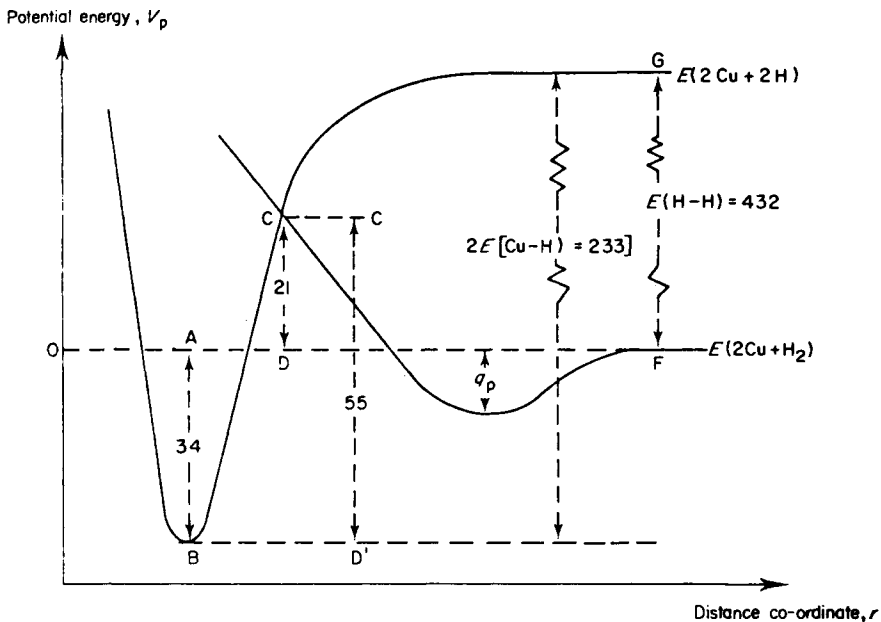


FIG. 1—Dissociative chemisorption energy curves for hydrogen on copper from Ref 1—energy units are in KJ/mol.

When the energy gained in forming the two metal-adatom bonds exceeds the dissociation energy of the free hydrogen molecule, that is

$$2E(M-H) > E(H-H),$$

where

E = energy,

M = metal

H = hydrogen

$M-H$ = metal-hydrogen bond

dissociative chemisorption is thermodynamically possible. The reference level of zero energy represents that of the molecule at infinite distance from the surface. The curve CF represents that for physisorption, while BCG depicts the energy states for dissociative chemisorption. GF is the dissociation energy of the free hydrogen molecules, CD the activation energy for chemisorption, AB the heat of chemisorption (binding energy), and CD the heat of desorption of hydrogen molecules. It is of significance that Point C, at which the curves cross, lies above the zero reference level, because in such a case a high activation energy is required.

The dissociative chemisorption of hydrogen on specific metals has been reviewed by Schlabbach, et al. [2], Speiser [3], and Shanabarger [4,5]. In general, physisorption and chemisorption curves for hydrogen adsorption on transition metals cross below the zero reference level in a dissociative chemisorption process, and hence there is essentially zero activation energy involved (there is a small activation energy, discussed in paragraphs that follow, which is necessary for the atom to move from the physisorbed to the chemisorbed state). The evidence is abundant that the hydrogen atom interacts with the unpaired "d" and "f" electrons in the transition metals [1,6-9]. Two of these authors [8,9] have used the change in magnetization of iron due to this interaction of adsorbed hydrogen atoms with the "d" shell electrons to study the kinetics of the adsorption process. Most nontransition metals, on the other hand [2,3,4], require an activation energy, thus chemisorption is limited or does not occur at all except at elevated temperatures and pressures.

The chemisorption of hydrogen on iron has been studied extensively, although adsorption curves such as shown in Fig. 1 for the hydrogen-copper system could not be located by the author. Shanabarger [4] has shown a simplified potential energy schematic curve for a hypothetical hydrogen-metal system. The height of the activation barrier E_a depends on where the physisorbed and chemisorbed curves cross and the depth of the precursor potential well (Fig. 2). The values for the actual binding energies are not shown here, but in another article [10] he quoted a value of 82.1 KJ/mol for the isotheric heat of adsorption of hydrogen on iron as measured by the surface coverage (resistance change) and by application of the Clausius-Clapeyron equation. This value is in general agreement with other measurements [11,12,6]. The physisorbed state is often called the precursor state although these two may be distinct, the latter referring to some type of charged molecule, for example, H_2^+ . Ransom and Ficalora [8], using changes in magnetization, have described the adsorption reaction on iron as a two-step process involving the formation of the H_2^+ adsorbed molecular precursor prior to the formation of the hydrogen ion. Below about 300°K, the formation of the H^- ion from the adsorbed precursor H_2^+ ion was the rate-controlling process in gaseous hydrogen embrittlement. At temperatures greater than about 300°K, the decreasing net adsorption of H_2^+ becomes the limiting process. The precursor state acts to mediate the adsorption-desorption reaction between the gas phase and the chemisorbed state.

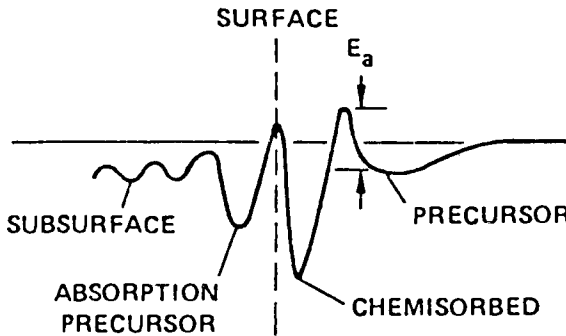


FIG. 2—Simplified energy curve for a hydrogen-metal system [4].

Inhibitors in the Gaseous State

In order to understand the role of inhibitors, it is convenient to use the concept of the sticking probability, which is defined as the ratio of the rate of capture of the molecules (or adatoms in the dissociative chemisorbed state) to the rate of collisions of the gaseous molecules with the surface. When a surface site is occupied by an inhibitor adatom or molecule, it may prevent the adsorption of hydrogen adatoms. Hydrogen adatoms themselves in effect can act as inhibitors because, as surface coverage increases, sites that are occupied are no longer available for adsorption of additional hydrogen. Thus the sticking probability decreases with exposure. It is possible for the time of the charged molecule in the precursor state to be of sufficient duration that the precursor "molecule" can diffuse along the surface until it finds an unoccupied site, and then it can become adsorbed as an adatom. In this case the sticking probability is almost independent of surface coverage. Chemisorption ceases when the adsorbate can no longer make contact with the surface and is, therefore, a monolayer process (Langmuirian). If the adsorption exceeds a monolayer, the second and higher layers are physically adsorbed. The beneficial effect of inhibitors on hydrogen embrittlement is simply that the inhibiting species have a higher binding energy to the iron than does hydrogen and, thereby, block sites for hydrogen adsorption.

Several articles have appeared in the literature on the use of additives in the gaseous state for inhibition of hydrogen entry into the metal of interest. Robertson [13] demonstrated that ethylene, ethane, and 1,2-dibromomethylene added to hydrogen reduced the permeation rate of hydrogen through high purity iron at 200°C by factors of 50 to 100. These effects were rationalized on the basis that adsorption of the inhibitor of adjacent metal sites blocked these sites to hydrogen adsorption. Frandsen and Marcus [14] showed that oxygen, carbon monoxide, and nitrous oxide prevented hydrogen-metal interaction and markedly decreased the fatigue crack propagation rate in hydrogen. Sulfur dioxide (SO₂) and carbon disulfide (CS₂) added to hydrogen stopped hydrogen-assisted crack growth in 4340 steel [15]. Hydrogen permeation through iron-, nickel-, and cobalt-based alloys was reduced an order of magnitude by the addition of 0.2 to 5% carbon dioxide (CO₂) [16].

Electronegative elements such as carbon (C), oxygen (O), and sulfur (S) on iron surfaces were reported [17] to reduce the extent, the heat, and the kinetics of dissociative hydrogen adsorption on iron, presumably by reducing the binding energy of hydrogen to the iron surface; that is, the sticking probability for hydrogen decreased. Vapor phase inhibitors such as hydrazine have been shown [18] to be very effective in reducing low-cycle fatigue crack propagation rates in 7075 aluminum alloy. Such cracking is believed to involve hydrogen.

Flitt and Bockris [19] pointed out that additives cannot be classified simply as promoters and inhibitors of hydrogen ingress but act through a balancing of several factors, some of which are

dependent on electrode potential and some which are not. Sulfur, for example, at increasing concentrations on ruthenium surfaces acts to block dissociation sites for hydrogen absorption and also recombination sites for hydrogen desorption [20]. Berkowitz et al. [21] have noted that elements which are hydrogen recombination catalysts are also hydrogen dissociation catalysts.

Inhibitors in Liquid State

Pressouyre [22] has recently reviewed and summarized the effects of many inhibitors, including the nitrites, organic nitrogen compounds, phosphates, chromates, and organic amines. All of these papers will not be reviewed here. Rather, I will attempt to cover recent ones and some that were omitted from his article.

Flitt and Bockris [19] studied the relation of adsorbed to absorbed hydrogen as a function of electrode potential and various solution constituents, namely naphthyanitrile, benzonitrile, naphthalene, hydrogen sulfide, and sodium dihydrogen phosphate in a 0.5-M sulfuric acid electrolyte. These additives were selected because nitriles were known to be general corrosion inhibitors while naphthalene was known as a promoter and hydrogen sulfide and phosphates as embrittling agents. All additives decreased the exchange current density and increased the content of internal hydrogen. Mechanical property effects were not determined. Oxidizing inhibitors such as hydrazine, which contains nitrite (NO_2^-) in solution, retarded crack growth rates in high-strength, low-alloy steels [23]. Bhansali et al. [24] have reported on a large number of inhibitors such as phosphates, chromates, nitrites, amines, and alcohols, and more recently [25] in detail on borax-nitrite, which was found to be the most effective of the lot. The effectiveness of the multifunctional borax-nitrite inhibitor system was observed in both sustained-load and cyclic-load experiments. Crack growth rates were lowered by an order of magnitude in the presence of the inhibitor. The results were not analyzed with respect to the possible mechanisms involved.

Metallic Thin Films

Metallic thin films can retard hydrogen entry into the substrate metal by virtue of their low solubility for hydrogen, low diffusivity for hydrogen, or surface effects involving adsorption, or by combinations of these mechanisms. In many studies the relative effects responsible for the permeabilities have not been separated. Also, permeabilities may be affected by the formation of thin oxide coatings on the metal film being studied. Such oxides generally have much lower diffusivities for hydrogen than do metals, thus giving misleading diffusivity and/or permeability data. In addition, oxides would be suspected to have lower sticking probabilities by virtue of their tightly bound valence electrons. Hydrogen diffusivity data through many metals have been compiled [26]. To establish reliability one would need to examine each experiment for possible surface oxide effects and/or the lack or presence of data as a function of thickness. If the diffusion of hydrogen through the metal film is the rate-controlling process, then the diffusivity should be a linear function of the reciprocal of the coating thickness, and the data should show zero diffusivity at infinite thickness. These diffusion data were not examined in such detail. Furthermore, we should be concerned about permeability rather than diffusivity since permeability is a product of the solubility and diffusivity. Pressouyre [22] compiled permeability data for hydrogen through a number of metals and compared these values to those for hydrogen through low alloyed and austenitic steels. Much of this data were originally published by Tison et al. [27]. The permeabilities of the metals studied, in decreasing order, are listed as follows: nickel (Ni), platinum (Pt), copper (Cu), molybdenum (Mo), aluminum (Al), silver (Ag), gold (Au), tungsten (W). Except for nickel, they were all less than that through the steels at temperatures less than about 300°C. The hydrogen permeability through nickel was somewhat greater than that through austenitic steels but less than that through the low-alloy steels. Except for nickel, where the hydrogen permeability was about one order of magnitude less than that for

alloy steels, the permeabilities of the other metals varied from a factor of 10^3 less for Pt to about 10^9 less for W. These differences would be even larger at room temperature assuming the linear relationship can be extrapolated that far. Extrapolation is probably valid if there are no surface oxides to interfere with permeation. Nevertheless, it appears that hydrogen permeability through a number of metals is sufficiently low that they can be considered as coatings for prevention of hydrogen embrittlement.

Chatterjee et al. [28] obtained a linear relationship of the permeability as a function of inverse thickness for hydrogen through copper coatings $\geq 0.5\text{-}\mu\text{m}$ thick and for nickel coatings $\geq 1.0\text{-}\mu\text{m}$ thick, indicating that diffusion was the rate-controlling process. Platinum, on the other hand, acted as a barrier at thicknesses of the order of $0.015\text{ }\mu\text{m}$ and was believed to act to influence the hydrogen evolution reaction rather than being a diffusion-controlled barrier. Using a partially covered electroplated surface, it was demonstrated that all three metals did reduce hydrogen ingress by acting as a catalyst for the hydrogen evolution reaction. Chatterjee et al. referenced several papers on other metallic films.

Stone [29] reported permeabilities of deuterium through a number of metallic films on 304L stainless steel. The 304L specimens were sputter etched to remove any oxide films and then sputter coated immediately with 100 nm of the metal of interest, in this case palladium (Pd), Pt, Ni, Al, and Au. Ni, Pt, and Pd all showed permeation rates sufficiently fast that they could supply hydrogen ions to satisfy the base permeation rate of the underlying stainless steel. The results on Pt differed somewhat from those of Tison et al. [27] in that the latter showed hydrogen permeability through platinum to be less than that through austenitic stainless steels. Pd films have been used by several investigators [30,31] to study hydrogen permeation of steels without the bothersome effects of oxide coatings. Pd also promotes hydrogen dissociation. In fact, much diffusion data are suspect when this procedure has not been used. The high diffusivity and solubility of Pd for hydrogen and its dissociative effects ensures that the hydrogen permeability or diffusivity of the metal substrate is indeed the rate-controlling process. In the work reported by Stone [29], gold films showed much lower permeabilities, by factors of 10 to 50 less than that of steel. Thus gold films could be considered as a protective barrier. Al films also showed a reduction in permeability by a factor of about 50.

Many studies have been made on cadmium (Cd) electroplated coatings on steel, but most have dealt with egress rather than hydrogen permeation of a previously coated steel. This stems, of course, from the fact that Cd serves to reduce general corrosion, but, in the plating process, hydrogen pickup occurs. Baking after plating has become a standard procedure to remove this hydrogen even though it has been pointed out [32] that conventional bakeout procedures cannot remove more than a fraction of the hydrogen dissolved in a coated steel. Hydrogen outgassing results have suggested [33] that Cd coatings not only serve as a permeability barrier but also influence surface reactions such as hydrogen recombination and desorption.

Nonmetallic Inorganic Films

One of the earlier papers on the low permeability of hydrogen through inorganic compounds appeared in 1960 [34]. There have been many reports in recent years that verify the impervious nature of such films to hydrogen. Piggott and Siarkowski [35] demonstrated that thermally grown oxide films on 302 and 347 stainless steels were barriers to hydrogen infusion and that diffusion coefficients for hydrogen through thin oxide films were of the order of $10^{-17}\text{ cm}^2/\text{s}^{-1}$ at ambient temperatures. In one of the more definitive experiments, Caskey [36] showed that the diffusivity of hydrogen through rutile (TiO_2) single crystals was very low and varied with crystallographic direction. Diffusivity values at 20°C of $1.9 \times 10^{-12}\text{ cm}^2/\text{s}^{-1}$ and $7.5 \times 10^{-16}\text{ cm}^2/\text{s}^{-1}$ were reported for the "c" and "a" crystallographic directions, respectively. Others [37-38] have demonstrated that oxide films on titanium are effective barriers to hydrogen penetration. Swansiger et al. [39] reported that increasing the film thickness had a minor effect on the permeability. Swansiger and Bastaz [40] reported that thin oxide films of the order of 15 nm

thickness chemically produced on stainless steel surfaces reduced the permeability of tritium and deuterium two to three orders of magnitude. One experiment in which palladium was deposited over the oxide on the upstream side (but not on downstream side) negated the effect of the oxide, suggesting that the oxide may have a significant surface effect. Stone [29] reported similar results. Van Deventer et al. [41,42] showed that sputtered aluminum-aluminum oxide films on 321 stainless steel and that thermally grown oxide films on Fe-Cr-Al alloys served to retard hydrogen permeation.

The data just cited led to experiments in our laboratories to determine if oxide films could prevent hydrogen embrittlement of the PH stainless steels. The PH stainless steels are particularly attractive for aerospace and marine applications due to their high strengths, generally in the 965 to 1400 MPa range (depending on aging treatment), good ductility, of the order of 65% reduction in area (RA) in room temperature tension tests, and good corrosion resistance. One of their chief drawbacks has been their susceptibility to hydrogen embrittlement.

Early experiments were conducted to assess their susceptibility by simply electrochemically charging tension specimens at room temperature with hydrogen and immediately testing for percent reduction in area. The fracture surfaces revealed a brittle external shell (Fig. 3) with a ductile interior [43]. Scanning electron microscope (SEM) examination showed the external shell to be predominantly intergranular mixed with some transgranular fracture (Fig. 4), while the internal core was of the microvoidcoalescence (MVC) type fracture. After charging for 16 to 24 h, depending on specimen strength, the entire fracture surface was of a brittle nature. It is of interest to note that the depth of the brittle shell, for a given charging time, was smaller for the higher strength aged condition. Assuming equal diffusivities, this implies a smaller hydrogen concentration for brittle failure for the higher strength condition. Of course, the higher strength could mean higher coherency strains and higher localized hydrogen concentration at the point of crack nucleation. The general picture of sensitivity to hydrogen embrittlement as a function of strength is depicted in Fig. 5. [44]. In this figure, and hereafter,

$$\text{ductility loss} = \frac{\% \text{ RA uncharged} - \% \text{ RA charged}}{\% \text{ RA uncharged}}$$

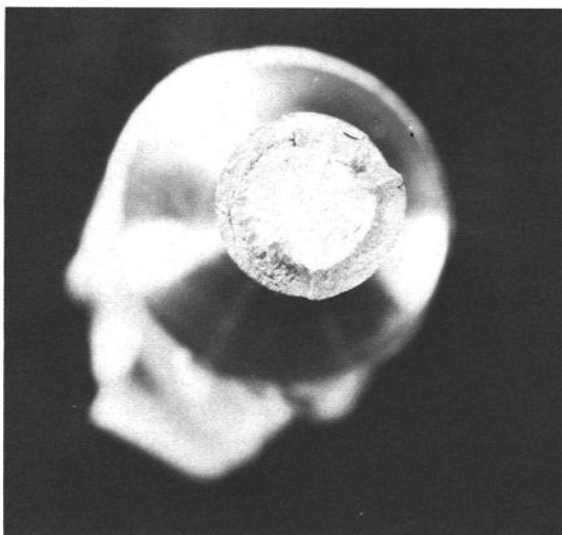


FIG. 3—Brittle shell on PH 13-8 Mo stainless steel (H1050 condition); charged 4 h, magnification $\times 10$.

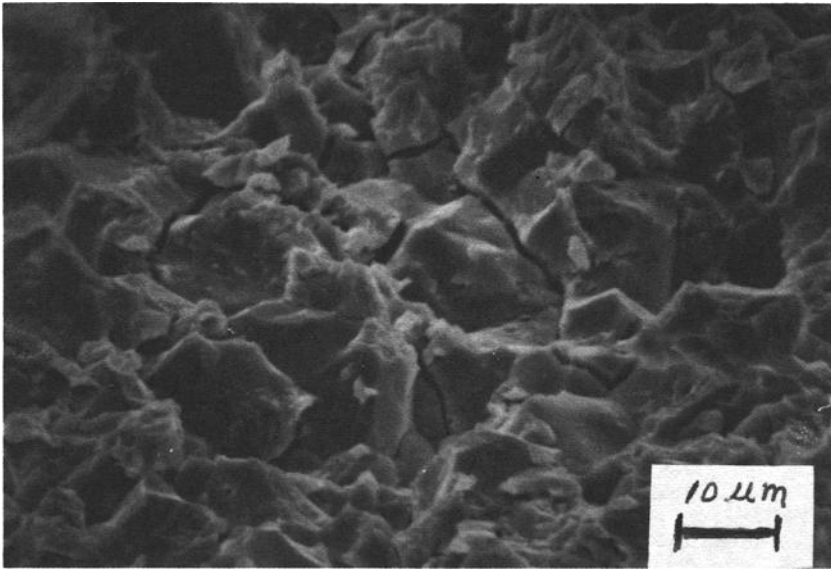


FIG. 4—SEM of brittle shell in Fig. 3.

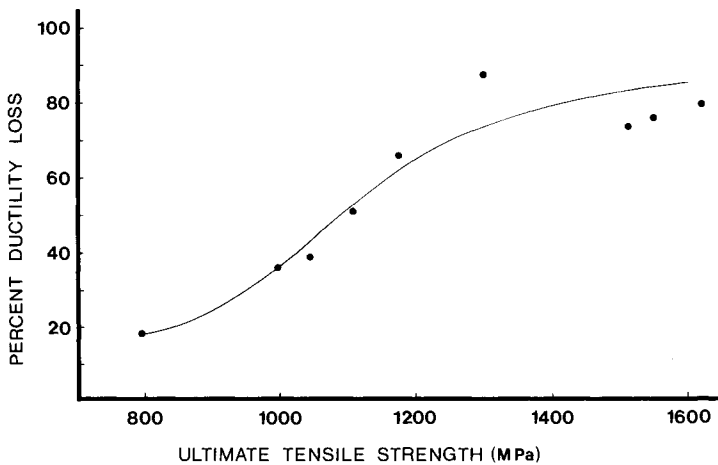


FIG. 5—Ductility loss versus ultimate tensile strength for PH stainless steels aged to different strength levels. Specimens were electrolytically charged with hydrogen for 2 h at 90 A/m² prior to testing.

The effect of a sputter-coated TiO₂ film on the hydrogen embrittlement of 15-5 PH² stainless steel, which had been aged for 4 h at 552°C (1025°F—referred to as H1025 condition), is shown in Fig. 6 [45]. Specimens were electrolytically charged with hydrogen at a current density of 90 A/m². A film of only 50 nm thickness showed ductilities in the vicinity of 60% RA, very close to the values of 68% RA obtained on noncoated, noncharged specimens. A 500 nm film gave

²Registered trademark of Armco Steel Corp.

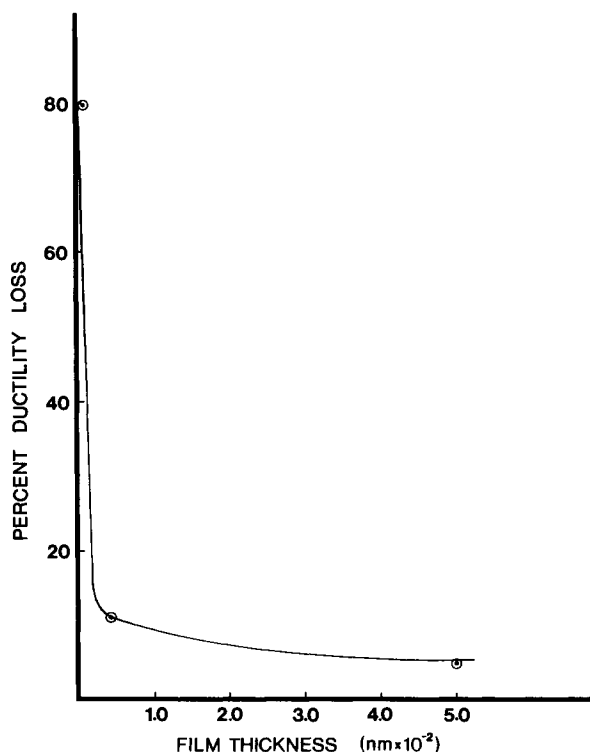


FIG. 6—Ductility loss versus TiO_2 film thickness. Specimens were 15-5 PH stainless steel in H1025 condition charged 4 h at 90 A/m^2 [45].

complete protection for the 4-h charging time. After charging for 40 h (Fig. 7) there is some evidence of hydrogen penetration based on ductility measurements. However, the fracture surface consisted of a few isolated regions of intergranular fracture, constituting less than 5% of the circumference and less than 0.01 cm in depth. It is not clear whether this result is due to hydrogen diffusing through the film or some type of defect formed in the film due to the excessive charging. Diffusion calculations, using the highest diffusivity found by Caskey [36], showed that the steel should be 3.3% of saturation after 4 h and 6.5% of saturation after 41-h charging time. Work is still in progress on this aspect of the results.

The protection offered by other nonmetallic films is depicted in Fig. 8 [46]. Alumina (Al_2O_3) films as thin as 50 nm prevented hydrogen embrittlement of 17-4 PH H-1050 condition (aged 4 h at 1050°F) stainless steel. Ductilities of noncoated, noncharged specimens averaged 66% RA.

Since sputter-coating is a somewhat impractical coating method for large parts, it was decided to investigate the protection offered by thermally grown oxides. Furthermore, it was decided to use temperatures of the solution annealing treatment (1038°C) and the common aging temperatures of about 565°C (1050°F) to grow the oxide since these temperatures, if successful, would avoid the introduction of additional processing steps.

The results obtained by forming the oxide during the solution annealing treatment are listed in Table 1. The industrial solution annealing process, that is 30 min in air at 1038°C (1900°F) followed by air cooling, was utilized. The specimens were machined to final dimensions of a nominal 0.64 cm diameter by a 2.54-cm gage length prior to the solution annealing treatment. The specimens exhibited considerable oxide flaking as a result of this high temperature anneal.

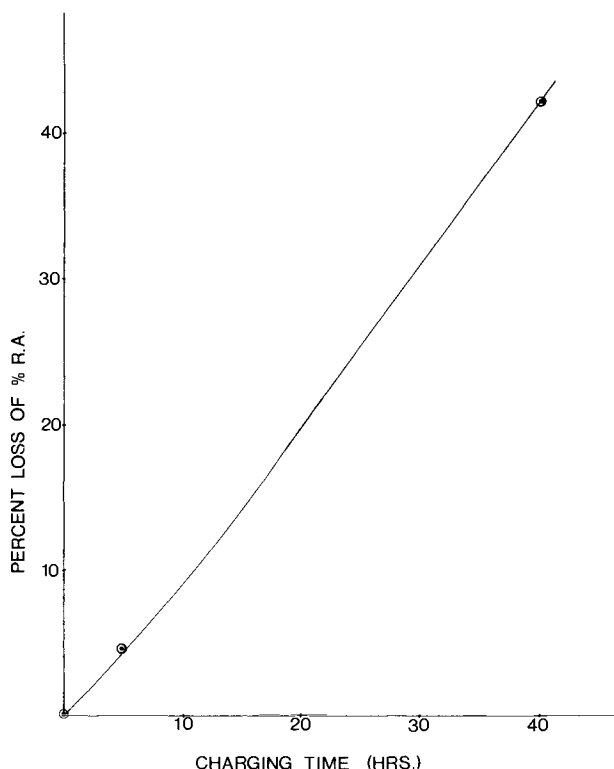


Fig. 7—Ductility loss versus hydrogen charging time for a 500 Å TiO_2 film [45].

Yet the oxide remaining was very tight and adherent. One specimen (Specimen 5) was severely abraded with steel wool to remove the loose oxide and also to test the ability of the remaining tight adherent oxide film to withstand ordinary scratching and handling that might occur in service. This adherent film was measured by SEM examination to be on the order of 3000 nm in thickness. This film gave complete protection to hydrogen charging compared to Control Specimens 1 and 2. Even after charging for 73 h (Specimen 6), the loss in ductility as measured by % RA compared to the control specimens was only 6%.

The normal commercial usage of the precipitation-hardening stainless steels is to purchase the alloy in the solution-annealed state, form and/or machine in this ductile state, then age the finished part to a higher strength level. Therefore, it was decided to attempt to thermally grow the oxide film during the aging process. Since Specimen 2 in Table 1 revealed that air aging would not produce a protective oxide film (similar results had been previously obtained on 15-5 PH and PH 13-8 Mo), aging was conducted in a stream of 50% oxygen-50% argon, and 100% oxygen. Flow rates of 0.4 m³/h (15 ft³/h) through an enclosed tubular furnace were maintained. The results are listed in Table 2.

Both the pure oxygen and the oxygen-argon mixture yielded similar results, that is, the % RA loss after charging for 16 h was the order of 33%. However, these films were protective for 4-h charging periods as evidenced by Specimen 9. The reasons for this lack of protection for longer charging times are unclear at this time and are still being investigated. SEM measurements indicate that the oxide films formed during aging in oxygen are of the order of Angstroms in thickness, but with rather wide variations in thickness. Yet the thinnest region was still several

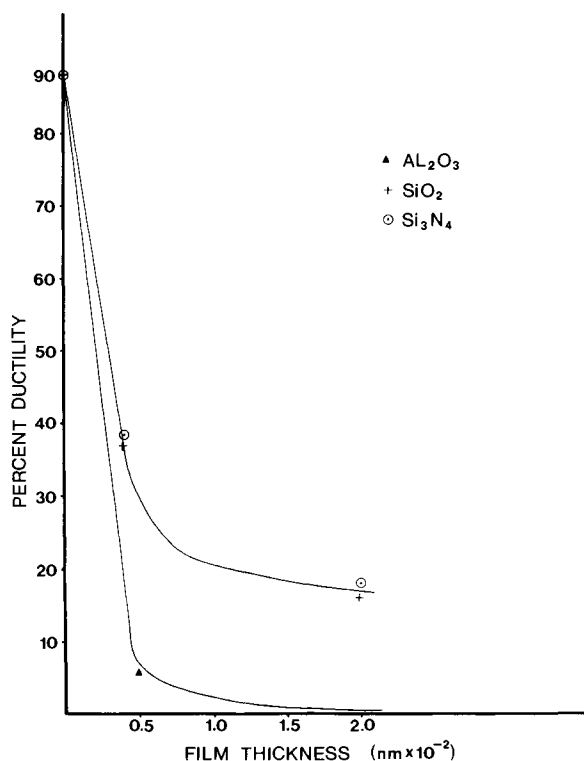


FIG. 8—Ductility loss versus film thickness for 17-4 PH, H1050 condition after hydrogen charging 16 h [46].

TABLE 1—Effect of oxide formed by solution annealing in air on hydrogen embrittlement of 17-4 stainless steel—H1050 condition [46].

Specimen Number	Treatment	% RA	% RA Loss
1	Solution annealed ^a , machined, aged 4 h in argon, uncharged (control)	66	0
2	Same as Specimen 1 except aged in air	66	0
3	Solution annealed, machined, aged 4 h in air, charged ^b 16 h	8	88
4	Machined, solution annealed, aged 4 h in air, charged 16 h	66	0
5	Machined, solution annealed, abraded with steel wool, aged 4 h in air, charged 16 h	66	0
6	Machined, solution annealed, aged 4 h in air, charged 73 h	60	6

^aSolution anneal—0.5 h in air at 1038°C (1900°F) followed by air cool.

^bCharged in 3.5% NaCl solution at 90 A/m².

hundred nanometres in thickness, that is of a much larger thickness than that of the protective films formed by reactive sputtering. Examination of the oxidized surface showed the presence of scattered pits, indicating that the films may be porous or incomplete in certain regions. However, the fractured surfaces of the subsequently charged specimens were of the ductile MVC type. The void size was not noticeably different from the uncharged specimens.

TABLE 2—Effect of oxide formed during aging in an oxygen atmosphere on hydrogen embrittlement of 17-4 PH stainless steel—H1050 condition [46].

Specimen Number	Treatment	% RA	% RA Loss
7	Solution annealed, machined, aged 4 h in 50% oxygen–50% argon, charged 16 h	42	36
8	Solution annealed, machined, aged 4 h in 100% oxygen, charged 16 h	44	33.3
9	Solution annealed, machined, aged 4 h in 100% oxygen, charged 4 h	65	1.5

Summary

A review of the literature on the efficacy of surface films for the prevention of hydrogen embrittlement of steels reveals a number of possible paths one can take. Inhibitors, both in gaseous and in liquid media, offer considerable protection through altering the surface adsorption characteristics. Borax-nitrite was one of the better performers of the lot. For both metallic and non-metallic surface coatings, there are several candidates. Tungsten has the lowest hydrogen permeability of the metals studied, while TiO_2 and Al_2O_3 nonmetallic coatings are protective in thin layers of the order of 50 nm. For stainless steels it is possible to thermally grow adherent oxide films of hundreds of nanometers thickness at temperatures in the vicinity of 1000°C. These films offer extensive protection and appear to be abrasion proof. The beneficial effects obtained from solid films may be derived from low diffusivities plus inhibition of surface adsorption, with the latter being the most probable mechanism in most cases.

Acknowledgment

Part of this work was sponsored by the Naval Weapons Center, China Lake, CA.

References

- [1] Tompkins, F. C., *Chemisorption of Gases on Metals*, Academic Press, New York, 1978, pp. 1–9.
- [2] Schlabach, L., Seiler, A., Stucke, F., and Siegmann, H. H., *Journal of Less Common Metals*, Vol. 73, 1980, p. 145–160.
- [3] Speiser, R. in *Metal Hydrides*, W. Muller, J. P. Blackledge, and G. G. Libowitz, Eds., Academic Press, New York, 1968, p. 53.
- [4] Shanabarger, M. R., in "Advanced Techniques for Characterization of Hydrogen in Metals," N. F. Fiore and B. J. Berkowitz, Eds., American Institute of Mining, Metallurgical, and Petroleum Engineers, Warrendale, PA, 1982, pp. 155–170.
- [5] Shanabarger, M. R., *Surface Science*, Vol. 150, 1985, pp. 451–479.
- [6] Hawyard, D. O. and Trapnell, B. M. W., *Chemisorption*, Butterworths, London, 1964, p. 8.
- [7] Pecora, L. M. and Ficalora, P. J., *Metallurgical Transactions Annual*, Vol. 8A, 1977, p. 1841.
- [8] Ransom, C. M. and Ficalora, P. J., *Metallurgical Transactions Annual*, Vol. 8A, 1980, p. 801,807.
- [9] Selwood, P. W., *Chemisorption and Magnetization*, Academic Press, New York, 1975, p. 35.
- [10] Shanabarger, M. R. in *Hydrogen Effects in Metals*, I. M. Bernstein and A. W. Thompson, Eds., American Institute of Mining, Metallurgical, and Petroleum Engineers, New York, 1981, p. 135–141.
- [11] Wedler, G. and Borgmann, B. B., *Physical Chemistry*, Vol. 78, 1974, p. 67.
- [12] Chornet, E., and Coughlin, R. W., *J. Cataloging and Classification*, Vol. 27, 1972, p. 246–265.
- [13] Robertson, W. M., *Metallurgical Transactions*, Vol. 11A, Nov. 1980, p. 1207.
- [14] Frandsen, J. D. and Marcus, H. L., *Metallurgical Transactions Annual*, Vol. 8A, Aug. 1977, p. 281.
- [15] Liu, H. W., Hu, Y. L., and Ficalora, P. J., *Engineering Fracture Mechanics*, Vol. 5, 1973, p. 281–292.

- [16] Stephens, R. A., Klopp, W. D., and Misencik, J. A., *NASA Technical Brief*, Vol. 5, No. 3, 1980, p. 331.
- [17] Benziger, J. and Madix, R. J., *Surface Science*, Vol. 94, 1980, p. 119.
- [18] Miller, R. N. and Smith, R. L. in *Environmental-Sensitive Fracture of Engineering Materials*, Z. A. Foroulis, Ed., American Institute of Mining, Metallurgical, and Petroleum Engineers, Warrendale, PA, 1979, pp. 628-638.
- [19] Flitt, H. J. and Bockris, J. O. M. in *Environmental Degradation of Engineering Materials in Hydrogen*, M. R. Louthan, R. P. McNitt, and R. D. Sisson, Eds., Virginia Polytechnic Institute Press, Blacksburg, VA, 1982, pp. 13-42.
- [20] Schwarz, J. A., *Surface Science*, Vol. 87, 1979, p. 525.
- [21] Berkowitz, B. J., Burton, J. J., Helms, C. R., and Polizzotti, R. S., *Scripta Metallurgica*, Vol. 10, 1976, p. 871.
- [22] Pressouyre, G. M. in *Current Solutions in Hydrogen Problems in Steels*, C. G. Interrante and G. M. Pressouyre, Eds., American Society for Metals, Metals Park, OH, 1982, pp. 19-34.
- [23] Parrish, P. A., AFML-TR-76-120, Air Force Materials Laboratory, Wright-Patterson Air Force Base, Dayton, OH, 1975.
- [24] Bhansali, K. J., Lynch, C. T., Vahldiek, F., and Summitt, R., in *Effect of Hydrogen on Mechanical Behavior of Materials*, Thompson, A. W. and Bernstein, I. M., Eds., American Institute of Mining, Metallurgical, and Petroleum Engineers, New York, 1976, p. 185.
- [25] Lynch, C. T., Vahldiek, F. W., Bhansali, K. G., and Summitt, R., in Ref. 18, pp. 639-658.
- [26] Volkl, J. and Alefeld, G. in *Diffusion in Solids*, A. S. Nowick and J. J. Burton, Eds., Academic Press, New York, 1975, p. 232.
- [27] Tison, P., Brouteur, R., Fidelle, J. P., and Hocheid, B., in *Second International Congress on Hydrogen in Metals*, Paper 1A4 Paris, France, 1977, Pergamon Press, Elmsford, NY.
- [28] Chatterjee, S. S., Ateys, B. G., and Pickering, *Metallurgical Transactions Annual*, Vol. 9A, March 1978, pp. 389-395.
- [29] Stone, J. M. in Ref 19, pp. 83-100.
- [30] Kumnick, A. J. and Johnson, H. H., *Metallurgical Transactions Annual*, Vol. 5A, 1974, p. 1199.
- [31] Kumnick, A. J. and Johnson, H. H., *Metallurgical Transactions Annual*, Vol. 6A, 1975, p. 1087.
- [32] Kargol, J. A., Fiore, N. F. and Paul, L. D. in Ref 19, pp. 55-67.
- [33] Kargol, J. A. and Paul, L. D. in Ref 22, pp. 91-97.
- [34] Huffman, C. L. and Williams, J. L., *Corrosion*, Vol. 16, 1960, pp. 430-432.
- [35] Piggott, M. R. and Siarkowski, A. C., *Journal of Iron and Steel Institute*, Vol. 210, 1972, pp. 901-904.
- [36] Caskey, G. R., *Material Science and Engineering*, Vol. 14, 1974, p. 110.
- [37] Covington, L. C., *Corrosion*, Vol. 35, No. 8, Aug. 1979, p. 378.
- [38] Shultz, R. W. and Covington, L. C., *Corrosion*, Vol. 37, No. 10, October 1981, p. 585.
- [39] Swansiger, W. A., Musket, R. G., Weirick, L. J., and Bauer, W., *Journal of Nuclear Materials*, Vol. 53, 1974, 307.
- [40] Swansiger, W. A. and Bastaz, R., *Journal of Materials*, Vol. 85/86, 1979, pp. 335-339.
- [41] Van Deventer, E. H., MacLaren, V. A., and Marani, V. A., *Journal of Nuclear Materials*, Vol. 88, 1980, p. 168.
- [42] Van Deventer, E. H. and Maroni, V. A., *Journal of Nuclear Materials*, Vol. 113, 1983, p. 65.
- [43] Murray, G. T., Honegger, H. H., and Mousel, T., *Corrosion*, Vol. 40, 1984, pp. 146-151.
- [44] Danks, D., Senior Project, California Polytechnic State University, San Luis Obispo, CA, unpublished, 1982.
- [45] Nelson, J. G., and Murray, G. T., *Metallurgical Transactions Annual*, Vol. 15A, March 1984, p. 597.
- [46] Murray, G. T., Bouffard, J. P. and Briggs, D. A., *Metallurgical Transactions Annual*, in press, 1986.

DISCUSSION

Mackor: Did you deposit your silicon nitrides by CVD on top of your steel?

Murray: No, those were reactively sputtered. All of those: TiO_2 , Al_2O_3 , SiO_2 , Si_3N_4 .

Mackor: I noted that there is very little difference between your SiO_2 and your Si_3N_4 . Normally you do not get silicon nitride without a large amount of silicon oxide in it.

Murray: I see. I did not know that. We did not examine the films in this respect.

Schwab: In your test that you ran here, did you see the brittle intergranular ring?

Murray: No, we did not see the thick brittle ring, but we did see a few brittle regions of very small thickness near the surface. The ductility loss may be associated with these regions, which were scattered around the periphery. That was also the case for the loss in ductility for the long charging time. It appears that the oxide may not be complete around the circumference.

Schwab: When you look at the fracture surfaces in the broken specimen, does it give you any clue as to what mechanism is causing a reduction in ductility?

Murray: We did observe spots of intergranular fracture around the surface looking at the cross section, but they were scattered and were not very thick. They were very small, apparently enough to reduce the ductility.

Schwab: Did you look at the structure of the oxide that you formed by thermal treatment?

Murray: We are looking at it now just to see if there are some cracks formed during charging. We have not looked at the structure by X-ray diffraction.

Schwab: I wonder if the oxide is cracked or crazed when you finally use it?

Murray: We are not sure at the moment. We are working on that right now.

Hydrogen Embrittlement and Relief Treatment Study of Zinc Phosphate-Coated Submunitions

REFERENCE: Voorhis, G. P., "Hydrogen Embrittlement and Relief Treatment Study of Zinc Phosphate-Coated Submunitions," *Hydrogen Embrittlement: Prevention and Control*, ASTM STP 962, L. Raymond, Ed., American Society for Testing and Materials, Philadelphia, 1988, pp. 318-334.

ABSTRACT: The effect of various zinc phosphating treatments on the hydrogen embrittlement susceptibility of high-strength steel artillery submunitions and the effect of subsequent thermal relief treatments were evaluated in this study.

The submunitions were two types of grenade bodies fabricated from AISI 4140 steel and AISI 15B41 steel. The first type of grenade body contained an embossed inside wall and was heat treated to a hardness Rockwell "C" (HRC) range of 38 to 45 HRC. The second type of grenade body contained a smooth inside wall and was heat treated to a hardness range of 44 to 50 HRC.

Test specimens, machined from the heat treated and zinc phosphate-coated components, were in the form of rings that were stressed to 65% of the nominal breaking load for 200 h. Specimens that failed the 200-h test were considered embrittled; specimens that did not fail were considered nonembrittled. Failed specimens were examined with a scanning electron microscope for the evidence of intergranular fracture, which substantiated that hydrogen embrittlement had occurred.

It was shown that the zinc-phosphated material was susceptible to hydrogen embrittlement. The susceptibility increased when the exposure time and the acid concentration of the zinc phosphate process increased. Thermal bake-out treatments at ambient and at elevated temperatures were effective in reducing the embrittlement effect. Thirty days at ambient temperature or 3 h at 93°C (200°F) were found to be adequate in eliminating hydrogen embrittlement. These relief treatments are not effective when the acid concentrations in the zinc phosphate-coating process are abnormally high.

KEY WORDS: hydrogen embrittlement, high-strength steels, zinc phosphate coatings, thermal relief treatments, bakeouts, delayed failure testing

It is known that steels, particularly those of high strength, are susceptible to hydrogen embrittlement when subjected to various acid cleaning and zinc phosphate coating immersion treatments [1,2]. The available hydrogen, in the form of free acid from the sulfuric acid (cleaning) and phosphoric acid (coating) solutions, readily diffuses into the high-strength steel, thereby causing the steel to embrittle, that is, lose in toughness or ductility or both. In general, as the strength of a steel increases, the hydrogen embrittlement susceptibility increases.

To alleviate the embrittlement effect from the zinc phosphate treatments, thermal relief treatments (hydrogen bakeouts) are used such as described in Federal Specification TT-C-490. Heating to 93°C to 99°C (200° to 210°F) for 15 min is cited as a hydrogen embrittlement relief treatment. Other specifications, such as DOD-P-1623F, cited 99° to 107°C (210° to 225°F) for 8 h or a room temperature bakeout for 120 h to be adequate. The conventional standard [3] for

¹Materials engineer, U.S. Army Armament Research, Development, and Engineering Center, Dover, NJ.

the bakeout of hydrogen at 190°C (375°F) cannot be applied to zinc-phosphated steels since a temperature above 107°C (225°F) will degrade the zinc phosphate coating.

The United States Army contracted six manufacturers to produce two types of artillery submunitions (grenade bodies) using AISI 4140 and 15B41 steels. The manufacturing process for the grenades consists of a six-step, cold-drawing operation of spheroidized annealed strip stock. One of the grenade types uses an embossed starting stock that produces an embossed inner wall on the grenade. This embossing is used to enhance the fragmentation of the grenade. During the drawing operation of the embossed grenade body, stress risers in the form of cracks developed at the root of the embossing notches. The second type of grenade is produced with a smooth wall and does not contain these stress risers.

The embossed and smooth-wall grenades were heat treated to hardness ranges of 38 to 45 HRC and 44 to 50 HRC, respectively. The choice of heat treatment, austemper or quench and temper, was at the manufacturer's discretion. The finished parts were cleaned in a phosphoric or sulfuric acid bath and then subjected to a zinc phosphate immersion treatment (containing phosphoric acid), which provides a corrosion-resistant coating. In many cases, the zinc phosphate treatment does not produce a satisfactory coating in a single exposure. In such cases a second and possibly a third exposure is necessary. The multiple exposures of the grenade bodies to the cleaning and coating baths increased the amount of hydrogen diffusing into the high-strength steel, thereby increasing hydrogen embrittlement susceptibility.

The finished grenade bodies are subjected to various hoop stresses during the press loading of the high explosive and final assembly. Any cracking of the grenade during this point in the production will go unchecked, and the grenades are directly loaded into the carrier artillery shells. Needless to say, an affected or cracked grenade presents a potential detonation problem during handling and firing when the grenades experience radial loading (crushing).

The purpose of this work is to determine the susceptibility of the grenade bodies to hydrogen embrittlement and to investigate the effect of thermal relief treatments at 96°C (205°F) and at room temperature [4].

Procedure

Specimen and Test Configuration

The specimens used in this work, shown in Fig. 1, were in the form of 0.89-cm (0.35-in.)-wide rings machined from the cupped end of the grenade bodies.

The breaking loads (in radial compression) of representative grenades from the various manufacturers were determined by loading specimens to failure in compression using an Instron Universal test machine. This type of loading creates tensile stresses located directly under the contact points on the inside surfaces of the specimen that is similar to what would occur if a grenade was crushed radially. A schematic of the loading configuration and a typical test result are shown in Fig. 2. From these tests, a mean deflection value that corresponded to 65% of the breaking load was determined. The 65% value was used to insure that the corresponding load was below the elastic or proportional limit of the ring's load-deflection curve.

The effect of hydrogen embrittlement on the acid-cleaned and zinc phosphate-coated grenade bodies was determined by delayed-failure tests. In these tests, the rings were compressed by C-clamps to the 65% breaking load-deflection point determined previously. This load configuration was similar to that used in the compression tests. The rings were held under load until failure occurred or for 200 h at which time the test was completed. The absence of a failure after 200 h of loading indicated that the grenade body was not embrittled by hydrogen. This test is somewhat of a modification of that test described in ASTM Method for Mechanical Hydrogen Embrittlement Testing of Plating Processes and Aircraft Maintenance (F 519-77), whereas the grenade rings are tested to evaluate the embrittling nature of the acid-cleaning and zinc phosphate-coating treatments and their effect on separately manufactured grenades.

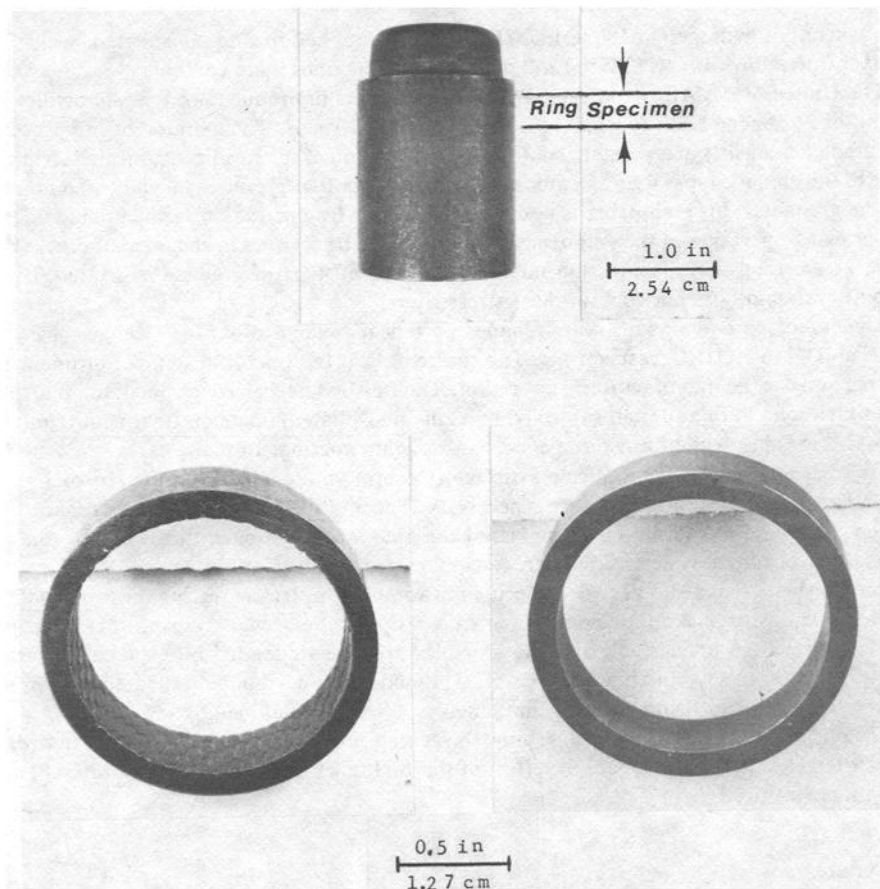


FIG. 1—Grenade body (upper) with the location from which each specimen was taken (about $\times 0.75$). Ring specimens from the embossed (bottom left) and smooth-walled (bottom right) grenade bodies (about $\times 1.6$). Note the embossed and smooth surfaces on the inside walls.

One drawback in testing these grenade bodies was that the specimens could not be tested immediately after the cleaning and coating treatments. In all cases, the grenade specimens were tested within 48 h of the treatments. This lag time was due to shipping and specimen preparation.

Test Program

Eight ring specimens from each manufacturer of grenade bodies were loaded to failure in radial compression. Of the eight specimens, four were uncoated, two were passed through the cleaning and coating process once, and two were passed through twice.

The delayed-failure test variables are listed in Table 1. Tests were performed on single- and double-processed specimens as well as uncoated specimens immersed in a 30% hydrochloric acid aqueous solution for 20 min. The latter tests were performed to provide classical hydrogen embrittlement fractures for scanning electron microscopy (SEM). Thermal relief treatments are also listed in Table 1.

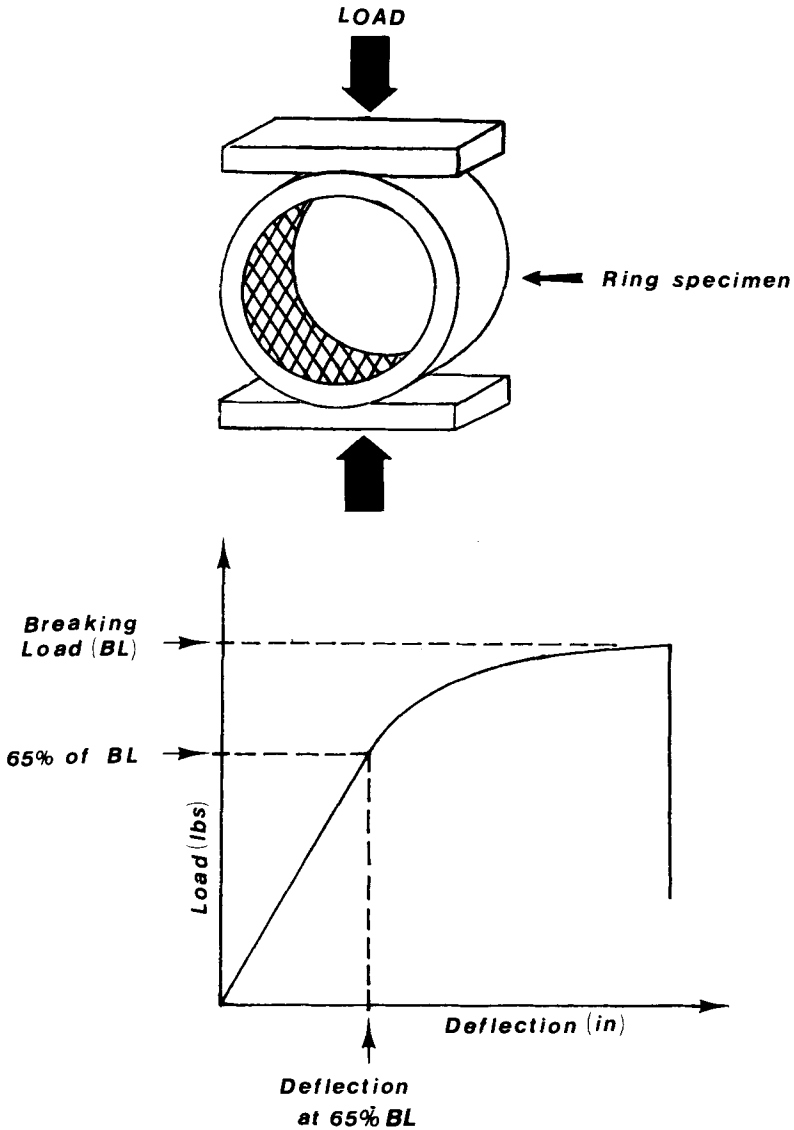


FIG. 2—Upper: The loading configuration of the ring specimens from the grenade bodies. Lower: Typical results of the radial compression test of the ring specimens. Load versus deflection curves and breaking loads are determined.

Tests were also performed on rings from uncoated (and acid-cleaned) grenade bodies to determine whether delayed failure would occur from factors other than hydrogen embrittlement.

The fracture surfaces on all ring specimens that failed during the delayed-failure tests were examined by SEM. The fracture surfaces of the compression-tested failures were also examined.

Hardness measurements and metallographic examinations were performed on each group (manufacturer) of grenade bodies.

TABLE 1—Test plan for the delayed failure testing of the as-received and the thermal relief treated embossed and smooth-walled grenade bodies.

Manu- facturer	Single Zinc Phosphated				Double Zinc Phosphated				Uncoated A/R	Uncoated w/HCl Pickled
	A/R	5 Day/RT	30 Day/RT	E	A/R	5 Day/RT	30 Day/RT	90 Day/RT		
A	E	E	E	E	E	E	E	...	E	E
B	E/S	E/S	E/S	...	E/S	E/S	E/S	E/S
C	E/S	E/S	E/S	...	E/S ^a	E/S	S ^a	S ^a	E/S	E/S
D	E	E	E	E	E	E
E	E	E	E	E	E	E	E	...	E	E
F	E/S	E/S	E/S	E/S	E/S	E/S

NOTE: E/S = both embossed and smooth walled; E = embossed only; S = smooth walled; A/R = as received; "... " = no test performed for that condition.

^aAdditional groups of double-phosphated grenade bodies from Manufacturer C with a thermal relief treatment of 96.1°C (205°F) for 15 min was also tested.

Results

Delayed-Failure Tests of Coated and Acid-Pickled Grenade Bodies

The results of the delayed-failure tests for the embossed wall grenades are shown in Table 2 with the hardness and compressive breaking loads listed for each grenade manufacturer. For confidentiality, the manufacturers will be referred to in this study as Manufacturer A, B, . . . F. The rings from the single and double zinc phosphate-processed (including either a sulfuric or phosphoric acid cleaning) grenades made by Manufacturers B and C did not fail. Single-processed grenade specimens from Manufacturers D and F also passed the 200-h test; however, failures occurred in the rings from double-processed grenades. The single and double zinc phosphate-processed rings from manufacturers A and E failed the 200-h test. In most cases the failures occurred within 48 h from the start of the test. All embossed grenade bodies subjected to the 30% hydrochloric acid solution failed within 24 h after loading.

The results of the delayed-failure tests for the smooth-wall grenade bodies are shown in Table 3. With the exception of the first lot of specimens from Manufacturer C, all smooth-walled

TABLE 2—*Delayed failure (hydrogen embrittlement) test results for the embossed ring specimens (as received); (F/N)^a hardness and breaking load values also listed.*

Manufacturer	Single Zinc Phosphate Coating	Double Zinc Phosphate Coating	Uncoated and Pickled in HCl ^b	Hardness, HRC	Breaking Loads, lb
(AISI Steel Type)					
A (4140)	2/4	2/4	4/4	42	1400 ± 150
B (4140)	0/4	0/4	4/4	41 to 43	1400 ± 150
C (15B41)	0/4	0/4	4/4	44	1420 ± 150
D (15B41)	0/4	1/4	4/4	40 to 45	1560 ± 190
E (15B41)	2/4	2/4	4/4	41	1450 ± 100
F (4140)	0/4	2/4	3/3	39 to 42	1500 ± 120

^aF/N = number of failures/number of specimens tested.

^bHydrochloric acid pickled in laboratory.

TABLE 3—*Delayed failure (hydrogen embrittlement) test results for the smooth-walled ring specimens (F/N)^a; hardness and breaking load values also listed.*

Manufacturer	Single Zinc Phosphate Coating	Double Zinc Phosphate Coating	Uncoated and Pickled in HCl ^b	Hardness, HRC	Breaking Loads, lbs
AISI Steel Type					
B (4140)	0/4	0/4	4/4	48	2330 ± 55
C, Lot 1 (15B41)	2/4	4/4	4/4	51	2640 ± 90
C, Lot 2 (15B41)	0/4	4/4	... ^d	48	2330 ± 75
F (4140)	0/4	0/4	4/4	48	2390 ± 90
C, Lot 1/B ^c (15B41)	0/4	0/4

^aF/N = number of failures/number of specimens tested.

^bHydrochloric acid pickled in laboratory.

^cUncoated grenade bodies from Manufacturer C, Lot 1, acid pickled and zinc phosphate coated by Manufacturer B.

^d"..." denotes that no test was performed for that condition.

grenade specimens passed the delayed-failure test. It was later determined that the cleaning and coating processes used on Lot 1 of the Manufacturer C grenade bodies had higher levels of free acid than that used on the Lot 2 grenade bodies. This was confirmed by retesting the Lot 1 bodies after being subjected to another manufacturer's (B) coating process. No failures occurred during this retest. All smooth-walled specimens pickled in the hydrochloric acid failed within one day of loading.

Delayed-Failure Tests of Specimens with Thermal Relief Treatments

The effect of a thermal relief treatment on reducing the number of delayed failures (due to hydrogen embrittlement) in the embossed grenade specimens is shown in Table 4. After a relief treatment of five days at room temperature, the number of failures was reduced for specimens from Manufacturers A and E. In addition, after 30 days at room temperature, no failures occurred. The failures observed in the initial testing of Manufacturers D and F (without a relief treatment) were eliminated after a five-day, room temperature, thermal relief treatment.

The effect of a thermal relief treatment in reducing delayed failures in the smooth-wall grenade bodies from Manufacturer C are shown in Table 5. A five-day thermal relief treatment at room temperature eliminated the failures in the single-coated grenade specimens; however, little or no embrittlement relief was achieved for those grenades processed twice [with and without an initial 96°C (205°F), 15-min bakeout performed by the producer]. The number of failures in the double-processed grenade bodies was reduced after 30 days at room temperature and was eliminated after 90 days at room temperature.

Delayed-Failure Tests of Uncoated Specimens

Uncoated grenade body rings from the six manufacturers were loaded to 65% of their respective breaking loads for 200 h and did not fail.

Fractography by Scanning Electron Microscopy

Hydrochloric Acid Pickle. In general, an intergranular fracture mode with hair-like features on the grain facets was observed on the fracture surfaces of all acid-pickled grenade bodies

TABLE 4—Delayed failure tests of the embossed ring specimens from grenade bodies subjected to hydrogen embrittlement relief thermal treatments (F/N)^a.

Manufacturer	Single Zinc Phosphate Coating		Double Zinc Phosphate Coating			
	5 Days at RT	30 Days at RT	5 Days at RT	30 Days at RT	(205°F) for ^b 15 min	(205°F) for 15 min. ^b and 5 Days at RT
A	1/3	0/3	0/3	0/3
B	0/3	...	0/3
C	0/3	...	0/3	...	0/4	0/3
D	0/3	...	0/3
E	0/3	0/3 ^c	1/3	0/3 ^c
F	0/3	...	0/3

^aF/N = number of failures/number of specimens tested.

^bRelief treatment at 96.1°C (205°F)/min performed by Manufacturer C.

^c40 days at RT.

"..." denotes that no test was performed at that condition.

TABLE 5—*Delayed failure tests of the smooth-walled rings from grenade bodies subjected to hydrogen embrittlement relief thermal treatments (F/N)^a.*

Manufacturer	Single Zinc Phosphate Coating	Double Zinc Phosphate Coating			Double Zinc Phosphate Coating, 96.1°C (205°F)/15 Min plus		
	5 Days at RT	5 Days at RT	30 Days at RT	90 Days at RT	5 Days at RT	30 Days at RT	90 Days at RT
B	0/3	0/3
C, Lot 1	0/3	3/3	2/3	0/3	2/3	1/3	0/3
C, Lot 2	0/3	0/3	0/3
F	0/3	0/3
C, Lot 1/B ^b	0/3	0/3

^aF/N = number of failures/number of specimens tested.

^bUncoated grenade bodies from Manufacturer C, Lot 1, acid pickled and zinc phosphate coated by Manufacturer B.

"..." denotes that no test was performed at that condition.

(embossed and smooth walled). The hair-like features are remnants of localized plastic deformation on the grain facets. This is a typical fracture mode for hydrogen-embrittled, high-strength steels (hardness greater than 39 HRC) [5,6].

In the embossed grenade bodies, the intergranular regions were more prevalent on those made from the boron steel (AISI 15B41), that is, Manufacturers C, D, and E, as compared to those made from AISI 4140 steel (Manufacturers A, B, and F). The intergranular regions in the 4140 steel fractures surfaces were smaller and less frequent; in the case of those grenades made by Manufacturer F, the intergranular regions were very difficult to locate. A common feature of all the embossed grenade bodies was that fracture initiation occurred by microvoid coalescence (a dimple ductile mode), followed by a combination of dimple ductile and patches of intergranular fracture. These features are shown in Figs. 3 and 4.

The intergranular fracture regions on the smooth-wall grenade bodies were as prevalent as those found on the boron steel, embossed grenade bodies. These regions were also surrounded by the dimple ductile fracture. Fractographs of a typical smooth-wall grenade fracture (acid pickled) are shown in Fig. 5.

Zinc Phosphate Coated. The fracture surfaces of the zinc phosphate-coated, embossed grenade bodies did not exhibit the classic examples of intergranular failure to the extent observed in the hydrochloric acid-pickled bodies. For example, of the four groups that experienced delayed failure, intergranular fracture was observed only in the grenade bodies from Manufacturer D and in very small amounts, as shown in Fig. 6. In the other three groups of grenade bodies made by Manufacturers A, E, and F, intergranular fracture was not readily detectable; only the microvoid coalescence (or dimple ductile) fracture mode was observed in the embrittled embossed region. The fracture surfaces of the embossed grenades subjected to a thermal relief treatment (five days at room temperature) were similar to those described above.

Examples of the fracture surfaces of the smooth-wall grenade bodies (Manufacturer C only) are shown in Figs. 7 and 8. The fracture surfaces exhibited a classical hydrogen embrittlement failure, containing large amounts of intergranular fracture.

Compression Tested. An example of a compression test failure is shown in Fig. 9. The fracture mode for each type of grenade was essentially the same. Fracture initiation occurred by a dimple ductile mode followed by quasicleavage in the fast fracture region. All fractures in the embossed grenade bodies initiated at the embossing. The smooth-wall grenade rings failed at the same stressed areas as the embossed rings.

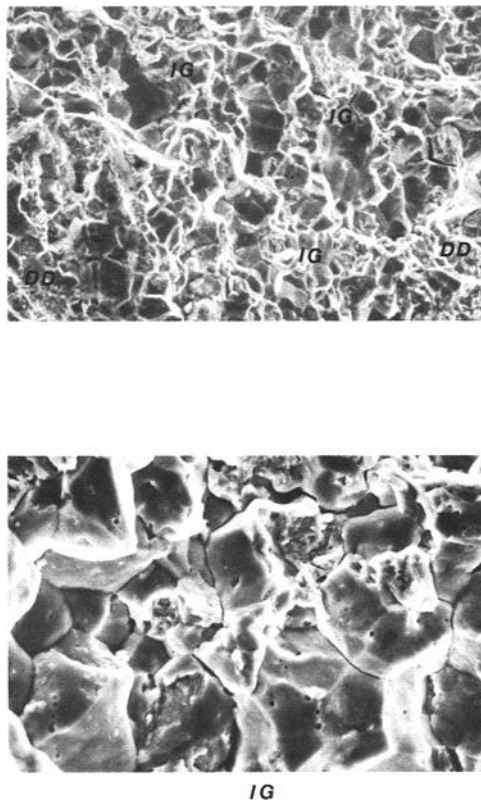


FIG. 3—Hydrochloric acid-pickled embossed grenade body (15B41 steel—Manufacturer E) examined by SEM. Upper fractograph shows a large patch of intergranular (IG) fracture surrounded by a dimple ductile (DD) mode (about $\times 300$). Lower fractograph shows the same region of intergranular fracture (about $\times 1000$).

Metallography

Typical examples of the embossed and smooth-wall grenade microstructures are shown in Fig. 10. The embossed grenade bodies made by Manufacturer A, AISI 4140 steel, quenched and tempered, contained a fine-tempered martensitic microstructure. The remainder of the embossed grenades, AISI 4140 and 15B41, austempered, contained bainitic microstructures.

The typical microstructure found in the austempered, AISI 4140 and 15B41 steel, smooth-wall grenade bodies consisted primarily of bainite with tempered martensite.

Discussion

Delayed Failure/Phosphate-Coated Bodies

It has been demonstrated that grenade bodies, as currently manufactured and zinc phosphate coated, can be susceptible to hydrogen embrittlement. This result is not surprising since two factors that promote hydrogen embrittlement in steel are present in these items: high strength and a source of hydrogen (sulfuric or phosphoric acid cleaning and zinc phosphating). A significant number of delayed failures of zinc phosphate-coated embossed bodies occurred,

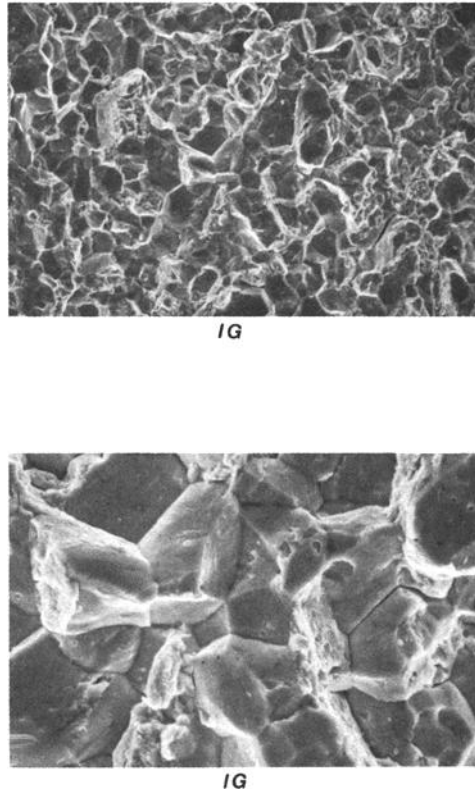


FIG. 4—Hydrochloric acid-pickled embossed grenade body (4140 steel—Manufacturer F) examined by SEM. Upper fractograph shows a small intergranular (IG) patch within a dimple ductile (DD) region (about $\times 1000$). Lower fractograph shows a region of intergranular fracture with typical features on grain facets (about $\times 2000$).

as well as a significant number of grenades that did not fail. Moreover, only one lot of smooth-wall grenade bodies failed during this test. However, for the purpose of this discussion, it will be assumed that the grenade bodies from all the manufacturers are susceptible to hydrogen embrittlement. The reasons for this are described below.

In the case of the embossed grenades, hydrogen embrittlement should always be considered a potential problem because of the embossing cracks, which increase the stress intensity (under load) and hence increase the tendency toward failure when hydrogen is present.

The susceptibility to hydrogen embrittlement of zinc phosphate-coated, smooth-wall grenades should also be considered as a potential problem because of the higher strength (and higher hardness). The maximum advisory hardness for these grenades is 50 HRC; in one case, Manufacturer C, Lot 1, the hardness was found to be slightly higher (51 HRC). The possibility of grenades with above normal hardness coupled with high levels of hydrogen (free acid) in the acid pickle cleaning and zinc phosphate coating baths can promote a greater tendency towards hydrogen embrittlement. For example, it is known [7] that without adequate control of the zinc phosphate bath pH, the free acid content will increase which, in turn, will increase the quantity of embrittling hydrogen entering the steel. The importance of proper control of the bath chemistry was demonstrated by the fact that no failures occurred in the grenade bodies made by Manufacturer C, Lot 1, when cleaned and zinc phosphate coated by Manufacturer B. Informa-

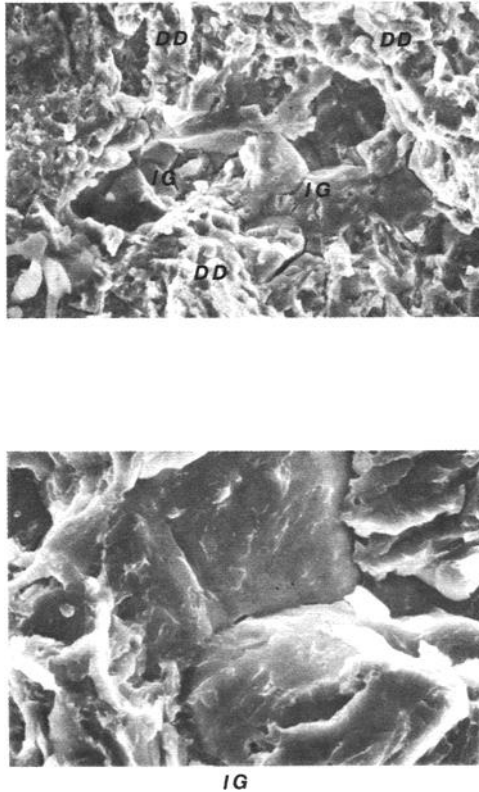


FIG. 5—Hydrochloric acid-pickled, smooth-walled grenade body (15B41 steel—Manufacturer C) examined by SEM. Upper fractograph shows a large patch of intergranular fracture surrounded by a dimple ductile (DD) mode, (about $\times 300$). Lower fractograph shows the same region of intergranular fracture (about $\times 1000$).

tion received from Manufacturer C indicated that the cleaning and coating bath chemistries were not routinely checked. This might explain why Manufacturer C, Lot 1, exhibited delayed failures, whereas Lot 2, as well as the smooth-wall bodies from Manufacturers B and D, did not fail.

Delayed Failures/Phosphate-Coated Bodies with Thermal Relief

It has been shown that some relief from hydrogen embrittlement in zinc phosphate-coated, embossed grenade bodies can be achieved from a room temperature-five day treatment. For those embossed bodies that experienced delayed failures, the room temperature-five day treatment either reduced or eliminated the number of failures. After a room temperature-thirty day treatment, all failures were eliminated. In the case of the failed smooth-wall grenade specimens (from Manufacturer C, Lot 1), single zinc phosphate coated, the five day-room temperature relief was also effective in eliminating the embrittlement effect. However, the same grenade bodies subjected to the cleaning and coating twice continued to fail even after a 30 day-room temperature relief treatment. An elevated thermal treatment of 96°C (205°F) for 15 min was

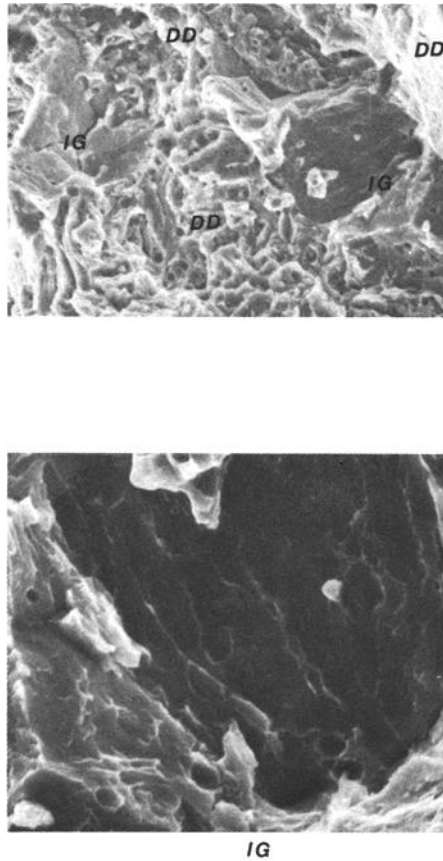


FIG. 6—Double zinc phosphate-treated embossed grenade body (15B41 steel—Manufacturer D). Upper fractograph shows small isolated regions of intergranular (IG) fracture surrounded by dimple ductile (DD) mode (about $\times 1000$). Lower fractograph shows the intergranular fracture with hair-like features on the grains facets (about $\times 3000$).

not totally satisfactory for relieving this lot of grenades. A 90 day-room temperature relief was adequate in eliminating the embrittlement in these grenades.

It should be noted that all of these thermal relief treatments are additions to the initial 48 h of relief that grenades experienced while in shipment to the testing laboratory and during specimen preparation. This 48 h of relief could be very significant in reducing the hydrogen content in grenades that were marginally embrittled by the coating process. It is believed that the number of delayed failures would be greater if the testing was performed within a few hours of coating.

Delayed Failure/Uncoated Bodies

It is significant that none of the uncoated embossed grenades failed the delayed-failure test. This is consistent with and confirms the belief that the delayed failures of the zinc phosphate-coated grenade bodies occurred as a result of hydrogen embrittlement.

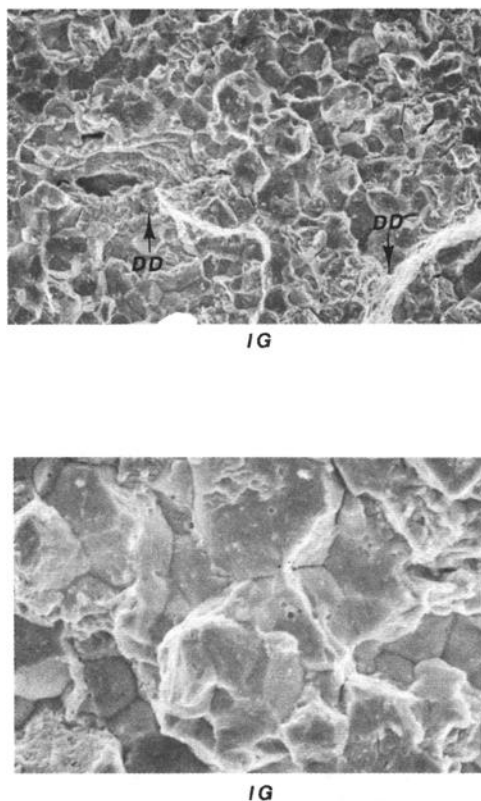


FIG. 7—Single zinc phosphate-treated, smooth-walled grenade body (15B41—Manufacturer C). Upper fractograph shows extensive intergranular (IG) fracture (about $\times 300$). Lower fractograph shows the same region (about $\times 1000$).

Fractography

It is worth noting that intergranular fracture, which is normally associated with hydrogen embrittlement, was not always detectable in all the fracture surfaces of the zinc phosphate-coated embossed grenade bodies. This suggests that the amount of intergranular fracture needed to cause a failure in the embossed grenades is very small. Therefore, the absence or lack of very small amounts of intergranular fracture for an embossed grenade would not necessarily imply the absence of hydrogen embrittlement.

In contrast, all fracture surfaces of the smooth-wall grenade bodies (Manufacturer C, Lot 1) exhibited intergranular fracture with distinctive hair-like features on the grain facets. The difference between the smooth-wall grenade fractures and those found in the embossed grenades is likely to be related to the difference in the grenade hardnesses (50 HRC for the smooth wall and 44 HRC for the embossed).

Microstructure

There was no detectable trend on the effect of microstructure due to heat treatment on hydrogen susceptibility of the embossed grenade bodies. Failures occurred in both the quenched and

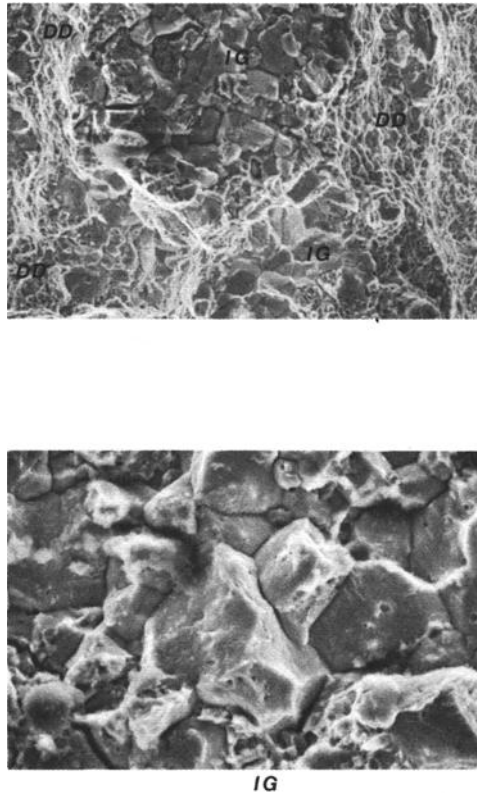


FIG. 8—Double zinc phosphate-treated, smooth-walled grenade body (15B41—Manufacturer C) with 15 min at 205°F (96°C) and 30 days at room temperature thermal relief. Upper fractograph shows patches of intergranular (IG) fracture within the dimple ductile (DD) region (about $\times 300$). Lower fractograph shows the intergranular region (about $\times 1000$).

tempered (martensitic) and austempered (bainitic) embossed grenade bodies. All of the smooth-wall grenades were austempered.

In summary, it is prudent to adopt the position that all the grenade bodies currently manufactured are susceptible to hydrogen embrittlement. Therefore, an embrittlement relief treatment such as a 30-day minimum storage at room temperature should be incorporated into the process to insure the elimination of the detrimental hydrogen content in the grenade. If an elevated temperature bakeout is more practical, then 93°C (200°F) for 2 to 3 h should be considered. The latter treatment provides about the same kinetics as 30 days at room temperature. These recommendations are contingent on quality controls of the zinc phosphate bath chemistries being implemented. Such controls are essential because they will insure the effectiveness of the thermal relief treatments.

Conclusions

1. The delayed failures of the embossed and smooth-wall grenade bodies subjected to the acid cleaning and zinc phosphate coating treatments occurred from hydrogen embrittlement.

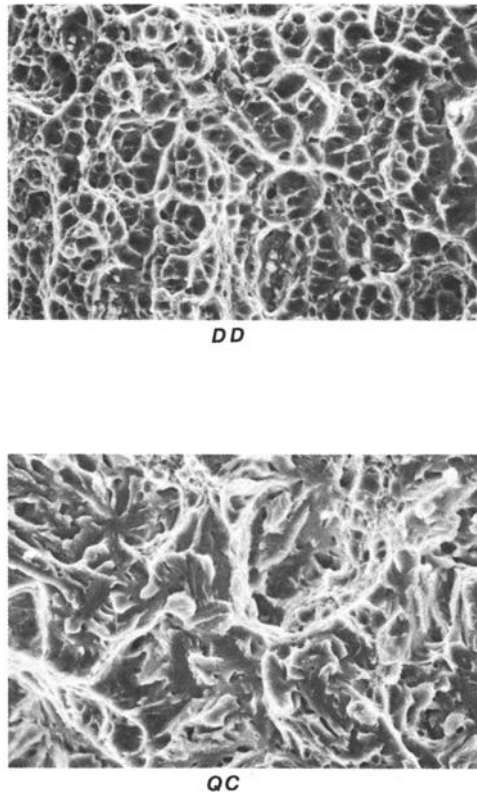


FIG. 9—Compression test to failure of an embossed grenade body (15B41—Manufacturer D) (about $\times 1000$). Upper fractograph shows the region of initiation—dimple ductile (DD). Lower fractograph shows fast fracture region—quasicleavage (QC).

The high hardness of the smooth-wall grenades and the stress concentration caused by the embossing cracks in the embossed grenades were significant factors in promoting these failures.

2. Effective thermal relief treatments of 30 days at room temperature, or 93°C (200°F) for 3 h, are adequate to eliminate hydrogen embrittlement in the grenade bodies when the acid cleaning and zinc phosphate bath chemistries are regularly maintained.

3. Better controls of the acid cleaning and zinc phosphate bath chemistries are needed to minimize the degree of hydrogen embrittlement in the grenade bodies.

4. In the case of the embossed grenade bodies, intergranular fracture was not readily detectable. Therefore, fractography cannot be used as a sole means of determining whether hydrogen embrittlement has occurred.

Acknowledgements

The author wishes to thank James V. Rinnovatore and Karl F. Lukens, Jr., U.S. Army ARDEC, Dover, New Jersey, for their invaluable technical assistance.

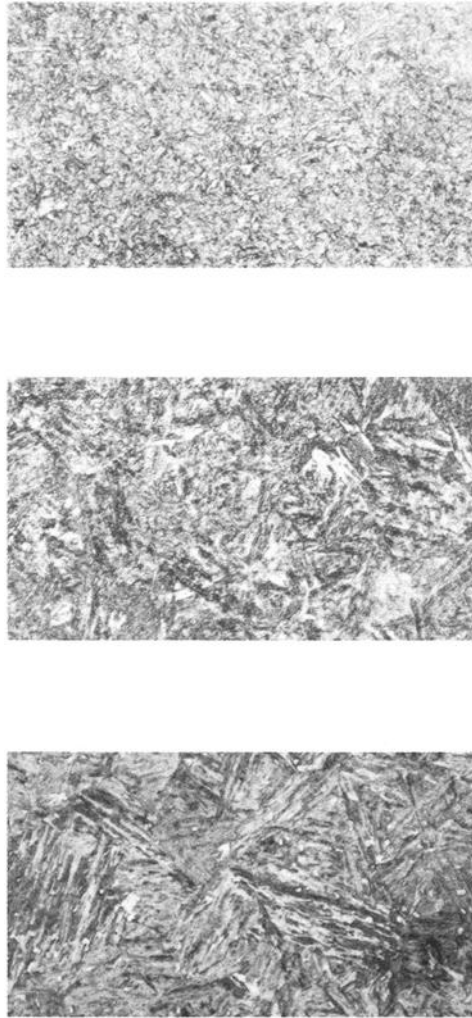


FIG. 10—Representative microstructures of the embossed and smooth-wall grenade bodies (about $\times 800$). Upper: Quenched and tempered 4140 steel embossed grenade body consisting of tempered martensite. Middle: Austempered 15B41 or 4140 steel embossed grenade body consisting of bainite. Lower: Austempered 15B41 or 4140 steel smooth-walled grenade body consisting primarily of bainite plus tempered martensite.

References

- [1] Croucher, T. R., "Delayed Static Failure," in *Metals Progress Source Book Failure Analysis*, American Society for Metals, Metals Park, OH, 1974, pp. 22-24.
- [2] Staehle, R. W., "Hydrogen-Damage Failures," in *ASM Metals Handbook Failure Analysis and Prevention*, Vol. 10, American Society for Metals, Metals Park, OH, 1975, pp. 230-238.
- [3] ASTM Method for Mechanical Hydrogen Embrittlement Testing of Plating Processes and Aircraft Maintenance Materials (F 519-77), American Society for Testing and Materials, Philadelphia, 1977.
- [4] Voorhis, G. P., "A Hydrogen Embrittlement Study of M42 and M46 Grenade Bodies," Report No. MMB-25-84, U.S. Army, ARDC, Dover, NJ, Feb. 1985.

- [5] Phillips, A. and Kerlins, V., "Analyzing Fracture Characteristics by Electron Microscopy," in Metals Progress Source Book *Failure Analysis*, American Society for Metals, Metals Park, OH, 1974, pp. 394-395.
- [6] Jensen, W., "Failures of Mechanical Fasteners," in ASM Metals Handbook *Failure Analysis and Prevention*, Vol. 10, American Society for Metals, Metals Park, OH, 1975, pp. 479-480.
- [7] Military Handbook for Phosphate and Black Oxide Coating of Ferrous Metals," MIL-HDBK-205, Department of Defense, Standardization Division, Washington, DC, June 1957.

Examination of Cadmium-Plated Aircraft Fasteners for Hydrogen Embrittlement

REFERENCE: Levy, M. and Bruggeman, G. A., "Examination of Cadmium-Plated Aircraft Fasteners for Hydrogen Embrittlement," *Hydrogen Embrittlement: Prevention and Control*, ASTM STP 962, L. Raymond, Ed., American Society for Testing and Materials, Philadelphia, 1988, pp. 335-342.

ABSTRACT: The Army Technology Materials Laboratory (AMTL) participated in a possible hydrogen embrittlement (HE) problem involving a variety of cadmium-plated AISI 4340 steel fasteners used in OH-58 and CH-47 helicopters. These fasteners were being reworked at an Army depot where cadmium plating was carried out according to Federal Specification QQ-P-416C. A three-month period was considered suspect for cadmium-plated items processed at the depot, and AMTL was supplied with a number of fasteners (bolts), both new and reworked at the depot during the suspect period, for evaluation. These fasteners were sustained load tested for evidence of HE. All of the bolts provided by the depot survived at least 200 h of testing without cracking or fracture. Several of the bolts which were plated during the suspect period and which had passed HE relief tests were deliberately fractured for examination of failure mode. The fracture topography showed no evidence of HE effects. Hardness and cadmium plating thickness measurements were consistent with specification requirements.

KEY WORDS: aircraft fasteners, high-strength steel, cadmium electroplate, hydrogen embrittlement, fracture, mechanical properties

The Army Materials Technology Laboratory (AMTL) was consulted by the Quality Assurance Division, New Cumberland Army Depot (NCAD), on a possible hydrogen embrittlement (HE) problem involving a variety of cadmium-plated AISI 4340 steel fasteners used in OH-58 and CH-47 helicopters. The OV-1 and U-21 fixed wing aircraft may also have been affected but to a lesser degree.

New Cumberland Army Depot has the responsibility for reworking the just-cited components. They have been plating components in accordance with Federal Specification QQ-P-416C but in August 1977 had instituted the requirement for hydrogen embrittlement testing to monitor their plating process. In addition to QQ-P-416C, MIL-STD-1501 and ASTM E 8 [ASTM Methods of Tension Testing of Metallic Materials (E 8-85)] were being utilized as the appropriate reference documents. Since NCAD does not have an on-site testing capability, a testing source was established at Warner Robins Air Force Command (ALC) Laboratories, Macon, Georgia. New Cumberland cadmium (Cd) plates and stress relieves certified notched round tension specimens to simulate critical processed aircraft components and then forwards specimens to Warner Robins ALC for testing. Four Cd-plated round notched tension specimens designated 7339-3 (CdI), 7339-4 (CdI), 7339-5 (CdII), and 7339-6 (CdII) were submitted to Robins Air Force Base (AFB) for testing. Cadmium plate Type I refers to specimens as plated.

¹Chief—Corrosion Science Branch, U.S. Army Materials Technology Laboratory, Watertown, MA 02172-0001.

²Director—Metals and Ceramics Laboratory, U.S. Army Materials Technology Laboratory, Watertown, MA 02172-0001.

Type II requires a supplementary chromate treatment. Their procedure included (1) static load testing at 75% of the notched ultimate tensile strength (UTS) for 200 h, (2) visual and macroscopic examination, and (3) electron fractography of failed specimens. The test report of 22 Feb. 1978 from Warner Robins ALC indicated specimens 7339-4 (CdI) and 7339-6 (CdII) had failed after 140 h. The remaining specimens completed the 200-h test without failure. It was also reported that visual and macroscopic examination of the two failed specimens revealed fractographic patterns indicative of overload failure over most of the failed surface. However, small areas near the origin of failure showed evidence of time-dependent fracture. Further, electron fractographic studies of the region near the origin revealed a very small area of intergranular faceting in each failed specimen. The faceted area contained a considerable amount of secondary cracking which is typical of hydrogen embrittlement (HE). Other areas showed a dimpled rupture topography typical of overload failure. Based on these results, a hold was placed on Cd plating of parts having hardnesses above HRC 40.

Subsequent troubleshooting and testing resulted in the following actions: (a) liaison with cognizant Navy and Air Force personnel indicated that brightener solution additives can introduce organic materials which, after gradual buildup, will adversely affect the plating process (that is, enhance the possibility of HE), and consequently, the affected Cd plating solutions were run through charcoal filters to remove the organics; (b) after filtration, four additional embrittlement specimens were processed in the Cd plating bath, stress relieved, and forwarded to Warner Robins ALC for the 200-h sustained load test, and on 22 Mar. 1978, NCAD was notified that all four specimens had successfully passed the test; (c) all Cd plating was resumed using charcoal-filtered plating solutions.

Those parts having hardnesses above HRC 40 which had been Cd-plated during the three-month period, 22 Nov. 1977 to 22 Feb. 1978, were considered suspect. The affected parts are identified in Table 1. Components/assemblies or aircraft processed through NACD during this critical time frame, in which the suspect items listed in Table 1 could have been installed, were declared unserviceable by the Army Troop Support Aviation Readiness Command. As a result many aircraft were grounded.

The Army Materials Technology Laboratory was asked to assess the problem and to recommend procedures which might demonstrate that components plated between 22 Nov. 1977 and 22 Feb. 1978 were or were not embrittled by hydrogen during the plating process. Further, one of the fasteners, the retainer latch, was in very short supply. Suspect retainer latches, therefore, had to be salvaged, if at all possible. Recommendations for salvaging these components were requested.

Procedure

The Army Materials Technology Laboratory recommended that sustained load testing of representative suspect Cd-plated fasteners (specifically bolts) be carried out in accordance with MIL-STD-1312, Test 5, at AMTL. Follow-on fractographic analysis would also be performed.

TABLE 1—*Parts cadmium plated during the suspect period.*

Aircraft	Item	Part Number
CH-47	Washer	(772720) 11 YR 2051
CH-47	Bolt	NAS 1304-13
CH-47	Bolt	NAS 1305-13
CH-47	Bolt	NAS 1306-3
OH-58	Latch	(97499) 206-010-121

Accordingly NCAD provided AMTL with representative parts for testing. Federal Specification QQ-P-416C requires that fastener hardware, where the maximum design yield load is not known or given, shall be tested in accordance with MIL-STD1312, Test 5. This test involves the application of an axial load of 75% of the minimum ultimate strength of the product in static load-type testing equipment for a period of 200 h. The development of cracks or failure by fracture constitutes failure of the product.

With respect to the retainer latches, it was recommended that suspect parts be given a bake at $190 \pm 3.8^{\circ}\text{C}$ ($375 \pm 25^{\circ}\text{F}$) for at least 48 h to mitigate possible HE. For the Type II plating (Cd plus chromate treatment) it was recommended that the chromate film (which loses corrosion protection upon heating) be removed prior to baking by using a very mild abrasive (a paste of levigated alumina rubbed on with the finger) and be subsequently rechromate-treated after baking.

Results

Hardness Measurements and Sustained Load Tests

Table 2 lists the bolts provided by NCAD along with the average hardness measured for each plated part, the corresponding ultimate tensile strength extrapolated from hardness conversion tables, and results of the sustained load tests. The applied load in the sustained load tests [941 MN/m^2 (136 ksi)] was based on an average hardness of HRC 40 and ultimate tensile strength of 1255 MN/m^2 (182 ksi). Initial hardness measurements made on Bolts NAS 1304-13, 6.35 mm (0.250 in.)-diameter, indicated the products were "dead soft." Follow-on measurements showed hardness values of HRC 37. The low readings obtained initially on these small diameter bolts were attributed to movement of the bolts in the V-block fixture during measurement. To insure accurate hardness measurement of small diameter bolts, the preferred practice is to grind the bolt flat and parallel. But this procedure would have precluded follow-on sustained load testing. Consequently, a single 6.35-mm (0.250-in.)-diameter bolt, designated "x" in Table 2, was ground flat and parallel, and the average hardness was found to be HRC 40.

All of the bolts tested survived at least 200 h of sustained load testing without cracking or fracture, that is, they passed the embrittlement relief test described in Section 4.5.4 of Federal Specification QQ-P-416C.

Fractographic Analysis

To further investigate the possibility that hydrogen may have been introduced into the bolt during the cadmium plating operation and may not have been adequately removed by the low-temperature embrittlement relief treatment, the 22.225-mm (0.875-in.)-diameter bolt No. 3 (no failure after 261 h of sustained load testing at 75% of UTS) was stressed at an increased load until fracture occurred in the threaded portion. The fracture load was higher than that anticipated from the estimated UTS, with the apparent fracture stress being 1613 MN/m^2 (234 ksi). It is possible that the plastic constraints in the threaded region could have resulted in a notch strengthening effect to give rise to the high apparent fracture stress. However, even had the UTS of the steel been underestimated, delayed failure due to hydrogen could nevertheless be experienced at the stress imposed in the sustained load test.

The fracture surface was examined with the scanning electron microscope to detect any evidence of intergranular fracture. Hydrogen-induced fractures in high-strength steels will usually initiate intergranularly. A scanning electron fractograph, typical of the entire fracture surface, is presented in Fig. 1. The fracture exhibits the dimpled rupture appearance, characteristic of a ductile fracture; no evidence of intergranular fracture was observed at the fracture origin or elsewhere.

Based upon the survival of the specimen under the sustained load test and the absence of the

TABLE 2—Hardness and sustained load test results.

Supplier	Part No.	MTL Number	Diameter, mm	Average Hardness, RC ^a	Ultimate Tensile Strength, Approximate MN/m ²	Sustained Load Test ^a
NCAD	Bolt 114D 2162-3	1	31.750	41	1296	NF 214 H ^a
NCAD	Bolt 114D 2162-4	2	31.750	40	1255	NF 201 H
NCAD	Bolt NAS 634	3	22.225	38	1182	NF 261 H
New	Bolt NAS 634	4	22.225	41	1296	NF 215 H
NCAD	Retainer latch	5	...	41	1296	Not tested
New	Bolt 114D-2162-3	6	31.750	41	1296	NF 200 H
New	Bolt 114D-2162-4	7	31.750	41	1296	NF 235 H
NCAD	Bolt NAS 1305-13	A	7.938	36	1117	NF 239 H
NCAD	Bolt NAS 1305-13	B	7.938	40	1255	NF 267 H
NCAD	Bolt NAS 1305-13	C	7.938	38	1182	NF 216 H
NCAD	Bolt NAS 1304-13	X	6.350	38	1182	Not tested
NCAD	Bolt NAS 1304-13	Y	6.350	36	1120	NF 210 H
NCAD	Bolt NAS 1304-13	Z	6.350	37	1145	NF 287 H

^aNF = no failure; RC = Rockwell C hardness; H = hours.

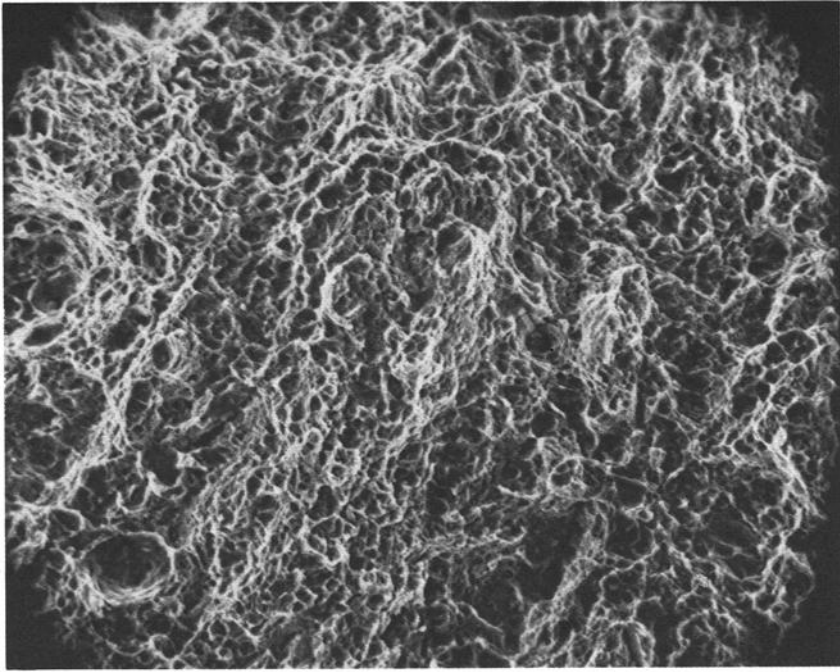


FIG. 1—Scanning electron micrograph of the fractured surface of Bolt NAS 634 (No. 3) $\times 1000$.

intergranular fracture mode in the bolt loaded to failure, it was concluded that insufficient hydrogen remained in the component to give rise to hydrogen embrittlement effects.

Cadmium Plating Thickness Measurement

Since one of the NAS 1304-13 bolts, AMTL designation "X," could not be sustained load tested (it had been ground flat and parallel for hardness measurements), it was decided to metallographically examine this bolt for thickness of cadmium plate. Figure 2 contains photomicrographs of the cross section along the shaft (*A*) and the thread area (*B*).

Note that the thickness of Cd plate is 0.0102 mm (0.0004 in.) and the plate is fairly uniform even at the root of the thread.

Discussion

Simply put, the action to ground aircraft which may contain suspect parts was based primarily on results of the sustained load tests of Cd-plated round notched tension specimens and follow-on fractography reported by Warner Robins ALC on 22 Feb. 1978. These tension specimens were Cd plated simultaneously with actual components being reworked to monitor the plating process. Even though the hardness of the components being plated at NCAD never exceeded HRC44 [1420 MN/m^2 (206 ksi)], yet the sustained load test was carried out on round notched tension bars which have been heat treated to HRC51 to 53. There is no doubt that the higher hardness material will be more susceptible to HE and that the sustained load behavior of HRC 51 to 53 test bars is not characteristic of components having a maximum hardness of HRC 44. This anomaly in test procedure must therefore be resolved.

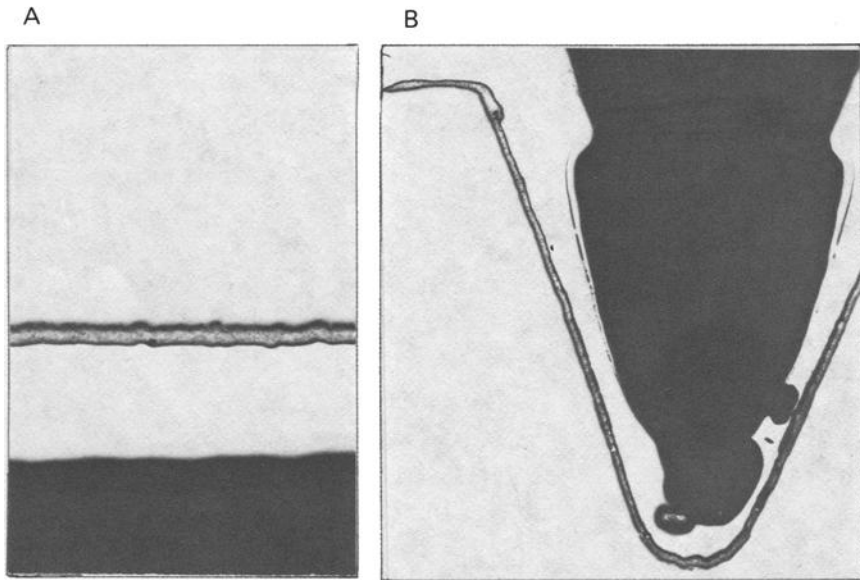


FIG. 2—Photomicrographs showing cadmium plating on Bolt NAS 1304-13 (No. X): (A) shaft area ($\times 200$); (B) threaded area ($\times 100$). Photos have been reduced 30% for printing purposes.)

Justification given for utilizing HRC 51 to 53 specimens for the embrittlement relief test was MIL-STD-1501 (Chromium Plating-Low Embrittlement, Electrodeposition). This standard prescribes that the specimens shall be heat treated to a tensile strength of 1793 to 1931 MN/m² (260 to 280 ksi), which is equivalent to HRC 51 to 53. Federal Specification QQ-P-416C Plating, Cadmium (Electrodeposited), Section 4.3.4 Production Control Specimens, requires that "specimens for the production control embrittlement relief test shall be four round notched steel specimens of alloy steel 4340 conforming to QQ-S-624, heat treated to the maximum tensile strength from one or more heats," etc. But maximum tensile strength representing production usage is implied (see Section 4.3.2 Preproduction Control). It was AMTL's view that Section 4.3.4 should be amended to read "maximum tensile strength representing production usage" to eliminate misinterpretation. Thus the hardness of round notch tension specimens should not exceed HRC 44, which represents the maximum hardness of components being plated at NCAD.

In retrospect, grounding of helicopters based on results of embrittlement relief tests utilizing HRC 51 to 53 specimens may not have been justified. On the other hand, it could not be definitely predicted that fielded Cd-plated 4340 steels parts (maximum hardness HRC 44) would not fail by HE since sustained load testing was not carried out with HRC 44 specimens Cd plated in the suspect bath containing brighteners. The suspect plating bath was not available for such tests because the brighteners had been removed from the bath prior to the involvement of AMTL. It should be noted that Amendment 1 to QQ-P-416C, dated 21 Sept. 1982, Section 3.2.7 Luster, specifies that "parts for aircraft and aerospace applications that are heat treated to HRC 40 and above, shall have a dull luster or finish." Therefore, brighteners should not have been used in the Cd plating bath at NCAD.

Summary

Fasteners, both new and reworked at NCAD during the suspect period, were sustained load tested for evidence of hydrogen embrittlement. All of the bolts provided by NCAD survived at least 200 h of test without cracking or fracture. One of the bolts which was plated at NCAD during the suspect period and which passed the hydrogen embrittlement relief test was deliberately fractured for examination of failure mode. The fracture topography showed no evidence of hydrogen embrittlement effects. Hardness and cadmium plating thickness measurements were consistent with specification requirements.

In order to salvage the retainer latches, it was recommended that suspect parts be given a bake at $190 \pm 3.8^\circ\text{C}$ ($375 \pm 25^\circ\text{F}$) for at least 48 h to mitigate possible HE. The hardness ambiguity in the test procedure for the sustained load test on round notched tension bars (QQ-P-416C, Section 4.3.4 Production Control Specimens) remains to be resolved. Test bars having a maximum hardness of RC 44 were recommended for consistency with production usage. But a compromise solution requiring testing of specimens of Hardness HRC 51 to 53 as well as hardness representative of product usage may be a viable alternative.

Since the correction of the NCAD plating process and adoption of the AMTL recommendation for reclaiming suspect fasteners, no further problems have been reported.

DISCUSSION

Schwab: It is interesting that these failures occurred so long ago, six years ago. The interpretation of the specific point you made as to what the "maximum tensile strength" should be, recently required that we contact the government agency that was responsible for issuing this specification and identify the technical experts, which, in this case, were at NADC in Warminster, Pennsylvania. NADC's interpretation was not at all the interpretation that you proposed here. NADC's interpretation was that "maximum tensile strength" means 260 to 280 ksi strength range, which is the maximum range prescribed for that material in MIL-6875.

It is unfortunate that since 1979 the very confusing language in QQ-P-416 has not been cleared up. We submitted seven pages, almost 40 comments, in review of QQ-P-416, D Revision, last August. I hope that whoever is responsible for this specification or has the influence to get it cleaned up, gets those instructions clarified so that people cannot make the mistake again, because it is very clear to me that anybody could make any of several mistakes in interpreting that specification as it is written today. Do you know what action is being taken to get that clarified?

Bruggeman: Let me say, I agree with you. First of all, this is a specification which is maintained by the Navy, not AMTL. Obviously, what I said does not agree with their interpretation. The specification that was being applied at the time of the incident that I described was QQ-P-416C. There is the D revision, which is being reviewed now. It was much to my dismay that I found, in reviewing QQ-P-416D, that the same language prevailed. I agree with you. I think that there should be something done to clean that up, and I think it would be the Army's position that it be made clear that we are really not talking about the 260 to 280 tensile strength heat treatment as being that required for the separate test bars. I really think that is unnecessary, as I have said. Since this has come to light in preparing this talk, I have gone to see what actual QQ-P-416D terminology was being used and, finding that the change that we had recommended was not incorporated, I intend to pursue that matter further with the appropriate Navy and Army specifications agency.

Schwab: Thank you.

Murray: Do you, by any chance, know what organic additives were in your brightener? Because some act as inhibitors and some may act as a poison.

Bruggeman: No, I do not, unfortunately. We would have liked to have gone back and tried to reproduce some of the alleged embrittling plating operations, but by the time we came on the scene, everybody had their act cleaned up and they were producing good parts again. Therefore, we could not do that, nor do I know what additives were being used.

Murray: It looks like it is something that prevents hydrogen recombination and there are a number of those.

Grobin: We have been experimenting with tests for fasteners since approximately 1965. We recently released our test to ASTM Committee B08, and that is now in balloting. We found that use of test specimens to test fasteners was rather questionable. They rarely related to what really happened to the fasteners. Direct tests on lots of fasteners can be accomplished using a 6° wedge. We have successfully used this test for a number of years and recently have used it in very critical application where it clearly separates embrittled lots from nonembrittled lots of fasteners. This can be applied on a lot-by-lot basis much more realistically. I suggest you get with Committee B08 and get in the circulation of this document. You might find it very useful.

Bruggeman: Thank you. I hope your earlier remark was that the test bars tend to overtest the condition.

Grobin: Yes.

Berman: Why can you not specify a tensile strength in psi because you are working in narrow ranges anyhow? Then there is no ambiguity, even if you are off by a couple of percent. Is that possible?

Bruggeman: We think that what is intended in the specification is that it be loaded to 75% of the ultimate tensile strength, whatever that may be.

Berman: Then if you have two materials, why not say 75% of 260 ksi? Or 75% of 200 ksi, whatever it is and put a number in?

Bruggeman: I would imagine fasteners can be made at any number of strength levels.

Berman: And then say of the fastener, not of the material, so the people know what it is.

Bruggeman: Prior to the remark of the gentleman who spoke just before you, I would have said that the test bars should be heat treated to the same strength level as the fasteners being plated. He is saying that applies an overly severe test, which the Department of Defense might want to continue to go with since they like to build a little margin of safety into their test procedures anyway. I think, however, they (Robins AFB) were building in too much of a margin of safety going with the 260 to 280 ksi. If you make it clear you are talking about 75% of the actual notched tensile strength of the parts being produced, it gives the producer the ability then to produce both fasteners and test specimens to whatever strength level is required by the application at hand.

Proof Test Logic for Hydrogen Embrittlement Control

REFERENCE: Krams, W. E., "Proof Test Logic for Hydrogen Embrittlement Control," *Hydrogen Embrittlement: Prevention and Control*, ASTM STP 962, L. Raymond, Ed., American Society for Testing and Materials, Philadelphia, 1988, pp. 343-349.

ABSTRACT: The embrittlement of production hardware due to the introduction of hydrogen into the hardware as a side effect of normal production processes, such as the plating of parts, has been a long-standing concern. Present nondestructive proof test methods cannot be used to individually qualify suspect parts since the excessive test loads may actually microscopically damage the hardware, rendering it unsafe for in-service applications. A proof test logic, applied to each piece of hardware, is offered based on fracture mechanics concepts to insure 100% reliability of the hardware for in-service applications. The proof test logic is proposed, and the efficacy of its implementation is examined by following the events of an actual case study.

KEY WORDS: proof test logic, hydrogen embrittlement, ASTM Standard F 519, Charpy impact energy, dynamic toughness, rising step load, subcritical crack growth, threshold stress intensity, critical crack size

Proof testing is conventionally a nondestructive test conducted on each piece of hardware prior to its use to establish its structural integrity. A load is applied above the maximum anticipated service load, and the ratio of the proof test load to service load establishes a margin of safety on rupture. Additionally, this ratio is often used to estimate the fatigue life.

ASTM Standard F 519

Hydrogen embrittlement control is generally maintained with a destructive test performed on representative coupons per ASTM Method for Mechanical Hydrogen Embrittlement Testing of Plating Processes and Aircraft Maintenance Chemicals (F 519). If the coupons fail, implying that the parts have been embrittled, the final recourse, before all of the parts are rejected, is to take the same sample size or "lot" of parts, such as pressure containers, fasteners, or springs, from the actual production hardware and test them in a fashion similar to F 519. Obviously, the assumption in testing a sample lot of parts is that each piece of hardware from the lot has been manufactured and processed identically, or, conversely, that no piece of hardware has been manufactured and processed individually.

Again, the intent is that the applied test load exceed the maximum anticipated service load. Consequently, the tested parts are often subsequently sacrificially loaded to destruction, and then the scanning electron microscope is used to verify that no subcritical crack growth has taken place.

¹Senior consultant, L. Raymond & Associates, Irvine, CA 92714.

Concern

Hydrogen embrittlement control test samples taken from the lot of actual hardware are never subsequently placed in-service even though they have passed a 200-h sustained load test because the test load is generally too excessive.

In performing a nondestructive proof test, some military specifications call for a sustained load on the part of 75% of the material's yield (see paper by Robert Dreher in this publication). Because the applied stress on the part is lower and its radius less acute than with a notched coupon (F 519 Type 1a), there is a distinct possibility that the sustained load qualification test applied to the actual part could produce stresses that would be high enough to cause damage during a 200-h test, but not high enough to cause fracture. The occurrence of microscopic damage to a part during this 200-h test would actually result in using a large portion of the parts life expectancy rather than in establishing its integrity. Therefore, any low sustained load stresses must be accompanied by other techniques such as acoustic emission in order to be able to monitor subcritical crack growth during the test.

If there is no traceability or it is suspected that all parts were not processed identically, then each part must be nondestructively proof tested to assure 100% reliability. Obviously, under these conditions, a new approach for hydrogen embrittlement proof testing is required since a proof test applied to each part in the manner just discussed would render all of the parts unavailable for service due to the concern over the damage produced by an excessive test load applied for 200 h.

Case Study

Here is an example to show the need for a nondestructive proof test logic. This actual case study clearly presents a classic example of the acceptance of the efficacy of an embrittlement relief treatment applied to a single lot of parts, based on the successful test results of five notched tensile coupons tested in accordance with ASTM F 519 (Type 1a). None of the test coupons failed after the 200-h test period, and the entire lot of parts was considered to be free of any residual hydrogen due to the plating operation. As a result, 285 helicopter hydraulic actuator pistons were accepted for service since all of the manufacturing quality assurance tests and inspections had been passed.

The parts were shipped in pairs. When the box containing these parts was opened just prior to installation on a helicopter, it was found that one of the pistons was broken. This discovery did not cause a great deal of immediate concern because the system is redundant; two pistons are available for safety. The two pistons were placed back in the box and returned to the manufacturer for a failure analysis on the broken piston. Upon arrival at the manufacturer's plant, the box was opened and both pistons were found to be fractured. So much for redundancy as related to hydrogen embrittlement.

A failure analysis conducted on the fractured pistons revealed that failure occurred by classic intergranular fracture, a surface morphology typical of hydrogen embrittlement. The fracture occurred across a fillet, which constitutes the narrowest cross section of the piston and is the local section plastically deformed in straightening the part.

With the aforementioned considerations in mind, the schematic diagram shown in Fig. 1 is presented to exemplify a typical piston assembly. The cadmium-plated piston is threaded on one end and is manufactured from a 1241 to 1379 MPa (180 to 200 ksi) Type 4340 ESR steel. The fillet region where the fracture occurred is located at the base of the shank just below the threads (see arrow). At installation, a preload occurs at the fillet due to the attachment of another assembly, which is held in place by a nut on the threaded end of the piston. The result is a sustained tensile load in the fillet region. The actual in-service loads result in the superposition of an alternating or fatigue stress onto the preload stress.

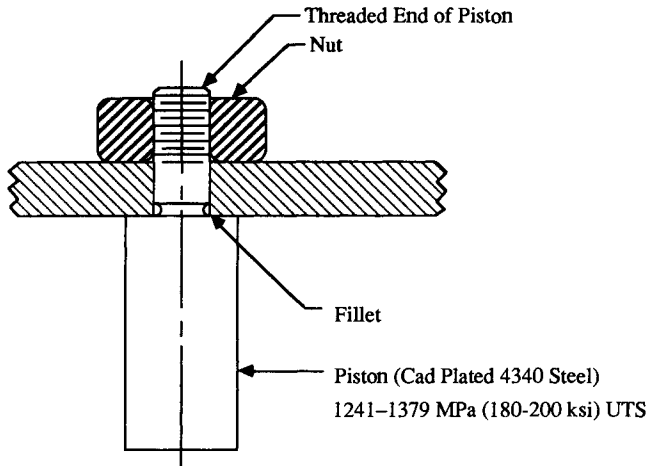


FIG. 1—Schematic illustration of piston assembly under sustained load.

At this point, the structural integrity of the entire inventory of pistons came into question. A trace of the entire lot would have to be conducted in order to establish the identity of the plater, the plating baths, and the conditions under which the parts were plated. Unfortunately, this kind of traceability could not be conducted, and a series of 200-h tests applied as a proof test on all of the actual parts was initiated.

After applying the specified load to these parts for 200 h, it was noted that the parts did not fail, and, therefore, they were considered to be in compliance with the military specifications. It was then decided to leave the parts loaded for a longer period of time. After 210 h, the parts began to fail. The concern was obvious. Is the attempt to establish the integrity of a part by the 200-h proof test only putting more damage into the part?

With the failure of the parts due to microstructural damage after 210 test h, the problem became one of determining a way to salvage the remaining lot of pistons and prove that they would be 100% reliable in-service. In response to this problem, the feasibility of establishing a method to determine the reliability of the remaining pistons was studied. As a result of this study, the necessity for a proof test logic based on fracture mechanics concepts was established. This logic must then be implemented to successfully apply a nondestructive proof test to each piece of processed hardware for subsequent use in-service in order to prevent hydrogen embrittlement failures.

Proof Test

Based upon this reasoning, a proof test sequence composed of the following steps was proposed to be applied to the remaining pistons to obtain 100% reliability:

1. Preload at room temperature and hold for 23 h.
2. Quench in liquid nitrogen.
3. Return to room temperature and retorque.

If a piston went through all of the just-cited steps and cracked, then it would fail the proof test. Also, if the retorque could not be obtained, then the piston would also fail to qualify. But if the retorque was finally obtained, then the piston would be considered 100% reliable.

Logic

A sustained load test period of 23 h was chosen on the basis of the curve developed by Troiano and reproduced in Fig. 2. Troiano's data was based upon 4340 steel with a notched tensile strength of 2069 MPa (300 ksi) and a yield strength of 1655 MPa (240 ksi). His test samples were baked out for different periods of time, thus representing different levels of hydrogen in the steel. Troiano conducted a series of tension tests for each baked lot by holding each specimen at a given load until failure occurred. Lowering the applied stress resulted in only relatively small increases in the time to failure until finally a threshold value of applied stress was reached, below which the time to failure approached infinity. These tests produced the precipitous family of curves shown in Fig. 2. Longer baking times (less hydrogen in the steel) resulted in higher thresholds of applied stress. Another way of describing the results is that it takes a longer period of time for a fracture to occur as the level of hydrogen in the steel is reduced. This family of curves then essentially describes, for each baking time period, a region of failure to the right and above the curve and a no fail region below the curve. From Fig. 2, it is evident that if a part is held for 23 h at 75% of the applied stress, it should fail or at least cause some incipient cracks to form unless there is very little residual hydrogen present in the steel. Therefore, 23 h was specified as the minimum time required for the preload test, which is consistent with the requirements of ASTM F 519.

While 23 h was considered to be sufficient time to initiate a fracture, a sufficient load must also be present. Presumably, when the torque was applied, whatever hydrogen was present in the piston would either cause a crack to initiate and grow subcritically or actually cause the part to fail under the applied stress during the 23-h test period.

The logic behind the remaining steps of the proof test sequence requires an analysis of the mechanical properties of the lot of pistons from a fracture mechanics perspective.

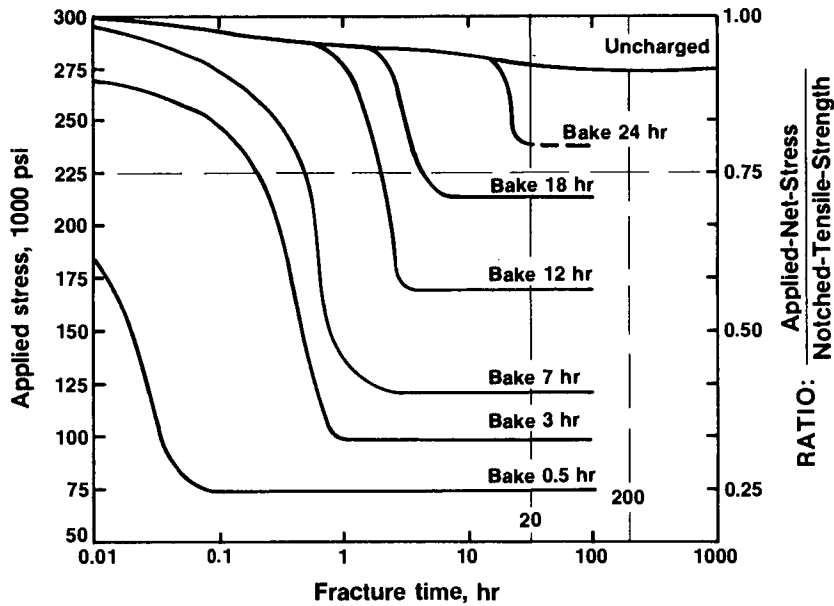


FIG. 2—Effect of hydrogen concentration in Type 4340 steel on fracture time and applied net tensile stress.

Analysis

In order to complete an analysis of the piston failure, tension tests were conducted on material taken from the fractured pistons to obtain the mechanical properties. Several Charpy V-notch specimens were also machined from the failed parts. One set of Charpy specimens was used to obtain the impact energy at room temperature, while another set was used to obtain the impact energy immediately after removal from a liquid nitrogen bath. The dynamic toughness of the material under these two temperature conditions was estimated from the correlation that relates impact energy to dynamic toughness developed by Rolfe and Barsom [1]. For steels above 1034 MPa (150 ksi), the dynamic toughness is roughly equivalent to the slow strain rate toughness. A third set of Charpy specimens was used to measure the threshold stress intensity in an aggressive hydrogen environment ($K_{I_{hem}}$ or $K_{I_{th}}$) utilizing a rising step load test system [2]. These properties were obtained in order to see if there was any merit to testing the part itself.

The results from the tests conducted on the Charpy specimens could be used as indicators of the relative fracture toughness of the material and therefore, its ability to withstand fracture. The Rolfe and Barsom relationship states that the dynamic toughness is proportional to the square root of the Charpy impact energy. If the Charpy impact energy of a material is known at room temperature and at a lower temperature, then the toughness at the lower temperature would be in the ratio of the square root of the Charpy energies times the toughness at room temperature. Knowing those properties, a curve can be constructed similar to the type of curve seen in proof testing for fatigue analysis. This curve, shown in Fig. 3, is based on the equation that relates stress intensity to applied stress (σ) and to a defect size (designated by "a").

The Charpy impact tests on the piston material correlated to a fracture toughness of about 132 MPa \sqrt{m} (120 ksi $\sqrt{in.}$) at room temperature and only about 44 MPa \sqrt{m} (40 ksi $\sqrt{in.}$) at the liquid nitrogen temperature. Obviously, the material goes from a very tough state at room temperature to a very brittle condition at the lower liquid nitrogen temperature. Lowering the fracture toughness essentially results in a shift in the plot of applied stress (σ) versus crack size ("a") as noted in Fig. 3. Therefore, for a given level of applied stress, the critical crack size becomes smaller at the lower temperature. The third curve in Fig. 3 was constructed from the results of

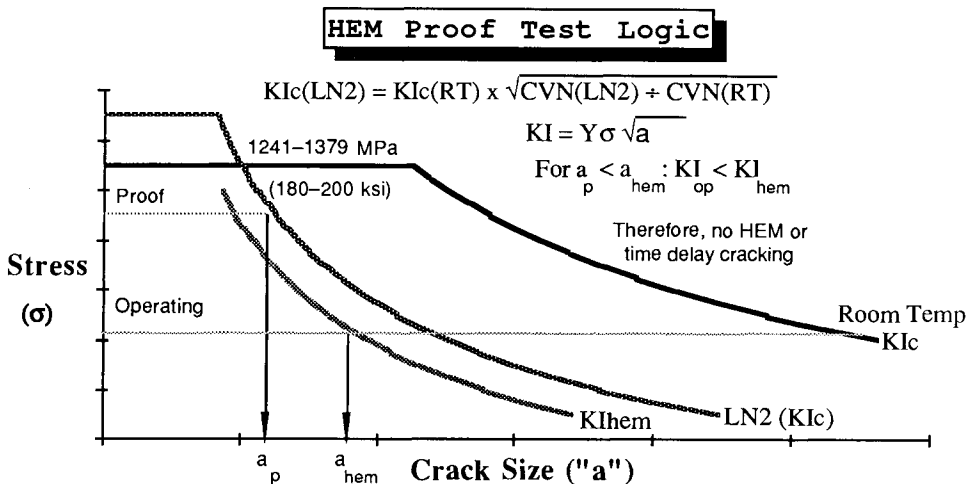


FIG. 3—Basis for proof test logic from measurement of stress intensity parameters for fracture and environmental cracking.

the $K_{I_{hem}}$ or threshold stress intensity test for hydrogen embrittlement at room temperature. This curve delineates the critical combination of applied stress and crack size that will cause subcritical or slow crack growth.

Application of the proof test preload at room temperature could conceivably initiate some cracks in the piston or even cause failure during the 23-h test period depending on the amount of residual hydrogen in the steel. If failure did not occur, immersion in liquid nitrogen with an applied stress level slightly above the operating stress level would then render the material very brittle and thus establish a critical crack size designated " a_p ," the proof test critical crack size. If the part broke in the liquid nitrogen, then that would mean that the crack size was greater than or equal to a_p , and if it did not break then it was less than that value. If fracture did not occur at the liquid nitrogen temperature, retorquing the piston after it returned to room temperature would indicate whether or not any slow crack growth had occurred, since crack growth would be accompanied by a drop in the applied load for a constant displacement test. However, the presence of any cracks at the liquid nitrogen temperature would produce very rapid crack growth resulting in nearly immediate fracture.

If the part survives the liquid nitrogen test and the operating stress level is below the proof test applied stress, then the combination of the operating stress and the crack size defined by the liquid nitrogen immersion is below the critical combination for subcritical crack growth at room temperature. This means that the necessary conditions of applied stress and crack size would not be present to cause a crack to grow in a hydrogen environment at room temperature. Presumably, this then assures that the part will be 100% reliable in-service since fracture mechanics has been used to rationalize that the potential for subcritical crack growth is not present.

Conclusion

To obtain 100% reliability for the prevention of hydrogen embrittlement failure, each and every part must be nondestructively tested. A proof test logic similar to that used to establish the fatigue life can be used to establish the structural integrity with regard to hydrogen embrittlement. For each piece of fracture critical hardware, the fracture toughness must be measured at both the operating and proof temperatures, and the threshold stress intensity for hydrogen stress cracking must be measured at room temperature. The specimens must be taken in the proper orientation from the as-processed parts. Then a proof test load can be established to insure against hydrogen embrittlement failure from processing with 100% reliability.

To avoid the introduction of other problems caused by this proof test procedure, due consideration should be given to the possibility of producing cracks in the plating or debonding of the plating due to the differences in the coefficients of thermal expansion.

Finally, and most importantly, the proof test logic for hydrogen embrittlement control must be conducted from a sound knowledge base, including the availability of sufficient test data, in order to establish the structural integrity of each piece of hardware.

References

- [1] Rolfe, S. T., and Barsom, J. M., *Fracture and Fatigue Control in Structures*, Prentice-Hall, Inc., Englewood Cliffs, NJ, 1977, pp. 167-204.
- [2] Raymond, L., *Tests for Hydrogen Embrittlement*, ASM Metals Handbook, 9th ed., Vol. 8, 1985, pp. 537-543.

DISCUSSION:

Schwab: Would you explain how you got that curve for K_{Isc} ? Was that done using your RIM HEM electrochemical test cell?

Krams: That is how I obtained K_{Isc} , with a Charpy-sized specimen using a potential of -1.2 V versus SCE in a 3.5% salt water solution.

Schwab: And then you assume that K_{Isc} determined in this way is the lowest stress intensity at which hydrogen embrittlement crack propagation will occur?

Krams: Yes.

Schwab: Are there other papers that would back that up? How do you know that? In one case you have stress corrosion and in the other case, hydrogen embrittlement.

Krams: The specimen is cathodically charged, so the mechanism is hydrogen embrittlement.

Schwab: If hydrogen was introduced into the steel during a plating operation and then the part was stressed, crack propagation might occur by hydrogen embrittlement, but in your test with the electrochemical cell, that is a different situation. How do you know that the stress intensity value would be the same in both cases?

Krams: It is absolutely not a different situation. We are cathodically charging the specimen, just as in a plating bath, making hydrogen available under the worst possible conditions, which means, while the specimen is under stress, so the test is definitely a hydrogen embrittlement test and not a stress corrosion test. The result is a hydrogen embrittlement threshold stress intensity and not a stress corrosion threshold under the test conditions we use, which is a negative potential of about -1.2 V.

Schwab: So, no corrosion can occur under those electrochemical conditions?

Krams: No, it is nice and polished and protected just like any steel that is cathodically protected. We are measuring a lower limit value because of the availability of hydrogen. It is available under stress, and that environment is the worse case condition. The test is similar to stressing a part in a plating bath; it will break. That is why, in Standard F 519, the specimens are unstressed when plated, removed, baked, and then the stress is applied.

Schwab: Is the charging rate important in determining K_{Isc} if you change the charging variable through the solution for anything?

Krams: We found that to be so in HY140 steels. As the open circuit potential is approached, the parent metal threshold stress intensity increased. This effect has not been studied that extensively in the higher hardness steels.

Schwab: Is there no standard procedure for the K_{Isc} ? Can you vary your electrode potentials, and so on?

Krams: Correct. We take the worst case condition, which is charging at a very high potential, to obtain a minimum value. The basis for stating that this is a minimum value under very severe testing conditions is based on the results of a Navy program. We tested and compared HY steels that were also tested with the wedge opening load (WOL) specimen in H₂S for 5000 to 10 000 h. Additional data was available with cantilever beam specimens of HY steels coupled to zinc in salt water, and these results gave threshold values higher than the WOL specimens. These results bring up the question of "how long do you wait?," but we found with our RIM HEM testing system our 8-h test results were comparable to the lowest values obtained with the WOL specimens. That is why I feel very confident about the test system producing a very conservatively low threshold value for hydrogen stress cracking.

Section 7: Research in Progress

Quantitative Analysis of Critical Concentrations for Hydrogen-Induced Cracking

REFERENCE: Pressouyre, G. M. and Faure, F. M., "Quantitative Analysis of Critical Concentrations for Hydrogen-Induced Cracking," *Hydrogen Embrittlement: Prevention and Control*, ASTM STP 962, L. Raymond, Ed., American Society for Testing and Materials, Philadelphia, 1988, pp. 353-371.

ABSTRACT: The purpose of this paper is to show how to evaluate the sensitivity of a given material to hydrogen-induced cracking through the use of a conventional electrochemical permeation technique. Prior to the cracking test itself, the permeation cell is used to compute the diffusion, solubility, and trapping characteristics of the material under study; then, hydrogen cracks are created in the disk-shaped specimen and the critical value at which damage appears is found from computed concentration profiles. Because of the numerous underlying theoretical assumptions for the calculation of critical concentrations, the obtained results are finally compared to data gathered from more conventional techniques (chemical analysis, mechanical testing). Critical concentration data for various materials and the use of this data to assess hydrogen embrittlement sensitivity are also discussed.

KEY WORDS: hydrogen, cracking, diffusion, solubility, trapping, low-alloy steels

A synthesis of recent hydrogen embrittlement (HE) theories [1-5] relates the nucleation of hydrogen-induced cracks (HIC) to a critical value, C_K , taken by the concentration of hydrogen trapped, C_H , on particular defects of the microstructure (for example, inclusions, particles, grain boundaries, dislocations, voids, etc.). Figure 1 illustrates this point [8]: hydrogen trapped on specific sites may increase the local stress, σ_T^H , introducing a new component to be added to the applied and/or residual stresses (σ_a^H , σ_R^H), and decrease the cohesive strength ($\sigma_c^H < \sigma_c^0$), so that when $C_K = C_H$, $\sigma_T^H = \sigma_a^H + \sigma_R^H \geq \sigma_c^H$. The C_K -value relative to a given defect is difficult to compute; it depends on a variety of parameters [8] (microstructure, inclusion shape, size, applied stress, etc.). The total critical hydrogen concentration, C_K^T , present in a volume surrounding the site on which a crack nucleates may, however, be calculated as will be shown hereafter; potential use of these results will also be discussed.

Experimental Setup and Procedure

The experimental setup used here is the well-known Devanathan and Stachursky [6] permeation cell. Disk-shaped specimens (diameter: 60 mm; thickness around 1 mm) are cathodically charged with hydrogen at constant current density on one side in 0.1 N sodium hydroxide

¹Senior research metallurgist, Division Head, Center for Materials Research, Creusot-Loire Industrie, 71208 Le Creusot, France.

²Consulting materials engineer, Materials Dept., Framatome, Tour Fiat, 92084 Paris La Defense, France.

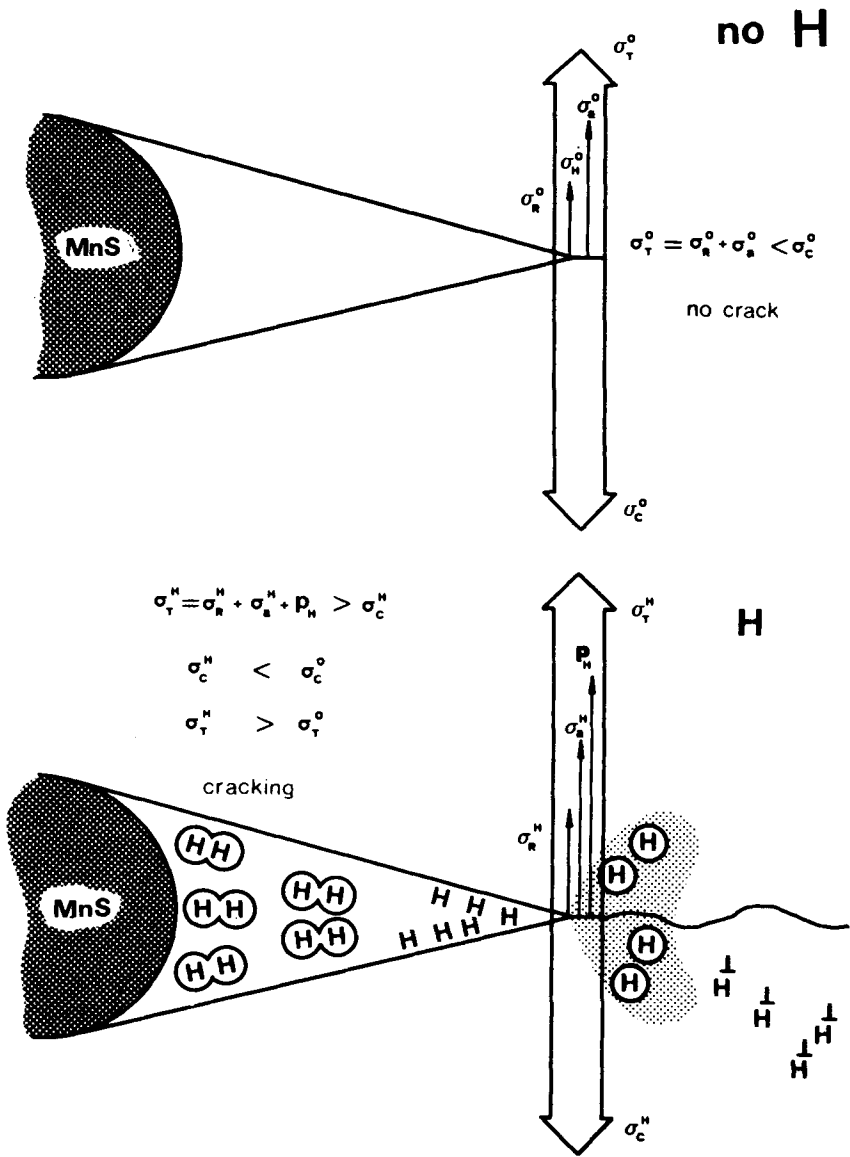
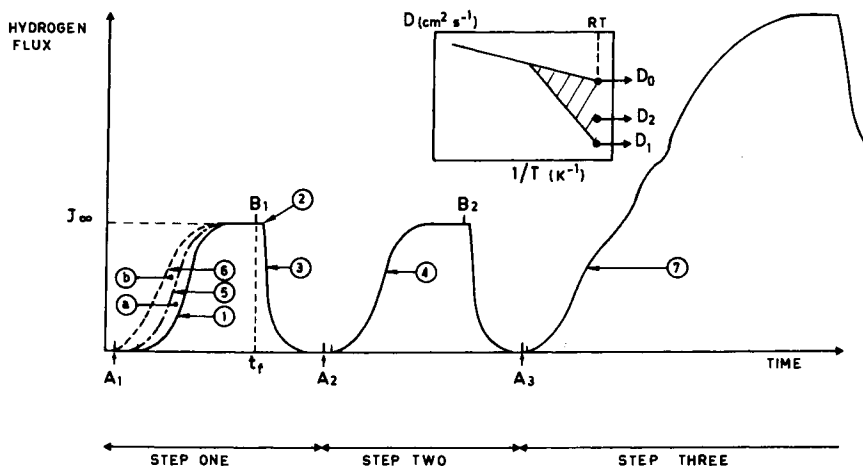


FIG. 1—Schematic illustration of the effect of hydrogen on crack initiation (from Ref 8).

(NaOH) or in acids [for example, 1 *N* sulfuric acid (H_2SO_4)]. Permeating hydrogen is measured on the other side thru a potentiostatic setup [6]: the current density necessary to maintain constant and applied potential between the disk and a platinum counter electrode (this potential serves to oxidize exiting hydrogen: $H \rightarrow H^+ + \bar{e}$) is a direct measure of the permeating hydrogen flux.

As described in more detail elsewhere [7], the calculation of C_K^T may be performed in several steps:



- J_{∞} = steady state flux,
 A_1 = start of first permeation and origin of translated curves,
 B_1 = end of first permeation and start of degassing,
 A_2 = start of second permeation,
 B_2 = end of second permeation,
 A_3 = start of "cracking permeation,"
 ① = first permeation curve for computation of D_1 ,
 ② = location of computation of D_0 ,
 ③ = degassing,
 ④ = second permeation curve for computation of D_2 ,
 ⑤ = translation of ④ to origin A_1 ,
 ⑥ = theoretical permeation curve drawn from D_0 (diffusible hydrogen) with origin A_1 ,
 a = area between ① and ⑤ used to compute C_i (irreversibly trapped hydrogen), and
 b = area between ⑤ and ⑥ used to compute C_R (reversibly trapped hydrogen).

FIG. 2—Schematic of the various experimental steps leading to the calculation of the critical concentration.

Step one. Electrochemical solutions at the input and output sides of the permeation cell are 0.1 N NaOH (distilled and deionized); the charging input density is low ($< 1 \text{ mA/cm}^2$) so as to allow hydrogen diffusion without cracking. A first permeation curve is then obtained, and when steady state is reached the disk is degassed by turning off the input current density. The degassing curve is also plotted.

Step two. With the same electrochemical solutions, and when degassing is completed, a second permeation is run at the same low charging current density. Degassing is also performed when steady state is reached. As shown later, all obtained permeation curves will be used to compute diffusion coefficients, quantities of irreversibly and reversibly trapped hydrogen, diffusible hydrogen, etc.

Step three. The charging solution on the input side used for permeation experiments (0.1 N NaOH) is replaced (after careful washing) by an acid solution (generally 1 N H_2SO_4). A new permeation experiment is then run with a high charging current density (for example, 5 to 10 mA/cm^2) until steady state is reached. Cracks are nucleated in the disk, and the shape of the permeation curve may exhibit humps (contrary to "normal" permeation curves as in Fig. 2). When steady state is obtained, the disk is diametrically cut in several parts, and the depth at which cracking occurs is metallographically measured on the etched and polished sections. C_K^T is then computed as shown later.

Parallel to these measurements using the electrochemical permeation technique, other techniques were used to check the validity of C_K^T calculations and to compare results to those of mechanical HE testing.

The validity of C_K^T computations was checked via fusion analysis of hydrogen contained in square plate specimens (2 by 2 by 0.1 cm). These specimens are each charged in 1 N H₂SO₄ at a given current density for a time sufficient to ensure complete saturation; half the specimen is fused for hydrogen analysis and the other half is cut and metallographically checked for cracks as shown in Fig. 3. Cutting is done at low temperature (usually in a mixture of acetone and dry ice) to minimize loss of hydrogen during the operation.

Another test, called F% test ("F" for "fragility"), was also run to relate the amount of introduced hydrogen to a degradation in mechanical properties. Round tension specimens are cathodically charged in 1 N hydrochloric acid (HCl) solution at 5 mA/cm². After charging, the percent reduction in area (% RA_c) is quickly evaluated and compared to that of uncharged specimens (% RA_{uc}). The F% index is given by

$$F\% = 100(\% RA_{uc} - \% RA_c)/(\% RA_{uc}) \tag{1}$$

Part of the specimen is also fused to measure the hydrogen content prior to testing. A large set of data, collected over the last 20 years [12] and in which lab results and field experience have been compared, has shown that problems arose in service whenever

$$F\% > 30\% \tag{2}$$

Hence, $F\% \geq 30\%$ was used as a criterion for the susceptibility of a given steel to HE.

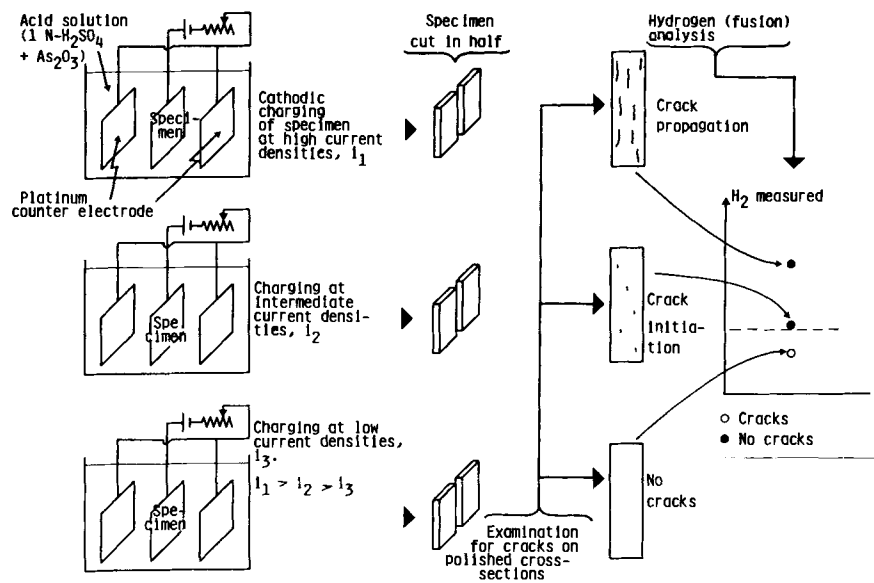


FIG. 3—Measure of critical concentration thru conventional analysis technique.

Theoretical Considerations

The theoretical basis for the calculation of C_K^T has been given elsewhere by the authors [7]. We will consider it here in more detail with the help of Fig. 2.

Hydrogen Diffusivity

A reasonable assumption about the population of hydrogen throughout the thickness of the permeation disk is to say that

$$C_T(x) = C_d(x) + C_R(x) + C_i(x) \quad (3)$$

where

$C_{T,d,R,i}(x)$ = total, diffusible, reversibly trapped, and irreversibly trapped concentrations of hydrogen at Depth x , respectively.

Reversibly trapped hydrogen is that amount of hydrogen that can leave trapping sites and the specimen (at the testing temperature) when the charging current density is turned off. On the contrary, irreversibly trapped hydrogen will stay in the specimen (at the testing temperature). This assumption is now well supported experimentally [9]; irreversibility at room temperature seems to be obtained whenever the trapping energy is greater than 0.8 eV [10].

Hence, the first permeation renders diffusion across a specimen in which both reversible and irreversible traps are active. After degassing, irreversible traps will stay filled up by definition. Thus the second permeation renders diffusion across a specimen whose only reversible traps are active.

This is why second permeation transients are usually developed faster than first permeation transients. The diffusion coefficients calculated from first and second permeations will be termed D_1 and D_2 , respectively; these coefficients will vary along the curve, at any time along the permeation curve, and at time-lag, for instance [9]

$$D_1 < D_2 \quad (4)$$

The diffusion coefficient with no traps, D_0 , that is, the diffusion coefficient with only untrapped-diffusible hydrogen, may be computed from the first instants of the degassing curve (Fig. 2). This follows from the assumption that, at that point, trapping is at saturation or at steady state, and that only diffusible hydrogen leaves first. This assumption is supported by the fact that D_0 calculated in this way and D_0 calculated from room temperature extrapolations of $D = f(1/T)$ compare well [since trapping disappears at high temperature, T (see Fig. 2)]. The corresponding permeation curve, with D_0 , may now be drawn from Fick's laws (no trapping) and obviously is the fastest one (Fig. 2).

Trapped Hydrogen Concentrations

Now, during the first permeation, the average concentration of hydrogen contained in the specimen between Time $t = 0$ and Time $t = t_f$ (Fig. 2), that is, \bar{C}_1 , is given by

$$\bar{C}_1 = \frac{1}{e} \left[\int_0^{t_f} J_0^1(t) dt - \int_0^{t_f} J_e^1(t) dt \right] \quad (5)$$

where $J_0^1(t)$ = input ($x = 0$) or output flux ($x = e$) of hydrogen during the first permeation.

In the same way, during the 2nd permeation

$$\bar{C}_2 = \frac{1}{e} \left[\int_0^{t_f} J_0^2(t) dt - \int_0^{t_f} J_e^2(t) dt \right] \quad (6)$$

using the same symbolism.

Since \bar{C}_1 represents irreversibly and reversibly trapped hydrogen, and \bar{C}_2 only reversibly trapped hydrogen, the average concentration of irreversibly trapped hydrogen is given by

$$\bar{C}_1 - \bar{C}_2 = \bar{C}_i = \frac{1}{e} \left\{ \left[\int_0^{t_f} J_0^1(t) dt - \int_0^{t_f} J_0^2(t) dt \right] - \left[\int_0^{t_f} J_e^1(t) dt - \int_0^{t_f} J_e^2(t) dt \right] \right\} \quad (7)$$

On the input side of the specimen ($x = 0$), and because of the fact that $C = C_0$ (at $t = 0$) is supposed instantaneous, the input fluxes J_0^1 and J_0^2 may rapidly be considered equal. This assumes that all reversible and irreversible traps are rapidly saturated. This is certainly true of reversible traps, since they may be considered (see later on) to be in equilibrium with C_0 , that is, instantaneously reached. Thus, according to Eq 7 and to the cancellation of input fluxes, \bar{C}_1 may be computed from the area between the first and second permeation transients (Fig. 2).

In the same way, it can be shown that the average concentration of hydrogen that is reversibly trapped, \bar{C}_R , may be computed from the area between the second permeation curve and the diffusible curve obtained with D_0 (Fig. 2).

Relationships Between Diffusible and Trapped Hydrogen Concentrations

Consider now the evolution of these various quantities with Depth x . For this, we may simply reason on a trapping reaction such as that of McNabb and Foster [11]

$$dn/dt = kC(1 - n) - pn \quad (8)$$

where

n = occupancy of trap sites,

k and p = trapping and detrapping (trap release) constants, and

C = concentration of diffusible hydrogen (C_d).

Equation 8 is a reversible trapping equation. At steady state ($dn/dt = 0$)

$$n_s(x) = \frac{kC_s(x)/p}{1 + kC_s(x)/p} \quad (9)$$

Hence, the amount of reversibly trapped hydrogen may be considered in equilibrium with the amount of diffusible hydrogen; for the sake of simplicity (generally, $kC_s(x)/p \ll 1$ [13])

$$K = \frac{C_R(x)}{C_d(x)} \quad (10)$$

In the case of irreversible trapping ($p = 0$), Eq 8 reads

$$dn/dt = kC(1 - n) \quad (11)$$

and at steady state

$$n_s(x) = 1 \quad (12)$$

That is, the amount of irreversibly trapped hydrogen is independent of C_d and x .

Now, C_d at steady state, C_d^S , may be found from Fick's law and is given by

$$C_d^S(x) = C_0(1 - x/e) \quad (13)$$

where C_0 = input side diffusible hydrogen concentration, and e = specimen thickness.

C_0 may be found from Fick's second law at steady state (that is, all traps saturated or at equilibrium) using D_0 as calculated before and the measured steady state flux J_∞

$$C_0 = J_\infty \cdot e / D_0 \quad (14)$$

Computation of the Critical Concentration

Let us now turn to the calculation of the critical concentration, C_K^T , as shown in Fig. 4. Assume that the disk specimen has been cut after having been submitted to various permeations followed by a "cracking" permeation (Step 3 of the experimental procedure just described), and that a single crack (barely nucleated) has been found at depth " x ." At this depth, the total critical concentration, $C_K^T(x)$, is the total amount of hydrogen, that is

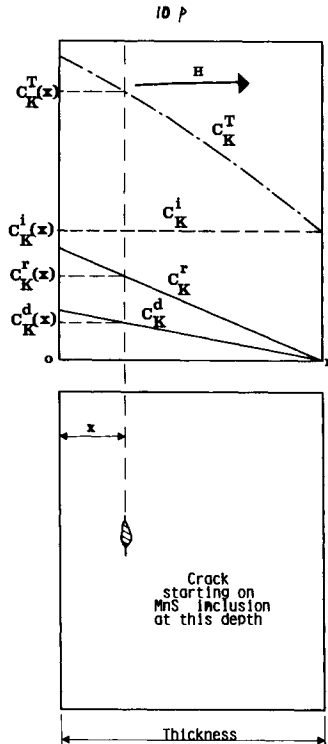


FIG. 4—Principles of the calculation of $C_K^T(x)$.

$$C_K^T(x) = C_K^d(x) + C_K^R(x) + C_K^i(x) \quad (15)$$

with the same symbolism as in Eq 3 for the critical concentration (Fig. 4).

The just-cited considerations now allow us to compute $C_K^d(x)$, $C_K^R(x)$, and $C_K^i(x)$.

Indeed:

$C_K^i(x)$. As shown in Eq 12, the value of $C_i(x)$ is constant throughout the thickness of the specimen and may be calculated from the area between the first and second permeation transients (Eq 7). Since irreversible traps have been saturated after the first permeation, they remain as such during the "cracking" experiment, and

$$C_K^i(x) = \bar{C}_i \text{ (from Area 1-2 permeation)}$$

$C_K^R(x)$. Contrary to $C_K^i(x)$, $C_K^R(x)$ is greater than $C_R(x)$ calculated from the permeation curves (without cracking), since it is in equilibrium with an increased diffusible concentration, $C_K^d(x)$, according to Eq 10

$$K = C_K^R(x)/C_K^d(x) \quad (16)$$

To compute $C_K^R(x)$, one needs to know K and $C_K^d(x)$. K may be computed by assuming that average concentrations of reversibly trapped hydrogen, \bar{C}_R , after permeation (without cracking) and average diffusible hydrogen, that is, $\bar{C}_d = C_0/2$ (from Fick's laws), are in the same equilibrium

$$K = \bar{C}_R/(C_0/2) \quad (17)$$

K may be calculated thus, since \bar{C}_R is measured from the area between the second permeation and the permeation with D_0 (Fig. 2) and C_0 is given by Eq 14.

In the same way, $C_K^d(x)$ is given by an equation similar to Eq 13, with C_0^K being the input diffusible concentration in the "cracking" experiment ($C_0^K = J_\infty^K \cdot e/D_0$), and x is the depth of the crack

$$C_K^d(x) = C_0^K(1 - x/e) \quad (18)$$

$C_K^T(x)$. $C_K^T(x)$ is then given by Eq 15, with all parameters known from permeation and cracking curves, as just discussed

$$C_K^T(x) = C_0^K(1 - x/e)[1 + \bar{C}_R/(C_0/2)] + \bar{C}_i \quad (19)$$

Discussion of Assumptions

This calculation is subjected to various assumptions and will also give rise to different values from specimen to specimen. In fact, these values will be indicative of the material diversity in terms of sites susceptible to nucleate cracks. Indeed, consider Fig. 5 where three sites have been distributed differently in the membrane thickness, with the following true C_K -values (value computed in a volume around the defect)

$$C_K^1 > C_K^2 > C_K^3 \quad (20)$$

Thus, Defect 3 is the most susceptible to nucleate cracks (lowest C_K -value). Consider now, with a total C_K^T profile as shown in the figure, the following cases:

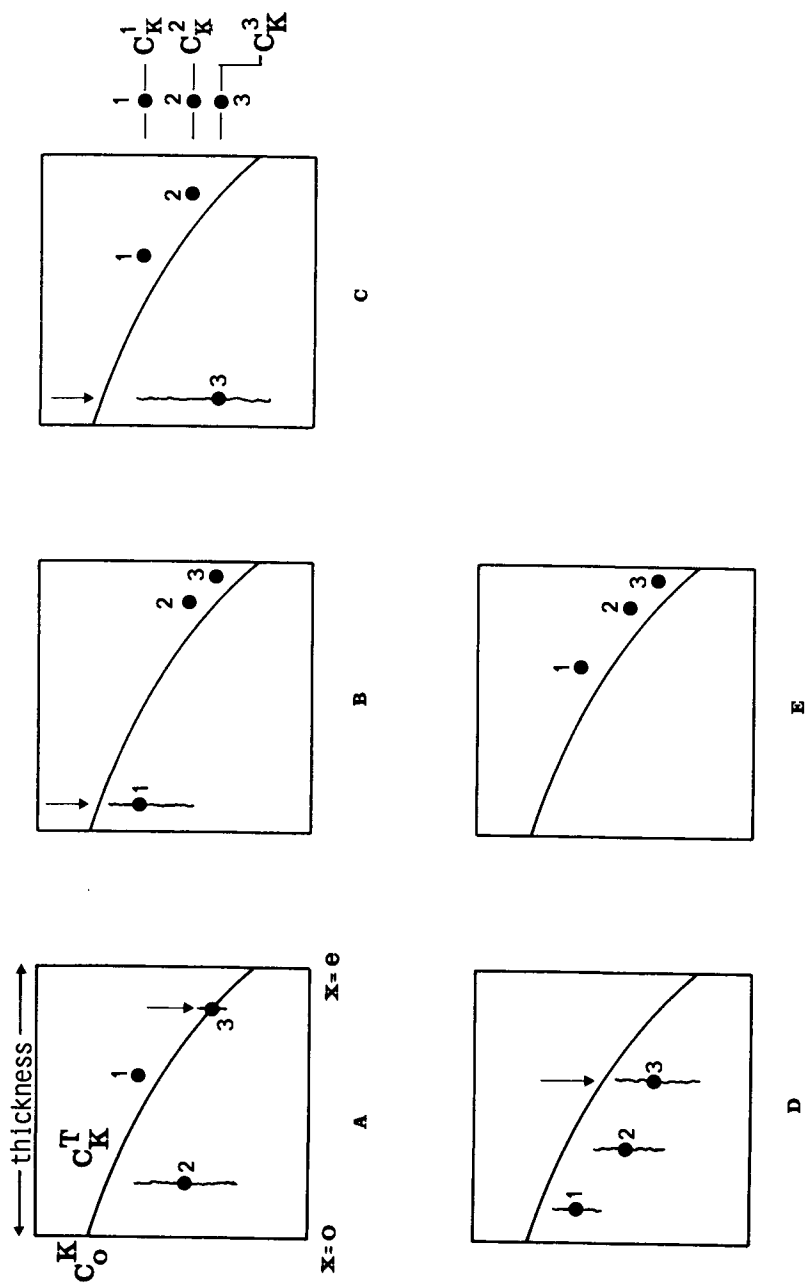


FIG. 5—Different cracking situations with a given C_K^T profile and three defects with $C_K^1 > C_K^2 > C_K^3$.

Case a. Only Defects 2 and 3 will nucleate cracks, since $C_K^T < C_K^1$. Defect 2 will propagate a large crack, since $C_K^T \gg C_K^2$. Defect 3 will barely nucleate a crack, since $C_K^T \approx C_K^3$ at Defect 3 depth. It is this last value that will be retained as the critical concentration of the material (that is, it is the lowest one at the greatest depth).

Case b. Only Defect 1 will crack, and C_K^T at that depth will be taken as the critical concentration for this specimen.

Case c, d. The critical concentration is taken to be the C_K^T -value at the depth of Defect 3.

Case e. No defect will crack, since all $C_K^{1,2,3}$ are greater than C_K^T at the depth at which defects are present. Since the "true" $C_K^{1,2,3}$ -values are unknown, this experiment will give the result that no crack happened for C_K^T -values between $C_K^T(x = 0)$ and $C_K^T(x = e)$.

With these examples, it is clear that a typical result, based on at least ten experiments, will look like that in Fig. 6:

Region A corresponds to hydrogen concentrations so low that even the most detrimental sites (with the lowest known C_K) will not nucleate a crack. Note that the upper limit, x , of the critical concentration below which no cracking occurs is best defined after a large number of experiments, that is, a high probability that the most dangerous defect could have been located favorably versus the concentration profile.

Region C corresponds to hydrogen concentrations so high that even the least detrimental site of the material will nucleate a crack, that is, cracking will always occur.

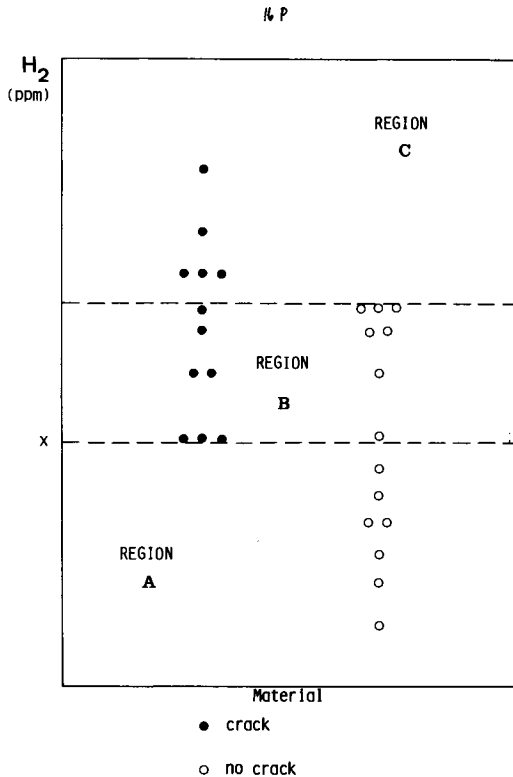


FIG. 6—Typical results on C_K^T calculations.

Region B is such that cracks will nucleate or not depending on the type of defects of the material and on their location versus the total hydrogen profile in the "cracking" experiment.

In fact, the value of practical interest here is that at "x" it corresponds to a crack barely nucleating on the most detrimental site and signals the lowest hydrogen concentration above which HIC will occur. Region B is a region of doubt: HIC will occur provided that the same kind of sites that crack for these concentrations will be present in the material and will see as much hydrogen.

Results

Correlation Between Critical Concentration Values Found with the Electrochemical Permeation Method and Those Measured with More Conventional Techniques

Figure 7 illustrates results obtained on a A508 Class 3 steel. It can be seen that the correlation between the two techniques is good, particularly for the upper limit of Zone B.

The conventional (fusion) technique is much simpler to use, but the electrochemical permeation technique offers the following advantages: (1) it allows a precise identification of the defect nucleating a crack at a particular C_K -value—because part of the specimen from which the hydrogen concentration is measured is fused, the conventional technique does not allow this

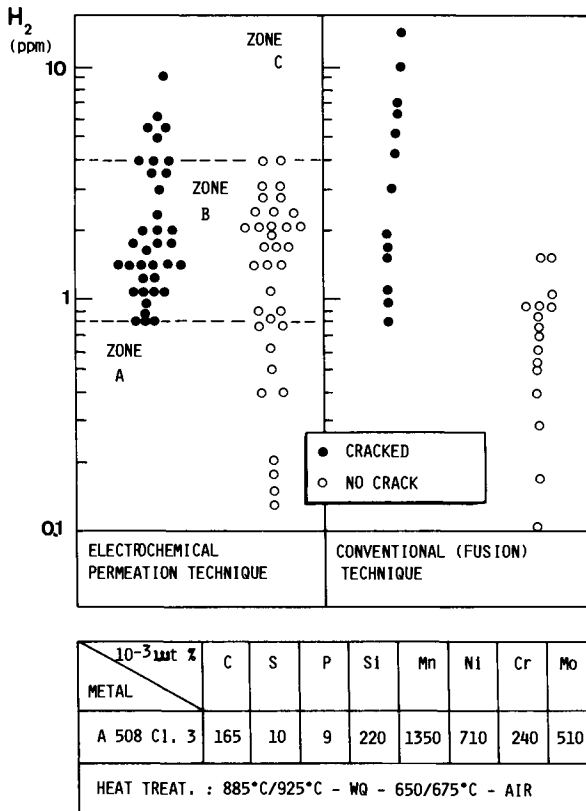


FIG. 7—Comparison between C_K^T -values from permeation (left) and from conventional technique (right).

precise identification; (2) it gives the amount of irreversibly/reversibly trapped versus diffusible hydrogen, which may be useful in the case where degassing may be considered for the materials; (3) it also gives useful information on diffusion coefficients. Also note that the good agreement found between the two techniques strengthens the validity of the assumptions made.

Correlation Between Critical Concentrations Given by the Electrochemical Technique and Results of the F% Test

Figures 8 to 10 illustrate these correlations for various steels: the left part of the diagram gives the critical concentration as calculated from permeation data, while the right part gives the evolution of F% versus the hydrogen content of the tension specimen measured by a conventional (fusion) technique. It is remarkable that the lowest hydrogen concentration for which F% reaches 30% is always close to the lower critical concentration value determined from electrochemical penetration data, that is, the upper limit of Zone A.

Thus, the criterion “F% > 30% means problems in service” is in fact related to the onset of cracking in the material. Loss of ductility due to internal hydrogen, without cracking, does not seem to lead to in-service problems, according to our experience.

Similar data are given in Fig. 11 for untempered (that is, “as welded”) simulated heat af-

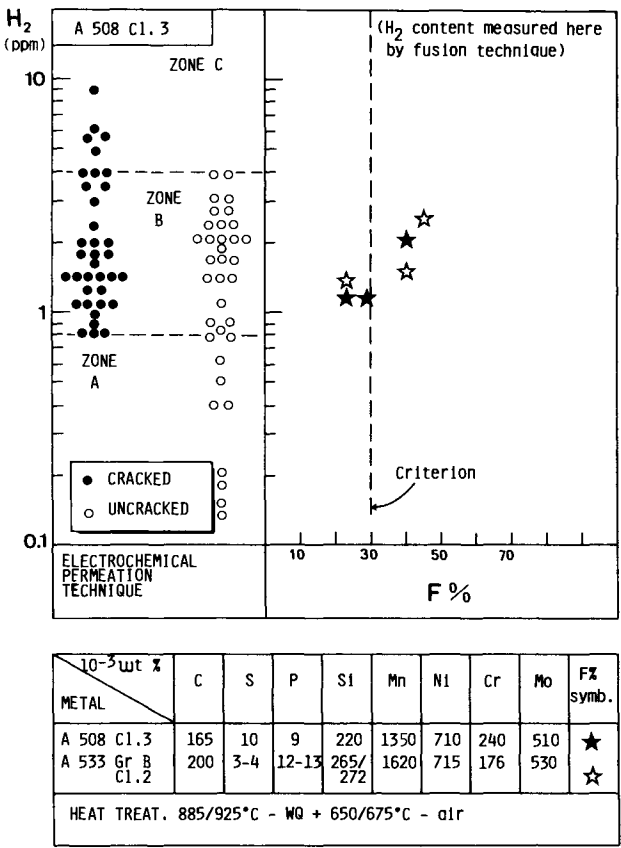


FIG. 8— C_K^T -values (permeation) versus F% test (A508 Class 3 and A533 Grade B Class 3).

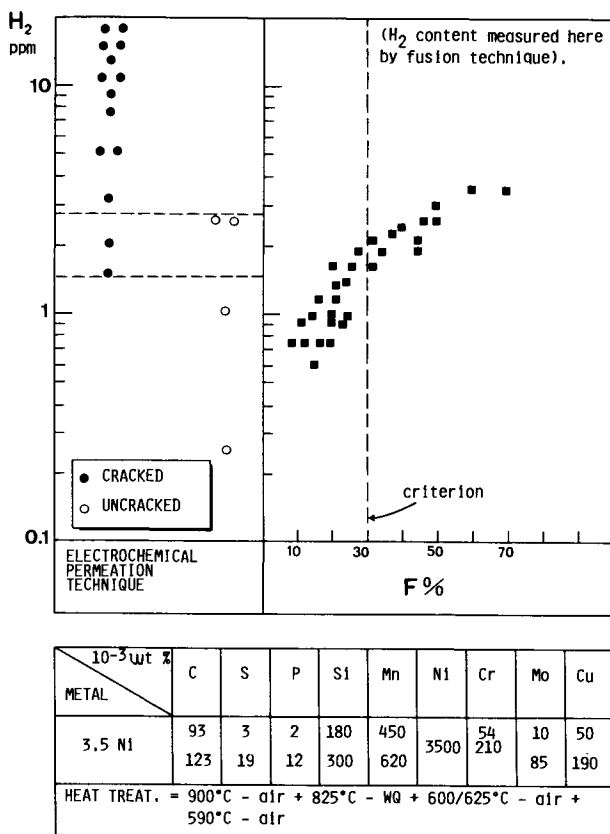


FIG. 9— C_K^T -values (permeation) versus F% test (3.5Ni steel).

affected zone (HAZ), but hydrogen concentrations in F% tests were then too high to make a useful correlation with critical concentrations given by the electrochemical permeation method.

Comparison Between Several Materials According to Critical Concentration Values

If one was to reason according to lowest critical concentration values (upper limit of Zone A), one would say from Figs. 8, 9, and 10 that carbon-manganese steel and A308 Class 3 behave the same, while 3.5Ni steel is better (C_K equal, 0.7 to 0.8 ppm versus 1.5 ppm). Although this may be true, reasoning in such a manner would be incorrect, particularly in the case when materials are exposed to the same external hydrogen activity. Indeed, according to Sievert's law

$$C(H_2) = k\sqrt{PH_2} \quad (21)$$

that is, the amount of hydrogen dissolved in a material, $C(H_2)$, depends both on the square root of hydrogen pressure, $\sqrt{PH_2}$, and on "k." This constant "k" depends on the type of steel considered; in particular, it may increase with trapping [10]. Furthermore, as said before, cracking depends on the position of hydrogen contained in the material versus the critical concentration. This means that a material may exhibit a relatively high C_K -value, but may absorb larger quantities of hydrogen than a material with a lower C_K -value. This point is illustrated in Fig. 12,

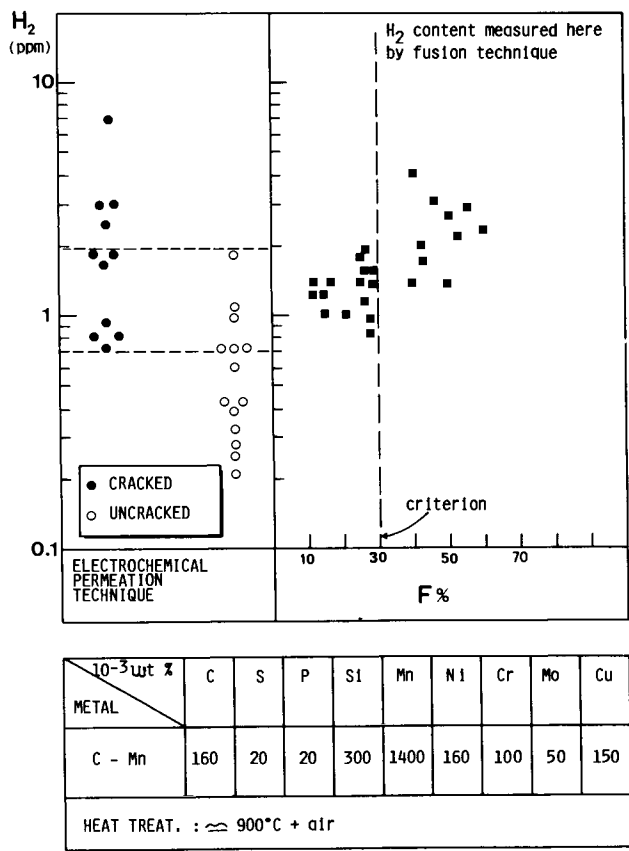


FIG. 10— C_K^T -values (permeation) versus F% test (C-Mn steel).

where C_0 values obtained by charging at 1 mA/cm² in 0.1 N NaOH (no cracks) are compared to the Region B (mixed crack-no crack region, Fig. 6) of C_K -values. Figure 12A compares values between various steels (A 508 Class 3, 3.5Ni, C1.2Mn steels), while Fig. 12B gives C_0 and C_K values for simulated HAZs of a A508 Class 3 steel. HAZ microstructures were simulated for the sake of homogeneous microstructure. HAZ simulation parameters are given in Table 1.

Figure 12 shows that:

1. In what concerns base metal steels (Fig. 12A), 3.5Ni steel has indeed a good (external) HIC resistance, as C_K is high and absorbed C_0 is low. For A 508 Class 3 steel, the ratio C_0/C_K mini (C_K mini being the lowest critical value, that is, the lower limit of Zone B, ///) is around 4.4×10^{-2} , while for the C1.2Mn, it is about 3.3×10^{-2} , compared to 10^{-2} for the 3.5Ni steel. But a high C_0/C_K mini ratio corresponds to a low C_K -value, or a high C_0 -value, or both, that is, little resistance to HIC with external hydrogen. Hence, the order of decreasing resistance will be: 3.5Ni steel followed by C-1.2Mn and A 508 Class 3 steels. Comparing C-1.2Mn and A 508 Class 3 steels on the basis of C_K alone would not have given the same ranking (in fact, both steels are quite close).

2. Turning to simulated HAZ, one will note that the C_0/C_K mini ratio is higher than A 508 Class 3 base metal (it goes from 4.6×10^{-2} to 3.4×10^{-1} , compared to 4.4×10^{-2} for base

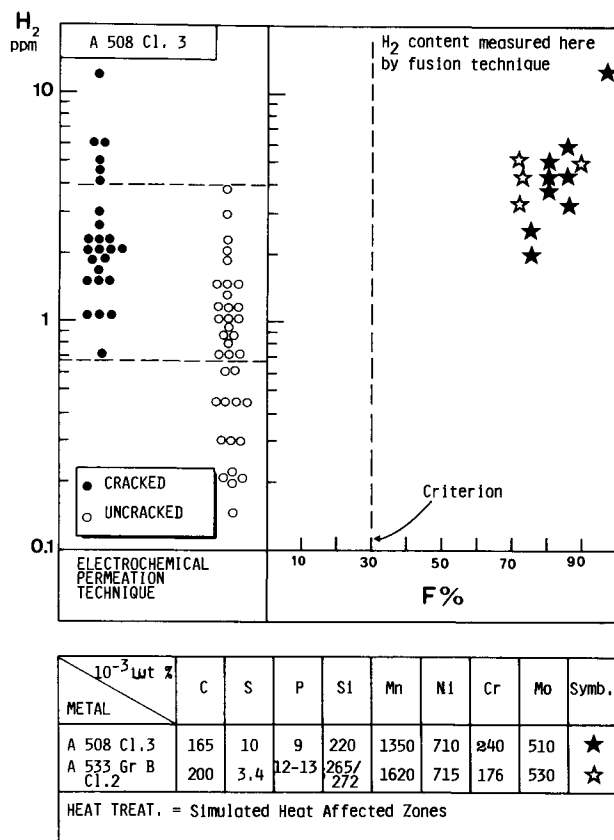


FIG. 11— C_K^T -values (permeation) versus F% test (simulated HAZ).

metal). Hence, HAZ are more sensitive to HIC. Also, Fig. 12B.5 shows that sensitivity to HIC with an external hydrogen atmosphere increases with increasing grain size [grain size number (G) increases³ from 6 to 1 (see Table 1)] and increasing hardness (HV), that is, with a decreasing G/HV ratio. This is a well-known hydrogen embrittlement evolution [8].

These remarks could also have been made in Fig. 11. With the same charging conditions, HAZs exhibit much higher F% values than base metals, not solely because C_K -values are much lower, but above all because hydrogen absorbed is much higher.

Identification of Sites Responsible for Crack Initiation

Figure 13 illustrates several cracking situations happening more or less deep in the thickness of disk-shaped specimens, that is, at various C_K -values. Usually, most dangerous defects and microstructures in C-Mn normalized or quenched and tempered steels are elongated manganese sulfides in segregated zones; such zones are highly enriched in both hardening elements (C, Mn, Mo, etc.) and tramps (S, P, etc.) and exhibit hard martensite or bainite-type microstruc-

³According to ASTM Methods for determining grain size (E 112-84), a low value for grain size number means a large grain size.

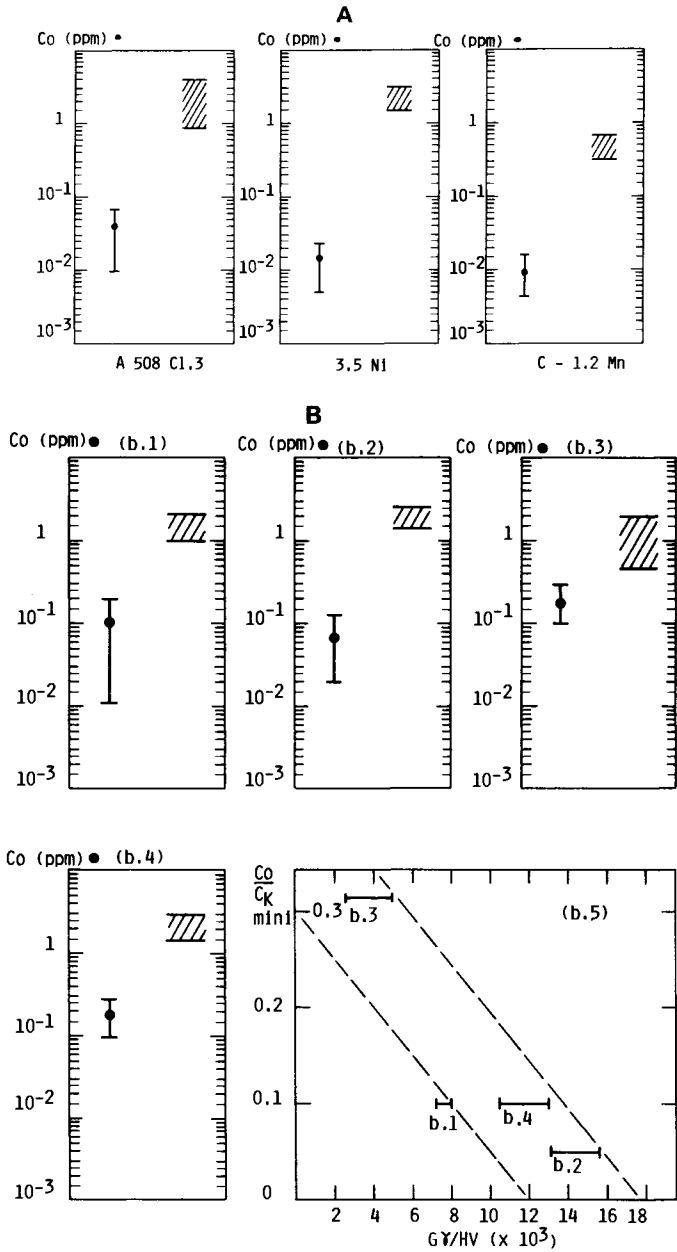


FIG. 12—(A) Comparison between diffusible hydrogen (C_0) after permeation test at 1 mA/cm^2 in 0.1 N NaOH and Region B of C_K^T -values for various steels. (B) Comparison between diffusible hydrogen (C_0) after permeation test at 1 mA/cm^2 in 0.1 N NaOH and Region B of C_K^T -values for HAZ microstructures of A508 Class 3. Figure b.5 plots the ratio C_0 over $C_{K\text{min}}$ (minimum C_K^T -value of Region B) versus the ratio of austenitic HAZ grain size number, G_V , over HAZ Vickers hardness, H_V .

TABLE 1—HAZ simulation parameters.

Parameters	HAZ b.1	HAZ b.2	HAZ b.3	HAZ b.4
Δt between 800 and 500°C, s	30	30	30	35
Peak temperature, °C	1250	1050	1300	1050
Time at peak, s	5	10	5	10
Hardness, HV	390	380	400	380
Austenitic (γ) grain size number according to ASTM E 112: G	3	5 to 6	1 to 2	4 to 5

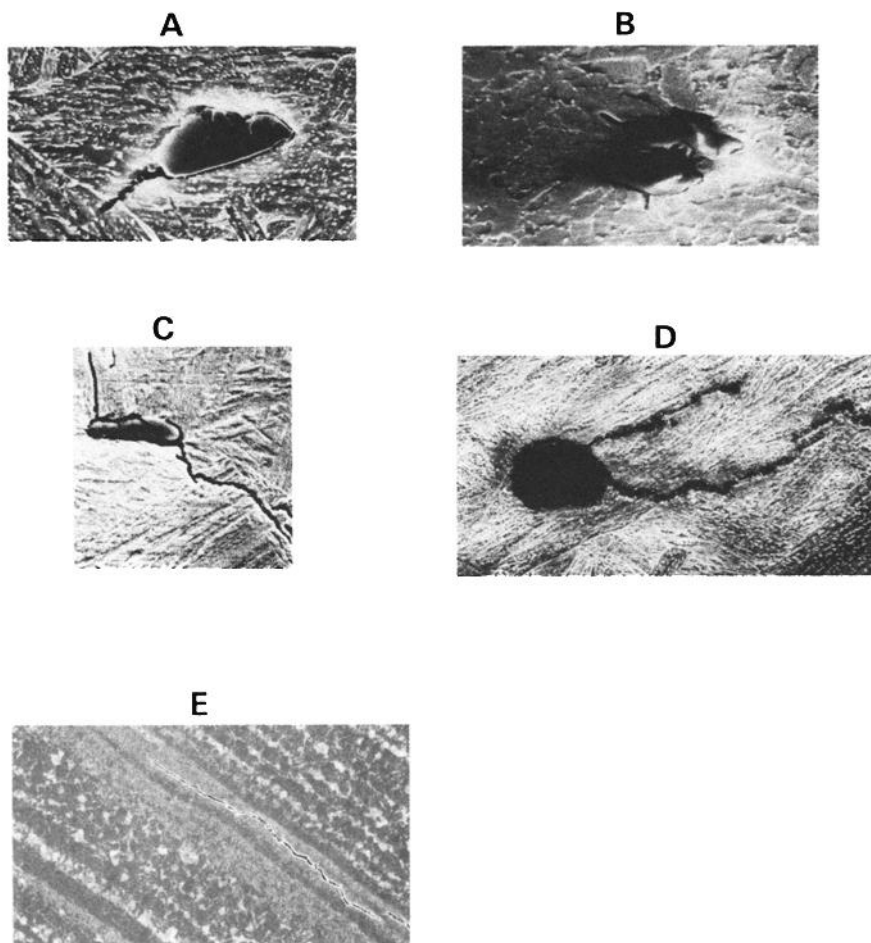


FIG. 13—Various cracking situations observed by scanning electron microscopy: (A) crack initiation on oxisulfide (C-Mn steel); (B) crack initiation on oxide (3.5Ni steel); (C) crack initiation on and propagation from manganese sulfide in HAZ of CMn steel; (D) crack initiation on and propagation from oxide in 3.5Ni steel; (E) crack propagation in segregated bands of a pearlitic CMn steel, with no obvious crack initiation site.

tures. Somewhat higher in C_K -values are elongated MnS stringers and oxide stringers in normalized structures. Round oxides and particles homogeneously distributed in the lattice resist at still higher hydrogen concentrations. Note also that it is sometimes difficult, particularly at high C_K -values (upper Zone B and Zone C), to identify precisely the defect responsible for a given crack; this is so because: (1) some crack propagation has taken place and the initiation site can only be suspected; (2) cracks may start on defects too small to be detected at SEM or light microscopy magnifications (for example, dislocations tangles).

Practical Value of C_K Knowledge

The knowledge of the critical concentration for crack initiation in a given material is of practical interest in many hydrogen embrittlement situations; for instance, if one knows that a given environment (say, sour gas in pipeline steels) will lead to an absorbed concentration in a material around 1 ppm, then all materials with C_K mini values less than 1 ppm will be rejected for use in that environment. Another example is pre- and postheat treatments for degassing hydrogen (among other things) out of a HAZ: the time and temperature of such treatments will be chosen so that the final amount of hydrogen in the HAZ will be less than C_K . Also note finally that the experiment described herein may be used to study the effect of stress on C_K -value [8]; one has to replace the disk specimens by flat tension specimens, for instance.

Conclusions

The well-known electrochemical permeation technique has been applied herein to the computation of the critical hydrogen concentration value necessary to initiate a crack on a given defect. The following concluding remarks can be made:

1. The calculation of the critical concentration requires the knowledge of various trapping characteristics of the material that are obtained through consecutive permeation experiments.
2. The necessary assumptions for such a calculation are somewhat strengthened by the good correlations found when it is compared to values obtained from more conventional analysis techniques.
3. There also exists a good correlation between critical concentration values and current criteria used to predict in-service performance of a given material through mechanical testing (F% test here).
4. Comparing different materials on the basis of their C_K -value alone is shown to be insufficient; knowledge of what the material can absorb under a given external hydrogen activity is also required.
5. An advantage of this technique is to pinpoint what defects of the material are really dangerous and should be avoided. For instance, a CMn type normalized steel containing elongated sulfide manganese stringers in segregated zones should contain less than 0.8 to 1 ppm hydrogen.
6. This technique could be applied to more complex cases, for example, when an external stress is applied on the specimen.

References

- [1] Zapffe, C. A. and Sims, C. E., *Metallurgical Alloys*, Vol. 11, 1940, p. 145.
- [2] Troiano, A. R., *Transactions of the American Society for Metals*, Vol. 52, 1960, p. 54.
- [3] Oriani, R. A., *Berichte der Bunsengesellschaft für Phisikalische Chemie*, Vol. 76, 1972, p. 848.
- [4] Petch, N. J., *Philosophical Magazine*, Vol. 1, 1956, p. 331.
- [5] Pressouyre, G. M., *Acta Metallurgica*, Vol. 28, 1980, p. 895.
- [6] Devanathan, M. A. V. and Stachursky, Z. O. J., *Proceedings of the Royal Society*, Vol. A 270, 1962, p. 90.

- [7] Pressouyre, G. M., *Conference on Environmental Degradation of Engineering Materials*, Virginia Polytechnic Institute, Blacksburg, VA, 1981.
- [8] Pressouyre, G. M., *Single Crystal Properties*, Vol. B1, 1982, p. 69.
- [9] Pressouyre, G. M. and Bernstein, I. M., *Metallurgical Transactions*, Vol. 9A, 1978, p. 1571.
- [10] Pressouyre, G. M., *Metallurgical Transactions*, Vol. 10A, 1979, p. 1571 and Vol. 14A, 1983, p. 2189.
- [11] McNabb, A. and Foster, P. K., *Metallurgical Society of the American Institute for Mining, Metallurgical, and Petroleum Engineers*, New York, Vol. 227, 1963, p. 618.
- [12] Bastien, P., Veron, H., and Roques, C., *Revue de Metallurgie*, LV, Nr. 4, 1958, p. 3.
- [13] Pressouyre, G. M. and Bernstein, I. M., *Metallurgical Transactions A*, Vol. 9A, 1978, p. 1571.

Assessment of the Degree of Hydrogen Embrittlement Produced in Plated High-Strength 4340 Steel by Paint Strippers Using Slow Strain Rate Testing

REFERENCE: Pollock, W. J. and Grey, C., "Assessment of the Degree of Hydrogen Embrittlement Produced in Plated High-Strength 4340 Steel by Paint Strippers Using Slow Strain Rate Testing," *Hydrogen Embrittlement: Prevention and Control*, ASTM STP 962, L. Raymond, Ed., American Society for Testing and Materials, Philadelphia, 1988, pp. 372-386.

ABSTRACT: The present work demonstrates how a slow strain rate test can be used to quantify rapidly the severity of hydrogen embrittlement produced in porous cadmium plated-and-baked high-strength 4340 steel by paint strippers. The results of multiple slow strain rate tests, conducted at a crosshead displacement rate of 2×10^{-4} mm/s using notched tension specimens in various paint strippers, show that a minimum mean fracture stress within the range of 1700 to 1850 MN/m² can be correlated with the pass/fail criterion for acceptability of paint strippers in standard notched C-ring tests. The advantages of using a slow strain rate test as a viable alternative to existing standard methods for hydrogen embrittlement testing are discussed.

KEY WORDS: low-alloy steel, high-strength steel, hydrogen embrittlement, strain rate, cadmium coatings, paint removers

Recent trends in alloy development in the aircraft industry have been directed towards the production of alloys with high strength-to-weight ratios. Although many high-strength, low-alloy steels have been developed for use in aircraft structure, a lack of proper consideration regarding the detrimental effect of environment on their load-bearing properties has sometimes been evident. In particular, absorption of small amounts of hydrogen (few parts per million) can cause severe embrittlement in steels, particularly if the strength level exceeds 1200 MN/m² (175 ksi). Hydrogen can be introduced into steel components by pickling and plating treatments, exposure to paint strippers and other maintenance chemicals, and by corrosion during service. The wide use of paint to protect high-strength steel components from the deleterious effects of environmental damage has prompted much research into the development of paint strippers that can effectively remove these coatings without damaging the steel. As a consequence of the necessity to prevent hydrogen entry into steel during paint stripping, a variety of mechanical tests have been developed to determine the degree of embrittlement produced by such processes. Although test methods are continually updated and modified to accommodate the latest developments in engineering practice, a number of differences are evident when comparing the various specifications [1-4] (Table 1):

¹Principal research scientist, Aeronautical Research Laboratory, Defence Science and Technology Organisation, Department of Defence, Melbourne, Australia.

²Experimental officer, Materials Research Laboratories, Defence Science and Technology Organisation, Department of Defence, Melbourne, Australia.

TABLE 1—Summary of some American and Australian standard specifications for hydrogen embrittlement testing of high-strength steels subjected to paint strippers.

Specification	Specimen Geometry	Material	Stress Concentration Factor	Type of Loading	Applied Stress, % NTS	Maximum Test Time, h	No. of Specimens (See Appendix)
MIL-R-83936B [2]	N.T.	N/S	3.9	C.L.	75	200	4
MIL-R-25134B [3]	N.T.	4340	2.5	C.L.	75	200	8
ASTM F 519-77 [4]	N.T.	4340	3.1	C.L.	45	150	3 (6)
ASTM F 519-77	N.T.	4340	2.8	C.D.	55	150	3 (6)
ASTM F 519-77	N.B.	4340	3.9	C.D.	45	150	3 (6)
ASTM F 519-77	N. C-ring	4340	4	C.D.	65	150	3 (6)
MIL-R-81294B [1]	N. C-ring	4340	4	C.D.	75	100	4
RAAF K-55 [15]	N. C-ring	4340	4	C.D.	75	100	4
Present work							
(Modified RAAF K-55)	N. C-ring	4340	4	C.D.	75	100	3 (6)
ASTM F 519-77	S. O-ring	4340	...	C.D.	80 (% UTS)	150	3 (6)

NOTE: N.T. = notched tensile; N. C-ring = notched C-ring; C.L. = constant load; N.B. = notched bend; S. O-ring = smooth O-ring; C.D. = constant displacement; N/S = not specified; UTS = ultimate tensile strength; NTS = notch tensile/bend strength.

1. The user must choose one of four specimen types: (a) notched tension, (b) notched bend, (c) notched C-ring, and (d) smooth O-ring. The majority of specifications favor the notched tension specimen (Table 1).

2. Some specifications require specimens to be manufactured from 4340 steel heat treated to a tensile strength of 1800 to 1930 MN/m² (260 to 280 ksi), whereas others specify use of any high-strength steel. It is known that 4340 steel in this heat-treated condition is particularly susceptible to hydrogen embrittlement, hence standard tests using this steel should provide a sensitive test for determining the severity of embrittlement produced by paint strippers.

3. The method of applying the paint stripper, the applied stress, and the test time all vary with each specification. A summary of test procedures for each specification listed in Table 1 is given in the Appendix.

In the specifications just outlined, tests produce a pass/fail result for the particular environmental condition under study. If all specimens fail, then the time to failure can provide some indication of the degree of embrittlement; however, if all specimens pass the test, there is no method of determining which environment induces the least amount of embrittlement. Consequently, little can be done to quantify the degree of embrittlement more precisely or treat the results in a statistically rigorous manner. Furthermore, since some tests can take up to 200 h to perform, these methods cannot be used on either a regular daily or even weekly basis.

It is apparent from this discussion that existing specifications: (a) define test methods that display significant differences between the various specifications, (b) can be time consuming, and (c) fail to provide a reliable estimate of the degree of embrittlement produced by paint strippers. Therefore, there is some justification for seeking an alternative mode of testing that will overcome the problems associated with the existing standard test methods.

Hydrogen embrittlement is known to involve a time-dependent diffusion process [5] and, hence, the rate of loading a specimen should provide a simple method for controlling the degree of severity of the test [6]. For steels not containing hydrogen, the rate of loading in a standard tension test does not usually affect the tensile properties of the steel. For specimens containing hydrogen in which the tension test is conducted sufficiently slowly, the hydrogen has time to diffuse to areas where the steel can become embrittled (usually grain boundaries), resulting in premature failure. If the loading rate is increased, the hydrogen has less time to damage the steel and the unembrittled properties of the steel are retained. Slow strain rate methods are used to assess the degree of embrittlement produced by paint strippers in cadmium-plated, high-strength 4340 steel using notched tension specimens. Results are then compared with those obtained using notched C-rings that are tested in accordance with standard test methods.

Experimental Procedures

The 9.5-mm round aircraft quality 4340 steel bar used in the present work complied with the MIL-S-5000E specification [7] and had a composition (weight %) of 0.43 carbon (C), 0.85 chromium (Cr), 0.84 manganese (Mn), 0.25 molybdenum (Mo), 1.78 nickel (Ni), <0.01 phosphorus (P), 0.29 silicon (Si), 0.009 sulfur (S), <0.05 aluminum (Al), with the remainder iron (Fe). Notched tension specimens were manufactured to comply with the reduced load requirements for the Type 1a specimen detailed in ASTM Method for Mechanical Hydrogen Embrittlement Testing of Plating Processes and Aircraft Maintenance Chemicals (F 519-77) (Fig. 1). This was accomplished by maintaining the notch stress concentration factor within the range 2.9 to 3.3. The notch was prepared by low-stress grinding after heat treatment. Specimens were austenitized at 815°C/1 h in salt, oil quenched to 40 to 60°C, and double tempered at 260°C/1 h with air cooling to 20°C between tempers to produce a steel with an ultimate tensile strength of 1845 MN/m².

Specimens were cadmium (Cd) plated to a thickness of 12 to 15 μ m in low-embrittlement Cd plating baths in accordance with either Qantas Processing Specification P65 [8] or Hawker de Havilland Process Specification HPS 1.03.00 [9]. Both specifications include baking at 190°C/

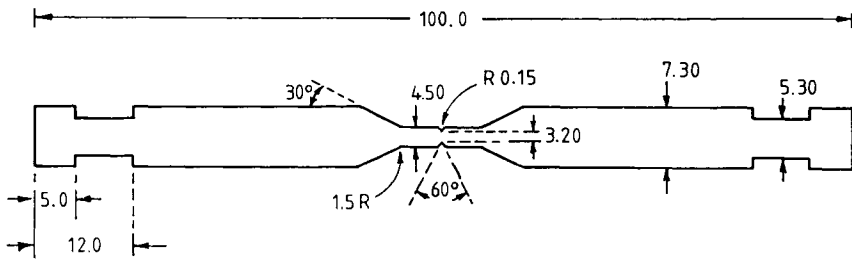


FIG. 1—4340 steel notched tension specimen: dimensions in mm.

23 h within 4 h of the plating treatment. Specimens were not chromate passivated after baking. The HPS 1.03.00 specification meets the hydrogen embrittlement requirements of the U.S. specifications MIL-STD-870A [10] and DPS 9.28 [11], whereas the Qantas P65 specification meets the intent of the specifications BAC 5718 [12], DPS 9.28 [11], QQ-P-416 [13], and AMS 2401C [14].

The embrittling properties of six propriety paint strippers (A,B,C1,C2,D,E) were investigated. Samples C1 and C2 were two different batches of the same paint stripper and had the same nominal composition. Paint Strippers A and B had a phenolic base, whereas the remainder were classified as nonphenolic. All paint strippers also contained a small quantity of water. The central 25-mm portion of the Cd-plated notched tension specimens were exposed to the paint stripper during slow strain rate tests conducted with a 20 kN motor-driven, hard-beam tension testing machine which had a variety of gears enabling tests to be conducted over a range of crosshead displacement rates varying from 10^{-2} to 10^{-6} mm/s. Fracture stress was calculated from the failure load and used to estimate the degree of embrittlement in specimens by comparison with the unembrittled fracture stress obtained by testing bare steel specimens in laboratory air at the same crosshead displacement rate. The mean fracture stress and standard deviation were calculated from the results of testing three specimens in an identical manner. The severity of embrittlement produced in 4340 steel by paint strippers was also assessed according to a modified version of the K-55 specification [15] (see Appendix) using three notched C-rings.

Electrochemical measurements were made in paint strippers using 7-mm-diameter cylindrical 4340 steel and electrolytic Cd specimens mounted to give a tight fit in a Teflon holder. After polishing to a 600-mesh finish, the open circuit potential of the steel and the coupled galvanic potential were measured with respect to a saturated calomel electrode (SCE) using a high impedance follower circuit. The pH of each paint stripper was also determined.

Results

The results of testing notched bare steel specimens in air showed that the fracture stress was independent of crosshead displacement rate over the range 2×10^{-3} to 2×10^{-6} mm/s. The results of 21 specimens taken from several specimen batches heat treated at different times produced a mean value of 2456 MN/m² with a standard deviation of 52 MN/m² (Fig. 2).

Slow strain rate tests conducted in air using specimens given the low-embrittlement, Cd-plating treatment followed by baking at 190°C/23 h resulted in fracture stresses within the range 2400 to 2500 MN/m² at all crosshead displacement rates except the lowest rate used (2×10^{-6} mm/s) (Fig. 2). This result confirmed that the degree of embrittlement produced by the porous Cd plating-and-baking treatment was minimal [16].

Results of notched C-ring tests with the six paint strippers indicated that Paint Strippers A,

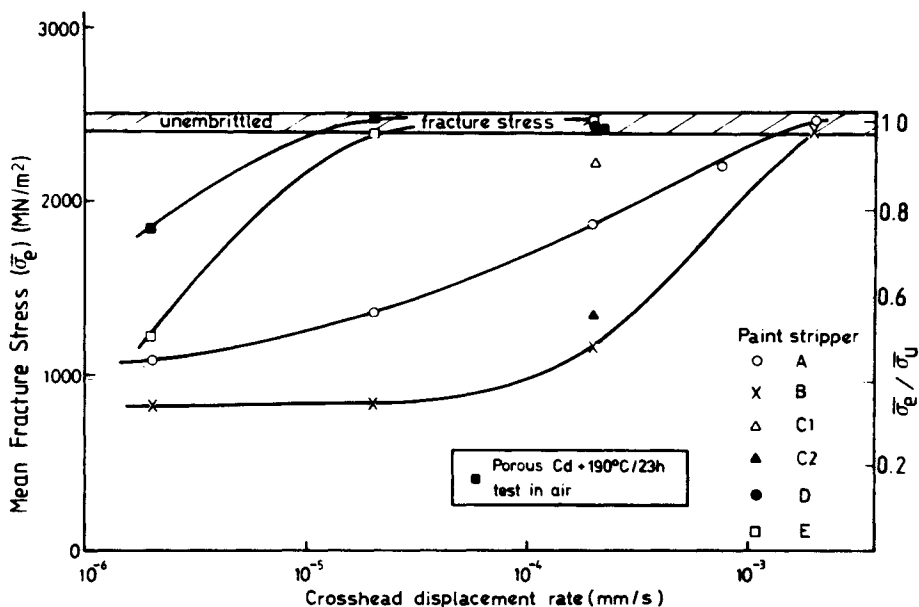


FIG. 2—Mean fracture stress ($\bar{\sigma}_c$) and mean fracture stress ratio ($\bar{\sigma}_c/\bar{\sigma}_u$) of Cd plated-and-baked 4340 steel notched specimens tested in paint strippers at various crosshead displacement rates, where $\bar{\sigma}_u$ is the mean unembrittled fracture stress.

C1, D, and E could be classified as “nonembrittling,” whereas Paint Strippers B and C2 could be labelled “embrittling” (Table 2).

The effect of crosshead displacement rate on the mean fracture stress of Cd plated-and-baked notched tension specimens tested in the various paint strippers is shown in Fig. 2. Although no paint stripper showed signs of embrittling the steel when specimens were tested at 2×10^{-3} mm/s, tests at lower crosshead displacement rates revealed significant variations in mean fracture stress between the various products. A satisfactory separation in mean fracture stress between the various paint strippers was observed at a crosshead displacement rate of 2×10^{-4} mm/s, and hence this rate of straining was chosen for all subsequent tests using notched specimens.

The effect of notch radius on mean fracture stress was studied for unplated specimens tested in air and for Cd plated-and-baked specimens tested in Paint Stripper A (Fig. 3). Results showed that a 100% increase in notch radius produced only an 8% increase in mean fracture stress for bare steel specimens tested in air, and a 33% increase for Cd plated-and-baked specimens tested in Paint Stripper A. The most significant change in mean fracture stress occurred when the notch stress concentration factor exceeded 3.3, and only small changes in fracture stress were obtained when specimen design was maintained within the limitations laid down in ASTM F 519-77 specification (notch stress concentration factor within the range 2.9 to 3.3).

Since Batches C1 and C2 of Paint Stripper C were found to be “nonembrittling” and “embrittling,” respectively, further slow strain rate and notched C-ring tests were carried out in various mixtures of Paint Strippers C1 and C2 and a critical mean fracture stress within the range 1700 to 1850 MN/m² was found to correspond with the pass/fail criterion in the notched C-ring tests (Fig. 4 and Table 2). Evaluation of the standard deviation for all paint stripper tests showed that the standard deviation was low for nonembrittling and highly embrittling paint strippers, whereas moderately embrittling paint strippers produced results with high scatter (Fig. 5).

TABLE 2—Results of notched C-ring tests in paint strippers—specimens loaded to 75% of notched breaking strength and held for 100 h (see Appendix, Method 6).

Paint Stripper	Time to Failure, h			Pass/Fail
	Specimen 1	Specimen 2	Specimen 3	
A	P	P	P	Pass
B	<1	<1	<1	Fail
C1	P	P	P	Pass
C2	<1	<1	1	Fail
D	P	P	P	Pass
E	P	P	P	Pass
50% C1 + 50% C2	20	20	60	Fail
65% C1 + 35% C2	24	24	48	Fail
75% C1 + 25% C2	P	P	60	Pass
75% C1 + 25% C2 (repeat)	P	P	P	

NOTE: P = specimen unbroken after 100-h. All specimens that passed the 100-h test were also found to be intact after 150 h.

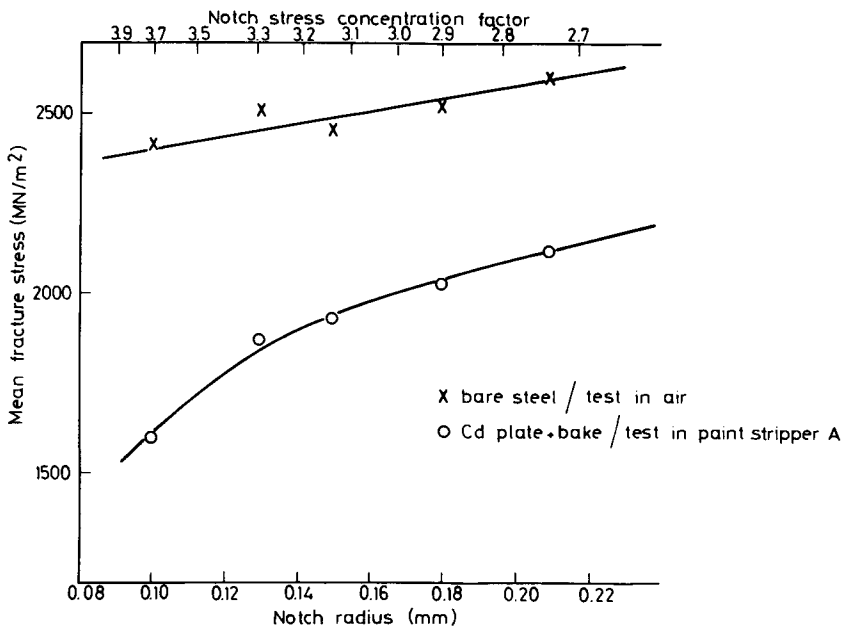


FIG. 3—Effect of notch radius on mean fracture stress of 4340 bare steel specimens tested in air and Cd plated-and-baked 4340 steel specimens tested in Paint Stripper A at a crosshead displacement rate of 2×10^{-4} mm/s.

Further tests with Paint Stripper B highlighted the role of Cd in causing embrittlement of the steel. In contrast to Cd-plated specimens, bare steel specimens showed no evidence of embrittlement when tested at a crosshead displacement rate of 2×10^{-4} mm/s in Paint Stripper B (Fig. 6). When a steel specimen was galvanically coupled to a piece of Cd of equivalent area during straining, premature failure of the steel specimen resulted (Fig. 6). Furthermore, expo-

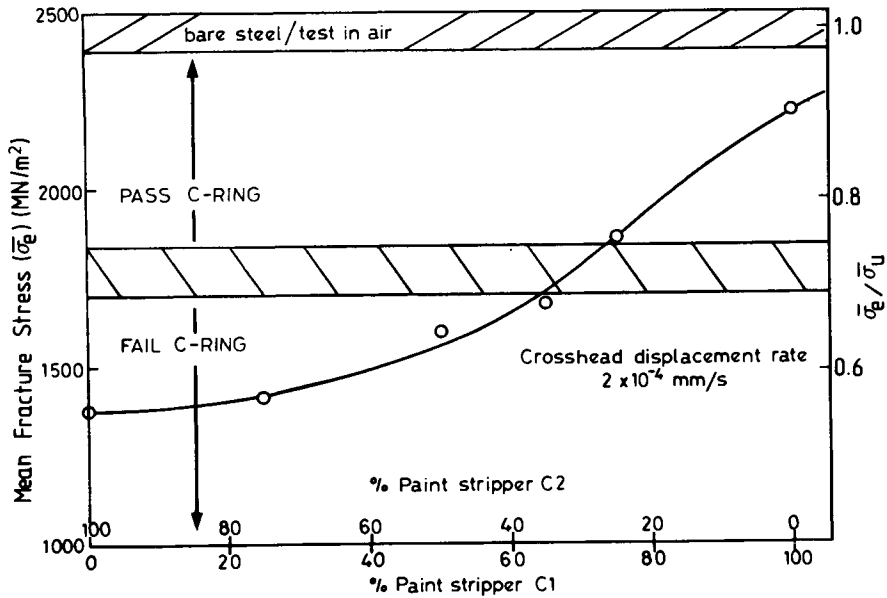


FIG. 4—Comparison of notched C-ring and slow strain rate results in mixtures of Paint Strippers C1 and C2.

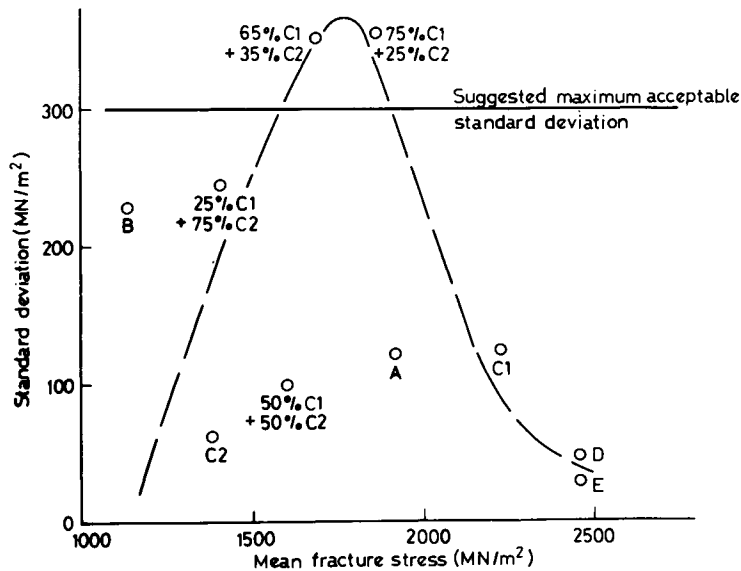


FIG. 5—Mean fracture stress and standard deviation of Cd plated-and-baked 4340 steel notched specimens tested in paint strippers at a crosshead displacement rate of 2×10^{-4} mm/s.

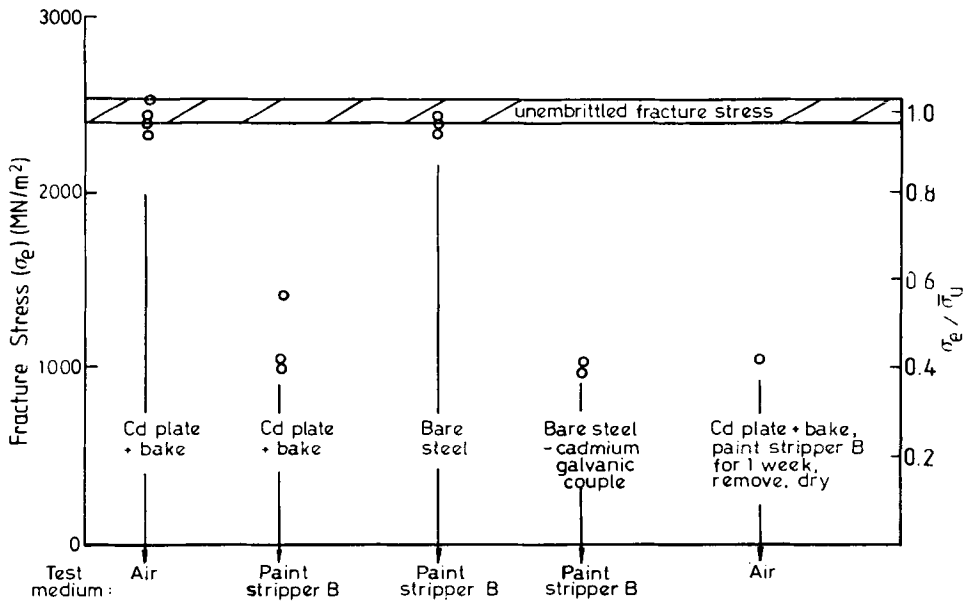


FIG. 6—Fracture stress (σ_f) and fracture stress ratio (σ_f/σ_u) of 4340 steel notched specimens tested under various conditions at a crosshead displacement rate of 2×10^{-4} mm/s.

sure of a Cd plated-and-baked specimen to Paint Stripper B for a week resulted in premature failure after the specimen was cleaned, dried, and subsequently tested in air (Fig. 6).

All paint strippers were alkaline with pH ranging from 8.0 to 11.5. Values of the Cd-steel galvanic potential for the six paint strippers ranged from -0.49V (SCE) to -0.93V (SCE). When all results were plotted on a Pourbaix diagram, only Paint Strippers B and C2 displayed galvanic potentials in the region where generation of hydrogen was expected (Fig. 7). The open circuit potentials for 4340 steel in the six paint strippers were all located in the water-stable region of the Pourbaix diagram and were significantly more positive than corresponding galvanic potentials.

Discussion

The present results confirm that the slow strain rate method can quantify the degree of hydrogen embrittlement in high-strength 4340 steel produced during exposure to paint strippers. Before a satisfactory comparison of the slow strain rate and notched C-ring test methods can be made, the problem of nonuniform scatter in the results of slow strain rate tests must be addressed. In multiple slow strain rate tests conducted at a crosshead displacement rate of 2×10^{-4} mm/s, values of fracture stress standard deviation pass through a maximum (~ 300 MN/m²) at mean fracture stresses within the range 1500 to 1900 MN/m² (Fig. 5). The high scatter is associated with the increased sensitivity of the slow strain rate test for detection of hydrogen embrittlement at intermediate values of fracture stress (Fig. 4). Since the pass/fail condition in standard notched C-ring tests corresponds to a value of mean fracture stress within the range 1700 to 1850 MN/m², the high degree of scatter associated with the slow strain rate tests would make a more precise evaluation difficult; however, since unreliable paint strippers are likely to lead to a standard deviation in excess of 300 MN/m², a minimum mean fracture stress of 1850 MN/m² and maximum standard deviation of 300 MN/m² are suggested as suitable criteria for

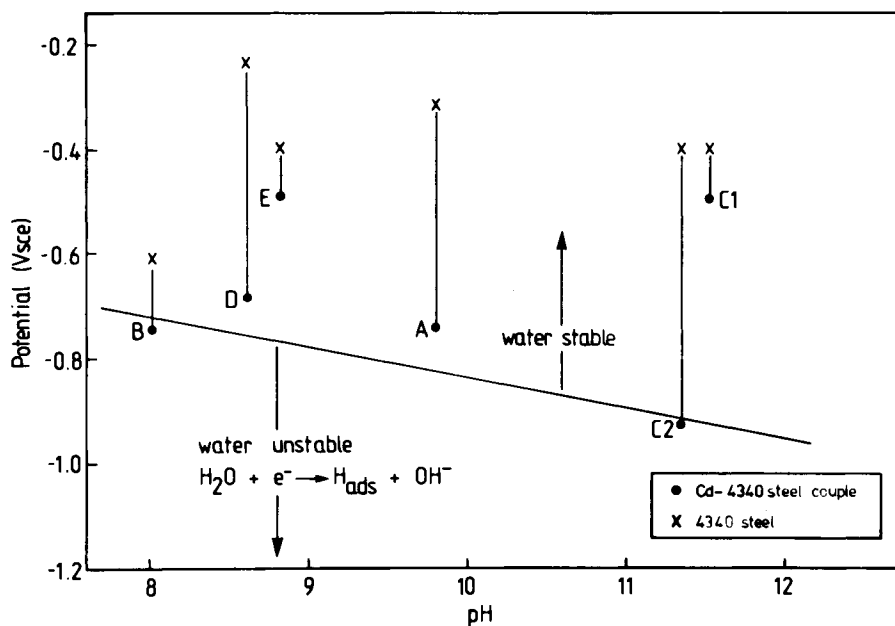


FIG. 7—Pourbaix diagram for 4340 steel-Cd galvanic couple in paint strippers.

acceptance of a paint stripper. Due to the significance of defining a minimum mean fracture stress and a maximum standard deviation as possible criteria for acceptance or rejection of products causing hydrogen embrittlement, it is suggested that better statistical values might be obtained from the results of five rather than three specimens. This method of assessing scatter of results is considered superior to the method of assessment laid down in ASTM F 519-77, where retesting of a further batch of three specimens is required if one specimen fails during testing of the initial batch. Furthermore, this latter procedure can take up to two weeks to complete compared with 2.5 h for a slow strain rate test performed at a crosshead displacement rate of 2×10^{-4} mm/s. Manufacturing costs for the notched tension specimen have also been found to be 50% less than for the notched C-ring specimen. This is due to the lower cost of machining (40%) and lower rejection rate for the notched tension specimen ($\sim 0.5\%$) compared with the notched C-ring specimen (5%).

The slow strain rate method could also be used to quantify the relative severity of other hydrogen embrittlement test methods defined in ASTM F 519-77, MIL-R-83936B Amendment 1, MIL-R-25134B, and MIL-R-81294B specifications. This could be done by conducting tests at a crosshead displacement rate of 2×10^{-4} mm/s and defining an appropriate minimum mean fracture stress and maximum standard deviation consistent with the pass/fail results of the standard specifications. Justification for this approach is evident from a comparison of calculated notch stress concentration factors in five notched tension specimens detailed in the standard specifications (Table 3). Stress concentration factors for the five specimen geometries are calculated assuming the notched specimen to comply with Neuber's solution for a grooved shaft loaded in tension [17] and found to vary from 2.5 to 3.9 (Fig. 8). Troiano [5] has demonstrated that time to failure of sharply notched embrittled steel specimens, loaded to the same percentage value of the unembrittled fracture stress, decreases with increasing notch stress concentration factor. Consequently, it is unlikely that the same pass/fail result would occur if all five specimen types were used to assess treatments producing the same degree of embrittlement.

TABLE 3—Specimen geometry and stress concentration factor (k_T) of notched tension specimens used in standard specifications for hydrogen embrittlement testing of ultrahigh-strength steels [17].

Specification	D , mm	d , mm	r , mm	d/D	r/D	k_T
MIL-R-83936B	12.50	8.84	0.25	0.707	0.020	3.9
ASTM F-519-77 (1a)	8.46	5.97	0.25	0.706	0.030	3.2
ASTM F-519-77 (1b)	4.78	2.27	0.15	0.476	0.032	2.8
MIL-R-25134B	9.07	5.72	0.64	0.631	0.071	2.5
Present work	4.50	3.20	0.15	0.707	0.033	3.1

NOTE: See Fig. 8 for definition of D , d , and r .

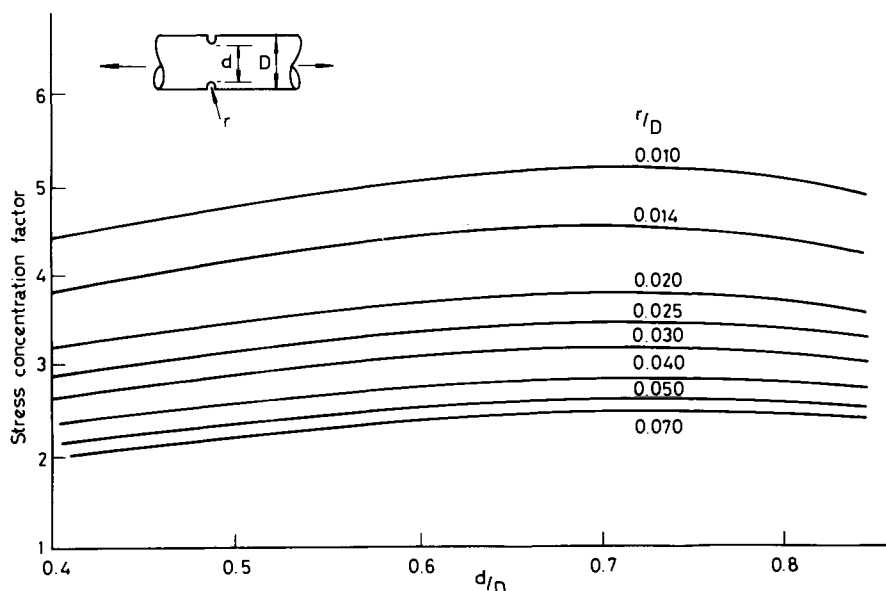


FIG. 8—Calculated values of stress concentration factor (k_T) for a grooved shaft in tension (R. E. Petersen, Stress Concentration Factors, Figs. 30 and 31) [17].

A comparison of the time to failure of chromium-plated notched tension and C-ring 4340 steel specimens also illustrates the difference in test severity exhibited by these two types of specimen (Fig. 9) [18]. Although both curves approach the same lower critical stress at long testing times, the shorter times to failure of notched C-ring specimens tested at the same applied stress demonstrate that this specimen type provides a more severe test compared with identical tests using notched tension specimens. This result is surprising since the notch stress concentration factor in the tension specimen is significantly higher than in the C-ring specimen. Consequently, it is possible that Cd plated-and-baked notched tension specimens tested in a moderately embrittling paint stripper in accordance with ASTM F 519-77 could pass the standard test, whereas notched C-ring specimens would fail the same test. At the present time, it is apparent that the degree of severity associated with the various specimens and test methods is a quantity that has been neither properly defined nor adequately investigated.

The present galvanic potential results show that only paint strippers that fail the standard notched C-ring tests have galvanic potential values in the region of the Pourbaix diagram where

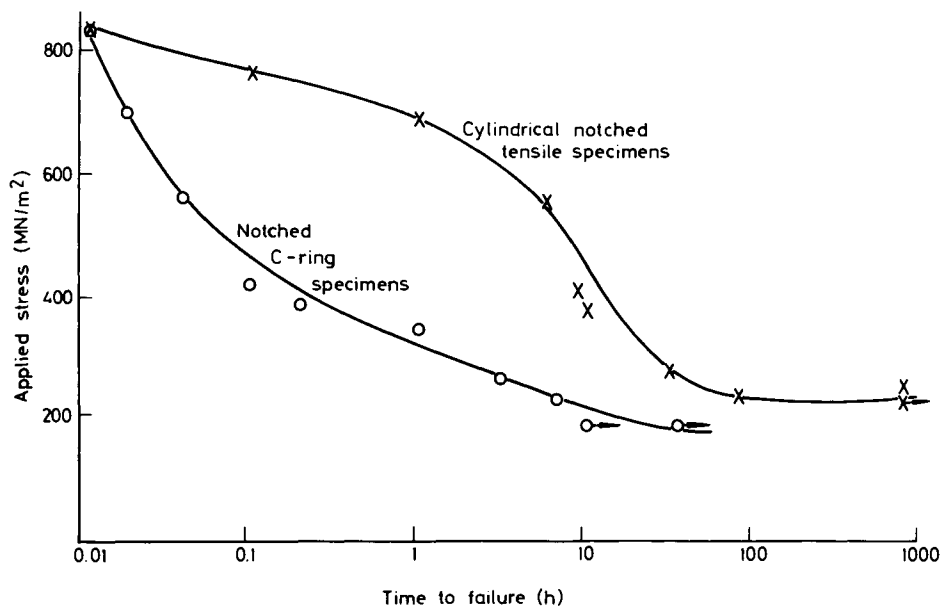


FIG. 9—Comparison of time to failure of notched C-ring ($k_T = 4$) and notched tension specimens ($k_T = 6.3$) chromium plated to a thickness of 0.05 mm and loaded in air to various values of constant applied stress [18].

cathodic reduction of water is expected. Although this approach therefore offers a rapid inexpensive test for predicting whether a paint stripper will seriously embrittle a plated high-strength steel, a more precise evaluation should be possible from in-situ potential measurements of plated specimens. Similarly, values of the steel open circuit potential can be used to predict whether a paint stripper will embrittle unplated steel components. In the present work, this approach successfully predicts that Paint Stripper B will not embrittle 4340 bare steel specimens (Fig. 6).

The highly porous Cd coating deposited in the low-embrittlement plating bath ensures that the paint stripper can penetrate to the steel surface. Since the anodic and cathodic currents must be equal, the large anodic area provides the driving force for high cathodic current densities at the small area of steel exposed to the paint stripper (Fig. 10). Since both slow strain rate and constant load tests are conducted in the presence of the paint stripper, hydrogen produced at the root of the notch can diffuse to the region of maximum triaxial stress ahead of the notch and cause delayed failure in a constant load test and a reduction in fracture stress in a slow strain rate experiment. If a critical concentration of hydrogen is not reached within the time scale of the constant load test, then failure does not occur. Under such circumstances, the test does not reveal the extent to which hydrogen might have been introduced into the steel. In some cases, only a small amount of additional hydrogen may be required to lead to a potentially dangerous situation. Since the paint stripper can also cause hydrogen to be generated at plated regions of the specimen remote from the notch, this hydrogen could ultimately diffuse to the region of maximum triaxial stress over longer periods of time and cause delayed failure. This interpretation may explain the results of experiments in which some notched C-rings passed the standard test for assessment of paint strippers, but which subsequently failed unexpectedly after many weeks.³ In practice, this additional hydrogen could also be generated by the exposure of plated

³C. Grey, unpublished results.

GALVANIC CORROSION
 ↓
 LOCALISED CATHODIC GENERATION OF H AT STEEL SURFACE

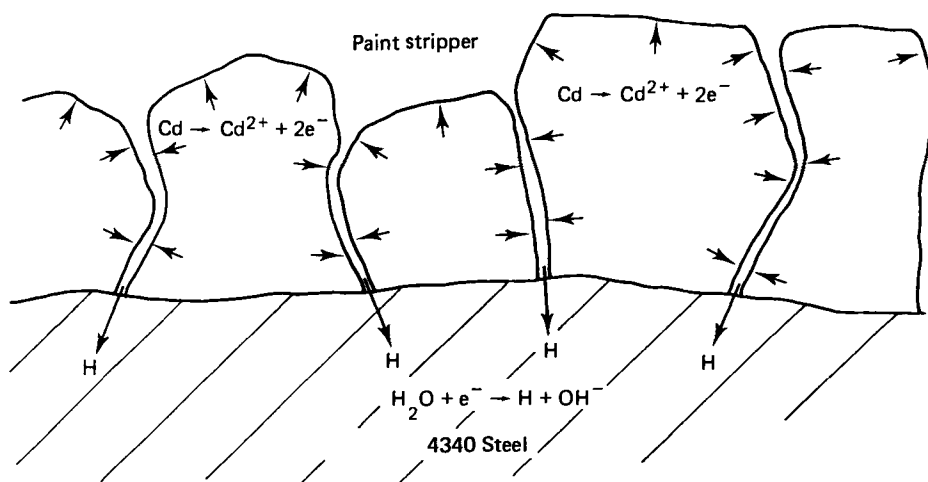


FIG. 10—Localized cathodic generation of hydrogen at steel surface in porous Cd plated-and-baked specimens immersed in paint strippers.

components to other deleterious environments during subsequent maintenance or service [19]. Since the slow strain rate method provides a quantitative measure of the degree of embrittlement produced by paint strippers irrespective of the pass/fail result in standard constant load tests, a more critical assessment can be made of the paint stripper under investigation. Reassessment of the current slow strain rate tests reveals Paint Stripper A to be suspect despite a pass in the standard notched C-ring test. Paint Strippers D and E exhibit a significantly lower tendency to embrittle 4340 steel.

The increasing demands by operators for improved protection schemes has led to the development of paints that are more durable to the effects of deleterious environments. Unfortunately, many of these new paint schemes require more sophisticated paint strippers to remove them. Furthermore, since the environmental hazards associated with phenolic-base paint strippers has led to the development of many new paint strippers that are less toxic, it is important to establish that they are also safe to use on high-strength steel components where hydrogen embrittlement can pose a threat to the integrity of structure. With so much at stake, it is important to optimize methods for quantifying the degree of hydrogen embrittlement in steel by paint strippers. It is believed that the results obtained in the present work using the slow strain rate technique provide some basis for achieving this goal.

Conclusions

A comparison of the slow strain rate method with standard constant load tests highlights many advantages of the former test in assessing the degree of hydrogen embrittlement produced in plated high-strength 4340 steel by paint strippers:

1. Slow strain rate tests can be done using a notched tension specimen that complies with the reduced load requirements in ASTM F 519-77.

2. The slow strain rate test with notched specimens utilizes the fracture stress as a simple parameter for assessing the degree of embrittlement.

3. The severity of the slow strain rate test can be controlled by altering the crosshead displacement rate.

4. For multiple testing of specimens at a crosshead displacement rate of 2×10^{-4} mm/s, a minimum mean fracture stress and maximum standard deviation can be specified for acceptance of a paint stripper.

5. Quantitative results can be obtained in less than 3 h with a slow strain rate test conducted at a crosshead displacement rate of 2×10^{-4} mm/s, compared with a maximum time of 100 to 300 h for tests defined in the standard specifications.

6. The slow strain rate technique could be used to quantify the relative severity of test procedures defined in the various standard specifications.

7. An overall manufacturing cost reduction of 50% can be achieved with the use of notched tension specimens compared with notched C-ring specimens.

The evidence cited in this paper strongly supports the view that the slow strain rate method should be adopted as an alternative standard method for assessing the severity of hydrogen embrittlement in high-strength, low-alloy steel during exposure to paint strippers. It is hoped that this approach will lead to better qualification of products used in the improved maintenance of aircraft components, thereby reducing the risk of failure by hydrogen embrittlement during subsequent service.

Acknowledgments

The authors wish to thank N. Matthews of the Royal Australian Airforce and N. E. Ryan for much encouragement and advice.

APPENDIX

Details of Specifications for Determination of the Degree of Hydrogen Embrittlement Induced by Paint Strippers in High-Strength, Low-Alloy Steels

1. ASTM F 519-77 [4]

Specification allows notched tension, notched bend, notched C-ring, and smooth O-ring 4340 steel specimens to be used. Specimens are porous Cd plated-and-baked and chromate passivated. A minimum of three specimens are loaded in air to the values shown in Table 1 and the notched region immersed in the paint stripper or fluid. If two or more specimens fail within 150 h, the environment is considered embrittling. If one specimen fails, a further three specimens are tested, and if any specimen fractures during retest, the environment is considered embrittling.

2. MIL-R-83936B Amendment 1 [2]

Four notched tension steel specimens are Cd plated-and-baked as outlined in MIL STD 870A [10]. Specimens are then immersed in paint stripper for 4 h, rinsed, dried, and loaded in air to 75% of the notch tensile strength. Failure of one specimen within a period of 200 h is sufficient to cause rejection of the paint stripper.

3. MIL-R-25134B [3]

Four unplated and four Cd plated-and-baked notched tension 4340 steel specimens are loaded in air to 75% of the notch tensile strength. The paint stripper is applied to the notched region of the specimen, wiped off carefully after 10 min, and the process repeated to give four full cycles per day at two hourly intervals until either 100 h has elapsed or until failure. If the specimens are still intact after the 100-h period, the load is maintained for a further 100 h, and if any specimens fail, the paint stripper is considered to be embrittling.

4. MIL-R-81294B [1]

Four Cd plated-and-baked 4340 steel notched C-rings are loaded to 75% of the notched breaking strength in air. The C-ring specimens are immersed for 60 s with the notched side down to a point where the ring is covered approximately 25 mm on either side of the notch. The rings are removed and allowed to hang notched side down in air for 100 h. Failure or cracking of any specimen within this period causes rejection of the paint stripper.

5. Australian RAAF Engineering Specification K55 [15]

Identical to the MIL-R-81294B specification [1] except that either 4340 steel or D6ac steel can be used. Ultimate tensile strength of D6ac steel is specified to be within the range of 1800 to 1930 MN/m².

6. Modified RAAF Specification K55

Identical to the K55 specification except that three notched C-rings are tested for 100 h, and if two or more specimens crack or fail within this period, the paint stripper is considered embrittling. If one specimen fails, a further three specimens are tested, and the paint stripper is considered acceptable only if all three specimens pass the 100 h test.

References

- [1] American Military Specification MIL-R-81294B (May 1977) for Remover, Paint, Epoxy and Polyurethane Systems.
- [2] American Military Specification MIL-R-83936B Amendment 1 (Aug. 1978) for Remover, Paint, Tank Type; for Aircraft Wheels, Landing Gear Components and other Aircraft and Age Components.
- [3] American Military Specification MIL-R-25134B (March 1972) for Remover, Paint and Lacquer, Solvent Type.
- [4] American National Standard ANSI/ASTM F 519-77 (1977), Method for Mechanical Hydrogen Embrittlement Testing of Plating Processes and Aircraft Maintenance Chemicals.
- [5] Troiano, A. R., *Corrosion*, Vol. 15, 1959, pp. 207t-212t.
- [6] Bowker, P. and Hardie, D., *Metal Science Journal*, Vol. 9, 1975, pp. 432-436.
- [7] American Military Specification MIL-S-5000E (Nov. 1982) for Steel, Chrome-Nickel-Molybdenum (E4340) Bars and Reforging Stock.
- [8] Qantas Process Specification P65 (1981), Low Hydrogen Embrittlement Cd Plate of High Heat Treat Steels.
- [9] Hawker de Havilland Australia Process Specification HPS 1.03.00 (1981), Cd Plating (Electrodeposited).
- [10] U.S. Military Standard MIL-STD-870A (USAF) (Aug. 1978), Cd Plating, Low Embrittlement, Electrodeposition.
- [11] Douglas Aircraft Co. Process Engineering Order DPS 9.28 (1973), Special Cd Plating for High Strength Steels.
- [12] Boeing Aircraft Co., Process Specification BAC 5718, Rev F (1976), Low Hydrogen Embrittlement Cd Plating.
- [13] Federal Specification QQ-P-416C (Aug. 1979), Plating, Cd (electrodeposited).
- [14] Aerospace Material Specification AMS2401C (1978), Cd Plating-Low Hydrogen Content Deposit.
- [15] Australian RAAF Engineering Specification K55, Issue 3 (March 1980), Paint Removers—Aircraft.
- [16] Pollock, W. J., "Assessment of the Degree of Hydrogen Embrittlement Produced in High-Strength 4340 Steel by Plating-and-Baking Processes Using Slow Strain Rate Testing, this publication.

- [17] Petersen, R. E., *Stress Concentration Factors*, J. Wiley and Sons, New York, 1974.
- [18] Williams, F. S., Beck, W., and Jankowsky, E. J., *Proceedings*, Vol. 60, 1960, ASTM, Philadelphia, pp. 1192-1202.
- [19] Pollock, W. J. and Hinton, B. R. W., "Hydrogen Embrittlement of Plated High-Strength 4340 Steel by Galvanic Corrosion," to be published in *Galvanic Corrosion, ASTM STP 978*, 1988.

The Hydrogen Embrittlement Susceptibility of Ferrous Alloys: The Influence of Strain on Hydrogen Entry and Transport

REFERENCE: Scully, J. R. and Moran, P. J., "The Hydrogen Embrittlement Susceptibility of Ferrous Alloys: The Influence of Strain on Hydrogen Entry and Transport," *Hydrogen Embrittlement: Prevention and Control*, ASTM STP 962, L. Raymond, Ed., American Society for Testing and Materials, Philadelphia, 1988, pp. 387-402.

ABSTRACT: The influence of strain and strain rate on hydrogen entry, transport, and trapping in high-strength ferrous alloys and the subsequent effects on hydrogen embrittlement are being investigated in this research program. Most hydrogen permeation measurements reported in the literature presume surface absorption kinetics to be sufficiently fast as to not influence observed changes in the permeation flux. It is interesting that hydrogen recombination poisons (enhancing absorption) are frequently used to observe permeation currents. It is also interesting that environmental slow-strain-rate plastic loading and cyclic loading at low frequency, possibly enhancing either absorption or bulk diffusion of hydrogen, have been observed to increase tendencies towards hydrogen embrittlement. In the present investigation a series of slow-strain-rate measurements, electrochemical measurements to investigate adsorption-absorption kinetics and eventually a combination of these, are being performed and will be described. A discussion of electrochemical techniques being utilized for adsorption-absorption studies is included. It is anticipated that once this program is completed, the influence of plastic deformation on the hydrogen absorption and apparent hydrogen diffusion rate for a high-strength steel will be assessed. Once the effects of surface absorption and bulk diffusion are differentiated, the influence of each will be correlated with the degree of hydrogen-stimulated environmental damage observed for AISI 4340 steel in chloride environments.

KEY WORDS: hydrogen, hydrogen embrittlement, adsorption, absorption, surface coverage, strain rate, diffusion, plasticity, permeability, film rupture, hydrogen trapping, solubility, concentration

Transport of hydrogen to embrittlement sites in alloys exposed in aqueous environments requires the electrochemical reduction of water, hydrogen adsorption, absorption, and movement of hydrogen to the embrittlement site either by lattice diffusion, short circuit path diffusion, or dislocation transport. Hydrogen may then concentrate at an internal interface where it influences an embrittlement event. All of these processes have an activation energy barrier, and, therefore, any one step or combination of steps may become rate controlling in the embrittlement event [1]. Further, mechanical deformation may change the rate determining step(s). Examples have been given in the literature where adsorption [2-4], diffusion [3], and crack growth [5-6] appear to be rate controlling. For the case of diffusion rate control, the possibility of enhancement [7] and the observation of diminishment [8,9] by dislocations formation move-

¹Formerly, Materials scientist, the David Taylor Naval Ship Research Center, Bethesda, MD (currently, Sandia National Laboratories, Albuquerque, NM).

²Associate professor, Department of Materials Science, The Johns Hopkins University, Baltimore, MD.

ment and trapping have both been demonstrated. Adsorption, absorption, and diffusion can perhaps be modified by plastic strain. Dislocation generation and movement certainly occur under plastic deformation when stress is applied to materials. Therefore, adsorption and diffusion must be studied under dynamic straining conditions as well.

For hydrogen embrittlement to become better understood, therefore, the rates at which hydrogen adsorption, entry, and transport processes occur under dynamic strain, along with rates of internal trapping, require clarification. Under a given set of conditions, the net hydrogen accumulation can be determined once the rate at which these processes occur is understood. Research on these topics has progressed for force-centered cubic (FCC) metals [10] but largely remains confused for the body-centered cubic (BCC) metals, or high-strength steels [10], which are obviously of technological interest.

The interplay of these three fundamental features (adsorption, absorption, and transport) is irrevocable and has been drawn upon by numerous investigators to explain the strong strain rate and temperature dependency of hydrogen embrittlement [11] as well as the delayed mode of cracking requiring "incubation times," [12] the discontinuous nature of crack propagation, and the dependency of Mode II cracking on hydrogen fugacity [2,13].

With regard to dynamic permeation and absorption experiments, it is appropriate to describe work that has been reported in order to clarify questions which remain unanswered. Latanision and coworkers have studied the effects of plastic deformation on the permeation rates of both single crystal and polycrystalline nickel as well as a steel alloy [14-17]. Single crystal nickel samples displayed evidence of dislocation transport of hydrogen in the easy glide region of plastic deformation [16]. The polycrystalline nickel material exhibited dynamic trapping occurring as a result of the formation of new dislocations [17]. This decreased the permeation flux over a range of strain rates with the exception of the lowest strain rate tested. At that strain rate a permeation increase was observed. This increase was attributed to an enhancement in the hydrogen concentration at the entry surface.

For the steel alloy a greater than 50% decrease in permeation flux was observed upon plastic deformation [15]. Bernstein and Hwang [18] studied hydrogen permeation in single crystal and polycrystalline iron. Using an analysis technique to separate dislocation transport from trapping, a weak correlation is shown supporting slight hydrogen transport by dislocations in the single slip region. The observed effect of hydrogen transport by dislocations is diminished further by duplex slip and work hardening. Heubaum and Berkowitz [9] have studied hydrogen permeation in AISI 4130 steel. These results indicate hydrogen trapping by dislocations as manifested by a 10% decrease in permeation flux upon plastic strain. Blundy et al. [19] have studied hydrogen permeation in steel under elastic and plastic strain. Under conditions of plastic strain, after a previous period of charging, permeation results show a rapid but transient permeation increase, followed by a trapping effect (gradual permeation decrease), followed by a gradual permeation increase at still longer times during plastic straining.

While some of the observations just described remain unexplained, all of the investigators have neglected the effects of adsorption and absorption, which may very well have influenced their measurements [8]. Indeed, permeation experiments generally assume rapid absorption, but these investigators have not attempted to separate effects of changes in adsorption or absorption on the permeation results. Bockris and Flitt [20] and Kim and Wilde [21,22] have studied adsorption, absorption, and the rate constant for absorption on iron and steel but have not performed these studies with simultaneous plastic deformation. Kim and Wilde did show an increase in the absorption rate constant for steel (10 to 15 s^{-1}) over that of the iron (3 to 5 s^{-1}) in a chloride environment over a similar range of cathodic current density. Thomas et al. [23] have studied hydrogen sulfide (H_2S) adsorption rates under plastic deformation and indicated a 100% increase in adsorption rate with strains up to 10%. Also of interest is the work of Smialowski [24], who studied the effect of a hydrogen promoter (recombination poison) added to a sulfuric acid (H_2SO_4) solution. The materials were iron, nickel, and iron carbon alloy wires

twisted in torsion. Addition of the promoter enhanced hydrogen entry and subsequent embrittlement greatly in static load experiments. The addition of the promoter was only slightly significant under torsional straining despite the evidence that the hydrogen entry and embrittlement were both enhanced under such straining (even without the poison). The implication is that the enhanced hydrogen entry and severe subsequent embrittlement in straining experiments (both with and without promoter) resulted from the creation of fresh, uncontaminated, and abundant surfaces at emerging slip steps. Thus, the emerging slip steps provided for either an increased rate constant for absorption or an increased surface coverage or both. Under these conditions mechanically accelerated absorption may have been observed independent of the properties of the poison. Since the materials tested consisted of thin iron-nickel wires, the surface-to-volume ratio was large, and diffusion and possible dislocation transport as rate determining steps appear implausible but nevertheless possible. These are precisely the distinctions which need clarification and are presently being pursued in the research investigation. Straining-diffusion experiments on slow-strain-rate specimens to investigate bulk dislocation effects are being combined with electrochemical testing techniques to study surface effects. The issue of enhanced entry versus bulk transport of hydrogen will hopefully be clarified. The experimental approach, the results to date, and a discussion of the results relative to the concepts just discussed are given in the following sections.

Experimental Procedures

Materials and Specimen Preparation

Specimens were produced from a single heat of AISI 4340 steel (UNS No. G43400) and heat treated to form tempered martensite. Specifically, the 2.54-cm-thick plate material was austenitized at 804°C (1479°F) for 1 h, quenched in oil, and tempered at 538°C (1000°F) for 1 h. The nominal composition is given in Table 1. These processes produced an alloy with a nominal yield strength of 1200 MPa, 10 to 12% elongation, and 40 to 50% reduction in area at failure in air. Mechanical properties are given in Table 2. One tenth-inch-diameter (0.254-cm)-reduced cross-section transverse-long (T-L) orientation tension specimens were produced. Gage lengths were finished with an alumina paste, producing a polished surface. An insulating lacquer was used to mask the specimen except for the gage length.

TABLE 1—*Chemical composition of 4340 steel, weight %.*

C	Mn	P	Si	Cu	Ni	Cr	Mo	V	Fe
0.44	0.78	0.014	0.21	0.18	1.95	0.74	0.17	0.05	95.466

TABLE 2—*Mechanical properties of AISI 4340 steel.*

Ultimate Strength, (ksi)	0.2% Yield Strength, (ksi)	Elongation, %
1270 (183.3)	1200 (174.2)	10.0 to 12.0

Slow-Strain-Rate Testing (SSRT)

SSR tests were performed at displacement rates ranging from less than 5×10^{-7} cm/s. During straining specimens were cathodically polarized under potentiostatic control using a straining polarization cell shown in Fig. 1. The cell can accommodate either hollow tension specimens for simultaneous straining permeation measurements, as shown, or conventional SSRT specimens. Tests were initially conducted over the range of strain rates from above 10^{-2} to 10^{-7} s $^{-1}$ based on 2.54-cm (1-in.) gage lengths. A strong correlation between the percentage of reduction in area at failure and strain rate, when dynamically tested at a constant cathodic potential of -1.0 V Standard Calomel Electrode (SCE) in ASTM artificial ocean water, was found. The transition range in these tests occurred below from 10^{-5} to 10^{-6} s $^{-1}$. All subsequent SSR tests were conducted below this range.

Hydrogen Permeation Studies

In the Devanathan-Stachurski cell experiment [25], after hydrogen enters the lattice, it is transported by diffusion across the concentration gradient created with respect to the entry surface. For the case of unidirectional diffusion at steady state across a steel membrane of thickness, L , where the charging or entry side is maintained at a fixed high concentration and the exit surface is maintained at a zero hydrogen concentration, the following expression [21,25] will describe the measured permeation flux, J

$$1/J = L \cdot K_{\text{rev}}/D \cdot \theta \cdot K_{\text{abs}} + 1/K_{\text{abs}} \cdot \theta \quad (1)$$

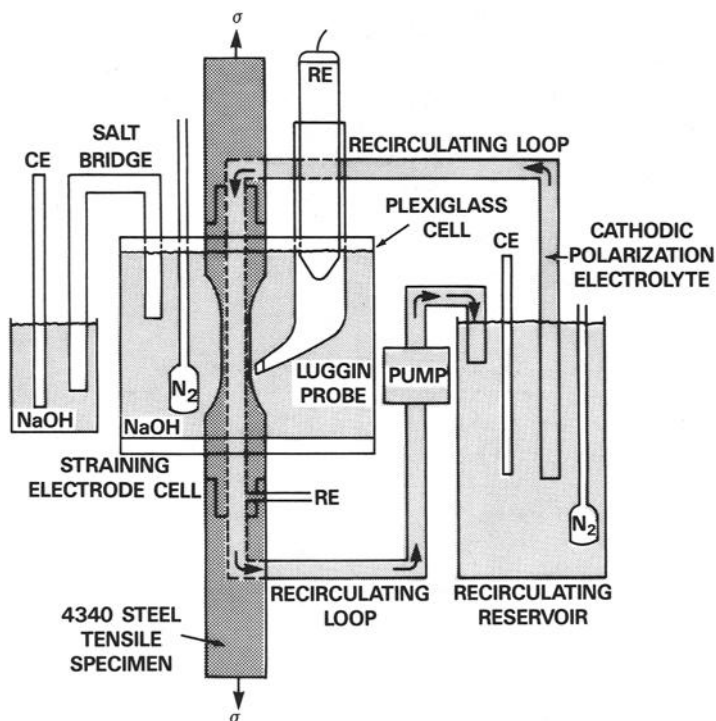


FIG. 1—Simultaneous devanathan—slow-strain-rate experiment.

where

- D = the diffusion coefficient,
 θ = the hydrogen surface coverage, and
 K_{abs} and K_{rev} = the forward and reverse rate constants for the reaction describing hydrogen entry.

Specimens utilized in this experiment were of transverse orientation and polished in the same manner as SSRT specimens. The exit surfaces of the specimens were plated with a thin layer of palladium. The solution utilized in the exit section of the cell was 0.1 M sodium hydroxide. Charging solutions consisted of ASTM artificial ocean water or 0.6 M sodium chloride (NaCl) adjusted to pH 9 to 10 with sodium hydroxide (NaOH).

Results and Discussion

The Influence of Strain Rate on the Degree of Environmental Damage

The influence of strain rate on the degree of environmental damage during in situ exposure has been observed by numerous investigators for a number of alloy electrolyte systems [11, 26–36]. Similar behavior is shown in Fig. 2 at two different cathodic protection levels. The strain rate effect has been attributed to a number of environmentally related phenomena. In the absence of oxide film formation in acid media or in cases where films are reduced cathodically, decreasing strain rates provide for longer exposure time, and this simply allows a greater net hydrogen accumulation at a greater depth in the specimen. In other cases, oxide film rupture can allow hydrogen entry, occurring as a function of a critical strain related to film ductility coupled with passive film breakdown-repassivation kinetics [29–32]. The anodic dissolution occurring after film rupture but before repassivation produces a minimum cathodic charge associ-

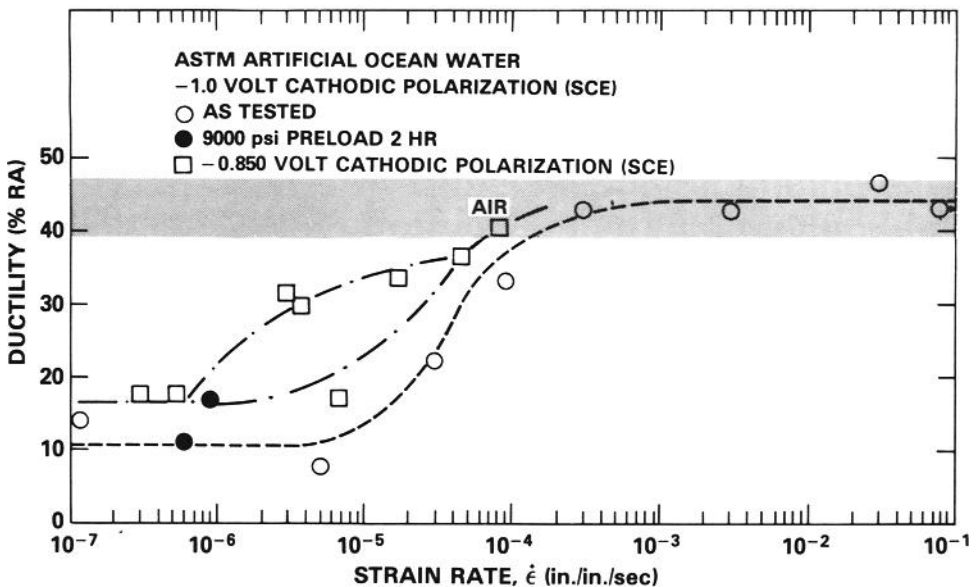


FIG. 2—Effect of strain rate on ductility of AISI 4340 steel under cathodic polarization in ASTM artificial ocean water.

ated with hydrogen entry. This is a modification, however, of the classical situation of stress corrosion cracking where a critical ratio of crack strain rate to anodic charge, relatable to crack tip dissolution rate, must be achieved but not exceeded [37-39]. Enhanced hydrogen surface entry as a result of slip step formation and dislocation transport of hydrogen are, also, phenomena where the total strain and strain rate magnitude are important in the cases of specimens charged simultaneous to straining. The significance of film rupture or slip step formation will be suggested by the following experiments. Additional SSR experiments were conducted after 100-h exposures of slow-strain-rate specimens under cathodic polarization (-900 mV versus SCE) without load. These specimens were then immediately strained to failure at susceptible strain rates (3×10^{-6} to $3 \times 10^{-7} \text{ s}^{-1}$) in air. The percent reduction in area was decreased only slightly from those of specimens tested in air which were never exposed to seawater. The 100-h cathodic protection period was longer in duration than the time of simultaneous cathodic polarization and straining during the conventional SSRT tests previously discussed (approx. 40 h to failure at $3 \times 10^{-7} \text{ s}^{-1}$). Even though partial hydrogen outgassing may have occurred during the air tests, the results suggest enhanced hydrogen entry under the simultaneous application of strain and cathodic polarization.

Electrochemical, Hydrogen Absorption, and Transport Considerations

Electrochemical

Hydrogen adsorption results from the reduction of water at potentials more electronegative than the reversible potential for hydrogen at the pH of interest.



The reversible potential for this reaction in pH 8.4 seawater is approximately -740 mV (SCE). This reaction leads to adsorption of hydrogen atoms and local alkalinization of the electrolyte. After adsorption, electrochemical or chemical combination and desorption of molecular hydrogen, precluding hydrogen entry, may result [40]. The exact electrochemical mechanism for this process is dependent upon solution chemistry and pH and must generally be determined for each alloy-electrolyte situation encountered [40]. Figure 3 illustrates the conditions of potential and pH under which hydrogen adsorption is thermodynamically possible [41]. Note that in the pH range of 8 to 14 and at potentials in the range of -750 at pH 8 decreasing to -1000 mV (SCE) at pH 13, or at more electronegative potentials, the following conditions are met: oxide films tend to be thermodynamically unstable and tend to dissolve or become reduced; anodic dissolution of iron is minimized or eliminated. Most importantly, reduction of water to form hydrogen is possible. Brown et al. [41] have shown that similar conditions of potential and pH can be met for an occluded cell crack tip in the case of a specimen cathodically polarized at the boldly exposed surface in a solution of neutral pH. Again the question may be raised as to the role of plastic strain in rupturing films and allowing hydrogen entry and/or providing clean surfaces for hydrogen adsorption/absorption at emerging slip bands.

With regard to hydrogen fugacities created at the specimen surface during cathodic electrochemical charging, the general relationship linking hydrogen overpotential and hydrogen fugacity is now given [42]

$$\eta = 30 \text{ mV} \cdot \log(f_{\text{H}_2}) \quad (3)$$

where

η = the hydrogen overpotential, and
 f_{H_2} = the hydrogen fugacity.

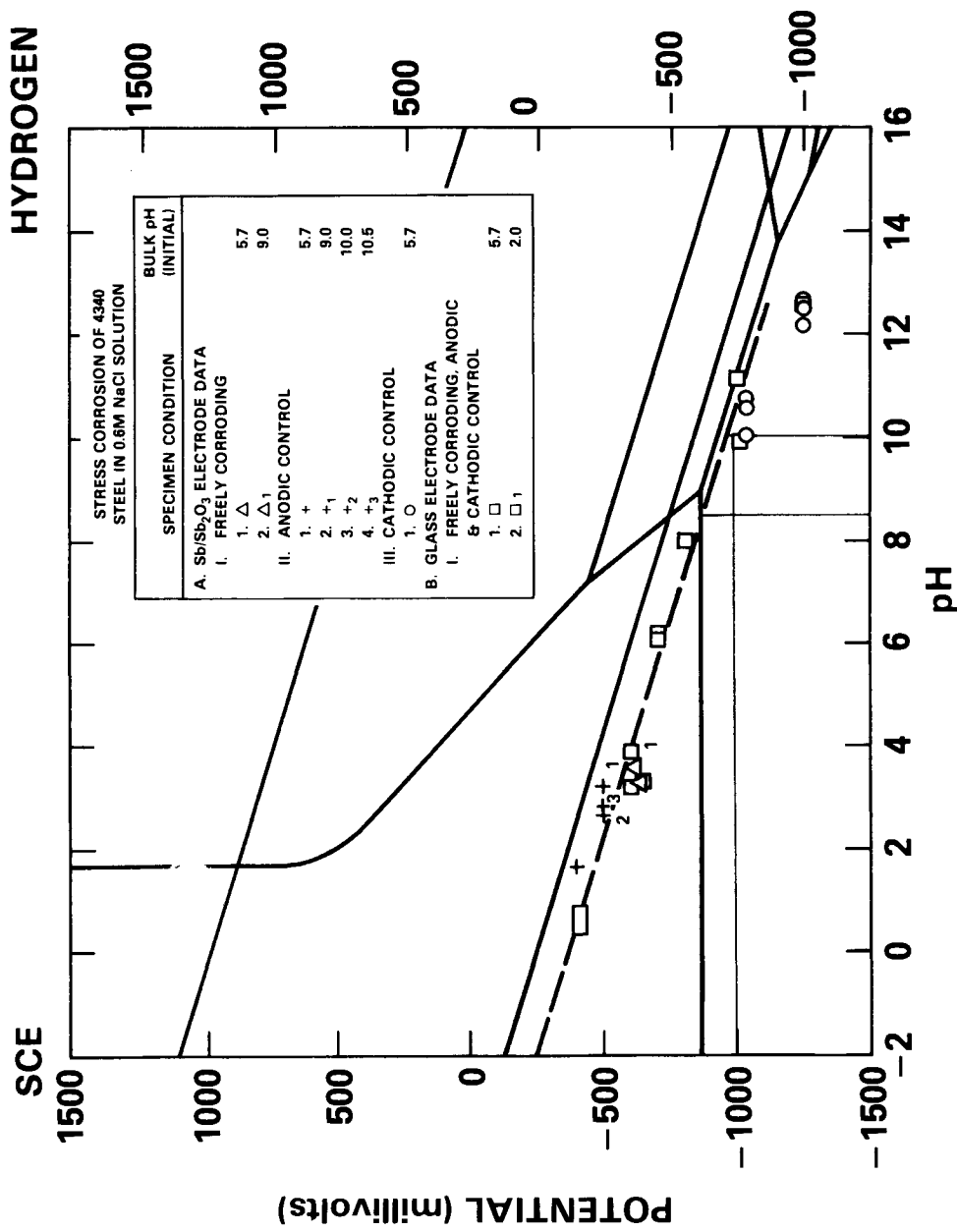


FIG. 3—The electrochemical condition for a propagating crack in AISI 4340 steel.

The exact relationship may change depending upon the specific electrochemical reaction mechanism [40]. Hydrogen fugacity will increase with increasing overpotential assuming that the electrolyte is maintained at a constant pH. A constant applied potential was maintained during the SSRT experiments by potentiostatic control. Increasing the hydrogen fugacity increases the hydrogen surface coverage, and this in turn increases the amount of hydrogen absorbed into the lattice [40]. The hydrogen subsurface concentration will increase approximately as a function of the hydrogen fugacity raised to the 0.5 power in the electrochemical experiment [40]. The relationship between hydrogen fugacity and ductility is shown in Fig. 4 for the 4340 alloy studied. A decrease from over 40 to 10% reduction in area is observed. Sacrificial zinc cathodic polarization in seawater to -900 mV (SCE) produces a square root fugacity of $316 \text{ atm}^{0.5}$ as shown. Cathodic protection with aluminum flame spraying to -850 mV (SCE) produces a square root fugacity of $46 \text{ atm}^{0.5}$. Both of these conditions can cause embrittlement for the AISI 4340 steel.

Hydrogen Absorption

Concerning the kinetics of hydrogen entry from aqueous media, the following reaction and rate constants describe this process, shown below at equilibrium [40]



where K_{abs} and K_{rev} describe the forward and reverse rate constants for a first order reaction. Described slightly differently [40]

$$[\text{Rate of Entry}] = \gamma \cdot \theta \cdot K_{\text{abs}} - C_H \cdot K_{\text{rev}} \quad (5)$$

where

θ = the fractional hydrogen surface coverage,

C_H = hydrogen concentration just below the surface, and

$\gamma = [H_{\text{ads}}]$, the surface concentration at $\theta = 1$.

The subsurface hydrogen content at equilibrium is also given by

$$C_H = \frac{K_{\text{abs}} \cdot \theta \cdot \gamma}{K_{\text{rev}}} \quad (6)$$

where

$$K' = \frac{K_{\text{abs}}}{K_{\text{rev}}}, \text{ and}$$

As previously discussed, one can control the applied potential and, thereby, partially the overpotential and the fugacity in a straining electrode experiment. To some extent this allows control of the hydrogen surface coverage; however, the surface coverage may increase at a fixed applied potential when the nature of the surface is altered chemically or mechanically. For instance, the surface coverage is generally thought to be greater at clean surfaces and at surface defects than at contaminated surfaces with the exception of those surfaces treated with a recombination poison. Increases in the effective surface coverage by whatever means will increase the subsurface hydrogen concentration, thus increasing the hydrogen permeation flux. The wide-

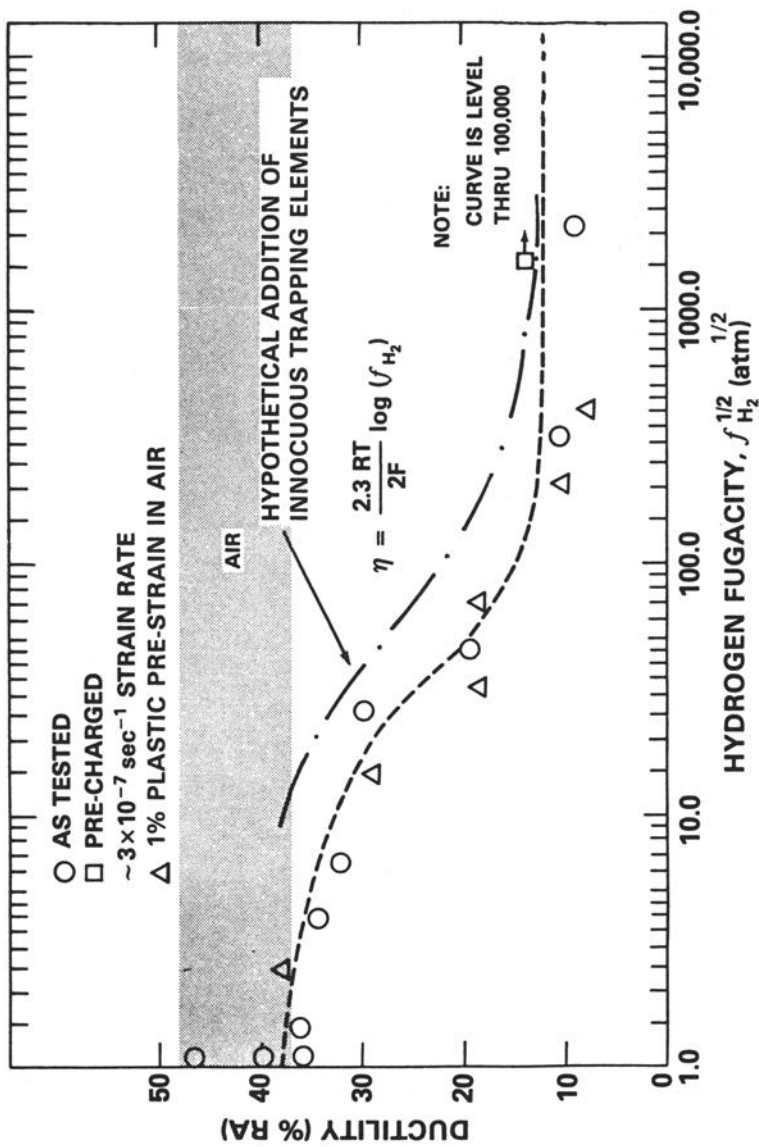


FIG. 4—Relationship between relative hydrogen fugacity and ductility of AISI 4340 steel in ASTM artificial ocean water.

spread use of recombination poisons to increase the permeation rate provides evidence of this effect.

There are several transient electrochemical techniques used to calculate the surface coverage [42-44]. Figure 5 illustrates this procedure as originally used by Bockris and coworkers involving a galvanostatic cathodic charging followed by an anodic galvanostatic pulse designed to oxidize hydrogen from the surface of the alloy. Kim and Wilde have utilized this technique for the study of iron and steel [21,22]. Some resulting data is summarized in Table 3. Bockris has modified the technique further, using a nonelectrochemical technique to measure the hydrogen solubility [20]. Note that, in all cases, the solubility must be determined separately, and with the

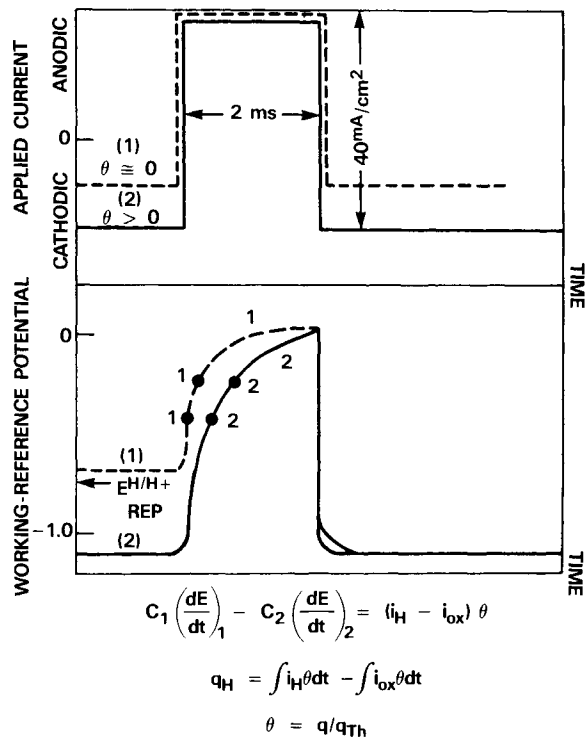


FIG. 5—Scheme for determining the partial surface coverage of hydrogen by galvanostatic technique.

TABLE 3—Absorption rate constants for hydrogen.

Metal/ Alloy	Electrolyte	Cathodic Current, μ A/cm ²	Over-potential, mV	Coverage, %	K_{abs} , s ⁻¹
Iron [21]	10 ⁻⁴ M NaOH and 0.1 M Na ₂ SO ₄	100	-335	6.65	5.1
		200	-363	8.24	4.2
		300	-385	9.95	3.5
C-Mn steel [22]	0.5 M NaCl pH 2	92 to 132	-575 to 600	22.00	11.8

exception of the Bockris study this is usually done using the steady state Devanathan permeation flux at a known value of the diffusion coefficient

$$J = D \cdot C_H / L \quad (7)$$

The overall reaction constant for hydrogen entry, K' , can thus be determined by combining the steady state Devanathan permeation experiment results with the transient experiments mentioned. Since $C_H = \gamma \cdot \theta \cdot K'$, K' can be determined if the surface coverage and solubility are known. Also, permeation measurements performed at various thicknesses, L , can be extrapolated to zero thickness to calculate the product $K_{\text{abs}} \cdot \theta$ [21, 25]. Figure 6 illustrates steady state permeation data for AISI 4340 as a function of specimen thickness and surface condition. The trend is in direct accordance with Eq 1. Departure from linear J versus $1/L$ data indicates surface control. Note that the presence of corrosion products reduces the value of the product $K_{\text{abs}} \cdot \theta$ and limits the quantity of hydrogen absorbed and permeated. Knowledge of θ using transient methods allows calculation of the forward rate constant directly from these data. For unstrained metals, K_{abs} is usually found to be fast (2 to $10 \text{ s}^{-1} \text{ s}^{-1}$) [21, 22]. Thus, absorption is assumed to be an unlikely rate-determining step as compared to diffusion. However, the use of poisons to increase hydrogen absorption indicates that the overall rate for hydrogen entry is finite, especially in the absence of strain or presence of corrosion products in alkaline environments. The data shown in Fig. 6 support this theory. Further, Gileadi and Berger have shown that K' for palladium is 1.5 to 15×10^{-4} , depending on the overpotential indicative of more hydrogen on the surface than in the bulk even for a material known as a rapid hydrogen absorber [43]. A calculation of the hydrogen entry rate constant under the condition of plastic strain has not been reported in the literature as known by the coauthors. Apparently the role of absorption is not necessarily minimal in determining the overall rate of hydrogen entry, particularly in alkaline environments at low cathodic current densities.

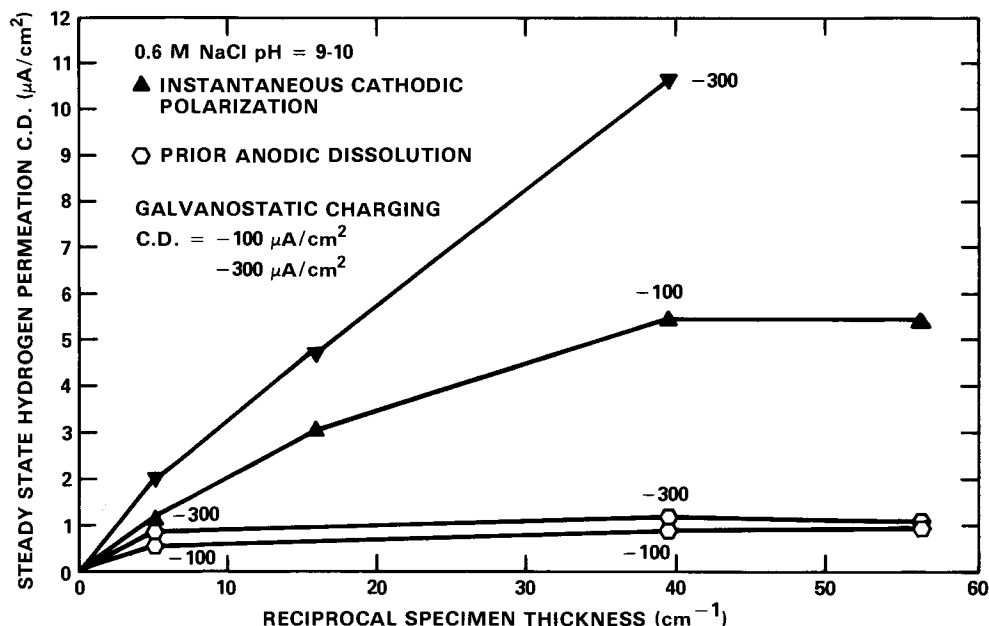


FIG. 6—Plot of the hydrogen permeation current against the reciprocal of the membrane thickness for AISI 4340 steel in 0.6 M NaCl solution (pH = 9-10).

Hydrogen Transport

In terms of relating hydrogen permeation to a reduction in mechanical properties, Figs. 7 and 8 clearly substantiate a direct relationship between increases in the hydrogen permeation flux and increases in the reduction area at failure. The SSRT specimens studied in Fig. 7 were tested at a strain rate of $3 \times 10^{-7} \text{ s}^{-1}$, previously identified as a susceptible strain rate (Fig. 2). Figure 8 graphs steady state permeation currents as a function of cathodic overpotential for non-strained permeation specimens. At the reversible hydrogen potential, the hydrogen fugacity is 1 atm and the permeation current is very low; consequently, only slight embrittlement is observed.

As mentioned previously, several investigators have performed the permeation experiment for the case of a mechanically strained specimen [9,14-17,19,45]. The results from these experiments are summarized schematically in Fig. 9. Note that increases in permeation flux have been attributed to lattice expansion and subsequently to a solubility increase for elastic strains [45] and to dislocation transport for the plastic case [15-17]. However, an increase in J could also be attributed to an increase in θ , K_{abs} , or both as suggested by the data plotted in Fig. 6. This would, subsequently, lead to an increase in the hydrogen concentration, which would enhance the concentration gradient for hydrogen transport. Alternatively, decreases in permeation flux due to the dynamic trapping of hydrogen, as a result of dislocation formation, although adversely affecting transport of hydrogen, may still have a deleterious effect on the material. This is the topic of the next section.

Metallurgical Trapping Effects

A general decrease in J , attributed to a decrease in the apparent diffusion coefficient, D , is brought about from the generation of new dislocations, which may be mobile traps in some

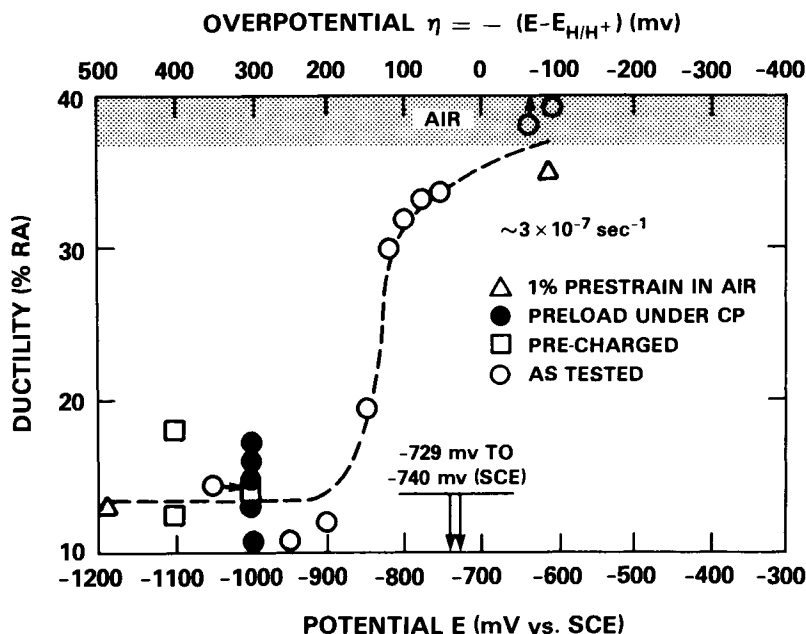


FIG. 7—Relationship between reduction in area at fracture and cathodic polarization level for AISI 4340 steel in ASTM artificial ocean water.

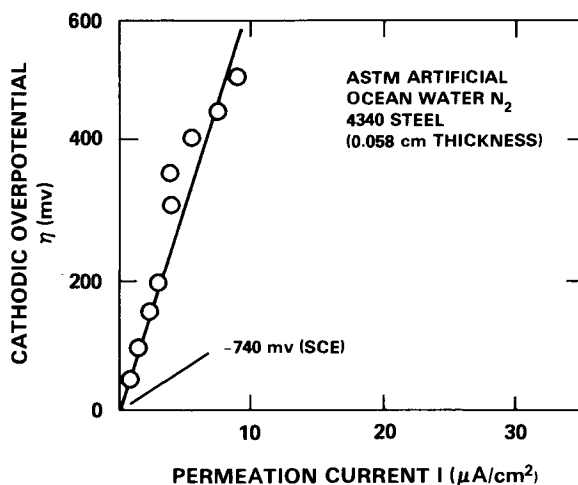


FIG. 8—Relationship between cathodic polarization level and hydrogen permeation rates for AISI 4340 steel in ASTM artificial ocean water.

instances but are rendered stationary when immobilized during work hardening. Figure 10 illustrates the effect of metallurgical features (trapping defects) in decreasing apparent diffusivity [46]. A similar type of plot has been shown for the case of D plotted versus percentage cold work for polycrystalline iron under a predeformed condition [47,48]. Thus, the formation of dislocations during straining of iron and steel creates additional trapping sites. In the case of mild steels, unlike quenched and tempered AISI 4340, some of these sites may serve as innocuous traps, particularly where dislocation networks are formed within grains, but not at grain boundaries. However, most dislocations in AISI 4340 will become immobilized at prior austenite grain boundaries, lath colonies, or at carbide particles. Enhanced delivery of hydrogen to these potentially dangerous embrittlement sites can occur if hydrogen is transported by dislocations during dynamic straining. Therefore, as Hirth has postulated [1], prior prestraining in air could improve embrittlement resistance under slow-strain-rate charging conditions for mild steels, but not necessary for AISI 4340. Dynamic straining or especially fatigue-type strains may degrade the properties of both mild steels and AISI 4340 [1]. The reason for this may be related to the short-range mobility of dislocations and their possible ability to transport hydrogen when mobile. Figure 4 illustrates the effect of prior 1% plastic prestrain in air. No appreciable change is seen for AISI 4340 in this case.

On the other hand, beneficial metallurgical trapping additions may be added to the material. One example of this would be the addition of trace amounts of rare earth metals to promote the formation of innocuous trapping particles, which may be able to compete with prior austenite grain boundaries and carbide particles to trap hydrogen [49].

Summary

The mechanisms for hydrogen entry and transport in alloys from aqueous solutions have been reviewed, as well as experimental methods capable of elucidating the role of each step in the overall transport process. It does seem likely that plastic deformation may increase the hydrogen entry rate at the surface. Three scenarios are possible which account for this effect. They include the formation of slip steps at the surface which either disrupt passive films acting as barriers to hydrogen entry or simply provide fresh clean surfaces. In addition, calcareous films

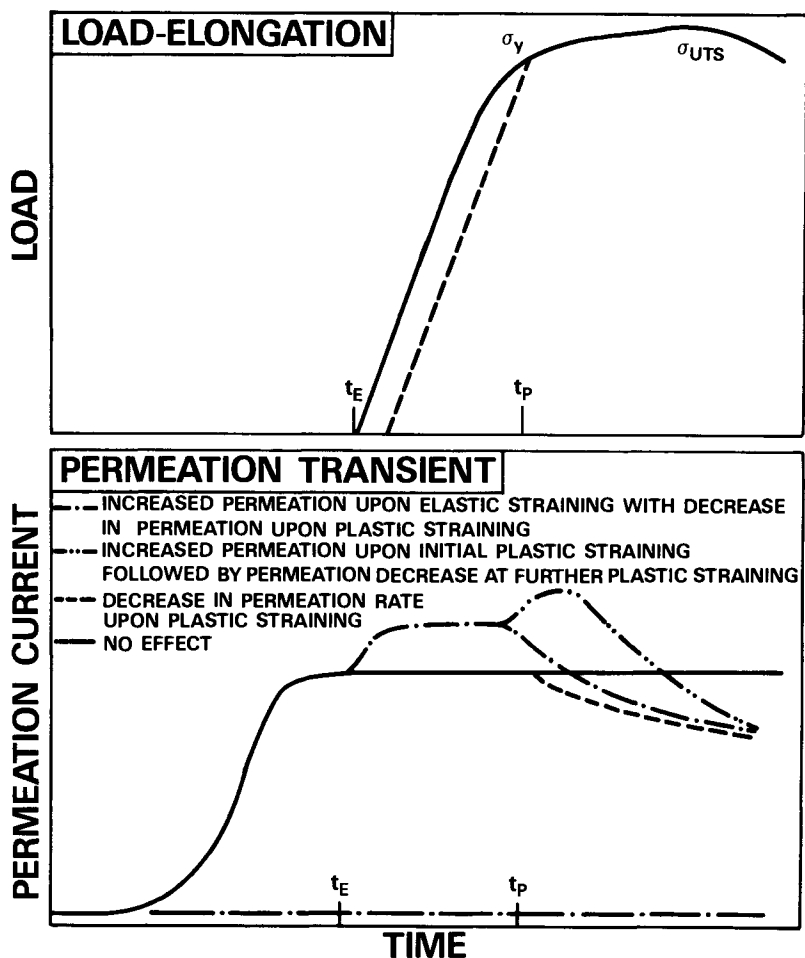


FIG. 9—Some effects of elastic and plastic deformation on hydrogen permeation through metals.

may be disrupted to promote hydrogen entry. Theory indicates that enhanced entry under such conditions would be related to the hydrogen surface coverage and absorption rate constant. Data have been given illustrating the role of these transport processes in the hydrogen embrittlement of AISI 4340 steel in ASTM artificial ocean water. In addition to the mechanistic information developed from the research underway, additional information pertinent to the mitigation of hydrogen embrittlement will result.

Future Opportunities

Solutions to the hydrogen embrittlement problems fall into two general categories. These are metallurgical modifications and surface modifications. Metallurgical modifications include additions of elements which form innocuous trapping particles homogeneously distributed in the lattice. These particles attract hydrogen away from metallurgically dangerous embrittlement sites. Surface modifications include the use of inhibitors. One role of the inhibitors would be to

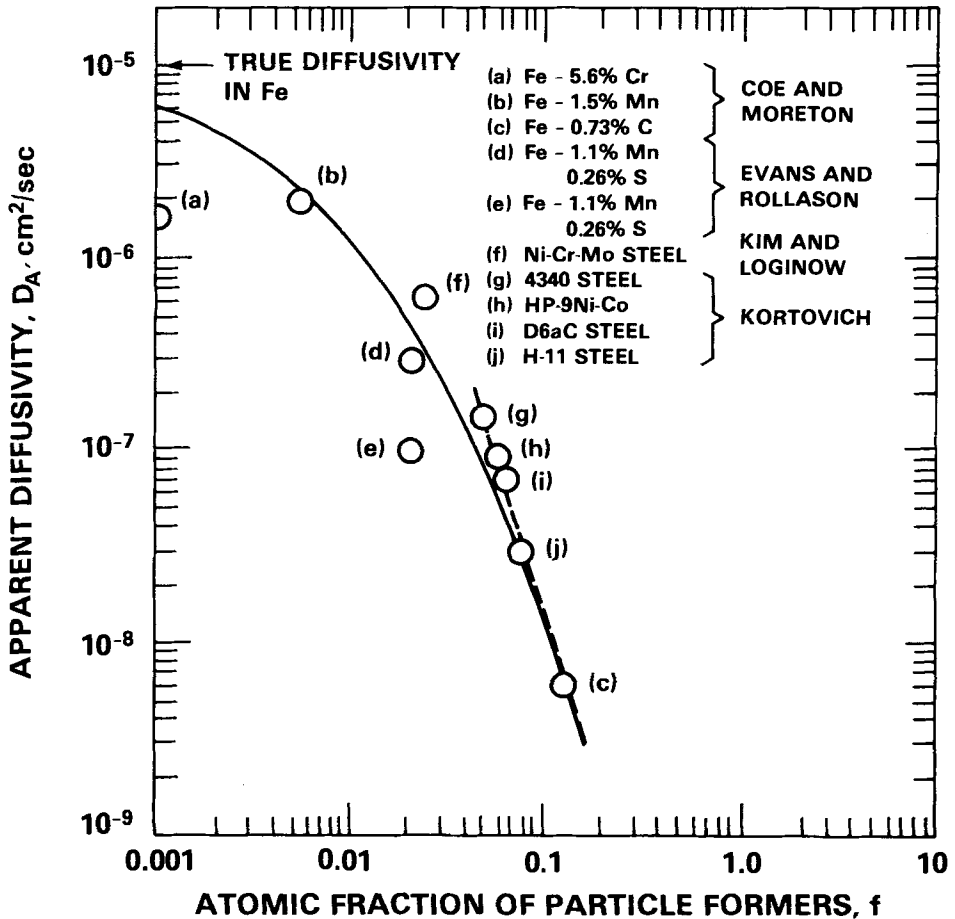


FIG. 10—Decrease in apparent hydrogen diffusivity with increasing fraction of precipitate particles.

lower the surface coverage by either physical blockage or by increasing the exchange current density which in turn lowers the hydrogen fugacity. Progress in the research described will aid in developing embrittlement solutions of these kinds.

References

- [1] Hirth, J. P., *Metallurgical Transactions Annual*, Vol. 11, 1980, p. 861.
- [2] Simmons, G. W., Pao, P. S., and Wei, R. P., *Metallurgical Transactions*, Vol. 9A, 1978, p. 1147.
- [3] Kerns, G. E. and Staehle, R. W., *Scripta Metallurgica*, Vol. 6, 1972, p. 631.
- [4] Nelson, H. G., Williams, D. P., and Tetelman, A. S., *Metallurgical Transactions*, Vol. 2, 1971, p. 953.
- [5] Oriani, R. A. and Josephic, P. H., *Acta Metallurgica*, Vol. 25, 1977, p. 979.
- [6] Nelson, H. G. and Williams, D. P. in *Stress Corrosion Cracking and Hydrogen Embrittlement of Iron Based Alloys*, National Association of Corrosion Engineers, Houston, TX, 1977, p. 390.
- [7] Tien, J. K., Thompson, A. W., Bernstein, I. M., and Richards, R. I., *Metallurgical Transactions*, Vol. 7A, 1976, p. 821.
- [8] Donovan, J., *Metallurgical Transactions Annual*, Vol. 7A, 1976, p. 145.

- [9] Heubaum, F. H. and Berkowitz, B. J. in *Atomistics of Fracture*, R. M. Latanision and J. Pickens, Eds., Plenum Press, New York, 1983, p. 823.
- [10] Bernstein, I. M. and Thompson, A. W. in *Atomistics of Fracture*, R. M. Latanision and J. Pickens, Eds., Plenum Press, New York, 1983, p. 813.
- [11] Toh, T. and Baldwin, W. M. in *Stress Corrosion Cracking and Embrittlement*, W. D. Robertson, Ed., J. Wiley & Sons, Inc., New York, 1976, p. 187.
- [12] Troiano, A. R., *Transactions of the American Society for Metals*, Vol. 52, 1960, p. 54.
- [13] MacDonald, D. D. and Chung, H. H., *Corrosion*, Vol. 41, No. 3, 1985, p. 151.
- [14] Kurkela, M. and Latanision, R. M., *Scripta Metallurgica*, Vol. 13, 1979, p. 927.
- [15] Kurkela, M., Frankel, G. S., Latanision, R. M., Suresh, S., and Ritchie, R. O., *Scripta Metallurgica*, Vol. 16, 1982, p. 45.
- [16] Frankel, G. S. and Latanision, R. M., *Metallurgical Transactions Annual*, Vol. 17, 1986, p. 869.
- [17] Frankel, G. S. and Latanision, R. M., *Metallurgical Transactions Annual*, Vol. 17A, May 1986, p. 861.
- [18] Hwang, C., Ph.D. thesis, Carnegie-Mellon University, Pittsburgh, PA, 1984.
- [19] Blundy, R. G., Royce, R., Pook, P., and Shreir, L. L. in *Stress Corrosion Cracking and Hydrogen Embrittlement of Iron Base Alloys*, J. Hochman and R. W. Staehle, Eds., National Association of Corrosion Engineers, Houston, TX, 1977, p. 636.
- [20] Flitt, H. J. and Bockris, J. O. M. in *Atomistics of Fracture*, R. M. Latanision and J. Pickens, Eds., Plenum Press, New York, 1983, p. 549.
- [21] Kim, C. D. and Wilde, B. E., *Journal of the Electrochemical Society*, February 1971, p. 203.
- [22] Wilde, B. E. and Kim, C. D., *Corrosion*, Vol. 37, No. 8, 1981, p. 449.
- [23] Thompson, M. T., Baer, D. R., and Jones, R. H. in *Atomistics of Fracture*, R. M. Latanision and J. Pickens, Eds., Plenum Press, New York, 1983, p. 1019.
- [24] Smialowski, M. in *Congre's International L'Hydrogene dans les Me'taux*, Editions Science, Paris, 1972, p. 300.
- [25] Devanathan, M. A. and Stachurski, Z., *Proceedings of the Royal Society*, A270, 1962, p. 90.
- [26] Wearmouth, W. R., Dean, G. P., and Parkins, R. N., *Corrosion*, Vol. 29, No. 6, 1973, p. 251.
- [27] Lyle, F. F., Jr. and Norris, E. B., *Corrosion*, Vol. 34, No. 6, 1978, p. 193.
- [28] Parkins, R. N. and Holroyd, N. J. H. in "Stress Corrosion Cracking of 70/30 Brass in Acetate, Formate, Tartrate, and Hydroxide Solutions," *Corrosion*, Vol. 38, No. 5, 1982, p. 245.
- [29] Parkins, R. N., Holroyd, N. J. H., and Fessler, R. R., *Corrosion*, Vol. 34, No. 8, 1978, p. 245.
- [30] Hardie, D. in *Proceedings of the 3rd International Conference on Hydrogen and Materials*, Paris, France, 1982, p. 7.
- [31] Bowler, P. and Hardie, D., *Metal Science*, Vol. 9, 1975, p. 432.
- [32] Craig, I. H. and Parkins, R. N., *British Corrosion Journal*, Vol. 19, No. 1, 1984.
- [33] Kawashima, A. A., Hashimoto, K., and Shimodaira, S., *Corrosion*, Vol. 32, No. 8, 1976, p. 321.
- [34] Dull, D. L. and Raymond L., *Metallurgical Transactions*, Vol. 4, 1973, p. 1635.
- [35] Graville, B. A., et al., *British Welding Journal*, 1967, p. 33.
- [36] Payer, J. E., Berry, W. E., and Boyd, W. K. in *Stress Corrosion—New Approaches*, ASTM STP 610, 1976, p. 82.
- [37] Vermilyea, D. A. in "Stress Corrosion Cracking of Iron Base Alloys," R. W. Staehle, Ed., National Association of Corrosion Engineers, Houston, TX, 1973, p. 208.
- [38] Scully, J. C., *Corrosion Science*, Vol. 15, 1975, p. 207.
- [39] Vermilyea, D. A. and Diegle, R. B., *Corrosion*, Vol. 32, 1976, p. 26.
- [40] Subramanyan, P. K. in *Comprehensive Treatise of Electrochemistry*, Bockris, Conway, Yeager and White, Eds., Plenum Press, New York, 1981, pp. 411-462.
- [41] Smith, J. A., Peterson, M. H., and Brown, B. F. in *ASM Source Book on Hydrogen Damage*, C. P. Beachem, Ed., American Society for Metals, Metals Park, OH, 1977, p. 255.
- [42] Gileadi, E., Kirova-Eisner, and Penciner, E., Jr. in *Interfacial Electrochemistry: An Experimental Approach*, Addison-Wesley Publishing Co., Reading, MA, 1975, p. 484.
- [43] Breger, V. and Gileadi, E., *Electrochimica Acta*, Vol. 16, 1971, p. 177.
- [44] Devanathan, M. A. V., Bockris, J. O'M., and Mehl, W., *Journal of Electroanalytical Chemistry*, Vol. 1, 1960, p. 143.
- [45] Beck, W., Bockris, J. O'M., McBreen, J., and Nanis, L. in *ASM Source Book on Hydrogen Damage*, C. B. Beachem, Ed., American Society for Metals, Metals Park, OH, 1977.
- [46] Gerberich, W. W. in *Hydrogen in Metals*, I. M. Bernstein, A. W. Thompson, Eds., American Society for Metals, Metals Park, OH, 1974, p. 115.
- [47] Kummich, A. J. and Johnson, H. H., *Acta Metallurgica*, Vol. 28, 1980, p. 33.
- [48] Johnson, H. H., Quick, N., and Kummich, A. J., *Scripta Metallurgica*, Vol. 13, 1979, p. 67.
- [49] Kortovich, C. S. in "Inhibition of Hydrogen Embrittlement of High Strength Steel," Technical Report No. ER-7814-2, prepared by TRWI Equipment Materials Technology for the Office of Naval Research, Washington, DC, Contract No. N00014-74-0365, February 1977.

Hydrogen Transport, Microstructure, and Hydrogen-Induced Cracking in Austenitic Stainless Steels

REFERENCE: Perng, T. and Altstetter, C., "Hydrogen Transport, Microstructure, and Hydrogen-Induced Cracking in Austenitic Stainless Steels," *Hydrogen Embrittlement: Prevention and Control*, ASTM STP 962, L. Raymond, Ed., American Society for Testing and Materials, Philadelphia, 1988, pp. 403-416.

ABSTRACT: Susceptibility to embrittlement in hydrogen gas was investigated for three types of stainless steel alloys having different microstructures. Both slow strain rate notched tension tests and constant load crack propagation tests were used to evaluate susceptibility at 0 to 200°C in hydrogen gas at 108 kPa (1 psig). The alloys were austenitic, ferritic, or austenite/ferrite mixtures produced by different thermomechanical treatments. The onset of embrittlement and crack propagation rates could be correlated with the microstructure of the alloys. Of particular importance to the understanding of the results are the marked hydrogen transport and solubility differences between the austenite and ferrite phases. The stress-induced transformation of austenite to body-centered cubic (bcc) martensite has particular relevance in rationalizing the behavior of various austenitic stainless steel alloys.

KEY WORDS: hydrogen embrittlement, austenitic, ferritic, duplex stainless steels, slow crack growth, stress-induced martensite, microstructure, hydrogen transport

Recently, hydrogen embrittlement in austenitic stainless steel has been extensively studied [1,2]. Austenitic stainless steel is, in general, less susceptible to hydrogen embrittlement than ferritic steels, presumably due to the slower hydrogen transport rate and higher solubility in austenite than in ferrite. Furthermore, stable austenitic steels such as AISI 310 are more resistant to hydrogen embrittlement than unstable ones such as AISI 301 and 304. This difference has often been ascribed to the stress-induced α' martensite in unstable alloys. Previous studies have shown that when notched unstable austenitic stainless steel alloys were tested in hydrogen gas or after cathodic charging, slow crack growth (SCG) under constant load was observed, and α' martensite was associated with the fracture path [3-7]. No SCG was observed for AISI 310.

Various theories have been proposed to explain the kinetics of hydrogen-induced SCG behavior in steels and other structural materials. It is frequently postulated that in order for a crack to initiate and propagate, hydrogen has to be transported to and accumulated in an "embrittlement region" at or near the crack tip. The rate of crack advance is controlled by the rate of supply and accumulation of hydrogen in that region [8-14]. Extrapolated permeability of hydrogen in annealed austenitic stainless steel at room temperature is 2 to 3 orders of magnitude less than that in a highly alloyed ferritic stainless steel [15]. Therefore, stress-induced α' in unstable austenitic stainless steel may act as a suitable medium for entry into and transport of hydrogen within the matrix. In addition, it may be inherently more susceptible to hydrogen-induced cracking.

¹Department of Metallurgy and Mining Engineering, University of Illinois at Urbana-Champaign, Urbana, IL 61801.

This paper discusses the correlation of hydrogen transport and microstructure with the kinetics of hydrogen-induced cracking in a number of stainless steels. The kinetics of SCG for annealed AISI 310 is compared with that for ferritic and duplex stainless steels. Specimens of AISI 301 which has been cold worked both above and below the M_D temperature² and room temperature-deformed specimens annealed just below the A_s temperature² are also compared. The mechanism of crack advance is also a very important consideration, but it will not be considered in this paper.

Experimental Studies

Three types of stainless steels were studied. These included austenitic (AISI 301), ferritic (AL 29-4-2³), and duplex (Ferrallium Alloy 255³). The latter alloy was tested with the loading axis at either 90 or 0° to the rolling direction, designated transverse or longitudinal tests, respectively. The chemical compositions of these alloys are shown in Table 1. Sheet specimens of 301 of dimensions 0.15 by 2.54 by 15.0 cm were annealed in vacuum for 1 h at 1100°C and then rapidly quenched in water. Specimens were then electropolished in a chilled (~2°C) solution of one part of perchloric acid and four parts of glacial acetic acid. Annealed sheet specimens of dimensions 0.15 by 2.54 by 20.0 cm for AL 29-4-2 and 0.20 by 2.60 by 20.0 cm for Ferrallium Alloy 255 were used in as-received condition. Some deformed 301 specimens, designated as 301C, 301H, and 301A, were also prepared. The annealed and electropolished sheet specimens were rolled either at room temperature or at 110°C (> M_D) with a 30% reduction in thickness. The room temperature deformed specimens (301C) contained approximately 57% α' , whereas less than 0.5% α' was detected for the 110°C deformed ones (301H). The α' was detected magnetically using a probe which registered the average amount in a volume of several cubic millimetres. Some 301C specimens were then annealed in vacuum at 450°C for 24 h. This annealing relieved ~40% peak stress but enhanced the α' content to ~65% [16]. These specimens were designated as 301A. Prior to testing, a saw cut, ~7 mm deep with a notch root radius of ~0.125 mm, was made in the middle of one edge of each specimen.

To investigate hydrogen embrittlement susceptibility, notched specimens were tension tested at room temperature in air and in 108 kPa (1 psig) of hydrogen gas using an Instron machine at a crosshead speed of 8.3×10^{-5} cm/s. To study the hydrogen-induced cracking kinetics, the notched specimens were fatigue precracked for an additional 1 mm to get a sharp crack tip and were then subjected to sustained load tests in hydrogen gas. For all specimens tested in hydrogen, the notched region was enclosed in a glass chamber (~7 cm high) and sealed with silicone rubber. The chamber was first evacuated to $\sim 5.0 \times 10^{-3}$ torr (0.7 Pa), then repeatedly purged with hydrogen and reevacuated at least ten times, and finally tested at 108 kPa of hydrogen. Ultrahigh purity hydrogen with $H_2 > 99.999\%$, $H_2O < 2$ ppm, and $O_2 < 1$ ppm was used. For all tests, the "gage length" of each specimen between the grips was 10 cm. The crack growth was followed microscopically, with a resolution of 2.5×10^{-3} cm.

The SCG behavior is presented as a plot of $\log da/dt$ versus K . The stress intensity K was calculated using the equation

$$K = Y \sigma \sqrt{a} \quad (1)$$

where Y is a geometric factor and is obtained from the following relation [17]

²The M_D temperature is the highest temperature at which martensite forms during deformation. The A_s temperature is the temperature at which martensite reverts to austenite upon heating.

³AL 29-4-2 and Ferrallium Alloy 255 are products of the Allegheny Ludlum Steel Corp. and the Cabot Corp., respectively.

TABLE 1—Chemical compositions (wt%) of the alloys used for SCG tests.

Material	C	Mn	P	S	Si	Cr	Ni	Mo	N	Cu	O	H
AISI 301	0.082	1.29	0.023	0.012	0.49	17.1	7.17	...	0.056	0.20	0.0079	1.1×10^{-6}
AL 29-4-2	0.0029	0.10	0.01	0.009	0.10	29.5	2.23	3.93	0.012
Ferrallium 255	0.03	0.61	0.021	0.003	0.55	25.6	5.59	3.01	0.16	1.63

$$Y = 1.99 - 0.41\left(\frac{a}{w}\right) + 18.70\left(\frac{a}{w}\right)^2 - 38.48\left(\frac{a}{w}\right)^3 + 53.85\left(\frac{a}{w}\right)^4 \quad (2)$$

where

w = the width of the specimen, and
 a = total crack length.

Results

The results of slow extension rate tension tests in air and 108 kPa of hydrogen for these alloys at room temperature are given in Table 2. They all exhibited some reduction in both notch tensile strength and ductility (expressed as percent elongation averaged over a length of 10 cm) in hydrogen. Deformation in AISI 301 greatly increased the strength but also reduced the ductility. The hydrogen embrittlement susceptibility for the deformed 301 was, however, less severe than the annealed one. The relative reduction in strength was about the same or slightly lower, while the reduction in ductility was substantially lower.

Sustained-load tests in hydrogen at 108 kPa (1 psig) at 0 to 125°C were performed to study the SCG behavior of AISI 301. While the stressing conditions in the sustained-load tests are presented in terms of stress intensity, the specimen geometry (1.5 mm thick) was such that plane-strain conditions were not expected. Only slight thinning was observed at lower temperature (0 to 50°C). The degree of thinning increased with increasing temperature (75 to 125°C). The SCG velocity as a function of stress intensity is shown in Fig. 1 for 0 to 75°C and Fig. 2 for 100 and 125°C. The curves in Fig. 1 followed the typical pattern of three-stage environment-assisted cracking. Rapid rupture by microvoid coalescence (MVC) occurred following the last point on each curve. This value of K is taken as the critical stress intensity, K_c , for crack instability. SCG appeared to gradually disappear between 75 to 100°C. When tested at 100°C (Fig. 2), the crack started to propagate at $K > K_{th}$. The SCG, however, was found to slow down and stop after a period of time. A slight increase in load was necessary to restart the crack. After a short increment of accelerating SCG, rapid fracture took place. A similar pattern repeated at 125°C, with the average crack velocity lower than at 100°C at the same applied stress intensity. At both 100 and 125°C considerable thinning of the specimen took place, so that the calculation of K from Eqs 1 and 2 is in error. That expression assumes uniform thickness.

The SCG behavior of AL 29-4-2 and Ferralium 255 (T and L) was also studied in the same temperature range. The complete results are presented elsewhere [18]. Only those for room

TABLE 2—Mechanical properties of alloys tested at slow strain rate in air and 108 kPa of hydrogen gas at 25°C.²

Material	Notch Tensile Strength			Ductility		
	Air, MPa	H ₂ , MPa	Loss in H ₂ , %	Air, %	H ₂ , %	Loss in H ₂ , %
AISI 301	379	289	24	7.4	2.3	69
301H	757	624	18	3.4	2.3	33
301C	979	732	25	2.9	2.2	23
301 A	1016	845	17	2.8	2.1	26
AL 29-4-2	604	502	17	5.8	2.9	50
Ferralium 255 L	795	606	24	6.0	4.0	34
Ferralium 255 T	769	614	20	6.3	4.1	35

^aCrosshead speed of 8.3×10^{-5} cm/s.

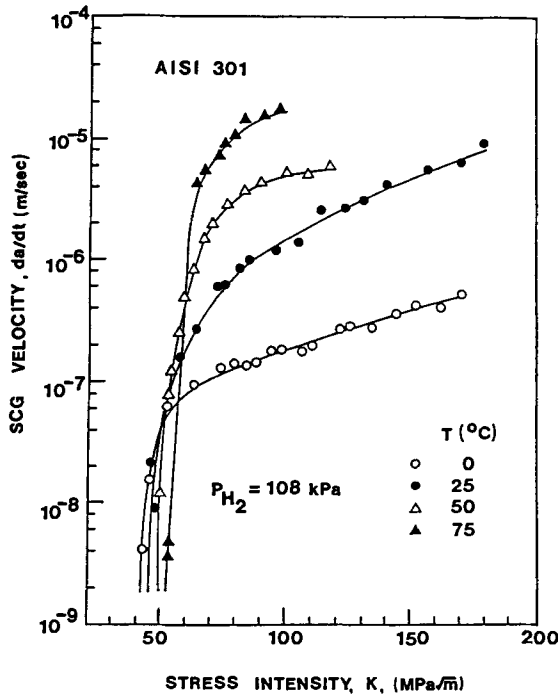


FIG. 1—Slow crack growth curve of AISI 301 tested in hydrogen gas at 108 kPa for 0 to 75°C.

temperature are shown in Fig. 3, where the SCG curve for AISI 301 is also included for comparison. It was found that AISI 301 exhibited the greatest hydrogen embrittlement and the duplex Ferralium 255 the least. The relative order of Stage II crack velocity was $301 > 255 \text{ T} \geq 29.4-2 > 255 \text{ L}$.

Figure 4 shows the SCG curves for the deformed 301 alloys tested at 25°C. With the same degrees of deformation, 301H had the highest Stage II cracking velocity and the lowest K_{th} , whereas the cold-worked and stress-relieved 301A had the highest K_{th} and the lowest cracking rate.

Discussion

When a metal is exposed to gaseous hydrogen, it is assumed that in order for SCG to occur, hydrogen has to dissociate and enter the matrix as individual atoms, then diffuse to and accumulate in the embrittlement region at the crack tip. SCG then occurs under the combined effect of stress and hydrogen on the metal. The crack propagation velocity is controlled by the rate of accumulation of hydrogen in the embrittlement region, which is determined by the slowest step in a series of processes. The cracking velocity of each alloy tested in this work can be rationalized in terms of the hydrogen transport parameters. For a simple estimate, the Stage II crack growth velocity is given as

$$\left(\frac{da}{dt} \right)_{II} \sim \frac{\delta_I}{t_c} \quad (3)$$

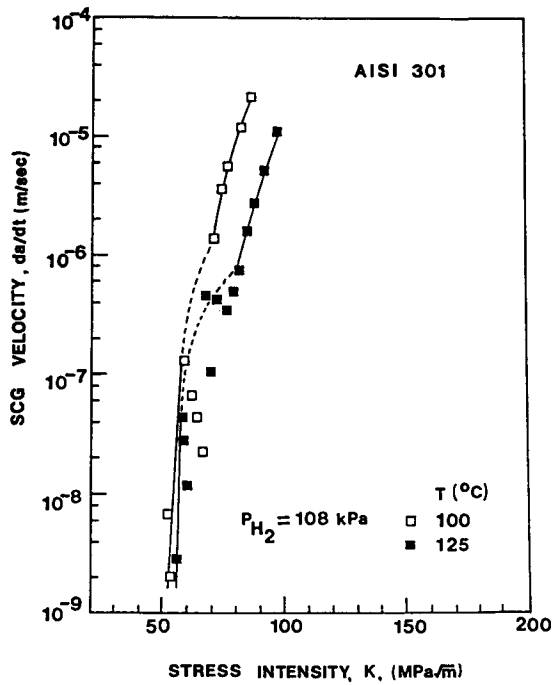


FIG. 2—Slow crack growth curve of AISI 301 tested in hydrogen gas at 108 kPa for 100 and 125°C. Dashed line indicates stress intensity range in which stress was incremented to maintain crack propagation.

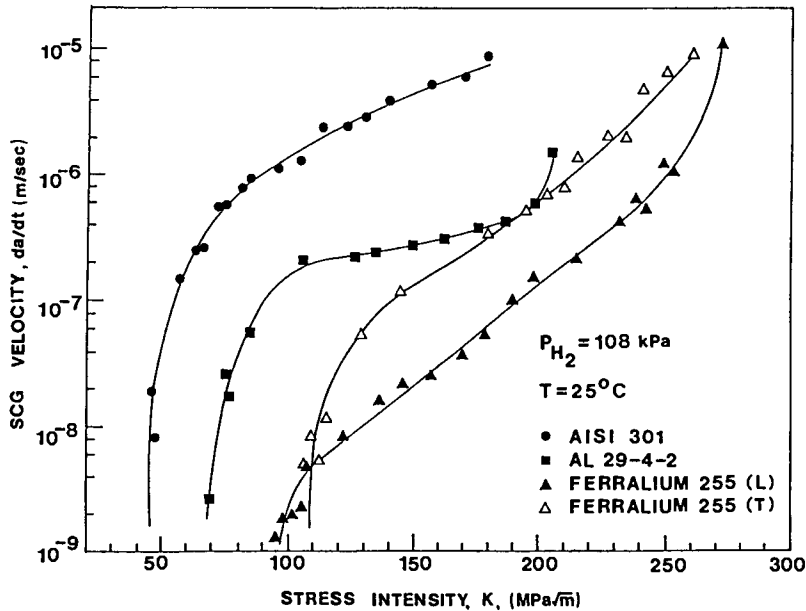


FIG. 3—Comparison of the SCG behavior for four stainless steels tested in hydrogen gas at 108 kPa and 25°C.

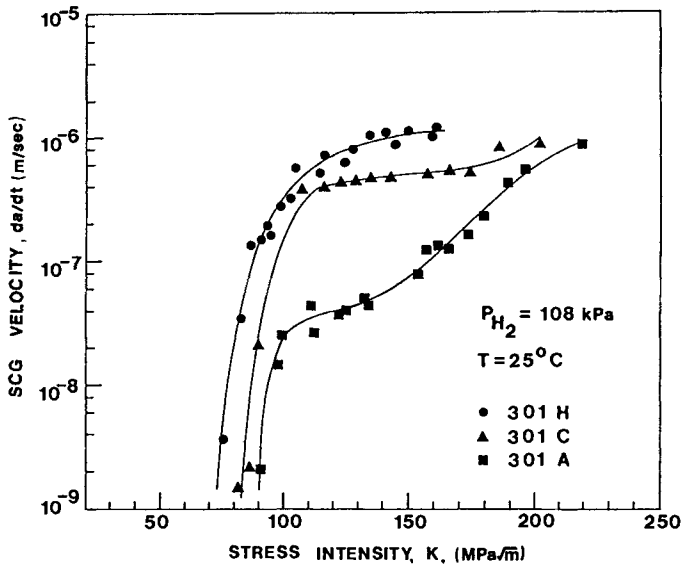


FIG. 4—Comparison of the SCG behavior for three 30% deformed AISI 301 alloys tested in hydrogen gas at 108 kPa and 25°C.

where t_c is the time to build up the critical hydrogen concentration C_c , and δ_t is the distance from the crack tip to the point of maximum triaxiality, which can be estimated as [19]

$$\delta_t = \frac{K^2}{2E\sigma_y} \quad (4)$$

The time t_c may be roughly estimated from the hydrogen diffusivity, D

$$t_c = \frac{\delta_t^2}{4D} \quad (5)$$

Equations 3 to 5 lead to

$$\left(\frac{da}{dt} \right)_{II} \sim \frac{4D}{\delta_t} = \frac{8DE\sigma_y}{K^2} \quad (6)$$

The hydrogen diffusivity in each alloy was obtained in a previous study on the same alloys [15]. Figures 5 and 6 show the effective hydrogen diffusivity and permeability in annealed and deformed AISI 301 and annealed AL 29-4-2, respectively. Deformation in AISI 301 resulted in various amounts of α' martensite, which enhanced the effective hydrogen diffusivity and permeability. The hydrogen diffusivities for the annealed 301 and AL 29-4-2 are used to approximate those for the austenite and ferrite, respectively, in Ferralium 255. If the extrapolated diffusivities to room temperature from Fig. 5 are substituted in Eq 6, the calculated Stage II crack velocity for AL 29-4-2 and Ferralium 255 (T and L) are found to be approximately 10^3 higher than the observed values (Fig. 3). This means that diffusion is sufficiently rapid to keep up with the observed crack advance. For AISI 301, however, the calculated values based on the hydrogen diffusivity in pure face-centered cubic (fcc) phase are about 10^2 below the observed ones for

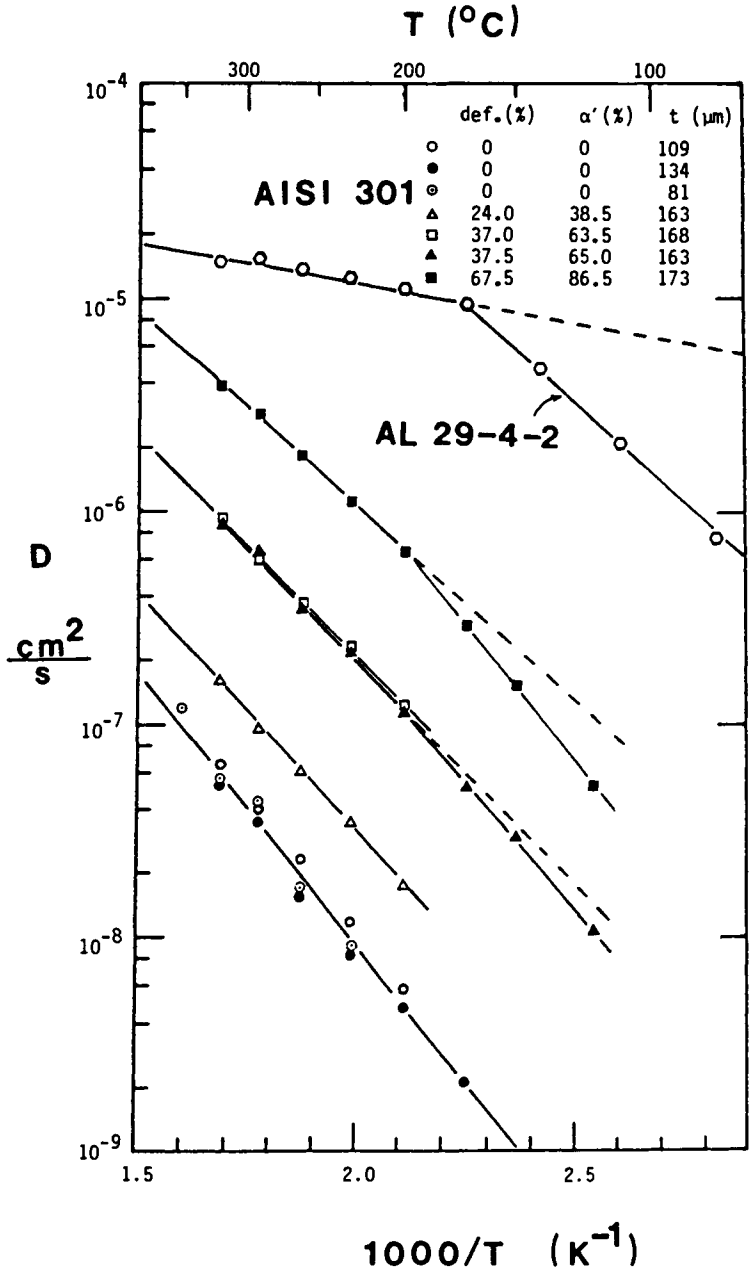


FIG. 5—Hydrogen diffusivity in annealed and deformed AISI 301 and in annealed AL 29-4-2 [15].

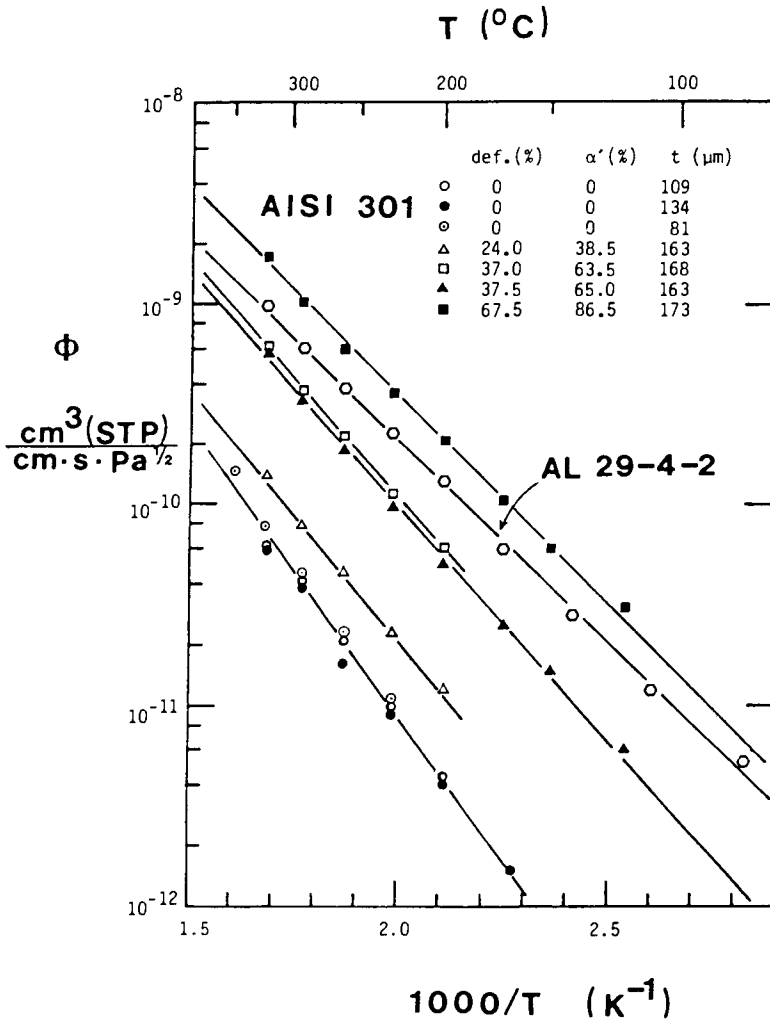


FIG. 6—Hydrogen permeability in annealed and deformed AISI 301 and in annealed AL 29-4-2 [15].

$T = 0$ to 75°C . When the effective hydrogen diffusivity for AL 29-4-2 is used to approximate that in the α' induced in AISI 301, the calculated values become $\sim 10^2$ higher than the experimental ones. This explains why AISI 301 does not show SCG, but 301 does. The stress-induced transformation of γ to α' is critical to the SCG process in 301. The higher calculated values of $(da/dt)_I$ arose primarily from Eq 5, where the value of t_c was the lower limit for a composition change. From diffusion theory, this equation only accounts for the time required for hydrogen to diffuse to the nucleation site. The time it takes to accumulate a critical concentration was not estimated here. This calculation, however, demonstrates that the hydrogen diffusion rate was high enough to allow hydrogen to diffuse to the crack tip, neglecting for the moment the additional amount of time to build up to a critical concentration.

To identify the rate-controlling process of the thermally activated SCG, the activation energy for SCG is often calculated and compared with those for hydrogen transport, adsorption, or other hydrogen-metal reactions [20, 21]. A direct comparison of these values in this work, how-

ever, may not be appropriate. For instance, Fig. 7 shows two sets of data for AISI 301 for $K = 80$ and $100 \text{ MPa} \cdot \text{m}^{1/2}$. Three regions of different crack rate were observed, in common with that reported for high-strength steels [20,21]. For K -values from 70 to $110 \text{ MPa} \cdot \text{m}^{1/2}$, the activation energy in the lower temperature region ($T < 75^\circ\text{C}$) ranged from 43.6 to 48.2 kJ/mol , with an average of 47. This value is found to be very close to the activation energy either for hydrogen diffusion or for hydrogen permeation in the deformed AISI 301 with 65 to 86.5% α' (Figs. 5 and 6) and far higher than the energy of migration of a hydrogen adatom on iron or nickel [20,22]. A more strict treatment has to consider the stress and stress gradient, the plasticity, the dislocation sweeping of hydrogen, and the α' content (which decreases when deformation temperature increases) ahead of the crack tip during the crack propagation. Because of these unknown but compensating factors involved in the SCG, it is difficult to use activation energies to establish whether the cracking is controlled by diffusion or permeation.

The previous calculations for hydrogen diffusion illustrated that hydrogen diffusion in fcc phase could not account for the observed SCG velocity in AISI 301. In this alloy, the fracture surface has been reported to be covered with α' to a depth of $\sim 1 \mu\text{m}$ [6, 7]. The content of α' further away from the crack surface decreased continuously. It is expected that the hydrogen diffusion path during the crack advance was confined to the primarily α' area. From Fig. 6, it was found that the deformed AISI 301 with 86.5% α' had higher hydrogen permeability than AL 29-4-2. Thus, a higher rate of accumulation of hydrogen in AISI 301 than in AL 29-4-2 would be expected if the diffusion path consisted of primarily α' phase and some undeformed γ . On the other hand, the effective hydrogen diffusivity in deformed AISI 301 was consistently less than that in AL 29-4-2 by a factor of ~ 50 . If the crack velocity were controlled by hydrogen diffusion, a higher SCG velocity in AL 29-4-2 would be expected. Experimental results showed

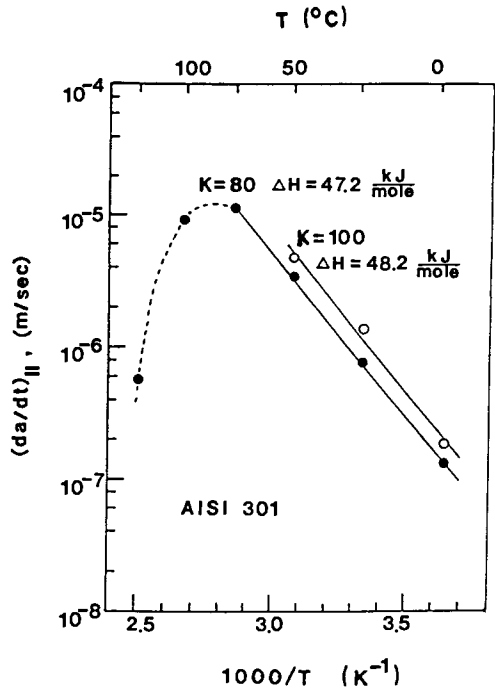


FIG. 7—Effect of temperature on Stage II cracking rate for AISI 301 tested in hydrogen gas at 108 kPa.

that the average SCG velocity in AISI 301 was higher than in AL 29-4-2 under the same test condition. This result suggests that hydrogen permeability rather than diffusivity controls the gaseous hydrogen-induced SCG, and the relatively high SCG rate for AISI 301 was controlled by the stress-induced α' martensite around the crack.

Three annealed alloys with four different microstructures have been studied. Figure 3 compares the SCG curves for these alloys tested at 25°C. The relative order of Stage II crack velocity was 301 > 255 T \geq AL 29-4-2 > 255 L. It is believed that the microstructure played an important role in determining this relative order of crack velocity in these alloys. In following paragraphs, the different SCG behavior at room temperature in these alloys will be discussed based upon the concept that the SCG velocity is controlled by the rate of accumulation of hydrogen in the embrittlement region. Schematic diagrams of microstructure for each alloy are shown in Fig. 8. For AISI 301, the stress-induced α' martensite is distributed along the crack surface and at the crack tip. The volume away from the crack remained in the fcc structure. Hydrogen atoms can easily get into the embrittlement region in front of the crack tip through the primarily α' phase. Once hydrogen has diffused to this region, it is difficult for it to move away from that region because hydrogen transport in fcc is slower by two orders of magnitude (Fig. 6). Hence a critical hydrogen concentration in the embrittlement region is built up relatively rapidly. Furthermore, since the γ phase dissolves more hydrogen than the α' phase, the hydrogen which has been dissolved in the γ phase near the crack path could possibly be incorporated into the α' region, because the γ phase directly ahead of the crack tip will later be transformed to α' phase and become part of the crack path. In these γ grains, the already dissolved hydrogen provides the higher initial concentration required for the next crack advance. The effect of γ in acting as a hydrogen reservoir might be important in helping to build up the hydrogen content for SCG.

In the case of AL 29-4-2, the matrix is α phase, hydrogen permeates rapidly into the embrittlement region, but there is also an appreciable flux into the surrounding volume. The rate of

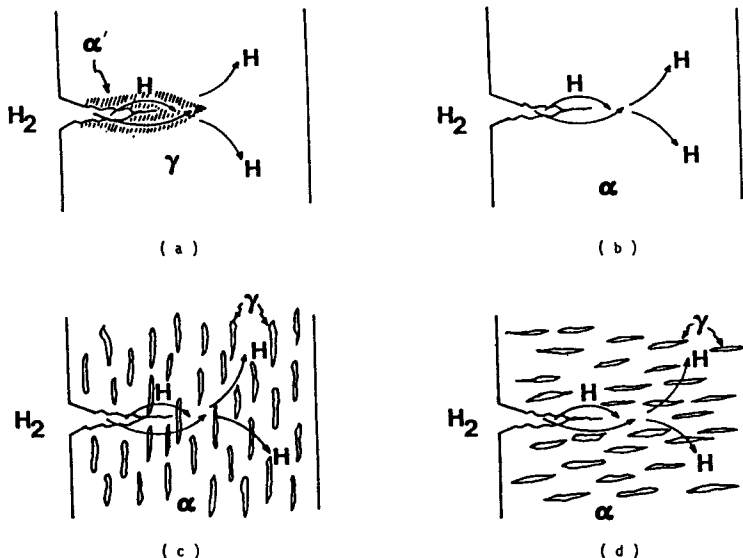


FIG. 8—Schematic microstructure and hydrogen transport path around the crack tip: (a) AISI 301, (b) AL 29-4-2, (c) Ferralium 255L, and (d) Ferralium 255T.

accumulation of hydrogen in AL 29-4-2 is expected to be slower than that in AISI 301. For this reason, a lower SCG velocity in AL 29-4-2 would be expected, and indeed this was the case.

The effect of different orientations of γ phase in the duplex Ferralium Alloy 255 on the rate of accumulation of hydrogen is even more striking. From Fig. 8(c), it can be seen that the γ grains are uniformly dispersed and elongated along the stress axis in Ferralium 255L. Some γ grains near or in front of the crack tip are perpendicular to the hydrogen flux to the embrittlement region, and hydrogen has to penetrate through the γ grains. Since the γ phase acts as a low permeability barrier for hydrogen, the rate of supply of hydrogen to the embrittlement region is significantly reduced. Although the γ grains ahead of the embrittlement region also somewhat reduce the escape rate of hydrogen, this effect, however, is less important than that of blocking the entry of hydrogen because the flux of hydrogen away from the crack tip is parallel to the austenite. Comparing the situation in Ferralium 255L with that in AL 29-4-2, one expects that the accumulation rate in 255L would be smaller than in AL 29-4-2, and therefore a smaller SCG velocity should be, and was, observed. For Ferralium 255T, Fig. 8(d), the γ grains are extended in a direction parallel to the crack path and so are parallel to the hydrogen flux to the crack tip. Hydrogen finds a continuous path in the α matrix to get into the embrittlement region. The γ grains ahead of the embrittlement region, however, are expected to limit somewhat the escape of hydrogen. It would be more difficult than in pure α (AL 29-4-2), but easier than in metastable γ (AISI 301) for hydrogen to escape from the embrittlement region. Furthermore, since the γ grains are parallel to the crack path and dissolve more hydrogen, they may act as a second source to supply hydrogen to the α phase along the crack path for SCG. The different behavior of Ferralium 255L and T can be rationalized even more clearly by a quantitative estimation of hydrogen permeation in these two alloys. If one uses the hydrogen permeabilities from AL 29-4-2 and AISI 301 to approximate those of the α and γ phases in Ferralium 255, a calculation for a lamellar composite material shows that parallel to the lamellae the permeability may be up to a factor of 9 larger than perpendicular to the lamellae at 200°C. The ratio depends on the volume fraction of each phase. Applying these calculations to the present case, it can be seen that the rate of entry of hydrogen in 255T (with the orientation of γ parallel to the incoming flux) can be greater than in 255L (series) by a factor of ~ 4 at 200°C. This factor can be even greater at room temperature. The extrapolated values from the high temperature region for 255T and 255L are 3.68×10^{-13} and 1.10×10^{-14} cm³ (STP⁴)/cm · s · Pa^{1/2}, respectively. A factor of 33 is obtained. The ratio in escape rates of hydrogen, on the other hand, would be roughly the reciprocal of the ratio for entry. This implies that it can be ~ 33 times lower in 255T than in 255L. The just-cited calculations assumed a two-dimensional structure of Ferralium 225. Since the γ grains do not extend across the entire thickness, the actual hydrogen permeability difference for these two orientations could be lower. It is obvious, however, that a duplex alloy tested along the transverse orientation is more susceptible to hydrogen damage than along the longitudinal direction. Based upon these arguments, one expects that the accumulation rate of hydrogen in Ferralium 255T would be higher than in both AL 29-4-2 and 255L, but lower than in AISI 301. The SCG velocity observed in this work followed this pattern.

To further elaborate the effect of microstructure on the SCG behavior, the results of the three deformed 301 alloys can be compared. When they were subjected to sustained load in hydrogen, α' martensite was formed at the crack tip in 301H. The average quantity detected by metallographic examination and magnetic measurement seemed to be higher than that in the annealed 301. Further increase of α' content around the crack tip was also observed for 301C and 301A. From Fig. 4, it is found that of these three alloys, 301H had the lowest K_{th} and the highest Stage II cracking velocity. 301A was just the opposite. A previous study showed that for AISI 310, deformation up to 80% did not change the hydrogen permeability in the austenite structure [15]. If this can be applied to the deformed austenite in 301H, it is expected that the just-cited

⁴STP = standard temperature and pressure.

argument for the annealed 301 may be applied to 301H, namely, hydrogen enters 301H rapidly through the stress-induced α' at the crack tip and has difficulty escaping from the stressed region because the surrounding austenite is a barrier for hydrogen transport. The hydrogen permeability in 301H at room temperature, extrapolated from the annealed 301, is $1.1 \times 10^{-15} \text{ cm}^3 (\text{STP})/\text{cm} \cdot \text{s} \cdot \text{Pa}^{1/2}$. For the uniformly deformed 301C with 57% α' , extrapolation from Fig. 6 shows that the permeability at room temperature is approximately $5.0 \times 10^{-14} \text{ cm}^3 (\text{STP})/\text{cm} \cdot \text{s} \cdot \text{Pa}^{1/2}$. As for 301A with 65% α' , the permeability is estimated to be $6.8 \times 10^{-14} \text{ cm}^3 (\text{STP})/\text{cm} \cdot \text{s} \cdot \text{Pa}^{1/2}$. However, the stress relief treatment at 450°C may further enhance the effective permeability. Hydrogen permeation measurements on AL 29-4-2 showed that deformation of 25 to 75% could reduce the hydrogen permeability by a factor of 10 to 20 [18]. This means that the actual hydrogen permeability in 301A would be higher than the just calculated value, $6.8 \times 10^{-14} \text{ cm}^3 (\text{STP})/\text{cm} \cdot \text{s} \cdot \text{Pa}^{1/2}$. It is expected, therefore, that the rate of accumulation of hydrogen in the critical stressed region would be 301H > 301C > 301A. The relative order of SCG velocity for these three alloys, again, followed this pattern. Annealing at 450°C for 301A seemed to substantially reduce the cracking velocity. It is also interesting to note from a practical viewpoint that cold work of AISI 301 not only enhanced the strength but also decreased the hydrogen embrittlement susceptibility.

Conclusions

1. Gaseous hydrogen-induced SCG behavior was investigated for three types of stainless steels. The relative order of cracking velocity at room temperature was 301 > 255T \geq 29-4-2 > 255L. In addition, with the same amount of deformation but different thermal treatment, 301H had the highest cracking rate and 301A the lowest.

2. AISI 301 had the highest SCG velocity among the three alloys. This was ascribed to the fast transport of hydrogen through the primarily stress-induced α' phase around the crack path and low escape rate of hydrogen through the γ phase in the surrounding region.

3. The kinetics of hydrogen-induced SCG in stainless steel can be rationalized in terms of hydrogen transport and microstructure. The microstructure determines the rate of supply and accumulation of hydrogen in the stressed region ahead of the crack tip necessary for crack advance. A higher accumulation rate of hydrogen leads to a higher cracking velocity.

Acknowledgment

This work was supported by the National Science Foundation under Contract NSF-DMR 83-03421.

References

- [1] *Stress Corrosion Cracking and Hydrogen Embrittlement of Iron Base Alloys*, Staehle, R. W. et al., Eds., National Association of Corrosion Engineers, Houston, TX, 1977.
- [2] *Hydrogen Effects in Metals*, Bernstein, I. M. and Thompson, A. W., Eds., TMS-AIME, Warrendale, PA, 1980.
- [3] Eliezer, D., Chakrapani, D. G., Altstetter, C. J., and Pugh, E. N., *Metallurgical Transactions, A*, 1979, Vol. 10A, p. 935.
- [4] Liu, R., Narita, N., Altstetter, C., Birnbaum, H., and Pugh, E. N., *Metallurgical Transactions, A*, 1980, Vol. 11A, p. 1563.
- [5] Narita, N. and Birnbaum, H. K., *Scripta Metallurgica*, 1980, Vol. 14, p. 1355.
- [6] Singh, S. and Altstetter, C., *Metallurgical Transactions, A*, 1982, Vol. 13A, p. 1799.
- [7] Schuster, G. and Altstetter, C., *Metallurgical Transactions, A*, 1983, Vol. 14A, p. 2085.
- [8] Oriani, R. A. and Josephic, P. H., *Acta Metallurgica*, 1974, Vol. 22, p. 1965.
- [9] Oriani, R. A. and Josephic, P. H., *Acta Metallurgica*, 1977, Vol. 25, p. 979.
- [10] Gerberich, W. W., Chen, Y. T., and St. John, C., *Metallurgical Transactions, A*, 1975, Vol. 6A, p. 1485.

- [11] Gerberich, W. W. and Chen, Y. T., *Metallurgical Transactions, A*, 1975, Vol. 6A, p. 271.
- [12] Gerberich, W. W., Garry, J., and Lessar, J. F. in *Effects of Hydrogen on Behavior of Materials*, A. W. Thompson, and I. M. Bernstein, Eds., TMS-AIME, 1976, p. 70.
- [13] van Leeuwen, H. P., *Corrosion*, 1973, Vol. 29, p. 197.
- [14] van Leeuwen, H. P., *Corrosion*, 1975, Vol. 31, p. 154.
- [15] Perng, T.-P. and Altstetter, C. J., *Acta Metallurgica*, 1986, Vol. 34, p. 1771.
- [16] Novak, C. J. in *Handbook of Stainless Steels*, D. Pecker, and I. M. Bernstein, Eds., McGraw-Hill, New York, 1977, p. 4-29.
- [17] Brown, W. F. Jr. and Srawley, J. E., *Plane-Strain Crack Toughness Testing of High-Strength Metallic Materials*, ASTM STP 410, ASTM, Philadelphia, 1966.
- [18] Perng, T.-P. and Altstetter, C. J., *Metallurgical Transactions A*, 1987, Vol. 18A, p. 23.
- [19] Rice, J. R. and Johnson, M. A., *Inelastic Behavior of Solids*, McGraw-Hill, New York, 1970, p. 641.
- [20] Williams, D. and Nelson, H., *Metallurgical Transactions*, 1970, Vol. 1, p. 63.
- [21] Wei, R. P., in *Hydrogen Effects in Metals*, TMS-AIME, Warrendale, PA, 1980, p. 677.
- [22] Oriani, R. A. in *Fundamental Aspects of Stress Corrosion Cracking*, R. W. Staehle, A. J. Forty, and D. Van Rooyen, Eds., National Association of Corrosion Engineers, Houston, TX, 1969, p. 32.

Temperature Dependence of Fatigue Crack Propagation in Niobium-Hydrogen Alloys

REFERENCE: Polvanich, N. and Salama, K., "Temperature Dependence of Fatigue Crack Propagation in Niobium-Hydrogen Alloys," *Hydrogen Embrittlement: Prevention and Control*, ASTM STP 962, L. Raymond, Ed., American Society for Testing and Materials, Philadelphia, 1988, pp. 417-427.

ABSTRACT: The effects of temperature on near-threshold fatigue crack growth rate have been investigated in niobium-hydrogen alloys. Fatigue tests were performed at 273 and 400 K on hydrogen-free specimens as well as on specimens containing hydrogen in solid solution and in the form of hydride. Compact tension specimens were tested using a tension-tension loading cycle at a frequency of 4 Hz and a load ratio of 0.05. At both temperatures, the results show that the threshold stress intensity range ΔK_{th} decreases with the addition of hydrogen and reaches a minimum value at a critical hydrogen concentration. As the hydrogen concentration exceeds the critical concentration, ΔK_{th} increases with the increase of the amount of dissolved hydrogen. The minimum threshold stress intensity range $(\Delta K_{th})_{min}$ also increases linearly with the increase in temperature. Analysis of results suggests that the presence of hydrides cannot be responsible for the embrittlement of niobium with hydrogen, and that some more mobile form of hydrogen clusters is likely to cause the embrittlement.

KEY WORDS: fatigue, crack propagation, temperature, threshold, hydrogen embrittlement, niobium, Group VB

Hydrogen effects on monotonic response of Group VB metals, niobium [1-4], tantalum [5], and vanadium [3,6], have been extensively investigated. These investigations indicate that, when pure, this particular group of metals has appreciable ductility over a wide range of temperature down to that of liquid nitrogen [7]. When hydrogen is dissolved, however, the mechanical properties of these metals are greatly affected. The ductility decreases sharply with decreasing temperature, resulting in an increase of the ductile-brittle transition temperature and embrittlement.

While these effects have been investigated extensively, little has been done to study the influence of hydrogen on fatigue crack propagation in Group VB metals. Wilcox [8] showed that hydrogen in solution and in the form of hydride significantly reduced the fatigue life of tantalum. He also concluded that hydrogen embrittlement was associated with the increased ease of both crack initiation and propagation. In contrast, Lee and Stoloff [9] reported significant improvements in high-cycle, tension-compression fatigue life when hydrogen was present in vanadium as a hydride. This work was further extended by Chung and Stoloff [10] to study the effects of hydrogen on fatigue crack initiation and the rate of crack propagation in vanadium-hydrogen alloys. The results were found to satisfy the Paris-Erdogan equation. Crack growth

¹Graduate student and professor of materials engineering, respectively, Mechanical Engineering Department, University of Houston, Houston, TX 77004.

rates were lowest in pure vanadium and dilute vanadium-hydrogen alloys and were not sensitive to the volume fraction of hydride in more concentrated alloys. No stress-induced hydrides were observed in vanadium-hydrogen (V-H) solid solution alloys. Chung and Stoloff [11] also studied the influence of hydrogen on the fatigue behavior of niobium and found again that hydrogen markedly improved the fatigue life in high-frequency stress control tests, while low-frequency strain control conditions resulted in decreased fatigue life with increasing hydrogen content. Crack initiation was found to occupy most of the fatigue life of hydrogenated niobium (Nb) and to a lesser extent unalloyed Nb. Crack growth rates are significantly greater when hydrogen is present.

At present, a limited number of researchers have concentrated on the effect of temperature on fatigue crack propagation in Group VB metals. For most materials, they find that fracture toughness decreases markedly with decreasing temperature [12]. In their study of the effect of temperature on fatigue crack growth rate in forged Ni-Mo-V steel, Clark and Trout [13] found that the crack growth rate for a given stress intensity factor decreases as the temperature decreases. Similarly, Rolfe and Munse [14] found that the fatigue crack growth rate of mild steel decreases as the test temperature decreases from 298 to 233 K.

While the general features of the embrittlement of Group VB metals by hydrogen are in relative agreement, no general understanding of the mechanisms involved has been established [15]. Several mechanisms have been considered as possible causes for hydrogen embrittlement in this group of metals. The first, namely hydrogen decohesion, was originally proposed by Troiano [16] for the embrittlement of high-strength steels. This concept was later reformed more explicitly in terms of fracture mechanics by several authors [17, 18], who demonstrated that the pressure field around a crack tip could account for long-range diffusivity of an interstitial such as hydrogen. More recent investigations [19] have added several new dimensions to this concept, where the stress intensity could be related to hydrogen concentration at the crack tip and also to material properties such as the monotonic yield strength.

The second mechanism deals with the other extreme, where a phase change at the crack tip occurs, and the metal hydride is formed. Group VB metals form metal hydrides at relatively low hydrogen concentrations [20], and these hydrides can also be stress induced at temperatures above those of stress-free transition. Westlake [21] has argued that the external stress-free solvus is not an indication of when the hydride phase is formed in a region of triaxial tension at the crack tip.

Earlier investigations on tantalum and vanadium [6] as well as on niobium and vanadium [3], however, attributed the hydrogen embrittlement in Group VB to two mechanisms. One is based on decohesion resulting from mobile hydrogen in solution or as clusters. This mechanism is responsible for the onset of embrittlement and the subsequent drop in ductility. At temperatures below those of equilibrium phase transition, the second mechanism manifests itself by the presence of the hydride phase that produces the loss of ductility. The presence of two mechanisms responsible for hydrogen embrittlement in Group VB has been also proposed by Farahani et al. [1] from their study on single crystal and polycrystalline niobium. They found that in Nb one mechanism is operative at the onset of embrittlement and involves the interaction between dislocations and hydrogen. The second mechanism has similar effects on both single crystals and polycrystals and is associated with the precipitation of the hydride phase. This was also confirmed by Fariabi et al. [22] from their studies on the effects of hydrogen on near threshold crack propagation in niobium.

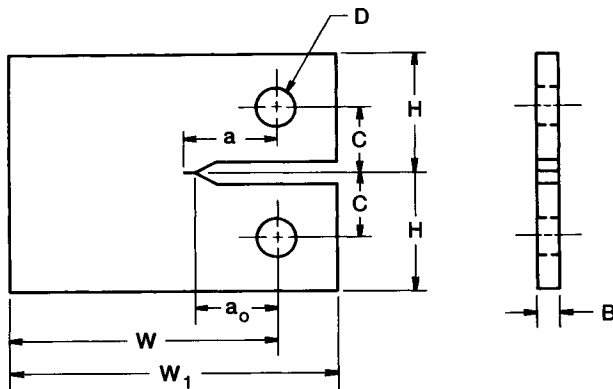
In this paper, the effects of hydrogen in solution and as hydrides on near threshold fatigue crack growth have been investigated in niobium at 273 and 400 K. At both temperatures, the results show that the threshold stress intensity range decreases with the addition of hydrogen and reaches a minimum at a critical hydrogen concentration where maximum embrittlement occurs. This critical hydrogen concentration increases as the temperature is decreased. Analysis of the results suggests that the presence of hydride cannot be responsible for the embrittlement of niobium, and a more mobile form of hydrogen cluster is likely to cause embrittlement.

Experimental

Specimens used in this investigation were made of pure niobium (99.85%) furnished by Tele-dyne Wah Chang Corp. in Albany, Oregon in the form of a sheet 50 cm long, 40 cm wide, and 1 mm thick. Typical composition of the niobium sheet (as received) is given in Table 1. Compact tension specimens were machined to the dimensions shown in Fig. 1, which satisfy plane stress conditions. Thus, no effect of crack curvature need be taken into consideration. Specimens were etched chemically and afterward were cleaned with benzene and acetone. They were then annealed in a vacuum of 10^{-11} MPa for 5 h at 1273 K and furnace cooled in vacuum. Average grain size after annealing was approximately 15 μm . Hydrogen was introduced into the specimens by thermal equilibrium using a modified type of Sievert's apparatus. An estimate of the amount of hydrogen dissolved in each specimen was determined using a calibrated microbalance. The exact amount, however, was determined after the fatigue test was performed using a modified Leco analyzing unit, along with standard samples supplied by the National Bureau of Standards. Alloy compositions of specimens and their designated numbers are listed in Table 2.

TABLE 1—Typical composition of niobium sheet
as received.

Element	Amount, ppm weight
C	<30
O	50 to 90
N	16 to 30
Ta	1080 to 1100
W	24 to 30
Zr	<100
Nb	Balance



$$W_1 = 6.78 \text{ cm.}, W = 5.46 \text{ cm.}, a_0 = 2.21 \text{ cm.}$$

$$H = 3.24 \text{ cm.}, C = 0.95 \text{ cm.}, D = 0.64 \text{ cm.}$$

$$B = 0.10 \text{ cm.}$$

FIG. 1—Compact tension (CT) specimen for fatigue crack growth experiments.

TABLE 2—*Hydrogen content in niobium-hydrogen alloys in ppm weight.*

273 K	400 K
0	0
13	60
103	86
213	296
361	445
508	742
787	1181
1108	

Fatigue tests were performed in tension-tension loading in a closed-loop electrohydraulic machine using a sinusoidal loading cycle of frequency 4 Hz. In these tests, the specimen was mounted in the machine with two Teflon side plates to prevent out-of-plane displacements at the crack tip. The tests were performed at a load ratio R (equals minimum load divided by maximum load) of approximately 0.05 and at test temperatures of 273 and 400 K. A temperature control system with an accuracy of ± 1 K was used to control and measure the temperature of the specimen. Tests were usually terminated when the crack length was about 60% of the specimen width. The stress intensity range ΔK was determined using the expression

$$\Delta K = \frac{\Delta P}{bW^{1/2}} f(a/W) \quad (1)$$

where

ΔP = the load range,

b and W = the thickness and the width of the specimen, respectively, and

$f(a/W)$ = the compliance function, given by

$$f(a/W) = \frac{(2 + a/W)}{(1 - a/W)^{3/2}} \times \left[0.866 + 4.64 \frac{a}{W} - 13.32 \left(\frac{a}{W} \right)^2 + 14.72 \left(\frac{a}{W} \right)^3 - 5.62 \left(\frac{a}{W} \right)^4 \right] \quad (2)$$

Crack extension was determined by measuring changes in the electrical potential at two points across the crack where a constant alternate current was applied. This is based on the principle that electrical resistance in specimens increases with crack extension. A schematic diagram for the a-c potential difference system used in this work is illustrated in Fig. 2. The system consists of a lock-in amplifier, a bipolar operational power supply (BOP), a strip chart recorder, and a resistance circuit box. The resistance box was designed to supply, in conjunction with BOP, a constant current (I_o) of approximately 8 A to the specimen. Initially, a calibration between the potential difference across the crack and the actual crack extension was made using a traveling microscope to measure the actual crack length. The change in electrical potential was recorded on the strip chart recorder that allowed continuous monitoring of the crack growth.

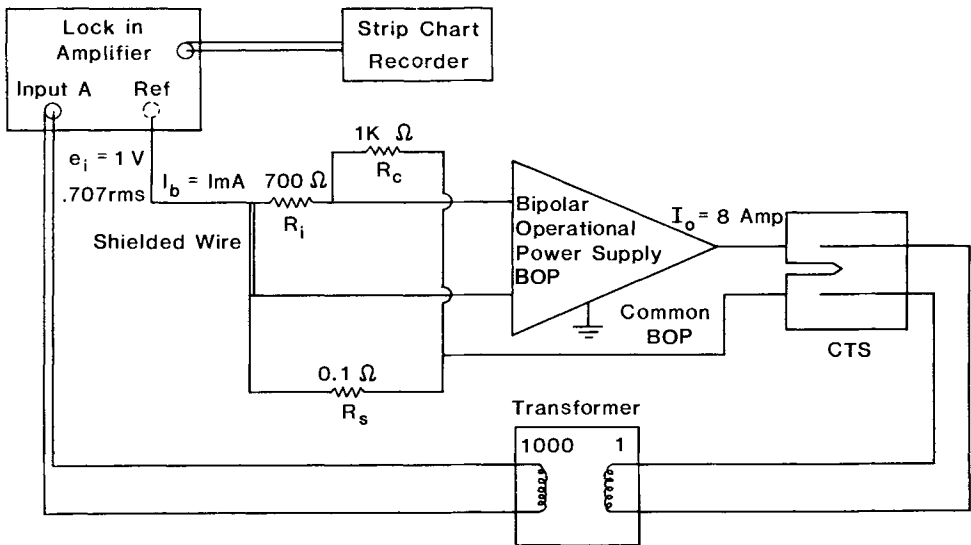


FIG. 2—Schematic for a-c potential difference system.

Results

Figure 3 shows the crack growth rate da/dN as a function of stress intensity range ΔK for all specimens tested in this investigation at 273 K. The crack growth rate da/dN was calculated using the increase in the crack length during the number of cycles N between successive crack tip readings. Results obtained at $T = 400$ K are shown in Fig. 4. The majority of the curves in both figures represents the crack growth rates in Stages I and II. From both Figs. 3 and 4, it can be seen that, at low growth rates (near threshold), there is a strong influence of hydrogen on ΔK_{th} . This region is followed by Region II where da/dN linearly increases with ΔK , and the slope of da/dN versus ΔK does not change much with hydrogen.

The near threshold stress intensity range, ΔK_{th} , as a function of hydrogen concentration for both 273 and 400 K, is plotted in Fig. 5. Also shown in this figure are the results obtained by Fariabi et al. at room temperature [22]. From Fig. 5, one can see that, at constant temperature, ΔK_{th} of hydrogen-free niobium is the greatest, but decreases rather sharply as hydrogen is increased. The decrease of ΔK_{th} with increased hydrogen is almost linear until it reaches a minimum value at a concentration of approximately 600 ppm weight at the test temperature of 273 K, 400 ppm weight at 296 K, and 280 ppm weight at 400 K. Above these hydrogen concentrations, ΔK_{th} increases as the amount of hydrogen dissolved is increased and levels off as the amount of hydrogen is further increased. Also observed in Fig. 5 is that the values of ΔK_{th} at 273 K are less than those obtained at 296 K. The latter values are also less than those at 400 K.

Discussion

From Fig. 5, one can see that for all temperatures ΔK_{th} decreases as the amount of hydrogen in the specimen is increased until ΔK_{th} reaches a minimum value, $(\Delta K_{th})_{min}$. This value represents the maximum embrittlement in the material at a given temperature. The hydrogen concentration at this maximum embrittlement may be considered as the critical concentration of

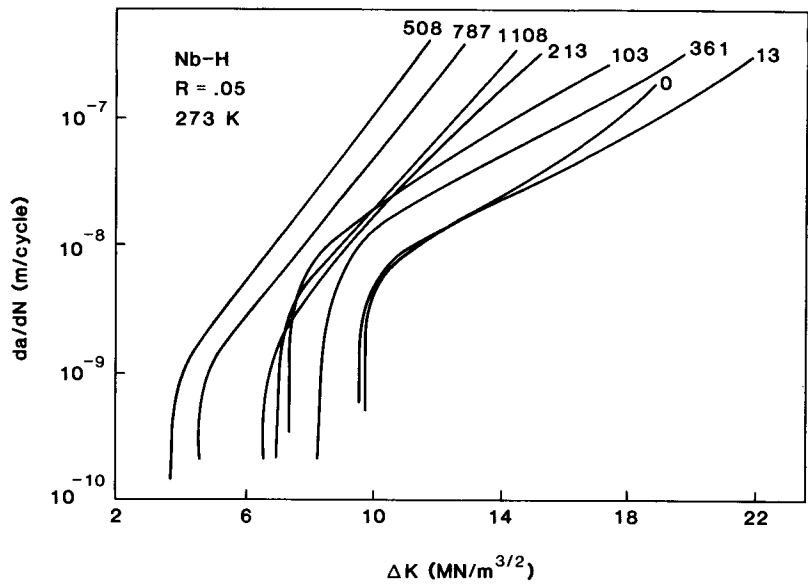


FIG. 3—Fatigue crack propagation rate, da/dN , versus stress intensity range, ΔK , in niobium-hydrogen alloys at stress ratio $R = 0.05$ and 273 K. Numbers above curves represent the amount of hydrogen dissolved in ppm weight.

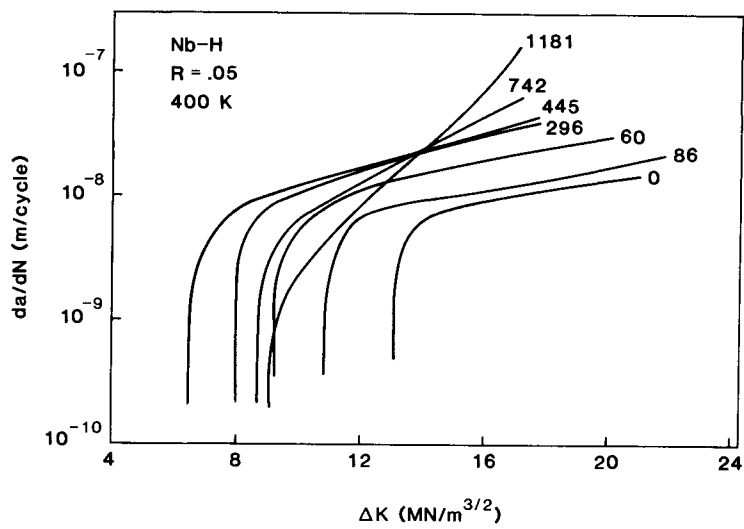


FIG. 4—Fatigue crack propagation rate, da/dN , versus stress intensity range, ΔK , in niobium-hydrogen alloys at stress ratio $R = 0.05$ and 400 K. Numbers at curves represent the amount of hydrogen dissolved in ppm weight.

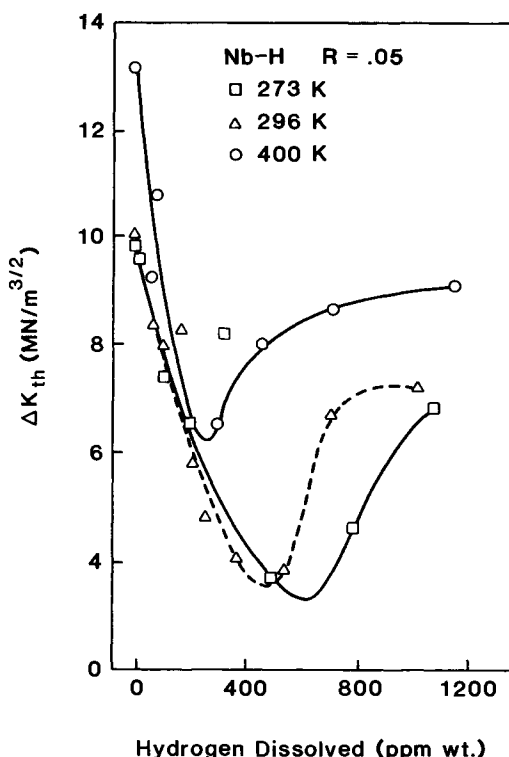


FIG. 5—Dependence of threshold stress intensity range, ΔK_{th} , on hydrogen concentration in niobium-hydrogen alloys. Stress ratio $R = 0.05$. The stress-free solubility of hydrogen in niobium at 273, 296, and 400 K are, respectively, 230, 350, and 1170 ppm weight.

hydrogen, C_r , required for embrittlement. As the amount of hydrogen dissolved exceeds C_r , ΔK_{th} increases as a function of hydrogen concentration and seems to reach a steady state value at very high concentrations. This behavior suggests that two mechanisms are responsible for the embrittlement of niobium with hydrogen. One causes the sharp decrease in ductility when the amount of hydrogen is less than C_r , while the other mechanism, which partially offsets the embrittlement occurring at lower concentrations, operates when the hydrogen concentration is greater than C_r . The effects of the two mechanisms become equal at C_r .

There is a possibility, however, that under plane stress conditions the effects of closure can be large and can account for or perhaps exceed the observed increase in ΔK_{th} at high hydrogen concentrations. In this case, ΔK_{th} would either remain constant or continue decreasing after the hydrogen concentration in the specimen exceeds C_r , and only one mechanism would be responsible for the behavior of ΔK_{th} with hydrogen concentration. At present, results to examine the extent of closure contributions to ΔK_{th} are not available, and we are in the process of developing the experimental capability to perform these measurements.

Figure 5 indicates that the maximum embrittlement occurs at approximately 600 ppm weight at 273 K, 400 ppm weight at 296 K, and 280 ppm weight hydrogen at 400 K. The stress-free solubility of hydrogen in niobium at these temperatures are, respectively, 230, 350, and 1170 ppm weight and indicates no correlation between C_r and the formation of stress-free hydride as reported earlier [22]. The possibility of stress-induced hydrides formed at the crack tip also seems to be remote since the differences between C_r and the solubility limit at some tempera-

tures are very great. Using the calculations of Grossbeck and Birnbaum [23] for the effects of external stress on the precipitation of hydrides, one finds that a biaxial stress of 0.2μ (μ is the shear modulus) is needed to shift the solubility limit 1170 ppm weight at 400 K to the value $C_r = 280$ ppm weight. Such stress (0.2μ) is greater than that likely to be generated at the crack tip. Accordingly, it may then be concluded that stress-induced hydrides cannot be also formed and that the decrease of ΔK_{th} with hydrogen will not be due to the presence of hydrides. If hydride, rather than some more mobile form of hydrogen, was responsible for embrittlement, ΔK_{th} would have reached a minimum value when the hydride phase began to form and then decreased precipitously after that. This argument also suggests that the two embrittlement mechanisms are operative when the hydrogen is in solid solution as well as in the hydride phase.

Also from Fig. 5, one can see that the minimum values of threshold stress intensity range for the three test temperatures follow the general behavior of fatigue fracture toughness of most materials where ΔK decreases as the test temperature decreases. Figure 6 is a plot of $(\Delta K_{th})_{min}$ as a function of Temperature T and indicates a linear relationship between the two quantities with a slope of $0.024 \text{ MN/m}^{3/2}$. The solute concentration buildup in a stress field, C_r , at a distance r has been given by Liu as [24]

$$C_r = C_o \exp \left[\frac{2(1 + \nu)}{\sqrt{2\pi r}} \cdot \frac{V_H \Delta K}{3RT} \right] \quad (3)$$

where

C_o = the solute concentration in the bulk,

V_H = the partial molal volume,

ν = Poisson's ratio, and

R = the gas constant.

From microhardness measurements at room temperature, Fariabi et al. [25] determined the plastic zone size, r_y in niobium specimens containing various amounts of hydrogen and found that r_y does not change much as a function of dissolved hydrogen C_o , and is in the order of approximately 1 mm. Those authors also found that the calculated hydrogen concentration C_r in the stress field around the crack increases linearly as a function of the amount of dissolved hydrogen C_o . If these results are valid at all temperatures, then $\Delta K/T$ will be constant and agrees with the plot in Fig. 6.

Using the values for $(\Delta K_{th})_{min}/T = 0.024 \text{ MN/m}^{3/2}/\text{K}$, $r = 1 \text{ mm}$, $\nu = 0.37$, $V_H = 1.7 \times 10^{-6} \text{ m}^3$, and $R = 8.3 \times 10^7 \text{ erg/mol. K}$, the quantity between brackets in Eq 3, is equal to 0.056. The ratio of the hydrogen concentrations at a distance r from the crack tip C_r and in the bulk C_o will then be equal to 1.06. This indicates that at $(\Delta K_{th})_{min}$, there will be no migration of hydrogen from the bulk to the crack tip stress field, and C_r represents the critical hydrogen concentration required for maximum embrittlement. This result supports the quantitative correlation obtained by Gerberich and Chen [19], who suggest the existence of ΔK_{th} , defined as the stress intensity below which no cracking will occur under hydrogen-assisted conditions. The agreement, however, is for the minimum values of ΔK_{th} or for maximum embrittlement at specific temperatures.

Figure 7 is a plot of the natural logarithm of hydrogen concentration (in percentage of atomic ratio) for maximum embrittlement, C_r , as a function of the inverse absolute temperature. As seen, a straight line passes through the data and can be described by

$$C_r = A \exp[Q/RT] \quad (4)$$

where A is a constant. The value of the activation energy, Q , calculated from Fig. 7, is 1400 cal/mol .

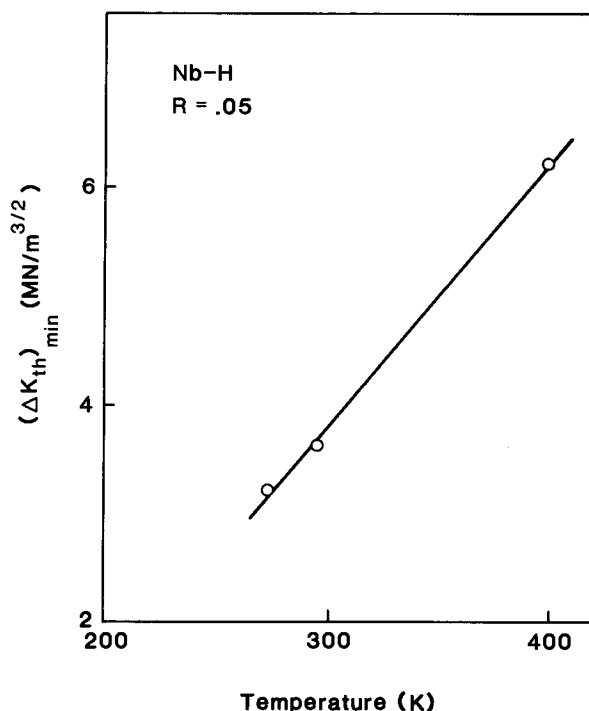


FIG. 6—Minimum threshold stress intensity range, $(\Delta K_{th})_{min}$, as a function of temperature.

From their anelastic studies of hydrogen diffusion in niobium, Baker and Birnbaum [26] found that, at low temperatures, hydrogen exists as pairs of hydrogen-hydrogen (H-H) clusters, and the energy of interaction of these pairs is 1265 ± 100 cal/mol. The agreement between their value and ours suggests that at $(\Delta K_{th})_{min}$, hydrogen at the crack tip may exist as pairs of H-H clusters, and the number of these clusters increases as the temperature is decreased. One of the mechanisms proposed earlier [5] for hydrogen embrittlement was based on decohesion resulting from mobile hydrogen in solution or as clusters. The presence of H-H clusters can also be more effective as obstacles to dislocation mobility. Earlier studies by Farahani et al. [1] and by Farabi et al. [22] gave evidence in support of dislocation-hydrogen interaction as a mechanism for hydrogen embrittlement in niobium.

Conclusions

From the fatigue crack propagation results obtained in this work, the following conclusions can be drawn:

1. The threshold stress intensity range, ΔK_{th} , of niobium decreases as the amount of dissolved hydrogen is increased and reaches a minimum, $(\Delta K_{th})_{min}$, at a critical concentration, C_r , where the maximum embrittlement occurs. As the hydrogen concentration exceeds this critical concentration, ΔK_{th} increases with the increase of hydrogen content. This behavior suggests that two mechanisms are responsible for the embrittlement of niobium with hydrogen.

2. $(\Delta K_{th})_{min}$ is found to be affected by temperature and decreases as the temperature is decreased. C_r , however, increases as the temperature is decreased.

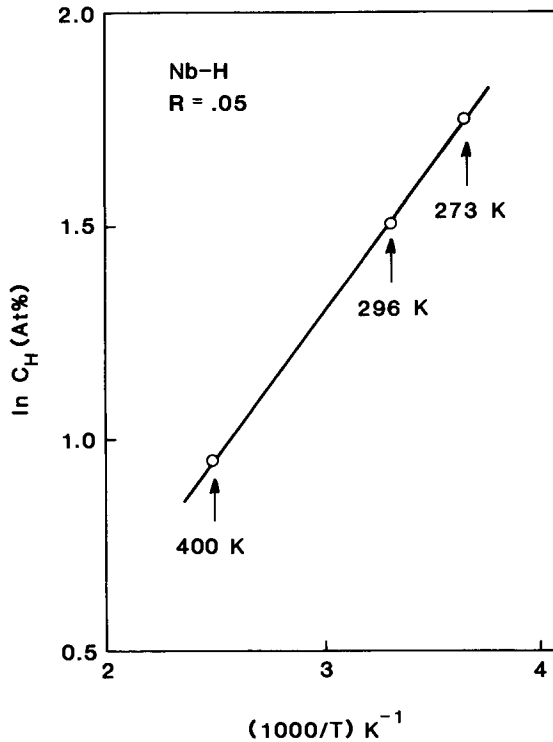


FIG. 7—Hydrogen concentration at maximum embrittlement versus inverse of absolute temperature.

3. The analysis of results supports the model of Gerberich and Chen for the existence of ΔK_{th} below which no cracking occurs under hydrogen-assisted conditions. The analysis also suggests that hydrides cannot be responsible for embrittlement of niobium, and some more mobile form of hydrogen clusters is likely to cause embrittlement.

Acknowledgments

The authors would like to thank C. C. Lin for his assistance with experiments. They also wish to thank the reviewers of the paper for their constructive criticisms and critical reading of the manuscript.

References

- [1] Farahani, M. M., Attia, F., and Salama, K., *Metallurgical Transactions Annual*, 1981, Vol. 12A, pp. 631-38.
- [2] Gahr, S., Grossbeck, M. L., and Birnbaum, H. K., *Acta Metallurgica*, 1977, Vol. 25, pp. 125-34.
- [3] Hardie, D. and McIntyre, P., *Metallurgical Transactions*, 1973, Vol. 4, pp. 1247-54.
- [4] Westlake, D. G. and Ockers, S. T., *Metallurgical Transactions Annual*, 1975, Vol. 6A, pp. 399-403.
- [5] Owen, C. V. and Scott, T. E., *Metallurgical Transactions*, 1972, Vol. 3, pp. 1715-26.
- [6] Westlake, D. G., *Transactions of TMS-AIME*, 1967, Vol. 239, pp. 1341-44.
- [7] Chandler, W. T. and Walter, R. J., *Proceedings of AIME Symposium on Refractory Metal Alloy*, I. Machlin, R. T. Begley, and E. D. Weisert, Eds., Plenum Press, New York, 1968, p. 197.
- [8] Wilcox, B. A., *Transactions of TMS-AIME*, 1964, Vol. 230, pp. 1199-200.

- [9] Lee, K. S. and Stoloff, N. S., *Effect of Hydrogen on Behavior of Materials*, A. W. Thompson and I. M. Bernstein, Eds., American Institute of Mining, Metallurgical, and Petroleum Engineers, New York, 1975, pp. 404-14.
- [10] Chung, D. W. and Stoloff, N. S., *Metallurgical Transactions Annual*, 1978, Vol. 9A, pp. 71-78.
- [11] Chung, D. W. and Stoloff, N. S., *Metallurgical Transactions Annual*, 1978, Vol. 9A, pp. 1387-99.
- [12] Gertzman, S. L. and Thurston, R. C. A., CIM Conference of Metallurgy, Halifax, Nova Scotia, 1972, Canadian Institute of Mining and Metallurgy.
- [13] Clark, Jr., W. G. and Trout, Jr., H. E., *Engineering Fracture Mechanics*, 1970, Vol. 2, p. 107.
- [14] Rolfe, S. T. and Munse, W. H., *Welding Research Council, Research Reports*, 1963, Vol. 42, p. 2525.
- [15] Birnbaum, H. K., *Environment-Sensitive Fracture of Engineering Materials*, Z. A. Foroulis, Ed., TMS-AIME, Warrendale, PA, 1979, pp. 326-60.
- [16] Troiano, A. R., *Transactions of the American Society for Metals*, 1960, Vol. 52, pp. 54-80.
- [17] St. John, C. and Gerberich, W. W., *Metallurgical Transactions*, 1973, Vol. 4, pp. 589-601.
- [18] Van Leeuwen, H. P., *Corrosion*, 1973, Vol. 29, pp. 197-204.
- [19] Gerberich, W. W. and Chen, Y. T., *Metallurgical Transactions Annual*, 1975, Vol. 6A, pp. 271-78.
- [20] Mueller, W. M., Blackedge, J. P., and Libowitz, G. G., *Metal Hydrides*, Academic Press, New York, 1968, pp. 592-607.
- [21] Westlake, D. G., *Transactions of TMS-AIME*, 1969, Vol. 245, pp. 287-92.
- [22] Fariabi, S., Collins, A. L. W., and Salama, K., *Metallurgical Transactions Annual*, 1983, Vol. 14A, pp. 701-707.
- [23] Grossbeck, M. L. and Birnbaum, H. K., *Acta Metallurgica*, 1977, pp. 135-147.
- [24] Liu, H. W., *Journal of Basic Engineering*, ASME, 1970, Vol. 92, p. 633.
- [25] Fariabi, S., Collins, A. L. W., and Salama, K., *Proceedings of the Sixth International Council on Fracture 6*, S. R. Valluri, D. M. R. Taplin, P. Rama Rao, and J. F. Knott, Eds., 1984, pp. 3997-4008.
- [26] Baker, C. and Birnbaum, H. K., *Acta Metallurgica*, 1973, pp. 865-872.

Author Index

A

Agarwala, V. S., 98
Altstetter, C., 403
Ancil, A. A., 8

B

Berman, D. A., 98
Blackburn, J., 217
Bruggeman, G. A., 335

C

Chionis, W. C., 287
Cialone, H. J., 134
Ciaraldi, S. W., 200
Clegg, E. T., 37
Coates, D. J., 55
Cox, D. O., 190
Crumly, W. R., 173

D

Dannecker, J. R., 247
de Kreuk, C. W., 90
DeLuccia, J. J., 17
Dreher, R. V., 60
Dubois, D. J. M., 219

F

Faure, F. M., 219, 353
Fidelle, J.-P., 153
Field, W., 303
Fricioni, R., 89, 128

G

Grey, C., 372
Grobin, A. W., Jr., 46

H

Holbrook, J. H., 134

K

Kawase, H., 105
Krams, W. E., 343

L

Leblond, J.-B., 219
Lemoine, V., 219
Levy, M., 335

M

Mackor, A., 90
McIntyre, D. R., 133, 178
Moran, P. J., 387
Murray, G. T., 304

O

Ohtsubo, T., 105

P

Perng, T., 403
Pollock, W. J., 68, 372
Polvanich, N., 417
Pressouyre, G. M., 219, 353

Q

Quintana, M. A., 247

R

Raymond, L., 1, 10

S

Saillard, P. R., 219
Salama, K., 417
Schoonman, J., 90
Scully, J. R., 387
Shewmon, P. G., 117
Siewert, T. A., 238
Sonnino, C., 7

V

Voorhis, G. P., 318

W

Wang, M., 117
White, D. R., 287
Wong, R. J., 274

Y

Yamazaki, S., 105

Subject Index

A

- Accelerated testing, 14, 60
- Acoustic emission testing, 14
- Adsorption, 387
- Aircraft fasteners, 55, 335
- Aircraft maintenance, 55
- Aluminum, 1, 17, 83
- American Bureau of Shipping glycerine test, 238
- ASTM
 - committees, 46, 127, 173, 190
 - standards
 - A 36: 57, 238
 - A 262-85: 202
 - A 304-79: 43
 - A 487: 190
 - B 602: 54
 - B 697: 54
 - E 8-85: 61, 335
 - E 8M-84: 43
 - E 399-83: 14
 - E 647-83: 137
 - E 813-81: 137
 - F 519-77: 1, 10, 14, 56, 61, 69, 319, 343, 374, 384
 - G 35-73: 202
 - G 44: 133
- American Welding Society standards, 57
- Amine solutions, 210
- Annealing, 7
- Anodic polarization, 82
- Atomic hydrogen, 37

B

- Bakeouts, 318
- Barnacle electrode test, 10, 26, 98
- Bending, 10
- Bent beam test method, 190
- Brittle failure, 37
- Bronze electrodes, 90

C

- Cadmium plating, 68, 98, 335, 372
- Cadmium-titanium plating, 68
- Carbon dioxide, 138
- Carbon monoxide, 138
- Charpy impact energy, 343

- Chemical analysis (*See* Testing)
- Chloride-induced stress-corrosion cracking, 209
- Coatings, zinc phosphate (*See also* Surface films; Platings), 318
- Cobalt alloys, 17, 162
- Computer analysis, 219
- Concentration cells, 90
- Copper, 17
- Corrosion, 17, 55, 178, 190, 200, 209
- Corrosion-resistant alloys, 178, 200
- Crack growth, subcritical, 343, 417
- Crack propagation, fatigue, 134, 417
- Crack size, critical, 343
- Crack tips, hydrogen in, 26
- Cracking
 - from chloride, 209
 - critical hydrogen concentrations, 353
 - in HY-80 steel, 274
 - from hydrogen sulfide, 55, 178, 190, 200
 - susceptibility screening, 173, 200
 - U.S. Government standards, 37

D

- Defense Specifications and Standards Program, 37
- Delayed failure testing, 318
- Department of Defense standardization, 37
- Diffusible hydrogen (*See* Hydrogen diffusion)
- Disk pressure test, 13, 153
- Dynamic toughness, 343

E

- Electrochemical sensors, 90
- Electrochemical test methods
 - barnacle electrode, 25, 98
 - hydrogen sensor, 90
 - permeation, 117, 353, 387
 - status, 10
- Electrochemistry of hydrogen embrittlement, 7, 17, 117
- Embrittlement (*See* Hydrogen embrittlement)
- Endothermic occluders, 17
- Environmental cracking (*See* Hydrogen embrittlement; Stress corrosion and cracking; Testing)
- Exchange current density, 18
- Exothermic occluders, 17

F

Fasteners, 53, 55, 335
 Fatigue crack propagation, 134, 417
 Ferrous alloys (*See also* Steels), 37, 387
 Film rupture, 387
 Fracture mechanics, 10, 134, 335, 343

G

Galvanic coupling, 15
 Gas chromatography, 238, 287
 Gas service, ranking materials for, 178, 200
 Glycerin, 238
 Group VB metals, 417

H

Hardness, 37
 Hydrogen, atomic, 37, 90
 Hydrogen, critical concentrations in metals, 353
 Hydrogen determination and measurement, 90, 98, 105
 Hydrogen diffusion
 in crack tips, 26
 critical concentrations, 353
 electrochemical measurement techniques, 10, 25, 90, 98, 117, 353, 387
 in ferrous alloys, 37, 387
 gas chromatography testing, 247
 solubility, 353, 387
 sources of, 17, 55, 372
 in steels (*See* Steels)
 testing (*See* Testing)
 in weld heat affected zones, 219
 in weld metal, 274, 287
 in welding electrodes, 238
 Hydrogen embrittlement
 electrochemistry, 7, 17, 117
 in ferrous alloys, 387
 mechanisms, 7, 17, 133
 by paint strippers, 372
 prevention techniques
 coatings, zinc phosphate, 318
 platings (*See* Platings)
 polarization, 82
 relief treatments, 37, 48, 51, 318
 surface films, nitride and oxide (*See also* Platings), 304
 slow crack growth, 403
 standards (*See* Standards)
 in steels (*See* Steels)
 test methods (*See* Standards; Testing)
 Hydrogen evolution kinetics, 17
 Hydrogen, gaseous, 134

Hydrogen permeation (*See* Hydrogen diffusion)
 Hydrogen-stress cracking, 37, 274, 353
 Hydrogen sulfide stress corrosion cracking resistance, 55, 190
 Hydrogen transport (*See* Hydrogen diffusion)
 Hydrogen trapping, 17, 353, 387

I

Implant test, 274
 Industrial Fasteners Institute standards, 10, 56
 Inhibitors, 134, 304
 International Institute of Welding test, 238
 ISO committees and standards, 46
 Iron, 17, 105

K

Kolachev effect, 160

L

Langmuir adsorption isotherm, 23

M

Maintenance chemicals, 10
 Mass spectrometry, 219
 Materials selection and ranking, 173, 200
 Mercury, 238, 270
 Metals, precious, 153
 Methane, 138
 Microstructure of austenitic stainless steels, 403
 Molten metal, 105
 Molybdenum bronze, 90

N

National Association of Corrosion Engineers standards, 58, 203
 Nickel, 17, 68
 Niobium-hydrogen alloys, 417
 Nitrogen, 138
 Numerical simulation, 219

P

Paint strippers, 372
 Palladium, 18, 90
 Permeability, 117, 387
 Petroleum industry materials selection, 178, 200
 Plasticity, 387

Platings (*See also* Surface films), 10
 aluminum, 83
 cadmium, 68, 98, 335, 372
 nickel, 68
 plating-and-baking processes, 68, 98
 U. S. Government standards, 37, 60

Platinum, 17
 Polarization, 22, 82
 Polythionic acid, 200
 Potential measurements, 90
 Precious metals, 17, 153
 Precipitation hardening, 304
 Proof tests, 343

R

Rust, 218

S

Sensors
 electrochemical, 90
 inert gas probe, 105
 Sievert's law, 287
 Silicone oil test, 240
 Silver, 17
 Slow strain rate test, 10, 68, 178, 372
 Society of Automotive Engineers standards, 55
 Solubility of materials, 353, 387
 Sour gas service, ranking materials for, 178, 200
 Specifications for testing (*See* Standards)
 Spectroscopy, 287
 Standards
 American Bureau of Shipping, 238
 ASTM
 A 36: 57, 238
 A 262-85: 202
 A 304-79: 43
 A 487: 190
 B 602: 54
 B 697: 54
 E 8-85: 61, 335
 E 8M-84: 43
 E 399-83: 14
 E 647-83: 137
 E 813-81: 137
 F 519-77: 1, 10, 14, 56, 61, 69, 319, 343, 374, 384
 F 606-85: 47
 G 35-73: 202
 G 44: 133
 American Welding Society, 57
 Australian RAAF, 385
 comparison, table, 76, 78

Industrial Fasteners Institute, 10, 56
 International Institute of Welding, 238
 ISO, 46
 Kaiser RYY 3-006: 64
 National Association of Corrosion Engineers, 58, 203
 Society of Automotive Engineers, 55
 U.S. Government, 10, 37
 MIL-C-23422: 63
 MIL-C-26074B: 62
 MIL-R-81294B: 385
 MIL-R-83936B: 384
 MIL-STD-1312: 335
 MIL-STD-1501: 335
 QQ-C-320: 64
 QQ-P-416C: 335

Steels

austenitic stainless, 157, 403
 carbon, 117
 castings, 190
 cold work, influence of, 165
 duplex stainless, 403
 electroslog refined, 117
 ferritic, 403
 hydrogen-induced cracking mechanisms, 133
 low alloy, 68, 178, 219, 353, 372
 martensitic, 153, 403
 mechanical properties, 335
 microstructure, 403
 pipeline, 134, 178, 200
 slow crack growth, 403
 sour gas service, ranking materials for, 178, 200
 stainless, 157, 304, 403
 stress-induced martensite, 403
 zinc phosphate coated, 318
 C-1.2Mn, 366
 3.5Ni, 365
 9 Ni cryogenic, 165
 15B41, 318
 20 CrNiMo 10, 162
 HS 25 Co, 168
 35 NCD 16, illus., 164
 35 NiCrMo 16, illus., 156
 HY-80, 274
 250 maraging, illus., 158
 A286, illus., 158
 300M, 83, 98
 301, 403
 302L, illus., 158
 304, 403
 310, 403
 Am 355, illus., 163
 410, 15
 A508, 219, 363

Steels (*cont.*)

- A533, 365
- SAL 2560, 290
- 4140, 318
- 4330 V, 60
- 4340, 10, 68, 175, 335, 344, 372, 387
- Step load testing, 10, 60, 173, 343
- Strain, in ferrous alloys, 387
- Strain rate testing, 68, 156, 173, 178, 372, 387, 403
- Strength, tensile, 37
- Stress corrosion and cracking (*See also* Hydrogen embrittlement)
 - in austenitic stainless steels, 403
 - from chloride, 209
 - critical hydrogen concentrations, 353
 - in HY-80 steel, 274
 - from hydrogen sulfide, 55, 178, 190, 200
 - from sulfide, 55, 178, 190, 200
 - susceptibility screening, 173, 200
 - U.S. Government standards, 37
- Stress-induced martensite, 403
- Stress intensity estimation, critical, 173, 343
- Stress relief methods, 51
- Stress testing, 173
- Subcritical crack growth, 343
- Submunitions, 318
- Sulfide stress cracking, 55, 178, 190, 200
- Surface coverage, 387
- Surface films, nitride and oxide (*See also* Coatings; Platings), 304
- Sustained load testing, 10

T

- Tantalum, 417
- Teapot test, 240
- Temperature dependence of fatigue crack propagation, 417
- Tensile strength, 10, 37
- Tension testing, 10
- Testing (*See also* Standards)
 - accelerated, 14, 60
 - acoustic emission, 14
 - ASTM and ISO committees involved, 46
 - barnacle electrode, 10, 26, 98
 - bent beam, 190
 - Charpy impact, 343
 - comparison of test methods, 238
 - computer analysis, 219
 - constant load, 403
 - disk pressure, 13, 153
 - 8-h test, 60
 - electrochemical
 - barnacle electrode, 25, 98

- hydrogen sensor, 90
- permeation, 117, 353, 387
- status, 10
- environmental cracking, 190, 200
- gas chromatography, 238, 247, 287
- glycerine test, American Bureau of Shipping, 238
- implant, 274
- in liquid iron, mass spectrometry, 105
- proof, 343
- rigidly restrained cracking, 284
- silicone oil, 240
- specifications, 55
- spectroscopy, 287
- stepped load, 14, 60, 173, 343
- strain rate, 10, 68, 156, 173, 178, 372, 387, 403
- stress intensity, critical, 173, 343
- sustained load, 10
- teapot, 240
- tension, 10, 417
- Thermal relief treatments, 37, 48, 51, 318
- Thorium, 18
- Threaded fasteners, 53
- Threshold stress intensity, 173, 343, 417
- Titanium alloys, 17, 68, 157, 162

V

- Vanadium, 18, 417
- Voids in steel, 117

W

- Weldability, 274
- Welding
 - electrode coating moisture, 238
 - electrode testing, 238
 - ferritic arc, 217
 - gas metal arc, 287
 - hydrogen arc atmosphere, 287
 - hydrogen in heat-affected zones, 219, 247, 274
 - prediction of hydrogen content, 287
 - rust, 218
 - shielded metal arc, 238
 - standards, 55
 - weld metal diffusible hydrogen, 274

Z

- Zinc phosphate coatings, 318
- Zirconium, 18



Lou Raymond
P.O. Box 7925
Newport Beach, CA 92658-7925